



The
University
Of
Sheffield.

**Tissue Engineering an *In Vitro* Model of
Osteoporosis**

Robert Owen

**A thesis submitted in partial fulfilment of the
requirements for the degree of Doctor of
Philosophy**

The University of Sheffield

Faculty of Engineering

**Department of Materials Science and
Engineering**

October 2017

Abstract

Postmenopausal osteoporosis is a skeletal disorder characterised by bone loss. Declining oestrogen levels postmenopause disrupt bone remodelling by overstimulating resorption. Although the disorder is currently studied in animals, we should aim to minimise their use. Therefore, this thesis explored the feasibility of developing an *in vitro* model of postmenopausal osteoporosis using tissue engineering principles.

The response of three osteoblast cell lines, MC3T3-E1, MLOA5, and IDG-SW3, to oestrogen was explored, finding only MC3T3-E1 was stimulated by the hormone. The ability of RAW264.7 to undergo osteoclastogenesis was strongly influenced by seeding density and proliferation. Additionally, tartrate-resistant acid phosphatase (TRAP) activity could be suppressed by oestrogen exposure. Due to its ability to support osteoclastogenesis in co-culture, IDG-SW3 was the most suitable osteoblast cell line for the model.

Bone-matrix deposition over 28 days on three scaffolds (PolyHIPE, polyurethane, Biotek) was compared to select the most appropriate for the model. PolyHIPE and polyurethane scaffolds supported significantly more matrix deposition than the Biotek. Mineralisation on the scaffold could be detected by micro-computed tomography; however, the presence of PBS interfered with this. Due to its cellular performance and ease of manufacture, the polyurethane scaffold was identified as the most suitable for the model.

Changes in mineral content, TRAP and alkaline phosphatase activity were confirmed as markers for osteoclast and osteoblast activity in co-culture. RAW264.7 pre-treatment with oestrogen to mimic pre-menopause had lasting effects on their ability to undergo osteoclastogenesis. 2D co-cultures using oestrogen withdrawal to mimic menopause resulted in increased resorption, analogous to the effect seen *in vivo*. From the conditions assessed in 3D co-cultures, no equivalent response was observed. This thesis demonstrates it is possible to imitate the onset of postmenopausal osteoporosis *in vitro*. However, a 3D system that uses human cells and longer time periods is necessary to provide a valid alternative to animal models.

Acknowledgements

I would like to thank my supervisor, Dr. Gwendolen Reilly, for providing me with the opportunity to undertake this PhD. Your support, input, encouragement, and belief has helped guide this project and my future career. Without your guidance, I would not be in the position I am in today. I would also like to thank Dr. Frederik Claeysens for his continued involvement and interest, your endless enthusiasm is an excellent source of motivation when everything seems to be going wrong. Thanks also to Prof. Sheila MacNeil for securing funding from the EPSRC and BBSRC, and the Leverhulme Trade Charities Trust whose continued support has been received most gratefully.

To my friends, I would like to thank you for all your advice, help in the lab, and trips to the pub. Will and Nat, thank you for all the memories over the last seven years since we started University together. Liam and Hossein, thank you for being the backbone of the lab, keeping everything running smoothly with an endless supply of tip boxes, and making conferences more exciting. Ross, without your help in the laser lab during second year I don't think I could have ever faced making a scaffold again. Adam, our never-ending discussions on everything in the world have helped solve so many problems. Claudia and Luke, thank you for the fruity ciders. Colin, your limitless knowledge of PolyHIPEs helped make this project possible. I also want to thank Ben for his help during his placement and Julie for making sure the lab doesn't fall apart.

To my parents, Gillian and Vernon, I would like to thank you for always encouraging me to pursue what makes me happy. I appreciate everything you have done for me. I'd like to thank Dr. Richard Owen for his insight into undertaking a PhD, as well as my Uncles and Grandfather for introducing me to engineering during my childhood. Finally, to my partner Rebecca, words will never be able to express my gratitude and thanks to you. Whether it was stressed late nights, tired early mornings or inconvenient weekends, you have always been there and put up with me and I wouldn't be here today without you. This thesis is dedicated to the memory of my beloved Grandfather, John R. Nelson. You were a brilliant man who inspired all that met you. I will try and emulate your shining example in all that I do. Thank you for everything.

“If I have seen further it is by standing on the shoulders of giants.”

-Sir Isaac Newton

Outputs

Publications

1. **Owen, R.**, Sherborne, C., Paterson, T., Green, N.H., Reilly, G.C., Claeysens, F., 2016. Emulsion templated scaffolds with tunable mechanical properties for bone tissue engineering. *Journal of the mechanical behavior of biomedical materials*, 54, pp.159-172.
 - a. A full copy of this publication is available in the appendix, §10.3.
2. **Owen, R.**, Sherborne, C., Reilly, G.C., Claeysens, F., 2015. Data for the analysis of PolyHIPE scaffolds with tunable mechanical properties for bone tissue engineering. *Data in brief*, 5, pp.616-620.
3. Wang, A.J., Paterson, T., **Owen, R.**, Sherborne, C., Dugan, J., Li, J.M., Claeysens, F., 2016. Photocurable high internal phase emulsions (HIPEs) containing hydroxyapatite for additive manufacture of tissue engineering scaffolds with multi-scale porosity. *Materials Science and Engineering: C*, 67, pp.51-58.
4. Baud'huin, M., Lamoureux, F., Jacques, C., Calleja, L.R., Quillard, T., Charrier, C., Amiaud, J., Berreur, M., Brounais-LeRoyer, B., **Owen, R.**, Reilly, G.C., Bradner, J.E., Heymann, D., Ory, B., 2017. Inhibition of BET proteins and epigenetic signaling as a potential treatment for osteoporosis. *Bone*, 94, pp.10-21.
5. Antonini, L.M., Kothe, V., Reilly, G.C., **Owen, R.**, Marcuzzo, J.S., Malfatti, C.F. Effect of Ti6Al4V surface morphology on the osteogenic differentiation of human embryonic stem cells. 2017. *Journal of Materials Research*. 32(10), pp. 3811-3821
6. Birru, B., **Owen, R.**, Bahmaee, H., Rao, P.S., Reilly, G.C. Design and assessment of a dynamic perfusion reactor for large bone tissue engineering scaffolds. *Applied Biochemistry and Biotechnology*.

7. Borg, S.A., Buckley, H., **Owen, R.**, Campos Marin, A., Lu, Y., Eyles, D., Lacroix, D., Reilly, G.C., Skerry, T.M., Bishop, N.J. Early life Vitamin D depletion alters the postnatal response to skeletal loading in growing and mature bone. *PLOS ONE*.

Publications in Preparation

1. Bhaskar, B., **Owen, R.**, Bahmaee, H., Wally, Z., Sreenivasa Rao, P., Reilly, G.C. Composite porous scaffold of polyethylene glycol (PEG)/polylactic acid (PLA) support improved bone matrix deposition in vitro compared to PLA-only scaffolds. *Submitted to Journal of Biomedical Materials Research: Part A.*
2. Glen, A., **Owen, R.**, Claeysens, F., Haycock, J.W., Enhanced Antibody Computed Tomography (ENACT) – A novel, non-destructive, molecularly specific method for the detection of cellular populations in three dimensional samples. *Submitted to Scientific Reports.*
3. Pashneh-Tala, S., **Owen, R.**, Bahmaee, H., Rekštytė, S., Malinauskas, M., Claeysens, F. Synthesis, Characterization and Structuring of a Photocurable Poly(glycerol sebacate) for Applications in Tissue Engineering. *Submitted to Biomacromolecules.*
4. **Owen, R.**, Reilly, G.C., In vitro models of bone remodelling and associated disorders.
5. Sherborne, C., **Owen, R.**, Reilly, G.C., Claeysens, F. The influence of surface skin formation on light-based additive manufacturing with emulsion templated resins.

Oral Presentations

1. PolyHIPE Scaffolds with Tunable Mechanical Properties for Bone Tissue Engineering. *21st Congress of the European Society of Biomechanics. Prague, Czech Republic. 5th – 8th July 2015*
2. PolyHIPE scaffolds with Tunable Mechanical Properties for Bone Tissue Engineering. *MEIBioeng15. Leeds, United Kingdom. 7th – 8th September 2015*
3. Multiscale Porosity Scaffolds for Bone Tissue Engineering. *17th Annual White Rose Work in Progress Meeting. York, United Kingdom. 15th December 2015.*
Winner – Best Oral Presentation
4. Multiscale Porosity Scaffolds for Osteochondral Repair. *22nd Congress of the European Society of Biomechanics. Lyon, France. 10th – 13th July, 2016.*
5. Bioreactors for Bone Tissue Engineering. *18th Annual White Rose Work in Progress Meeting. 14th December 2016.* **Winner – Best Oral Presentation**
6. Can We Tissue Engineer an *in vitro* model of Osteoporosis? *Advances in Cell and Tissue Culture 2017. Manchester, United Kingdom. 22nd – 24th May 2017*
7. Tissue Engineering an *in vitro* Model of Osteoporosis. *Tissue Engineering and Regenerative Medicine International Society (TERMIS) – EU 2017. Davos, Switzerland. 26th – 30th June 2017*

Poster Presentations

1. Mechanical Characterisation of PolyHIPEs. *BOSE User Group Meeting 2014. Sheffield, United Kingdom. 24th June 2014.* **Runner up – Best Poster**
2. PolyHIPE Scaffolds with Tunable Mechanical Properties for Bone Tissue Engineering. *16th Annual White Rose Work in Progress Meeting. Sheffield, United Kingdom. 15th December 2014.* **Winner – Best Abstract Image**
3. Tissue Engineering an *In Vitro* Model of Osteoporosis. *INSIGNEO Showcase 2015. Sheffield, United Kingdom. 8th May 2015*
4. Multiscale Porosity Scaffolds for Osteochondral Repair. *INSIGNEO Showcase 2016. 11th May 2016.*

Contents

Abstract	iii
Acknowledgements	iv
Outputs	v
Publications	v
Publications in Preparation	vii
Oral Presentations	viii
Poster Presentations	viii
Contents	ix
List of Figures	xviii
List of Tables.....	xxvi
Abbreviations	xxviii
1. Introduction	37
2. Background	39
2.1 Bone – Physiology, hierarchy and healing.....	39
2.1.1 Anatomy and function.....	39
2.1.2 Macrostructure	39
2.1.3 Micro and nanostructure	42

2.1.4 Cell biology of bone.....	48
2.1.5 Bone remodelling.....	54
2.1.6 Bone tissue engineering	60
2.2 Osteoporosis.....	63
2.2.1 Prevalence and clinical consequence	63
2.2.2 Aetiology, pathogenesis and risk factors	64
2.2.3 Diagnosis and current treatments.....	68
2.2.4 Animal models of osteoporosis.....	73
2.3 Bone remodelling <i>in vitro</i>	78
2.3.1 The need for <i>in vitro</i> models.....	78
2.3.2 Remodelling fundamentals	86
2.3.3 Remodelling models	95
2.3.4 Pathological models.....	102
2.4 Summary.....	107
2.5 Project aims and objectives.....	108
3. Materials and Methods.....	109
3.1 Materials	109
3.2 Methods.....	109
3.2.1 Osteoblast cell lines	109

3.2.2 Osteoclast cell lines.....	111
3.2.3 Culture media preparation.....	111
3.2.4 General osteoblast culture.....	113
3.2.5 General osteoclast culture.....	114
3.2.6 Resazurin reduction assay.....	115
3.2.7 Cell digestion.....	115
3.2.8 Alkaline phosphatase activity.....	116
3.2.9 DNA quantification.....	116
3.2.10 Cell fixing.....	117
3.2.11 Alizarin Red S staining.....	117
3.2.12 Direct Red 80 staining.....	117
3.2.13 TRAP staining.....	118
3.2.14 TRAP activity.....	118
3.2.15 Scanning electron microscopy.....	119
3.2.16 Statistical analysis.....	119
4. Response of bone cells to oestrogen.....	121
4.1 Introduction.....	121
4.2 Aims and objectives.....	124
4.3 Materials and Methods.....	125

4.3.1 Preparation of oestrogen supplement.....	125
4.3.2 Alternative cell digestion protocols	125
4.3.3 Polyurethane scaffold preparation	126
4.3.4 Polyurethane scaffold seeding	126
4.3.5 RANKL and OPG ELISA.....	126
4.3.6 Preparation of Vitamin D3 supplement	127
4.3.7 Assessment of osteocytogenesis	127
4.3.8 Fluorescence microscopy.....	127
4.3.9 Resorption pit quantification.....	128
4.3.10 TRAP activity – lysates	128
4.3.11 Preparation of trabecular bone and dentine substrates.....	128
4.4 Results.....	129
4.4.1 Phenol red only affects oestrogen responsiveness at low concentrations	129
4.4.2 Oestrogen withdrawal does not further enhance MC3T3-E1 activity	131
4.4.3 Mineralisation capacity of MC3T3-E1 can be increased with varied supplementation	132
4.4.4 Oestrogen withdrawal has no effect of MLOA5.....	133
4.4.5 Oestrogen exposure has no effect on MLOA5 even at extreme concentrations	134

4.4.6 Oestrogen exposure has no effect on IDG-SW3	136
4.4.7 Varied temperature and media type can hold IDG-SW3 as osteoblasts .	138
4.4.8 RANKL:OPG Ratio	140
4.4.9 RAW264.7 mature in the presence of sRANKL.....	146
4.4.10 TRAP activity is dose dependent and is significantly reduced by digestion	149
4.4.11 Seeding density affects osteoclastogenesis	151
4.4.12 Oestrogen inhibits osteoclast viability and activity	152
4.4.13 IDG-SW3 support osteoclastogenesis in direct co-culture	154
4.4.14 RAW264.7 failed to resorb <i>ex vivo</i> tissue.....	156
4.5 Discussion	157
4.6 Summary	169
5. Development of a suitable substrate for an <i>in vitro</i> model of osteoporosis.....	171
5.1 Introduction	171
5.1.1 Scaffold requirements	171
5.1.2 Fabrication techniques	174
5.1.3 Microstereolithography	174
5.1.4 PolyHIPE materials for tissue engineering	175
5.2 Aims and objectives	179

5.3 Materials and methods	180
5.3.1 PolyHIPE nomenclature.....	180
5.3.2 HIPE synthesis	180
5.3.3 Coverslip functionalisation	182
5.3.4 Bulk HIPE polymerisation.....	182
5.3.5 Mechanical characterisation.....	182
5.3.6 Physical characterisation.....	183
5.3.7 PolyHIPE scaffold fabrication	184
5.3.8 Plasma modification of scaffolds.....	185
5.3.9 General hES-MP culture	186
5.3.10 PolyHIPE scaffold sterilisation.....	186
5.3.11 PolyHIPE scaffold seeding	186
5.3.12 Polyurethane scaffold preparation	187
5.3.13 Polyurethane scaffold seeding	187
5.3.14 Biotek scaffold seeding.....	187
5.3.15 Micro-computed tomography	188
5.3.16 Tissue sectioning and staining	191
5.4 Results.....	193
5.4.1 Wet mechanical properties are the same as dry	193

5.4.2 The degree of openness is linearly related to the internal phase proportion	194
5.4.3 Batch production significantly reduces manufacture time.....	196
5.4.4 Air and acrylic acid plasma treatments are equally effective at supporting cells	198
5.4.5 Substrate stiffness only affects differentiation under certain conditions	201
5.4.6 Stiffer PolyHIPE scaffolds retain their architecture without a glass base	202
5.4.7 Printing resolution is improved using a UV light absorber.....	206
5.4.8 Tinuvin is not cytotoxic in an EHA/IBOA PolyHIPE	209
5.4.9 PolyHIPE and polyurethane scaffolds are equally suitable for the model	211
5.4.10 Micro-computed tomography	216
5.4.11 Generation 3 PolyHIPE – improved architecture and reproducibility ..	224
5.4.12 Cells do not fully penetrate the internal porosity within 3 weeks.....	228
5.5 Discussion	230
5.6 Summary	246
6. Modelling osteoporosis <i>in vitro</i>	247
6.1 Introduction	247
6.2 Aims and objectives	248
6.3 Materials and methods	249

6.3.1 Co-culture medium	249
6.3.2 Evaluation of mineral resorption in co-cultures.....	249
6.3.3 Parathyroid hormone preparation	250
6.4 Results.....	251
6.4.1 Parathyroid hormone has a predominantly catabolic effect on IDG-SW3	251
6.4.2 Mineralisation and ALP and TRAP activity are appropriate co-culture markers.....	257
6.4.3 Oestrogen affects co-cultures in TCP and scaffolds	262
6.4.4 Co-cultures are not stable over extended time periods	264
6.4.5 Density of osteoclast precursors affects mineral resorption	268
6.4.6 Oestrogen pre-treatment of RAW264.7 has lasting effects after seeding	272
6.4.7 Oestrogen withdrawal increases mineral resorption in monolayer co- cultures.....	274
6.4.8 Mineral staining fails to detect changes in resorption following oestrogen withdrawal in 3D.....	278
6.5 Discussion.....	282
6.6 Summary	297
7. General discussion and future work.....	299
8. Conclusion	311

9. References	312
10. Appendix	359
10.1 Standard curves	359
10.2 Figure permissions	360
10.3 Emulsion templated scaffolds with tunable mechanical properties for bone tissue engineering.....	362

List of Figures

<i>Figure 2.1: Macroscopic and microscopic anatomy of an adult long bone</i>	41
<i>Figure 2.2: Hierarchical structure of cortical bone</i>	43
<i>Figure 2.3: Synchrotron image of a transverse cross section of a bone</i>	45
<i>Figure 2.4: Network of Haversian (white arrows) and Volkmann's (red arrows) canals</i>	46
<i>Figure 2.5: Synchrotron image of the microstructure of cortical bone</i>	47
<i>Figure 2.6: Osteoblastic and osteoclastic cell lineages</i>	49
<i>Figure 2.7: Schematic representation of an embedded osteocyte within its lacuna</i> .	51
<i>Figure 2.8: Colourised scanning electron micrograph of an active osteoclast and a resorption pit</i>	53
<i>Figure 2.9: Bone multicellular units in (top) trabecular and (bottom) cortical bone</i>	55
<i>Figure 2.10: Diagram of how the RANKL/RANK/OPG axis and M-CSF direct osteoclastogenesis and activation</i>	56
<i>Figure 2.11: The five stages of bone remodelling</i>	59
<i>Figure 2.12: Vertebral cancellous bone of a (A) 21-year old male and (B) 65-year old female</i>	65
<i>Figure 2.13: The central role of oestrogen in postmenopausal osteoporosis</i>	66
<i>Figure 2.14: Different methods of co-culturing cells</i>	79

Figure 2.15: Schematic summarising the effects of different factors on bone balance	94
Figure 4.1: Effect of phenol and oestrogen on MC3T3-E1	130
Figure 4.2: Effect of oestrogen withdrawal on MC3T3-E1.....	131
Figure 4.3: Effect of varied osteogenic supplementation of MC3T3-E1.....	132
Figure 4.4: Effect of oestrogen withdrawal on MLOA5.....	133
Figure 4.5: Effect of oestrogen exposure on MLOA5-S	134
Figure 4.6: Effect of oestrogen exposure on MLOA5-K.....	135
Figure 4.7: Comparison of MLOA5-K and MLOA5-A.....	136
Figure 4.8: Response of IDG-SW3 to oestrogen	137
Figure 4.9: Effect of varied temperature and media composition on IDG-SW3.....	139
Figure 4.10: Day 7 RANKL and OPG production in various osteoblastic cell lines	140
Figure 4.11: Effect of Vitamin D on RANKL production in MC3T3-E1 and IDG-SW3	142
Figure 4.12: The effect of oestrogen and osteocytogenesis on RANKL expression	144
Figure 4.13: Composite images of IDG-SW3 GFP fluorescence.....	145
Figure 4.14: Effect of RANKL on RAW264.7	147
Figure 4.15: Analysis of RAW264.7 resorption.....	148
Figure 4.16: Comparison of digestion protocol on apparent TRAP activity	150

Figure 4.17: TRAP activity in response to varied RANKL concentrations and seeding number	151
Figure 4.18: Effect of oestrogen on RAW264.7	153
Figure 4.19: Day 7 TRAP activity for co-cultures of (A) MLOA5-K and RAW264.7 and (B) IDG-SW3 and RAW264.7	155
Figure 4.20: Composite of multiple SEM images of RAW264.7 on trabecular bone and dentine (bottom right).	156
Figure 4.21: A hypothetical diagram showing how seeding density affects when osteoclastogenesis occurs in RAW264.7	167
Figure 5.1: SEM of an acrylate-based PolyHIPE demonstrating the interconnected porous network.....	177
Figure 5.2: Young's moduli under dry and wet conditions of the three PolyHIPE compositions selected for cell culture	193
Figure 5.3: Effect of composition and porosity on degree of openness	195
Figure 5.4: SEM images of an EHA0P80 4-layer 'woodpile' scaffold.....	197
Figure 5.5: Effect of PolyHIPE composition, media and plasma treatment on cell proliferation	200
Figure 5.6: Effect of PolyHIPE composition, media and plasma treatment on osteoblastic differentiation.....	201
Figure 5.7: SEM images of an EHA0P75 free standing scaffold.....	204
Figure 5.8: Growth and differentiation of hES-MPs on generation 2 scaffolds	205
Figure 5.9: SEM images of an EHA0P80-0.1wt% Tinuvin scaffold	208

Figure 5.10: Metabolic activity on EHA0P80 scaffolds with or without Tinuvin for (A) 21 days or (B) 18 weeks	210
Figure 5.11: SEM images of the macrostructure of the three scaffold types evaluated. (A) PolyHIPE (B) Biotek (C) polyurethane	213
Figure 5.12: Comparison of proliferation and matrix deposition on the three scaffold types.....	214
Figure 5.13: Distribution of calcium as shown by ARS staining before destain with perchloric acid for (Top) PolyHIPE (Bottom) Biotek.....	215
Figure 5.14: MicroCT comparison of unseeded, D21 and D28 VOIs for each scaffold type	216
Figure 5.15: Comparison of GSI for all three scaffolds at D21 and D28 with scaffold included in the threshold.....	217
Figure 5.16: Comparison of GSI for all three scaffold types at D21 and D28 with minimum GSI set to exclude scaffold material.....	219
Figure 5.17: Comparison of GSI when MLOA5-K are cultured in SM or BM	220
Figure 5.18: Comparison of wet (A) and dry (B) unseeded PU VOIs.....	222
Figure 5.19: MicroCT and SEM images of the Biotek and PolyHIPE woodpiles ..	223
Figure 5.20: Render showing polymer addition for generation 1 and 2 scaffolds..	224
Figure 5.21: Effect of polymer addition method on fibre architecture	225
Figure 5.22: SEM images of generation 3 PolyHIPE scaffolds.....	226
Figure 5.23: Bespoke seeding well plate for generation 3 scaffolds.....	227
Figure 5.24: Generation 3 PolyHIPE scaffolds supported (A) cell growth and (B) mineralised extracellular matrix production over a three-week period	227

Figure 5.25: Representative photographs of ARS stained single phase PolyHIPE scaffolds	228
Figure 5.26: Optical microscope images of generation 3 PolyHIPE scaffold sections stained with H&E.....	229
Figure 5.27: Confocal microscopy (A and B) images of a EHA100P80 scaffold showing cells completely covering fibres and filling the spaces between the fibres	233
Figure 5.28: Ingrowth of hES-MPs into PolyHIPE microparticles on day (A) 15 and (B) 60	236
Figure 5.29: a) 3D CAD model of the intended geometry of the Biotek scaffold. b) scaffold design specifications provided by the manufacturer	241
Figure 5.30: (A) typical structure of a mosaicplasty graft (B) SEM image of an example biphasic scaffold produced by a non-continuous fabrication technique ...	244
Figure 6.1: Response of IDG-SW3 to a range of PTH concentrations and treatment duration.....	252
Figure 6.2: Effect of a range of PTH concentrations and treatment frequencies on IDG-SW3	254
Figure 6.3: Effect of a range of PTH concentrations and treatment frequencies on RAW264.7	256
Figure 6.4: Schematic showing the co-culture regimen when RAW264.7 were added after 24 hours.....	257
Figure 6.5: Comparison of day 7 (A) DNA (B) ALP activity (C) TRAP activity for co-cultures of IDG-SW3 and RAW264.7 where osteoclasts were added on day 1	258
Figure 6.6: Schematic showing the co-culture regiment when RAW264.7 were added after seven days.....	259

Figure 6.7: Comparison of day 10(+7) (A) DNA (B) ALP activity (C) TRAP activity for co-cultures of IDG-SW3 and RAW264.7 where osteoclasts were added on day 7	260
Figure 6.8: Photograph taken at 10× magnification on an optical microscope of ARS stained day 10(+7) co-cultures of IDG-SW3 and RAW264.7	261
Figure 6.9: Schematic showing the co-culture regimen from preliminary oestrogen-exposed co-cultures.	262
Figure 6.10: Comparison of (A) DNA (B) ALP activity (C) TRAP activity in day 10(+7) co-cultures of IDG-SW3 and RAW264.7 in TCP or 3D	263
Figure 6.11: (A) Metabolic and (B) TRAP activity of RAW264.7 over 28 days.....	264
Figure 6.12: Schematic showing the co-culture regimen for oestrogen exposure and staggered withdrawal in TCP co-culture.	265
Figure 6.13: (A) DNA (B) ALP activity (C) TRAP activity of IDG-SW3 and RAW264.7 co-cultures over 28 days	266
Figure 6.14: Photographs of RAW264.7 cultures on day (A) 7 and (B) 28	267
Figure 6.15: Schematic showing the TCP co-culture regimen with varied RAW264.7 seeding number and oestrogen exposure.	268
Figure 6.16: Effect of varied RAW264.7 seeding number and oestrogen on (A) DNA (B) ALP activity (C) TRAP activity over time in IDG-SW3 and RAW264.7 co-cultures	269
Figure 6.17: Effect of varied RAW264.7 seeding number in TCP co-cultures and oestrogen on (A) TRAP activity (n=7) and (B) resorption by quantifying remaining mineral	271
Figure 6.18: Schematic showing the oestrogen pre-treatment regimen for RAW264.7 do determine whether it has lasting effects after withdrawal	272

Figure 6.19: Effect of oestrogen pre-treatment on RAW264.7 TRAP activity	273
Figure 6.20: Schematic showing the various regimens of oestrogen treatment to be applied to the co-culture	274
Figure 6.21: Effect of oestrogen pre-treatment and withdrawal on (A) DNA (n=3). (B) ALP activity (n=3) (C) TRAP activity (n=6) (D) remaining mineral (n=6).	276
Figure: 6.22: Pictures of multinucleated cells on day 10 of co-culture.....	277
Figure 6.23: Effect of oestrogen pre-treatment and withdrawal on mineral resorption in 3D co-cultures.....	278
Figure 6.24: Representative optical microscope pictures of the 3D co-culture	280
Figure 6.25: Optical microscope images of day 10 3D co-culture sections stained with H&E	281
Figure 6.26: PTH can have anabolic or catabolic effects on bone depending on application modality.	282
Figure 6.27: Schematic showing the expected and actual ability of RAW264.7 to form multiple generations of mature osteoclasts.....	288
Figure 6.22: XY plot of mean±SD of TRAP activity vs. ARS staining for co-cultures exposed to 0 nM or 100 nM oestrogen.....	290
Figure 6.28: A diagram illustrating the role of the JNK pathway on osteoclast precursor differentiation.....	293
Figure 7.1: Ability of colourimetric analysis to discern between different ARS concentrations.....	305
Figure 7.2: Schematic showing a potential layout of a bioreactor system used for long term co-cultures. A peristaltic pump is used to flow and recirculate media through the chambers.	308

Figure 10.1: *Standard curves for the ALP, DNA, ARS and DR80 assays.....*359

Figure 10.2: *Reprint permissions granted via RightsLink®.*360

Figure 10.3: *Written permissions for figures not available through RightsLink®.* 361

List of Tables

<i>Table 2.1: Various treatments for osteoporosis available on the NHS and their approximate annual cost per patient</i>	70
<i>Table 2.2: Common osteoclastic lineage cell types used in vitro.....</i>	80
<i>Table 2.3: Common osteoblastic lineage cell types used in vitro.....</i>	81
<i>Table 2.4: Common factors analysed during in vitro bone cultures.</i>	83
<i>Table 3.1: Cell lines used in this thesis and their respective culture media.</i>	112
<i>Table 5.1: The difference in requirements for a tissue engineering scaffold and in vitro model scaffold.</i>	173
<i>Table 5.2: Proportions of the HIPE constituent materials.....</i>	181
<i>Table 5.3: MicroCT scanning parameters for the three different scaffolds.....</i>	188
<i>Table 5.4: MicroCT analysis parameters for the three different scaffolds</i>	190
<i>Table 5.5: Conditions to be examined to determine the effects of plasma treatment, media composition and substrate stiffness on hES-MPs.....</i>	198
<i>Table 5.6: Summary of the different attempts to create a free standing PolyHIPE scaffold.....</i>	203
<i>Table 5.7: Summary of the effects of different Tinuvin concentrations on EHA0P80 scaffolds.</i>	207
<i>Table 5.8: Comparison of key features and properties of the three scaffolds compared for the model.</i>	212

Table 6.1: *A summary of the different oestrogen treatments applied to RAW264.7 monocultures and co-cultures of RAW264.7 and IDG-SW3.....295*

Abbreviations

2D	Two-dimensional
3D	Three-dimensional
AA-2P	Ascorbic acid 2-phosphate
AFM	Atomic force microscopy
ALP	Alkaline phosphatase
AMTs	Additive manufacturing techniques
ANOVA	Analysis of variance
ARS	Alizarin red S
BCa	Breast cancer
BM	Basal Media
BMD	Bone mineral density
BMHC	Bone marrow derived haematopoietic cells
BMI	Body mass index
BM-MSC	Bone marrow derived mesenchymal stem cell
BMP	Bone morphogenetic protein
BMU	Bone multicellular unit
BRC	Bone remodelling compartment

CAB	Cell assay buffer
CAD/CAM	Computer aided design/Computer aided manufacture
CB2	Cannabinoid type 2
CCD	Cleidocranial dysplasia
CDB	Cell digestion buffer
c-fms	Colony-stimulating factor-1 receptor
CGRP	Calcitonin gene-related peptide
COL-1 α 1	Collagen type 1 alpha 1
CTX/NTX	Carboxy-/amino-terminal telopeptides of collagen type 1
DAPI	4', 6-diamidino-2- phenylindole dihydrochloride
Dex	Dexamethasone
DFC	Dental follicle cells
diH ₂ O	Deionised water
DMSO	Dimethyl sulfoxide
DOK3	Downstream of tyrosine kinase 3
DOO	Degree of openness
DR80	Direct red 80
dsDNA	Double stranded deoxyribonucleic acid
DXA	Dual-energy X-ray absorptiometry

ECM	Extracellular matrix
EDTA	Ethylenediaminetetraacetic acid
EGME	Ethylene glycol monomethyl ether
EHA	2-ethylhexyl acrylate
ELISA	Enzyme-linked immunosorbent assay
EM	Expansion media
ER α	Oestrogen receptor alpha
ER β	Oestrogen receptor beta
FBS	Foetal bovine serum
FDA	US Food and Drug Administration
GAGs	Glycosaminoglycans
GAL-8	Galectin-8
GC	Ovarian follicular granulose cell
GFP	Green fluorescent protein
GGA	Geranylgeranoic acid
GIP	Glucose-dependent insulinotropic peptide
GM-CFU	Granulocyte-macrophage colony forming cell
GM-CSF	Granulocyte macrophage-colony stimulating factor
GSI	Greyscale index

H&E	Haematoxylin and eosin
hAFMSC	Human amniotic fluid mesenchymal stem cell
HBSS	Hank's balanced salt solution
HEPES	4-(2-hydroxyethyl)-1-piperazineethanesulfonic acid
hES-MPs	Human embryonic stem-cell derived mesenchymal progenitors 002.5
hFGF	Human fibroblastic growth factor
HIPE	High internal phase emulsion
HLB	Hydrophilic-lipophilic balance
HMDS	Hexamethyldisilazane
hMSC	Human mesenchymal stem cell
hOB	Primary human osteoblast
hPBMC	Human peripheral blood monocyte
HRT	Hormone replacement therapy
HSC	Haematopoietic stem cell
HUVEC	Human umbilical vein endothelial cell
IBOA	Isobornyl acrylate
IBSP/BSP-II	Integrin binding sialoprotein/Bone sialoprotein
ICAM	Intercellular adhesion molecule
IFN- γ	Interferon- γ

IL	Interleukin
JNK	Jun N-terminal kinase pathway
KO	Knockout
LPS	Lipopolysaccharides
MAPK	Mitogen-activated protein kinase
MAPTMS	3-methylacryloxypropyltrimethoxysilane
M-CSF	Macrophage colony stimulating factor
MEM	Minimum essential medium
MP	Mesenchymal progenitor
MicroCT	Micro-computed tomography
MIPE	Medium internal phase emulsion
MK-4	Menaquinone-4
MM	Multiple myeloma
MMP-9	Matrix metalloproteinase 9
mOB	Primary murine osteoblast
MP	Mesenchymal progenitors
mRNA	Messenger ribonucleic acid
NFATc1	Nuclear factor-activated T cells c1
O/W	Oil-in-water

OA	Osteoarthritis
OFF	Oscillating fluid flow
OIM	Osteogenesis induction media
ONJ	Osteonecrosis of the jaw
OPG	Osteoprotegerin
Oscar	Osteoclast associated receptor
OSX	Osterix
OVX	Ovariectomy
P1CP/P1NP	Carboxy-/amino-terminal propeptides of collagen type 1
PBS	Phosphate buffered saline
PC	Phenol containing
PCa	Prostate cancer
pcAir	Air plasma clean
PCL	Poly(ϵ -caprolactone)
pdAAc	Plasma deposited acrylic acid
PDL	Periodontal ligament
PF	Phenol free
PFF	Pulsatile fluid flow
Pi	Inorganic phosphate

PLGA	Poly(lactic-co-glycolic acid)
PLLA	Poly(lactic acid)
PMSF	Phenylmethanesulfonyl fluoride
pNP	Para-nitrophenol
pNPP	Para-nitrophenol phosphate
pOB	Porcine osteoblast
PolyHIPE	Polymerised high internal phase emulsion
PPi	Inorganic pyrophosphate
PTH	Parathyroid hormone
PTH1R	Parathyroid hormone 1 receptor
QCT	Quantitative computed tomography
RANK	Receptor activator of nuclear factor kappa-B
RANKL	Receptor activator of nuclear factor kappa-B ligand
RBC	Red blood cell
ROI	Region of interest
RR	Resazurin reduction
RT-PCR	Reverse transcriptase-polymerase chain reaction
RUNX2	Runt-related transcription factor 2
SEM	Scanning electron microscopy

sema4D	Semaphorin 4D
SERM	Selective oestrogen receptor modulator
siRNA	Small interfering ribonucleic acid
SM	Supplemented media
SVF	Stromal vascular fraction
TCP	Tissue culture plastic
TGF- β	Transforming growth factor beta
TMPTA	Trimethylolpropane triacrylate
TNF	Tumour necrosis factor
TRAP	Tartrate-resistant acid phosphatase
TSA	Trichostatin A
UHMWPE	Ultra-high molecular weight polyethylene
uPAR	Urokinase receptor
UTS	Ultimate tensile stress
VDR	Vitamin D3 receptor
VOI	Volume of interest
W/O	Water-in-oil
WT	Wildtype
β GP	Beta-glycerolphosphate

μSL Microstereolithography

Φ Internal phase volume ratio

1. Introduction

Osteoporosis is a skeletal disease common in the elderly population which is often underdiagnosed and undertreated. Demographics are changing, resulting in more people above the age of 60 in the population, thereby increasing the incidence of this disorder. An estimated three million people in the United Kingdom have osteoporosis, with health and social care costs for associated hip fractures alone being approximately £2.3 billion each year [1]. Osteoporosis occurs when the balance of bone resorption and formation is disrupted. Endocrine changes associated with ageing result in an over-stimulation of bone resorption and inhibition of bone formation. This results in a reduced bone mineral density and strength, as well as a deterioration of the microarchitecture. When the bone mineral density falls below a certain threshold, the patient is classed as having osteoporosis [2].

Current treatments for osteoporosis are physical, dietary or pharmacological. However, despite these approaches reducing fracture risk and increasing bone mineral density, they are associated with side effects ranging from gastrointestinal problems for bisphosphonates, to cardiovascular complications with hormone replacement therapy, and osteosarcoma from parathyroid hormone treatments [3]–[5]. From this it is clear that a better understanding of the disease mechanisms, improvements to current treatments, and an understanding of how to prevent osteoporosis is essential in reducing its prevalence and improving patients' quality of life.

The most common method of studying osteoporosis and testing new therapeutics is through the use of animal models due to their ability to provide a uniform approach to research with a level of experimental control that is not possible in humans. In fact, the US Food and Drug administration (FDA) requires a new osteoporosis drug to be preclinically tested on a rodent and a validated large animal model [6]. Although viewed as the gold standard for testing the safety and efficacy of new therapies and are an essential step in preclinical development, differences between animal and human physiology means that they cannot accurately model the human response. The use of *in vivo* models should align with the principles of the '3Rs' – replacing, reducing and refining animal testing [7]. In addition to these principles, in September 2010 the EU Directive 'Directive 2010/63/EU – Legislation for the protection of animals used for scientific purposes' was adopted. This supports the principles of the

3Rs, widening their scope and laying down standards for housing and care of animals. In addition to this, it establishes a Union reference laboratory for the validation of alternatives to animal models in order to promote their development, validation and implementation [8]. This directive is in fact part of the impetus behind this project; if aspects of *in vivo* models can be replicated *in vitro* then certain facets of animal testing can be replaced.

Previous work within the Reilly group has shown that culturing osteoblastic cells on porous polymer scaffolds can induce the formation of an immature mineralised bone-like matrix [9]. This thesis focuses on combining this with osteoclast culture and a regimen of oestrogen treatments to investigate whether an applicable model of postmenopausal osteoporosis can be developed *in vitro*.

2. Background

2.1 Bone – Physiology, hierarchy and healing

2.1.1 Anatomy and function

Bone performs several roles. It provides support, protects vital organs, facilitates movement by acting as levers, stores minerals such as calcium and phosphorus, contains cells that produce blood such as haematopoietic red marrow, and stores energy in the form of lipid filled yellow marrow. There are two types of osseous tissue, cortical bone (also known as compact bone) and cancellous bone (also known as trabecular or spongy bone). Cortical bone makes up approximately 80% of the bone mass of an adult skeleton and usually has a porosity below 5% [10], [11]. Cancellous bone makes up the remaining 20% and has much higher porosity, approximately 50-90%. It contains thin (50-400 μm), interconnecting rods and plates of bone termed trabeculae. Rods give an open cell structure and plates a closed cell structure, and the spaces between the trabeculae are filled with bone marrow and blood vessels. This high porosity results in a much lower compressive strength but a greatly increased surface area in comparison to cortical bone [12]–[15].

2.1.2 Macrostructure

The adult human skeleton contains 206 bones which are classified by shape to give five types: long, short, irregular, flat, and sesamoid. Long bones are longer than they are wide, act as levers, and are typically found in the legs and arms but also in the fingers and toes. They consist of three regions, the diaphysis, epiphysis, and metaphysis. The diaphysis is the hollow shaft that connects to the proximal and distal epiphyses via the proximal and distal metaphyses. It is formed from a hollow tube with the outside constructed from cortical bone and the medullary cavity filled with bone marrow. The epiphysis is the end of the bone, and has a specialised shape depending on the location and function. It is predominantly cancellous bone with an outer surface composed from cortical bone. The metaphysis, also known as the epiphyseal plate, is part of the growth plate, the portion of bone that grows during childhood.

Short bones are normally cubic, with approximately equal dimensions in all three axes. They give stability and allow limited movement and are only found in the wrists and ankles. They have a trabecular centre covered with cortical bone. Flat bones are composed of a layer of cancellous bone between two layers of cortical bone. Found predominantly in the skull, shoulder blades, sternum, and ribs, they provide protection. Irregular bones do not meet the requirements of the previous categories, for instance the vertebrae or facial bones containing the sinuses. Their complex shapes afford protection and support. Finally, the sesamoid bones are small, round bones that occur in tendons. Their formation is pressure dependant, developing when large compressive forces are exerted onto a tendon. This means that the number and location of sesamoid bones varies from person to person, with the exception of the patellae.

With the exception of articular cartilage covering joint surfaces, the outer surface of bone is covered by connective tissue termed the periosteal membrane. Formed from two layers, the outside contains dense, irregular collagenous tissue containing blood vessels and nerves and the inside is a single layer of bone cells. The outer layer is continuous with attached tendons and ligaments, and some collagen fibres (Sharpey's fibres) even penetrate the periosteum and bone tissue, strengthening the attachment. Blood vessels within the periosteum also penetrate the bone through nutrient foramina, minute holes within the tissue. Endosteum is a connective tissue membrane which lines the inner surface of bone and is also formed from a layer of bone cells [14], [16]. (Fig. 2.1)

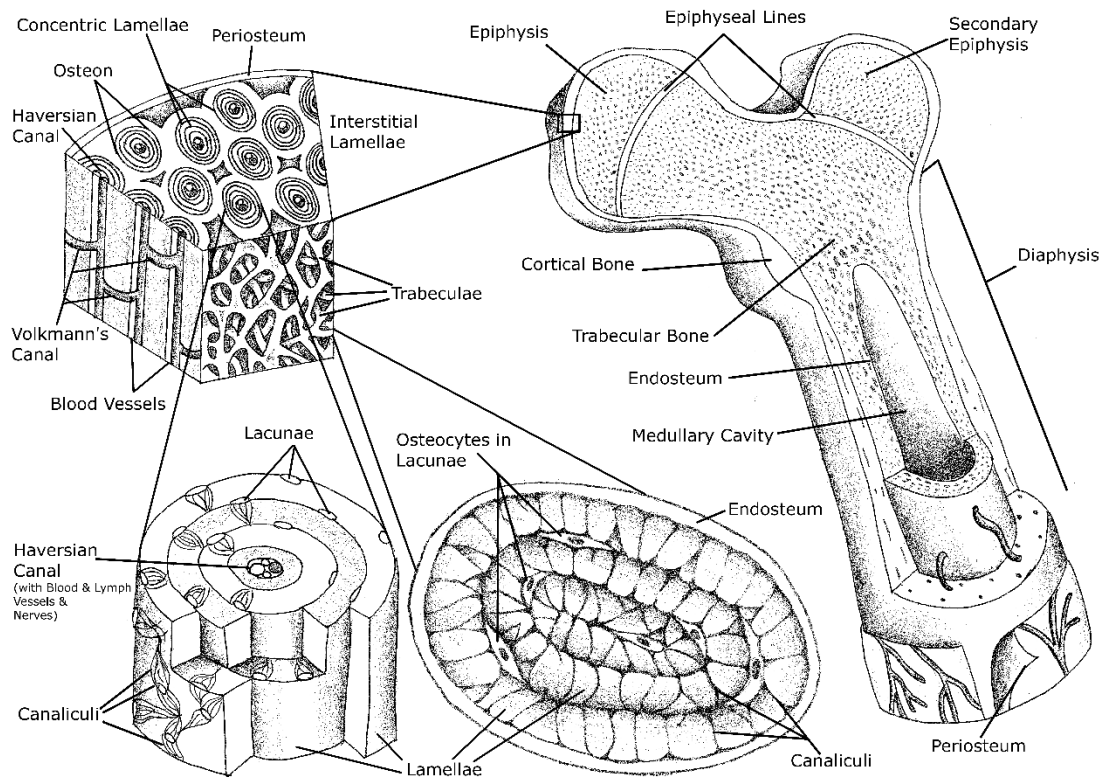


Figure 2.1: Macroscopic and microscopic anatomy of an adult long bone. (Right) Macroscopic view of an adult femur. (Top left) Cross section view of the intersect between cortical and trabecular bone. (Bottom left) Cut away of a single osteon. (Bottom centre) cross section of a single trabeculae. Image used with the kind permission of Rebecca O'Neill.

2.1.3 Micro and nanostructure

Osseous tissue is a composite material with an organic phase, inorganic phase, and cellular phase. The organic phase provides bone with its tensile strength and reduces the brittleness allowing for bending, and the inorganic phase gives compressive strength. The combination of these two phases is known as the bone matrix or osteoid and the cellular phase deposits, maintains, and resorbs this. By dry weight, osseous tissue is one third organic and two thirds inorganic. The inorganic phase is mainly constituted from hydroxyapatite (~85%), but there is also calcium carbonate (~10%), and small amounts of other minerals [16].

The organic phase is predominantly type I collagen (~90%) with trace amounts of type III and V, but is also formed from ~10% non-collagenous proteins such as glycosaminoglycans, proteoglycans, and glycoproteins. The majority of these have a high affinity for calcium ions due to their aspartic and glutamic acid residues [17]. Examples of these proteins include osteocalcin, osteopontin, osteonectin and alkaline phosphatase. Osteocalcin, a skeletal gla protein, can be used as a late-marker of osteogenic differentiation and is implicated in bone remodelling. Additionally, its inhibition may be used in the control of mineralisation [18], [19]. Osteopontin is a sialoprotein involved in cell attachment to bone matrix and bone remodelling [20], and osteonectin is a glycoprotein which is likely involved with mineralisation due to its binding affinity to calcium, hydroxyapatite and collagen.

Alkaline phosphatase (ALP), specifically tissue non-specific alkaline phosphatase, is an enzyme secreted from osteoblasts which promotes hydroxyapatite crystal formation within the bone matrix, and it is considered to be a highly specific marker of bone-forming osteoblasts [18], [21]. Therefore, ALP activity is often used during *in vitro* analyses as an early indicator of osteogenic differentiation [22]. However, the exact mechanism of its involvement is unknown. The key substrate for ALP in bone is thought to be inorganic pyrophosphate (PPi). PPi inhibits hydroxyapatite formation, but its hydrolysis by ALP provides inorganic phosphate (Pi) which is required for the formation of hydroxyapatite [23], [24].

Osseous tissue has a hierarchical structure. The cortical and cancellous bone form the macrostructure, the microstructure (500 μm – 10 μm) is composed of osteons and trabeculae. The sub-microstructure (10 μm – 1 μm) is the lamellae, the nanostructure (1 μm - ~500 nm) is the collagen fibres, and the sub-nanostructure (below ~500 nm) is the fibrils and molecules that form collagen fibres (Fig. 2.2).

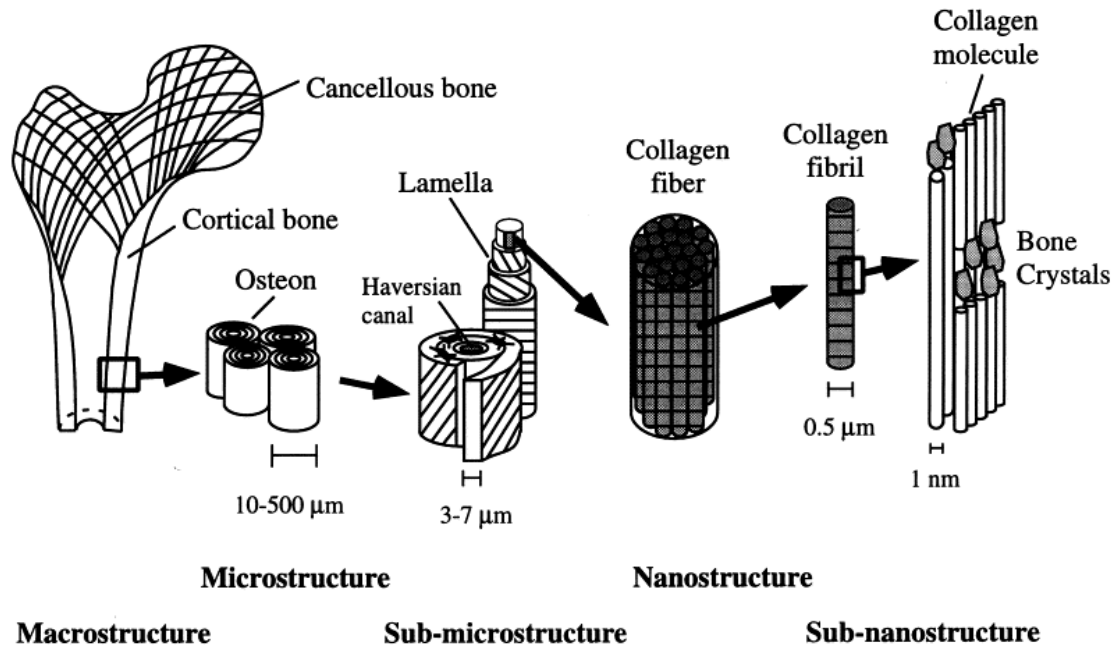


Figure 2.2: Hierarchical structure of cortical bone. Reprinted from Rho, et al., with the kind permission of Elsevier [25].

Depending on the organisation of collagen fibrils within the osteoid, osseous tissue can be classified as either woven or lamellar bone. The former contains randomly orientated collagen and is formed during foetal development or fracture repair. It is the only type of bone that can be formed *de novo*, and does not contain any osteons. It is laid down randomly and rapidly in response to the need for a stiff tissue to be formed in a short period of time. This disorganisation gives isotropic mechanical properties and increases flexibility. Conversely, lamellar bone has highly organised collagen fibrils which are formed in alternating orientations. Each layer (lamellae) is between 3 and 7 μm thick and within each layer collagen fibres lie parallel. In adjacent layers, collagen fibres also lie parallel, but at an angle to neighbouring lamellae. This high level of orientation yields anisotropic mechanical properties, meaning its mechanical performance depends on the direction of the applied force. This results in lamellar

bone being much stronger than woven bone in the long axis of the collagen fibres, but also less flexible [13], [14].

The microstructure of cortical and trabecular bone is notably different (Fig. 2.3). The microstructure of cortical bone consists of lamellae wrapped concentrically around a blood vessel canal. The combination of lamellae and the canal within which the blood vessel and nerves reside forms an osteon, the building block of cortical bone. Osteons can be divided into two groups, primary and secondary. Primary osteons occur during the mineralisation of cartilage as bone tissue is formed for the first time, and secondary osteons occur when existing bone is replaced during bone remodelling and are also known as Haversian systems. These tend to have more lamellae and larger canals than primary osteons. Cancellous bone also contains lamellae; however, these are not concentric, meaning that there are no osteons.

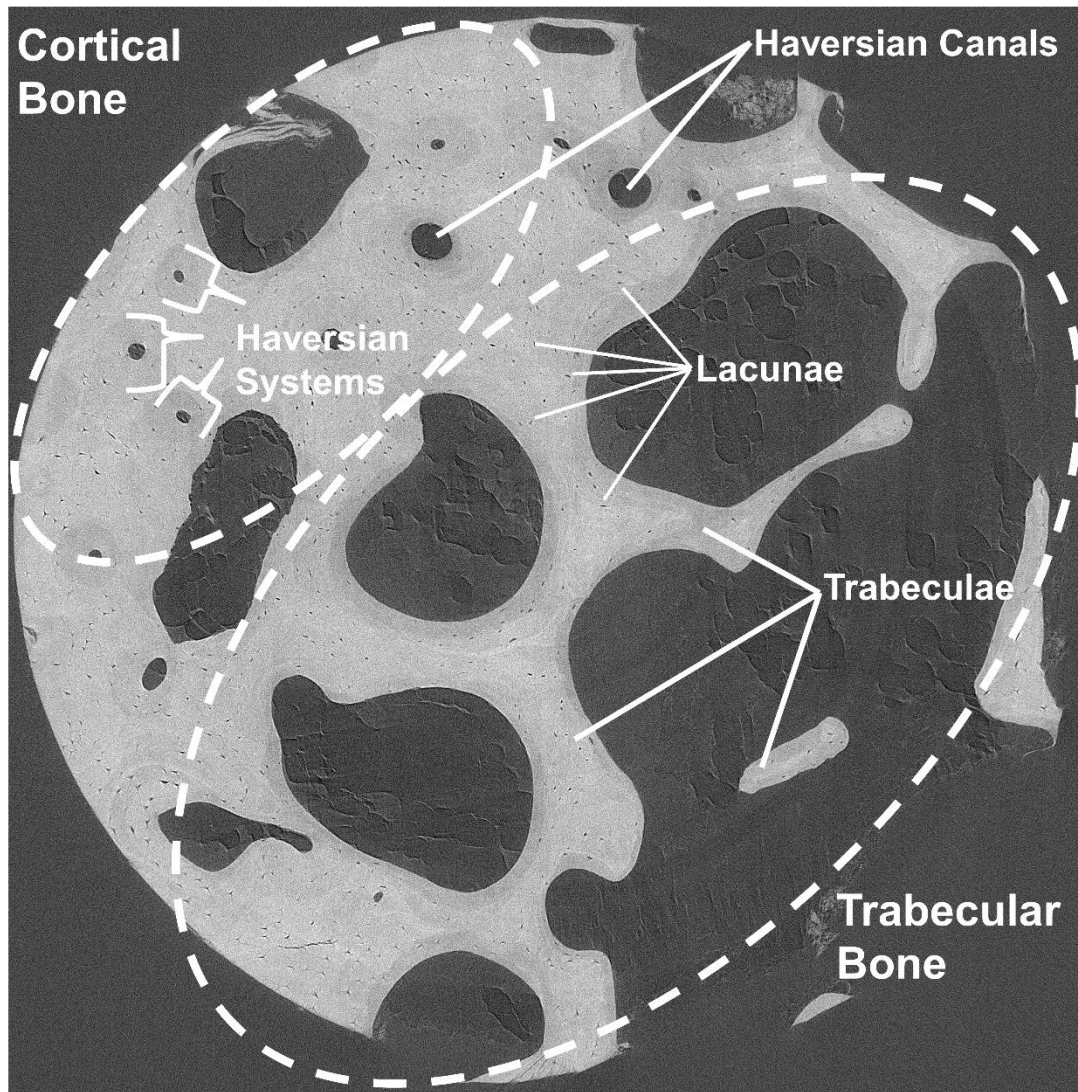


Figure 2.3: Synchrotron image of a transverse cross section of a bone. Sample taken from the lower trochanter of a 101-year-old human female revealing the microstructure of cortical and trabecular bone. Haversian systems their canals are only visible in the cortical region. Osteocyte lacunae are present throughout. 3 mm diameter sample. Image acquired by author at Diamond Light Source I13-2, experiment MT15886.

Osteons run parallel to the long axis of the bone and are joined via Volkmann's canals (Fig. 2.4). Haversian and Volkmann's canals contain blood vessels, nerves and lymph vessels. Lacunae are found between the lamellae and are connected by canaliculi. The lamellae underlying the periosteum and endosteum of cortical bone are termed circumferential lamellae, and any residual lamellae remaining after remodelling that lie between osteons are referred to as interstitial lamellae (Fig. 2.5).

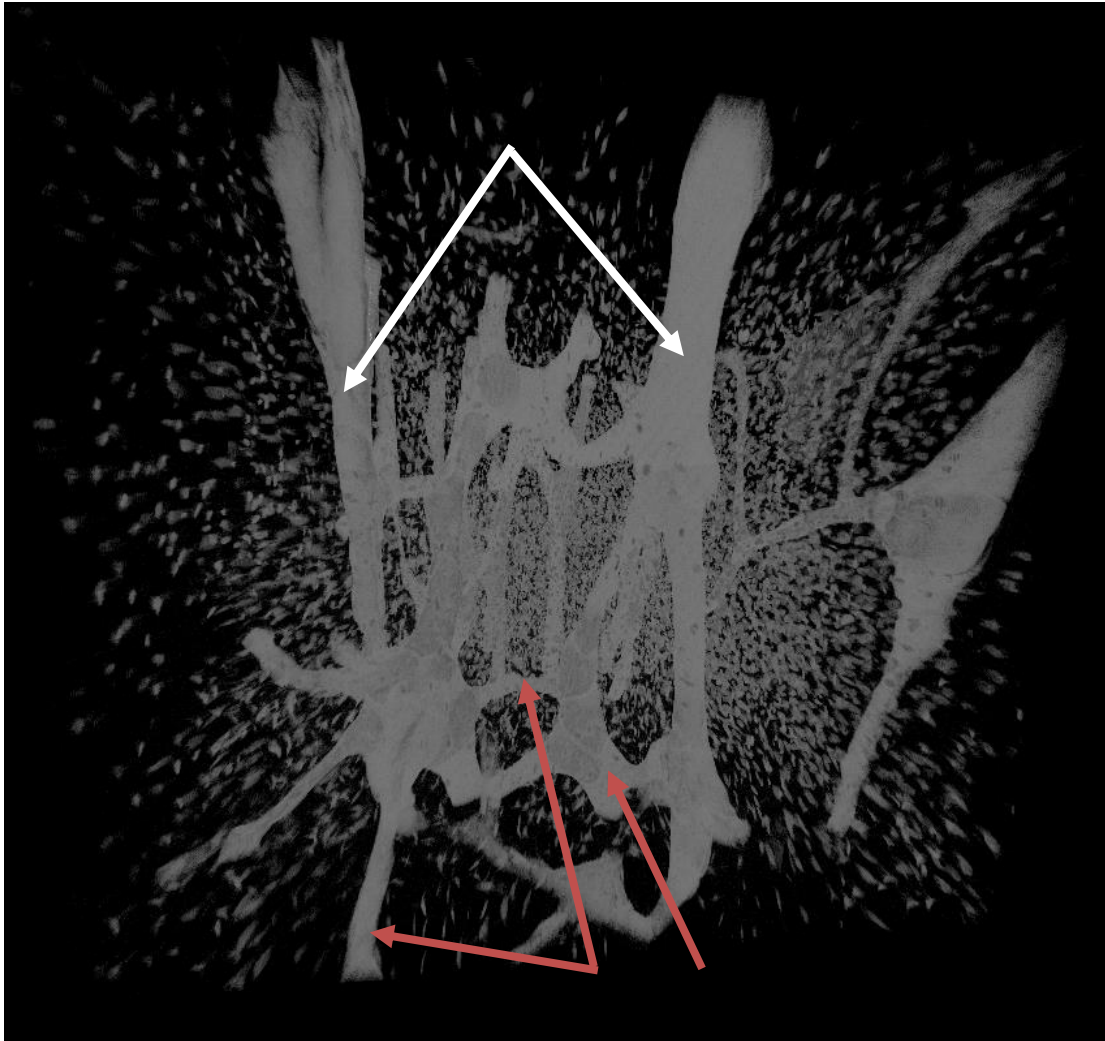


Figure 2.4: Network of Haversian (white arrows) and Volkmann's (red arrows) canals. Reconstructed volume from a synchrotron scan of a cortical bone sample taken from the femoral midshaft of an 86-year-old male. By thresholding for opacity only the empty volumes are left visible. The small volumes surrounding the network are osteocyte lacunae. Image acquired by author at Diamond Light Source I13-2, experiment MT15886.

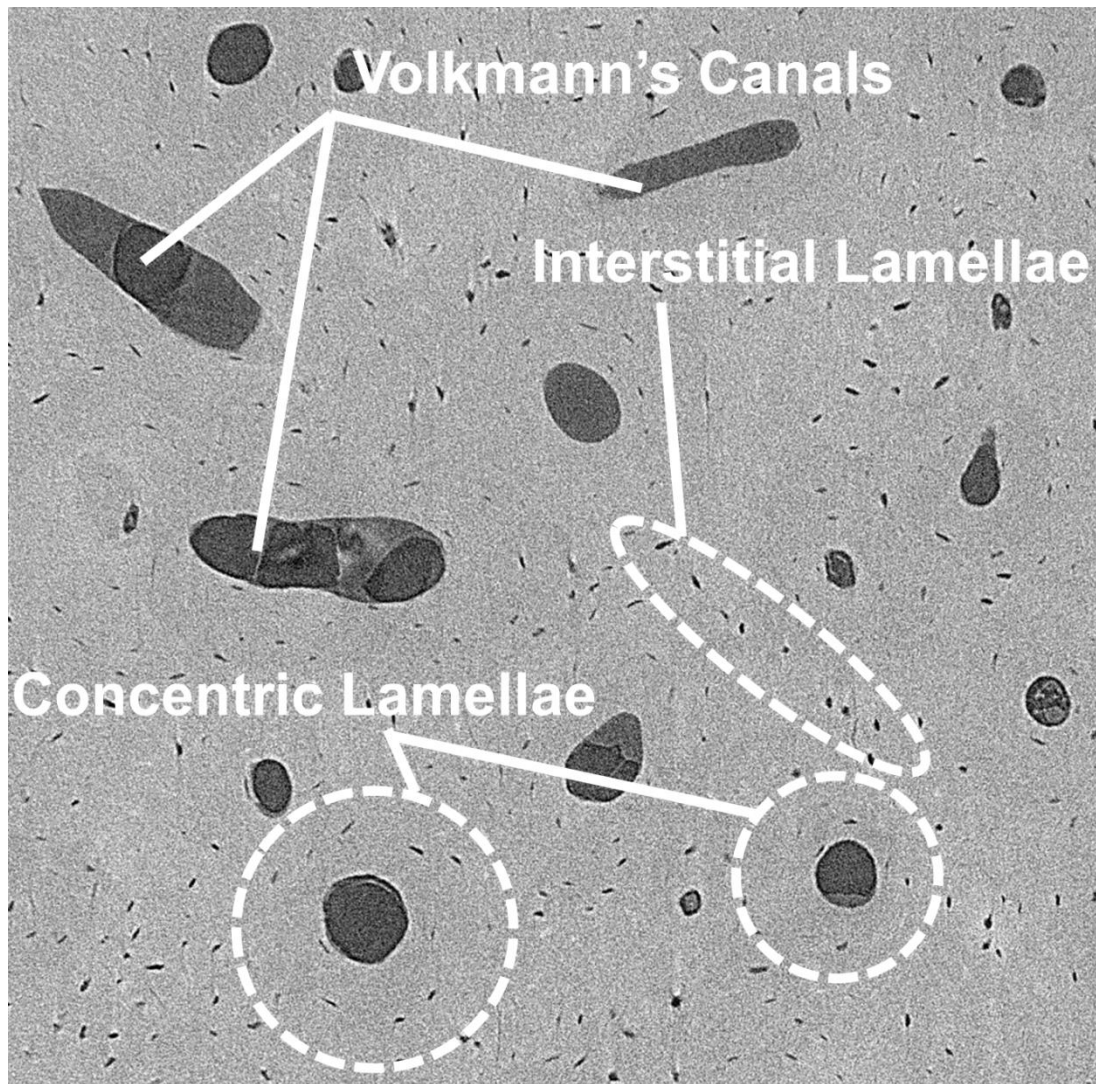


Figure 2.5: Synchrotron image of the microstructure of cortical bone. Transverse cross section of a sample taken from the femoral midshaft of an 86-year-old male. Volkmann's canals appear as elliptical Haversian canals where they span between two osteons. Lamellae are not immediately visible, but their path can be traced by viewing lacunae. Concentric lamellae can be seen around osteons and interstitial lamellae between them. Field of view is 1 mm. Image acquired by author at Diamond Light Source I13-2, experiment MT15886.

2.1.4 Cell biology of bone

There are four main cell types present within bone, mesenchymal progenitors, osteoblasts, osteoclasts, and osteocytes, with each performing a different role and function. Mesenchymal progenitors, osteoblasts and osteocytes are all of the same osteoblastic lineage, where mesenchymal progenitors undergo osteogenesis and differentiate into pre-osteoblasts and osteoblasts, a subset of which ultimately terminally differentiate into osteocytes with the remainder undergoing apoptosis or becoming bone lining cells (Fig. 2.6a) [26]. In contrast, osteoclasts are derived from haematopoietic stem cells (HSCs).

The differentiation of mesenchymal progenitors into osteoblasts can occur by two different processes depending on where it occurs in the skeleton. Direct differentiation from mesenchymal progenitor to osteoblast occurs during intermembranous ossification. In mammals, this mechanism is limited to certain skull bones and the clavicle. All other parts of the skeleton are formed by endochondral ossification. Here, mesenchymal progenitors initially differentiate into chondrocytes and perichondral cells. At first these chondrocytes are proliferative; however, they then exit the cell cycle and become hypertrophic. This triggers the differentiation of osteoblasts from the perichondral cells (Fig. 2.6b) [13], [26]. Due to the ability of mesenchymal progenitors to differentiate into osteogenic cells and the ease with which they can be isolated and expanded in culture, they hold a great deal of promise in the field of bone tissue engineering. However, their proliferative and differentiation capability decreases during *ex vivo* expansion which limits their clinical use but inspires research into overcoming these limitations [27].

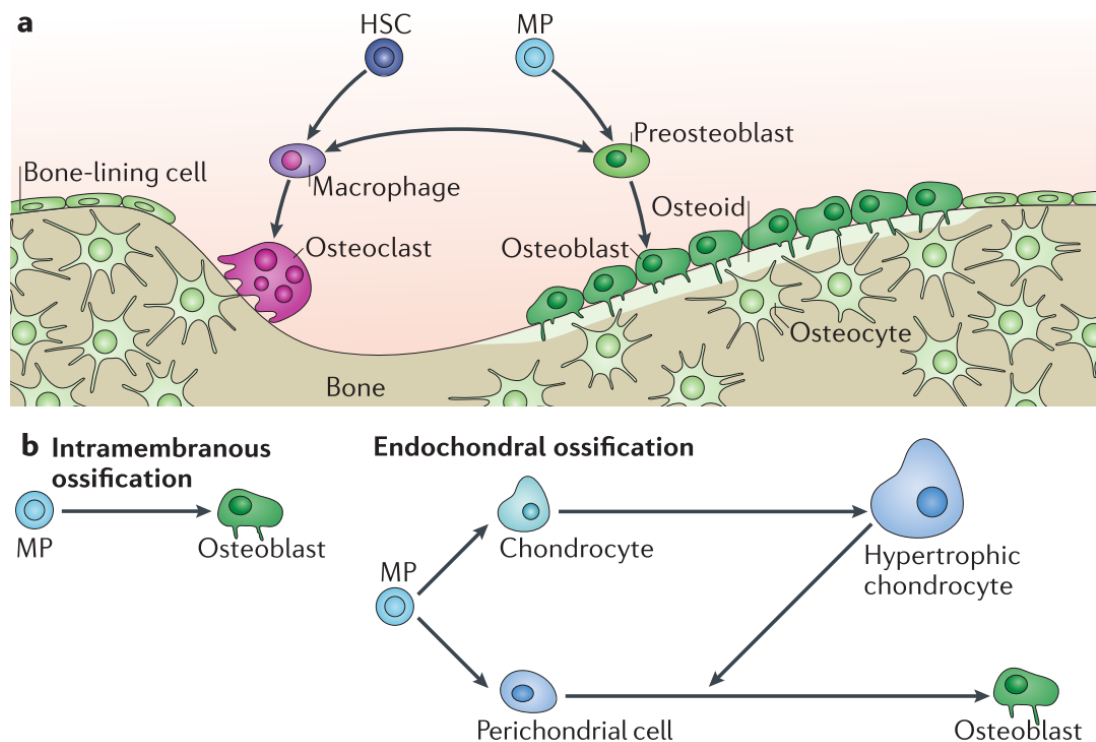


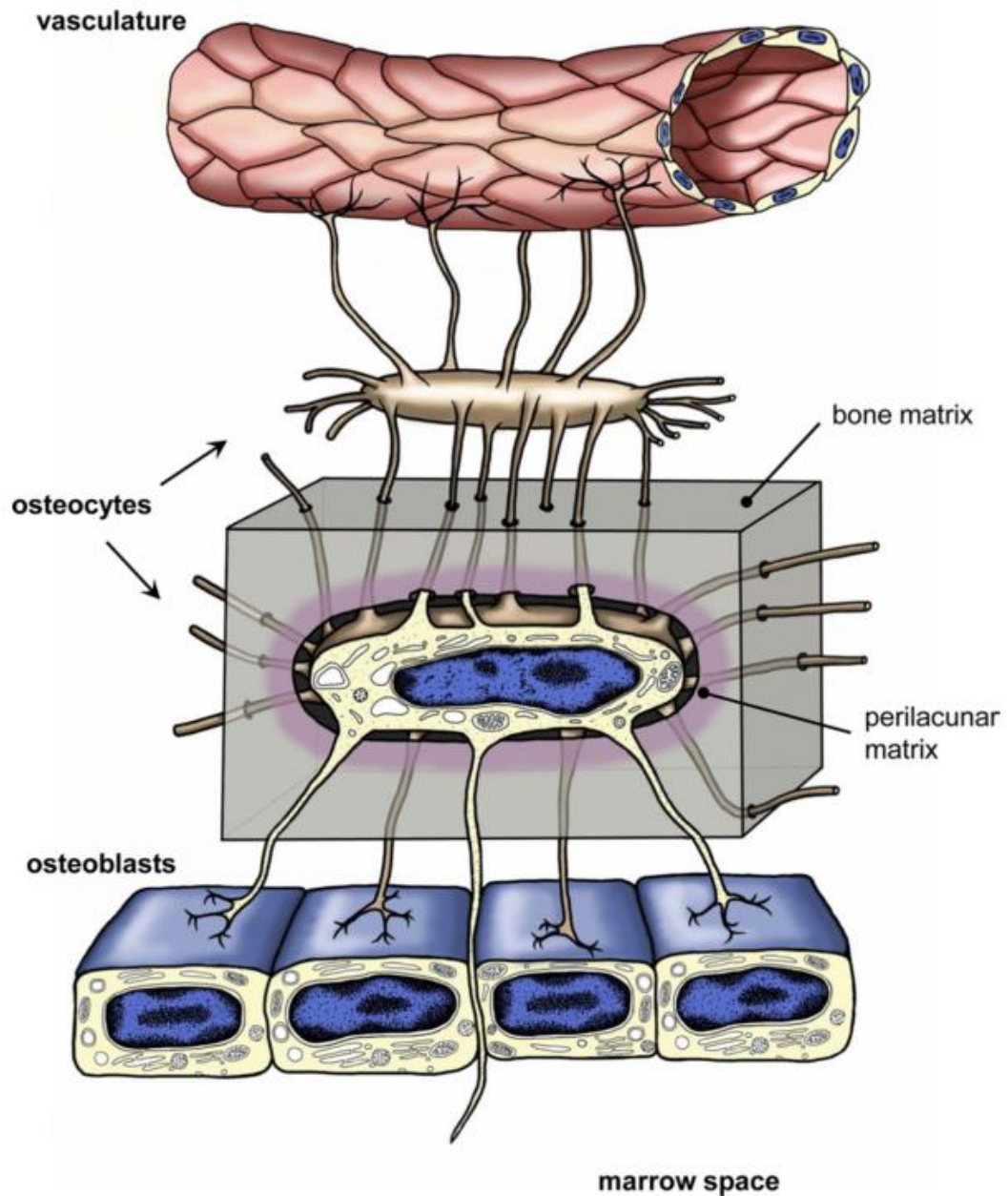
Figure 2.6: *Osteoblastic and osteoclastic cell lineages.* (a) Osteoclasts are derived from haematopoietic stem cells (HSCs) and pre-osteoblasts, osteoblasts, osteocytes and bone lining cells from mesenchymal progenitors (MPs). (b) Different pathways of osteoblastic differentiation from mesenchymal progenitors (MP). *Reprinted from Long, with the kind permission of Nature Publishing Group [26].*

Osteoblasts are mononucleate, deposit the extracellular matrix of bone at a rate of 0.5 – 1.5 μm per day and regulate its mineralisation [28]. Identifiable by their cuboidal morphology and located on the surface of the osteoid, they produce the collagen and non-collagenous proteins that form the organic phase of bone. They are anchorage dependent and require cell-matrix and cell-cell contacts to maintain function. This is achieved through either specific receptors for signalling molecules, such as cytokines, hormones and growth factors, or transmembranous proteins, for instance connexins, cadherins and integrins. If osteoblasts become fully embedded and trapped within their own calcified osteoid, they change phenotype and develop into osteocytes [13], [28].

It is widely reported that once the differentiation through the osteoblastic lineage has progressed to the osteoblast phenotype, these mature osteoblasts are post-mitotic [29]–[32]. Therefore, mature osteoblasts can only be created via mesenchymal progenitor differentiation. Although this lineage of cells is classically divided into four

phenotypes (progenitor, pre-osteoblast, osteoblast, and osteocyte) due to these discrete divisions being useful when discussing bone biology, progression through the lineage is a continuous process meaning that there are not well defined identities for each phenotype [26]. As osteoblastic lineage cells differentiate from mesenchymal precursors, there is a period of active proliferation and mitotic activity as demonstrated by expression of cell cycle and cell growth genes. At this time, genes associated with extracellular matrix production (e.g. type I collagen) that are fundamental to the osteoblast phenotype are also expressed. In the subsequent stages of differentiation, these proliferation genes are downregulated and DNA synthesis declines whilst ALP expression rapidly increases as the extracellular matrix is prepared for mineralisation. Therefore, it appears that this cessation of proliferation is required for the genes specific to bone mineralisation to be activated [33].

Osteocytes reside within the lacunae and account for 90% of all cells in the human skeleton. They can survive for decades and although derived from osteoblasts, have a markedly different function and morphology. They are smaller than osteoblasts, have a reduced number of organelles but an increased nucleus-to-cytoplasm ratio, and are star shaped (stellate) with multiple cytoplasmic extensions (Fig. 2.7) [34]. These processes penetrate the canaliculi that connect the lacunae and make contact with other osteocytes, osteoblasts, cells lining the bone surface, and vasculature via gap junctions [35]. Surrounding the osteocytes in the lacunocanalicular network is interstitial fluid. As the osteocyte network has no vascular supply, it relies on diffusion through this fluid to provide oxygen and nutrients to the osteocytes [36]. This network of osteocytes forms a complex communication system that enables them to sense and respond to stresses placed upon the bone. Currently, it is thought that this is achieved by bone deformation causing the interstitial fluid surrounding the osteocytes to flow from regions of high pressure to those of low pressure. This flow is sensed by osteocytes, stimulating them to produce signalling molecules that regulate resorption and formation activity in osteoclasts and osteoblasts, respectively [37]. The lacunae/canaliculi system has a huge surface area that signalling molecules produced by osteocytes can affect. Even though it contains only 1% of the bone fluid volume, it has a surface area 400 times greater than the Haversian and Volkmann's systems combined, and 133 times greater than cancellous bone [38].



osteocyte

Figure 2.7: Schematic representation of an embedded osteocyte within its lacuna. Processes can be seen penetrating the canaliculi within the bone matrix. These interconnect via gap junctions with other osteocytes, osteoblasts, the marrow space and vasculature to allow nutrients to diffuse through the interstitial fluid. Reprinted from Dallas, et al., with the kind permission of Oxford Academic [36].

Unlike osteoblasts and osteocytes, osteoclasts are ultimately derived from haematopoietic stem cells [39]. They are multinucleated bone resorbing cells formed from fused monocyte progenitors. Their average lifespan is 15-20 days before undergoing apoptosis, and they degrade osteoid using hydrogen ions and enzymes. Initially hydrochloric acid dissolves the mineral content of the matrix before proteolytic enzymes, such as tartrate-resistant acid phosphatase (TRAP), matrix metalloproteinase 9 (MMP-9), gelatinase, and cathepsin K, degrade the organic component. The result is visible resorption cavities in the bone called Howship's lacunae [40]. An active osteoclast can resorb bone at a rate of up to 200,000 $\mu\text{m}^3/\text{day}$; to replace this volume of bone takes up to ten generations of osteoblasts [28]. When resorbing, osteoclasts tightly attach to bone through a sealing zone created through cytoskeleton rearrangement to form a ring of actin. Within this ring the plasma membrane enlarges and becomes convoluted forming a ruffled membrane with finger-like projections to increase surface area and therefore contact with the bone matrix. The acids and enzymes are secreted through the ruffled border to degrade the bone below, forming the resorption cavities (Fig. 2.8) [28], [41]–[43].

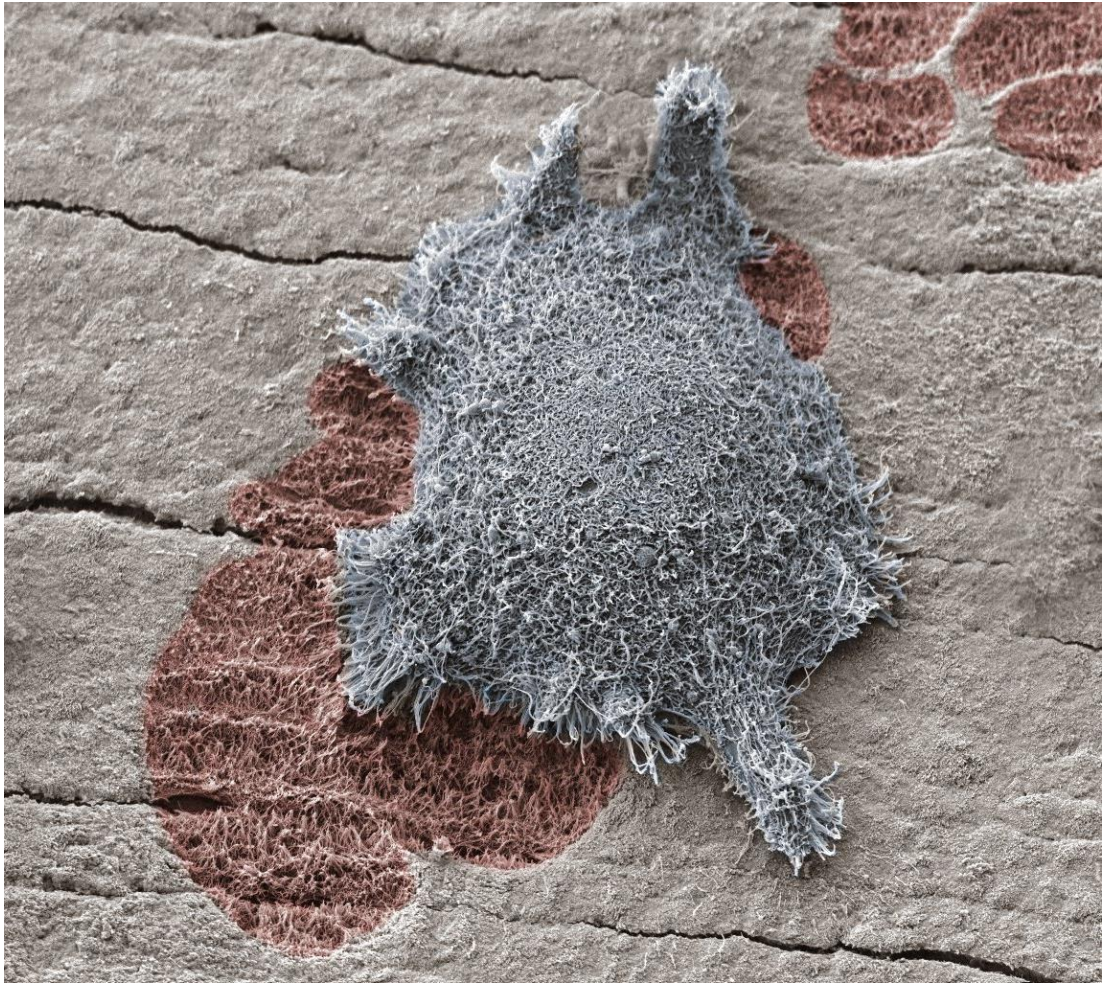


Figure 2.8: *Colourised scanning electron micrograph of an active osteoclast and a resorption pit. Image used with the kind permission of Prof. Timothy Arnett, University College London. Original image available on boneresearchsociety.org.*

2.1.5 Bone remodelling

Bone remodelling occurs throughout life and is an essential physiological process. It maintains or improves bone strength by replacing primary, immature bone and old, micro-damaged or fractured bone, as well as maintaining calcium homeostasis. The resorption and formation processes are balanced, and remodel approximately 5% of cortical and 20% of trabecular bone each year. Whilst the latter accounts for only 25% of the total bone volume, the increased surface area to volume ratio results in a ten times higher metabolic rate. Bone remodelling is a continuous event throughout life, but the balance between resorption and formation changes. In healthy individuals, formation dominates for the first three decades until peak bone mass is achieved. This bone mass is then maintained for approximately 20 years until resorption begins to outweigh formation and mass declines [44].

Remodelling occurs via basic multicellular units (BMUs). These are composed from discrete packets of osteoclasts and osteoblasts accompanied by a blood supply and supporting connective tissue. BMUs form and refill tunnels through cortical bone and in trabecular bone they create trenches on the surface. The osteoclasts are at the front, forming the cutting cone or hemicone in the case of trabecular BMUs, with osteoblasts behind forming the closing cone or hemicone. The BMU can move in all three axes in cortical BMUs and two axes in trabecular BMUs as they are on the surface [13], [45] (Fig. 2.9).

The action of osteoblasts and osteoclasts within the BMU is tightly coupled via biochemical pathways. Once osteoclast precursors have arrived at the remodelling site from the bloodstream or surrounding marrow, two factors are predominantly responsible for their maturation into osteoclasts: macrophage-colony stimulating factor (M-CSF) and receptor activator of nuclear factor kappa-B ligand (RANKL). These factors bind to their respective receptors on the precursors, colony-stimulating factor-1 receptor (c-fms) and receptor activator of nuclear factor kappa-B (RANK) and initiate osteoclastogenesis.

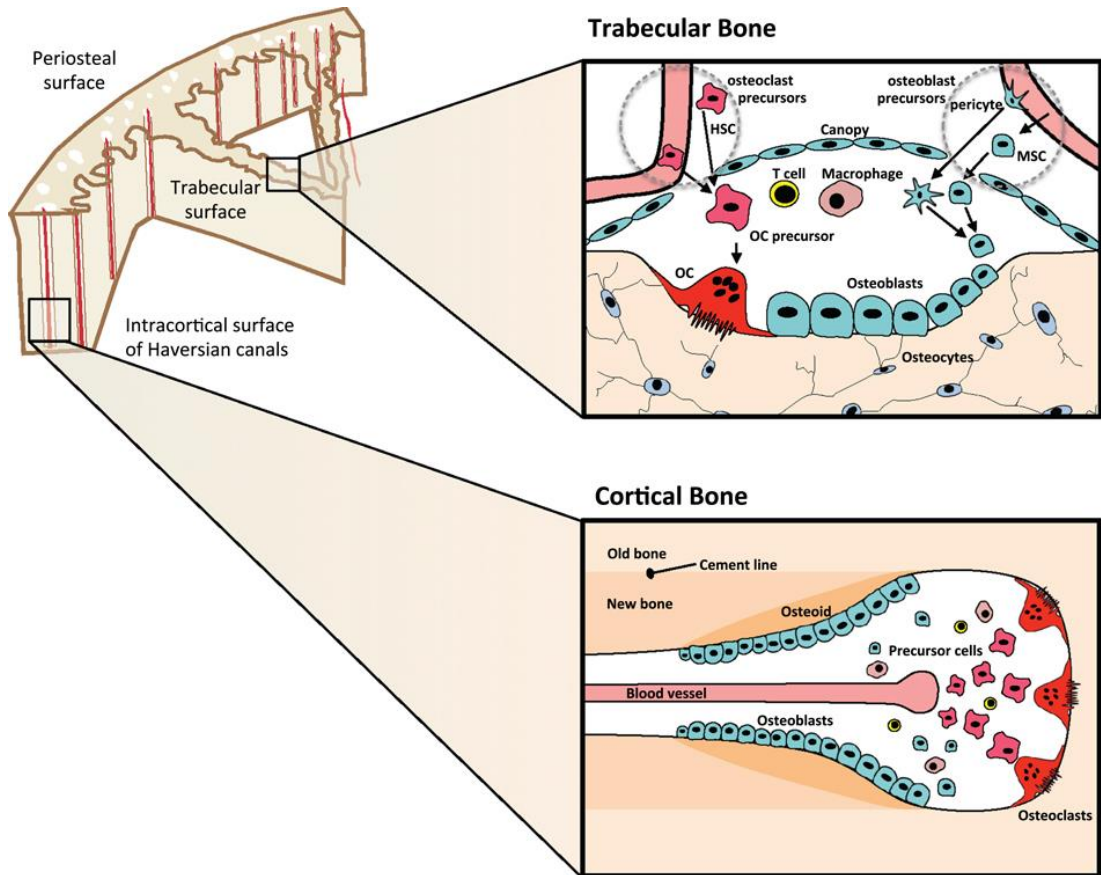


Figure 2.9: Bone multicellular units in (top) trabecular and (bottom) cortical bone. In trabecular bone they initiate underneath bone remodelling canopies and in cortical bone at points within Haversian canals. Reprinted from Sims and Martin, with the kind permission of Nature Publishing Group [46].

The earliest haematopoietic precursor that can give rise to an osteoclast is the granulocyte-macrophage colony forming cell (GM-CFU). M-CSF is produced by osteoblasts and stromal cells and its activation of c-fms promotes the survival and proliferation of the GM-CFU [47], [48]. RANKL is expressed by osteoblasts, T cells and endothelial cells and its conjugation with RANK commits the GM-CFU to the osteoclast lineage, upregulating key markers such as TRAP. Continued exposure to both factors stimulates the preosteoclasts to fuse, and once activated, they bind to the bone surface and express markers specific to osteoclasts such as cathepsin K [49]. The binding of RANKL to RANK can be antagonised by osteoprotegerin (OPG), a decoy receptor for RANKL that inhibits osteoclastogenesis. Therefore, whether and how much resorption occurs is determined by the RANKL:OPG ratio [50]. Like RANKL, OPG is also produced by osteoblasts meaning that they have a key role in controlling the balance between bone formation and resorption (Fig. 2.10).

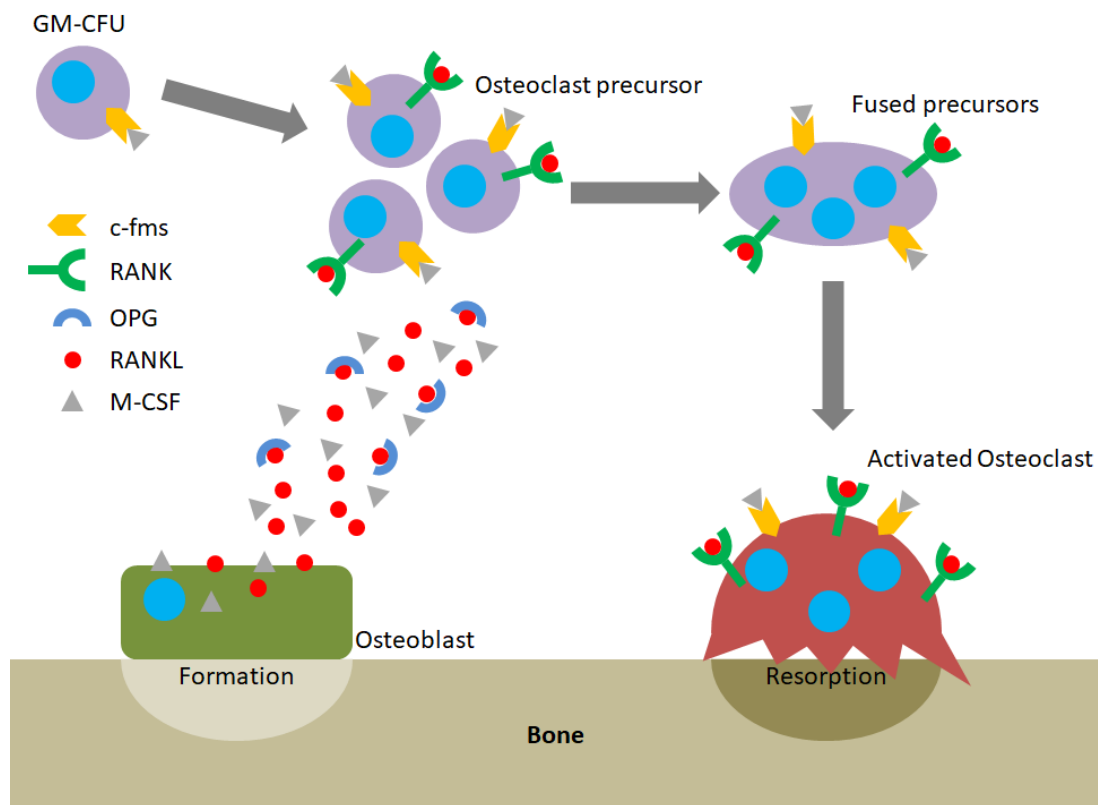


Figure 2.10: Diagram of how the RANKL/RANK/OPG axis and M-CSF direct osteoclastogenesis and activation.

Through the use of tetracycline dyes, the rate of longitudinal BMU advance is calculated to be approximately 25 μm per day and they can continue for between 6 and 9 months. As the lifespans of the constituent cells of the BMU are much shorter, they must be continuously replaced for the unit to operate correctly [51]. There are approximately 35 million BMUs operating within the skeleton at any one time, with 5-10% of the existing bone being replaced each year. This means that every 10 years the skeleton is entirely renewed [44].

It has recently been discovered that trabecular BMUs are separated from the surrounding bone marrow by a canopy to create a bone remodelling compartment (BRC). These canopies are likely formed by an extension of the bone-lining cells due to their expression of typical osteoblastic markers. The BRC generates a unique microenvironment conducive to paracrine signalling and facilitates BMU formation and function. It allows control over osteoblast-osteoclast coupling and ensures tightly regulated bone remodelling. BRCs cover practically all resorptive surfaces and over 50% of formative surfaces, indicating that they form as resorption initiates and are closed as formation completes. Capillaries penetrate the BRC and are thought to serve as conduits for the precursor cells needed to form and maintain BMUs as their lifespan is 6 to 9 months, much longer than the constituent cells (osteoclasts 2 weeks, osteoblasts 3 months). Disruption of the BRC negatively affects bone turnover and can result in uncoupled remodelling, where bone is resorbed without being replaced [52]–[58].

There are five stages in bone remodelling: the quiescent, activation, resorption, formation, and mineralisation phases (Fig. 2.11). During the quiescent phase the bone is inactive. It is not known exactly what factors initiate remodelling, but the most likely causes are micro-fracture, to maintain normocalcaemia during pregnancy or a deficient diet, or a change in the mechanical loading of the tissue sensed by osteocytes. This results in the production of factors such as insulin growth factor-1, tumour necrosis factor- α , parathyroid hormone and interleukin-6 which activate the bone lining cells [59], [60]. The activation phase prepares the surface of the bone for resorption. Bone lining cells, elongated mature osteoblasts on the endosteal surface, retract and the endosteal membrane is broken down by collagenase, exposing the mineralised bone matrix. Mononuclear monocyte-macrophage osteoclast precursors are recruited from the circulation and activated, which fuse to form multinucleate osteoclasts. These bind to the exposed bone matrix through interactions between

integrin receptors in the cell membrane and peptides containing RGD (arginine, glycine, asparagine) in the matrix [13].

The resorption phase then begins, with osteoclasts using a combination of hydrogen ions and lysosomal enzymes to degrade and dissolve the matrix, forming resorption cavities. Osteoclasts then undergo apoptosis and macrophages complete this process, facilitating the release of growth factors from within the matrix [44]. At the end of resorption there is a transition to the formation phase which can take up to five weeks. This is sometimes classed as the reversal phase. When resorption is completed the resorption cavities contain monocytes, osteocytes that have been freed from within the matrix, and preosteoblasts. It is not yet known what signals couple resorption and formation phases, but it is likely bone matrix-derived factors [61].

Formation and mineralisation can be viewed as a two-step process. Preosteoblasts are recruited to the resorption cavity by the chemotactic growth factors released from the matrix. They synthesise a cementing substance on the surface which acts as a foundation for new tissue and express bone morphogenetic proteins responsible for differentiation. After a few days, osteoblasts first deposit the collagenous organic matrix then regulate its mineralisation, filling the resorption cavity with osteoid. Once the collagen has been secreted, mineralisation is triggered by the osteoblasts releasing membrane-bound vesicles termed matrix vesicles which establish conditions conducive to mineralisation. This involves increasing the concentration of calcium and phosphorus ions and degrading inhibitors of mineralisation, such as some proteoglycans present in the organic matrix. Mineralisation begins 30 days after osteoid deposition and finishes after 90 or 130 days later for cancellous and cortical bone, respectively. As this occurs, some osteoblasts become embedded and undergo osteocytogenesis. After completion, the remaining osteoblasts either undergo apoptosis or become bone lining cells [12], [44], [61], [62].

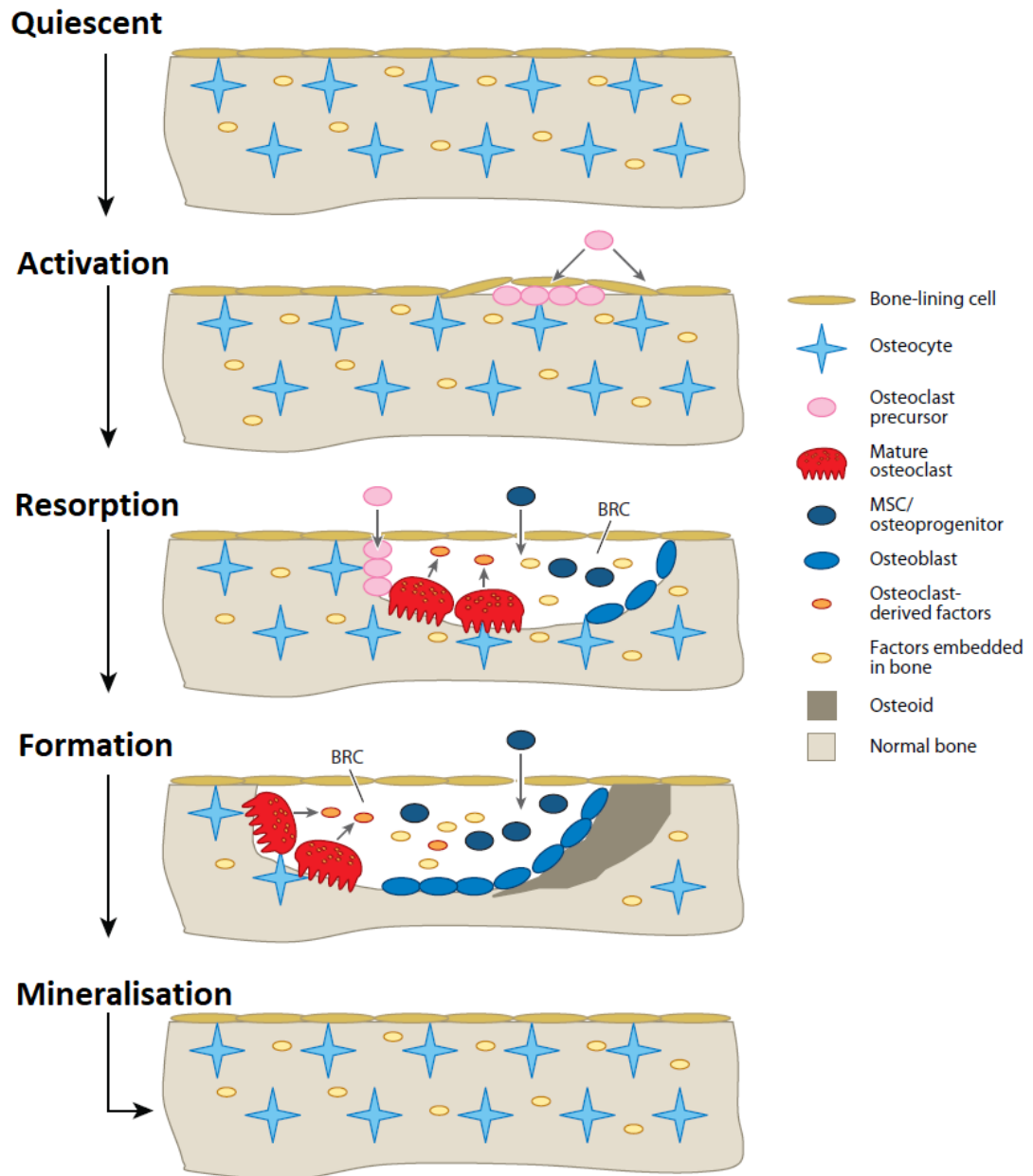


Figure 2.11: The five stages of bone remodelling. Reprinted and adapted from Feng and Macdonald under the Creative Commons Attribution Licence [63].

At the completion of remodelling there should be no net loss or gain of bone. Any difference in resorption and formation is referred to as the ‘bone balance’. BMUs on the periosteal surface of cortical bone have a marginally positive bone balance; therefore, with ageing, the circumference of the periosteal surface increases as the net gain from each remodelling cycle accumulates. Conversely, endosteal BMUs have a marginally negative bone balance; therefore, the marrow cavity circumference

increases with age. However, the net loss on the endosteal surface is greater than the net gain on the periosteal surface, resulting in cortical thinning with age. This, combined with a slightly negative bone balance on the surface of the trabeculae resulting in thinning of the cancellous bone, increases the fracture susceptibility of bones with large surface area, such as the vertebrae or distal radius. Therefore, bone remodelling in the elderly results in a loss of bone, which can eventually manifest as osteopenia or osteoporosis depending on the severity [12], [44], [61], [62].

2.1.6 Bone tissue engineering

In the United Kingdom the incidence of bone fractures is 3.6 per 100 people per year, with 38.2% of people experiencing a bone fracture in their lifetime [64]. Fractures can be divided into two categories, pathologic/fragility fractures and traumatic fractures. The former are fractures of diseased bone at a stress lower than that required to fracture a healthy bone, and are associated with conditions such as osteoporosis. Traumatic fractures are the result of excessive force on the bone due to events such as falls and vehicle accidents [16]. The treatment method for bone fractures is dependent on the severity of the break, and the options range from pain management to surgery. A bone graft may be necessary for the most complex fractures, facial and cranial reconstruction, and defects caused by bone cancer. There are estimated to be 2.2 million bone grafts performed each year, making it the second most transplanted tissue after blood [65].

Tissue engineering aims to improve on current medical treatments and therapies by imitating nature; creating, repairing and regenerating tissues and organs to restore the original function. In order to achieve this successfully, engineering principles are applied to the life sciences, drawing knowledge from a wide range of fields including physics, chemistry, engineering, biology, materials science and medicine [19], [66].

Autologous bone grafts are considered the gold standard. Commonly sourced from the iliac crest, these grafts contain osteoblasts, osteoid, and factors such as bone morphogenetic proteins. This results in an osteogenic (causes bone formation because of the implantation of viable cells), osteoinductive (stimulates bone to form when implanted, typically inducing osteoblastic differentiation) and osteoconductive (composition, shape or surface topology promotes bone formation along its surface) graft which when implanted at the injury site, promotes a bone healing response [67]. Autografts are also relatively cheap when compared to commercial alternatives, there

are no concerns regarding disease transmission, and fusion rates are relatively high. However, there is limited tissue availability, donor site morbidity and pain, as well as multiple surgeries required for the procedure [68].

Allografts are an alternative to autografts which use bone tissue from cadavers. Bone is readily available; however, there are concerns with disease transmission, immune rejection, and tissue compatibility. The success rate of these grafts is lower than autografts and although transmission of pathogens from donor to host is infrequent, it is possible [19], [68]. Between 1999 and June 2007 in the United States, improper donor evaluation was the most common reason for allograft recall (67.2%), followed by contamination (21.5%) and recipient infection (14.6%) [69].

Xenogeneic grafts are bone harvested from one species and implanted into another. Tissue is readily available as with allografts and due to similar structures of hydroxyapatite between bovine and human mineral, they have a potentially better suitability for bone grafting than synthetic materials. As with allografts, processing procedures such as donor cell and antigen removal and the elimination of pathogens are essential. However, it is important not to damage the natural biological properties, such as mechanical strength and osteoinductivity [70]. In addition, strong immune responses preclude the use of most xenografts resulting in allografts being generally considered more effective [71]. For both allografts and xenogeneic grafts, sterilisation and freeze-drying techniques diminish osteoinductive and mechanical properties of the graft.

Synthetic bone grafts or bone graft substitutes aim to achieve the osteoinductive, osteoconductive, biocompatible, bioresorbable nature of natural bone grafts whilst removing the possibility of immune rejection and pain associated with donor site morbidity. Ceramics, bioactive glasses, glass ionomers and hydroxyapatite derivatives are just a small selection of materials attempted for use as a bone graft substitute. Bioactive glasses are osteoinductive, and it is this biological activity that encourages their use as bone graft substitutes [72]. Bioactive glasses can also be combined with polymers, such as poly(lactic-co-glycolic acid) (PLGA), to improve its osteoinductivity and mechanical properties. The resulting composite can be used for bone tissue engineering as the superior mechanical properties make it more suitable for load-bearing applications [73]. Depending on the type of bioactive glass used, the resulting composite material can either promote or inhibit osteoblast and osteoclast

activity *in vitro* [74], [75], and are capable of inducing ectopic bone formation *in vivo* as a demonstration of their osteoinductivity [76].

However, synthetic bone graft substitutes are yet to be as successful as natural bone grafts due to poor wear properties and brittleness limiting their use in locations with considerable shear stress, torsion or bending [77], [78]. As a result they are usually provided as granules [79], [80]. Synthetic substitutes also have minimal biological activity, acting as defect fillers with osteoconductive properties that promote osseointegration. To improve biological activity synthetic grafts may be incorporated with auto- or allografts, creating a composite. Ideally, synthetic grafts would have the ability to act as a delivery system for factors that regulate bone remodelling at the defect site, resulting in a graft with a controlled resorption and delivery rate that has sufficient mechanical properties to act as a framework for bone formation [71], [81].

Bone tissue engineering is an emerging field that is a promising alternative to bone grafting as it could overcome the associated limitations. The general principle is to obtain cells from the patient, expand them in culture, seed them onto a scaffold, and implant the scaffold back into the patient where it will resorb over time [82]. These scaffolds are biodegradable, and provide physical and chemical cues that direct cell differentiation, adhesion, and growth, forming three-dimensional (3D) tissues [83]. Despite tissue engineering and regenerative medicine being hailed as the future of medicine, with the exception of the medical device and implant industry, it is yet to fulfil expectations [66]. Whilst there are products in the market, they are mainly skin substitutes and tissue engineering remains a fledgling industry. This is due to the technical challenges of creating effective “off the shelf” products that contain cells, but which also have an appropriate shelf life and can still treat millions of different individuals. The properties and mechanisms of the scaffolds also need to be improved, such as preserving mechanical strength whilst retaining adequate porosity for sufficient and timely vascularisation of scaffolds after implantation [84], and *in vitro* experiments need to retain their efficacy when scaled up to clinical applications [85].

2.2 Osteoporosis

2.2.1 Prevalence and clinical consequence

Osteoporosis is a systemic disease which affects bone, reducing its strength through a reduction in mass and deterioration of the microarchitecture. This results in an increase in fragility and an increased susceptibility to fracture [86]. The World Health Organisation state that the deterioration of bone mass and quality is classed as osteoporosis when the bone mineral density (BMD) is 2.5 standard deviations below the mean for young normal healthy adults (T score of -2.5). However, how to utilise this criterion properly is unclear when diagnosing individuals of different gender, ethnicity and age [2]. Osteoporosis refers to a group of conditions, rather than a specific, single entity. It is traditionally classified as primary or secondary, with primary type being subdivided into two further categories. Primary type I is the most common form of the disorder and is often referred to as postmenopausal osteoporosis. This disorder is common within the postmenopausal demographic as decline in oestrogen levels as a result of menopause is an important factor in the pathogenesis. Primary type II osteoporosis, also known as senile or age-related osteoporosis, is associated with both men and women and the onset is associated with ageing. Finally, secondary osteoporosis refers to when the disorder is present as a consequence of an adverse response to a medication, change in physical activity, or another medical condition. Common examples of this iatrogenic condition include glucocorticoid- and immobilisation-induced osteoporosis [63].

There are an estimated three million people in the United Kingdom with osteoporosis, and approximately three hundred thousand fragility fractures per year [1]. Currently, fifty percent of women and twenty percent of men over the age of fifty will have a fragility fracture, with the health and social care costs for treating hip fractures alone currently exceeding £2.3 billion per year in the United Kingdom. However, the demographics of western countries are changing with an increasing proportion of the population exceeding fifty years of age, thus further increasing the incidence and cost each year [87].

Hip fractures are often considered the most devastating, accounting for around one in five osteoporotic fractures and 20% of these cases resulting in fatality within the first year [1]. However, the adverse effects of vertebral fractures due to osteoporosis can often be underestimated and underdiagnosed. They are an often-neglected

consequence of the disorder that can result in substantial pain and disability and increased mortality risk. They are also an indicator of future fracture risk [88]. Multiple thoracic fractures and lumbar fractures can result in restrictive lung disease and changes in the abdominal anatomy, respectively. The latter can lead to pain, a reduction in appetite and the patient feeling sated prematurely [89]. Wrist fractures are also common in osteoporotic patients; however, relevant data is sparser than for the previous types, perhaps due to the mortality rate being similar to that of the general population [90]. As a consequence of osteoporotic fracture, there may also be psychological effects on the patient due to the pain, disability and changes in appearance, resulting in depression, reduced self-esteem and anxiety [91].

2.2.2 Aetiology, pathogenesis and risk factors

Bone strength is dependent on two key factors: density and quality. Skeletal fragility can be a result of improper development during growth resulting in sub-optimal mass and strength, excessive resorption which decreases mass and deteriorates the microarchitecture, and/or insufficient formation in response to resorption [86]. Osteoporosis is diagnosed when the BMD falls below a certain threshold. However, this may not be the optimum diagnostic criterion as it does not take bone quality into account. The geometry, microarchitecture and material properties all affect the strength of bone and its susceptibility to fracture. In postmenopausal osteoporosis, abnormalities in bone remodelling affect all these properties. If a diagnostic approach integrated all of these and was combined with bone turnover markers, it may be superior and able to evaluate more accurately bone strength and fracture risk than BMD alone [89]. In healthy tissue, bone turnover is balanced with complimentary amounts of osteoclastic resorption and osteoblastic formation. Postmenopause, the rate of bone turnover increases and remains elevated, resulting in progressive bone loss in both cortical and cancellous bone that deteriorates the bone strength (Fig. 2.12).

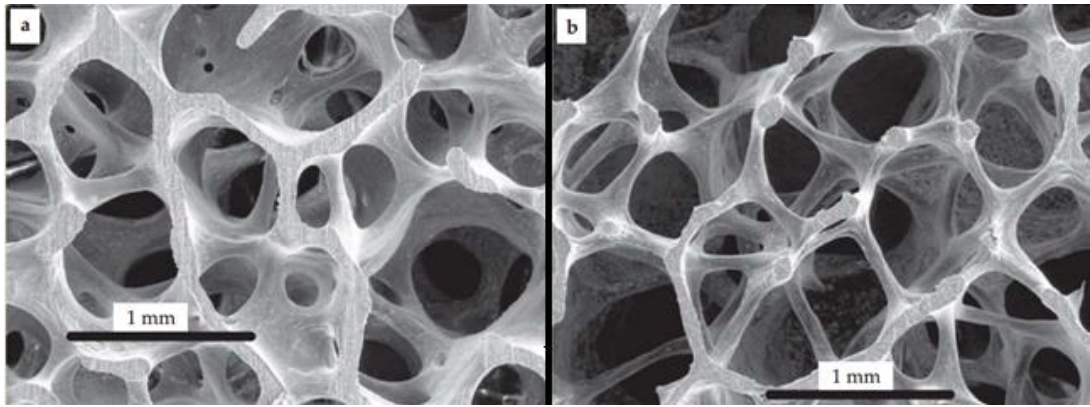


Figure 2.12: Vertebral cancellous bone of a (A) 21-year old male and (B) 65-year old female. Adapted from Ritchie, et al., and reprinted with the kind permission of Dr. James Weaver, Wyss Institute, Harvard University [92].

The pathogenesis of primary type I osteoporosis is predominantly due to the decline in oestrogen caused by cessation of ovarian function. This hypothesis was first proposed in the 1940s when it was demonstrated that postmenopausal women have a negative calcium balance [63]. Although initially believed that the deficiency resulted in insufficient formation, later work showed that it is increased resorption that impairs bone quality [93]. Although both aspects of bone turnover are increased postmenopause, resorption exceeds formation causing a negative bone balance [94]. Once identified as playing a central role in the pathogenesis of the disorder, investigations into the mechanisms by which this occurs have been investigated in order to better understand the disease and develop new therapies (Fig. 2.13).

Studies in the 1980s found that osteoclastogenesis is regulated by several cytokines such as interleukin (IL)-1 and IL-6, tumour necrosis factor (TNF), and M-CSF. IL-1 and TNF are powerful stimulants of bone resorption and inhibitors of formation. They enhance osteoclast formation by stimulating the proliferation of precursors and can also induce other cytokines, such as IL-6, which regulate precursor differentiation into mature osteoclasts [95]. Oestrogen inhibits these cytokines, indicating it may perform a protective role by modulating their production.

The discovery of the interaction of RANK/RANKL/OPG in the 1990s was a significant milestone in understanding the pathogenesis of postmenopausal osteoporosis, as well as other bone metabolic disorders [63]. RANKL binds to its receptor, RANK, but OPG can compete with RANK for binding to RANKL,

antagonising its function. The interactions between these three regulate osteoclast formation and function [96]. During normal bone remodelling, cells from the osteoblast lineage, such as osteoblasts and osteoprogenitors, express M-CSF and RANKL which conjugate with their respective receptors on osteoclast precursors, c-fms and RANK, stimulating osteoclast formation. Oestrogen stimulates the expression of OPG which reduces formation; therefore, deficiency results in increased osteoclastogenesis [97]. Additionally, the expression of RANKL is elevated postmenopause, demonstrating the role of this system in osteoporosis pathogenesis [98]. Oestrogen has also been shown to modulate osteoclast life span by promoting apoptosis, further indicating its preventative role against osteoporosis [99].

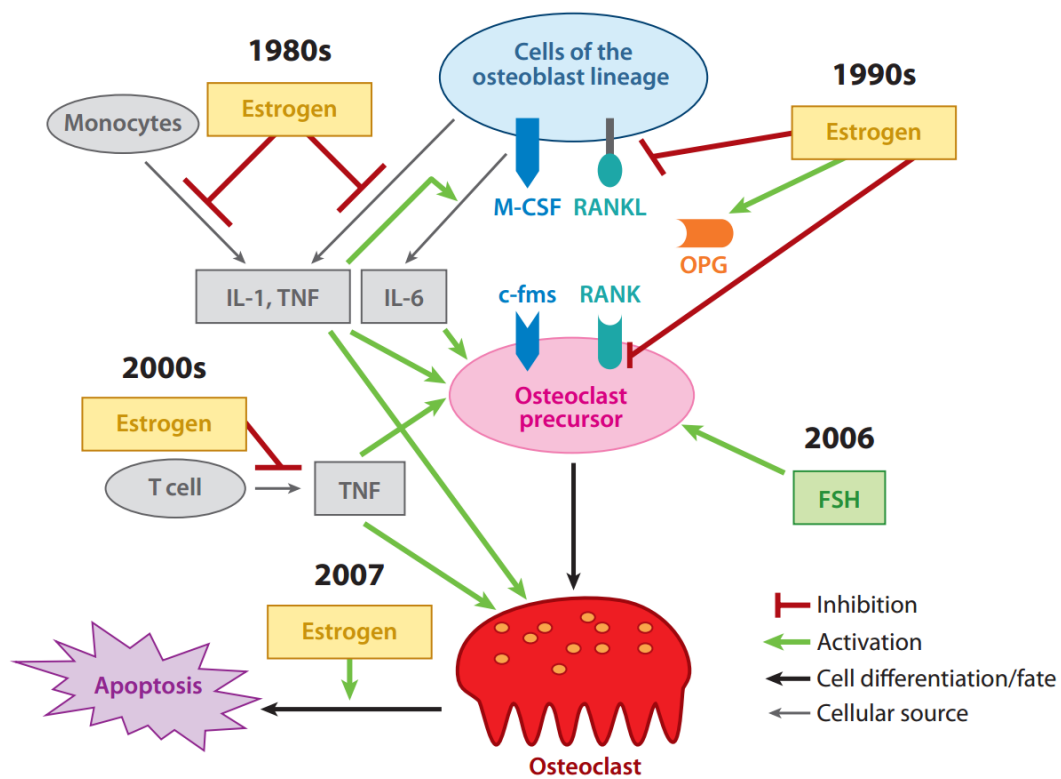


Figure 2.13: The central role of oestrogen in postmenopausal osteoporosis. Dates indicate when effects were discovered. Reprinted from Feng and Macdonald under the Creative Commons Attribution Licence [63].

The likelihood of developing postmenopausal osteoporosis is dependent on a large number of risk factors, including clinical, medical, behavioural, nutritional and genetic variables. The major determinant is the peak bone mass which typically occurs during the third decade of life, with the majority of bone mass attained during adolescence. After the cessation of ovarian function, the rate of bone turnover increases and remains elevated causing BMD to continually decline. Therefore, ageing itself is a risk factor for bone loss and osteoporosis [89].

Postmenopausal women with low body weight, percentage body fat, or body mass index (BMI) are also at an increased risk of osteoporosis due to the positive correlation between body mass and bone size [100]. Medical risk factors are therapies or disorders that would cause secondary osteoporosis, the most commonly implicated of which is glucocorticoids. Postmenopausal women who have low BMD that are not yet at the threshold for being classed as osteoporotic will achieve this sooner when taking glucocorticoids than those who are not. Several behaviours, including smoking [101] and a low level of physical activity [102], have been correlated with increased bone loss. With regards to nutrition, dietary calcium is correlated with BMD in women with low BMI, and in the elderly vitamin D deficiency increases bone turnover resulting in bone loss, as well as adversely affecting mineralisation, reducing bone strength and elevating fracture risk [102], [103].

Genetic risk factors for osteoporosis have also been identified. Race is a determinant of BMD, with white and Asian women at the highest risk of fracture above the age of 50 [89]. From studies involving twins and families, the heritability of BMD is estimated to be between 50 and 85% [104]. In exceptionally rare circumstances, osteoporosis can be inherited in a Mendelian manner. For example, osteoporosis can be caused by the inactivation of the oestrogen receptor α gene [105]. More commonly, multiple genes each constituting a modest effect on BMD cumulatively account for the individual's genetic risk factor. These include genes coding for vitamin D receptors and type I collagen [104]

2.2.3 Diagnosis and current treatments

A diagnosis of osteoporosis is typically given by assessing the BMD using a radiological approach. The gold standard for this is dual-energy X-ray absorptiometry (DXA) as quantitative measurements of BMD can be derived quickly and relatively cheaply from all locations within the body with radiation levels 90% lower than a standard chest X-ray [89]. However, surrounding soft tissues can introduce measurement errors, it cannot distinguish between cortical and cancellous bone so an 'integral' BMD is given, and variations in bone size affect measurements as density is expressed as areal BMD (g/cm^2) [106]. DXA studies are usually reported as T scores.

Quantitative computed tomography (QCT) is an alternative to DXA which can also be used to measure BMD. It can only be used on the lumbar spine or peripheral locations and involves relatively high doses of X-ray (2,000 μSV versus 5 μSV for DXA for scans of two vertebrae). However, it can differentiate between cortical and cancellous bone, is less prone to errors from soft tissue, and can measure volumetric BMD (mg/cm^3). 3D volumetric images can also be used to evaluate changes in bone geometry [107]. Whilst these two radiological techniques are excellent at determining BMD for diagnosing osteoporosis, their use when determining fracture risk is limited as it does not take bone quality into account, a key determinant of bone strength. In fact, approximately 50% of osteoporotic fractures occur in patients with a BMD above defined thresholds [108].

Biochemical markers of bone formation, such as alkaline phosphatase and osteocalcin, and bone resorption, such as hydroxyproline from collagen degradation and tartrate-resistant acid phosphatase, are measured in research and clinical trials of new therapies as a method of determining efficacy. Whilst they will never be a replacement for radiological evaluation of BMD, they could potentially be used as a predictor of future fracture risk and monitor drug efficacy in patients [89], [109].

The National Osteoporosis Foundation guidelines for clinicians recommend that all women greater than 65 years of age have their BMD measured and postmenopausal women between 50 and 69 if their risk factor profile raises concern. Once patients are being treated for osteoporosis, their BMD should be reassessed every 2 years [110]. Non-pharmacological approaches to treatment are typically behavioural, for instance smoking cessation and limiting alcohol and caffeine intake, as well as physical exercise and nutritional advice to ensure adequate vitamin D and calcium intake [111].

Bisphosphonates are typically the first-line therapy when a patient is diagnosed with osteoporosis as they have been shown to reduce bone turnover; increasing BMD and lowering fracture risk in postmenopausal women. However, orally administered bisphosphonates have gastrointestinal side effects including dyspepsia and abdominal pain, and intravenous bisphosphonates can result in influenza-like side effects. These can result in a lack of patient compliance and persistence with the therapy [3]. With oral bisphosphonates, such as sodium alendronate or sodium risedronate, doses are limited by the gastrointestinal side effects due to the low bioavailability of the drug, whereas intravenous alternatives, such as zoledronate, have increased potency which reduces bone turnover for longer and do not have to be administered as often. However, these are generally more expensive than oral alternatives (Table 2.1).

Hormone replacement therapy (HRT) has been shown to reduce the risk of hip and vertebral in patients with osteoporosis as well as reducing menopausal symptoms such as reduced libido, vaginal dryness and hot flushes [112]. However, oestrogen based HRT has been associated with an increased risk of stroke, and oestrogen-progesterone based HRT with breast cancer and heart disease [4]. From this, many organisations recommend HRT is only used at the minimum effective dose after in-depth discussion with the patients so they can consider carefully the risk to benefit ratio [113].

Table 2.1: Various treatments for osteoporosis available on the NHS and their approximate annual cost per patient [114].

Drug	Type	Approximate annual cost to the NHS
Generic sodium alendronate	Oral bisphosphonate	£14
Fosamax® - branded sodium alendronate	Oral bisphosphonate	£296
Generic sodium risedronate	Oral bisphosphonate	£220
Zometa® or Aclasta® - branded Zoledronate	Intravenous bisphosphonates	£174 / £253
Protelos®	Strontium ranelate	£330
Prolia® - Denosumab	Denosumab	£366
Evista®	Raloxifene	£220
Forteo®	Teriparatide	£3,540

Strontium ranelate has been shown to reduce bone resorption and increase formation as well as reducing vertebral, non-vertebral, and hip fracture risk over a period of five years when compared to a placebo [115]. A periodic safety update report on the drug produced by the European Medicines Agency in November 2012 showed that patients treated with strontium ranelate are at increased cardiovascular risk, and therefore it should not be prescribed to patients with a history of cardiovascular disease [116] [117]. In February 2014, they recommended further restricting the use of the medicine to patients who cannot be treated by any other approved drug, and those who do continue should be regularly monitored for heart and circulatory problems [118].

Denosumab is a human monoclonal antibody that inhibits RANKL. It is administered via a subcutaneous injection of either 60 mg twice or 30 mg four times per year. Over a 36 month trial it has been shown to reduce the risk of vertebral, non-vertebral and hip fracture [119]. Romosozumab is another monoclonal antibody-based treatment that is currently undergoing clinical trials for treating osteoporosis. Rather than targeting RANKL, it binds to sclerostin, a protein released by osteocytes that inhibits bone formation. The phase 2 clinical trial found that a one year treatment with Romosozumab administered by monthly subcutaneous injection significantly increased BMD and lowered markers of bone turnover and the risk of vertebral fracture [120].

Raloxifene, a selective oestrogen receptor modulator (SERM), inhibits bone resorption but does not stimulate the uterine endometrium. It has been approved for use in the prevention and treatment of postmenopausal osteoporosis and has been shown to increase BMD in the spine and femoral neck, reducing vertebral fracture risk by 30 – 50% in comparison to a placebo, but has not been demonstrated to significantly lower fracture risk at other anatomical locations. Bazedoxifene, another SERM, was also shown to reduce vertebral fracture risk, as well as fracture incidence at other anatomical sites in women characterised as having higher fracture risk [113], [121]. The most common adverse reactions of SERMs are vasomotor effects such as hot flushes and leg cramps. However, as with HRT, patients are also at a heightened risk of venous thromboembolism [122]. These side effects combined with limited clinical data on its effect on fracture risk render SERMs a second line approach to osteoporosis treatment.

Teriparatide (human recombinant parathyroid hormone 1-34) is an anabolic analogue of PTH administered via a once daily subcutaneous injection. Unlike antiresorptives, this biologic increases formation and resorption; however, in doing so changes the bone balance of the BMUs to positive, resulting in increased BMD [123]. Bone quality also improves, with cortical thickening and increased cancellous bone connectivity [124]. It has been shown to increase BMD and reduce the risk of vertebral and non-vertebral fractures by 65 - 69% and 35 – 40%, respectively [113]. Use of teriparatide is typically reserved for patients with severe osteoporosis, primarily due to the high cost and inconvenience of daily injections [125]. Treatment may increase the incidence of nausea, dizziness and leg cramps, but in comparison to other treatments, it has an acceptable side effect profile. Maximum treatment duration of two years is recommended due to limited evidence of treatment efficacy beyond this duration and long term toxicology concerns due to the development of osteosarcoma in rats [5].

2.2.4 Animal models of osteoporosis

Animal models provide a uniform approach to research with a level of experimental control that is not possible in humans. Compared to human trials, the cost is much lower and the time frame much shorter. Osteoporosis is a disorder with slow progression which means that human studies have a duration of several years, slowing data acquisition. Therefore, even if only a small representation of human function is made within an animal model, it can still be of use.

Postmenopausal osteoporosis only occurs naturally in humans and some non-human primates. Therefore, to study this disorder in other animals, it has to be induced. This is typically done by ovariectomy (OVX), surgical removal of the ovaries to suppress oestrogen production in order to simulate the postmenopausal condition. Other methods or combinations of approaches can be used to induce osteoporosis, such as restricted diet, glucocorticoids, immobilisation and breeding, but this review will focus on the main OVX animal models that simulate postmenopausal osteopenic/osteoporotic bone [87].

Animal models are essential to ongoing osteoporosis research, but this presents a paradox - how can we design a good animal model of a disorder we do not fully understand? [126]. Furthermore, osteoporosis is not a disease caused by a single factor; it is a description of the remaining bone after a multitude of factors has altered its metabolism. As a result, there is no single animal model that represents the entire condition. Instead, each is able to mimic a specific aspect. Therefore, selection of a suitable animal model presents a challenge. The key factors to be considered were rationally defined by Rogers, et al., who state that the model should be convenient, relevant to the human condition, and appropriate to the particular phenomenon you are investigating, with the limitations candidly stated [127].

In vivo models of osteoporosis can be divided into two categories; small and large animal models. Typically, mice and rats are selected for small animal models whilst sheep or non-human primates are used for large animal studies. When introducing a new osteoporotic drug the FDA require preclinical evaluation that involves testing at clinical dose and five times clinical dose on a rat as well as a validated, large animal model [6].

The rat animal model of postmenopausal osteoporosis is by far the most common. In contrast to large animal studies there is relatively minimal public opposition to its use, housing, handling and feeding costs are reduced and ethical implications are in general, lower [128]. OVX rats are frequently used when efficacy and toxicity of new potential therapies are beginning to be evaluated [129]. After surgery, bone balance initially becomes negative resulting in bone loss. However, bone turnover eventually becomes balanced again, meaning that the BMD stops decreasing and settles, albeit at a much lower level than pre-OVX. Significant loss of bone is seen after 14 days in the proximal tibial metaphysis, 30 days in the femoral neck, and 60 days in the lumbar vertebrae [130]–[133].

Two types of rat are used, aged and mature. Aged rats have reached skeletal maturity (~12 months); therefore, skeletal changes post-OVX can be regarded as a response to oestrogen deficiency. Mature rats are simply those that have reached sexual maturity (~3 months) and therefore are capable of responding to oestrogen and its deficiency. However, skeletal changes due to aging are still taking place so changes seen post-OVX may not be attributed exclusively to reduced oestrogen [126]. With age, the mechanism by which bone turnover occurs in the rat skeleton changes. Bone turnover can occur by two mechanisms; remodelling and modelling. Bone remodelling is the coupled, both spatially and temporally, action of formation and resorption by BMUs. Bone modelling is independent, uncoupled formation and resorption of bone at a specific site that occurs separately over extended time periods [134]. As rats age they transition from modelling to remodelling, with the latter becoming the dominating mechanism at 12 months. Although aged rats have more of the ideal characteristics for an *in vivo* model, they are more expensive, availability is limited, and substantial bone loss post-OVX may not be seen for several months [129]. This is not the case for mature rats, which are cheaper, more readily available, and skeletal changes can be seen within weeks.

A potential limitation of rat models is that they lack Haversian remodelling, a feature that is present in large animal models. In humans, osteons form the majority of the cortical porosity, but these units are not present with rat cortical bone. Despite this, performing OVX on adult rats still results in a condition similar to postmenopausal osteoporosis in humans, with an altered bone balance that leads to increased bone remodelling and bone loss at the endosteal surface and the trabeculae [135]. It is bone loss at these sites that is the hallmark of postmenopausal osteoporosis, rather than intracortical bone loss within the osteons [136].

Murine models of osteoporosis have the same size based limitations as rat models. Skeleton size does not scale linearly with body size and as a proportion of total body mass, a human skeleton is much larger than a mouse or rats. Furthermore, the proportion of trabecular bone mass in rodents is much smaller than in humans. Clearly, this makes these models incapable of being used for surgical or implant based studies for osteoporotic fracture. Despite this, mouse models are ideally suited to studying the genetic contribution to bone remodelling, allowing specific factors, proteins and pathways to be elucidated, an important tool in understanding metabolic bone disorders. However, just because a gene or factor can affect bone mass does not mean it is necessarily linked to osteoporosis.

Whilst the value of genetically modified mouse models is clear, justification for the use of murine OVX models is not well established. Post-OVX, trabecular bone is lost and this effect can be mitigated with oestrogen replacement in the form of 17 β -estradiol [137]. However, whilst bone turnover is affected by OVX, the effects are highly strain dependent, and are much less consistent than in rats [136]. This, in combination with the small amount of trabecular bone available making accurate analysis of changes in bone volume extremely challenging, results in the use of murine OVX models being less reliable than rat models.

Many large animals have been used for OVX models of osteoporosis, including dogs, cats, sheep, monkeys and apes. Public opposition to the use of dogs and cats is high as they are seen as companion animals. Despite dogs having extensive BMU based remodelling, they are of limited use when studying postmenopausal osteoporosis due to an apparent skeletal resistance to oestrogen deficiency. They only ovulate twice annually and therefore have very low oestrogen levels for most of the year; however, increased skeletal fragility is not seen. Similarly, many owners have their cat's ovaries removed to prevent unwanted breeding, yet as with dogs, fragility fractures are rare. Therefore, cats and dogs are of more use when studying secondary osteoporosis [6].

Ovine animal models are well established in orthopaedic research. They are docile, compliant, relatively cheap in terms of acquisition and maintenance, and society has low opposition to their use as they are seen as food animals, reducing the emotional attachment in comparison to cats and dogs. In addition to this, sheep have similar bone architecture to humans. Both have cortical and trabecular bone, Haversian systems, and remodelling is performed by BMUs. However, sheep have higher BMD and mineral content than humans which increases the mechanical stability of their bones,

meaning that fragility fractures post-OVX are rare. They also have a variable oestrus cycle and a much lower oestrogen peak, meaning that OVX has a reduced effect on bone mass and structure in comparison to humans [138]. It is also worth noting that the biomechanical loads experienced by quadrupeds are clearly different to those experienced by bipeds, especially in the spine where humans have an inward curvature (lordotic) whereas sheep have an outward curvature (kyphotic) [139].

Post-OVX, BMD is reduced three months after surgery in sheep [140], [141]. However, this bone loss is not always sustainable, with several groups reporting bone turnover and BMD stabilising then returning to pre-OVX levels due to bone formation also increasing [140], [142]–[144]. Other groups still detected significant changes in BMD and structure up to 24 months after OVX [145], [146]. Therefore, ovine bone metabolism seems similar to human and OVX results in rapid bone loss for three months, although this reduction may eventually be restored by increased formation. Conflicts in these results may be due to variations in BMD with the seasons. Humans have lower bone mass in winter than in summer, and bone turnover in sheep also changes throughout the year [147].

Unsurprisingly, non-human primates have been used extensively to create *in vivo* models of osteoporosis. Their gastrointestinal and endocrine systems closely resemble humans, with macaques and baboons having a 28-day and 33-day menstrual cycle, respectively, and both having similar oestrogen and progesterone patterns. There is also Haversian-based osteon remodelling, age-related bone loss, and natural menopause in some species [148]. Furthermore, they have similar physiological loading due to their upright posture and comparable immune systems, all of which combine to make them the most relevant model of human physiology [128].

Although primates undergo natural menopause, acquisition of aged animals is prohibitively expensive. Therefore, OVX is often performed on skeletally immature animals [6]. Non-human primate OVX models have been performed since 1986 and have become established as the best characterised large animal model in osteoporosis research [149]. Multiple primate species have been used in osteoporosis research, including cynomolgus, rhesus, baboon, and African green monkeys, with cynomolgus being the most common due to its availability, smaller size, lower relative cost, and extensive characterisation [150]. In ovariectomised cynomolgus, bone turnover is increased and rapid bone loss ensues, stabilising 8-9 months later [151].

Primate models have been used extensively to test therapies such as bisphosphonates and parathyroid hormone (PTH) in order to assess efficacy and safety, as well as their treatment mechanism [152], [153]. However, there are very few laboratories worldwide that can legally perform these studies and the associated costs are tremendous. Primates for research are often wild-caught and can be aggressive, which increases the risk of zoonotic disease transmission to humans [154]. Public opposition to their use is extreme; therefore, they are not standard animal models and are of most use during final preclinical testing before human trials, after investigations on other large animals have been performed.

Animal models are viewed as the gold standard for testing the safety and efficacy of new therapies and are an essential part of the preclinical development of new medicines. However, their use should align with the principles of the ‘3Rs’ – replacing, reducing and refining, in order to conduct humane animal research [7]. No animal model is the perfect representation of postmenopausal osteoporosis and all have clear advantages and limitations. Therefore, it is realistic that some of the work currently performed *in vivo* could be replicated *in vitro*, reducing the number of animals required as well as the cost of drug development. Indeed, this directive is part of the impetus behind this research project; if aspects of animal models can be replicated or even improved *in vitro*, then this should be pursued.

2.3 Bone remodelling *in vitro*

2.3.1 The need for *in vitro* models

In 2015, 2.08 million experimental procedures were performed on animals in the United Kingdom. 1.1 million were for basic research purposes, with 25,381 of these within the field of musculoskeletal research. 89% of these studies were conducted on mice and rats [155]. The popularity of rodent models for bone disorders arises from a relatively minimal public opposition to their use, as well as low cost and ease of housing in comparison to other, larger animal alternatives [128]. Furthermore, their size makes them amenable to non-invasive, high resolution *in vivo* imaging techniques such as x-ray micro-computed tomography (MicroCT) [156], [157] and the application of mechanical loading *in vivo* [158]. However, despite becoming a fundamental component of pre-clinical research, animal physiology does not accurately represent the human condition, with many aspects of human anatomy not well represented in a rodent model. This is demonstrated by the poor translation of pre-clinical efficacy in animal models to human clinical trials and the vast majority of promising discoveries failing to enter routine clinical use [159]–[162].

Although *in vivo* models are viewed as the gold standard for studying diseases and testing new therapies, their use should align with the philosophy of the 3Rs [7]. The limitations of *in vivo* models gives rise to the development of *in vitro* alternatives. However, the clinical relevance of these systems should be interpreted with caution as they lack the complexity of *in vivo* physiology. Despite this, if aspects of preclinical testing can be replicated or improved upon *in vitro* before proceeding to *in vivo* then the use of some animals can be reduced.

Reviews of *in vitro* models of bone diseases such as osteoarthritis have been performed previously [163]; however, to the author's knowledge, no such summary of *in vitro* models of bone remodelling has been completed. To perform this review, a search in PubMed for “in vitro AND osteoblast AND osteoclast AND (co-culture OR co culture) AND remodelling”, limiting results to relevant original research articles written in English (last updated: 17/07/2017). The resulting papers were divided into three categories: remodelling fundamentals; which explore bone cell signalling, differentiation and matrix formation/degradation to elucidate key pathways in bone remodelling, remodelling models; which attempt to mimic the process *in vitro* as a tool for understanding physiology or drug/material testing, and disease-orientated

models; which introduce additional cells or factors (e.g. cancer cells or inflammatory molecules) to the osteoblast-osteoclast co-culture to investigate their effects on bone remodelling.

In cell culture, co-cultures of different cell types can be performed either indirectly or directly. Indirect methods include conditioned media and the use of transwell inserts. The former takes media from one cell type and adds it to another, whereas the latter uses a permeable insert to provide two culture surfaces in the same well, allowing exchange of soluble factors but no cell-cell contact between the two types. Direct methods co-culture both cell types on the same surface, be it a planar, two-dimensional (2D) tissue culture well or a three-dimensional scaffold (Fig. 2.14). Common osteoclastic and osteoblastic cell types featured in the following review are summarised in tables 2.2 and 2.3, respectively, and proteins, genes and molecules referred to throughout this review are summarised in table 2.4.

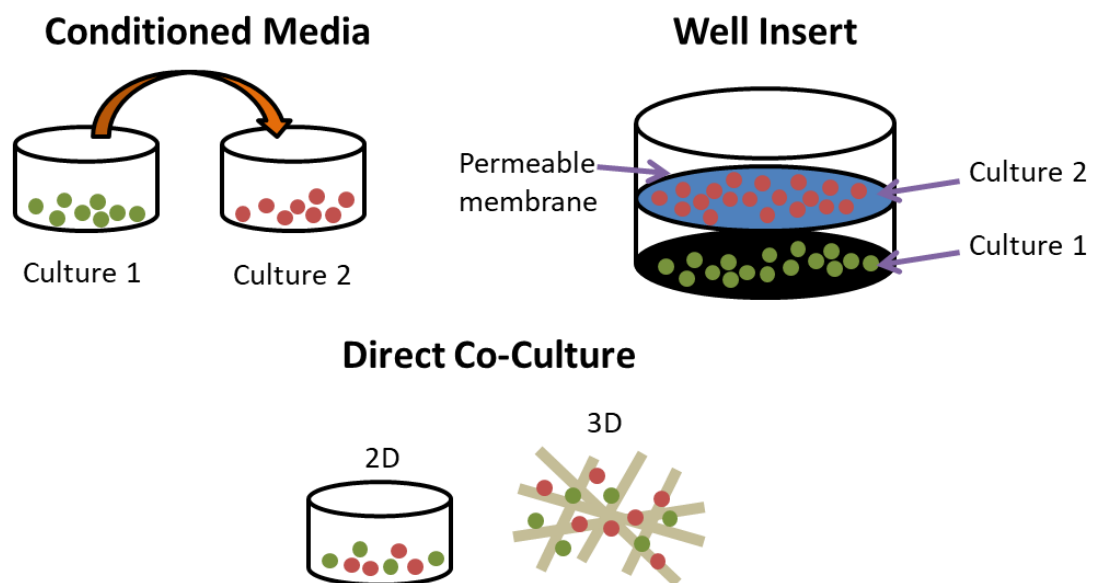


Figure 2.14: Different methods of co-culturing cells. Conditioned media transfers media used in one culture to another. Well inserts culture cells in the same well but only soluble factors can exchange between cell types. Direct co-cultures can be performed in 2D or 3D and permit membrane bound and soluble factors to exert influence.

Table 2.2: Common osteoclastic lineage cell types used in vitro.

Name	Abbreviation	Description
Human Peripheral Blood Monocyte	hPBMC	Mononuclear cells isolated from peripheral blood. Typically via density gradient centrifugation and negative selection using magnetic-activated cell sorting. Purity can be confirmed by flow cytometry using antibodies against CD14 and CD45 [164], [165]
RAW264.7 (ATCC® TIB-71™)	RAW264.7	Murine leukemic monocyte macrophage cell line that can undergo osteoclastic differentiation by RANKL exposure. A key advantage over other precursors is that they do not require co-stimulation with M-CSF [166], [167]
THP-1	THP-1	Human monocytic cell line derived from the blood of a boy with acute monocytic leukaemia [168]

Table 2.3: Common osteoblastic lineage cell types used in vitro.

Name	Abbreviation	Description
Primary Human Osteoblast	hOB	Osteoblast-like cells typically extracted from human trabecular bone fragments [169], [170]
Primary Murine Osteoblast	mOB	Osteoblast-like cells typically extracted from murine calvaria [171], [172]
SaOS-2	SaOS-2	Human osteosarcoma cell line reported to be derived from the primary osteosarcoma of an 11-year-old Caucasian female [173]
MG-63	MG-63	Human osteosarcoma cell line derived from the osteosarcoma of a 14-year Caucasian old boy [174]
Immortalised osteoblast precursors from human bone marrow stroma	hMS(2-15)	Osteoblast precursor cell line developed from human bone marrow stromal fraction [175]

ST-2	ST-2	Clone of murine stromal cells isolated from BC8 mice that develop an osteoblastic phenotype when cultured with ascorbic acid [176]
MC3T3-E1	MC3T3-E1	Spontaneously immortalised clonal osteoblast precursor cell line generated using the 3T3 passaging protocol from the calvaria of newborn C57BL/6 mice by Kodama, et al. [177]
Human periodontal ligament cells (between alveolar bone and the tooth root)	PDL	Osteoprogenitor cells of periodontal ligament connective tissue [178], [179].
MLO-Y4	MLO-Y4	Osteocyte cell line cloned from cells isolated from murine long bones [180]

Table 2.4: Common factors analysed during *in vitro* bone cultures.

Name	Abbreviation	Description
Receptor activator of nuclear factor $\kappa\beta$	RANK	Receptor for RANKL expressed on osteoclast-lineage cells [181]
Receptor activator of nuclear factor $\kappa\beta$ ligand	RANKL	Member of TNF cytokine family. Ligand for RANK receptor predominantly produced by osteoblast-lineage cells, but also by stromal and T cells [181]
Osteoprotegerin	OPG	Decoy receptor that prevents RANK activation by binding with RANKL [181]
Macrophage colony stimulating factor	M-CSF	Cytokine that influences differentiation and survival of haematopoietic precursors, produced by osteoblasts and stromal cells [47]
Alkaline phosphatase	ALP	Enzyme secreted from osteoblasts which promotes hydroxyapatite crystal formation within the bone matrix. Considered a highly specific marker of bone-forming osteoblasts [23]

Collagen type 1 alpha 1	COL-1 α 1	Protein that constitutes ~90% of the organic phase of bone [17]
Runt-related transcription factor 2	RUNX2	Key transcription factor associated with osteoblast differentiation [182]
Osterix	OSX	Transcription factor also known as Sp7 required for bone formation, works downstream of RUNX2 [183]
Osteopontin	OPN	OPN is an extracellular matrix glycoprotein. During remodelling, it anchors osteoclasts to the bone matrix [184]
Integrin binding sialoprotein/Bone sialoprotein-2	IBSP/BSP-II	Human variant of BSP, significant component of bone extracellular matrix [185]
Tartrate-resistant acid phosphatase	TRAP	Enzyme secreted by osteoclasts. Activity strongly correlates with bone resorption and TRAP knockout mice develop osteopetrosis [186]
Cathepsin K	Cathepsin K	Osteoclastic protease that catabolises bone by breaking down elastin, collagen and gelatine [187]

Matrix metalloproteinase-9	MMP-9	Osteoclastic enzyme that degrades extracellular matrix components such as collagen, fibronectin and laminin [188]
Osteoclast associated receptor	Oscar	An IgG-like receptor that is an important osteoimmunological mediator and acts as a co-stimulatory receptor for osteoclast differentiation [189]
Tumour necrosis factor alpha	TNF- α	A pro-inflammatory cytokine that can upregulate RANKL production and directly stimulate osteoclast precursor differentiation [190], [191]
Parathyroid hormone	PTH	A hormone that can indirectly stimulate osteoclastogenesis by action on osteoblasts. Depending on concentration and frequency of application, it can have a catabolic or anabolic effect [192]
1 α ,25(OH) ₂ D ₃	Vitamin D3	1 α ,25-dihydroxyvitamin D3 is the active form of vitamin D3. It has been shown to stimulate RANKL expression in osteoblasts and osteocytes [193]–[195].

2.3.2 Remodelling fundamentals

It was discovered in the 1980s that osteoblasts were producing factors that stimulate osteoclastic resorption, and *in vitro* conditioned media experiments were essential in their elucidation. For example, in the discovery of interleukin-6 and M-CSF, as well as the RANKL/RANK/OPG axis that mediates osteoclast formation and function [63], [95], [196]–[199], and that M-CSF and RANKL can be produced as either membrane bound (mM-CSF/mRANKL) and/or secreted, soluble forms (sM-CSF/sRANKL).

One of the first events in bone remodelling is an increase in osteoclastic resorption. One way osteoclasts can form is by the adhesion of osteoclast precursors to osteoblasts or bone marrow stromal cells. To investigate this mechanism *in vitro*, Tanaka, et al., investigated how the expression of intercellular adhesion molecule (ICAM)-1 mediates this process. They found that hOBs could easily be identified as ICAM-1 positive or negative, and that hPBMCs in co-culture tightly adhered to the ICAM-1⁺ cells even in the presence of anti-RANKL monoclonal antibodies, indicating that mRANKL alone is not sufficient for a high affinity adhesion. Furthermore, ICAM-1⁺ osteoblasts highly expressed RANKL and stimulated the formation of TRAP positive, multinucleated osteoclasts, indicating that it is this subgroup that is predominantly involved in osteoclastogenesis [169].

The production of sM-CSF can be upregulated in osteoblasts by the presence of TNF- α and PTH [200], [201]. Yao, et al., found that upregulation of mM-CSF is also seen in the presence of PTH and TNF- α in SaOS-2 and MG-63, respectively; however, in hOB cultures, only TNF- α resulted in an increased expression with PTH having no significant effect. Furthermore, they found that mM-CSF alone is sufficient to induce osteoclast formation, as NIH3T3 murine fibroblasts transfected to produce only mM-CSF co-cultured with murine bone marrow cells consistently formed osteoclasts [202]. However, this is inconsistent with majority of the literature concerning the role of M-CSF, where the consensus is that its role is in the proliferation and survival of osteoclast precursors. In an attempt to define the biological role played by mM-CSF, Yao, et al., generated mM-CSF knockout (KO) mice, which have increased bone mineral density (BMD) *in vivo*. The formation of osteoclasts when KO osteoblasts were co-cultured with wild type (WT) osteoclasts was reduced in comparison to WT osteoblasts, indicating that the increased BMD was due to reduced resorption [203].

The urokinase/urokinase receptor (uPAR) axis is most commonly activated in response to inflammatory, tissue remodelling, or cancerous diseases in order to regulate extracellular proteolytic cascades and activate intracellular signalling pathways [204]. Anaraki, et al., investigated whether this system was also involved in the regulation of osteoblast-osteoclast communication and osteoclastogenesis. Lentivirus-based silencing of uPAR in human mesenchymal stem cells (hMSCs) significantly reduced the expression of M-CSF mRNA and both mM-CSF and sM-CSF protein production. However, it did not affect RANKL expression. Conditioned media from uPAR silenced hMSCs and co-cultures of hMSC with hPBMCs using well inserts generated significantly fewer TRAP positive osteoclasts resulting in less resorption, indicating reduced osteoclastogenic potential with uPAR loss in osteoblasts. Using the same silencing technology on monocultures of hPBMCs and THP-1, uPAR deficient osteoclast precursors generated fewer TRAP positive osteoclasts and reduced resorptive capability. Double-deficient co-cultures reduced osteoclastogenesis even further, confirming the dual action the uPAR receptor has on bone remodelling [165].

In addition to its effect on osteoblasts, TNF- α can also affect osteoclast precursors. When applied to rat bone marrow depleted of stromal cells it can induce the formation of TRAP positive mononuclear pre-osteoclasts and upregulate cathepsin K mRNA expression. Co-culture of these pre-osteoclasts with primary rat osteoblasts on dentine resulted in the formation of significantly more multinucleated osteoclasts and greater resorption with the application of TNF- α [205].

Bone is a vascular tissue, and this blood supply is essential for bone development, remodelling and cell recruitment. In fact, human microvascular endothelial cells (HMVECs) express mRNA transcripts for RANKL and OPG. Collin-Osdoby, et al., found that unlike RANKL and OPG of osteoblast-origin, the production of these factors is not modulated by PTH and vitamin D₃, but rather by inflammatory molecules such as TNF- α in a dose-dependent manner, and that RANKL expression steadily increases over time whereas OPG peaks and then declines. RANKL protein expression on HMVECs was found to be in the form of mRANKL. It was capable of forming bone resorbing osteoclasts from hPBMCs and its action could be halted by addition of OPG. Interestingly, sections of human osteoporotic bone had higher RANKL staining on HMVECs near areas when resorbing osteoclasts were active [206]. Osteoblastic and vascular endothelial cells are not the only types capable of influencing osteoclastogenesis. Adipocytes found within bone marrow cultured with

dexamethasone have increased RANKL expression compared to untreated controls, and when co-cultured in direct contact with osteoclast precursors, treated adipocytes significantly enhanced osteoclast formation. However, when the cell types were separated using a well insert, no osteoclastogenesis was observed indicating soluble isoforms of RANKL were not being synthesised [207].

Interleukin-1 (IL-1) is a pro-inflammatory cytokine that can act on a wide variety of tissues, and can regulate bone remodelling through action on both osteoblasts and osteoclasts by stimulating RANKL expression and inducing fusion of osteoclast precursors as well as enhancing osteoclast resorptive activity. IL-1 KO mice have increased bone mass and BMD in comparison to WT due to decreased resorption, and co-cultures of their IL-1 KO bone marrow cells with either WT or KO osteoblasts resulted in significantly decreased osteoclast formation *in vitro*. Interestingly, this decrease is seen despite high levels of RANKL in the WT osteoblast / KO osteoclast co-culture, and more efficient formation is seen in KO osteoblast / WT osteoclast co-cultures which have low RANKL and high IL-1, indicating both IL-1 and RANKL are required for effective osteoclastogenesis [208].

Immune system T cells are capable of producing a range of osteoclastogenic factors, such as TNF- α , IL-6, IL-7 and RANKL, as well as molecules that inhibit osteoclast formation, such as transforming growth factor- β (TGF- β), granulocyte macrophage-colony stimulating factor (GM-CSF) and interferon- γ (IFN- γ). Co-cultures of SaOS and hPBMC generate TRAP positive multinuclear osteoclasts, but the addition of T cells completely inhibits their formation via GM-CSF and IFN- γ production. Addition of fixed T cells has no inhibitory effect, indicating that cytokines expressed by the T cells, not molecules on their surface, are necessary for this inhibition [209].

Although RANKL and OPG are produced by cells of the osteoblastic lineage, their expression varies depending on the progression of their differentiation from precursor to osteocyte. Culture of hMS(2-15) in osteogenic medium over 21 days sees an increase in ALP activity and mineralised matrix production over time. During this period, RANKL mRNA levels decrease and OPG mRNA levels increase in comparison to cultures in basal media, decreasing the RANKL:OPG ratio. Undifferentiated hMS(2-15) with a greater RANKL:OPG ratio are able to differentiate murine osteoclast precursors into TRAP positive multinucleated osteoclasts in co-culture, whilst differentiated cells could not without the further addition of exogenous sRANKL [210].

However, the ability to generate osteoclasts does not necessarily diminish as osteoblastic cells continue to differentiate. Osteoblasts that terminally differentiate into osteocytes and become embedded within the mineralised matrix of bone have the ability to modulate bone remodelling. MLO-Y4 can induce the formation and activation of osteoclasts capable of resorbing dentine in co-culture with murine spleen or marrow cells without the addition of any exogenous factors, although supplementation with vitamin D₃ enhances their production. However, conditioned media from MLO-Y4 cannot generate osteoclasts, despite producing sM-CSF. This indicates that M-CSF alone cannot induce osteoclastogenesis, and that MLO-Y4 must stimulate osteoclast formation through the mRANKL detected on their surface and dendritic processes, meaning that direct cell contact is required [211]. It is thought that osteocytes inhibit bone resorption in areas of high mechanical loading by producing signalling molecules in response to changes in fluid flow that occur within the tissue [212]. Kulkarni, et al., applied pulsatile fluid flow (PFF) to MLO-Y4, finding that this decreased their ability to induce osteoclastogenesis in murine bone marrow cells by decreasing the RANKL:OPG ratio [213]. Kim, et al., also investigated the effect of fluid flow on RANKL and OPG expression by applying oscillating fluid flow (OFF) to co-cultures of ST-2 and RAW264.7. OFF decreased the RANKL:OPG ratio by decreasing RANKL and increasing OPG mRNA expression, resulting in decreased osteoclast formation in comparison to a static control [214]. Cells can also be stimulated via direct mechanical loading. Using a transwell co-culture system where RAW264.7 were cultured on a membrane above mechanically strained MC3T3-E1, Zhang, et al., found that loading of the osteoblasts resulted in higher ALP activity and lowered osteoclast activity, as demonstrated by a decline in TRAP activity, resorption, cathepsin K and MMP-9 expression, in comparison to static controls. This was due to a decreased RANKL:OPG ratio by increased OPG expression [215].

To investigate how osteocytes may regulate osteoclast activity, Gu, et al., cultured primary rat osteoclasts on rat calvarial slices that had been stripped of the periosteum and endosteum to leave predominantly osteocytes in the samples. These were either cultured to maintain living cells or devitalised using water and sonication or freeze-thawing. Cultures on devitalised bone produced significantly more and deeper resorption pits in comparison to living bone, and conditioned media from living bone samples inhibited osteoclast resorption, indicating the live osteocytes were preventing resorption. Inducing osteocyte apoptosis via glucocorticoid application prior to osteoclast culture increased resorption in comparison to untreated calvaria [216]. The

alteration of this ratio over time may help co-ordinate the osteoblasts and osteoclasts during the remodelling cycle.

There are a wide range of factors which can modulate the RANKL:OPG ratio and therefore osteoclastogenesis and bone remodelling. Retinoids are important for normal bone growth and development. Geranylgeranoic acid (GGA), a synthetic acyclic retinoid, can promote a positive bone balance through a dual action of stimulating osteoblast differentiation and inhibition of osteoclast formation, as demonstrated by Wang, et al., who found it suppressed MC3T3-E1 proliferation whilst increasing ALP activity, reduced osteoclast formation in co-cultures of murine bone marrow cells and osteoblasts, and upregulated OPG mRNA expression in ST-2 cells after it has been chemically suppressed. Furthermore, it inhibited osteoclast formation in sRANKL and sM-CSF treated bone marrow cultures, indicating it can act on both osteoblasts and osteoclasts [217].

Hydrolysed collagens have also been shown to promote a positive bone balance *in vitro*, with 2 kDa hydrolysed collagen molecules increasing ALP activity and decreasing resorption in co-cultures of mOBs and bone marrow cells [218]. Omentin-1, an adipokine also known as intelectin-1, decreases the formation of TRAP positive, multinucleated osteoclasts in co-cultures of hOBs and hPBMCs as well as MC3T3-E1 and RAW264.7 through stimulation of OPG and inhibition of RANKL protein expression [170]. Lactoferrin is a glycoprotein that has an anabolic effect on bone by promoting osteoblast proliferation and differentiation as well as decreasing osteoclast formation [219], [220]. By coupling it to hydroxyapatite nanocrystals, Montesi, et al., showed that these two compounds can work synergistically act as a bone anabolic by increasing OSX and IBSP mRNA expression in osteoblasts, reducing osteoclast formation, and downregulating Oscar and cathepsin K mRNA expression in co-cultures of MC3T3-E1 and RAW264.7 [221].

Galectins are glycan-binding proteins that can link ECM components and cell-surface receptors. Vinik, et al., investigated how galectin-8 (GAL-8) can regulate RANKL production by co-culturing mOBs from calvaria with murine bone marrow cells and treating with GAL-8, finding that the protein stimulates a six-fold increase in RANKL mRNA expression and a 2.5-fold increase in sRANKL production whilst reducing OPG expression by 30%, resulting in a 15-fold increase in TRAP positive, multinucleated osteoclast generation. Furthermore, osteocytes extracted from the same calvaria treated with GAL-8 also had increased RANKL expression [172].

Glycosaminoglycans (GAGs) are found in the extracellular matrix (ECM) of bone and have been used in biomaterial applications to stimulate osteogenesis. Salbach-Hirsch, et al., used GAGs and sulphated-GAGs (sGAGs) to create artificial ECMs for culturing RAW264.7 in the conditioned media of mOBs generated from MSCs. They found that sGAG matrices significantly increased ALP, osteocalcin and OPG expression as well as mineralized matrix deposition. However, supernatants could not induce osteoclast formation due to the absence of sRANKL and the high level of OPG. Addition of exogenous sRANKL permitted osteoclast formation, but the lowest levels of differentiation and resorption were seen in the sGAG groups due to the increased OPG production, indicating that GAGs can have an anabolic effect on bone through action on the osteoblasts [222].

Downstream of tyrosine kinase (DOK) 3 is an adapter protein that limits tyrosine kinase-mediated signalling downstream of cell surface receptors on osteoclasts [223]. Cai, et al., found that DOK3 KO mice are osteoporotic due to an increase in TRAP positive osteoclasts. *In vitro*, osteoclasts differentiated from KO bone marrow had increased sensitivity to RANKL resulting in increased osteoclastogenesis, larger osteoclasts with more nuclei, and increased resorptive capability. Osteoblasts derived from DOK3 KO mice produce less mineralised matrix and reduced expression of Runx2, OSX, COL-1 α 1 and ALP mRNA, as well as reduced RANKL and increased OPG expression in comparison to WT. In direct co-culture, WT osteoblasts induced the formation of more osteoclasts from KO precursors than WT precursors, and KO osteoblasts induced fewer osteoclasts from KO and WT precursors than WT osteoblasts. This indicates that DOK3 promotes osteoblastogenesis and impedes osteoclastogenesis [224].

Parathyroid hormone (PTH) plays a major role in calcium and phosphate homeostasis. Continuous production of PTH, for example in hyperthyroidism, has a catabolic effect on bone, whereas intermittent application can have an anabolic result by increasing formation in both cancellous and cortical regions. Intermittent PTH increases bone formation by promoting osteoblast differentiation through activation of Wnt signalling in osteoblasts, inhibiting sclerostin in osteocytes, and stimulating the mitogen-activated protein kinase (MAPK) and phospholipase A and D pathways. This results in activation and differentiation of bone lining cells, as well as increasing osteoblast lifespan by inhibiting apoptosis. In contrast, continuous exposure to PTH inhibits the expression and synthesis of extracellular matrix proteins, such as collagen I, osteocalcin, and ALP [192], [225]. Despite this decrease in matrix formation, PTH

mediated catabolism of bone is not primarily due to decreased osteoblast function, but increased osteoclast activity. However, this is not through direct action on osteoclasts as they are not thought to have a PTH receptor. Instead, it is an indirect response to altered osteoblast function as continuous PTH increases RANKL and decreases OPG expression, increasing the RANKL:OPG ratio [226].

β -arrestin2 is an adaptor/scaffold protein that can regulate intracellular signalling initiated by the PTH-receptor. In comparisons of β -arrestin2 KO versus WT bone marrow cultures, increased osteoclastogenesis is seen in the KO phenotype due to an increased RANKL:OPG ratio [227]. Lössdorfer, et al, co cultured PDL cells with RAW 264.7 in the presence of intermittent PTH, finding that the response is dependent on the maturity of the PDL cells. When applied to co-cultures containing mature, confluent PDL cells, an upregulation of TRAP and cathepsin K expression, an increase in the RANKL:OPG ratio, and higher resorptive activity was observed. However, with less mature, pre-confluent cells, the opposite was seen, with downregulation of resorptive genes and a decrease in the RANKL:OPG ratio and amount of resorption. Similar results were seen when treating RAW 264.7 with conditioned media from the PDL cells, indicating the PDL cells can produce sRANKL and their response to PTH is dependent on cell maturity [228].

Serum is added to cell culture media as it contains a variety of proteins that help cells grow, divide and survive. However, its composition is not fully defined and therefore varies between batches [229]. This can give rise to inconsistencies in results due to the influence of unknown factors in the medium. Atkins, et al., attempted to develop a human-derived co-culture in a defined serum-free medium. They found that in serum-replete medium that supported the formation of osteoclasts from hPBMCs in co-culture with ST-2, osteoclastogenesis did not occur when the osteoblastic component was replaced with hOBs. However, when repeated in a defined, serum-free medium, co-culture of hOB with osteoclast precursors resulted in functional osteoclast formation, indicating some factor(s) may have been present in the serum that inhibited osteoclastogenesis [230].

The concentration of calcium and phosphate in the media can also affect osteoclastogenesis. Co-culture of MC3T3-E1 murine pre-osteoblasts with murine bone marrow cells on segments of bovine tooth-roots with calcium concentrations ranging from 0 to 2.5 mM resulted in increased TRAP staining and resorption with decreased calcium [231]. The same group found that as MC3T3-E1 ALP activity and

therefore extracellular inorganic phosphate increases over time there is a decrease in osteoclast formation, and that increasing concentrations of β -glycerolphosphate (β GP) and exogenous ALP in the media has a similar effect [232]. Shin, et al., also investigated the effect of extracellular calcium on osteoclastogenesis, looking at a higher range of concentrations ranging from 1.8 mM to 10 mM on co-cultures of murine calvarial osteoblasts and murine bone marrow cells. They found that osteoclastogenesis increases with extracellular calcium in a dose-dependent manner when no other osteoclastogenic factors are added. However, in the presence of exogenous vitamin D₃, sM-CSF and/or sRANKL, the opposite is seen and the number of TRAP positive, multinucleated osteoclasts decreases. This was likely due to the presence of calcium increasing the RANKL:OPG ratio by continuously upregulating RANKL expression but only transiently increasing OPG, whereas co-application of calcium and vitamin D₃ decreased the ratio by not affecting RANKL and increasing OPG expression [233].

In addition to chemical stimulus, environmental factors can also mediate osteoclastogenesis. Dandajena, et al., indirectly co-cultured hOBs from calvaria with hPBMCs using well inserts in either normoxic (21% O₂) or hypoxic (2.5% O₂) conditions, finding that low oxygen significantly upregulated RANKL production in comparison to normoxia, and that TRAP positive, resorptive osteoclasts only formed in hypoxic co-cultures [234].

Although the relationship between osteoblasts and osteoclasts is perhaps often considered to be one-sided, with the former producing factors that modulate the latter's behaviour, there is evidence that osteoclasts can also effect osteoblasts. Garimella, et al., co-cultured primary murine calvarial osteoblasts with murine bone marrow cells in order to generate TRAP positive, multinucleated osteoclasts. Using *in situ* hybridisation and immunohistochemistry, they were able to detect bone morphogenetic protein (BMP) -2, -4, and -6 mRNA and protein, respectively, within the osteoclasts. Reverse transcriptase-polymerase chain reaction (RT-PCR) confirmed that the osteoclasts could synthesise mRNAs for BMP-2, -4, -6, and -7, with BMP-6 having the highest expression [235]. Osteoclastic BMPs are possibly involved in the initiation of the anabolic phase of bone remodelling, recruiting and activating osteoprogenitor cells [236]. Further evidence for the influence of osteoclasts on osteoblasts comes from Luo, et al., who also co-cultured primary murine calvarial osteoblasts with murine bone marrow cells, albeit in a transwell configuration resulting in no direct osteoblast-osteoclast contact. Their findings demonstrated

greater ALP staining and activity in osteoblasts co-cultured with osteoclasts in comparison to monocultures. Furthermore, the osteogenesis related genes RUNX2, ALP and COL-1 α 1mRNA expression were all upregulated in the co-culture, indicating the anabolic role osteoclasts can have on osteoblasts [237].

A summary of the factors that can influence bone remodelling is given in figure 2.15.

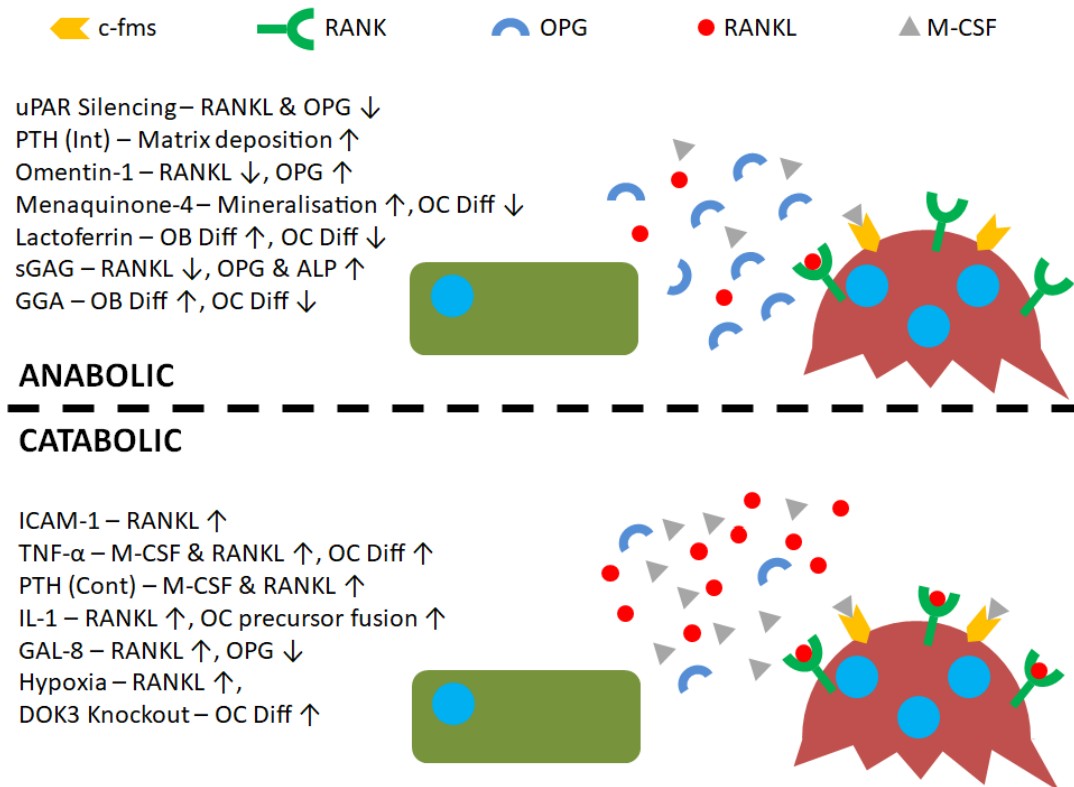


Figure 2.15: Schematic summarising the effects of different factors on bone balance. Factors that result in a positive bone balance shown on top, negative bone balance below. Legend: Osteoblast (OB) Osteoclast (OC) Differentiation (Diff) Intermittent (Int) Continuous (Cont).

2.3.3 Remodelling models

The majority of the work done on the fundamentals of bone remodelling *in vitro* has been performed through the use of either conditioned media experiments, indirect co-culture using well inserts that keep the osteoblasts and osteoclasts separate, or in direct 2D co-culture, where osteoclasts are plated onto a monolayer of osteoblasts grown on tissue culture plastic. Whilst these studies have revealed a plethora of factors and molecules involved on bone remodelling, they fail to replicate the 3D architecture of native bone tissue. This results in differences in cell morphology, polarity and receptor expression, as well as a lack of diffusion gradients and unrepresentative substrate stiffness that in combination fail to represent the *in vivo* condition [238]. Therefore, to produce a viable model of bone remodelling *in vitro*, the co-culture should be performed in three dimensions. The development of the field of bone tissue engineering has resulted in a multitude of polymer, ceramic and metal scaffolds being produced that support the formation of mineralised extracellular matrix [239], [240]. These studies primarily focus on the action of osteoblasts, but can be adapted to create *in vitro* models of bone remodelling.

Nakagawa, et al., appear to be the first to attempt to co-culture osteoblasts and osteoclasts in a scaffold *in vitro*. Collagen-coated porous PLGA scaffolds were precultured with porcine osteoblasts (pOBs) for two weeks before the addition of porcine osteoclast precursors and a further two weeks of culture in a rotational bioreactor. At the end of the culture, mature osteoclasts with ruffled borders and actin rings were visible on top of the mineralised surface synthesised by the osteoblasts, showing for the first time that studying remodelling *in vitro* is a realistic ambition [241].

Domaschke, et al., were the first to demonstrate remodelling *in vitro* and recognise its potential to reduce the need for animal studies. hPBMCs were cultured on mineralised collagen tapes containing hydroxyapatite for 24 hours before the addition of ST-2 and cultured in media supplemented with exogenous RANKL and M-CSF. Osteoclasts generated were able to resorb the scaffold-substrate and osteoblasts were able to deposit new mineralised matrix, a key element that distinguishes remodelling from resorption [164]. Further work by Bernhardt, et al., utilised the same substrate but replaced the murine ST-2 cells with primary hMSCs. However, here osteoblasts were seeded on one set of scaffolds and monocytes on another, keeping them separate from one another using well inserts. Osteoblasts proliferated at a faster rate and ALP mRNA

expression was higher in co-culture than monoculture. TRAP activity was lower on scaffolds and osteoclasts were smaller in size in the co-culture in comparison to monocyte monocultures, although there was no difference in cathepsin K and TRAP mRNA expression. Interestingly, across multiple donors, MSCs underwent less adipogenic differentiation in co-culture than in monoculture, as evidenced by fatty acid binding protein 4 expression and Oil Red O staining [242]. This indicates that without direct contact, the presence of osteoblasts can have an inhibitory effect on osteoclasts, perhaps via the increase in extracellular phosphate in the media as seen by Takeyama, et al. [232]. Furthermore, the presence of osteoclasts in indirect co-culture upregulated the proliferation and ALP activity of osteoblasts and inhibited adipogenesis, which agrees with the finding of Luo, et al. [237].

Following the initial work of Domaschke, Tortelli, et al., developed an *in vitro* remodelling model using primary murine cells. They used Skelite®, a commercial bone graft substitute, formed into discs to create a porous ceramic substrate and compared it to tissue culture plastic (TCP) using co-cultures that were seeded in a 1:1 ratio of calvarial mOBs and osteoclast precursors from murine bone marrow. These cultures were maintained for 30 or 60 days, 2-4 times longer than Domaschke, without exogenous RANKL or M-CSF before analysis. Mature, TRAP positive, multinucleated osteoclasts and deposited, mineralised extracellular matrix were detectable after 60 days in 2D and 3D, with a more organised bone-like matrix deposited in 3D. Runx2, OSX and osteocalcin expression were analysed as markers of early, middle, and late osteoblast maturation, and cathepsin K and TRAP expression as markers of osteoclast differentiation. 3D cultures reached a maximal expression of Runx2 and OSX within ten days, whereas 2D cultures took 40, and osteocalcin expression was 19-fold higher in 3D by day 40, indicating osteogenesis started immediately in 3D but was delayed in 2D, and that osteoblasts fully differentiated in 3D. Cathepsin K, TRAP and RANKL expression were significantly higher in 2D than 3D, whereas OPG expression was lower [171]. These results combine to imply that osteoblasts in the earlier stages of osteoblastic differentiation have higher osteoclastogenic potential than more mature osteoblasts due to an increased RANKL:OPG ratio, and that 2D culture retains osteoblasts in an earlier phenotype due to a lack of physical stimuli, which agrees with the findings on Gori, et al., [210].

Although bone turnover at various time points can be analysed by histology, PCR and enzyme activity, it is difficult to determine exactly how a scaffold has been resorbed and remodelled by the cells, and it is impossible to see how bone tissue volume on the

same scaffold changes over time due to the destructive nature of these techniques. Ruggiu, et al., repeated the same co-culture as Tortelli, et al., on the same substrate but in addition to histological techniques, examined the scaffold before and after culture by synchrotron MicroCT to enable image registration. In comparison to mOB monocultures, co-cultures formed a more organised bone tissue with clear segregation between mineralised ECM and non-mineralised osteoid. Using MicroCT, increased mineralised and non-mineralised matrix deposition was seen in co-cultures, as well as scaffold degradation due to osteoclast activity which was not visible in mOB monocultures [243].

The use of MicroCT as a non-invasive imaging technique to monitor bone remodelling *in vitro* has also been utilised by Rubert, et al., who co-cultured hMSCs and hPBMCs on previously mineralised and decellularised bone-like tissues in a spinner flask for up to 35 days in media supplemented with RANKL and M-CSF. By evaluating dynamic morphometric parameters using sequential MicroCT scans, co-cultures had a significantly decreased mineralising surface and almost 200% increase in bone resorption rate in comparison to hMSC mono-cultures. By registering images over time, regions of clear bone resorption and formation could be seen in the co-culture [244].

In addition to improving our understanding of the remodelling process, *in vitro* systems can also inform us how potential bone tissue engineering scaffolds will degrade and be remodelled *in vivo* prior to animal testing. Jones, et al., co-cultured MC3T3-E1 and primary mOC precursors on vapour or methanol stabilised silk fibroin, chitosan and poly(lactic acid) (PLLA) films to determine their suitability for bone tissue engineering. Cultures were seeded at a 1:100 (OB:OC) ratio and maintained in media containing exogenous RANKL for ten days. Silk and chitosan films supported the formation of greater numbers of TRAP positive osteoclasts in comparison to PLLA, and by comparing surface roughness using atomic force microscopy (AFM), the most resorption occurred on vapour stabilised silk films. This indicates their potential for remodelling studies and use in bone tissue engineering [245].

Hayden, et al., also utilised silk-based substrates in multiple studies attempting to develop an *in vitro* bone remodelling model. Initially, they used lentiviral transduction to tether ligands known to alter bone metabolism to hMSCs differentiated into hOBs; either PTH or glucose-dependent insulinotropic peptide (GIP). Green fluorescent protein (GFP) was used as a control.

Tethered osteoblasts were co-cultured with THP-1 in media with exogenous RANKL on silk films, porous silk sponges, or TCP for up to 5 weeks before surface roughness and calcium deposition quantification was performed to analyse resorption and matrix deposition. Tethering of PTH increased mineral deposition in comparison to the GFP control in the TCP co-culture. This was possibly due to the feedback mechanism of osteoclasts to osteoblasts as their activity is raised. Increased surface roughness was seen on silk films with PTH-tethered co-cultures due to the production of larger mineral deposits, whilst GIP-tethered co-cultures decreased roughness, as GIP lowers osteoclast activity and as a result osteoclastic stimulation of matrix deposition by osteoblasts. Similar surface roughness trends were seen in the 3D sponges, but due to their more complex architecture it was harder to quantify [246].

Following this, Hayden, et al., extended the duration of the co-culture with regular hMSCs and THP-1 and exogenous RANKL on the silk films to up to 32 weeks to characterise long term bone remodelling on the substrate. Films were characterised by SEM and MicroCT imaging prior to seeding. Mineralisation in co-culture in comparison to monoculture was continuous over the surface of the film, rather than in discrete patches. They also had higher surface roughness indicating more remodelling, as well as an increase in volume as quantified by MicroCT [247]. Finally, they looked to apply their *in vitro* model to a metabolic bone disease by investigating the effect of two bisphosphonates, a common therapeutic for patients with osteoporosis. Here the silk films were incorporated with hydroxyapatite and loaded with either clodronate or alendronate before co-culture of hMSCs and THP-1 with exogenous RANKL for up to 12 weeks. They identified concentrations of clodronate that could upregulate osteoblast ALP activity whilst diminishing osteoclast activity, a combination alendronate could not achieve [248]. Whilst this *in vitro* system can be used to evaluate potential osteoporosis therapeutics, it is a model of bone remodelling, not osteoporosis.

Heinemann, et al., also developed an *in vitro* biomaterial testing system that utilised an all-human origin, direct contact, co-culture that compared TCP with a silica-collagen-hydroxyapatite xerogel. hMSCs were first cultured for 13 days before the addition of hPBMCs and a further culture of up to 4 weeks without exogenous RANKL or M-CSF. Differentiation of MSCs into osteoblasts was confirmed by ALP activity. RANKL was synthesised as evidenced by RANKL mRNA expression and TRAP activity of the differentiated osteoclasts, which were also able to upregulate BSP-II gene expression in osteoblasts. In 3D, MSCs proliferated and differentiated,

forming layers of cells that covered the entire sample which had spherical, multinucleated osteoclasts with actin rings embedded within [249].

A further *in vitro* bone model that only used human-origin cells co-cultured in direct contact was developed by Papadimitropoulos, et al. However, in contrast to Heinemann, they used human adipose tissue-derived stromal vascular fraction (SVF) cells that can commit to osteoblastic and endothelial lineages. These were co-cultured with hPBMCs on porous hydroxyapatite/ β -tricalcium phosphate ceramic scaffolds in a perfusion bioreactor, with the SVF cells cultured for 5 days before the addition of the monocytes and the culture then maintained for 21 days in media supplemented with exogenous RANKL and M-CSF. After 21 days, osteoblastic, osteoclastic and endothelial cells were identifiable in the culture, with TRAP positive osteoclasts adhered to the deposited ECM. Culture supernatants were analysed to assess bone turnover, confirming matrix deposition by the presence of C-terminus procollagen-I, and resorption by the presence of N-telopeptides of collagen type-I, changing phosphate levels and TRAP activity. When replacing exogenous supplementation of RANKL and M-CSF with Vitamin D₃ co-cultures still underwent osteoclastogenesis, resulting in self-regulation of the model [250].

Although scaffolds provide a 3D environment and physical cues for cells, the natural and synthetic materials used to fabricate them are foreign to natural bone tissue and may obstruct the investigation of the actual sequence of cellular events that occurs *in vivo* during bone remodelling. This interference is greater if the scaffolds incorporate bioactive factors like BMPs. Therefore, Clarke, et al., attempted to create a scaffold-free three-dimensional *in vitro* bone model by forming tissue aggregates in a rotational bioreactor. Tissue constructs were formed by culturing hOBs and hPBMCs at a 2:1 ratio in media supplemented with exogenous RANKL and M-CSF with the rotational speed varied to alter initial aggregate size and keep the aggregate in free-fall for up to 21 days. Mineralised, solid to the touch, aggregates up to 4 mm in diameter could be formed after 3 weeks. These contained a mineralised core with structures that resemble trabeculae which contained embedded cells that express sclerostin, indicating they may have become osteocytic. Surrounding the core a morphologically different perimeter that contained active osteoblasts and osteoclasts expressing osteocalcin and TRAP, respectively, was apparent that appeared to have resorption pits. BMP-2, -4, and -7 expression was also detectable [251]. A clear advantage of this *in vitro* model is the potential presence of the three main cell types; osteoblasts, osteocytes and

osteoclasts. However, it relies on exogenous supplementation to induce osteoclastogenesis rather than these factors being inherently produced.

Penolazzi, et al., also utilised a rotational bioreactor in their *in vitro* remodelling system to simulate the jawbone microenvironment in the study of osteonecrosis of the jaw (ONJ), a very rare side effect associated with bisphosphonate therapy. They extracted hOBs from either healthy donors or patients undergoing treatment for ONJ and co-cultured them with hPBMCs either indirectly or directly without exogenous RANKL and M-CSF. Indirect cultures were performed using well inserts. Direct co-cultures were either static or dynamic. Direct-static cultures were performed by generating spheroids of hOBs and hPBMCs in a 1:2 ratio on agarose-coated well plates. Direct-dynamic aggregates were formed in a rotational bioreactor at the same ratio. The indirect co-culture was capable of generating multinucleated, TRAP and cathepsin K positive osteoclasts, indicating the production of sRANKL. Static and dynamic direct cultures had no difference in cell viability. As with Clarke, et al., aggregates within the rotational reactor had a much more defined, better organised structure with three distinct regions. Osteoblast markers osteopontin (OPN), OSX, Runx2 and calcium staining by alizarin red S (ARS) were all higher in the dynamic culture, as were osteoclast markers TRAP and cathepsin K. Osteoblasts from ONJ patients were lower in quality but still able to form mineralising, TRAP positive aggregates [252].

The same group used this rotational bioreactor system to explore the effect of menaquinone-4 (MK-4), a member of the vitamin K2 family that can regulate calcium homeostasis and may have an anabolic effect on bone formation. Human amniotic fluid MSCs (hAFMSCs) were co-cultured with hPBMCs in a 2:1 ratio without exogenous RANKL and M-CSF. In conventional 2D and dynamic 3D monocultures of hAFMSCs, 10 μ M of MK-4 significantly increased mineralisation, as well as ALP, RUNX2, osteocalcin, COL-1 α 1 and OPN mRNA expression without affecting cell viability. In dynamic 3D co-culture, hAFMSCs supported osteoclastogenesis without exogenous factors, again in the outer perimeter of the aggregate. In the presence of MK-4, there were significantly fewer TRAP positive osteoclasts formed and a significant increase in mineralised matrix deposition [253].

Young, et al., explored how the surface features of the substrate can influence bone remodelling *in vitro* by performing co-cultures on a polycarbonate surface either with or without their previously developed 'NSQ50' nanotopography shown to increase

osteoblast differentiation. Human bone marrow was aspirated and separated into BM-MSCs and BM-haematopoietic cells (BMHCs). BM-MSCs were cultured on the substrates for one week before the addition of BMHCs, and then cultures were maintained for a further three weeks with no exogenous osteoclastogenic supplements. After 21 days, large, TRAP positive, multinucleate osteoclasts with actin rings were visible on both substrates, as well as smaller TRAP positive mononuclear macrophages. There were no significant differences in osteoclastogenesis between planar and NSQ50 substrates, as quantified by microscopy and TRAP, OSCAR and cathepsin K mRNA expression. However, the patterned substrates stimulated increased bone mineral deposition over the planar surfaces as demonstrated by alizarin red s and osteopontin staining. RANKL, OPG and IL-6 expression were significantly increased on the NSQ50 surfaces but by equal amounts, maintaining the RANKL:OPG ratio [254]. Increasing osteoblast activity and mineral production without a subsequent increase in osteoclast activity suggests that certain nanotopographies can be selectively bioactive, influencing only one cell type. Furthermore, this work has potential applications in implant osseointegration and biomaterials that can stimulate bone restoration in patients with osteoporosis.

Healthy bone remodelling requires a delicate balance between formation and resorption by BMUs. These are comprised of osteoblasts and osteoclasts, but also a blood supply which is essential for delivery of nutrients, precursors and waste removal. However, due to the complexity of replicating angiogenesis *in vitro*, this aspect of bone remodelling is often overlooked. We know that the microvascular cells at sites of bone turnover can influence osteoclastogenesis, and therefore including vascularisation is essential in the attempt to mimic bone remodelling *in vitro* [206]. To address this, Bongio, et al., tetra-cultured human umbilical vein endothelial cells (HUVECs), BM-MSCs, BM-MSCs differentiated into hOBs, and hPBMCs within collagen/fibrin hydrogels incorporated with calcium phosphate nanoparticles in media supplemented with exogenous RANKL and M-CSF. Formation of microvessels was confirmed in hydrogels in co-cultures of HUVECs and BM-MSCs. Monocultures of osteoblasts expressed increased proliferation, ALP activity and mineralisation over time, and monocultures of osteoclasts became TRAP positive and were able to resorb the matrix, releasing phosphate into the media. Comparing vascularisation in HUVEC-BM-MSC co-cultures versus the tetra-culture, the presence of osteoblasts and osteoclasts appeared to diminish overall hydrogel vascularisation, with fewer but longer microvessels in the network. BM-MSC cells appeared to differentiate into mural cells to support the vascular network. Comparing osteoblast/osteoclast co-

cultures to the tetra-culture, the latter increased osteoblast and osteoclast differentiation over co-cultures, as indicated by ALP and TRAP activity and phosphate release [255]. The presence of MSCs and HUVECs within the culture positively influenced osteogenic and osteoclastic differentiation, with all four cell types synergistically influencing each other.

2.3.4 Pathological models

Simpler, two-dimensional co-cultures of osteoblasts and osteoclasts can help us elucidate factors that regulate the remodelling process, and by moving to more physiologically relevant three-dimensional systems we have seen the creation of increasingly complex *in vitro* models of the entire process. These will become invaluable in understanding how this intricate process occurs as well as evaluating potential new therapeutics and implants. However, they also have the capacity to be adapted to study various pathologies, including cancer, osteoporosis, dental disorders and implant rejection.

Multiple myeloma (MM) is a type of cancer characterised by accumulation of plasma cells in the bone marrow and formation of osteolytic lesions due to increased osteoclast activity and reduced osteoblast activity [256]. Bone remodelling compartments (BRCs) typically separate the BMU from the bone marrow to regulate the microenvironment and tightly control osteoblast-osteoclast coupling, ensuring balanced remodelling [55]. However, in biopsies from patients with MM, there are areas of uncoupled and therefore excessive resorption, which eventually results in the formation of osteolytic lesions. These lesions have compromised BRCs which permit the passage of MM cells. Uncompromised areas had normal bone remodelling as the BRCs acted as a barrier to the cancerous cells [54]. To elucidate whether the formation of these lesions was indeed due to compromised BRCs, Anderson, et al., attempted to create an *in vitro* model of the scenario. They utilised a confluent G₀-arrested monolayer of MC3T3-E1 to simulate the BRC. Direct contact with OPM2 MM cells decreased the surface area covered by the MC3T3-E1, whereas indirect co-culture using a well insert had no effect. Conversely, direct co-culture with hPBMC-derived osteoclasts increased the area covered [257]. This indicates that MM cells may be able to disrupt the BRC in direct cell contact.

Prostate cancer (PCa) is one of the most common cancers and has a high mortality rate due to the development of hematogenous metastases. Approximately 90% of these

occur within bone, with 85-100% of patients who die from prostate cancer having bone metastases [258]–[260]. In order to better understand how PCa cells interact with the tissue, Nordstrand, et al., developed an *in vitro* co-culture model where monolayers of either PC-3, an osteolytic human PCa cell line, or LNCaP, a human PCa cell line with a mixed/osteoblastic phenotype, were cultivated beneath a freshly harvested murine calvarial bone that still contained osteoblasts and osteoclasts. PC-3 upregulated cathepsin K, TRAP, MMP-9 and RANKL mRNA expression whilst inhibiting OPG, ALP and osteocalcin expression, causing a negative bone balance by increasing the RANKL:OPG ratio and decreasing osteoblast activity. In contrast to the osteolytic activity of PC-3, LNCaP increased ALP and osteocalcin expression and had no significant effect on the RANKL:OPG ratio in comparison to control calvarial cultures, indicating a small shift towards a positive bone balance [261]. By utilising *ex vivo* tissue in the co-culture the natural heterogeneity of the cell population in the bone tissue was maintained, allowing for an *in vitro* model that can study the interaction between PCa cells and bone to be produced. Lil, et al., also utilised PC-3 and C4-2B, a subline of LNCaP, to examine how PCa metastases influence bone remodelling. In both cell lines, TGF- β increased RANKL expression and RAW264.7 differentiation, indicating PCa cells can induce osteoclastogenesis [262].

Breast cancer (BCa) is another very common cancer that regularly metastasises to bone. These metastases cause a negative bone balance by increasing osteoclast activity. This releases cytokines and growth factors from the resorbed bone, which in turn stimulates cancer cell proliferation, further exacerbating the resorption. This vicious cycle results in significant bone loss, pain and morbidity [263], [264]. To investigate this, Krishnan, et al., introduced metastatic breast cancer cells to an *in vitro* bone remodelling model. Using a bioreactor they developed for long-term (<10 months) osteoblast culture, they maintained MC3T3-E1 for 60 days before the addition of pre-osteoclasts harvested from murine bone marrow [265]. MDA-MB-231-GFP BCa cells were added to the co-culture after a further ten days. Cultures were maintained in media containing exogenous RANKL and M-CSF. After 60 days, the MC3T3-E1 had created and become embedded in a thick, collagenous ECM. After a further 21 days of osteoclast culture, multinucleated, TRAP positive osteoclasts that resorbed the ECM and formed pits were visible. Subsequent addition of new MC3T3-E1 resulted in the refilling of the resorbed areas, completing the remodelling process. After the initial 60 days, the ECM was 20 μm thick. This was reduced to 16.5 μm by the addition of osteoclasts and 14.5 μm by osteoclasts and BCa cells. The metastatic cells penetrated the ECM and formed osteoclast-BCa aggregates, as well as increasing

osteoclastogenesis and downregulating osteoblast differentiation in comparison to co-cultures [266], [267]. This model without the BCa cells includes the major processes of remodelling, albeit requiring the addition of new osteoblast pre-cursors, and provides a way of studying the process over long time periods. The addition of BCa cells provides a simplified platform for the study of how the major cellular constituents of breast cancer metastases interact.

The cannabinoid type 2 (CB2) receptor has been implicated with regulating tumour growth and bone remodelling. By agonising this receptor with JWH133 or HU308, Sophocleous, et al., determined that the growth of three BCa cell lines could be inhibited, but that the agonists have no effect on the proliferation of murine calvarial osteoblasts or bone marrow-derived osteoclasts. In co-cultures of the bone cells, conditioned media from the cancer cells upregulated osteoclastogenesis in comparison to untreated controls; however, treatment with the CB2 agonists further increased osteoclast formation by increasing the RANKL:OPG ratio. Treatment of osteoclast monocultures with the agonists and conditioned media increased osteoclast formation, TRAP and cathepsin K expression and resorption in comparison to conditioned media alone [268]. These findings indicate that although CB-2 activation has been shown to suppress cancer cell proliferation and tumour growth at certain concentrations, ones lower than this enhanced osteolysis in this study. Therefore CB-2 inhibition may protect the skeleton in cases of BCa metastases [269].

Trichostatin A (TSA) is an antibiotic that acts as an inhibitor of histone deacetylase enzymes that regulate chromatin remodelling and transcription activity, rendering it a potent anticancer drug. In co-cultures of primary calvarial mOBs and red blood cell (RBC) free murine bone marrow cells, 10 nM TSA significantly reduced osteoclast formation but it did not alter the RANKL:OPG ratio. Instead, it acts directly on osteoclast precursors by downregulating c-fos, a transcription factor essential in osteoclastogenesis. *In vivo*, they found TSA can mitigate IL-1 induced bone loss, indicating this drug may also have potential in reducing inflammatory bone loss [270].

Osteoporosis is the most common metabolic bone disorder, but as it stands there is no *in vitro* model of the disorder that can be used for the study of the disease. Despite this, *in vitro* models of remodelling can be used to study potential new anabolic therapeutics. Icariin is a flavonoid in *Herba epimedii* that can stimulate bone formation and inhibit osteoclastogenesis [271]. Liu, et al., investigated whether it can have a synchronised dual effect on osteoblasts and osteoclasts by performing a direct co-

culture of murine BM-MSCs and RAW264.7 with exogenous RANKL and M-CSF, and indirectly culturing this with ovarian follicular granulosa cells (GC) in a well insert above. Co-cultures had increased ALP staining in comparison to mOB mono-cultures, indicating osteoclastic upregulation of osteoblasts. This was further increased when GC cells were present, and the co-culture increased the estradiol production of the GC cells. There was no increase in TRAP positive osteoclast formation in co-culture over osteoclast monoculture. Icariin was compared to common osteoporosis drugs to evaluate its efficacy. In co-culture, alendronate reduced both TRAP and ALP activity and PTH increased both TRAP and ALP activity. However, Icariin decreased TRAP and increased ALP activity, indicating its potential as an anabolic therapeutic for osteoporosis. A similar effect was seen when substituting RAW264.7 for murine peripheral blood monocytes [272].

Semaphorins are a class of membrane-bound or secreted proteins involved in osteoclast-osteoblast communication. Osteoclast-derived semaphorin 4D (sema4D) binds to its receptor Plexin-B1 on osteoblasts, inhibiting bone formation [273]. Therefore, it has the capability to regulate bone turnover, and overexpression of sema4D is observed in osteoporosis. Zhang, et al., utilised siRNA to interfere with sema4D and create a targeted drug delivery system. By applying the siRNA to co-cultures of mOBs with bone-marrow derived osteoclast precursors, they found that application of the siRNA does not influence osteoclast number or function, but ALP, COL-1 α 1 and osteocalcin mRNA expression and mineralised matrix formation are increased in silenced cultures. When used *in vivo* in OVX mice, regular administration of the siRNA significantly increased the number of active osteoblasts and total bone volume, indicating sema4D silencing as a potential therapeutic option for osteoporotic patients [274].

Remodelling models have also been used to study dental disorders. Cleidocranial dysplasia (CCD) is a congenital disorder that affects bone and tooth development due to mutations in the RUNX2 gene. For a tooth to erupt a path has to be cleared through the bone above via resorption. Eruption is delayed in patients with CCD, therefore Lossdörfer, et al., investigated whether this was due to PDL cells from CCD patients having reduced capability to induce osteoclastogenesis. Human PDL cells from healthy of CCD patients were co-cultured with RAW264.7 in a 1:1 ratio. Vitamin D₃ increased the RANKL:OPG ratio in both healthy and diseased PDL cells. Conditioned media from healthy PDL cells produced significantly more TRAP positive, multinucleated osteoclasts. In direct co-culture, PDL cells from CCD patients reduced

TRAP and cathepsin K expression in comparison to healthy PDL cells [275]. Yan, et al., also investigated the delayed eruption of teeth in CCD by co-culturing primary human dental pulp cells (DPCs) from healthy or CCD patients with hPBMCs. ALP expression and formation of mineralised nodules was reduced in CCD DPCs. In co-culture, TRAP, cathepsin K and MMP-9 expression were all reduced in comparison to healthy DPCs due to a 92% decrease in the RANKL:OPG ratio [276]. The findings of Wang, et al., agree with both these studies. They co-cultured healthy or CCD patient dental follicle cells (DFCs) with hPBMCs, finding that diseased cells had a reduced capability to induce osteoclast formation through a reduction in the RANKL:OPG ratio. However, vitamin D₃ was only able to increase the RANKL:OPG ratio in DFCs from healthy donors as its stimulation of RANKL production is mediated principally by a RUNX2 dependant pathway [277]. These data combine to indicate that the primary teeth retention associated with CCD may be due to a reduced capacity of osteoblast-like dental cells to induce osteoclastogenesis and create a path for teeth to emerge through.

In vitro models of bone remodelling can also be used to predict how successfully implants will integrate into the bone tissue. Osteolysis can occur at the bone-cement interface resulting in loosening of the implant. Granchi, et al., found that PMMA bone cements increase the RANKL:OPG ratio in MG-63 [278]. This could increase osteoclastogenesis and exacerbate implant loosening. Calcitonin gene-related peptide (CGRP) is thought to have an inhibitory effect on the inflammation induced osteolysis that occurs around implants. Jablonski, et al., examined this by co-culturing MG-63 with THP-1 without exogenous RANKL or M-CSF, aggravating the cultures with either ultra-high molecular weight polyethylene (UHMWPE) particles or bacterial lipopolysaccharides (LPS), then treating with CGRP. Both UHMWPE particles and LPS induce an inflammatory response by the THP-1 cells in the co-culture as indicated by the release of TNF- α . This response could be suppressed by the addition of CGRP. Interestingly, UHMWPE and LPS had no significant effect on the RANKL:OPG ratio or ALP activity [279]. This indicates that onset of inflammatory periprosthetic osteolysis is due to actions on osteoclastogenesis rather than osteoblast activity.

Wu, et al., examined how magnesium based implants influence bone turnover by co-culturing the human MSC cell line SCP-1 which had been differentiated into osteoblasts with hPBMCs and exposing them to varied concentrations of magnesium with no exogenous RANKL or M-CSF. The highest magnesium concentrations were toxic to hPBMC mono-cultures, but the presence of osteoblasts at the same

concentration played a protective role. High magnesium concentrations increased osteoblast proliferation, ALP activity and mineralisation whilst decreasing osteoclastogenesis [280]. This dual action on osteoblasts and osteoclasts highlights why *in vitro* assessment of potential implant materials should be performed using co-cultures of osteoblasts and osteoclasts, not just osteoblast monocultures, as they are more representative of *in vivo* physiology.

2.4 Summary

Postmenopausal osteoporosis is a skeletal disorder caused by a decline in oestrogen that results in increased bone resorption. This occurs due to an increase in osteoclast activity and lifespan. To date, the progression of osteoporosis and potential new therapeutics for the disease have been predominantly studied in animals. Bone tissue engineering aims to combine the culture of osteoblasts with three-dimensional substrates to create a bone graft substitute that results in the restoration of the original tissue. Work in this area can be combined with the culture of osteoclasts to create an *in vitro* model of bone remodelling. Whilst this has been attempted for normal, healthy bone remodelling, an attempt to utilise this to study postmenopausal osteoporosis has not yet been performed. However, there have been studies into the response of various osteoblastic and osteoclastic cell lines to oestrogen. Development of such a model would reduce the reliance on animal models during drug development by providing a cheaper and more ethical approach.

2.5 Project aims and objectives

The main aim of the work presented in this thesis was to determine to what extent an *in vitro* model of postmenopausal osteoporosis could be developed by utilising the principles of bone tissue engineering. This contributes to the long-term goal of reducing our reliance on rodent models for musculoskeletal research, as a human-based *in vitro* model of postmenopausal osteoporosis has the potential to generate more relevant data through the use of human cells, as well as being cheaper and more ethical than the use of OVX animal models.

To achieve this aim, the project was divided into the following objectives:

1. Determine the response of various bone cell lines to oestrogen.
 - a. Compare various osteoblast cell lines and their response to oestrogen, considering its effect on viability and mineral deposition.
 - b. Investigate the response of RAW264.7 osteoclast precursors to oestrogen, considering its effect on viability and resorption.
 - c. Select the most appropriate cell lines for the model based on the previously stated criteria.
2. Select a suitable substrate for an *in vitro* model of osteoporosis.
 - a. Confirm the amenability of a novel, emulsion templated scaffold to bone tissue engineering.
 - b. Compare it to at least two other bone tissue engineering scaffolds, considering cell viability, bone-matrix deposition, fabrication method, reproducibility and cost.
 - c. Select the most appropriate substrate for the *in vitro* model based on the previously stated criteria.
3. Evaluate the feasibility of a tissue engineered *in vitro* model of osteoporosis.
 - a. Confirm applicable markers of osteoblast and osteoclast activity in co-culture.
 - b. Utilise the findings of the previous two objectives to develop a two-dimensional and three-dimensional co-culture of osteoblasts and osteoclasts.
 - c. Evaluate the response of the co-culture to oestrogen exposure and subsequent withdrawal to mimic postmenopausal osteoporosis.
 - d. Apply common therapeutics for osteoporosis to the model and compare the effects to those seen *in vivo*.

3. Materials and Methods

This section contains the materials and methods necessary for the protocols common to the following chapters. Specific protocols relevant to only one section can be found in the respective chapter.

3.1 Materials

All reagents were purchased from Sigma-Aldrich (UK) unless otherwise stated. Tissue culture plastic was obtained from Thermo Fisher Scientific (UK).

3.2 Methods

3.2.1 Osteoblast cell lines

Three different murine osteoblast cell lines were used in this thesis: MC3T3-E1 subclone 4 (kindly donated by Dr. Peter Grabowski, University of Sheffield), IDG-SW3 (purchased from Kerfast, USA) and MLOA5.

MLOA5 were all originally from the laboratory of Dr Lynda Bonewald (University of Missouri) but were sourced from different locations:

- MLOA5-S: kindly donated by Dr. Lynda Bonewald, University of Missouri
- MLOA5-K: kindly donated by Prof. Alicia El Haj, University of Keele
- MLOA5-A: purchased from Kerfast, USA

MC3T3-E1 subclone 4 are derived from the clonal osteogenic cell line MC3T3-E1, which is a spontaneously immortalised osteoblast precursor cell line generated using the 3T3 passaging protocol from the calvaria of newborn C57BL/6 mice by Kodama, et al. [177]. Although originally a clonal cell line, prolonged passaging resulted in a phenotypically heterogeneous population, and in 1999 Wang, et al., took advantage of this and isolated ten subclonal MC3T3-E1 cell lines, with subclone 4 exhibiting high levels of osteoblastic differentiation and mineralised extracellular matrix production when cultured with ascorbic acid and inorganic phosphate [281]. MC3T3-E1 have been used extensively since their creation due to being one of the most physiologically

relevant and convenient osteoblast cell lines, with a search for MC3T3-E1 limited to journal articles on PubMed yielding over 4,000 results [282]. However, the subclone used is not commonly reported, therefore differences in results may be due to investigators using different subclones and different stages of differentiation

IDG-SW3 are a comparatively new cell line, developed in 2011 as an osteoblast-osteocyte cell model [283]. They proliferate when cultured at 33 °C in the presence of IFN- γ due to the expression of a temperature-sensitive mutant of a tumour antigen that induces continuous proliferation and immortalisation. However, when returned to 37 °C and IFN- γ is removed they resume their osteoblast/osteocyte behaviour and undergo osteocytogenesis. IDG-SW3 were isolated from 3-month-old transgenic mice that express green fluorescent protein (GFP) when DMP-1 is expressed, allowing observation of osteocyte differentiation by microscopy. Initially, they display typical late-osteoblastic characteristics, such as high ALP expression, collagen type 1 deposition, and production of mineralised extracellular matrix. However, over time they undergo osteocytogenesis. During this process, their rate of mineralisation and ALP activity decreases, and as early osteocytes, they are capable of expressing the osteocyte specific proteins E11/gp38, DMP-1 MEPE and Phex. As they progress to late osteocytes they develop a dendritic, stellate morphology and express sclerostin and FGF-23.

MLOA5 represent a post-osteoblast/pre-osteocyte cell type and are capable of rapidly depositing mineralised extracellular matrix in sheets rather than nodules [284]. They have very high expression of bone sialoprotein, osteocalcin and ALP (higher than IDG-SW3) all hallmarks of the post-osteoblast phenotype [285]. Unlike IDG-SW3, during culture they do not continue to differentiate into osteocytes, meaning that their ALP activity and mineralisation capability remains high.

Human embryonic stem-cell derived mesenchymal progenitors 002.5 (hES-MPs), a human cell line capable of undergoing osteogenic differentiation, were also used for some studies. They are a cell line developed from human embryonic stem cell lines by consecutive enzymatic passaging that is able to undergo osteogenic, chondrogenic and adipogenic differentiation. Phenotypically, they resemble mesenchymal stem cells, with a fibroblast-like morphology [286].

3.2.2 Osteoclast cell lines

The osteoclast pre-cursor cell line RAW264.7 (ATCC® TIB-71™) used in this thesis was kindly donated by Dr. Peter Grabowski, University of Sheffield, and was used for all osteoclast experiments.

RAW264.7 is a murine leukemic monocyte macrophage cell line that can be induced to undergo osteoclastic differentiation by exposure to RANKL. A key advantage they have over other osteoclast precursors is that they do not require co-stimulation with M-CSF to induce osteoclastogenesis as they express both M-CSF and the c-fms receptor [166], [167]. Osteoclasts generated from RAW264.7 are multinucleate, TRAP positive, express cathepsin K and are capable of resorbing a matrix [287].

3.2.3 Culture media preparation

Cell lines and their respective culture media are presented in table 3.1. Basal media (BM) refers to the simplest formulation of medium each cell line is cultured in and consists of a minimum essential medium (MEM), foetal bovine serum (FBS), glutamine, and antibiotics. Two types of MEM are used in this thesis; minimum alpha medium without l-glutamine (α -MEM, Lonza, UK, cat# BE02-002F) and minimum alpha medium with ultraglutamine and nucleosides (α -MEM+nuc, Lonza, UK, cat# BE12-169F).

For the MC3T3-E1, MLOA5 and RAW264.7 cell lines, BM is used during passage to expand cell number. However, when IDG-SW3 cell number is being expanded at 33 °C, they are cultured in expansion media (EM), which is their BM supplemented with IFN- γ . hES-MPs also require an expansion media during passage, which is their BM supplemented with human fibroblastic growth factor (hFGF).

Differentiation media is referred to as supplemented media (SM), which is BM with additives that promote mineralised extracellular matrix formation (beta-glycerol phosphate (β GP) and ascorbic acid 2-phosphate (AA-2P)), or osteogenesis induction media (OIM) which is the same as SM but also contains the corticosteroid dexamethasone (Dex) to stimulate osteogenic differentiation.

Table 3.1: Cell lines used in this thesis and their respective culture media.

Cell Line	Basal Media (BM)	Expansion Media (EM)	Differentiation Media
MC3T3-E1 Subclone 4 (Osteoblast)	α -MEM, 10% FBS, 2 mM L-glutamine, 100 U/mL penicillin, 100 μ g/mL streptomycin	N/A	OIM (BM + 5 mM β GP, 50 μ g/mL AA-2P, 10 nM Dex)
MLOA5-S (Osteoblast)	α -MEM, 10% FBS, 2 mM L-glutamine, 100 U/mL penicillin, 100 μ g/mL streptomycin	N/A	SM (BM + 5 mM β GP, 50 μ g/mL AA-2P)
MLOA5-K (Osteoblast)	α -MEM, 10% FBS, 2 mM L-glutamine, 100 U/mL penicillin, 100 μ g/mL streptomycin	N/A	SM (BM + 5 mM β GP, 50 μ g/mL AA-2P)
MLOA5-A (Osteoblast)	α -MEM+nuc, 5% iron supplemented bovine calf serum (cat# 11551831, Fisher Scientific), 5% heat inactivated FBS (cat# 12350273, Fisher Scientific), 100 U/mL penicillin, 100 μ g/mL streptomycin	N/A	SM (BM + 5 mM β GP, 50 μ g/mL AA-2P)

IDG-SW3 (Osteoblast)	α -MEM+nuc, 10% FBS, 100 U/mL penicillin, 100 μ g/mL streptomycin	BM + 50 U/mL INF- γ	SM (BM + 5 mM β GP, 50 μ g/mL AA- 2P)
hES-MP (Osteoblast)	α -MEM, 10% FBS, 2 mM L-glutamine, 100 U/mL penicillin, 100 μ g/mL streptomycin	BM + 4 nM hFGF	OIM (BM + 5 mM β GP, 50 μ g/mL AA- 2P, 100 nM Dex)
RAW264.7 (Osteoclast)	α -MEM, 10% FBS, 2 mM L-glutamine, 100 U/mL penicillin, 100 μ g/mL streptomycin	N/A	BM + 25-50 ng/mL RANKL

3.2.4 General osteoblast culture

MC3T3-E1 were expanded in T75 flasks, MLOA5-S, MLOA5-K and IDG-SW3 in gelatine coated T75 flasks, and MLOA5-A in collagen coated T75 flasks in BM. All were cultured until ~90% confluent with media changes every 2-3 days.

To detach cells for passage or seeding, media was removed from the T75 flasks which were then washed two times with PBS. 2.5 mL of trypsin (Trypsin-EDTA solution) was then added and incubated under standard conditions for 5 minutes to detach the cells. Flasks were checked under the microscope before adding 5 mL of BM to inhibit the enzyme, and then the suspension was centrifuged for 5 minutes at 1,000 rpm. The supernatant was then removed and the remaining cell pellet resuspended in a known volume of BM. 20 μ L of the suspension was combined with 20 μ L of Trypan Blue® in a 1.5 mL tube to selectively dye dead cells so that only viable cells appear bright when viewed under a microscope. This was then added to a haemocytometer and counted under a light microscope. From this, the viable cell density was determined.

Cell storage over long time periods was performed in liquid nitrogen at -196°C. When freezing down, after counting, the cell density of the cell suspension was adjusted to

1×10^6 cells/mL of freezing medium (10% DMSO, 90% FBS). 1 mL aliquots were transferred to freezing vials and placed into an isopropanol-jacketed freezing container at -80°C for 24 hours before transferring to liquid nitrogen.

To reanimate cells, partially thawed cells were immediately placed into 20 mL of warm medium and mixed before adding to a T75. After 24h, a full media change was performed to remove any residual DMSO.

3.2.5 General osteoclast culture

RAW264.7 were expanded in T75 flasks in 25 mL of BM and grown until 70-80% confluent. It is essential cultures do not overgrow as the cell line contains a sub-population of strongly adherent motile cells amongst a main population of semi-adherent static cells. Overgrowth can result in the dilution and removal of the motile sub-population within only a few passages. Similarly, splitting too early can also alter the balance between the two.

To detach cells for passage, all but 10 mL of BM was removed from the flask. A cell scraper was then used to detach the cells and the suspension aspirated and returned to the flask multiple times to disperse clumps of cells. 2 to 4 mL of suspension was then transferred to a new T75 flask and BM added to a total volume of 25 mL. Media was changed every 2-3 days by removing 75% of the BM and replacing with fresh to conserve factors produced by the cells. To detach for seeding, all but 5 mL of BM was removed from the flask, which was subsequently scraped and aspirated the same way. 20 μL of the suspension was combined with 20 μL of Trypan Blue® and a haemocytometer used to determine viable cell density.

To freeze down, the same protocol as that in §3.2.4 was used, except cells were frozen at a density of 5×10^6 cells/mL.

After seeding, RAW264.7 were maintained in media containing RANKL to induce osteoclastogenesis. Human RANKL was purchased from R&D Systems, UK (cat# 390-TN-010). A stock solution was created by dissolving 10 μg RANKL in PBS containing 0.1 wt/vol% bovine serum albumin. The stock solution was aliquoted and stored at -20°C .

3.2.6 Resazurin reduction assay

In order to evaluate cell viability, RR assays were performed. Resazurin sodium salt is reduced to resorufin by metabolically active cells, changing the colour of the media from a non-fluorescent blue to a highly fluorescent pink. The intensity of the fluorescence is correlated with metabolic activity [288].

A RR working solution was made by dissolving 10 vol% resazurin stock solution (1 mM resazurin sodium salt in diH₂O) in BM. To perform the assay on 2D experiments, media was removed from each well and replaced with a known volume of the working solution. The well plate was then wrapped in aluminium foil and incubated for 4 hours under standard conditions. For 3D experiments, scaffolds were transferred to a new well plate before adding the working solution so only cells adhered to the scaffold were analysed. In both protocols, after 4 hours 200 μ L of the reduced solution was transferred in triplicate to a 96-well plate and read on a plate reader (Tecan infinite 200-pro) at λ_{ex} : 540 nm and λ_{em} : 590 nm. Finally, wells and scaffolds were washed once with PBS before media was replaced.

3.2.7 Cell digestion

To produce lysates for ALP activity, TRAP activity and DNA assays, cells were digested. For 2D samples, media was removed and the cells washed twice in PBS. 1 mL of CDB (10 vol% CAB (1.5 M Tris-HCL, 1 mM ZnCl₂, 1 mM MgCl₂ in diH₂O) in diH₂O with 1 vol% Triton-X100) was added to the well and incubated for 30 minutes. Wells were then scraped and the lysates transferred to 1.5 mL tubes. These were vortexed briefly and refrigerated overnight. For scaffolds, media was removed and the scaffolds washed twice with PBS. 1 mL of CDB was added to a 1.5 mL tube and the scaffold drained and transferred to the CDB. These were then incubated for 30 minutes and refrigerated overnight. The following day, lysates underwent a freeze-thaw cycle (-80°C 10 mins, 37°C 15 mins) three times, vortexing for 15 seconds and the end of each cycle. Samples were then centrifuged at 10,000 rpm for 5 minutes before vortexing again. If evaluation was not done on the same day then samples were stored at -80°C directly after overnight refrigeration.

3.2.8 Alkaline phosphatase activity

To quantify ALP activity, a Pierce™ pNPP Substrate Kit (Thermo Scientific) was used according to manufacturer's instructions. Briefly, one tablet containing 5 mg para-nitrophenol phosphate (pNPP) was dissolved per 5 mL of 20 vol% diethanolamine buffer in diH₂O to form the assay substrate. 20 μL of cell lysate (§3.2.7) was added in triplicate to a 96 well plate. To this, 180 μL of ALP substrate was added. The well plate is then incubated at 37°C until a colour change from colourless to yellow is observed or 30 minutes has passed. The absorbance of each well was measured at 405 nm every minute for 30 minutes in a plate reader (Tecan infinite 200-pro). Activity is expressed as nmol para-nitrophenol (PNP) per minute (nmol PNP/min), where one absorbance value equals 19.75 nmol of product (K, standard curve in Appendix §10.1), the volume of the sample is the volume of digestion buffer added (V_{Sample}) and the measured volume is the volume combined with the pNPP phosphatase solution ($V_{Measured}$) (Eqn. 1).

$$ALP\ Activity = \frac{Maximum\ slope \times K \times V_{Sample}}{V_{Measured}} \quad (1)$$

3.2.9 DNA quantification

ALP activities were always determined in parallel with DNA quantities to allow normalisation to cell number using the same lysate. DNA was quantified using a Quant-iT® high sensitivity dsDNA assay kit according to manufacturer instructions. Briefly, the Quant-iT® reagent was diluted 1:200 in the Quant-iT® assay buffer to create a working solution. 90 μL of the working solution was added in triplicate to a black 96 well plate. 10 μL of the lysate was then added to this. The well plate was then shaken for 15 seconds with a linear amplitude of 1 mm, left for 10 minutes at room temperature to allow the DNA and reagent to conjugate and shaken again before the fluorescence was measured (λ_{ex} : 485 nm, λ_{em} : 535 nm). Shaking and fluorescence was performed and measured using a plate reader (Tecan infinite 200-pro). Fluorescence was converted to ng of DNA using a standard curve (Appendix §10.1), then similarly to ALP activity, whole sample DNA was calculated (Eqn. 2).

$$Total\ DNA\ (ng) = \frac{DNA\ in\ 20\ \mu L\ (ng) \times V_{Sample}}{V_{Measured}} \quad (2)$$

3.2.10 Cell fixing

To fix samples for histological evaluation, media was removed and the samples washed twice with PBS. Samples were then submerged in 3.7% formaldehyde for either 20 minutes for 2D cultures or 30 minutes for scaffolds. The fixative was then removed and the samples washed twice in PBS and then refrigerated in PBS until needed.

3.2.11 Alizarin Red S staining

Alizarin red S (ARS) is an organic dye that has a high affinity for calcium, and therefore can be used to stain mineral deposited by osteoblasts. A key advantage of this technique is that the dye can be extracted and assayed colourimetrically, allowing quantification of how much stain, and therefore calcium, is present [289].

To prepare the stain, ARS was dissolved at 1 w/v% in diH₂O. The solution was filtered using a 0.45 µm filter to remove undissolved particulates and the pH adjusted to 4.1. Fixed samples were rinsed twice with diH₂O before submerging in a known volume of ARS stain and leaving for 30 minutes. The stain was then removed and the samples washed with diH₂O every five minutes whilst orbitally shaking at 100 rpm until the wash-water remained clear. A known volume of 5% perchloric acid was then added to destain the samples and left on the orbital shaker at 100 rpm for 15 minutes. 150 µL was then added in triplicate to a 96 well plate and read at an absorbance of 405 nm. (Tecan infinite 200-pro). The concentration of ARS was determined via a standard curve (Appendix §10.1) created by serially diluting the staining solution in the destain. From this, the absorbance units can be converted to a quantity of ARS.

3.2.12 Direct Red 80 staining

To determine collagen production, DR80 staining was performed. To prepare the stain, DR80 was dissolved in saturated picric acid at 1 w/v%. The solution was filtered using a 0.45 µm filter to remove undissolved particulates. Depending on whether samples were being stained after fixing or ARS staining, samples were washed twice or thrice, respectively. After washing, samples were submerged in a known volume of DR80 stain and left for 18 hours on an orbital shaker at 100 rpm. The staining solution was then removed and the samples washed with diH₂O every five minutes whilst orbitally shaking at 100 rpm until the wash-water remained clear. A known volume of

0.2 M NaOH and MeOH in a 1:1 ratio was then added to destain the samples and left on the orbital shaker at 100 rpm for 20 minutes. 150 μ L was then added in triplicate to a 96 well plate and read at an absorbance of 405 nm. (Tecan infinite 200-pro). The concentration of DR80 was determined via a standard curve (Appendix §10.1) created by serially diluting the staining solution in the destain. From this, the absorbance units can be converted to a quantity of DR80.

3.2.13 TRAP staining

2D cultures were stained for TRAP using the Acid Phosphatase Leukocyte (TRAP) Kit (387A), adapting the manufacturer's instructions for *in vitro* staining. Cells were fixed by submersion in the fixative solution (citrate solution, 37% formaldehyde and acetone in a 25:8:65 ratio) for 30 seconds. They were then rinsed in diH₂O before adding the staining solution (diH₂O, diazotized Fast Garnet GBC solution, Naphthol AS-BI Phosphate solution, acetate solution and tartrate solution in a 45:1:0.5:2:1 ratio) and incubating at 37°C protected from light for 1 hour. Samples were then rinsed in diH₂O and counterstained in Haematoxylin solution, Gill No. 3, before blueing the nuclei in alkaline tap water. Samples were air-dried before imaging.

3.2.14 TRAP activity

TRAP staining is a qualitative measure of TRAP production and is not suitable for 3D cultures. Therefore, an assay to measure its activity in a sample is also necessary. For 2D samples, a modified protocol of that outlined by Dugard, et al. was used [290]. Media was removed from the wells and a known volume of the assay substrate (2.5 mM Naphthol AS-BI phosphate in 100 mM sodium acetate buffer containing 50 mM potassium hydrogen (+) tartrate, 2% IGEPAL and 1% ethylene glycol monomethyl ether (EGME) buffered to pH 5.6) was added. This was incubated for 35 minutes at 37°C before adding the stop solution (0.3 M NaOH). The volume of stop solution is half the volume of assay substrate. The solution was then transferred in triplicate to a 96 well plate and read at an absorbance of 405 nm (Tecan infinite 200-pro).

3.2.15 Scanning electron microscopy

Samples were mounted on a carbon tab, sputter coated with gold (SC500, emscope) and imaged using a Philips XL-20 SEM with a beam energy of 15 kV. To prepare scaffolds with cells for SEM, cells were fixed in accordance with §3.2.10, then dehydrated in ethanol at increasing concentrations (50/70/80/90/100/100 vol% in diH₂O) with a 10 minute exposure at each concentration. Finally, cells were immersed in 100% hexamethyldisilazane (HMDS) for 3 minutes before air drying overnight. Samples were then mounted, coated and imaged using the above protocol.

3.2.16 Statistical analysis

All statistical analysis was undertaken in Graphpad Prism (version 7.00). Data was tested for normality (D'Agostino-Pearson omnibus normality test) and outliers removed (ROUT method, Q = 1%). Normally distributed data was analysed by analysis of variance (ANOVA). Depending on whether a response was affected by one or two factors, either one or two-way ANOVA was performed with Tukey's multiple comparisons test to evaluate significant differences. Data which did not fit a Gaussian distribution was analysed by a Kruskal-Wallis non-parametric test with Dunn's multiple comparisons test to evaluate significant differences. Differences were considered significant when $p < 0.05$. All graphs are presented as mean \pm standard deviation unless otherwise stated and notable significant differences are indicated on the graphs or in the legends. All experiments were performed a minimum of two times in triplicate for each condition where possible. The total number of replicates (n) is stated in the figure legend.

4. Response of bone cells to oestrogen

4.1 Introduction

Decline in oestrogen levels following the onset of postmenopausal osteoporosis is associated with increased bone turnover and a loss of bone, resulting in weaker whole bone mechanical properties [131], [291]. However, although whole bone mass and strength is clearly reduced, it has been shown that the remaining tissue has increased stiffness and strength in comparison to normal tissue in OVX rats due to an increase in tissue-level mineral content [292]. Subsequent work studying mineral distribution in proximal femurs from OVX sheep and human female vertebrae found that the distribution of tissue-level mineral is altered during osteoporosis, with it becoming more heterogeneous, which in turn may affect the mechanics of the tissue [144], [293]. The mechanism by which this increase in mineralisation is initiated is unknown, but it may occur in an attempt to compensate for the overall loss of bone [294]. Although this compensation may increase the stiffness of the bone, it does not necessarily increase the toughness and therefore does not reduce the risk of fracture. Bisphosphonates can reduce fracture risk by up to 50%; however, their use is also associated with atypical femoral fractures due to increased mineralisation and therefore brittleness. It has been shown that the fracture toughness and crack-initiation toughness are lower in bisphosphonate treated patients in comparison to untreated patients [295].

The changes in osteoclast activity after the onset of menopause are well documented, but the effects of menopause on osteoblasts are less well known. There is evidence to suggest that following the decline in oestrogen at the onset of menopause, the first cell type affected is the osteoblast, with changes in osteoclast activity and increased resorption being later events [296], [297]. 17β -estradiol is the primary type of oestrogen produced by the ovaries; therefore, it is this form of oestrogen that is typically used in scientific studies. Oestrogen receptor α (ER α), rather than ER β , is the key receptor for oestrogen in bone [298]. Investigations into the response of osteoblasts to oestrogen have yielded contradictory results. For example, it has been shown to both accelerate [299], [300] and slow down [301] cell proliferation, upregulate ALP activity [299], [301], [302] but suppress osteocalcin production [299], [301], and both enhance [303] and not affect [304] mineralisation. In contrast to its effect on

osteoclasts, oestrogen is an anti-apoptotic factor for osteoblasts [305]. Interestingly, Rao, et al., found only intermittent, not continuous, exposure to oestrogen increased mineralisation in comparison to untreated controls [300], and Park, et al., found blocking oestrogen receptors with the oestrogen agonist fulvestrant reduces mineralisation [306].

Significantly for this project, it has been shown that osteoblasts cultured *in vitro* with oestrogen that subsequently undergo withdrawal respond in a similar way to cells from OVX mice, as indicated by an increase in IL-6 production [307]. From this, Brennan, et al., performed a subsequent study investigating whether altered mineral production occurs as a result of withdrawal, finding that MC3T3-E1 osteoblasts exposed to oestrogen for two weeks before withdrawal had significantly higher ALP activity and mineralisation than cultures with maintained oestrogen, and that this effect could be abrogated by fulvestrant [308].

The pathogenesis of postmenopausal osteoporosis is primarily due to the decline in oestrogen caused by the cessation of ovarian function. Although bone formation by osteoblasts may be increased slightly, the increase in resorption by osteoclasts is the most prominent change in bone cell activity postmenopause. This causes resorption to greatly exceed formation resulting in a strongly negative bone balance which impairs bone quality [93], [94]. Once oestrogen was identified as having a central role in the progression of osteoporosis, the mechanisms by which it affects bone turnover were investigated in order to understand the disorder better and develop treatments.

Several cytokines, such as IL-1, IL-6, TNF and M-CSF, can regulate osteoclastogenesis. IL-1 and TNF stimulate resorption and inhibit formation by enhancing osteoclast formation. This occurs by stimulating proliferation of precursors and inducing other cytokines, such as IL-6, that in turn regulate maturation of precursors into osteoclasts [95]. Oestrogen is an inhibitor of these cytokines, performing a protective role by modulating their production.

The RANK/RANKL/OPG axis is important in understanding the effect of oestrogen on osteoclasts [63]. RANKL binds to its receptor, RANK, but OPG can competitively bind to RANKL, antagonising its function [96]. In normal bone remodelling, cells from the osteoblast lineage express RANKL and M-CSF which conjugate with their receptors, RANK and c-fms, on osteoclast precursors, stimulating their maturation. Oestrogen increases OPG and decreases RANKL production by osteoblastic cells, as

well as modulating osteoclast lifespan by activating apoptosis. In addition to its action on the production of osteoclastogenic factors by osteoblasts and its effects on osteoclast lifespan, oestrogen also directly affects protein transcription downstream of the RANK receptor, directly inhibiting osteoclastogenesis [309], [310]. Therefore, reduced oestrogen results in less inhibition of osteoclastogenesis, meaning more mature osteoclasts are generated that in turn live longer due to a reduction in apoptosis. The result is the large increase in bone resorption seen in osteoporosis [97]–[99].

4.2 Aims and objectives

Oestrogen has an anabolic effect on bone *in vivo* by increasing osteoblast and decreasing osteoclast activity. The aim of this chapter was to explore the response of different osteoblast and osteoclast cell lines to oestrogen *in vitro*. From this, an appropriate osteoblast and osteoclast cell line can be selected for use in the *in vitro* model of postmenopausal osteoporosis developed in chapter 6. To achieve this, the following objectives were addressed:

1. Assess whether 17β -estradiol affects osteoblast proliferation, differentiation and matrix production *in vitro*.
2. Assess whether 17β -estradiol affects the RANKL:OPG ratio *in vitro*.
3. Determine the effects of 17β -estradiol on osteoclastogenesis and osteoclast activity *in vitro*.
4. Identify a suitable osteoblast and osteoclast cell lines for the *in vitro* model.

4.3 Materials and Methods

Further to the materials and methods outlined in §3, the following are used in this chapter.

4.3.1 Preparation of oestrogen supplement

17 β -estradiol (cat# E2257) was purchased from Sigma Aldrich, UK. A 100 μ M stock solution was created by dissolving 1 mg 17 β -estradiol in 1 mL of absolute ethanol then diluting in 35.7 mL of α -MEM. The stock solution was aliquoted and stored at -20°C. The same amount of vehicle was added to all wells regardless of the drug concentration used.

4.3.2 Alternative cell digestion protocols

To compare to the protocol used in §3.2.7, cells were also digested in the following ways:

To digest in PBS, media was removed and the cells washed twice in PBS. 1 mL of PBS with 1 vol% Triton-X100 was added to the well and the well plate refrigerated overnight. The following day, whole well plates underwent a freeze-thaw cycle (-80°C 10 mins, 37°C 15 mins) three times, before scraping and the lysates transferred to 1.5 mL tubes. These were vortexed briefly, then centrifuged at 10,000 rpm for 5 minutes before vortexing again. Samples were stored at -80 °C until use.

For enhanced digestion, cells were scraped in their culture media and the suspension transferred to microcentrifuge tubes. These were spun at 300 g for 7 minutes, the supernatant aspirated and the pellet resuspended in ice-cold PBS. This was centrifuged at 300 g for 7 minutes, the supernatant removed and the pellet resuspended in cell extraction buffer (CEB, Thermo Fisher Scientific, UK, cat# FNN0011) supplemented with 1 mM Phenylmethylsulfonyl fluoride (PMSF, 0.3 M stock solution in DMSO stored at -20 °C) and 5 vol% protease inhibitor cocktail (Sigma, UK, cat# P-2714). The suspension was then transferred to a new microcentrifuge tube and kept on ice for 30 minutes, vortexing every ten minutes. The lysate was then spun at 13,000g for ten minutes to clarify the extract, which was transferred again to a new clean tube. Samples were stored at -80 °C until use.

4.3.3 Polyurethane scaffold preparation

Polyether polyurethane foam (Caligen Foam Ltd) was cut into 5 × 5 mm (diameter × height) cylinders using a hole punch and scalpel in a similar method to Sittichokechaiwut , et al. [9]. Once cut, they were submerged in 0.1 w/v% gelatine solution and autoclaved at 121 °C for 30 minutes to sterilise and improve cell attachment.

4.3.4 Polyurethane scaffold seeding

Before seeding, scaffolds were soaked in BM for 30 minutes. To seed, the BM was aspirated and replaced with a seeding suspension of 600 cells/0.31 μL BM per mm³. Cells were left for 45 minutes to attach for 45 minutes before submerging in BM overnight. The following day, scaffolds were transferred to a new well plate and cultured in the appropriate medium for the remainder of the experiment. Media was changed every 2-3 days.

4.3.5 RANKL and OPG ELISA

RANKL and OPG enzyme-linked immunosorbent assay (ELISA) kits were purchased from R&D Systems (Cat# MTR00 and MOP00, respectively) and performed according to manufacturer instructions. Samples analysed were either cell culture supernatant for soluble isoforms of the cytokines or lysates produced using enhanced cell digestion for the membrane-bound variants (§4.4.2). Cell-culture supernatant was stored at -20°C until use. For the assay, supernatants or lysates were thawed and added to microplates with an affinity purified polyclonal antibody specific for RANKL or OPG coated onto the wells which binds the respective cytokine. Unbound substances are washed away before adding an enzyme-linked polyclonal antibody for either RANKL or OPG. After washing again, a substrate solution is then added which yields a blue product that turns blue upon addition of the stop solution. The intensity of the stopped reaction is compared to a standard curve to determine the quantity present. Both kits are supplied with a control concentration of the appropriate cytokine that is also tested during the ELISA to ensure that the assay is performed correctly.

4.3.6 Preparation of Vitamin D3 supplement

1 α ,25-dihydroxyvitamin D3 (vitamin D3) was purchased from Sigma Aldrich, UK. A 10 μ M stock solution was created by dissolving 10 μ g vitamin D3 in 2.4 mL of absolute ethanol. The stock solution was aliquoted and stored at -80 °C. The same amount of vehicle was added to all wells regardless of the drug concentration used.

4.3.7 Assessment of osteocytogenesis

DMP-1-GFP is a marker for osteocyte differentiation in IDG-SW3 [311]. To assess its production and therefore osteocytogenesis, GFP fluorescence was quantified in live cells using a microplate reader (Tecan infinite 200-pro). To take the measurements, media was removed, cells washed with PBS, and Hank's Balanced Salt Solution (HBSS) added to cover the cells. Multiple measurements were taken (λ_{ex} : 485 nm, λ_{em} : 535 nm) in the central region of experimental wells as well as wells containing just HBSS in order to subtract the background.

4.3.8 Fluorescence microscopy

Fluorescent images were obtained with a Ti-E Nikon inverted microscope (Nikon, Japan). Image capture and stage control were performed with MetaMorph® Microscopy Automation & Image Analysis Software (Molecular Devices LLC).

To stain live cell nuclei, Hoechst 33342 stock solution was created at 10 mg/mL in PBS and stored at -20 °C. Media was removed and the wells washed twice with PBS. The stock solution was diluted 1:2,000 in PBS to create a working solution, which was added for five minutes before aspirating and washing two further times in PBS. Cells were imaged (λ_{ex} : 360 nm, λ_{em} : 460 nm) in PBS before replacing with fresh media.

Fixed cell nuclei were stained with 4', 6-diamidino-2- phenylindole dihydrochloride (DAPI, Sigma Aldrich, UK). A DAPI stock solution was created at 4 mg/mL in PBS and stored at 4 °C. After fixing, cells were permeabilised and stained in a solution containing 0.1 vol% Triton X-100 in PBS and 400 ng/mL DAPI for five minutes. This solution was aspirated and replaced with PBS before imaging (λ_{ex} : 360 nm, λ_{em} : 460 nm). GFP synthesised by the IDG-SW3 did not require exogenous staining to image (λ_{ex} : 470 nm, λ_{em} : 525 nm)

4.3.9 Resorption pit quantification

To assess the resorptive capability of the osteoclasts, cultures were performed on the Corning® Osteo Assay Surface under standard conditions. At the end of the experiment, cells were removed by bleaching (1.2 g sodium hypochlorite/100 mL) for 5 minutes before rinsing twice with diH₂O and leaving to air dry for three hours.

To enhance contrast, the remaining phosphate in the wells was stained with either 1% toluidine blue in water for 2 minutes before washing until clear, or by using Von Kossa staining. Here, 2% silver nitrate solution was added and exposed to strong UV for 30 minutes before rinsing with water and adding 5% sodium thiosulphate for 5 minutes before rinsing again. Images were then captured using brightfield on a Ti-E Nikon inverted microscope (Nikon, Japan).

4.3.10 TRAP activity – lysates

In addition to the TRAP activity protocol detailed in §3.2.14, TRAP activity was also quantified from lysates. Here, 250 µL of lysate was combined with 250 µL of assay substrate (2.5 mM Naphthol AS-BI phosphate in 100 mM sodium acetate buffer containing 50 mM potassium hydrogen (+) tartrate, 2% IGEPAL and 1% EGME buffered to pH 5.6) and incubated for 35 minutes at 37°C before adding the 250 µL of stop solution (0.3 M NaOH). The solution was then transferred in triplicate to a 96 well plate and read at an absorbance of 405 nm (Tecan infinite 200-pro).

4.3.11 Preparation of trabecular bone and dentine substrates

3 mm diameter bovine trabecular bone or dentine cylinders were kindly provided by Dr. Enrico Dall'Ara, University of Sheffield. To prepare the bone samples for osteoclast culture, any marrow or debris was removed via ultrasonication for 15 minutes in deionised water before insertion into a 200 µL pipette tip and cleaning with a dental water jet. Discs were then removed from the tip and ultrasonicated for a further 15 minutes. Dentine discs were ultrasonicated for 15 minutes in deionised water. Both discs were then sterilised in 70% ethanol for 90 minutes before washing three times in sterile PBS before seeding with 20,000 RAW264.7 in 75 µL of BM in a 96 well plate. After 30 minutes, a further 125 µL of BM containing 50 ng/mL RANKL was added and the cultures maintained for 16 days before SEM analysis, with half the media changed every 2-3 days.

4.4 Results

4.4.1 Phenol red only affects oestrogen responsiveness at low concentrations

Phenol red is a pH indicator used in most culture media. However, it has a structural resemblance to some oestrogens and has been shown to affect oestrogen responsive cell lines [312]. To see whether the presence of phenol red was affecting the responsiveness of MC3T3-E1 to oestrogen, cultures were performed in phenol free media. There is no phenol free equivalent of the α -MEM produced by Lonza; therefore, a phenol-containing (PC) and phenol free (PF) version of a different α -MEM were used (Gibco, cat# 12571063 & 41061029, respectively). The effects of oestrogen added at different concentrations to OIM composed of these two media and the regular α -MEM were investigated over 21 days in MC3T3-E1. Cell viability, ALP activity and ARS were measured (Fig. 4.1).

MC3T3-E1 proliferated in all three media formulations at all time timepoints. Proliferation was significantly faster in the PF and PC media than the Lonza. There was no significant difference in metabolic activity at any time point between the PC and PF for any oestrogen concentration.

In all three media, normalised ALP activity increased with oestrogen concentration. ALP activities and total DNA were significantly higher in the PC and PF media in comparison to Lonza (data not shown), as expected from the metabolic activity; however, the normalised ratios remained similar. At 0.1 nM, normalised ALP activity was significantly higher in the PF media than PC and Lonza, but not at 10 or 100 nM. Furthermore, the difference between 0 and 0.1 nM was greatest in the PF group. Therefore, it appears that phenol red can mask the effect of very low concentrations of oestrogen, but at higher concentrations this effect is lost. Mineralisation was also higher in the PC and PF formulations, but oestrogen had no significant effect in any media type. Therefore, the Lonza α -MEM was used for all subsequent work.

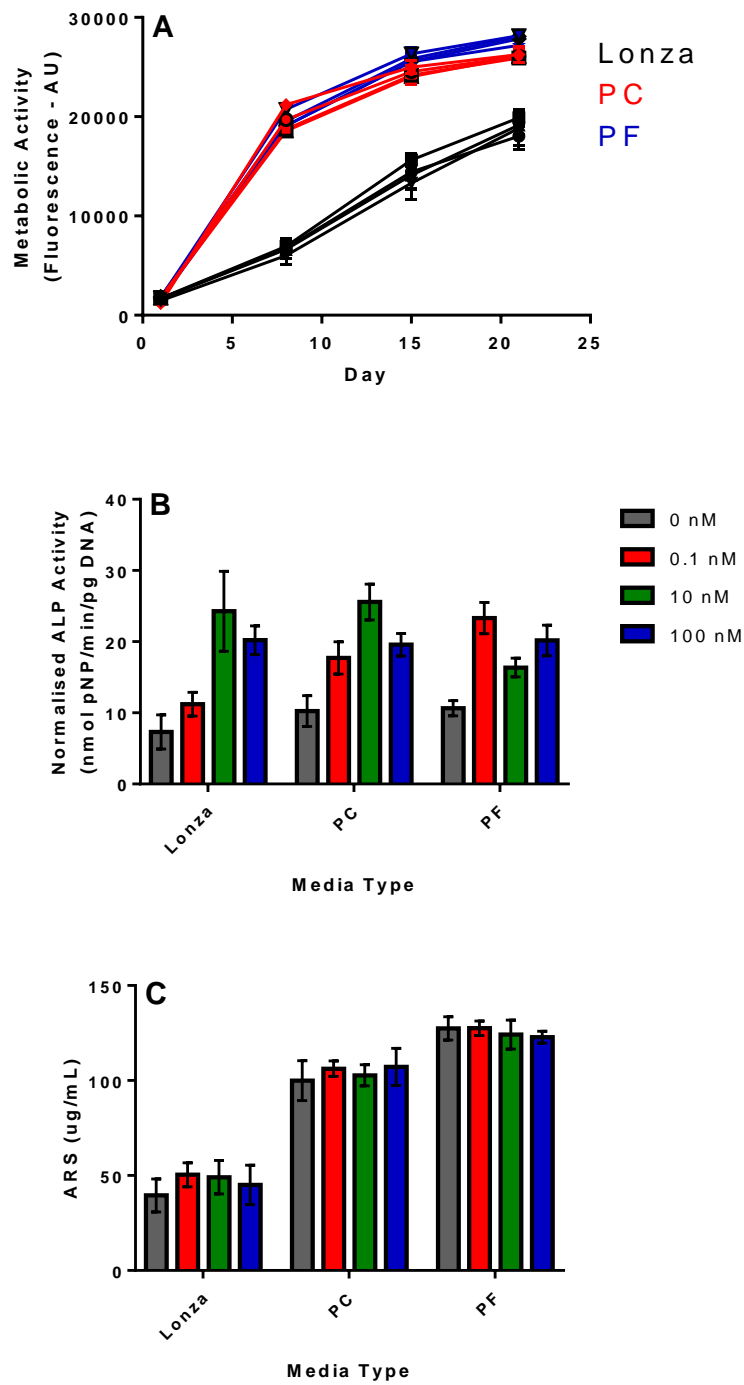


Figure 4.1: Effect of phenol and oestrogen on MC3T3-E1. Comparison of Lonza, phenol containing (PC) and phenol free (PF) media with different concentrations of oestrogen, examining (A) metabolic activity (B) day 21 ALP activity (C) day 21 ARS. For clarity, a legend for each individual growth curve is not given, instead each media type is coloured differently (n=6).

4.4.2 Oestrogen withdrawal does not further enhance MC3T3-E1 activity

It has been shown in the literature that exposing MC3T3-E1 osteoblasts to oestrogen for a prolonged period then withdrawing it results in a greater increase in ALP activity and mineralisation than exposure alone [308]. Here, cells were passaged in the presence of 10 nM oestrogen (17 β -estradiol) for 14 days. They were then seeded and the oestrogen level either maintained at 10 nM (E2), reduced to 0.1 nM (E1), or withdrawn (E-) (Fig. 4.2).

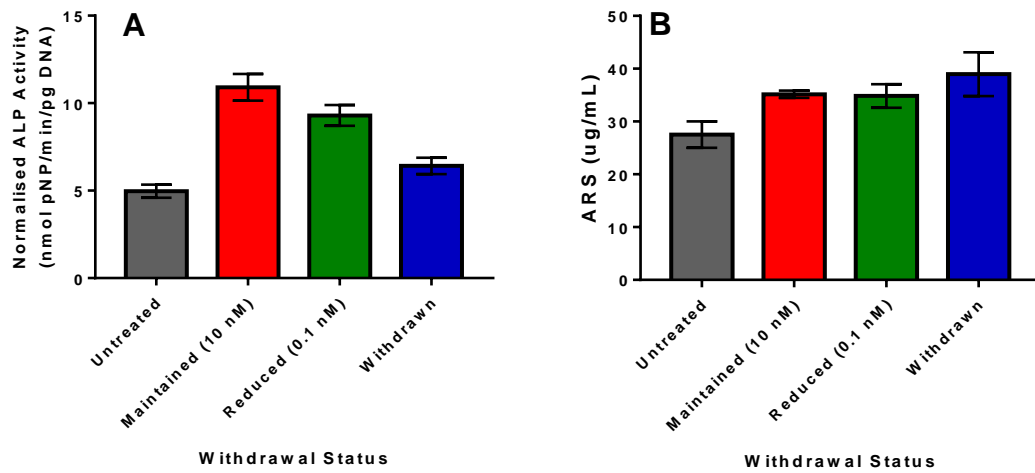


Figure 4.2: Effect of oestrogen withdrawal on MC3T3-E1. Day 14 (A) ALP (all groups significantly different to each other ($p < 0.01$)) (B) ARS (maintained, reduced withdrawn not significantly different to each other but all significantly higher than untreated control ($p < 0.001$)) ($n = 6$).

All oestrogen exposed groups had higher ALP activity and mineralisation than the untreated control. Maintained oestrogen had the highest normalised ALP activity and withdrawn was still significantly higher than untreated. There was no significant difference in mineral between oestrogen exposed groups, possibly due to the very low levels of mineralisation.

4.4.3 Mineralisation capacity of MC3T3-E1 can be increased with varied supplementation

The mineralisation capacity of MC3T3-E1 is far lower than other cell lines, such as MLOA5 [284]. As production of resorbable mineral is essential in an osteoporosis model, it is imperative that sufficient levels are deposited. Although the concentrations of β GP and AA2P added to OIM here are in line with that reported in the literature, higher levels are used by some groups. Therefore, the effect of increasing the concentrations typically used were examined by adding either normal (1X) or double (2X) concentrations of β GP and AA2P (Fig. 4.3).

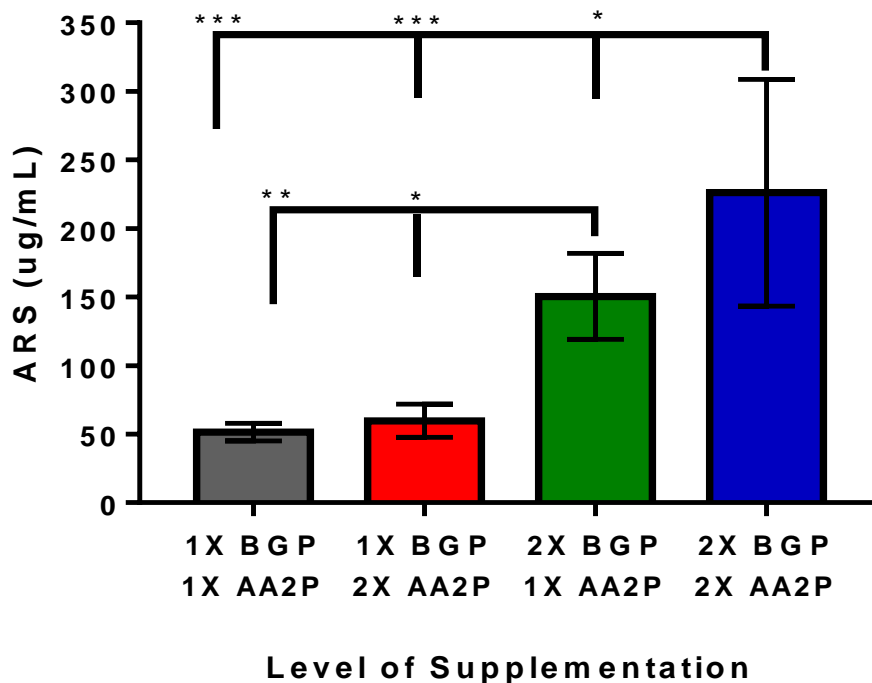


Figure 4.3: Effect of varied osteogenic supplementation of MC3T3-E1. Day 21 ARS staining for varied supplementation in OIM on MC3T3-E1 cells. 1X is normal supplementation, 2X is doubled. * = $p < 0.05$, ** = $p < 0.01$, *** = $p < 0.0001$ ($n = 6$).

Doubling the BGP concentration led to significantly higher mineralisation whereas doubling only AA2P did not. The combination of two times BGP and AA2P caused four times the amount of mineralisation in a three-week period in comparison to regular OIM.

4.4.4 Oestrogen withdrawal has no effect of MLOA5

To the author's knowledge, the oestrogen responsiveness of MLOA5 has not previously been tested. Initially, the withdrawal experiment in §4.4.2 was repeated with MLOA5-S (Fig. 4.4).

No effect of oestrogen was seen on MLOA5-S, with no significant difference in ALP activity or mineralisation for any of the oestrogen exposed groups in comparison to the untreated control. The MLOA5-S cell line was prone to cell sheet detachment once confluent. This meant that mineral deposition in the reduced group could not be quantified.

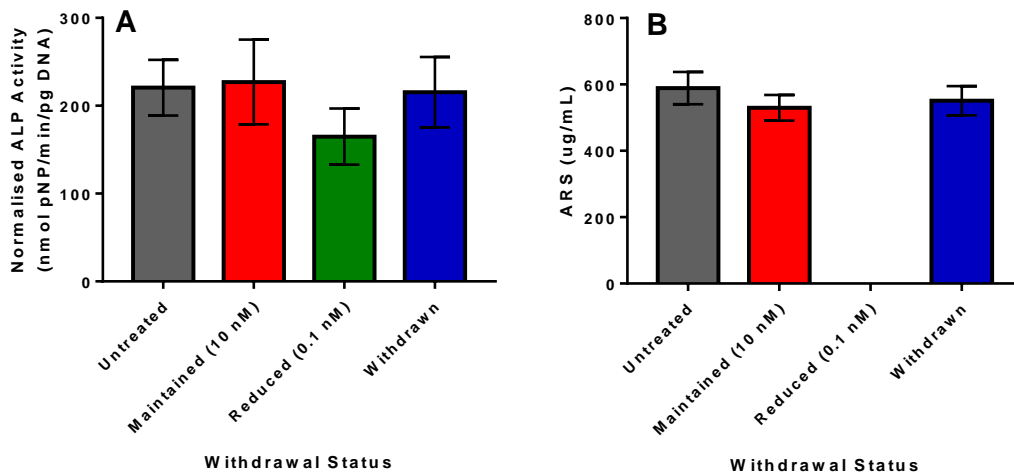


Figure 4.4: Effect of oestrogen withdrawal on MLOA5. Mean \pm SD on day 14 for (A) ALP (no significant different between groups) (B) ARS (no significant difference between groups with the exception of reduced vs. all others) ($n=6$).

4.4.5 Oestrogen exposure has no effect on MLOA5 even at extreme concentrations

Due to MLOA5 being much more metabolically active than MC3T3-E1, it was possible that 10 nM was not a sufficiently high concentration of oestrogen to have an effect. Therefore, their response to concentrations ranging from 0 nM to 10,000 nM was studied over seven days on MLOA5-S (Fig. 4.5) and 14 days on MLOA5-K (Fig. 4.6).

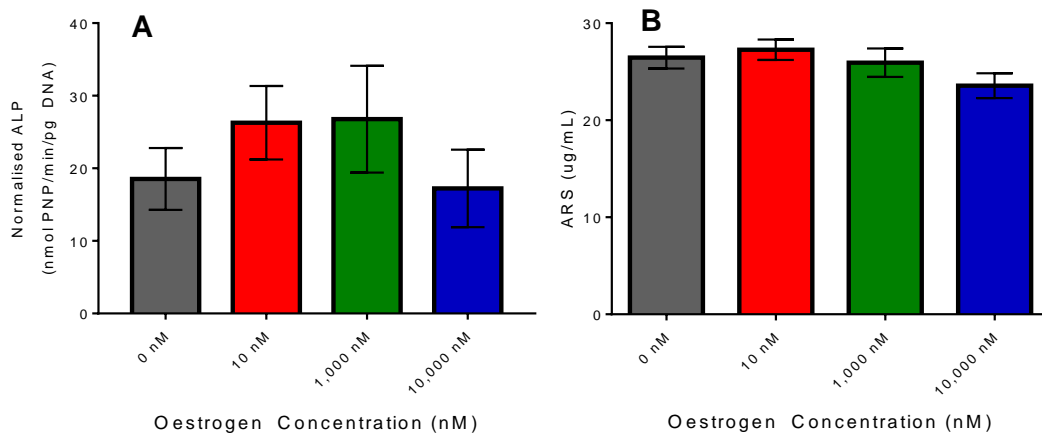


Figure 4.5: Effect of oestrogen exposure on MLOA5-S. Mean \pm SD on day 7 for (A) ALP (no significant difference between groups) (B) ARS (no significant difference between groups with the exception of 0 nM vs 10,000 nM ($p < 0.01$) for MLOA5-S ($n=6$)).

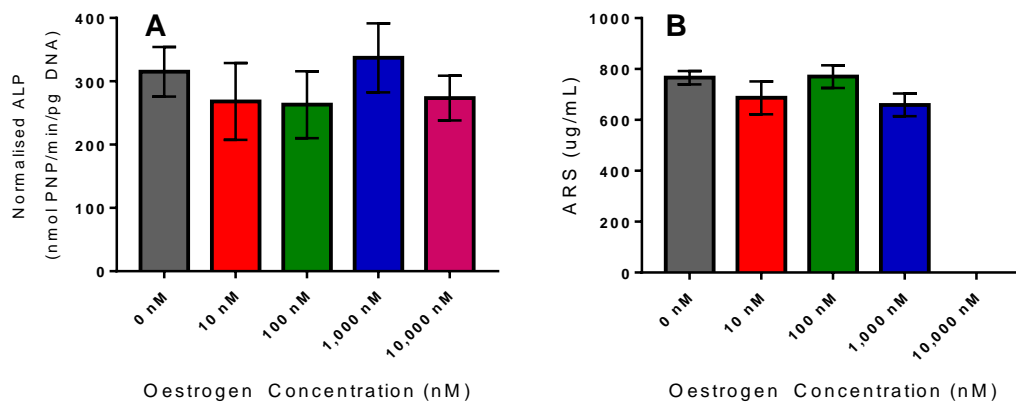


Figure 4.6: Effect of oestrogen exposure on MLOA5-K. Mean \pm SD on day 14 for (A) ALP (no significant difference between groups) (B) ARS (no oestrogen exposed group was significantly higher than the 0 nM group) for MLOA5-K (n=6).

Oestrogen had no effect on the ALP activity or calcium production of MLOA5-S or MLOA5-K. Detachment of the cell line once confluent again meant that mineral quantification could not be performed for all groups. Due to both MLOA5-S and MLOA5-K not behaving as described in the original literature about the creation of the MLOA5 cell line, a new source of MLOA5 (MLOA5-A) was purchased. However, these also did not function as described in literature and although there were still metabolically active cells after seven days, it was clear that a large proportion of the MLOA5-A cells were dying in comparison to MLOA5-K; therefore, the experiment was ended and oestrogen responsiveness not assessed (Fig. 4.7).

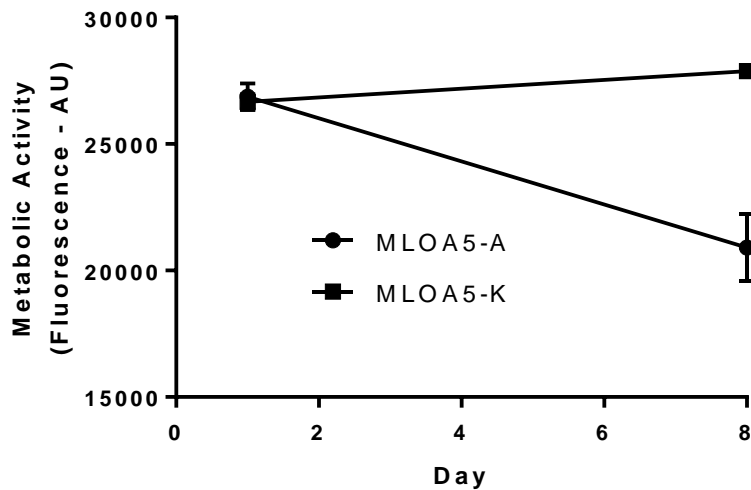


Figure 4.7: Comparison of MLOA5-K and MLOA5-A. Cell metabolic activity of MLOA5-A compared to MLOA5-K over eight days (n=6).

Despite seeding at a density just below confluent as stated by Kerfast, it seems that the MLOA5-A cells begin to die once confluent. Therefore, cells were seeded at a lower density (100,000 per well vs. 335,000 per well) initially to see whether this influenced how well they survived. Cells were discernibly dead before day 7 therefore the growth curve is not included.

4.4.6 Oestrogen exposure has no effect on IDG-SW3

Due to the low mineralisation capacity of MC3T3-E1 and the lack of reproducibility of MLOA5, an alternative cell line was sought. IDG-SW3 was identified as an appropriate cell line for these studies. Its oestrogen responsiveness was assessed by exposure to 0 – 100 nM for three weeks and quantifying ALP activity, total DNA, mineralisation and osteocytogenesis by measuring GFP expression (Fig. 4.8).

As with MLOA-5, there was no significant effect of oestrogen on the proliferation, ALP activity or mineralisation of IDG-SW3. Furthermore, there was no significant effect of oestrogen on osteocytogenesis, as indicated by GFP expression. However, the mineralisation capacity of IDG-SW3 is far superior to MC3T3-E1, and the behaviour of the cell line appeared to be more consistent than MLOA5.

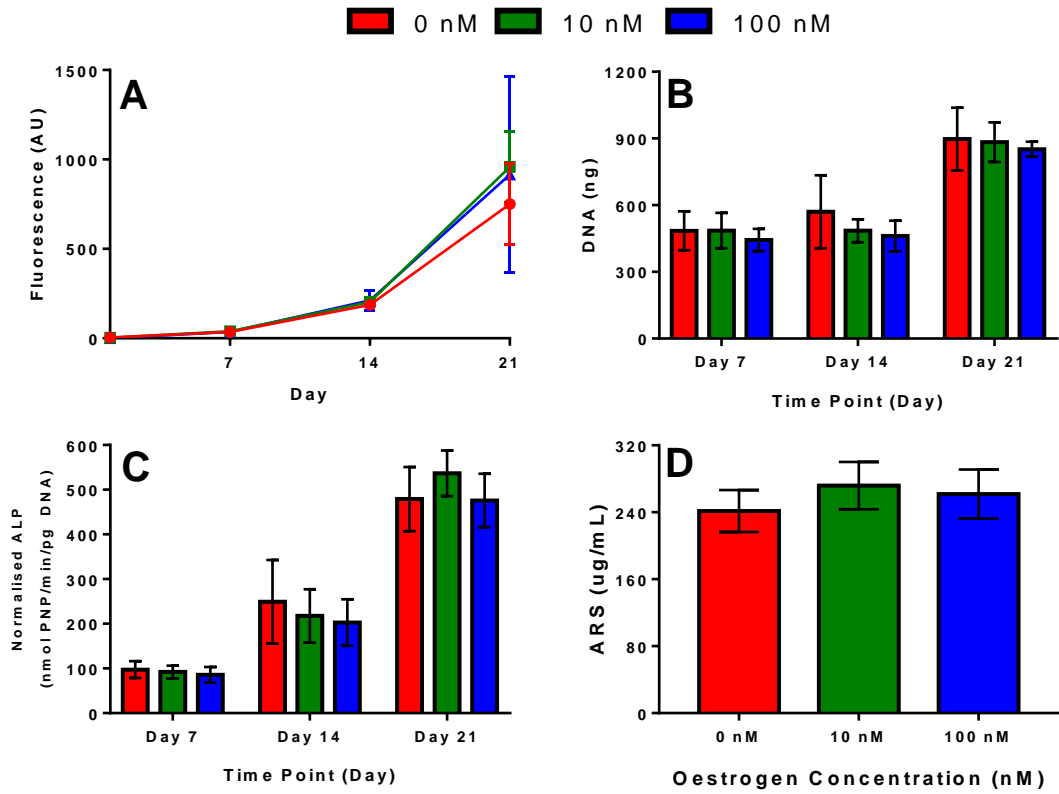


Figure 4.8: Response of IDG-SW3 to oestrogen. (A) GFP expression indicating osteocytogenesis (no significant difference) (B) total DNA (no significant difference) (B) Normalised ALP (no significant difference) (C) ARS (no significant difference) ($n=6$).

4.4.7 Varied temperature and media type can hold IDG-SW3 as osteoblasts

IDG-SW3 have been designed to proliferate at 33 °C in EM and undergo osteocytogenesis at 37 °C in SM. At 33 °C in the presence of IFN- γ , they express a temperature-sensitive mutant of a tumour antigen that induces continuous proliferation and immortalisation, but at 37 °C without IFN- γ they resume their normal proliferative ability [283]. To examine the effects of temperature and media supplementation, IDG-SW3 were seeded at 25,000 cells per well in a 48 well plate and cultured at 33 °C in EM for three days until confluent. They were then maintained for a further 28 days at either: 33 °C in EM (33-EM), at 33 °C in SM (33-SM), at 37 °C in EM (37-EM), or at 37 °C in SM (37-SM). Metabolic activity, ALP activity, DNA, GFP expression and calcium deposition were analysed at various time points (Fig. 4.9)

As expected, the highest metabolic activities and total DNA were found in cultures maintained in EM, with the highest total DNA in the 33-EM group at all time points. Interestingly, the highest ALP activities were found in the 33-SM group, rather than the 37-SM group. This pattern occurs even after normalising to total DNA. GFP expression is highest in the 33-SM group by day 14, but normalising to total DNA to account for variation in cell number shows that the condition that stimulated the highest amount of osteocytogenesis was 37-SM. By 28, cultures maintained in 37-SM had GFP expression approximately 4 times higher than 33-SM, indicating that osteocytogenesis occurs at the highest rate in week four. Cultures maintained in EM have no significant change in GFP expression.

Mineralisation was significantly higher in the 33-SM group at day 21 and day 28, although substantial mineralisation still occurred at 37-SM. Cultures maintained in EM did not mineralise. These results indicate that SM is clearly needed for mineralised matrix production and osteocytogenesis. However, at 33 °C in SM the osteoblast phenotype capable of mineralising with high ALP activities is maintained, whereas at 37-SM, IDG-SW3 become osteocytes, decreasing ALP and increasing GFP expression.

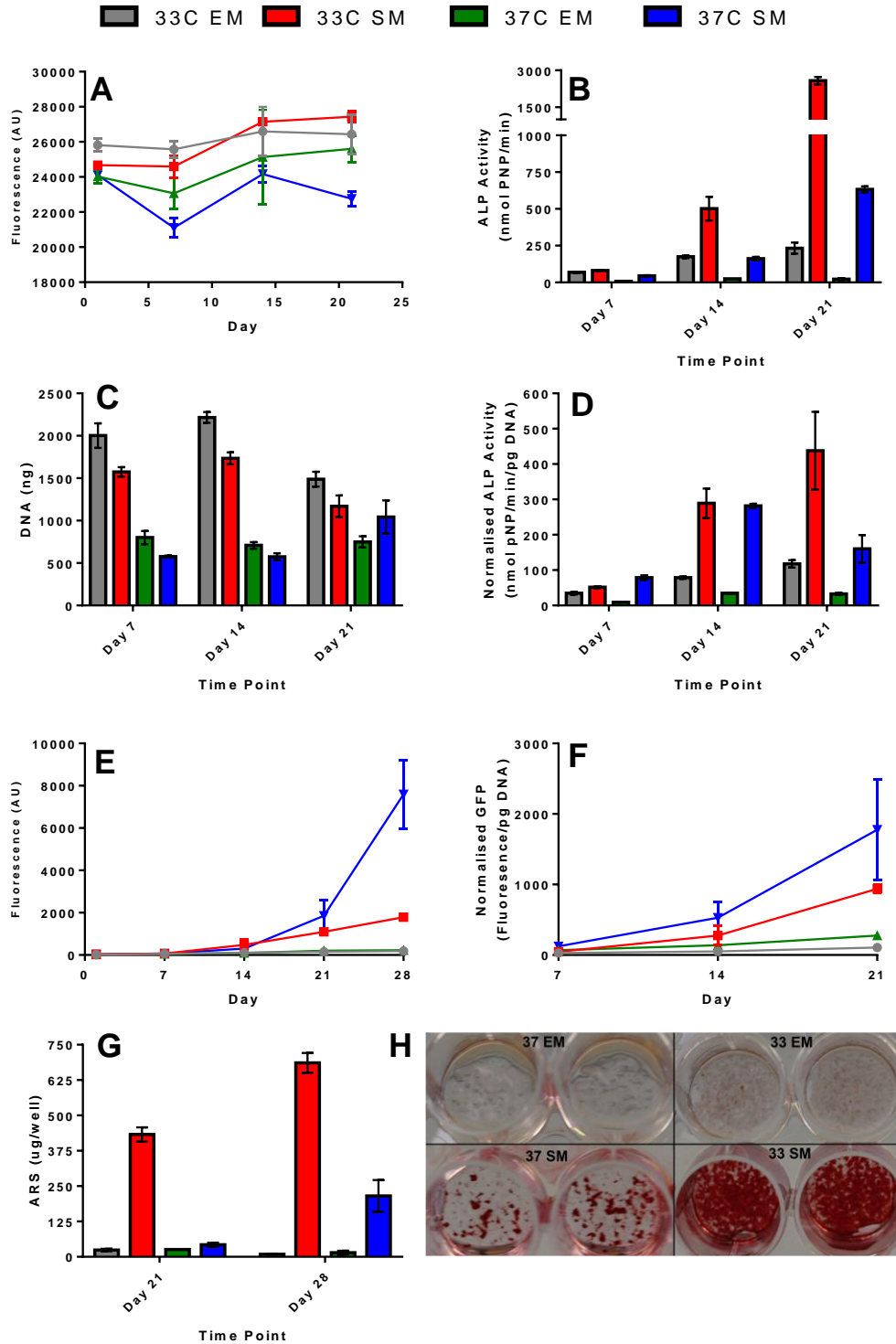


Figure 4.9: Effect of varied temperature and media composition on IDG-SW3. (A) metabolic activity (B) ALP activity (C) total DNA (D) normalised ALP activity (E) GFP expression and (F) normalised GFP expression (H) photograph of ARS staining before quantification in IDG-SW3 (n=4).

4.4.8 RANKL:OPG Ratio

The ratio of RANKL to OPG is an important determinant of whether osteoclastogenesis will occur. To compare the ratios of the three cell lines, all three were seeded either as a monolayer in a well plate at 200,000 per well in a six well plate or in a 5 × 5 PU scaffold at 60,000 per scaffold and maintained for seven days in their differentiation media. 1 mL of the media was then taken for ELISA analysis (Fig. 4.10).

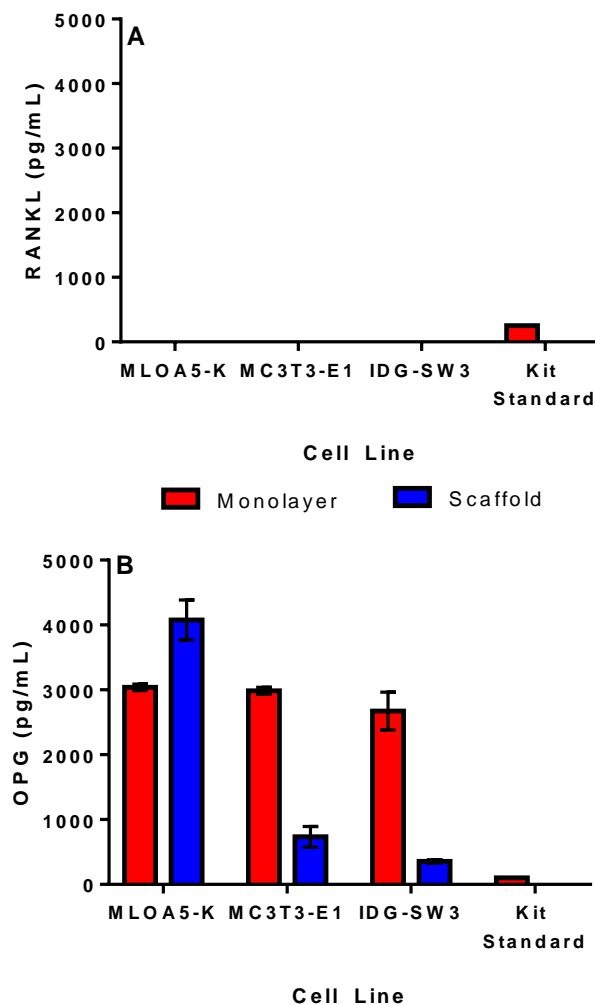


Figure 4.10: Day 7 RANKL and OPG production in various osteoblastic cell lines. Concentrations of (A) sRANKL and (B) OPG as determined by ELISA on day 7. No detectable sRANKL in any condition. OPG not significantly different in monolayer, MLOA5-K significantly higher in scaffolds than MC3T3-E1 and IDG-SW3 ($n=3$).

No RANKL was detectable from any cell line in monolayer or scaffolds culture. The ELISA was performed correctly as evidenced by the standard curve produced and the control kit standard provided being in the correct range. OPG production was not significantly different for any cell line in 2D; however, levels were significantly lower in 3D for MC3T3-E1 and IDG-SW3 in comparison to MLOA5-K.

Performing ELISAs on cell culture media can only evaluate the presence of soluble/secreted isoforms of the cytokines. Vitamin D3 has been shown to induce RANKL production. Therefore, MC3T3-E1 and IDG-SW3 were cultured with or without 10 nM vitamin D3 for seven days and media samples taken prior to digestion using the cell extraction protocol in §4.3.2. ELISAs were then performed on the media and lysates for RANKL. Normalised ALP activities were also determined from the lysates. The addition of vitamin D3 was found to cause cell death in the IDG-SW3, whereas the addition of the vehicle control did not. From changes in media colour this appeared to be due to a pH change; therefore, the effect of the addition of 10 mM of (4-(2-hydroxyethyl)-1-piperazineethanesulfonic acid) (HEPES) pH buffer was also evaluated (Fig. 4.11).

Neither cell type produced a detectable amount of RANKL in either the media or lysate whether vitamin D3 was present or not, indicating that neither cell type produces either the soluble or membrane-bound isoform. The addition of vitamin D3 had no effect on the ALP activity of MC3T3-E1. However, the presence of vitamin D3 significantly reduced the ALP activity of IDG-SW3 ($p < 0.01$). The presence of HEPES had no significant effect on ALP activity whether vitamin D3 was present or not. Media containing vitamin D3 was visibly more orange 24 hours after addition in comparison to vehicle-only controls, indicating a more acidic pH. By comparing the cell phenotype using an optical microscope, there were clearly dead or dying cells in wells treated with vitamin D3. Total DNA values on day 7 were approximately 50% lower by day 7 in treated wells. No such effect was seen on MC3T3-E1.

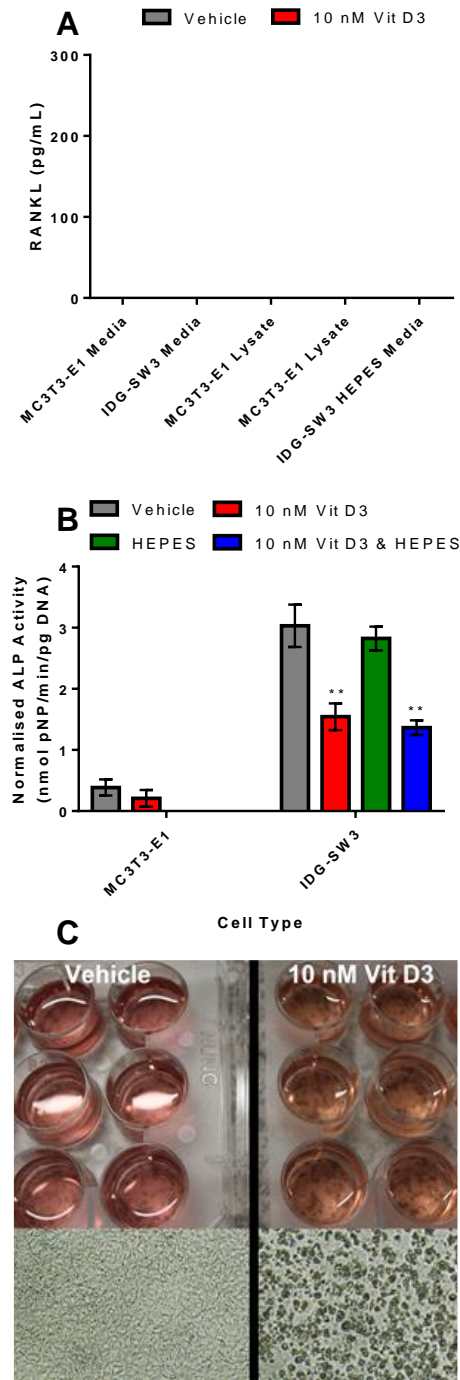


Figure 4.11: Effect of Vitamin D on RANKL production in MC3T3-E1 and IDG-SW3. (A) sRANKL and mRANKL concentrations of MC3T3-E1 and IDG-SW3 with and without vitamin D3 and (B) effect of vitamin D3 on normalised ALP activity of MC3T3-E1 and IDG-SW3 on day 7 (n=3) (C) Photo culture medium and cell phenotype after addition of vehicle and 10 nM vitamin D3.

The expression and ratio of RANKL and OPG expressed by osteoblastic cells changes as they progress from progenitor to osteocyte. Osteoblast precursors typically have a high RANKL:OPG ratio (high RANKL and low OPG), which decreases as they differentiate and produce osteoid (RANKL decreases, OPG increases), reducing their ability to induce osteoclastogenesis [210]. However, osteoblasts that become embedded in the bone and terminally differentiate into osteocytes are capable of inducing osteoclast differentiation through RANKL expression, showing that the RANKL:OPG ratio does not continually decline. MLO-Y4 osteocytes have been shown to induce osteoclastogenesis in direct cell-cell contact as they produce mRANKL [211].

The ELISAs performed thus far have tested the supernatants and cell extracts of osteoblasts which are thought to have the lowest RANKL expression in comparison to the rest of the osteoblast lineage. IDG-SW3 are capable of undergoing osteocytogenesis. To determine whether this differentiation results in a change in their ability to synthesise RANKL, the experiment exploring the effect of oestrogen on IDG-SW3 in §4.4.6 was continued to fully allow osteocytogenesis to occur [283]. GFP expression was measured and media supernatants collected each week for RANKL and OPG ELISA. On day 35, cells were digested using the enhanced digestion technique, allowing mRANKL to be determined.

The greatest increase in osteocytogenesis occurred in the fourth and fifth weeks of culture (Fig. 4.12). In the first four weeks of culture there was no significant effect of oestrogen on osteocytogenesis. However, at day 35, 100 nM of oestrogen had significantly higher GFP expression than 0 nM ($p < 0.01$). Through fluorescence microscopy, GFP expression was found to localise to areas of mineralisation (Fig. 4.13).

No sRANKL was detectable at any time point. OPG expression increased at each time point, and was over the detection limit of the ELISA on days 28 and 35. mRANKL was only detectable on day 35 in cultures containing oestrogen, with 100 nM oestrogen having the highest mRANKL expression of approximately 0.75 ng/mL.

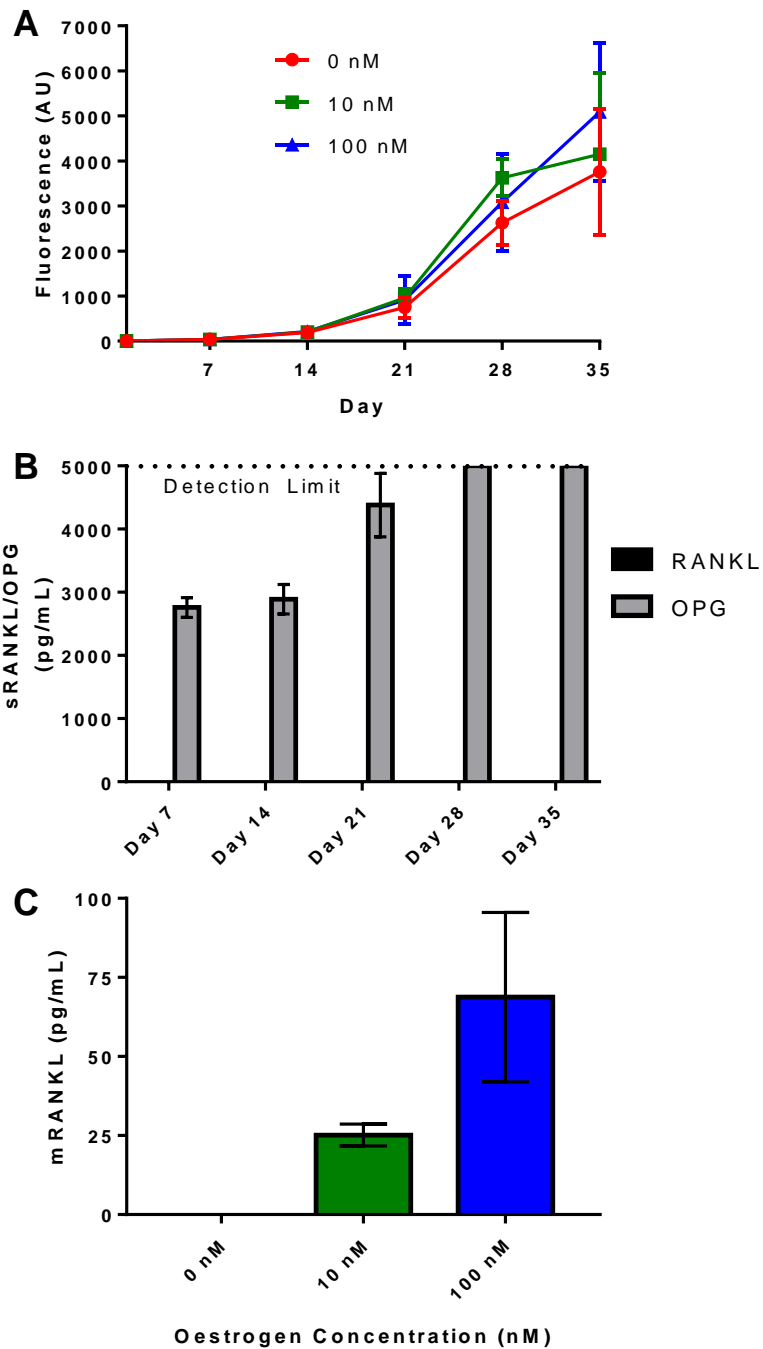


Figure 4.12: The effect of oestrogen and osteocytogenesis on RANKL expression. (A) oestrogen had no significant effect on GFP expression at any time point, except D35 where 100 nM was significantly greater than 0 nM ($p < 0.01$) ($n = 6$) (B) OPG expression increased at each time point and was above the detection limit on D28 and 35. No sRANKL detectable at any time point ($n = 3$) (C) Oestrogen exposure was necessary for mRANKL detection on day 35 ($n = 3$).

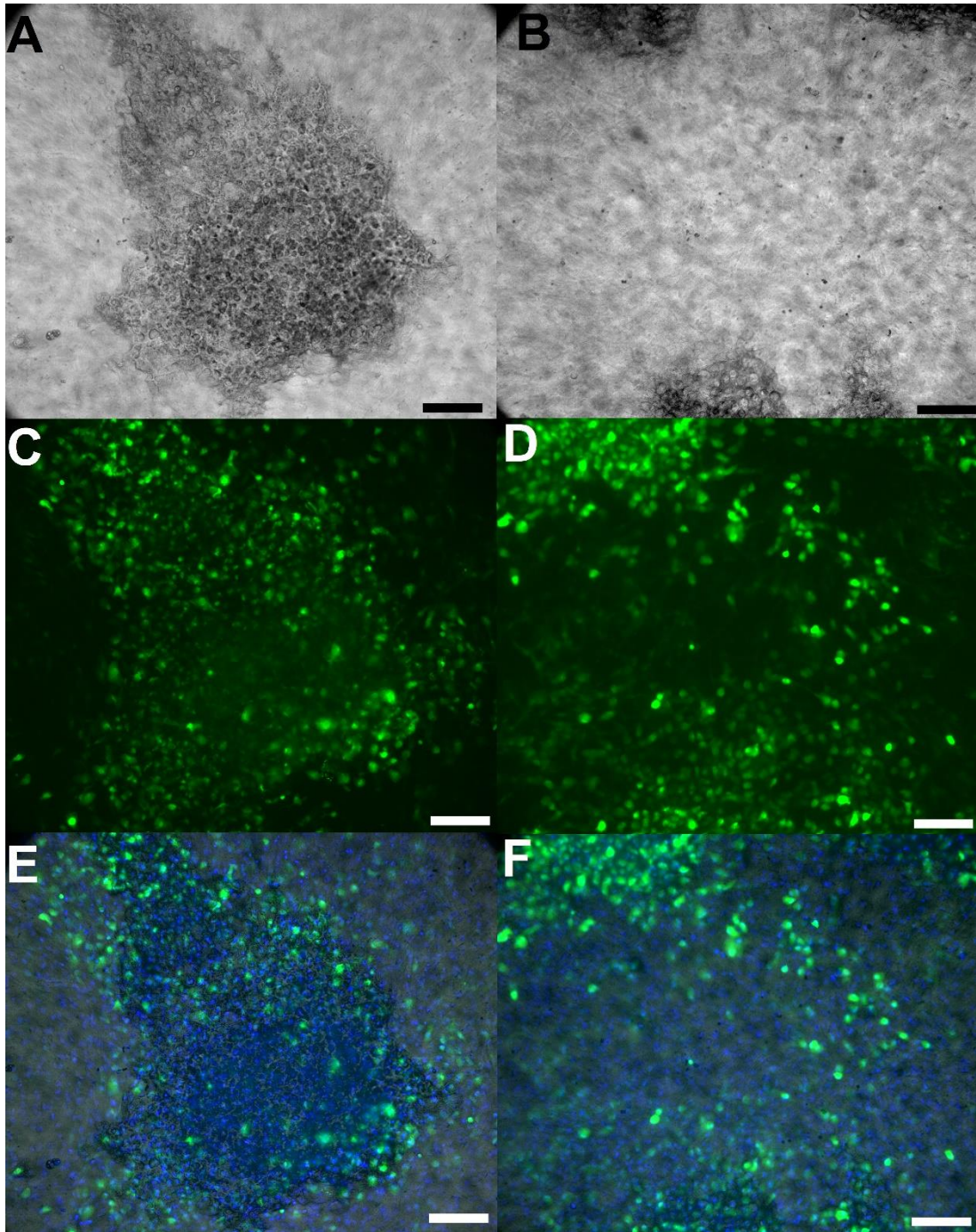


Figure 4.13: Composite images of IDG-SW3 GFP fluorescence. GFP fluorescence localises to regions of mineralisation. Left column: mineral in centre, Right column: mineral at top and bottom only. (A&B) Brightfield images (C&D) GFP fluorescence (E&F) Composite of brightfield, GFP and DAPI nuclei staining. All at 10 \times magnification, same exposure for each wavelength. Scale bar 200 μ m.

4.4.9 RAW264.7 mature in the presence of sRANKL

To mature osteoclast precursors into osteoclasts they need to be stimulated with M-CSF and RANKL. RAW264.7 inherently produces M-CSF; therefore, only exogenous supplementation with RANKL is necessary to stimulate osteoclastogenesis. Mature was defined as a large, multinucleated, TRAP positive osteoclast capable of resorbing a substrate.

To ensure that the source of RAW264.7 used was capable of undergoing osteoclastogenesis they were initially seeded at 20,000 cells/well in a 6 well plate and cultured with 25 ng/mL RANKL for six days (Fig. 4.14A-C). Clear purple staining for TRAP was only visible in cultures with RANKL. In cultures with RANKL, large, multinucleated osteoclasts were visible and well as smaller, TRAP positive macrophages. To confirm multinucleation, cultures were stained with Hoechst 33342 and imaged on day 6. Overlays of brightfield and fluorescent images show that multinucleation only occurs with RANKL (Fig. 4.14D-F). From the position of the nuclei around the perimeter of the large osteoclasts, it is possible to see the typical ring shape formed by actin, another marker of osteoclast maturity.

Osteo Assay Surface plates have a thin film of inorganic crystalline calcium phosphate on the culture surface to mimic bone material. In the presence of mature osteoclasts, areas of this film will be removed, leaving visible pits in the surface. RAW264.7 were seeded onto Osteo Assay Surfaces at 20,000 cells per well and cultured in either 0, 25 or 50 ng/mL of RANKL for 12 days before bleaching. Wells were either left unstained, or stained with toluidine blue or Von Kossa (Fig. 4.15). Whole wells were imaged at 10 × magnification using automated stage control software (MetaMorph®, Molecular Devices LLC). Images could not be stitched to create a composite image due to a lack of discernible features in each image for an algorithm to identify. Therefore, ten images were selected at random for each well using a random number generator to assess resorption pit formation. Cultures without RANKL did not mature and no resorption pits were detectable. Cultures with 25 ng/mL RANKL formed multinucleated osteoclasts, but resorption pits were small and sparse. 50 ng/mL RANKL resulted in frequent, large resorption pits over the entire culture surface. Due to the film being only microns thick, staining was not found to enhance contrast.

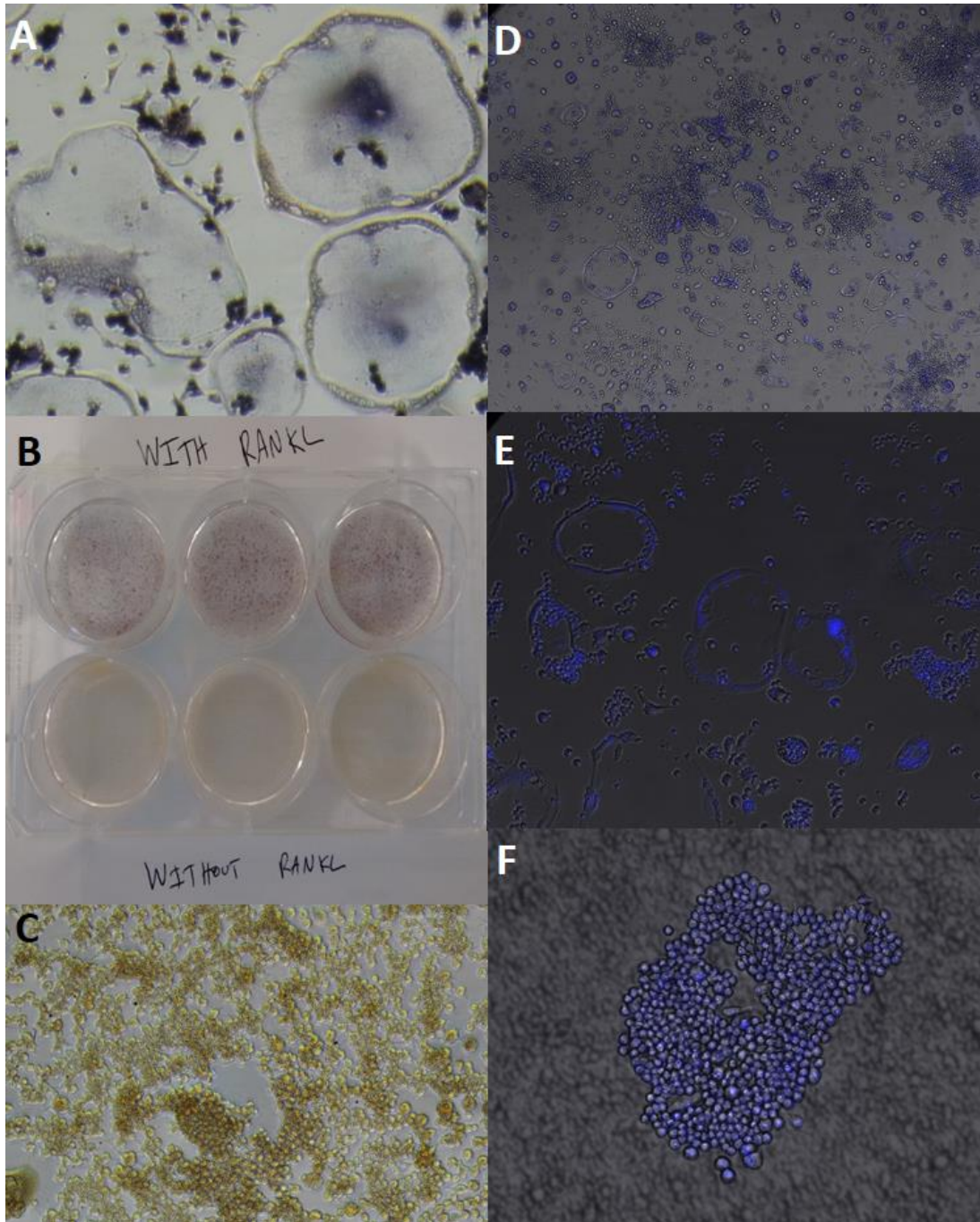


Figure 4.14: Effect of RANKL on RAW264.7. TRAP staining of RAW264.7 (A) cultured with 25 ng/mL RANKL at high magnification (B) whole well plate view showing clear positive staining with RANKL (C) without RANKL at the same magnification as (A). Hoechst 33342 staining day 6 (D) 6 × magnification with RANKL (E) 15 × magnification with RANKL (F) 6 × magnification without RANKL.

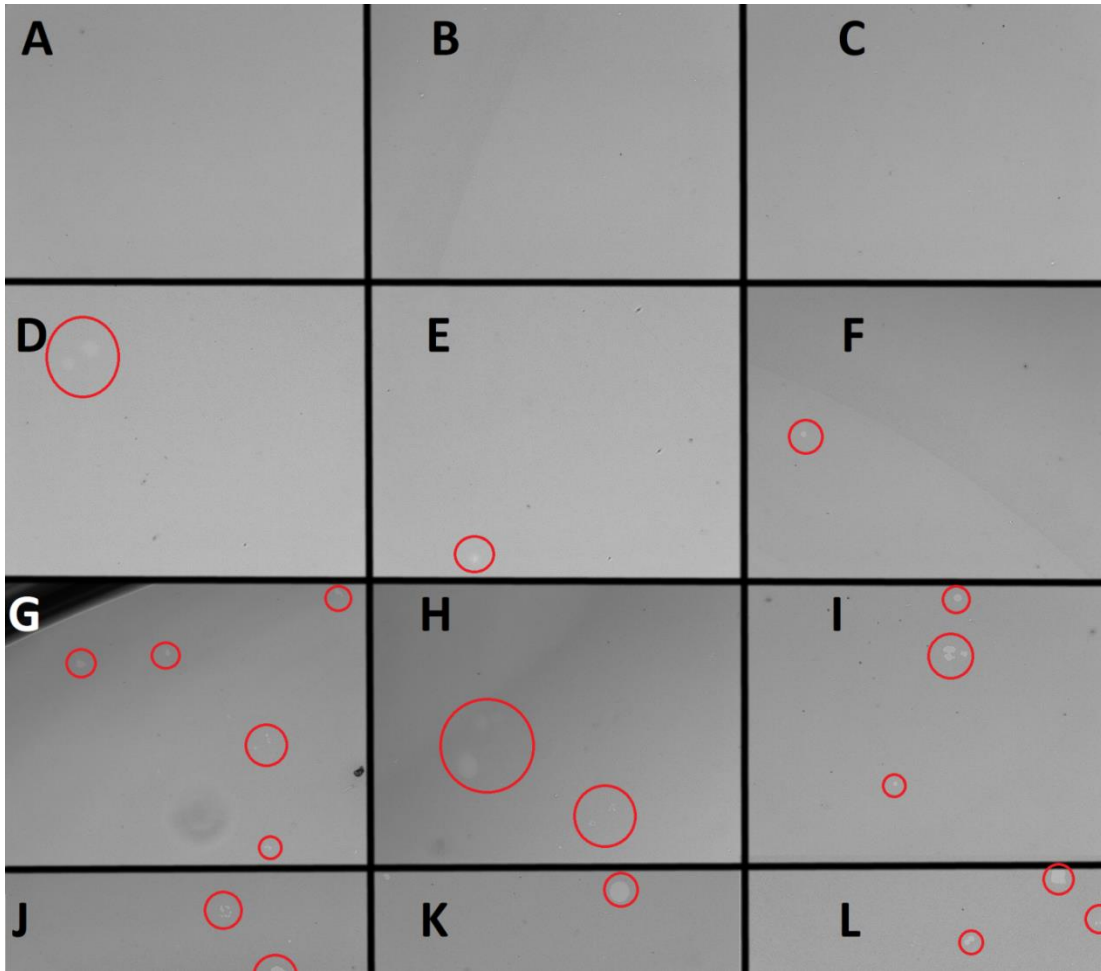


Figure 4.15: Analysis of RAW264.7 resorption. Brightfield images of randomly selected well regions. Resorption pits circled in red. (A-C) 0 ng/mL RANKL, no pits detected. (D-F) 25 ng/mL RANKL. Some pits, sparse, small. (G-L) 50 ng/mL RANKL, multiple pits, often in groups, range of sizes from very small to large. Present throughout well.

4.4.10 TRAP activity is dose dependent and is significantly reduced by digestion

As with ALP activity, it is also possible to quantify TRAP activity from cell lysates, rather than qualitatively staining. The advantage of this is that ALP and TRAP activity and total DNA can be quantified for the same sample, which reduces the number of experimental wells/scaffolds needed as a separate one is not needed for each assay. To determine the most efficacious method of quantifying TRAP activity, RAW264.7 were seeded at 5,000 cells per well in a 24 well plate in 25 ng/mL of RANKL and cultured for ten days. TRAP activity was then determined by either direct application of the assay substrate, as outlined in §3.2, or by digesting using the standard, PBS or enhanced method and combining the lysates with the assay substrate, as outlined in §4.3 (Fig. 4.15A&B). To determine the effect of RANKL on TRAP activity, RAW264.7 were seeded at 5,000 cells per well in a 24 well plate in either 0, 25 or 50 ng/mL of RANKL and cultured for six days before digesting using the PBS method and determining TRAP activity (Fig. 4.16).

There were no significant differences in the TRAP activities of the normal, PBS or enhanced digestion protocols. Direct measurement of TRAP yielded a significantly higher apparent TRAP activity than any of the digestion protocols. Cells were digested in 1 mL of digestion buffer and 250 μ L was analysed, therefore it was anticipated that the TRAP activity would be one quarter of the direct method. However, direct measurement is 8 times higher than the highest digestion method (direct mean 0.19 vs PBS mean 0.02375). Therefore, half of the apparent TRAP activity is lost by digesting. This could be due to loss of the amount of enzyme during the digestion process or a loss of enzyme efficacy because of the digestion process. Visually, no discernible yellow colour change is observed for the lysate activities after adding the stop solution.

TRAP activity increases with RANKL concentration. Due to the significant reduction in apparent TRAP activity in cell lysates, all TRAP activity described in the rest of this thesis was performed using the direct method.

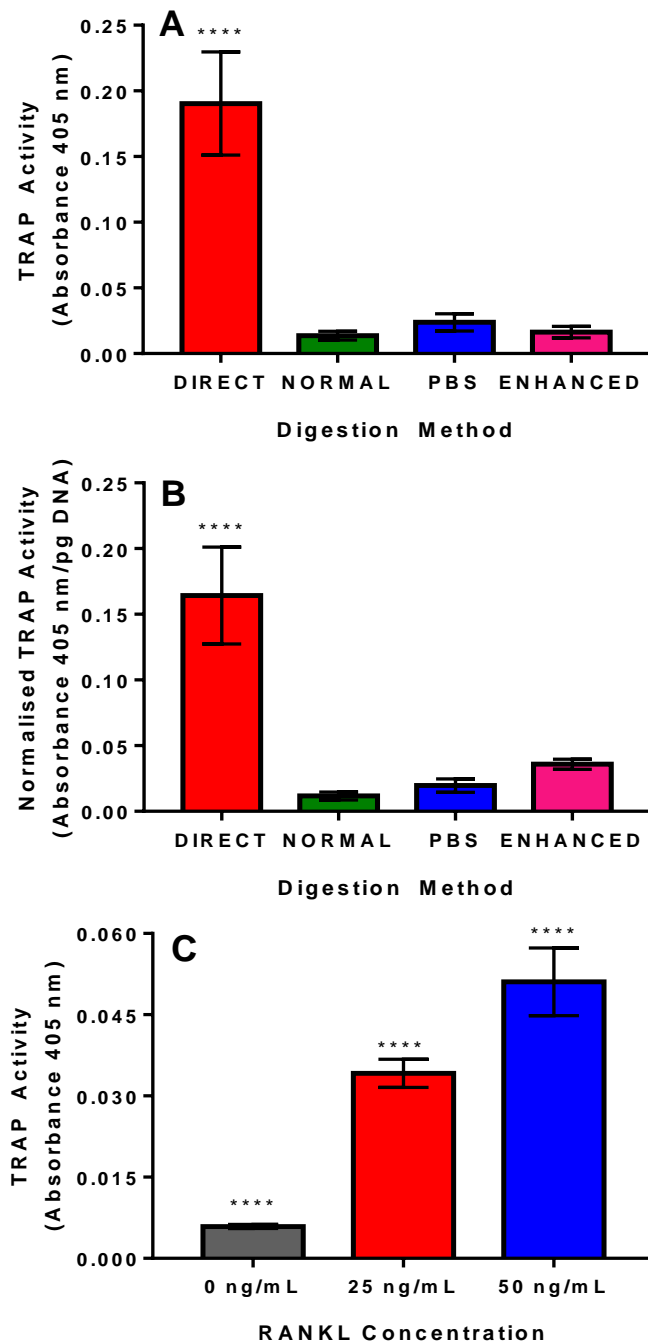


Figure 4.16: Comparison of digestion protocol on apparent TRAP activity. Mean \pm SD of (A) TRAP and (B) Normalised TRAP activity for different digestion methods. DIRECT TRAP normalised to NORMAL digestion DNA. DIRECT significantly higher ($p < 0.0001$) than all other methods. No significant difference between any digestion method. (C) TRAP activity at 0, 25, or 50 ng/mL RANKL. Activity significantly increases with RANKL concentration ($n=6$).

4.4.11 Seeding density affects osteoclastogenesis

To assess the effect of seeding density on the ability of osteoclast precursors to mature, RAW264.7 were seeded at either 400 to 5,000 cells per well in a 96 well plate and cultured for six days in either 0, 25, or 50 ng/mL of RANKL before determining TRAP activity (Fig. 4.17).

As seen in when using digestion, response to RANKL is dose-dependent. No TRAP activity was present without RANKL and 50 ng/mL RANKL resulted in significantly higher TRAP activity at every seeding number than 25 ng/mL. For both RANKL exposures, there was no significant difference between 400 and 1,000 cells and between 2,500 and 5,000 cells. For both concentrations, 400 and 1,000 were significantly higher than 2,500 and 5,000 cells. The culture surface area of a 96 well plate is 0.32 cm²; therefore, the optimal seeding density is approximately 3,000 cells/cm².

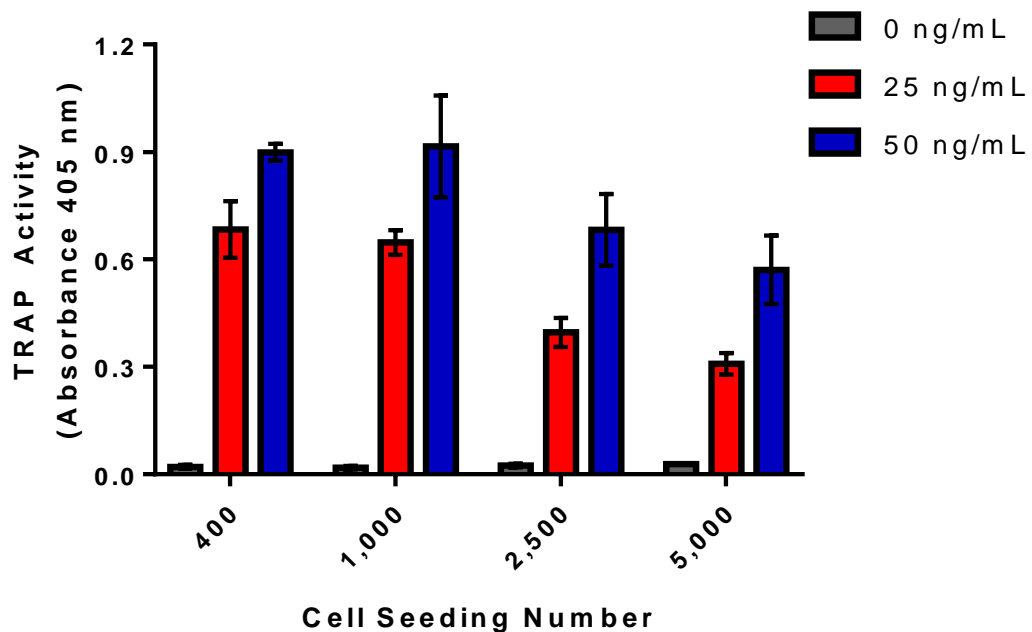


Figure 4.17: TRAP activity in response to varied RANKL concentrations and seeding number. 50 ng/mL significantly higher than 25 ng/mL for every seeding number. No significant difference between 400 and 1,000 cells at 25 or 50 ng/mL. 400 and 1,000 significantly higher than 2,500 and 5,000 at 25 and 50 ng/mL (n=4).

4.4.12 Oestrogen inhibits osteoclast viability and activity

Oestrogen inhibits the RANK/RANKL pathway and upregulates osteoclast apoptosis. To determine its effects on RAW264.7, cells were seeded at 20,000 cells per well in a six well plate and cultured with 50 ng/mL RANKL and either 0, 10 or 100 nM 17 β -estradiol for sixteen days. Metabolic activity was assessed by RR on days 1, 5, 12, and 16 and TRAP activity and total DNA quantified on day 7 (Fig. 4.18).

10 nM oestrogen had no significant effect on metabolic activity at any time point. 100 nM significantly lowered metabolic activity from day 5 onwards, with a dramatic decrease on day 16. 10 nM did lower the total DNA in comparison to 0 nM, but not significantly, whereas the reduction at 100 nM was significant. 100 nM oestrogen also significantly reduced the total TRAP activity. Interestingly, the reduction in DNA and TRAP activity at day 7 was 28% and 27%, respectively, meaning that normalised TRAP activities were similar and indicating that the reduced activity may be due to the effect on cell lifespan.

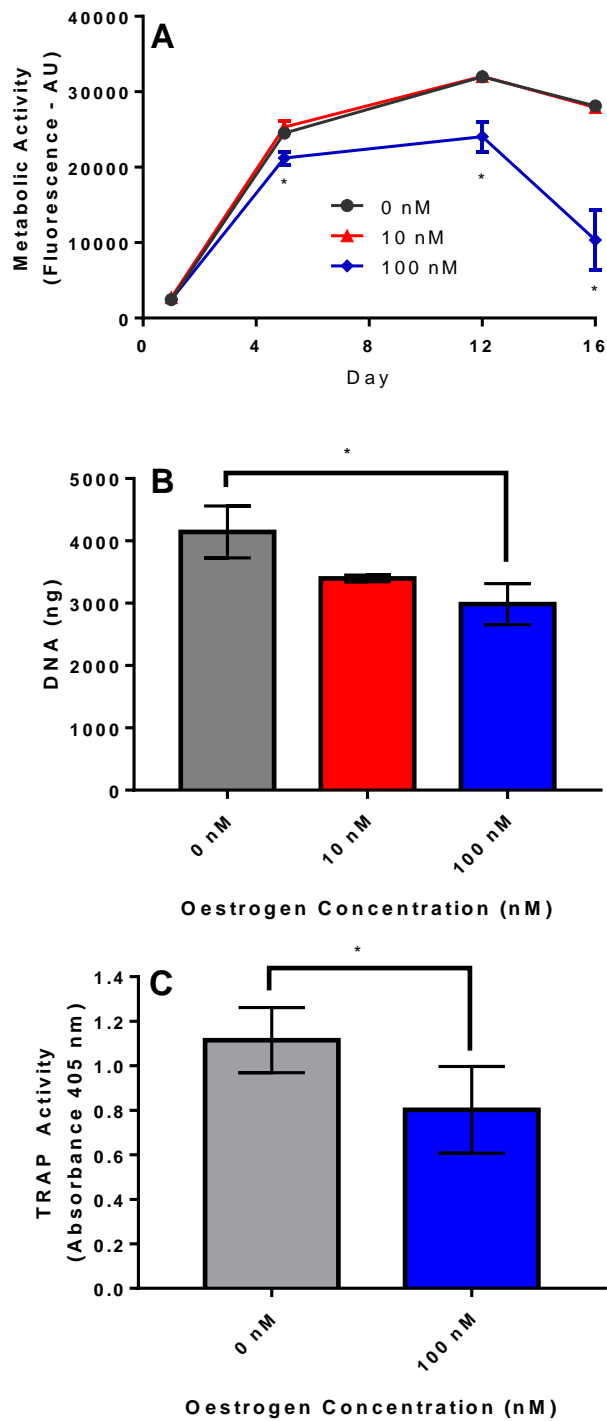


Figure 4.18: Effect of oestrogen on RAW264.7. (A) metabolic activity - significantly lower at 100 nM from day 5 onwards, no difference between 0 and 10 nM (B) DNA – only 100 nM significantly lower (C) TRAP activity – 100 nM significantly lower (n=3-6).

4.4.13 IDG-SW3 support osteoclastogenesis in direct co-culture

As seen by the RANKL ELISA, none of the potential osteoblast cell lines secrete detectable sRANKL or mRANKL. This means that in the co-cultures performed in the *in vitro* model of postmenopausal osteoporosis developed in chapter 6, exogenous RANKL will have to be added to induce osteoclastogenesis. However, they do produce OPG, an antagonist for RANKL. This means that the RANKL:OPG ratio will still be affected by the presence of osteoblasts.

As OPG has the potential to completely negate the effects of RANKL at high enough concentrations, co-cultures of MLOA5-K or IDG-SW3 with RAW264.7 were performed to determine which cell line has a RANKL:OPG ratio amenable to osteoclastogenesis. MC3T3-E1 were not used due to their low level of mineralisation. Osteoblasts were seeded at 1,500 cells/cm² in a 12 well plate before the addition of 3,000 RAW264.7/cm² 24 hours later. The cultures were maintained for 7 days with either 0 or 50 ng/mL RANKL and compared to monocultures of osteoblasts or RAW264.7 (Fig. 4.19).

For both co-cultures, no TRAP activity was present without exogenous RANKL addition, confirming that neither mRANKL or sRANKL are being produced by the osteoblasts. In co-culture with MLOA5-K, osteoclastogenesis did not occur as the TRAP activity was not significantly different to the MLOA5-K monoculture. Exogenous RANKL did not increase the co-culture activity, potentially due to overwhelming OPG production. In co-culture with IDG-SW3, TRAP activity was significantly higher when exogenous RANKL was added but significantly lower than the RAW264.7 monoculture. This could be due to OPG production by the osteoblasts, but in smaller quantities than MLOA5-K.

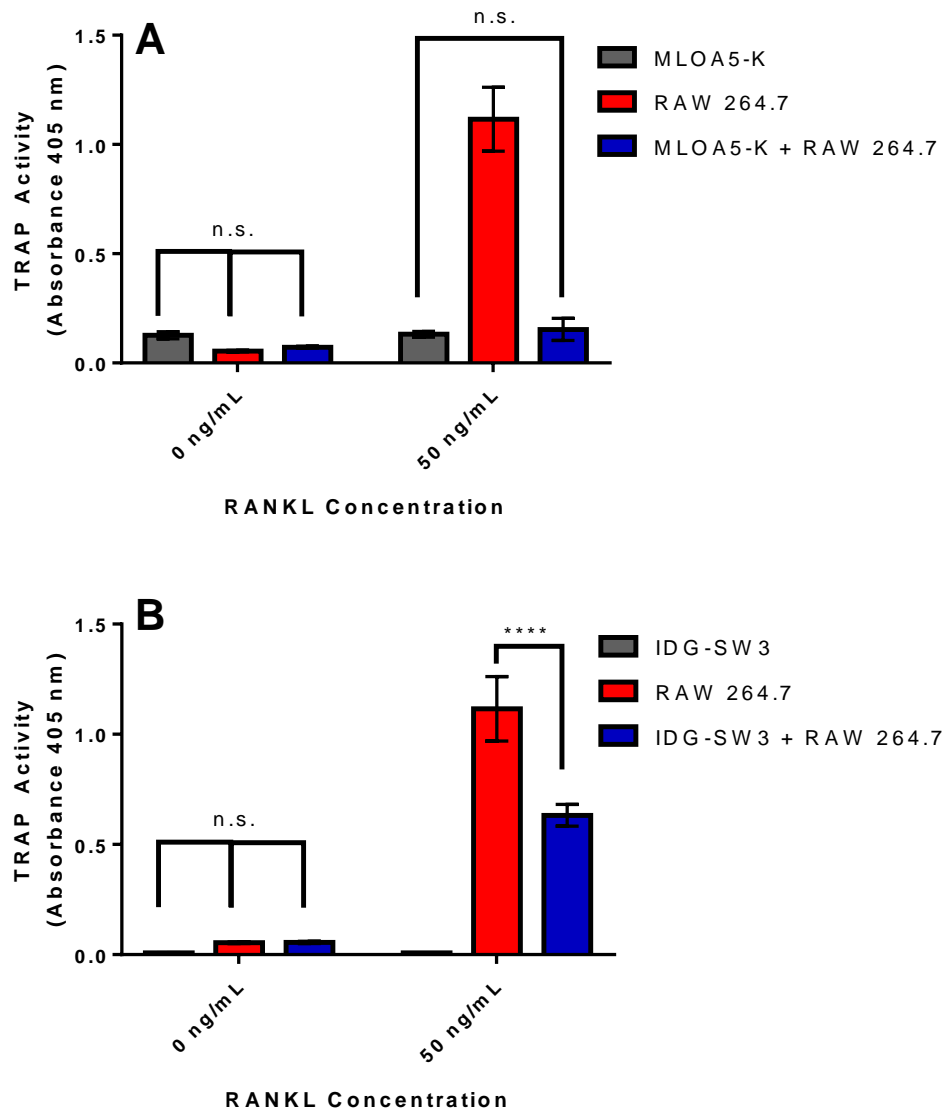


Figure 4.19: Day 7 TRAP activity for co-cultures of (A) MLOA5-K and RAW264.7 and (B) IDG-SW3 and RAW264.7. Neither osteoblast could stimulate osteoclastogenesis without exogenous RANKL. MLOA5-K inhibited osteoclastogenesis in co-culture. TRAP activity was lower in co-culture with IDG-SW3 than mono-culture, but still substantial (n=6).

4.4.14 RAW264.7 failed to resorb *ex vivo* tissue

In addition to quantifying resorption on the Osteo Assay Surface, RAW264.7 were also cultured on bovine trabecular bone and dentine to see whether resorption pits could be identified. Cultures were maintained for 16 days with 50 ng/mL (bone) or 100 ng/mL (dentine) RANKL before SEM examination (Fig. 4.20).

From the SEM images, it is clear that osteoclasts were able to adhere, mature and grow. However, it was not possible to identify clear resorption pits on either substrate.

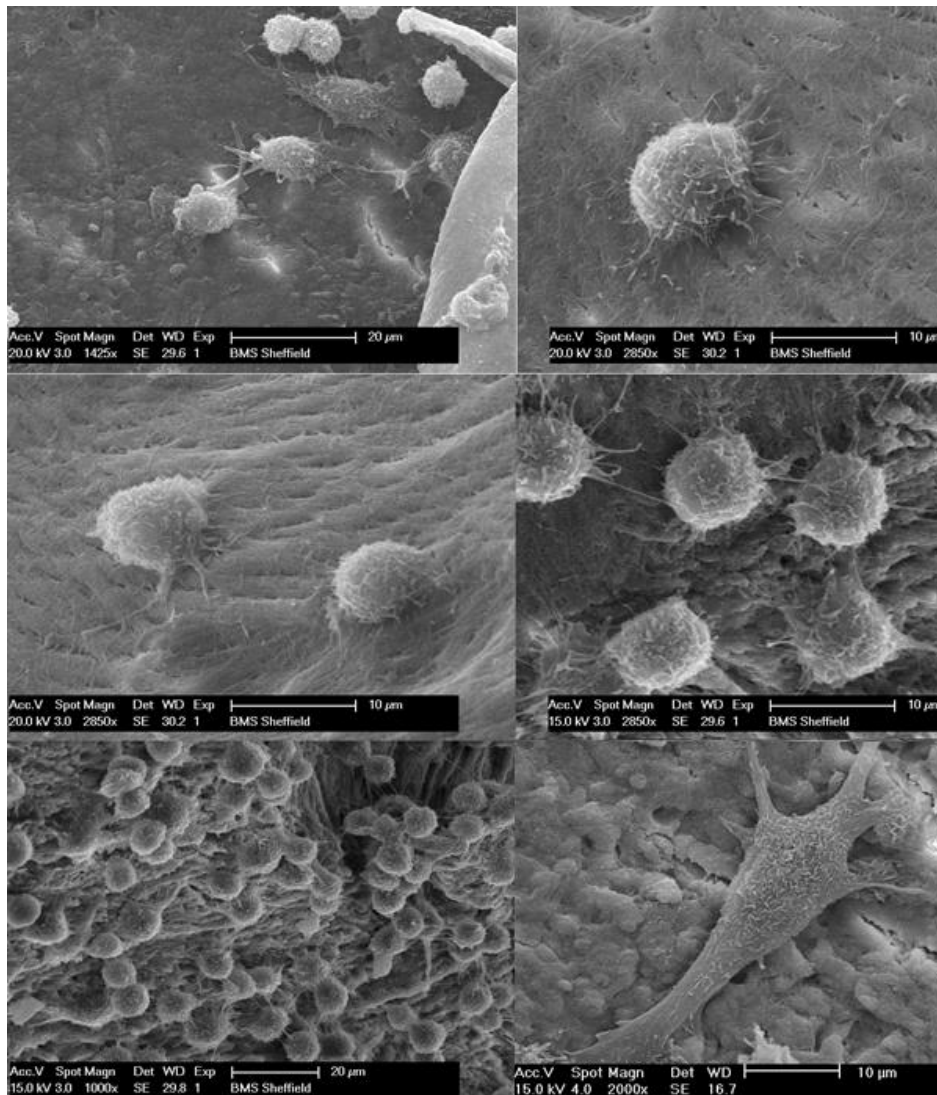


Figure 4.20: Composite of multiple SEM images of RAW264.7 on trabecular bone and dentine (bottom right).

4.5 Discussion

The work performed in this chapter primarily aimed to determine the effects of oestrogen on a range of bone cell lines with the aim of selecting an osteoblast and osteoclast cell line suitable for an *in vitro* model of postmenopausal osteoporosis. First, the effect of potentially oestrogenic factors in culture media was considered, then a range of common osteoblast cell lines were exposed to various oestrogen concentrations and treatment regimens and the effects on their activity evaluated. The effect of oestrogen and varied seeding density on RAW264.7 osteoclastogenesis was then examined, and finally, preliminary co-cultures of osteoblasts and osteoclasts were performed to allow the most suitable cell lines to be selected.

Initially the effect of phenol red in the media was assessed. Phenol red is a pH indicator commonly found in cell culture media. It has structural similarities to some non-steroidal oestrogens and can have oestrogenic effects, for example strongly promoting cell proliferation, progesterone receptor expression and susceptibility to chemotherapy in MCF-7 breast cancer cells [312]–[314]. Additionally, it has been found to have oestrogenic effects on bone cells *in vitro* [315]. However, other work suggests that its concentration in culture media is not sufficient to cause oestrogenic effects [316]. The PC and PF media used here both resulted in a higher proliferation rate of MC3T3-E1 than the regular BM. This is likely due to them being more ‘complete’ compositions of α -MEM as they contain ribonucleosides and deoxynucleosides. ALP activity is normalised to DNA, therefore the differences in cell number due to differences in proliferation rate are accounted for. It can be seen that there is no significant difference in ALP activity per cell between media types at 0 nM and 100 nM oestrogen. Mineralisation is higher in the PC and PF media due to the greater cell number. However, there is no significant difference in mineralisation at different oestrogen concentrations. Although the absolute values differ between PC and PF for ALP activity and mineralisation, the same response to oestrogen is seen whether phenol red is present or not, even at 0.1 nM. Therefore, it does not seem necessary to use phenol free culture medium. In addition to the oestrogen added to the cultures, it is likely that it is also present in the FBS added to the media. This effect could be removed by charcoal stripping FBS, removing hormones, growth factors and cytokines from the serum [317]. However, this process will cause differences in cellular performance in comparison to non-stripped FBS due to the removal of these factors, and as an effect of oestrogen can be seen without charcoal stripping, it seems unnecessary in this work. A better alternative to charcoal-stripping would be to use a serum-free or chemically

defined medium. This allows confidence that none of the factors being studied are already present in the culture medium and that no unknown factors are masking effects that would otherwise be observed. However, due to the high comparative cost and difficulties in identifying suitable media, it was instead decided to use a single batch of FBS for all experiments to maintain the same concentration of factors within the serum.

Although the effects of oestrogen withdrawal on MC3T3-E1 are not in full agreement with the work by Brennan et al., who showed that withdrawal significantly increased activity [308], the response seen here would still be applicable for the *in vitro* model. It is believed that postmenopause, osteoblast activity increases. However, due to the much greater increase in osteoclast activity, the net result is bone loss and therefore the increase is not evident, with the possible exception of increased mineral content in certain regions of the skeleton [144], [292], [293]. Therefore, if in the model to be developed oestrogen withdrawal does not promote osteoblast activity, the net effect will be similar as the amount of bone will reduce. This means that MC3T3-E1 could have been applicable for the model if they were able to mineralise sufficiently. Although mineralisation can be increased by doubling the osteogenic supplementation, these high phosphate concentrations have been related to detection of non-cell produced mineralisation as a result of spontaneous precipitation of calcium phosphate [318]. These deposits have a reduced ratio of calcium and phosphate ions in the mineral deposited in comparison to hydroxyapatite *in vivo*, where the ratio is approximately 1:1.63 [319]. As this spontaneous mineralisation does not represent what happens physiologically, where the mineral deposition is performed by osteoblasts, it would be more suitable to use an osteoblast cell line that had a higher mineralisation capacity at 5 mM β GP.

MLOA5 are capable of rapidly depositing mineralised extracellular matrix in sheets and have a typical post-osteoblast phenotype [284]. However, both MLOA5-S and MLOA5-K were found to not respond to oestrogen withdrawal or oestrogen exposure in the same way as MC3T3-E1, with no significant effect on ALP activity or ARS staining). This could have been due to much higher metabolic activity than MC3T3-E1; however, as a response was not seen at a concentration 100,000 \times greater than that used to stimulate MC3T3-E1 this seems unlikely. Furthermore, this concentration of 17 β -estradiol is many orders of magnitude higher than the levels found in serum in mice, whereas 10 – 100 nM is more physiologically relevant [320]. It seems more likely that this cell line is already producing ALP and mineralising at its maximum

capacity, and therefore cannot be further stimulated using oestrogen. This inability to further upregulate ALP activity and mineral deposition in the MLOA5 cell lines agrees with the findings of Wittkowske during a parallel project, who found that mechanical stimulation was unable to upregulate these processes, despite published results showing their responsiveness [321], [322].

It is possible that the detachment observed in some MLOA5 cultures was due to an increase in cell proliferation in response to oestrogen exposure. At the start of puberty when oestrogen levels begin to increase, epiphyseal growth is promoted causing the characteristic 'growth spurt', indicating the effects it can have on osteoblast-lineage cell proliferation [323]. Furthermore, *in vitro*, oestrogen has been shown to accelerate cell proliferation [299], [300]. However, it does not always promote proliferation, as high oestrogen levels towards the end of puberty promote bone maturation and epiphyseal fusion, and there are also *in vitro* studies that show it can slow down cell proliferation [301]. Therefore, due to the conflicting effects of oestrogen on cell proliferation, the sporadic nature of MLOA5 detachment, and the very high proliferation rate of the cell line even prior to treatment, it seems more likely that the detachment overserved was due to the inherent tendency of the cell line to overgrow in monolayer cultures regardless of any treatment applied.

One potential reason for MLOA5 being unable to respond to oestrogen is that they may lack ER α . To date, no study has explored whether this cell line responds to oestrogen or has oestrogen receptors, and it was not mentioned in the original literature detailing its development [284]. However, as the cell line was developed from a mouse and there is no good reason that the protocol used would have removed ER α , it seems unlikely that the original MLOA5 would have lacked the receptor.

Three different sources of MLOA5 were assessed in this work. MLOA5-K seem to be the variant most similar to that originally described by Kato, et al. [284]. However, in comparison to the original literature, none of the MLOA5 variants, including that purchased directly from the original developer, behave as originally described. All of the variants were provided at a high passage (minimum 20); therefore, differences may be explained by careless passaging where the fastest proliferating cells have unintentionally been selected for, similar to how multiple subclones of MC3T3-E1 were developed [281]. Furthermore, passage number is a poor description of a cell lines age as it does not take into account splitting at different ratios or confluences. Where possible, all work done in this thesis was from cell banks created before

experiments began to ensure that all cells seeded for experiments were the same age. Where new cell lines were purchased, passage doubling level rather than passage number was recorded so that an accurate record of the cell 'age' could be kept.

IDG-SW3 is a relatively newly developed cell line. As with MLOA5, to date the effect of oestrogen on their activity has not been explored. Here it has been found that oestrogen has no significant effect on proliferation, ALP activity or mineralisation. However, the findings that only one out of three osteoblast cell lines responded positively to oestrogen is not unthinkable. Reports on the effects of 17β -estradiol on osteoblast behaviour are varied and contradictory [299]–[304], and reports on response to oestrogen withdrawal *in vitro* are sparse. Furthermore, although there is evidence for increased tissue mineralisation in a heterogeneous manner to counteract whole bone weakening post-OVX, this is not a well-established response and does not occur in all bone tissues. This change in tissue-level mineral distribution was seen in ovine proximal femurs and human vertebrae, both of which undergo high physiological loads, whereas cultures here were performed under static, unloaded conditions [144], [293], [294].

IDG-SW3 are designed to proliferate at 33 °C in EM and undergo osteocytogenesis at 37 °C in SM. At 33 °C in the presence of IFN- γ they undergo continuous proliferation and are immortalised due to the presence of a temperature-sensitive mutant of the SV40 large tumour antigen that is controlled by an IFN- γ inducible promoter [283]. Once they are transferred to 37 °C and cultured in media without IFN- γ that is supplemented with β GP and AA2P they resume their normal proliferative ability and undergo osteocytogenesis. Here it was found that the control of the proliferation was predominantly due to temperature rather than the presence of IFN- γ due to the relative differences in total DNA and metabolic activity between 33-EM and 33-SM compared to 33-EM and 37-EM. ALP activity and mineralisation were an order of magnitude greater when cultured at 33-SM in comparison to 37-SM on day 21, even after normalising to account for differences in cell number. By day 28, 33-SM is still highest, but 37-SM deposited a substantial amount of mineral. As expected, the presence of osteogenic supplements, not the change in temperature, is the driving factor for their osteoblastic activity. Conversely, the highest number of osteoblasts undergoing osteocytogenesis occurred at 37 °C in SM, although SM at any temperature did induce some osteocytogenesis. This indicates that the lower temperature in combination with SM appears to hold IDG-SW3 in their osteoblast phenotype, whereas the higher temperature in combination with SM promotes

osteocytogenesis as a lower ALP activity and less mineralisation is observed. This is likely due to the cells production of sclerostin as they become osteocytes, a known inhibitor of bone formation [324].

It was observed that the most mineralised areas had the highest proportion of GFP positive IDG-SW3, indicating that there were also the most osteocytes. This finding agrees with the work of Wittkowske, who also noted that osteocytogenesis predominantly occurred in mineralised regions in IDG-SW3 cultures [322]. This finding may seem surprising as osteocytes produce sclerostin, an inhibitor of mineralisation. However, the mineralisation and osteocytogenesis processes are thought to be linked as *in vivo* osteocytes differentiate when osteoblasts become embedded in the bone matrix [325]–[327]. Therefore, it seems likely that these mineral deposits are necessary for osteocytogenesis to occur.

RANKL was not detectable in the cell culture supernatants of MLOA5-K, MC3T3-E1 or IDG-SW3 in 2D or 3D cultures at day 7. At this time point all three of these cell lines have an osteoblastic phenotype. As the expression and ratio of RANKL and OPG expressed by osteoblastic cells changes as they progress from progenitor to osteocyte, it was thought that this lack of detection may have been due the differentiative state of the cell line [210]. Therefore, the cell culture supernatants of IDG-SW3 cultures differentiated into osteocytes were tested for RANKL. As MLO-Y4 osteocytes have previously been shown to only express mRANKL, cell extracts were also analysed [211]. From GFP measurements and fluorescent images it was clear that numerous osteocytes were present after 35 days of culture; however, sRANKL and mRANKL were not detectable at any time point. However, cultures maintained in 10 nM and 100 nM oestrogen were positive for very low levels of mRANKL, indicating that the hormone may have induced its synthesis. Oestrogen is a hormone that is viewed as protecting bone; therefore, its ability to upregulate RANKL synthesis seems unlikely. It has previously been shown to upregulate OPG [328] and decrease M-CSF [95] and RANK [309] expression, but found to have no effect on RANKL production [329], [330]. It is worth noting that although it was detected, the concentration was only 25-50 pg/mL, over 100 times lower than the OPG detectable at the same time point, and 1,000 times less than the exogenous RANKL added to the media during RAW264.7 cultures. Therefore, in terms of RANKL:OPG ratios, it was not a quantity that could be utilised to induce osteoclast differentiation without exogenous additions, as the RANKL:OPG ratio would have been only 1:100, rather than 10:1.

Other studies have looked into the RANKL expression of the cell lines investigated here. MLOA5 have previously been shown to express RANKL mRNA [331]. Delgado-Calle, et al., reported detecting both RANKL mRNA and sRANKL production from MLOA5 using the same ELISA kit used here. However, their reported values are below 5 pg/mL which is the minimum detectable dose of the ELISA kit used, meaning that this may be a false positive [332]. MLO-Y4, an osteocyte cell line developed by the same group as MLOA5 and IDG-SW3, has also been shown to express RANKL mRNA and have RANKL on their cell surface and dendritic processes [211]. Sufficient amounts of RANKL are present on MLO-Y4 to stimulate TRAP positive osteoclast formation on RAW264.7 [333]. However, this cell line is unable to mineralise and therefore was not considered for the *in vitro* model. As with MLOA5, RANKL mRNA expression has also been reported in IDG-SW3 [334]–[336]. However, to the author’s knowledge, confirmation that the protein is successfully produced has not been performed. MC3T3-E1 have previously been shown to express both RANKL mRNA and produce sRANKL via ELISA, both with and without vitamin D3 in MC3T3-E1.

1 α ,25-dihydroxyvitamin D3 is the active form of vitamin D3 and is metabolised from 25-hydroxyvitamin D3 by the 1 α -hydroxylase enzyme [337]. It has previously been shown to stimulate RANKL expression in osteoblasts and osteocytes, and therefore increase osteoclast formation [193]–[195]. This is likely due to the role of vitamin D in maintaining normocalcaemia, as increased osteoclast activity can raise serum calcium through bone resorption. Paradoxically, vitamin D is administered as a therapeutic for osteoporosis due to its protective effects on BMD through suppressing bone resorption. The reasons why the opposite effects are seen *in vitro* and *in vivo* are not clear, but possible explanations include alteration of the calcium endocrine system when active vitamin D compounds are repeatedly administered, direct action on osteoblasts to suppress RANKL expression, or through action on osteoclast precursors [338].

Here the presence of vitamin D3 did not induce the production of sRANKL or mRANKL in MC3T3-E1 or IDG-SW3. It has previously been shown that all three cell types have the vitamin D3 receptor (VDR) [339], [340]. MLOA5 have been shown to be able to metabolise 25-hydroxyvitamin D3 to the active form [331] and that the presence of this can increase their mineralisation [341]. In MC3T3-E1, Song, et al., demonstrated that vitamin D3 could augment the effects of 17 β -estradiol. Here oestrogen enhanced cell proliferation, viability, differentiation and matrix production,

and these were further promoted when vitamin D3 was also added. However, it had no effect when added by itself [342]. St. John, et al., examined the effects of vitamin D3 exposure on IDG-SW3, finding that concentrations of 1 – 100 nM strongly inhibited mineralisation of IDG-SW3 by day 14. Furthermore, a 24h hour application on day 35 had a different effect on the transcriptome to when it is applied on day 3, indicating that osteoblasts were responding differently to osteocytes [340]. However, they did not report any negative effect on cell viability of vitamin D3 on IDG-SW3.

The effect that vitamin D3 can have on cells of the osteoblast lineage is clearly variable. It has been shown to regulate transcription, proliferation, differentiation and mineralisation, as well as increasing the RANKL:OPG ratio by altering the production of both cytokines [343]. Furthermore, it can also facilitate the adhesion of osteoclast precursors to osteoblasts by upregulating ICAM-1 expression [344]. Although RANKL is produced by most cells in the osteoblast lineage, it has been reported that it is expressed preferentially in immature osteoblasts and that levels decrease as they mature [345]. However, it seems that expression may increase again as they become osteocytes as it has been shown that they are better-able to support osteoclastogenesis in co-culture with osteoclast precursors that mature osteoblasts [346]. Furthermore, it has been shown to both negatively and positively influence matrix formation. Therefore, whether vitamin D3 affects RANKL and matrix synthesis seems dependant on the maturity of the cell type.

Vitamin D has also been shown to affect osteoclast precursors and is one potential reason it may have an anti-resorptive effect on osteoclasts *in vivo*. For example, monocyte precursors possess the enzyme required to metabolise vitamin D into the active form. Kogawa, et al., found that during RANKL-induced osteoclastogenesis, production of this enzyme is increased, and that the active metabolite increased osteoclast formation [337]. Vincent, et al., also demonstrated that when vitamin D3 is administered to RAW264.7 with RANKL, TRAP positive osteoclast formation is enhanced in comparison to RANKL-only osteoclastogenesis between concentrations of 1 and 20 nM [347]. During this thesis, the effect of vitamin D3 on RAW264.7 was also investigated; however, there were no significant difference in TRAP activity between 0 nM and 10 nM vitamin D3 by day 10 (n=6, data not shown).

The apparent lack of response to vitamin D3 in this study could have been due to a variety of reasons. It could have been that the cell types could have lacked VDR, either due to it not being present or cell line degradation. This seems unlikely as all four cell

lines have been reported to respond to vitamin D in the literature and, with the exception of MLOA5-K, all cell lines were sourced relatively recently from a supplier. Therefore, perhaps the most likely reason is the interference of factors in the FBS used during the experiments. Vincent, et al., studied the effect of vitamin D3 on RAW264.7 performed in serum-replete and serum-free conditions. They found vitamin D3, fibronectin, various growth factors and hormones within FBS, all of which can influence osteoclastogenesis [347]. The concentrations and presence of these factors varies between batches, and although only one batch was used during these experiments, it was not possible to accurately define its composition and analyse potential competing factors to the ones added exogenously [229].

There was no significant difference in OPG production in monolayer culture between the three cell types. By day 7 all cell types were confluent and therefore had similar cell numbers. In contrast, OPG levels were significantly higher in MLOA5-K than MC3T3-E1 and IDG-SW3 when cultured in scaffolds. Due to the higher proliferation rate of the MLOA5 cells than MC3T3-E1 and IDG-SW3, the higher OPG concentration in the media is most likely due to increased cell number. However, it could also be due to the phenotypic changes in cells when cultured in scaffolds in comparison to a monolayer, as 3D culture has been shown to increase expression of OPG and lower expression of RANKL [171]. It is important to know the total OPG, rather than the OPG per cell, as it is this concentration in the media that will affect the RANKL:OPG ratio.

It is well established that RANKL induces osteoclastogenesis in RAW264.7, indeed one of their main advantages for studying osteoclastogenesis is that you only need RANKL instead of both RANKL and M-CSF to induce osteoclastogenesis [166]. Osteoclast formation was confirmed by microscopy to view multinucleation, TRAP activity and resorption, the three essential characteristics of a mature osteoclast. Due to the difficulties with counting nuclei of individual cells in co-culture, especially in 3D, TRAP activity and resorption were used to quantify osteoclast activity in all successive experiments. TRAP activity correlates very strongly with counts of multinucleated osteoclasts and therefore is a valid substitution for manual counts [348].

TRAP activity is intrinsically linked with osteoclast activity, but its precise role is unknown. *In vivo*, TRAP activity strongly correlates with the rate bone resorption and TRAP knockout mice develop osteopetrosis [186]. It is a non-specific enzyme,

meaning it can act on a wide range of substrates, which has both intra- and extracellular functions. Outside the cell, it is able to cleave phosphate groups from bone matrix proteins such as osteopontin, bone sialoprotein and osteonectin [349]. Osteopontin allows osteoclasts to adhere to the bone surface by binding with integrins, therefore its disruption by TRAP implies a possible regulatory role for osteoclast adhesion, possibly enabling migration of the osteoclasts to sites adjacent to where is currently being resorbed. Furthermore, TRAP can release inorganic pyrophosphate from the matrix, an inhibitor of bone formation [23], [24], [40]. Intracellular TRAP is localised to transport vesicles within the osteoclast that move the organic products of bone resorption from the ruffled border to the functional secretory domain where they can both be removed [350]. This results in the increased concentration of TRAP seen in the serum with increased bone resorption. In addition to this, TRAP appears to catalyse the formation of free radicals that actively resorb the matrix and can degrade the proteins within the transcytotic vesicle [350], [351]. These observations combine to indicate that TRAP may have an indirect role on bone resorption, rather than a direct ability to degrade the tissue.

When analysing TRAP activity, it is important to ensure that your conditions and substrate are specific to the osteoclastic TRAP enzyme. There are many different acid phosphatases *in vivo* that can be generated by almost all cell types in the body [40]. Acid phosphatase 5b, more commonly known as TRAP5b, is specific to osteoclast activity, but another isoform, TRAP5a, predominantly produced by immune cells also exists. When using TRAP concentration in the serum as a marker of bone turnover, the 5b isoform can be preferentially selected for by increasing the pH to 6.1 as the optimum pH for 5a is 4.9-5.2. *In vitro*, where no immune cells are present, the optimum pH of 5b (5.5-6.0) can be used to maximise hydrolysis of the substrate [352], [353].

Relying on changing pH alone is not sufficient to ensure you are only measuring TRAP5b activity; the substrate must also be carefully selected. One of the most common substrates to assess acid phosphatase activity is para-nitrophenol phosphate (pNPP), the same substrate as that used when quantifying ALP, an alkaline phosphatase. pNPP is hydrolysed to produce para-nitrophenol (pNP), a yellow chromogen that can be analysed colourimetrically. However, this can be hydrolysed by non-TRAP5b acid phosphatases; therefore, it is better to use naphthol-ASBI-phosphate, a substrate specific to TRAP5a and 5b. When hydrolysed naphthol-ASBI

is produced which can also be quantified colourimetrically, and in serum quantification 5b can be preferentially selected for by increasing the pH [354].

Seeding density of osteoclast precursors affects their ability to mature and rate of maturation. However, when the seeding density of RAW264.7 is stated in the literature, it varies extensively from 1562.5/cm² [355] to 15,000/cm² [356], [357], 20,000/cm² [310], even up to 35,000/cm² [358]. Osdoby, et al., found that in the range of 100-500/cm² osteoclast formation is delayed due to a lack of precursors, and that above 450,000/cm² the density is so high that osteoclastogenesis is inhibited [167]. Although they recommend using 1,000-30,000/cm² for evaluating the effects of various agents on osteoclast formation, it has been found here that even increasing from 1,250-15,625/cm² affects this. This is because when precursors are too sparse, they cannot fuse readily, but as they become denser maturation occurs more quickly, generating osteoclasts sooner. However, these then undergo apoptosis at an earlier time point than those seeded at lower densities. This makes it difficult compare results between studies if different seeding densities are used as the peak osteoclast activity shifts, meaning it may have already happened, be happening, or be yet to occur (Fig. 4.21).

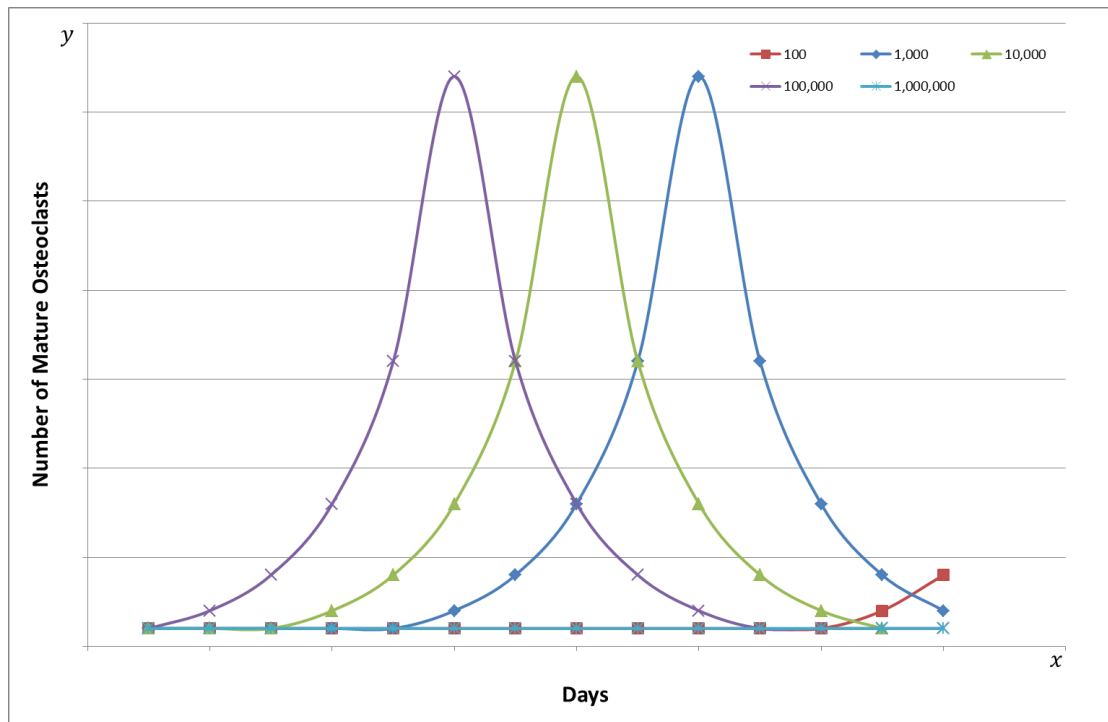


Figure 4.21: A hypothetical diagram showing how seeding density affects when osteoclastogenesis occurs in RAW264.7. At the lowest seeding density, fusing of precursors is delayed, as the density increases the peak shift to the left as multinucleation occurs sooner. At the highest density, precursors are too dense to be able to fuse.

The primary role of oestrogen in bone remodelling is its action on osteoblasts and the RANKL:OPG ratio; however, it can also act directly on osteoclasts. Palacios, et al., confirmed the expression of ER α but not ER β on RAW264.7, finding that osteoclastogenesis could be reduced by ER agonists. 17 β -estradiol and two non-steroidal ER agonists all reduced proliferation and TRAP expression of RAW264.7, with 10 nM estradiol being the most potent [310]. In contrast to this study, here 10 nM oestrogen did not have an effect on proliferation or osteoclastogenesis, requiring 100 nM for a significant reduction to occur. As the method for preparing and storing the stock solution is not given it is difficult to discern the reasons for the discrepancy, but it is likely due to differences in cell line age or in the potency of the oestrogen solution.

Both MLOA5 and IDG-SW3 were unable to promote osteoclast formation without exogenous RANKL. This is unsurprising considering that the ELISA indicated that neither cell line produced the cytokine. When RANKL was added, MLOA5

completely inhibited osteoclast formation. This could be due to the large amount of OPG produced by the cell line completely overwhelming the concentration of RANKL added. Alternatively, the very high metabolic activity and proliferation rate of MLOA5 could have resulted in RAW264.7 either being unable to have sufficient space and/or nutrients to proliferate and fuse. IDG-SW3 did support osteoclastogenesis; however, the TRAP activity of the co-culture was significantly lower than the RAW264.7 monoculture. As a substantial TRAP activity was still present, this inhibition is likely due to the OPG produced by the IDG-SW3 reducing the effective concentration of sRANKL.

Interestingly, it was not possible to identify resorption pits on trabecular bone and dentine slices. The ability of RAW264.7 to resorb a substrate does diminish with extended passaging; however, the cells used were only recently acquired from the ATCC and were capable of resorbing calcium phosphate films. RAW264.7 have previously been shown to resorb both bone and dentine [359], [360] at concentrations of RANKL ranging from 25 – 100 ng/mL. Here, 50-100 ng/mL RANKL was added and mature osteoclasts were generated; therefore, the lack of resorption pits may have been due to the osteoclasts being unable to form a sealed zone over the substrate, prohibiting resorption, possibly due to an unamenable surface roughness from the striations left by the saw when cutting the samples.

4.6 Summary

- Phenol red at the levels available in the culture media did not act as an oestrogen receptor agonist.
- Oestrogen only has an effect on MC3T3-E1, no changes are seen with MLOA5 or IDG-SW3.
- Different phenotypes of IDG-SW3 can be achieved by modulating temperature and media supplementation.
- None of the potential cell lines produced RANKL, meaning it will have to be added exogenously.
- MC3T3-E1 and IDG-SW3 have the lowest OPG production, giving them the highest RANKL:OPG ratio.
- RAW264.7 can be matured into multinucleated, TRAP positive, bone resorbing osteoclasts.
- The maturation of RAW264.7 into osteoclasts is highly dependent on seeding density.
- Oestrogen inhibits RAW264.7 proliferation and osteoclastogenesis.
- IDG-SW3 permit osteoclastogenesis in co-culture.
- IDG-SW3 and RAW264.7 are the most suitable osteoblast and osteoclast cell lines for the *in vitro* model aimed to be developed in chapter 6.

5. Development of a suitable substrate for an *in vitro* model of osteoporosis

5.1 Introduction

5.1.1 Scaffold requirements

In tissue engineering, 3D scaffolds are used to guide cell growth and tissue formation [82]. Scaffold properties and performance are dependent on material selection, architecture, and fabrication technique; factors that can be altered to fulfil scaffold requirements. First, the general requirements for implantable bone tissue engineering scaffolds are discussed, before considering whether all these properties are desirable for an *in vitro* model of osteoporosis, as well as any specific additional requirements.

Perhaps the single most important requirement of an implantable scaffold is biocompatibility, as without this cell growth and tissue integration cannot occur. Biodegradability is also a requisite property for tissue engineering scaffolds as ideally they biodegrade into biocompatible products at a similar rate to tissue formation, allowing complete tissue regeneration [19]. Porosity, which can be subdivided into percentage porosity, pore size, and pore interconnectivity, is important for cell attachment, cell growth and penetration into the scaffold, nutrient diffusion and metabolic waste removal, matrix production and vascularisation [361]. Each of these processes require different types of porosity. For example, nutrient and waste diffusion and tissue integration need a highly interconnected porosity, whereas it is recommended to incorporate pore sizes of at least 50 μm but ideally greater than 300 μm for osseous tissue deposition as this also permits vascularisation [362]–[365]. Therefore, the ideal scaffolds contain porosities on multiple length scales (hierarchical porosity), ranging from micron to millimetre, as well as a high level of interconnectivity.

Porosity also influences mechanical properties, another key characteristic. There is a trade-off between these two, as increased porosity and pore size are detrimental to mechanical strength. Mechanical properties of bone tissue engineering scaffolds are important as they must not fail during normal patient activities [366]. Additionally, as

bone formation is force dependent [16], scaffolds need to retain their strength until remodelling is complete. Finally, the surface properties of the material are important to permit cell attachment and proliferation.

The requirements outlined for implantable bone tissue engineering scaffolds are similar to those needed for scaffolds used in an *in vitro* model of osteoporosis, but there are some key differences (Table 5.1). Clearly, biocompatibility, a suitable surface chemistry and porosity are still essential for creating an appropriate scaffold as cell must be able to attach, survive and proliferate over the structure. Appropriate mechanical properties are also still important; however, 'appropriate' now refers to properties that permit dynamic culture through the use of bioreactors without undergoing irreversible, plastic deformation. However, biodegradability is no longer a necessary or desirable feature as it is with implantable scaffolds. This is because it is important to have a high level of control over related properties such as scaffold surface area to ensure that variation due to cell number or scaffold size between repeats are minimised. Furthermore, there are additional properties for an *in vitro* model scaffold that are not required for clinical applications. Perhaps the most important of these is reproducibility of their architecture, again to minimise variation between scaffolds. Although implantable scaffolds do need to be reproducible to an extent, due to the variation in defect sizes they will be used to treat as bone graft substitutes, there is no need for scaffolds to be identical on the micro-scale. Related to this is the desirability of an *in vitro* model scaffold to be easily modelled computationally. It is well known that fluid flow shear stress can be used to modulate bone cell activity [322]. To predict the stresses applied in complex structures it is necessary to use computational fluid dynamics; therefore, an architecture that is easily replicated *in silico* is advantageous [367], [368].

Table 5.1: The difference in requirements for a tissue engineering scaffold and in vitro model scaffold.

Property	Tissue Engineering	In Vitro Model
Biocompatible	✓	✓
Biodegradable	✓	✗
Porous	✓	✓
Regular architecture	Not essential	✓
Approved materials	✓	Not essential
Reproducible architecture	Not essential	✓

5.1.2 Fabrication techniques

3D scaffold fabrication techniques can be divided into two categories depending on whether they produce a random or user-controlled microstructure [82]. Random structures, produced using techniques such as solvent casting and particulate leaching, are generally easier to produce in bulk; however, there is less control over their microarchitecture and properties [369]. Additive manufacturing techniques (AMTs), such as stereolithography and fused deposition modelling, have an architecture defined by computer aided design and manufacture (CAD/CAM), which allows investigation into the effects of topology on cells by altering geometrical parameters [361]. AMTs create 3D structures by repeatedly depositing 2D cross sections. This results in a tightly controlled, reproducible architecture that has high levels of pore interconnectivity without the use of solvents.

Scaffolds produced by a casting or leaching approach that have a random microarchitecture can have limited pore interconnectivity and varied pore size [370], [371]. The low pore interconnectivity arises at lower porosities when there are not sufficient porogens to have a continuous porosity, and are the result of a 'skin' forming around the pores during solvent evaporation. In an attempt to alleviate this, samples are often thin to ensure even pore dispersal and adequate porogen removal [369]. Polymerised High Internal Phase Emulsions (PolyHIPEs) have a random porous microarchitecture and excellent interconnectivity without the use of solvents. However, thin monoliths can still only be produced as cellular penetration is dependent on pore size ($\sim 50 \mu\text{m}$) and thickness, with penetration rarely seen beyond 1 mm [372], [373].

5.1.3 Microstereolithography

Microstereolithography (μSL) is an AMT that was first explored in the 1980s [374]. It creates structures from photocurable monomers by use of a laser. Common approaches for this technique are projection μSL , direct-write μSL and scanning μSL . Projection μSL can create scaffolds with a resolution of 1 to 25 μm by reflecting laser light off a digital micromirror device which is set to only permit the reflection of an image of the cross-section of the scaffold. This image is focused onto a z-stage within a receptacle containing a photocurable prepolymer. The stage slowly moves downwards within the receptacle, allowing a 3D structure to be formed from the bottom up [375]. A direct-write approach uses a computer-controlled stage that can

travel in all three planes to move a photocurable liquid whilst a laser is focussed into a single focal spot that crosslinks the prepolymer. This creates a complex architecture one layer at a time [376]. This can be done using two-photon polymerisation, where resolutions of 120 nm can be achieved [377], or using a single-photon polymerisation, which trades resolution for fabrication speed allowing writing to occur one to two orders of magnitude faster [378]. Scanning μ SL is similar to direct-write, except the focal spot of the laser is translated rather than the prepolymer [379]. In order to create 3D structures, consecutive layers of polymer are cured through either manual or automated addition. Once fabrication is complete, any uncured prepolymer is washed away to reveal the structure.

5.1.4 PolyHIPE materials for tissue engineering

Emulsions form when water and oil are mixed in the presence of an emulsifier or surface active agent (surfactant). They consist of an internal and continuous phase, where the internal phase forms droplets within the continuous. Whether an emulsion is oil-in-water (O/W) or water-in-oil (W/O) can generally be determined using the Bancroft rule which states that whichever phase the surfactant is more soluble in is the continuous phase [380]. Surfactants lower the interfacial tension between the two phases by being amphiphilic, consisting of both hydrophilic and lipophilic groups. This enables them to adsorb at the oil-water interface and stabilise the emulsion, preventing the phases from separating. As surfactants are amphiphilic, they can be water or oil soluble. Their solubility is calculated by determining the hydrophilic-lipophilic balance (HLB) which is expressed on a scale of 0 to 20, where 3 – 6 represents hydrophobic, oil soluble W/O surfactants, and 12 – 16 represents hydrophilic, water soluble O/W surfactants [381]. As inversion for O/W to W/O or vice versa can occur at high internal phase volumes, it is important to carefully select an appropriate surfactant [382].

A high internal phase emulsion (HIPE) is an emulsion where the internal phase volume ratio (Φ) exceeds 0.7405. This is because at this Φ , droplets are forced to interact. If the most efficient manner of packing monodisperse rigid spheres into a cube is considered, they will occupy 74.05% of the volume. As monodisperse internal phase droplets are not rigid bodies, when this Φ is exceeded droplets are forced to change, becoming either polydisperse or polyhedral in shape [383]. When the continuous phase of a HIPE contains one or more monomers and polymerisation is initiated, a PolyHIPE is formed. This preserves the internal shape and structure of the emulsion

as a porous polymer (Fig. 5.1). The internal phase forms pores within the polymer, and the nominal percentage porosity is simply Φ multiplied by 100%. Depending on the level of surfactant present, PolyHIPEs have either a closed or open pore structure, where closed pores are completely contained trapping the internal phase, and open pores fully interconnect with each other allowing the internal phase to be removed [384]. Open porosity PolyHIPEs are permeable polymers with a highly interconnected microarchitecture and a low bulk density. Interestingly, this effect of surfactant on pore openness occurs even at internal phase volume ratios as high as 0.97. From this, it would appear that increased surfactant thins the internal-continuous phase interface, and at a threshold concentration this causes interconnects to appear between droplets during polymerisation. In an attempt to elucidate the mechanism by which this occurs, scanning electron microscopy has been used to view PolyHIPEs that have been frozen at different stages of polymerisation. These images indicated that the contraction of the continuous phase during conversion from monomer to polymer causes interconnects to occur [385]. However, an alternate theory proposed is that the cured PolyHIPEs still have thin films covering the interconnects after polymerisation which then rupture during washing, as evidenced by images of partially sealed interconnects [386].

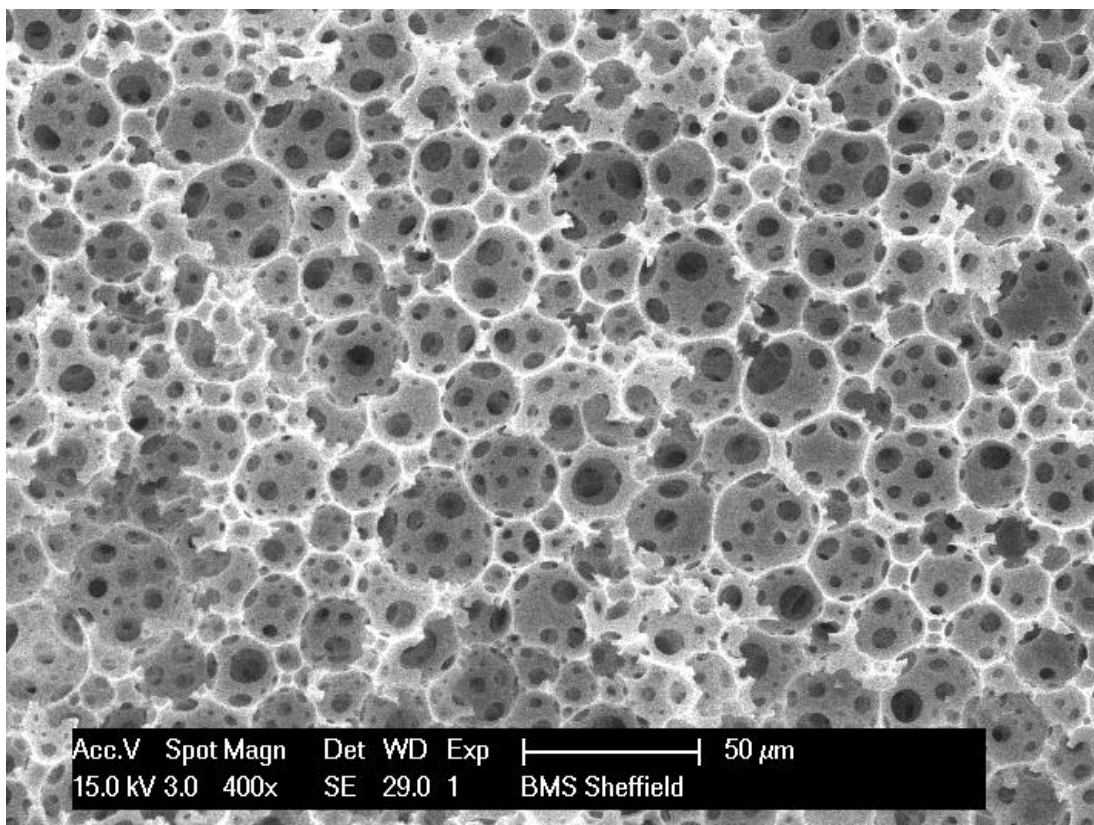


Figure 5.1: SEM of an acrylate-based PolyHIPE demonstrating the interconnected porous network. Image captured by author.

HIPEs are typically cured from acrylates or methacrylates via a radical initiated addition reaction. This process can be activated either thermally or photochemically by introducing a photoinitiator into the continuous phase. Photocurable HIPEs lend themselves to structuring via μ SL [375]. This combination allows the formation of scaffolds with multi-scale porosity that combine a bottom-up and top-down approach to introducing porosity, where the microstructure of the scaffold struts have an inherent porosity controlled by emulsion templating and the macrostructure is governed by AMT. Combining AMTs and emulsion templating has previously been used to create hierarchically porous structures, both through projection μ SL fabrication of HIPEs [375], [387] and Digital Light Process printing of O/W emulsions [388].

During previous work by the author, twenty acrylate-based PolyHIPE formulations were mechanically characterised and selected compositions structured using single-photon direct-write μ SL to fabricate hierarchically porous scaffolds [389]. The proportions of two monomers; 2-ethylhexyl acrylate (EHA), an elastomer, and

isobornyl acrylate (IBOA), which gives brittle characteristics, were varied from 100% EHA to 100% IBOA at 25% intervals. At each of these five compositions, HIPEs with Φ of 0.75, 0.80, 0.85, and 0.90 were synthesised [240]. Further work investigated introducing hydroxyapatite into these structures to determine its effects on osteogenesis [390]. These scaffolds will be evaluated and developed during this thesis.

5.2 Aims and objectives

The aim of this chapter was to compare multiple scaffolds, evaluating their ability to support extracellular matrix deposition, reproducibility and ease of manufacture. From this, an appropriate substrate can be selected for use in the *in vitro* model of postmenopausal osteoporosis to be developed in chapter 6. To achieve this, the following objectives were addressed:

1. Continue to improve and develop the PolyHIPE scaffolds previously designed by evaluating their ability support bone matrix deposition, examining the effects of substrate stiffness and surface coating, and improving its architecture.
2. Compare the cellular performance and physical characteristics of the PolyHIPE scaffold with two alternatives; a polyurethane foam and a polycaprolactone scaffold produced by fused deposition modelling.

5.3 Materials and methods

Further to the materials and methods outlined in §3, the following are used in this chapter.

5.3.1 PolyHIPE nomenclature

PolyHIPEs will be referred to by their monomer composition and porosity. All PolyHIPEs produced use only two monomers, EHA and IBOA; therefore, these will be referred to by their weight percentage of EHA and nominal porosity. For example, a 100% EHA composition at 85% porosity will be referred to as EHA100P85 and a 15% EHA composition at 80% porosity will be referred to as EHA15P80. If any further additions are made to the composition, this will be added to the end of the description.

5.3.2 HIPE synthesis

The proportions of the constituent materials to synthesise the HIPE are summarised in table 5.2. Briefly, the continuous phase is synthesised first before adding the internal phase. The continuous phase has an organic component consisting of the monomers EHA and IBOA and the crosslinker trimethylolpropane triacrylate (TMPTA) at 26.96 wt% of the monomers. A surfactant (Hypermer B246-SO-(MV), Croda, UK) was added at 3 wt% of the organic mass and left to dissolve in a sonic water bath. Finally, a photoinitiator (2,4,6-trimethylbenzoyl)-phosphine oxide/2-hydroxy-2-methylpropiophenone, 50/50,) was added at 5 wt% of the organic mass. When the UV light absorber Tinuvin® 234 (2-(2H-Benzotriazol-2-yl)-4,6-bis(1-methyl-1-phenylethyl)phenol) was included in the HIPE, it was introduced to the continuous phase of the emulsion at 0.1 wt% of the organic component.

To create the HIPE, the internal phase (deionised water) was added dropwise at a constant rate to the continuous phase whilst stirring at 350 rpm using a paddle stirrer (Pro40, SciQuip, UK) in a 50 mL beaker. Once added, the HIPE was stirred for a further five minutes before transferring to a foil wrapped tube. If HIPEs were not used on the day of synthesis, they were respun at 350 rpm for five minutes before use.

Table 5.2: Proportions of the HIPE constituent materials.

Phase	Material	Proportion
Continuous	Monomer(s)	N/A
Continuous	Crosslinker	26.96 wt% of monomers
Continuous	Surfactant	3 wt% of monomers and crosslinker
Continuous	Photoinitiator	5 wt% of monomers and crosslinker
Continuous	Light absorber	0.1 wt% of the monomers and crosslinker
Internal	Deionised water	75-90 vol%

5.3.3 Coverslip functionalisation

When the PolyHIPE was required to bind to a glass coverslip they were functionalised. Initially, coverslips were submerged in piranha solution (80 vol% H₂SO₄, 20 vol% H₂O₂ (30 wt% in water)) for thirty minutes. This powerful oxidiser removes any organic matter or residue and exposes surface hydroxyl groups. Coverslips were then rinsed in deionised water before washing in methanol and drying. Once dry, they were submerged in a solution of 10 wt% 3-methylacryloxypropyltrimethoxysilane (MAPTMS, Polysciences Inc) in toluene to add methacrylate groups to the surface and left overnight. Before use these were washed in methanol and dried.

5.3.4 Bulk HIPE polymerisation

To create sheets of the PolyHIPE material, bulk polymerisation was performed using a UV belt curer (GEW Mini Laboratory, GEW engineering UV). A Teflon sheet was added to the base of a glass petri dish before filling with HIPE. This was passed multiple times under the UV lamp at 10 m/min until cured. The resulting sheets were washed in acetone for 24 hours before drying until constant mass.

5.3.5 Mechanical characterisation

To create tensile specimens, PolyHIPE monoliths were laser cut (Mini 19 Laser, Epilog Laser) at a power of 8%, speed of 70% and frequency of 2,500 Hz in accordance with ASTM D638-10. However, the length of the specimens was reduced by a factor of 3.83 due to the maximum sample size of the testing machine.

Samples were tested on a BOSE ElectroForce 3200 mechanical testing machine using a 450 N load cell, an extension rate of 0.02 mm/sec, a grip distance of 10 mm, and a maximum extension of 6 mm. Young's modulus was determined using the linear region of the force-displacement curve. The initial point was always at an extension of 0.02 mm and the final point taken at yield.

5.3.6 Physical characterisation

In order to physically characterise the PolyHIPEs, SEM images of the 20 compositions were analysed and the degree of openness (DOO) of each determined [391]. For imaging, each sample was mounted on a carbon tab, sputter coated with gold (SC500, emscope) and imaged using a Philips XL-20 SEM with a beam energy of 20 kV. Images were taken at 400× and analysed using Image J [392].

DOO is the ratio of open surfaces (S_o) within a pore/cavity of the PolyHIPE to the total surface of the cavity (S_c). S_c is calculated from the measured diameter of the pore (D_m). However, as it is unknown where the pore has been bisected, this is multiplied by a statistical correction factor to give the equatorial pore diameter (D_e) (Eqn. 3) [393].

$$S_c = \pi \left(\frac{2D_m}{\sqrt{3}} \right)^2 \quad (3)$$

In order to determine the area of S_o , the diameters of visible interconnects within the pore are averaged (D_i) and this value used to calculate the average area. This is multiplied by the number of visible interconnects (N), then by 2 as the pore has been bisected, then by the statistical correction factor as we do not know where this has occurred. From these two values, the DOO can be calculated (Eqn. 4).

$$\text{Degree of Openness (DOO)} = \frac{\text{Open Surface of Cavity}}{\text{Total Surface of Cavity}} = \frac{N * 2 * \frac{2}{\sqrt{3}} * \pi \left(\frac{D_i}{2} \right)^2}{\pi D_e^2} \quad (4)$$

For each of the twenty PolyHIPE compositions, ten pores were analysed and the average DOO for each composition calculated.

5.3.7 PolyHIPE scaffold fabrication

Scaffolds were manufactured using single-photon direct write microstereolithography. Regardless of the HIPE composition, the following method was used; a subnanosecond pulse duration passively Q-switched DPSS microchip laser (PULSELAS-P355-300, ALPHALAS, Germany) controlled using a laser diode and thermoelectric cooler driver (LDD1-1BT-D, ALPHALAS, Germany) emitting wavelengths of 1064, 532 and 355nm was used as a source, with a Pellin-Broca prism (ADB-10, THORLABS, UK) used to separate a single wavelength of 355nm. Beam delivery was controlled with a shutter (UNIBLITZ LS6, VincentAssociates, Canada) linked to a shutter driver (VCM-D1, VincentAssociates, Canada), and a pinhole was used to modulate the beam intensity. Finally, the beam was focused through a microscope objective (EC-Plan NEOFLUAR 10x, Carl Zeiss Ltd, UK), and a high precision stage with the ability to move in all three planes (ANT130-XY, Aerotech, UK, for *xy* translation & PRO115, Aerotech, UK, for *z* translation) commanded by a motion controller and software (A3200 Software-Based Machine Controlled, Aerotech, UK) was used to translate the focal spot. To fabricate the scaffold, a known volume of HIPE was pipetted onto the coverslip which was placed onto the stage. The first layer was then written, followed by the addition of additional HIPE and the writing of the next layer after adjusting the *z* height accordingly. This was repeated until the scaffold was completed. The laser was focused just above the coverslip-HIPE interface for the bottom layer and the fibre-HIPE interface for each subsequent layer in order to write the scaffold.

For HIPE compositions without Tinuvin, a current of 2.20 μA and a pinhole size of 3.1 mm was used, resulting in a scaffold with $\sim 350 \mu\text{m}$ fibres and $\sim 650 \mu\text{m}$ spacing. For HIPE compositions with Tinuvin, a current of 2.65 μA and a pinhole size of 4.0 mm was used, resulting in a scaffold with $\sim 325 \mu\text{m}$ fibres and $\sim 325 \mu\text{m}$ spacing.

For clarity, the development of the PolyHIPE scaffold resulted in experiments with three separate ‘generations’ of scaffold. The first-generation scaffold is a four layer woodpile scaffold attached to a functionalised coverslip. The second generation is a four-layer scaffold with the incorporation of Tinuvin that has improved architecture and can be removed from the coverslip making it free standing. The third generation is a 6 to 12-layer scaffold with further improved architecture and reproducibility.

5.3.8 Plasma modification of scaffolds

As the continuous phase of the HIPEs is inherently hydrophobic in order to form an emulsion with water, it is necessary to alter the surface chemistry to promote cell attachment, spreading, and proliferation. This is achieved through plasma modification of the scaffold either using an air plasma clean (pcAir) or air plasma clean followed by plasma deposited acrylic acid (pdAAc).

Treatments were applied to the scaffolds by placing them on an aluminium foil wrapped platform in the centre of a cylindrical plasma chamber with stainless steel endplates wrapped with a coiled wire connected to a 13.56 MHz frequency generator (Coaxial Power Systems Ltd, UK). The gas/monomer inlet is controlled by a needle valve (LV10K, Edwards, UK) and a gauge (APG100 Active Pirani Vacuum Gauge, Edwards, UK) with a gauge controller (AGC Active Gauge Controller, Edwards, UK) used to monitor the pressure. An isolation valve (Speedivalve, Edwards, UK) is present between the plasma chamber and vacuum pump.

To apply the pcAir treatment, the pressure was lowered to 1.8×10^{-1} mbar and the power set to 50 W to generate the plasma. Samples were treated for 5 minutes. To apply the pdAAc treatment, samples were kept in the chamber after air plasma exposure and liquid nitrogen added to the cold trap. The pressure was lowered to 3.0×10^{-3} mbar, and then a flask (JY Sample Flask with O-Ring and Plain Arm, GPE Scientific, UK) of acrylic acid (Sigma Aldrich, UK) attached to the inlet. The pressure was then stabilised at 3.0×10^{-2} mbar and the flow rate (F) calculated by closing the isolation valve and recording the initial pressure (ρ_i) and the pressure after 30 seconds (ρ_f) (Eqn. 5). Δ is a constant specific to the plasma rig and always equals 6.2.

$$F = \Delta(\rho_f - \rho_i) \quad (5)$$

For all pdAAc treatments, a flow rate of 2.4-2.5 sccm⁻¹ was used by adjusting the initial pressure until the flow rate was within this range. Once achieved, this process was repeated a further two times to ensure stability, and then acrylic acid was deposited for 10 minutes at a power of 15 W. Samples were used for cell culture on the same day the plasma treatment was applied.

5.3.9 General hES-MP culture

hES-MPs (Cellartis, Sweden) were passaged at 37°C, 5% CO₂ in expansion media (EM), consisting of BM (α -MEM, 10% FBS, 2 mM L-glutamine, 100 mg/mL penicillin/streptomycin supplemented with 4 ng/mL of human fibroblastic growth factor (hFGF, Life Technologies, UK) in gelatine-coated T75 flasks. Media was changed every 2-3 days. Passaging, counting, freezing down and reanimating was performed using the general osteoblast culture protocol (§3.2.4).

Experiments with hES-MPs were seeded in BM. The following day media was exchanged for OIM (BM supplemented with 5 mM β GP, 50 μ g/mL AA-2P and 100 nM dexamethasone), with the exception of experiments where the influence of substrate stiffness on osteogenic differentiation was evaluated. Here, experiments were maintained in SM (BM supplemented with 5 mM β GP and 50 μ g/mL AA-2P), as it does not contain dexamethasone, a steroid which induces osteogenesis, but still has the osteogenic supplements required for mineralisation.

5.3.10 PolyHIPE scaffold sterilisation

Scaffolds were sterilised for use in cell culture experiments. They were soaked in 70 vol% ethanol under vacuum for 1.5 hours before rinsing three times with sterile PBS. Scaffolds were never stored, plasma treatment, sterilisation and seeding was always performed on the same day. Scaffolds which do not sink during sterilisation are discarded due to their hydrophobicity.

5.3.11 PolyHIPE scaffold seeding

To seed, generation 1 and 2 scaffolds were transferred to a non-treated 24 well plate and 75,000 cells at a density of 1,500,000 cells/mL were added and left for 45 minutes to attach. Scaffolds were then submerged in 1 mL BM and incubated overnight. The following day, scaffolds were transferred to a 12 well plate and cultured in 2 mL of

the appropriate medium for the remainder of the experiment. Medium was changed every 2-3 days.

Generation 3 scaffolds were seeded with 100,000 cells in 100 μ L of basal media (BM) in a bespoke 3D printed grid to maximise seeding efficiency. Grids were designed in Solidworks and printed using an Ultimaker 2 go using Acrylonitrile butadiene styrene (ABS) plastic. Cells were left to attach for 2 hours before transferring scaffolds to a well plate and submerging with BM overnight. The following day, appropriate medium was added for the remainder of the experiment. Medium was changed every 2-3 days.

5.3.12 Polyurethane scaffold preparation

Polyether polyurethane foam (Caligen Foam Ltd) was cut into 6 \times 10 mm or 5 \times 5 mm (diameter \times height) cylinders using a hole punch and scalpel in a similar method to Sittichockechaiwut , et al [9]. Once cut, they were submerged in 0.1 w/v% gelatine solution and autoclaved at 121 $^{\circ}$ C for 30 minutes to sterilise and improve cell attachment.

5.3.13 Polyurethane scaffold seeding

Before seeding, scaffolds were soaked in BM for 30 minutes. To seed, the BM was aspirated and replaced with a seeding suspension of 600 cells/0.31 μ L BM per mm^3 . Cells were left for 45 minutes to attach for 45 minutes before submerging in BM overnight. The following day, scaffolds were transferred to a new well plate and cultured in the appropriate medium for the remainder of the experiment. Media was changed every 2-3 days.

5.3.14 Biotek scaffold seeding

For comparison to the PolyHIPE and polyurethane scaffolds, osteoblasts were also cultured on the 24 well compatible 3D InsertTM-PCL, a commercial poly(ϵ -caprolactone) (PCL) woodpile scaffold produced by 3D Biotek. It has fibre diameter

and spacing of 300 μm , a diameter of 14 mm and a height of 1.5 mm, making it 6 layers in height. Biotek scaffolds were seeded according to manufacturer instructions. Briefly, 75,000 cells were added in a volume of 270 μL and left to attach for 3 hours. Scaffolds were then submerged in a further 370 μL of BM and left overnight. The following day, scaffolds were transferred to a new well plate and cultured in the appropriate medium for the remainder of the experiment. Media was changed every 2-3 days.

5.3.15 Micro-computed tomography

To evaluate the 3D architecture of the scaffold and mineralised matrix deposition, micro-computed tomography (MicroCT) was performed on a Skyscan 1172 (Bruker, Belgium). A polystyrene foam cube with a hole milled to the shape of the scaffold and glued to a brass platform supplied with the MicroCT was used to stop any artefacts associated with sample movement during scanning. Scanning parameters for the three different scaffolds are given below (table 5.3)

Table 5.3: *MicroCT scanning parameters for the three different scaffolds.*

Scanning Parameter	PolyHIPE	Polyurethane	Biotek
Voltage (kV)	38	51	59
Amperage (μ A)	173	165	167
Power (W)	7	8	10
Rotational step ($^{\circ}$)	0.7	0.7	0.7
Averaging	2	2	2
Total sample rotation ($^{\circ}$)	180	180	180
Voxel size (μm^3)	10	10	10
Filter	No filter	No filter	No filter
Camera size	Medium	Medium	Medium

All scans were reconstructed using Nrecon (v.1.6.10.2, Bruker, Belgium). Reconstructions were then aligned to counter any tilt present in the scan and a region

of interest that contained the entire scaffold was saved using DataViewer (v.1.5.2.4, Bruker, Belgium). These were analysed using CTAn (v.1.15.4.0, Bruker, Belgium) by selecting a volume of interest (VOI) within the centre of the scaffold, thresholding, and exporting the grayscale index histogram for the entire VOI. Analysis parameters are given in table 5.4. This histogram can be used to analyse differences in density. Reconstructions and VOIs were visualised using CTvox (v.3.0.0r114, Bruker, Belgium). To minimise reconstruction artefacts, samples underwent misalignment compensation, ring artefact reduction and beam-hardening correction. These settings are only relevant to the particular MicroCT scanner used and were kept consistent for each scanning session. Where comparisons are made, samples were scanned concurrently in the same session to allow accurate, quantitative comparisons.

Table 5.4: *MicroCT analysis parameters for the three different scaffolds. GSI is greyscale index.*

Analysis Parameter	PolyHIPE	Polyurethane	Biotek
Volume of interest (diameter × height, mm)	5 × 0.5	5 × 5 scaffold: 2 × 2	8 × 1
		6 × 10 scaffold: 3 × 3	
Thresholding with scaffold (GSI)	45 - 255	50 - 255	40 - 255
Thresholding without scaffold (GSI)	120 - 255	155 - 255	80 - 255

5.3.16 Tissue sectioning and staining

For histological analysis, some scaffolds were sectioned using a microtome. Samples were fixed in formaldehyde in accordance with §3.2.10 before being submerged in tissue freezing medium (Leica) and frozen by submerging in liquid nitrogen. Samples were then stored in a -80 °C freezer for a minimum of 24 hours before sectioning. Sections were obtained using a cryostat (Leica CM1860 UV) at -24 °C at 8 µm thickness.

Sections were mounted onto a glass slide and stained with haematoxylin and eosin (H&E) by rinsing in diH₂O to dissolve residual freezing medium, submerging in haematoxylin solution for 1 minute, washing in gentle running tap water for 4 minutes, counterstaining in 1% eosin solution for 5 minutes, briefly rinsing in diH₂O, dehydrating in 70%, 90% and 100% ethanol for 2 minutes at each stage before finally clearing in xylene for 1 minute. Sections were preserved by mounting with a coverslip attached using DPX mountant.

5.4 Results

Results in §5.5.1 to §5.5.5 have been published [240]. A full copy of this publication is available in the appendix, §10.3. Where the same figures have used, they are reprinted under the Creative Commons Attribution licence.

5.4.1 Wet mechanical properties are the same as dry

Previous work fully mechanically characterised 20 EHA/IBOA PolyHIPE compositions. Young's moduli between 63.01 ± 9.13 (EHA0P75) and 0.36 ± 0.04 (EHA100P90) MPa, Ultimate tensile stress (UTS) between 2.03 ± 0.33 (EHA25P75) and 0.11 ± 0.01 (EHA75P90) MPa, and percentage elongation at failure between 21.86 ± 2.87 (EHA50P90) and 2.60 ± 0.61 (EHA0P85) % were measured [389]. From this, three compositions, EHA0P80, EHA50P80, and EHA100P80, were selected for cell culture. To determine whether cell culture conditions affect the mechanical properties, wet mechanical testing was performed on these compositions to determine whether this would affect the stiffness by soaking the tensile specimens in BM for one hour prior to testing (Fig. 5.2).

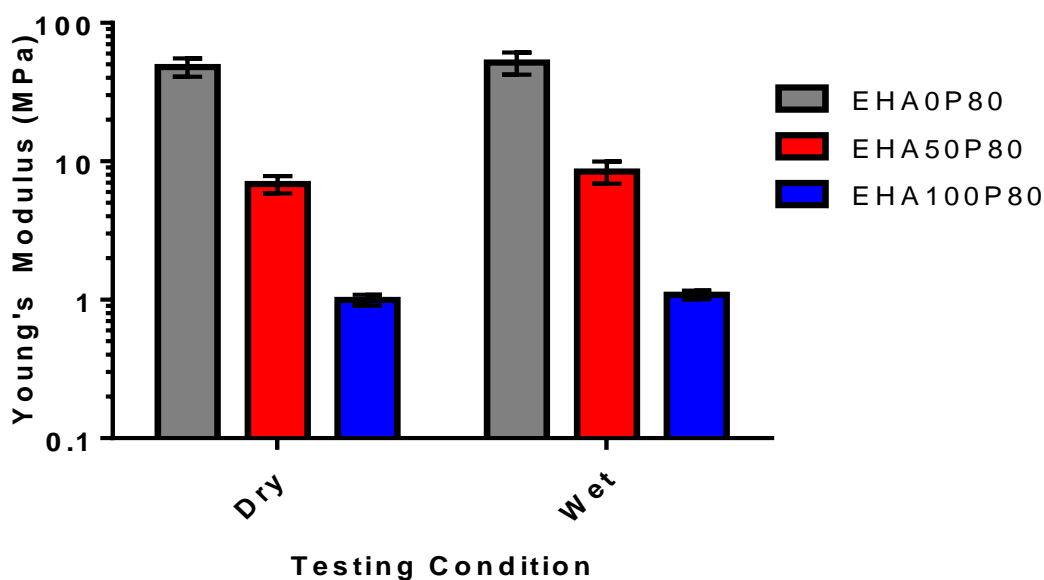


Figure 5.2: Young's moduli under dry and wet conditions of the three PolyHIPE compositions selected for cell culture. No significant difference for dry vs. wet for any composition ($n=13$).

The dry Young's moduli for the three compositions were 48.13 ± 7.25 MPa (EHA0P80), 6.85 ± 0.97 MPa (EHA50P80), and 1.00 ± 0.09 MPa (EHA100P80). The corresponding 'wet' moduli were 51.80 ± 9.45 MPa, 8.43 ± 1.52 MPa, and 1.09 ± 0.08 MPa, respectively. There was no significant difference between dry and wet moduli for any of the three compositions.

5.4.2 The degree of openness is linearly related to the internal phase proportion

The DOO of each of the 20 PolyHIPE compositions was calculated to determine whether the physical characteristics of the PolyHIPEs was affected by the monomer composition as well as the percentage porosity (Fig. 5.3).

DOO increased with porosity for all compositions. At a given porosity comparing monomer proportions, there was no significant difference between 0.75, 0.80, and 0.90 Φ ($p < 0.05$). For 0.85 Φ , only EHA25P85 vs. EHA50P85 and EHA50P85 vs. EHA75P85 were significantly different ($p < 0.05$). At every monomer composition, the largest increase in DOO was seen when increasing nominal porosity from 0.75 to 0.80 Φ . The lowest DOO at 0.75 Φ is because an emulsion is only classed as high internal phase at 0.7405 Φ , below this it is a medium internal phase emulsion (MIPE). Here, water droplets are not forced to interact resulting in negligible pore interconnectivity and therefore, a DOO of zero. The increase in DOO is not linearly correlated with the increase in nominal porosity. However, this is because the required internal phase addition exponentially increases with nominal porosity. If nominal porosity is not viewed as Φ , but rather the volume of internal phase addition required per 1 mL of continuous phase to achieve Φ , a linear relationship is seen. This is because the porosity of the HIPE is reciprocal to the amount of polymer.

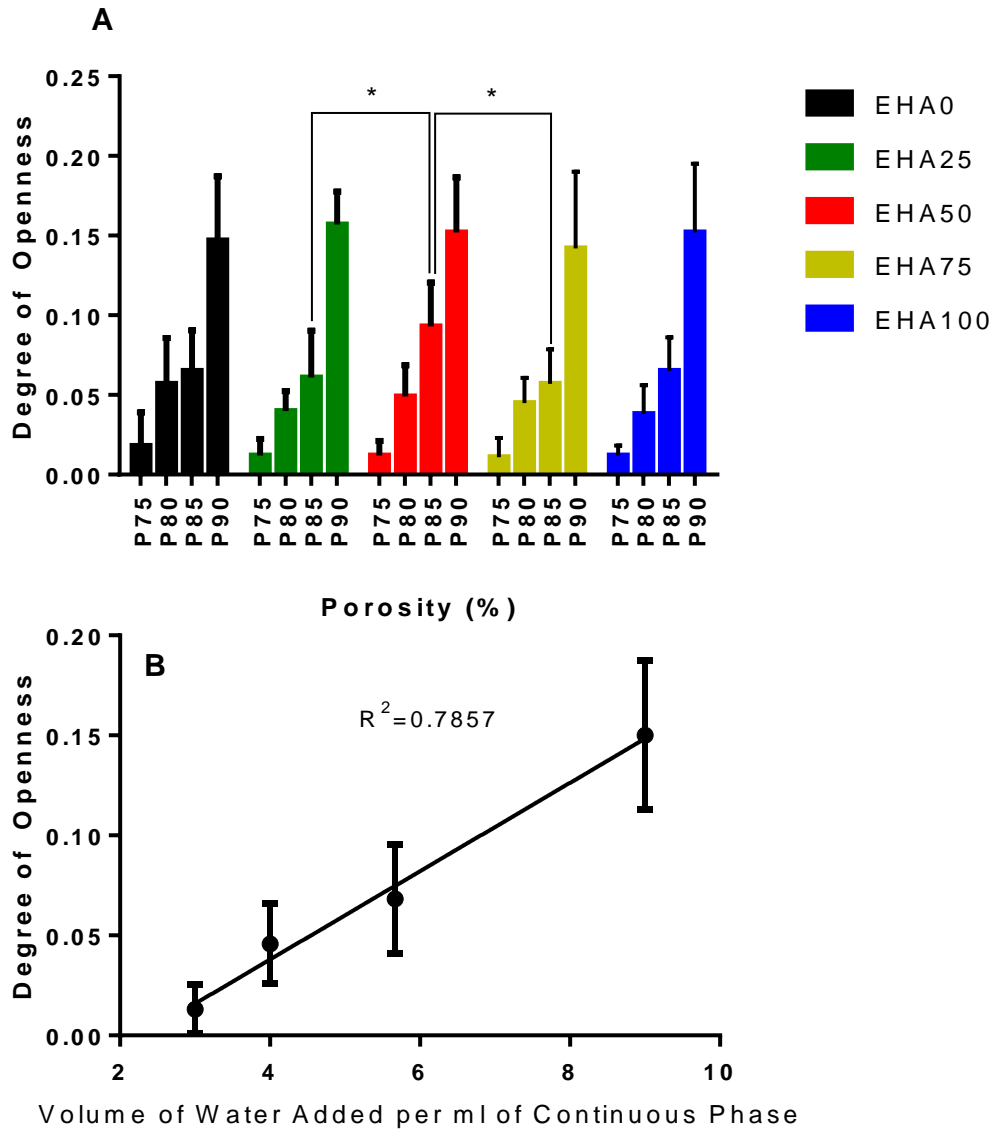


Figure 5.3: Effect of composition and porosity on degree of openness. (A) Mean \pm SD of the DOO for each of the 20 compositions (* = $p < 0.05$). (B) Average DOO vs. Φ expressed as the volume of internal phase per 1 mL of continuous phase. Nominal porosities combined for compositions. R^2 calculated using linear regression, slope is significantly non-zero ($p < 0.0001$).

5.4.3 Batch production significantly reduces manufacture time

Generation 1 scaffolds were fabricated from three HIPE compositions (EHA0P80, EHA50P80, EHA100P80). These four-layer scaffolds had an approximate fibre diameter of 350 μm and spacing of 650 μm . The third and fourth layers were offset by 500 μm so that the fibres lay directly above the gaps of the first and second layer (Fig. 5.4). Due to the large number of scaffolds required, batch production was investigated before production commenced. Rather than producing individual scaffolds with a manufacture time of approximately 15 minutes, a 3 \times 3 grid of scaffolds was initially attempted. This would produce 9 scaffolds in approximately 105 minutes, reducing the equivalent manufacture time per scaffold to 11.5 minutes. However, due to the long time periods between layers it was found that water from the internal phase evaporated. This results in scaffolds that did not have the correct composition and adversely affected the architecture. Therefore, a 2 \times 2 grid was attempted. Each layer was sufficiently fast for the HIPE to not be affected and the per scaffold manufacture time was reduced to 13 minutes. A saving per scaffold of 2 minutes per scaffold seems minimal, but in total 336 generation 1 scaffolds were produced to evaluate the effect of stiffness and plasma modification, reducing the total manufacture time by approximately 11 hours.

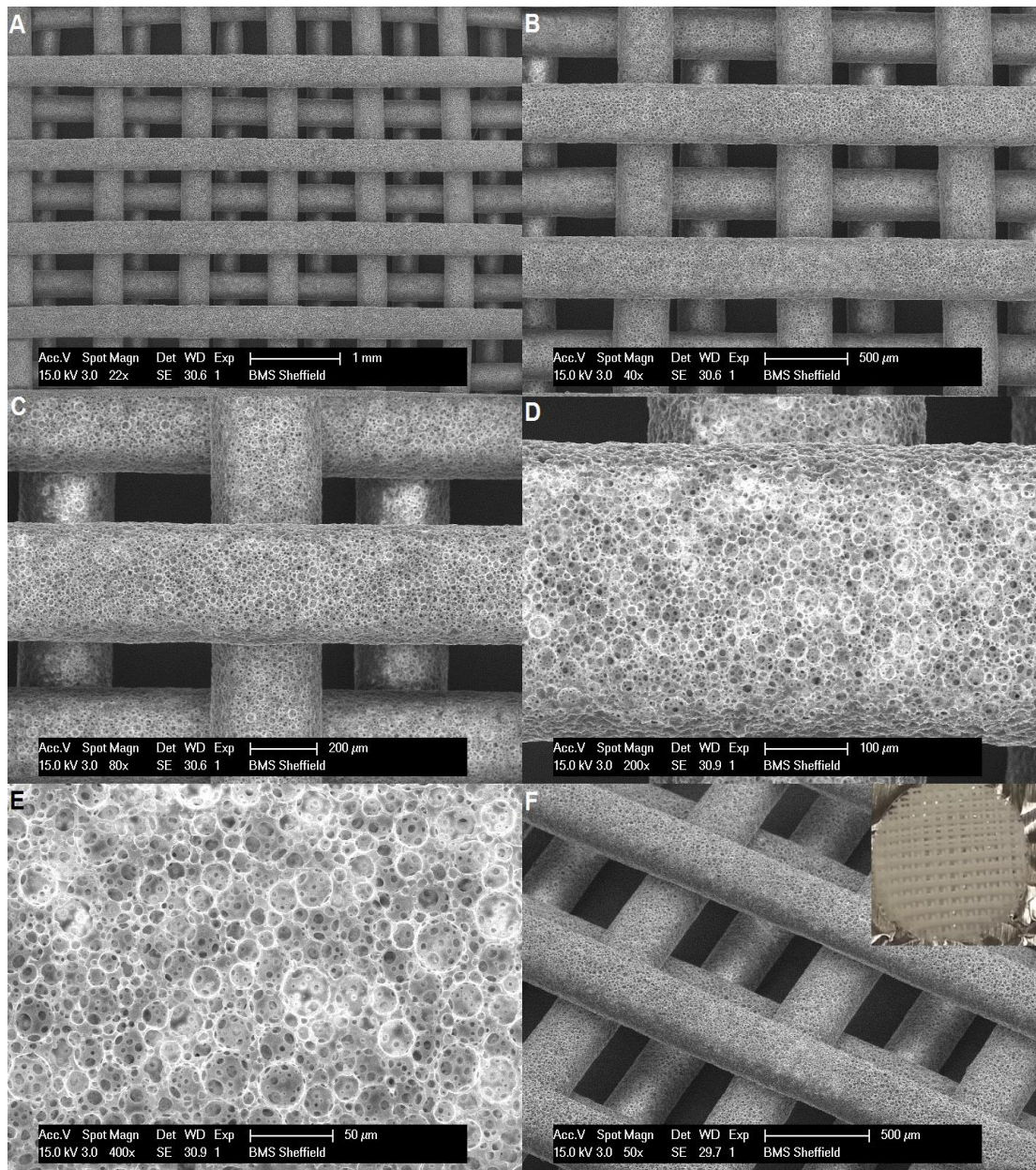


Figure 5.4: SEM images of an EHA0P80 4-layer ‘woodpile’ scaffold. (A-E) Magnification of the same point from 22× to 400×, showing the inherent macroscopic and microscopic porosity of the structure. (F - Main) A side view of one of the fibres showing the offset of the upper two layers. (F-Insert) Photograph of a single scaffold (13 mm diameter).

5.4.4 Air and acrylic acid plasma treatments are equally effective at supporting cells

Initially, the effects of plasma treatment, media composition and substrate stiffness on cell growth were examined over 15 days in all possible combinations (Table. 5.5).

Table 5.5: Conditions to be examined to determine the effects of plasma treatment, media composition and substrate stiffness on hES-MPs. All compositions are treated with each plasma and cultured with both media types.

PolyHIPE Compositions	Plasma Treatments	Media Compositions
EHA0P80 – ‘Stiff’	Untreated	Osteogenesis Induction Media (OIM)
EHA50P80 – ‘Medium’	pcAir	Supplemented Media (SM)
EHA100P80 0 ‘Soft’	pdAAc	-

Untreated scaffolds were unable to support cell attachment and growth (Fig. 5.5A). Both pcAir and pdAAc plasma treatments clearly enhanced the viable cell number on all scaffolds (Fig. 5.5B,C,D). The metabolic activity on plasma modified scaffolds was significantly higher on days 8 and 15 regardless of PolyHIPE composition or media type ($p < 0.05$). Interestingly, there was no significant difference at any time point and composition between pcAir and pdAAc scaffolds, showing that both treatments supported similar levels of metabolic activity. As previously described by Delaine-Smith, et al., there is no significant difference observed between the two cell culture media (SM and OIM) [321].). Comparisons between scaffolds with the same plasma treatment but different wt% EHA indicated that EHA0 scaffolds supported the lowest metabolic activity, with the highest metabolic activity achieved on pcAir-treated EHA100 scaffolds and pdAAc-modified EHA50 substrates. There were no significant differences between compositions at day 8, but by day 15 significant differences with regards to composition were observed between EHA0P80 pcAir vs. EHA100P80 pcAir and EHA0P80.

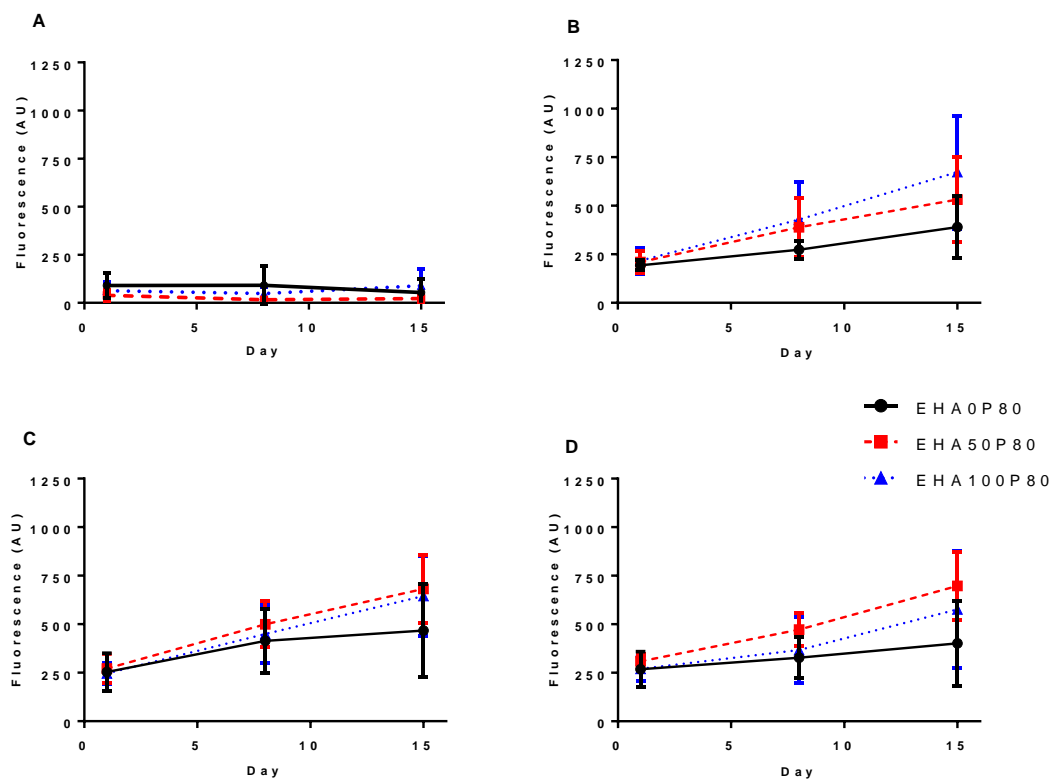


Figure 5.5: Effect of PolyHIPE composition, media and plasma treatment on cell proliferation. RR assay fluorescence for (A) untreated (B) pcAir (C) pdAAc OIM (D) pdAAc SM samples. Untreated scaffold did not support cell attachment and growth. pcAir and pdAAc had similar increases in metabolic activity. The highest metabolic activity appeared to occur in compositions containing EHA. Metabolic activity was not affected by differences in media composition (OIM vs. SM) ($n=6$).

5.4.5 Substrate stiffness only affects differentiation under certain conditions

In addition to determining the effects on metabolic activity, ALP activity was quantified on day 8 and 15 (Fig. 5.6).

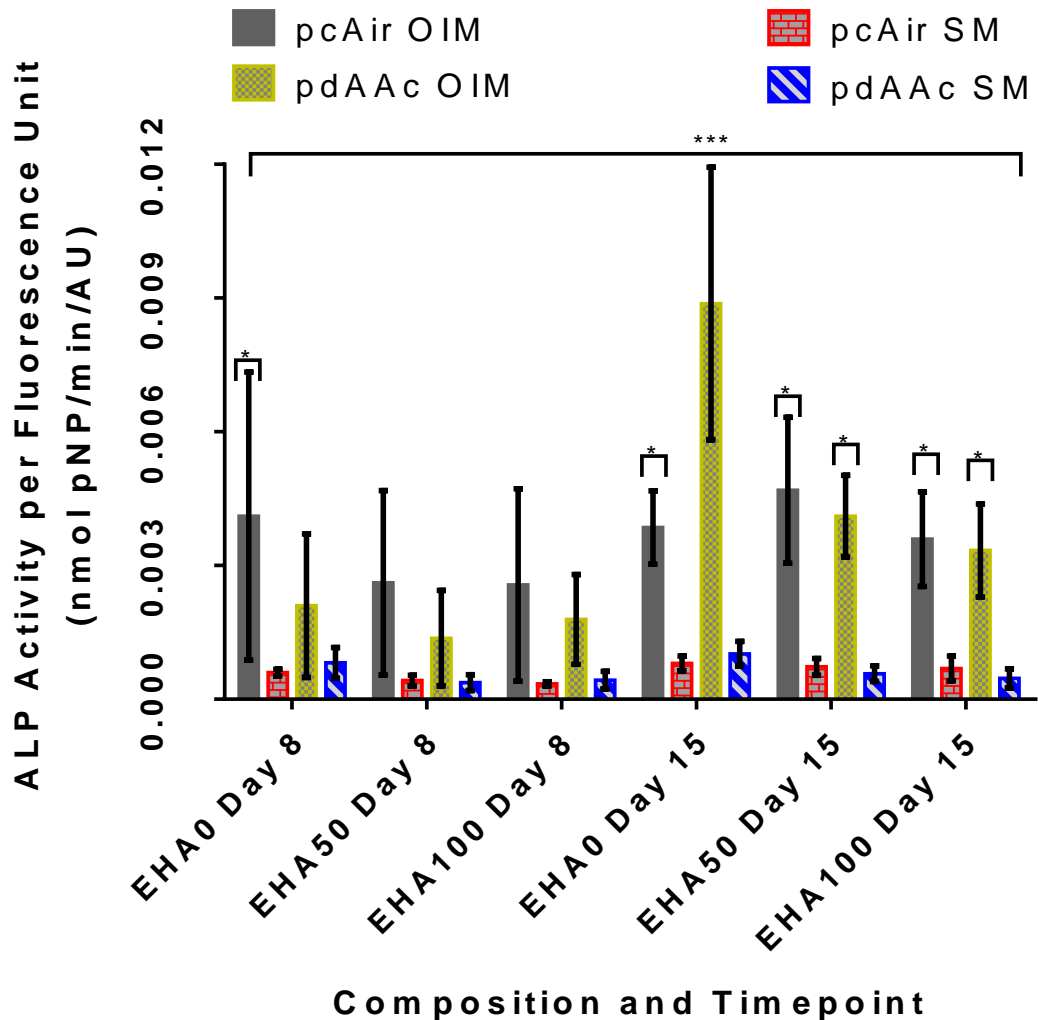


Figure 5.6: Effect of PolyHIPE composition, media and plasma treatment on osteoblastic differentiation. ALP activity normalised to DNA fluorescence. hES-MPs cultured in OCM had higher ALP activity than their NOCM counterparts at all time points (* = $p < 0.05$). None of the substrates or plasma treatments were seen to significantly induce higher osteogenic differentiation, with the exception of pdAAc modified EHA0 scaffolds, which by day 15 were found to be significantly higher than all other groups (***) = $p < 0.001$).

In OIM, normalised ALP activity increased over time . On day 8, normalised ALP activity was similar for both plasma treatments at each composition, with pcAir only being significantly higher on EHA0 scaffolds ($p < 0.05$). On day 15, there was no significant difference between pcAir and pdAAc for EHA50 and EHA100 scaffolds. However, normalised activity on pdAAc EHA0 scaffolds was significantly higher than pcAir for the same composition ($p < 0.001$), as well as significantly higher than both pdAAc and pcAir EHA50 and EHA100 scaffolds ($p < 0.001$). Normalised activity in SM was lower than in OIM in all instances and did not increase over time. This indicates that the stiffness of the substrate did not affect osteogenic differentiation when dexamethasone was not present in the media.

5.4.6 Stiffer PolyHIPE scaffolds retain their architecture without a glass base

The functionalised glass coverslip base of the generation 1 PolyHIPE scaffolds provided a useful platform for developing the manufacturing technique and investigating the effects of the polymer composition. However, this design is not suitable for tissue engineering as the glass is not implantable and it acts as a barrier, limiting nutrient diffusion and flow through the scaffold.

Initially, attempts to fabricate scaffolds using the same method but with a normal, non-functionalised coverslip were performed. Without the MAPTMS on the surface, the PolyHIPE cannot bond to the surface so the scaffold can be removed afterwards. A summary of these attempts is given below (Table 5.6).

EHA0P75 free standing scaffolds were analysed by SEM (Fig. 5.7). The bottom layer of fibres did not lie parallel as there was no anchoring to hold them in position. By looking at fibre cross sections, the interconnected porous network within the fibre can be seen, as well as a skin that forms around the edge of the fibres. This results in only the top surface of the fibre having open pores. This is due to the HIPE curing with an air interface on the top surface, with the side and underside of the fibres curing with a HIPE-polymer or HIPE-glass interface.

Table 5.6: Summary of the different attempts to create a free standing PolyHIPE scaffold.

PolyHIPE Composition	Reasoning	Result
EHA50P80	Able to undergo high strains (~20%) before failure, a useful property in dynamic culture	Unable to hold its structure, forms a ball during washing due to low stiffness
EHA50P30-60	Lower porosity (medium internal phase emulsion - MIPE) increases stiffness with minimal effect on strain at failure	Although a stiffer material, still unable to retain its architecture. MIPEs have closed porosity, which stops effective washing
EHA25P75	Higher proportion of IBOA increases stiffness of the PolyHIPE	Increased stiffness improves architecture, but the scaffold warps during drying
EHA0P75	Highest stiffness of PolyHIPE fabricated	Successfully formed free standing scaffolds with the same architecture as generation 1.

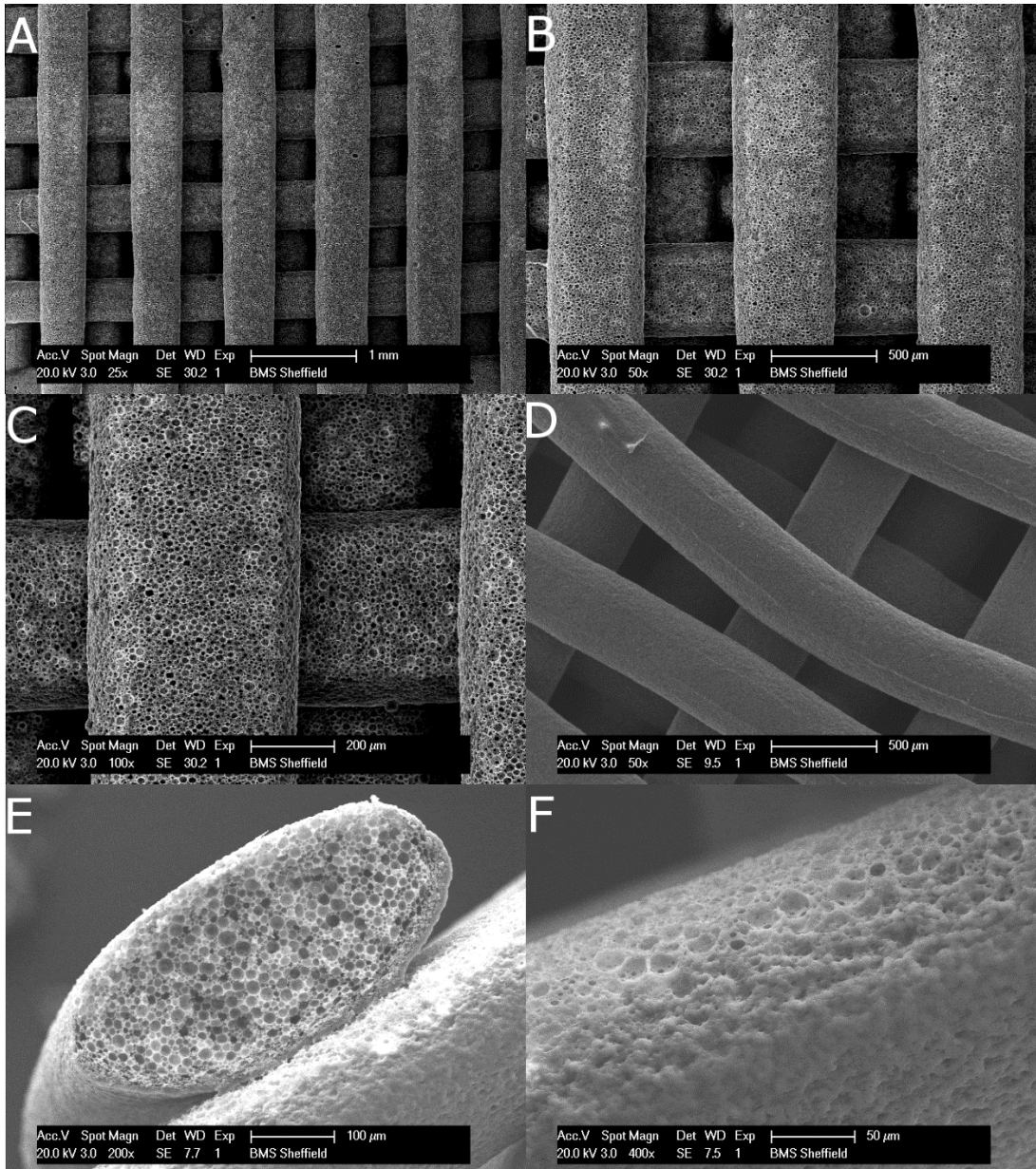


Figure 5.7: SEM images of an EHA0P75 free standing scaffold. (A-C) magnification of the same point from 25× to 100× (D) underside of the scaffold (E) fibre cross-section (F) side skin.

To confirm that these generation 2 PolyHIPE scaffolds could support cell growth over extended time periods, they were seeded using the same protocol as generation 1 scaffolds and maintained for 28 days, assessing metabolic and ALP activity (Fig. 5.8).

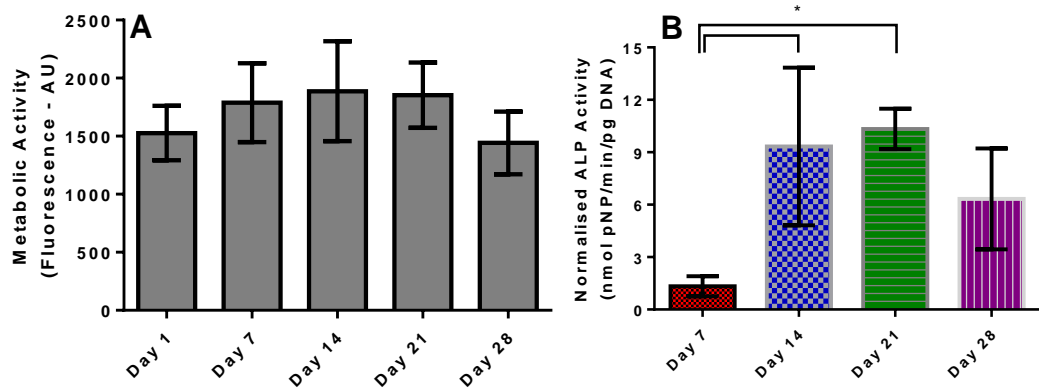


Figure 5.8: Growth and differentiation of hES-MPs on generation 2 scaffolds. Mean \pm SD for (A) RR fluorescence and (B) normalised ALP activity. * indicates $p < 0.05$ ($n=3$).

hES-MPs adhered and remained viable on the generation 2 scaffolds over the 28 day period although no time point was significantly different to any other. In comparison to generation 1, seeding efficiency was 60% lower as cells were not retained within the scaffold by a glass base. This low initial viability limited proliferation throughout the scaffold. ALP activity increased, showing that hES-MPs were still undergoing osteoblastic differentiation, with a peak between day 14 and 21.

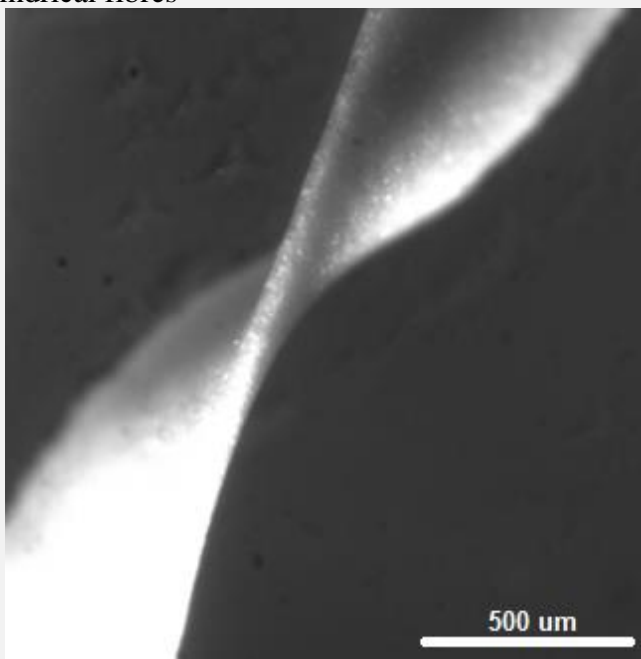
5.4.7 Printing resolution is improved using a UV light absorber

The fibre spacing in generation 1 and 2 PolyHIPE scaffolds is ~650 μm . When it is set to less than this, polymerisation occurs between the fibres resulting in a sheet being formed. A 355 nm laser beam in the UV wavelength is used to initiate polymerisation. Therefore Tinuvin, a UV light absorber, in the continuous phase should reduce or eliminate the polymerisation of material outside the focal spot of the laser. Furthermore, by reducing this partial polymerisation, the surface skin on the scaffold fibres should be reduced.

To determine the concentration of Tinuvin required, attempts to fabricate scaffolds with concentrations ranging from 0.1 to 4 wt% were added to EHA0P80 PolyHIPEs . A summary of these attempts is given below (Table 5.7).

Fibres with a depth similar to PolyHIPEs without UV light absorbers was attainable when using 0.1 wt% Tinuvin. In order to achieve this, the write speed was reduced to 1.50 mm/sec from 1.75 mm/sec, and the laser current increased to 2.65 μA which increases the power. The pinhole diameter remained at 3.1 mm. Fibre spacing was reduced from 650 μm to 450 μm , with a fibre diameter of 400 μm . The incorporation of Tinuvin also affected the side skin formation, as open pores can be seen on a higher percentage of the fibre surface area. However, it did not appear to reduce the thickness of the skin in the regions where it was still present (Fig. 5.9).

Table 5.7: Summary of the effects of different Tinuvin concentrations on EHA0P80 scaffolds.

Tinuvin Concentration	Effect
4 wt%	Unable to polymerise with maximum laser power and pinhole size
2 wt%	Unable to polymerise with maximum laser power and pinhole size
0.5 wt%	Polymerised, but formed thin ribbons rather than cylindrical fibres 
0.1 wt%	Polymerised and formed cylindrical fibres

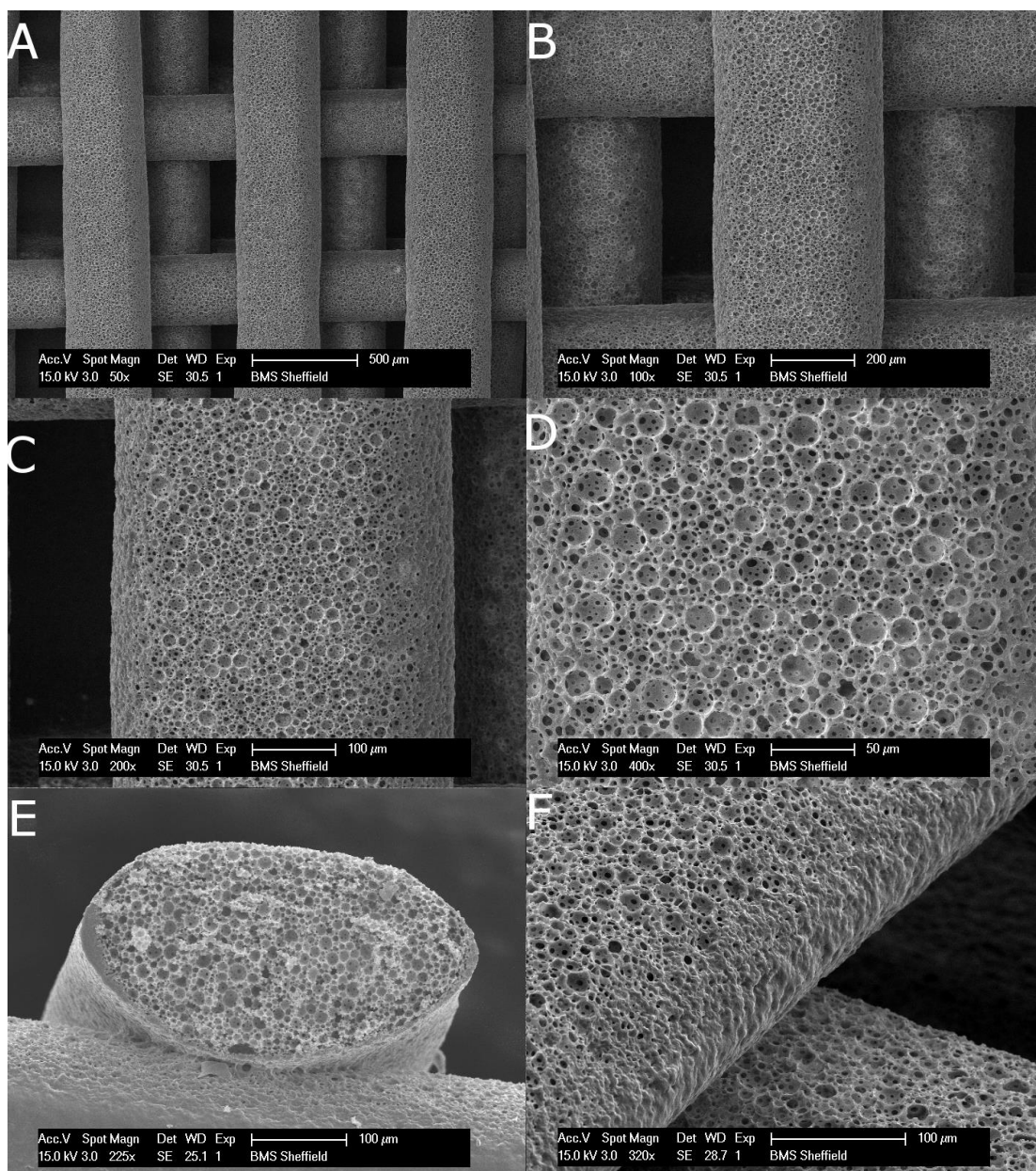


Figure 5.9: SEM images of an EHA0P80-0.1wt% Tinuvin scaffold. (A-D) magnification of the same point from 50× to 400× (E) fibre cross section (F) side skin.

5.4.8 Tinuvin is not cytotoxic in an EHA/IBOA PolyHIPE

Tinuvin is assumed to be cytotoxic and therefore would not be suitable in a biodegradable scaffold. However, the EHA/IBOA PolyHIPEs are non-degradable and therefore this effect may be mitigated. To assess cytotoxicity, MLOA5-S cells were seeded onto EHA0P80 scaffolds fabricated with either 0 or 0.1 wt% Tinuvin. To control for differences in surface area, fabrication parameters were changed for the composition with Tinuvin to match the fibre diameter and spacing of that without the light absorber. Metabolic activity was measured weekly for 18 weeks (Fig. 5.10). No loss of viability was seen with the incorporation of Tinuvin, even over extended time periods, indicating it is not cytotoxic in this polymer and does not leach out over time.

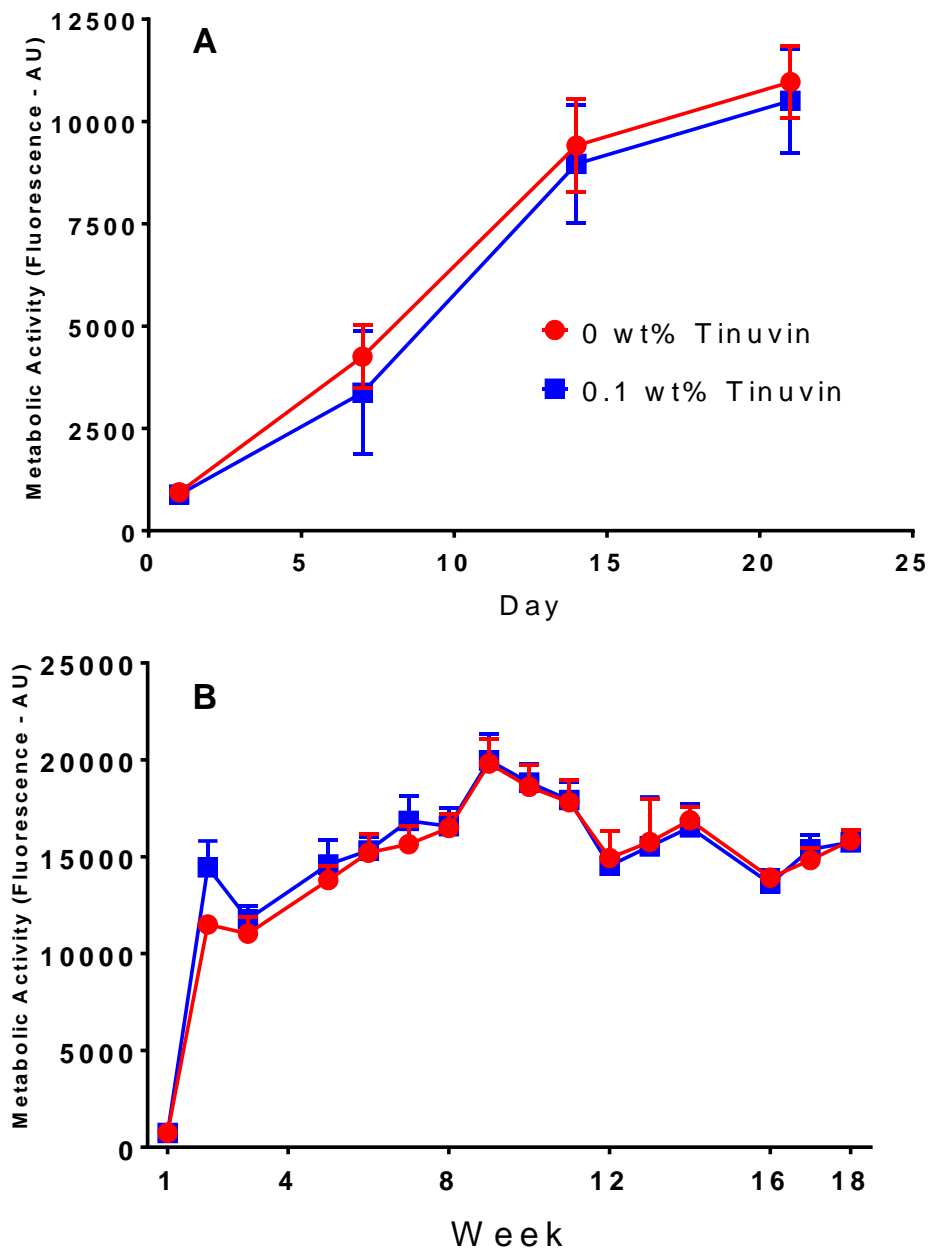


Figure 5.10: Metabolic activity on EHA0P80 scaffolds with or without Tinuvin for (A) 21 days or (B) 18 weeks. No significant difference with the light absorber (n=6).

5.4.9 PolyHIPE and polyurethane scaffolds are equally suitable for the model

To determine the most suitable scaffold for the *in vitro* model, multiple bone tissue engineering scaffolds were compared that fitted the requirements outlined in §5.1.1. Since the advent of bone tissue engineering a plethora of scaffolds have been developed from materials including ceramics, natural and synthetic polymers, glasses, metals and composites of combinations of these using a wide range of fabrication techniques [239], [394]. Clearly this gives a wide range of potential substrates; however, as the main scope of this thesis was the application of the scaffold rather than its development, comparisons were limited to three prospective scaffolds; the generation 2 PolyHIPE, a polyurethane scaffold, and the Biotek 3D Insert™-PCL (Biotek). Unlike some other scaffolds materials, for example electrospun PCL [395], the PolyHIPE and polyurethane scaffolds require a surface treatment before use which increases the processing time. Despite this, these materials were still pursued as the pcAir plasma treatment for the PolyHIPEs is relatively high throughput and the resulting hydrophilicity aids the sterilisation process, whilst the gelatine coating stage for the polyurethane scaffolds is combined with the autoclave sterilisation, making it a facile step.

The PolyHIPE scaffold developed thus far was selected due to the promise these emerging emulsion templated materials have shown in the field of bone tissue engineering to date [240], [389], [390], [396], [397]. The Biotek scaffold was chosen as it has a similar macroarchitecture to the PolyHIPE scaffold but lacks the inherent microporosity of the PolyHIPE material in the fibres, allowing its influence to be assessed. The Biotek scaffold has previously been used for bone tissue engineering studies [398], [399], as well as many other cell types including haematopoietic [400] and adipose-derived [401] stem cells. Finally, the polyurethane scaffold was selected due to its previous use in bone tissue engineering studies [9], [402], [403], as well as the use of other polyurethane scaffolds in the field [404]–[407]. A summary of their key properties and differences is given in table 5.8. Representative SEM images are shown in figure 5.11.

In order to determine which scaffold supports the most mineralised matrix deposition, each scaffold was seeded with 25,000 MLOA5-S and maintained for 28 days. Cell metabolic activity, calcium staining and collagen production were assessed (Fig. 5.12).

Table 5.8: Comparison of key features and properties of the three scaffolds compared for the model.

Parameter	PolyHIPE	Biotek 3D Insert™ - PCL	Commercial Polyurethane
Fibre Diameter	300 µm	300 µm	43 - 96 µm
Fibre Spacing/ Pore Size	350 µm	300 µm	150 – 1000 µm
Number of Layers/ Height	4	6	10 mm
Diameter	13 mm	14 mm	6 mm
Micro-porosity	Yes	No	No
Material	Acrylate PolyHIPE	Polycaprolactone	Polyurethane foam

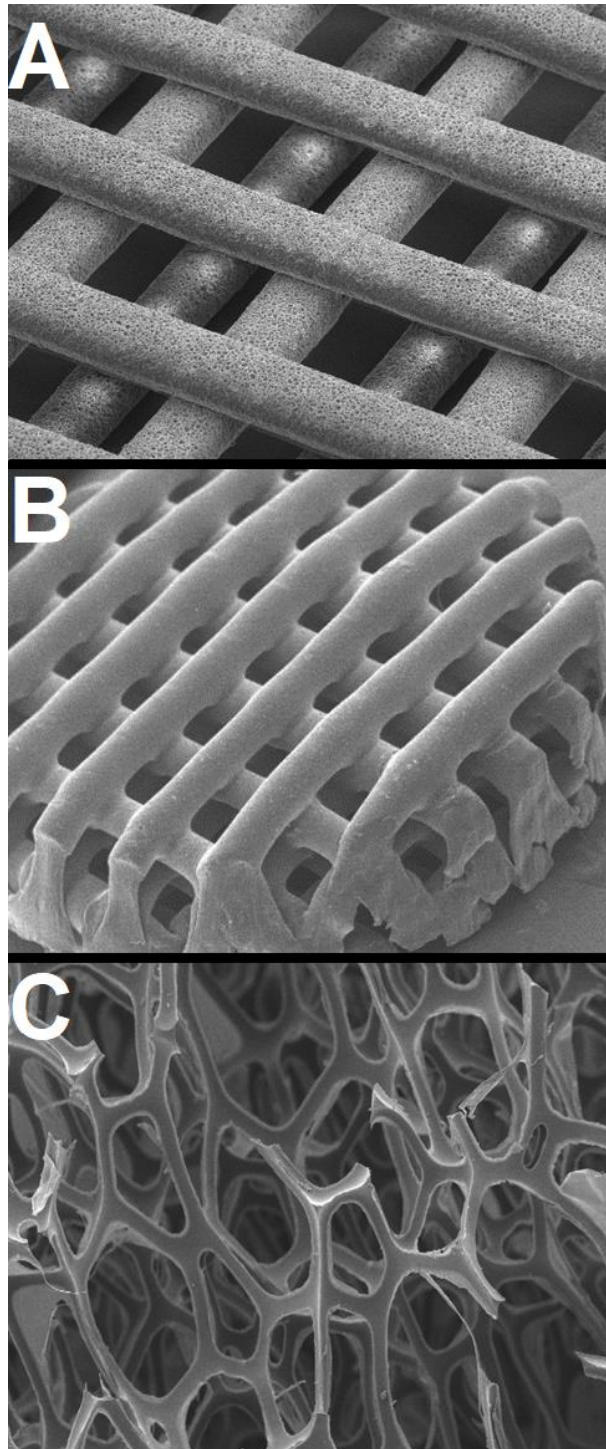


Figure 5.11: SEM images of the macrostructure of the three scaffold types evaluated. (A) PolyHIPE (B) Biotek (C) polyurethane. Images not to the same scale.

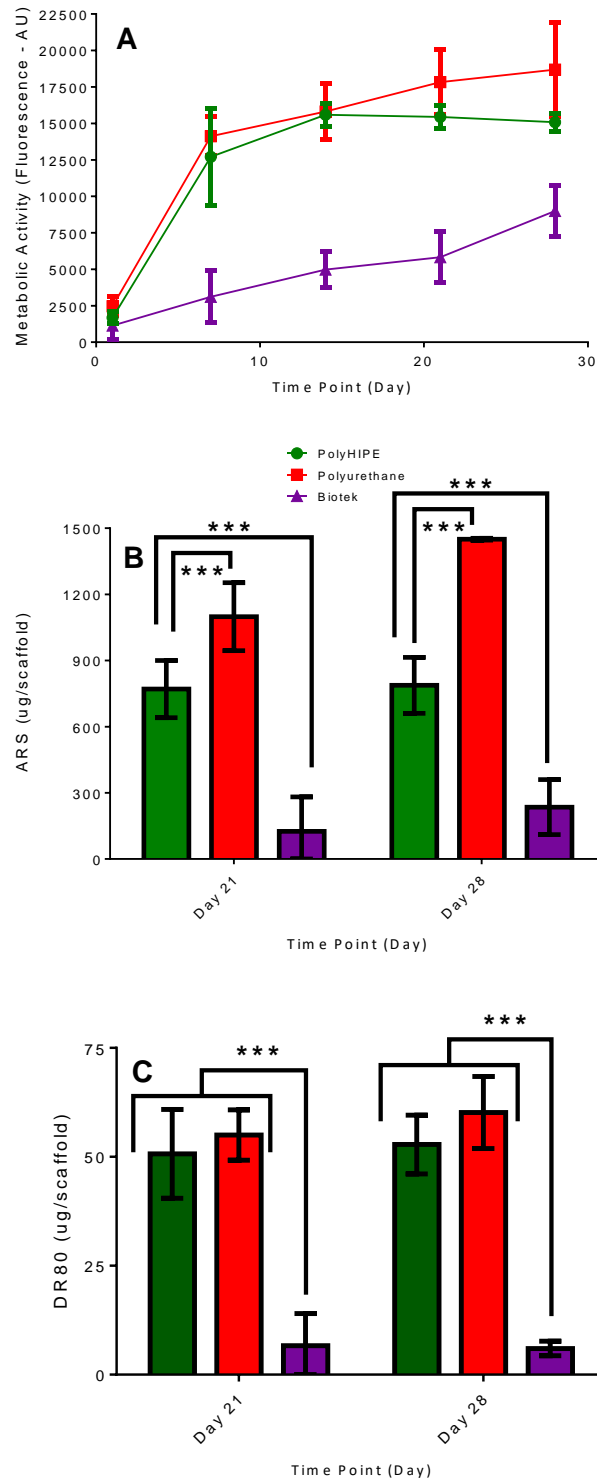


Figure 5.12: Comparison of proliferation and matrix deposition on the three scaffold types. Mean \pm SD for (A) viability (B) ARS staining (C) DR80 staining. *** indicates $p < 0.001$. PolyHIPE vs PU DR80 not significant at D21 or D28. (n=6).

PolyHIPE and polyurethane scaffolds supported cell proliferation at similar rates. The PolyHIPE scaffold reached a plateau sooner, as indicated by the flattening of the growth curve, whereas the polyurethane supported significantly higher metabolic activity (cell number) on days 21 and 28. The Biotek scaffold did not permit cell growth up to a plateau at the time points investigated, but cell number continued to increase throughout the culture period. From day 7 onwards, cell numbers were significantly lower than both other scaffold types.

The PolyHIPE and polyurethane scaffolds had significantly higher mineralisation than the Biotek scaffolds, with the polyurethane having the highest calcium staining on both day 21 and day 28. Mineralisation did not significantly increase between day 21 and day 28 on the Biotek or PolyHIPE scaffold. This is likely due to the cells on the Biotek scaffold being in the growth phase, and cells on the PolyHIPE scaffold having limited volume in which to deposit mineral, as shown by the matrix distribution (Fig. 5.13).

There was no significant difference in collagen production between the PolyHIPE and polyurethane scaffolds on day 21 or 28, but both contained significantly more collagen than the Biotek scaffold.

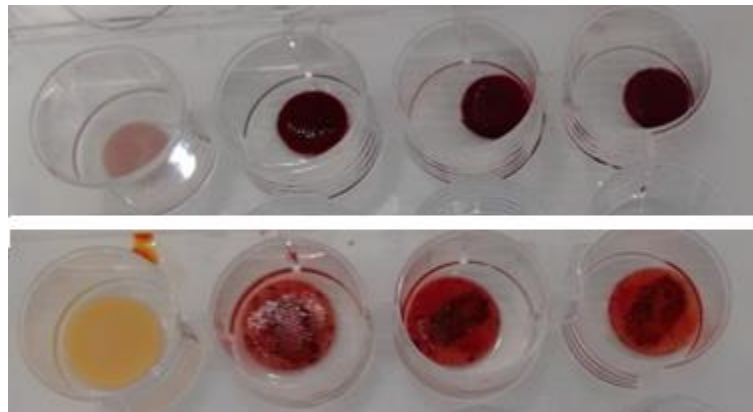


Figure 5.13: Distribution of calcium as shown by ARS staining before destain with perchloric acid for (Top) PolyHIPE (Bottom) Biotek. The far left scaffold in each image is the no-cell control.

5.4.10 Micro-computed tomography

In order to evaluate architecture and determine whether the spatial distribution on mineralised matrix deposition could be quantified accurately, scaffolds were scanned using MicroCT. MLOA5-K were cultured on all three scaffolds in accordance with the experiment outlined in §5.5.9. Scans were performed on seeded and unseeded scaffolds on day 21 and day 28 on all three scaffold types. Before scanning, samples were fixed in accordance with §3.2.10 and kept refrigerated in PBS until analysis. Before mounting in the polystyrene holder, scaffolds were blotted with paper towel to remove excess PBS. The VOIs for each scaffold and time point are given in figure 5.14.

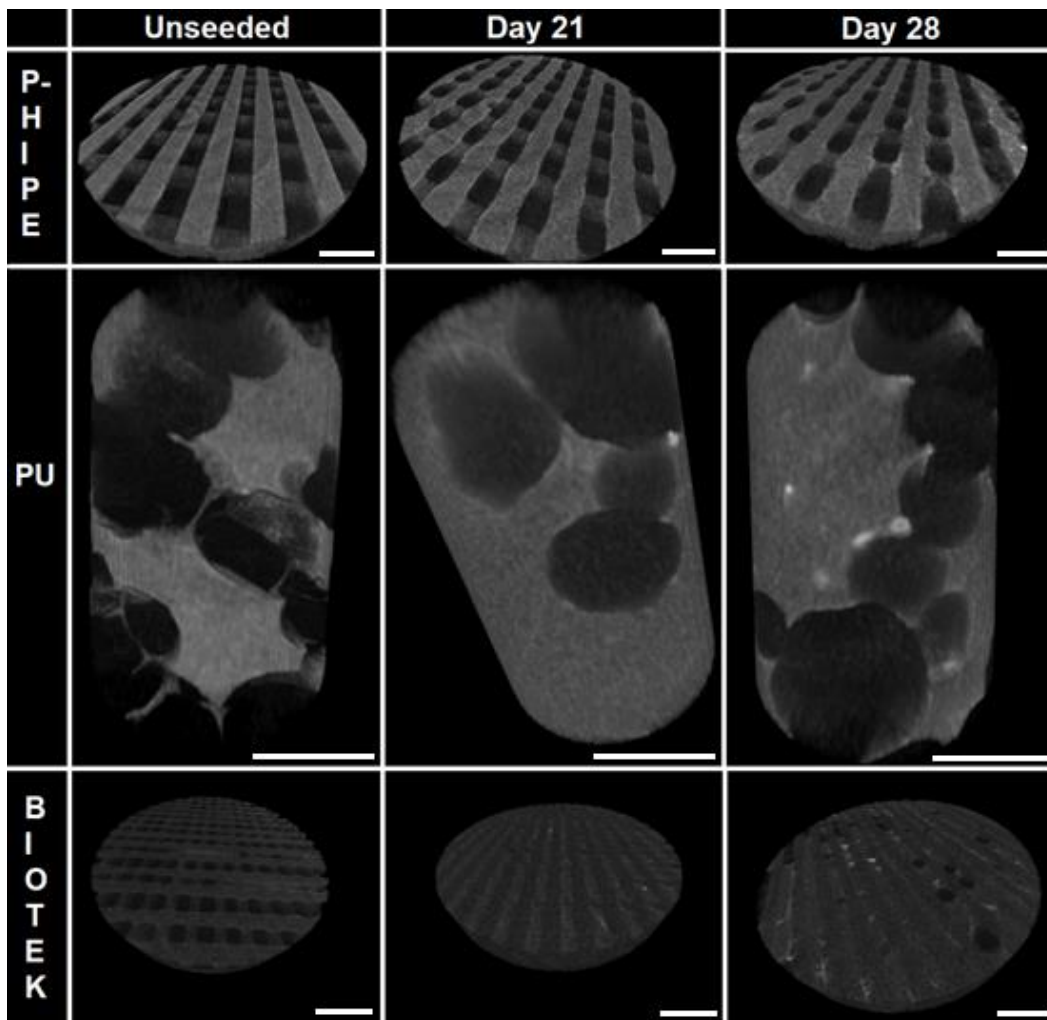


Figure 5.14: MicroCT comparison of unseeded, D21 and D28 VOIs for each scaffold type. Bright spots visible on seeded scaffolds are the high density mineral deposits. Scale bars: PolyHIPE & Biotek – 1 mm, PU – 3 mm.

From figure L it is clear that there are mineral deposits detectable on each scaffold type. In order to quantify this, greyscale index (GSI) histograms were compared to determine whether there were a higher percentage of denser voxels in the seeded scaffolds than the unseeded using a protocol similar to that of Puwanun, et al. [395]. This was done by two different methods, with the minimum threshold either being set as the scaffold GSI (Fig. 5.15) or a GSI above the scaffold density (Fig. 5.16). The former should allow you to see the scaffold and any deposited mineral, whereas the latter only shows deposited mineral.

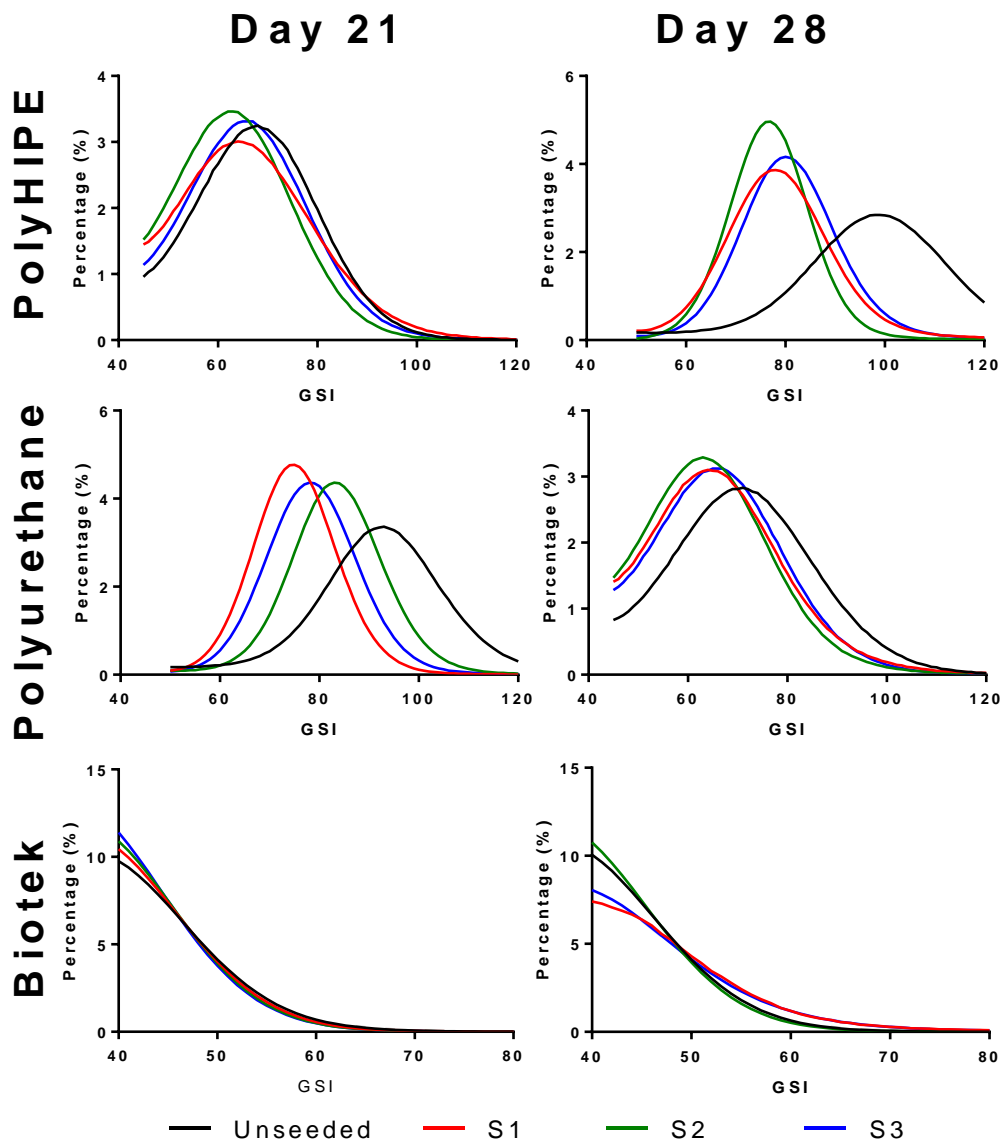


Figure 5.15: Comparison of GSI for all three scaffolds at D21 and D28 with scaffold included in the threshold (n=3).

From comparing the GSI of seeded and unseeded scaffolds (Fig. 5.15) it is not clear that seeded scaffolds are denser. In fact, for the PolyHIPE and polyurethane scaffolds the unseeded scaffolds have a higher percentage of higher GSIs, with the peak for the seeded scaffolds occurring at a lower density, and no discernible difference in GSI for the Biotek scaffolds. This peak may be due to the presence of PBS in the scanned sample, with more being retained in the PolyHIPE and polyurethane scaffolds due to the comparatively higher level of extracellular matrix deposited in these scaffolds as seen by calcium and collagen staining, and the fact that the polyurethane scaffold acts as a sponge.

By adjusting the minimum threshold so that minimum GSI is set as a density greater than the scaffold and comparing the distribution of GSIs above this point, the effect of the water and scaffold material should be removed (Fig. 5.16). Using this protocol, all three scaffold types have a higher percentage of denser GSIs in seeded scaffolds when compared to the control. This difference is most noticeable in the polyurethane scaffolds on day 28 and the Biotek scaffolds at both time points, with the difference in the PolyHIPE scaffolds being barely noticeable at day 21, but more pronounced at day 28.

To ensure that the MicroCT was indeed detecting mineralised matrix, cultures on polyurethane scaffolds were repeated; however, this time some were maintained in BM rather than SM, meaning that the osteogenic supplements were not present. Comparisons of ARS and DR80 staining and MicroCT scanning were performed on days 21 and 28, with thresholds set to exclude scaffold material (Fig. 5.17).

Cultures only mineralised in SM, as indicated by ARS staining, although there was no significant difference in collagen production at either time point. Seeded scaffolds were only denser when maintained in SM, confirming that the MicroCT is detecting mineralised extracellular matrix, rather than just the presence of cells.

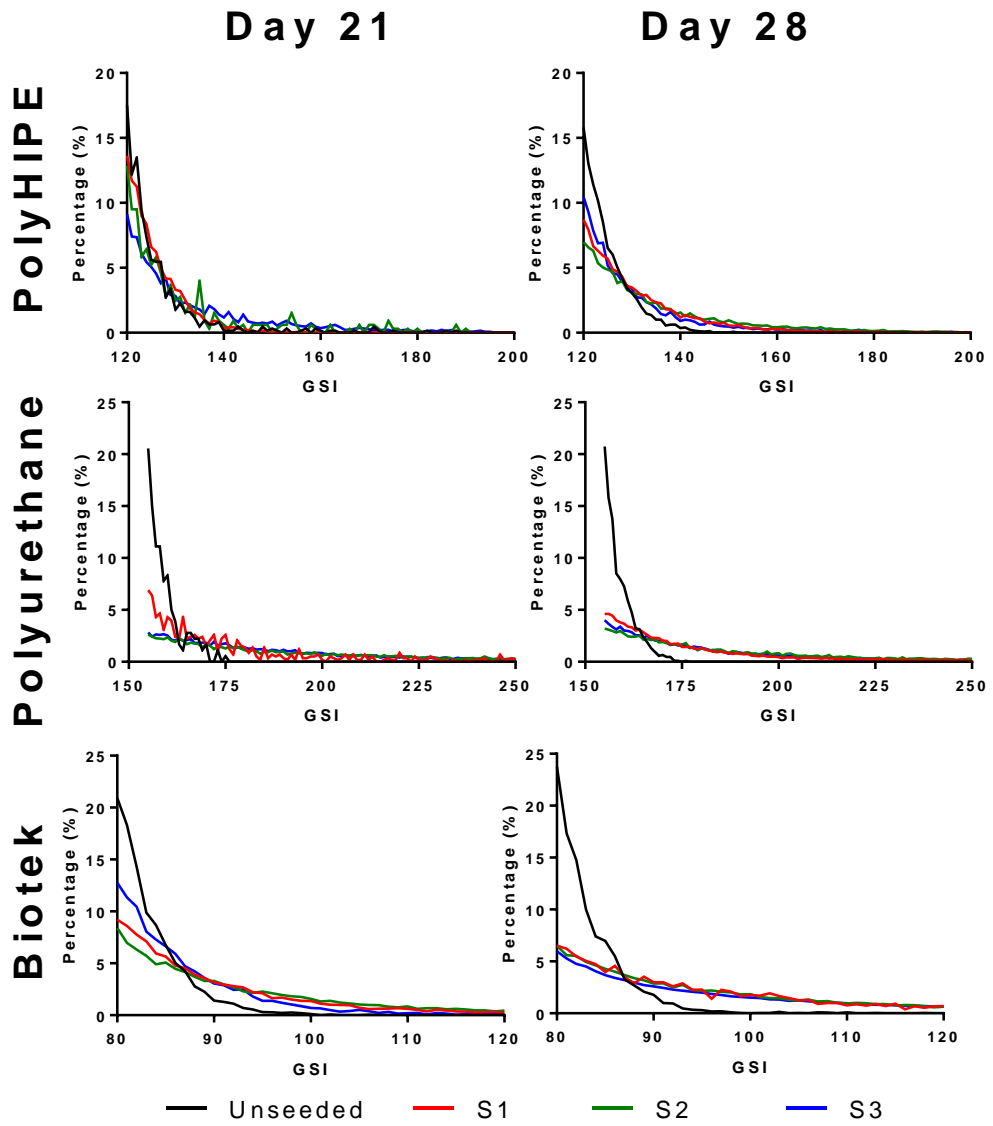


Figure 5.16: Comparison of GSI for all three scaffold types at D21 and D28 with minimum GSI set to exclude scaffold material (n=3).

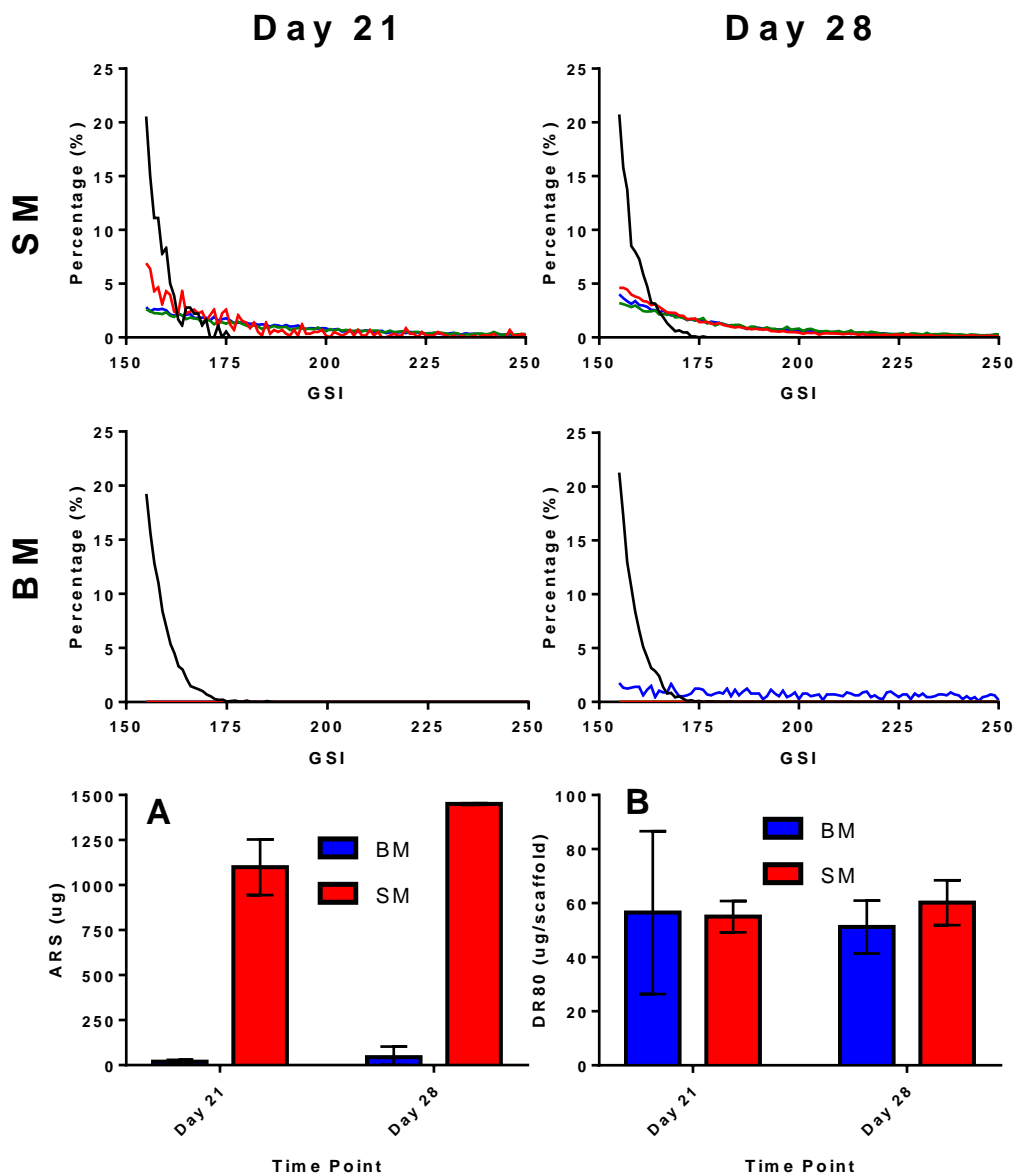


Figure 5.17: Comparison of GSI when MLOA5-K are cultured in SM or BM. Density greater than the scaffold only detectable in SM. (A) ARS and (B) DR80 comparison of SM and BM culture (n=6).

To examine whether it is indeed the presence of PBS that was affecting the GSI distribution, 5×5 polyurethane scaffolds were seeded with 60,000 IDG-SW3 and maintained in EM for three days before a further culture of 21 days in SM. Scaffolds were then fixed using the normal protocol (§3.2.10) before being dehydrated. This was performed by submerging scaffolds in increasing ethanol concentrations (50, 70, 80, 90, 100, 100 vol%) for ten minutes at each concentration before submerging samples in HMDS for three minutes then leaving to air dry in a fume cabinet overnight. Samples were then scanned using MicroCT using the standard protocol (§5.4.14), but the GSI threshold was set at 30-255. This includes the scaffold material and the mineralised matrix.

Comparison of wet and dry polyurethane VOIs clearly demonstrates the influence PBS was having on the scanned samples. Furthermore, in dry scaffolds, the percentage intensity of the GSIs is able to reveal the mineralised matrix deposition without the need to threshold out the scaffold material (Fig. 5.18).

As well as detecting mineral deposition, MicroCT can also reveal the architecture of the entire scaffold in a non-destructive manner. Both the Biotek and PolyHIPE scaffold are designed to be woodpile structures. To determine whether the final product matches the initial design, scans of the entire scaffold were performed, reconstructed, and electronically cross-sectioned using CTvox. These were compared to SEM images of scaffolds cut with a scalpel to examine microarchitectures (Fig. 5.19).

From the MicroCT and the SEM of the Biotek scaffold it is clear that it does not have the described architecture. The edge of the scaffold has merged where it has been stamped from a larger sheet and the layers of fibres do not alternate properly, meaning that there is not a regular porosity throughout. MicroCT images of the PolyHIPE scaffold have very poor contrast due to them being 80% air and MicroCT being a density-based imaging modality. Despite this, it can be seen that these scaffolds have retained their fibre offset, resulting in a regular macroporosity throughout. This is confirmed by the SEM images of the PolyHIPE scaffold, where the offset can clearly be seen, as well as the internal microporosity. However, the perimeter of the scaffold suffers from fibre merging, resulting in all four layers of fibres combining (Fig. 5.19, bottom left).

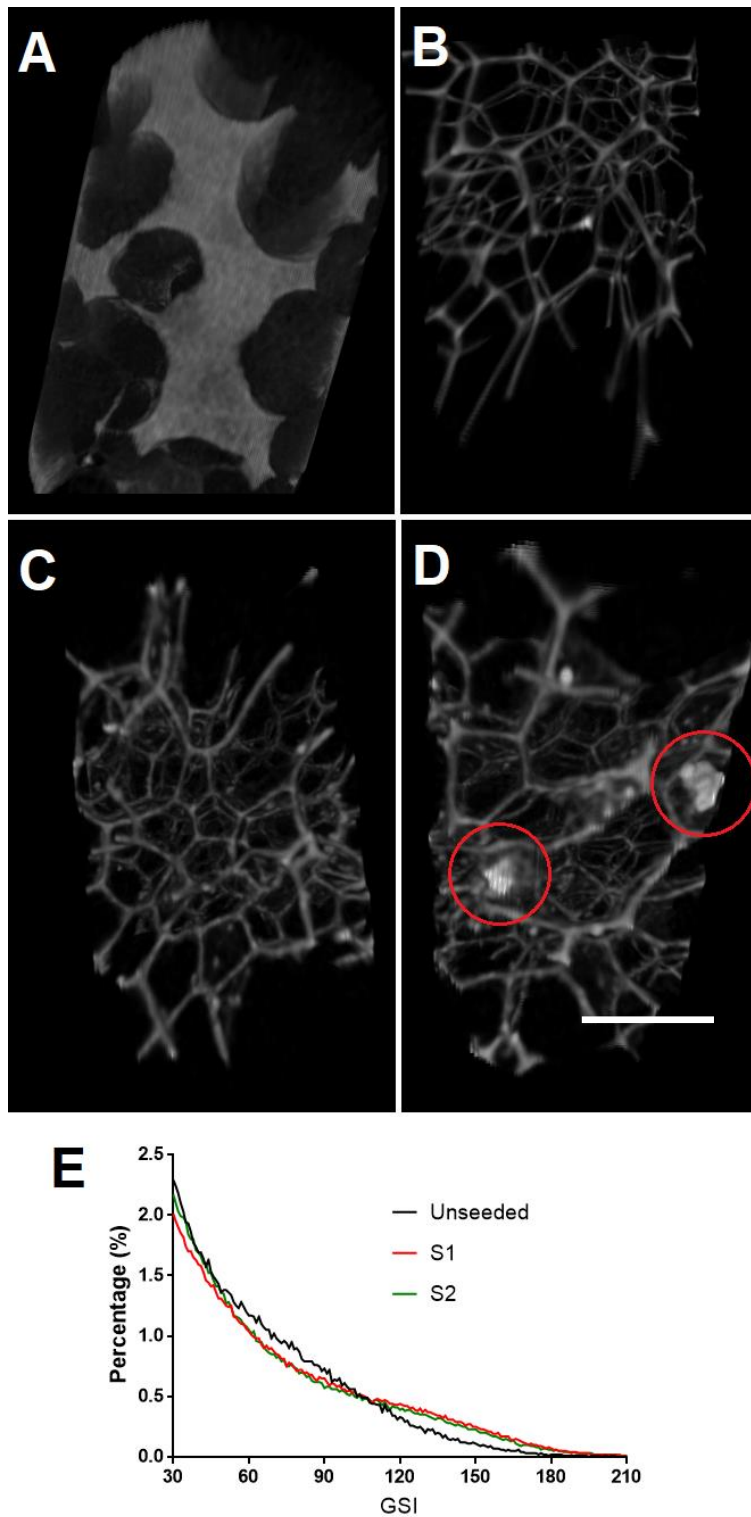


Figure 5.18: Comparison of wet (A) and dry (B) unseeded PU VOIs. On seeded, dried VOIs, scaffold struts are clearly denser (brighter) and mineral deposits are even visible (circled in red, C & D). This higher density is also clear in the GSI histogram without thresholding out the scaffold (E). Scale bar: 2.5 mm.

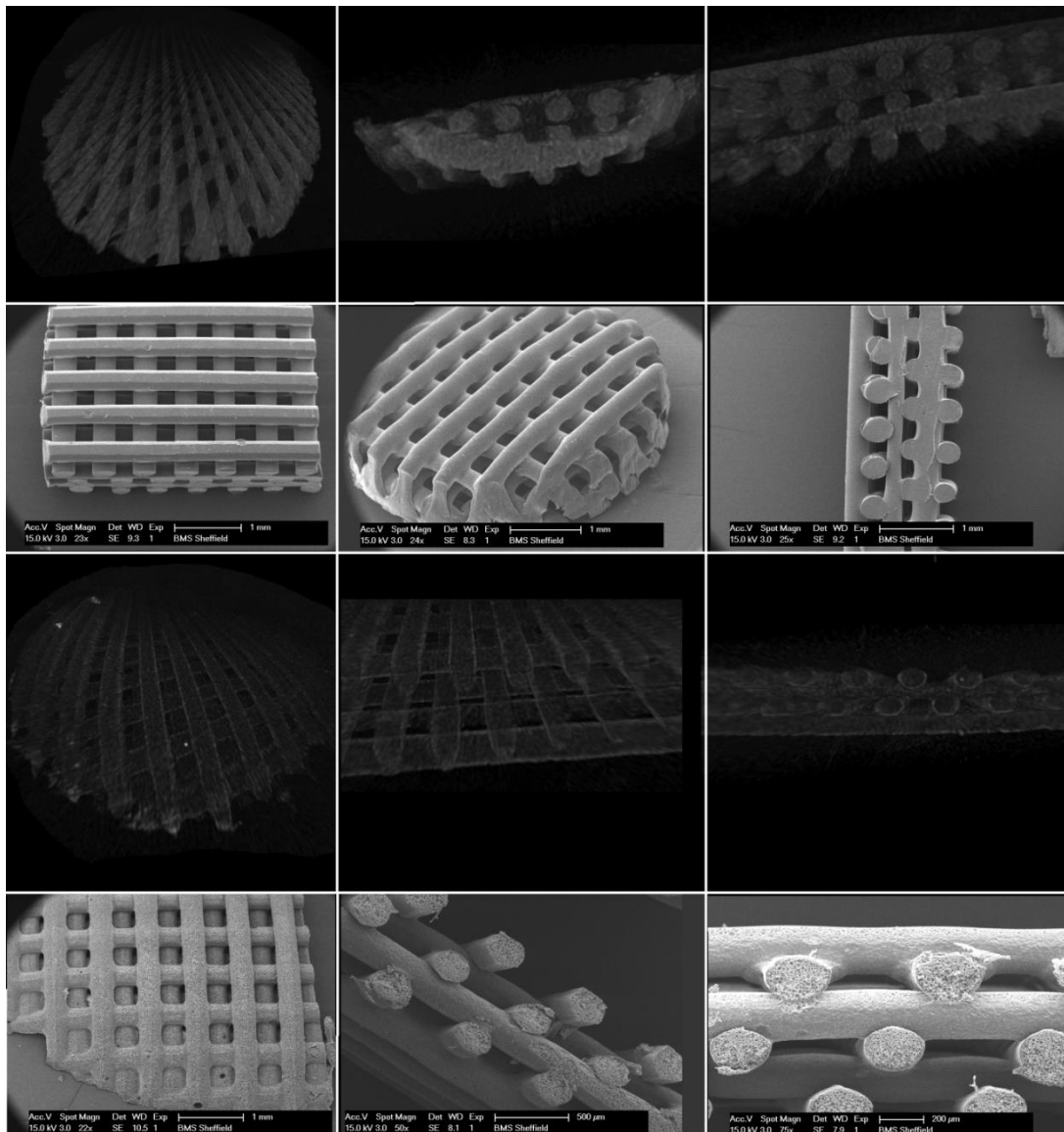


Figure 5.19: MicroCT and SEM images of the Biotek and PolyHIPE woodpiles. Top Row: MicroCT of whole (left), edge (centre) and cross-section (right) of Biotek. Second Row: SEM of Top (left), whole (centre) and cross-section (right) of Biotek. Third Row: MicroCT of whole (left), and two cross-sections (centre & right) of PolyHIPE. Fourth Row: SEM of edge (left), and two cross sections (centre and right) of PolyHIPE.

5.4.11 Generation 3 PolyHIPE – improved architecture and reproducibility

The generation 1 PolyHIPE scaffold was the four-layer woodpile attached to the functionalised coverslip. The second generation reduced the fibre spacing through the incorporation of Tinuvin and permitted the removal of the scaffold from the coverslip, resulting in it being free standing. However, the method of polymer addition during the fabrication relies on surface tension to stay in place, limiting the height of the scaffold to four layers and compromising its architecture at the perimeter (Fig. 5.20).

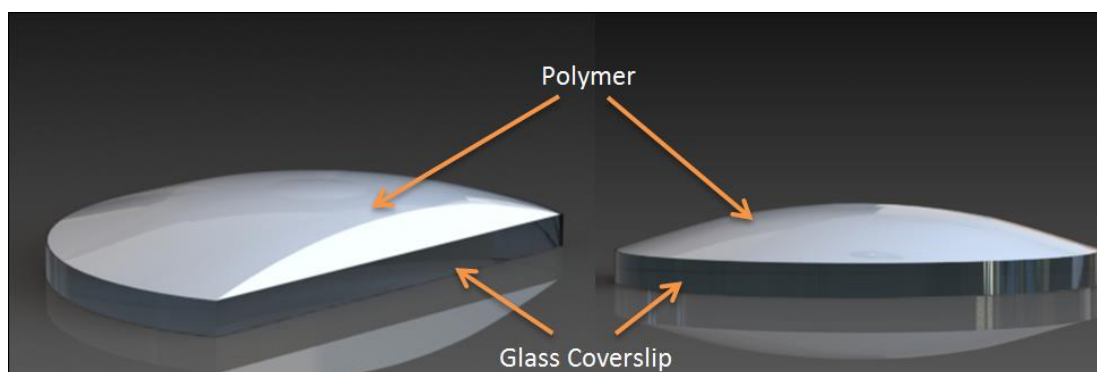


Figure 5.20: Render showing polymer addition for generation 1 and 2 scaffolds. Technique relies on the HIPE droplet staying on the coverslip through surface tension. This results in a 'contact lens' shaped scaffold that is exacerbated as more layers are added. CAD render used with the kind permission of Ross Burdis.

The effect of this method of polymer addition can be seen in figure 5.21. Although the architecture is retained in the centre of the scaffold, at the edge there is not sufficient HIPE on the preceding layer for the subsequent layer to form from, resulting in fibre merging.

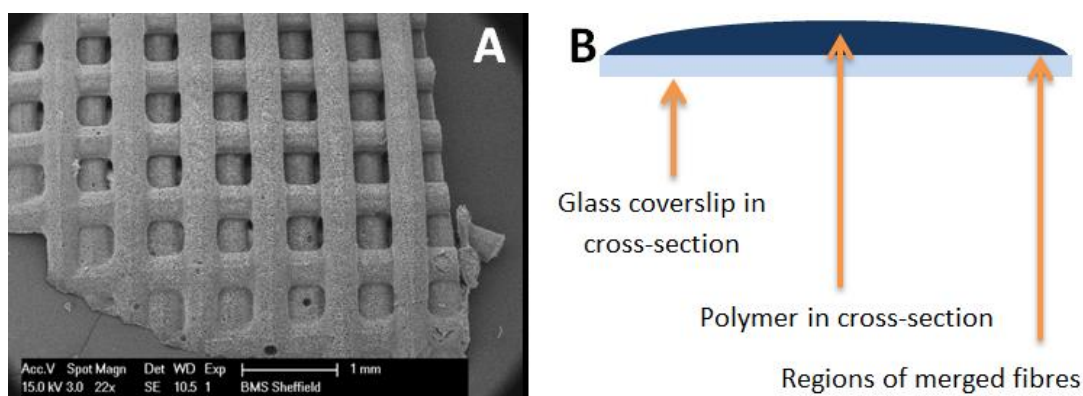


Figure 5.21: Effect of polymer addition method on fibre architecture. (A) SEM image of a second generation scaffold. (B) schematic identifying the regions where fibre merging occurs. CAD render used with the kind permission of Ross Burdis.

In order to overcome this, HIPE needs to be added in a manner which does not rely on surface tension. Therefore, a custom 15×15 mm square well was 3D printed in ABS. In the base of this, a square glass coverslip was placed which was covered with a layer of HIPE. After the first layer of fibres was written, HIPE could again be added that covered the entire well, negating the effects of surface tension.

To avoid surface tension, HIPE covered the entire base of the ABS well. To mitigate fibre merging between layers, HIPE was always added evenly over the entire area of the well. To keep the bottom layer of fibres aligned and parallel, a perimeter the length and width of the scaffold was written first, inside which the first layer of fibres were polymerised. Subsequent layers of HIPE were added with a 22g hypodermic needles for precise spatial and volumetric delivery. Only HIPES in the range of EHA0P80 to EHA15P80 with 0.1 wt% Tinuvin produced scaffolds with acceptable architecture. Above 15 wt% EHA, polymerisation between fibres occurred, producing sheets rather than distinct fibres.

This optimised protocol allowed scaffolds to be produced without fibre merging up to 22 layers in height. The final dimensions of the third generation scaffolds were 6.75×6.75 mm squares, 6 layers in height, with a mean fibre diameter and spacing of $325 \mu\text{m}$ and $315 \mu\text{m}$, respectively (Fig. 5.22). There was no significant difference in diameter and spacing between the EHA0P80 and EHA15P80 compositions. Reproducibility and architecture were significantly improved.

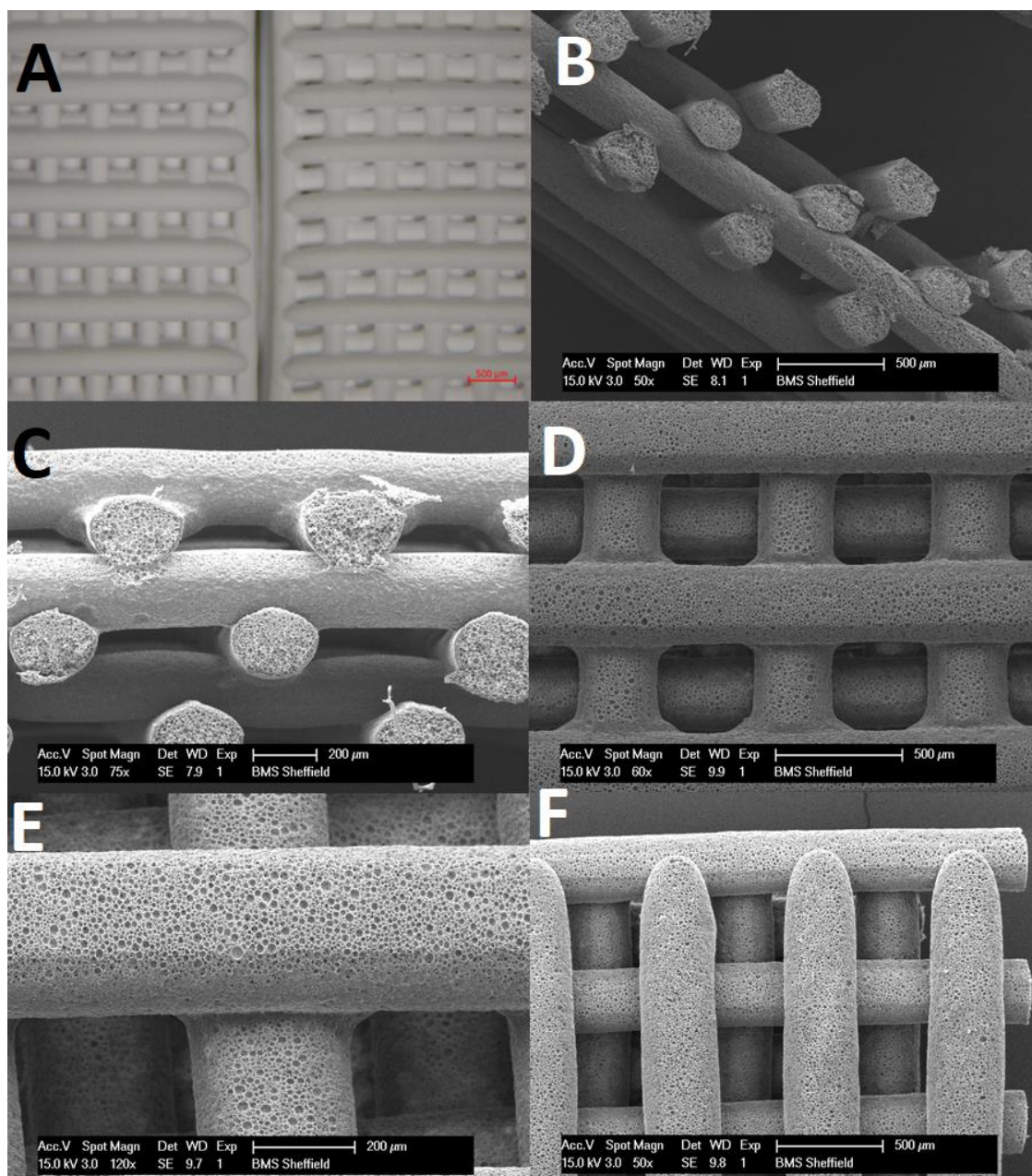


Figure 5.22: SEM images of generation 3 PolyHIPE scaffolds. (A) microscope image showing two third generation scaffolds (B-G) SEM of 6-layer EHA0/EHA15P80 generation 3 scaffolds.

Cellular performance of the generation 3 scaffolds was evaluated by seeding with 25,000 MLOA5-K in 100 μL of BM in a bespoke well plate to maximise seeding efficiency (Fig. 5.23). Each well is 7 × 7 mm and completely filled when a scaffold and 100 μL of media is added. Metabolic activity and mineralisation were assessed over a 3-week period (Fig. 5.24).

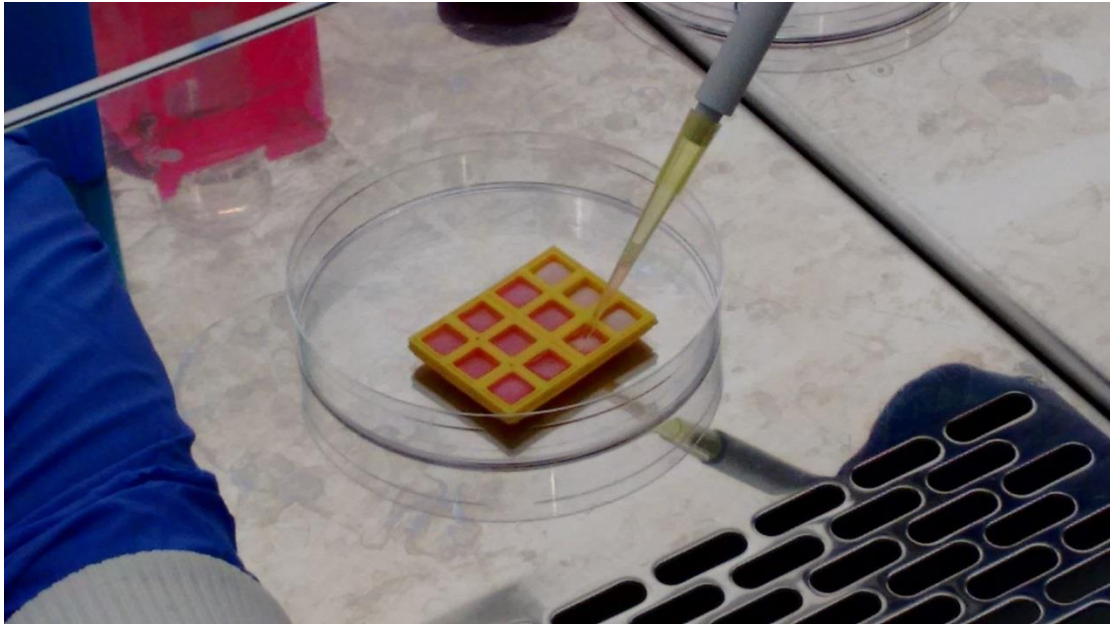


Figure 5.23: Bespoke seeding well plate for generation 3 scaffolds.

Cell metabolic activity significantly increased at each time point. By day 21, there was substantial mineralised matrix deposition, as indicated by high levels of ARS and DR80 staining. Direct comparisons to generation 2 scaffolds are not possible due to the significantly different architecture.

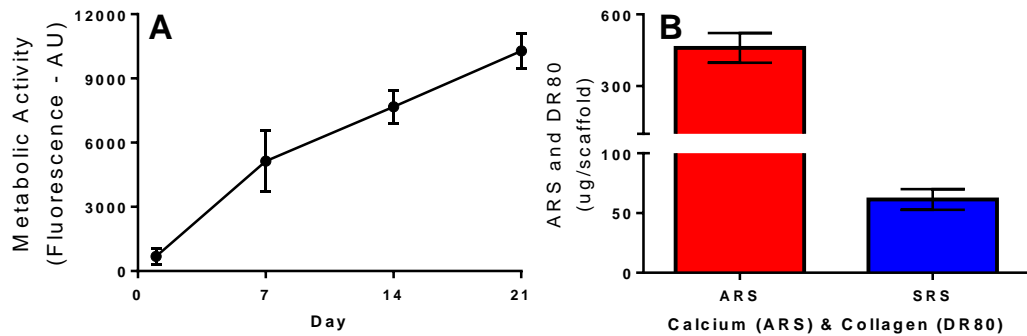


Figure 5.24: Generation 3 PolyHIPE scaffolds supported (A) cell growth and (B) mineralised extracellular matrix production over a three-week period (n=5).

5.4.12 Cells do not fully penetrate the internal porosity within 3 weeks

Ingrowth into the internal porosity of the fibres of the generation 3 PolyHIPE scaffolds was assessed using histology. 200,000 hES-MPs were seeded onto 6-layer EHA0P80 generation 3 scaffolds in BM then maintained for 21 days in OIM. Scaffold mineralisation was assessed via Alizarin Red S staining (Fig. 5.25) and ingrowth by sectioning and H&E staining (Fig. 5.26).

ARS staining revealed mineralised nodules on the fibres and in the matrix deposited between the scaffold fibres. hES-MPs appeared to have an elongated phenotype that ran parallel with the fibre direction.

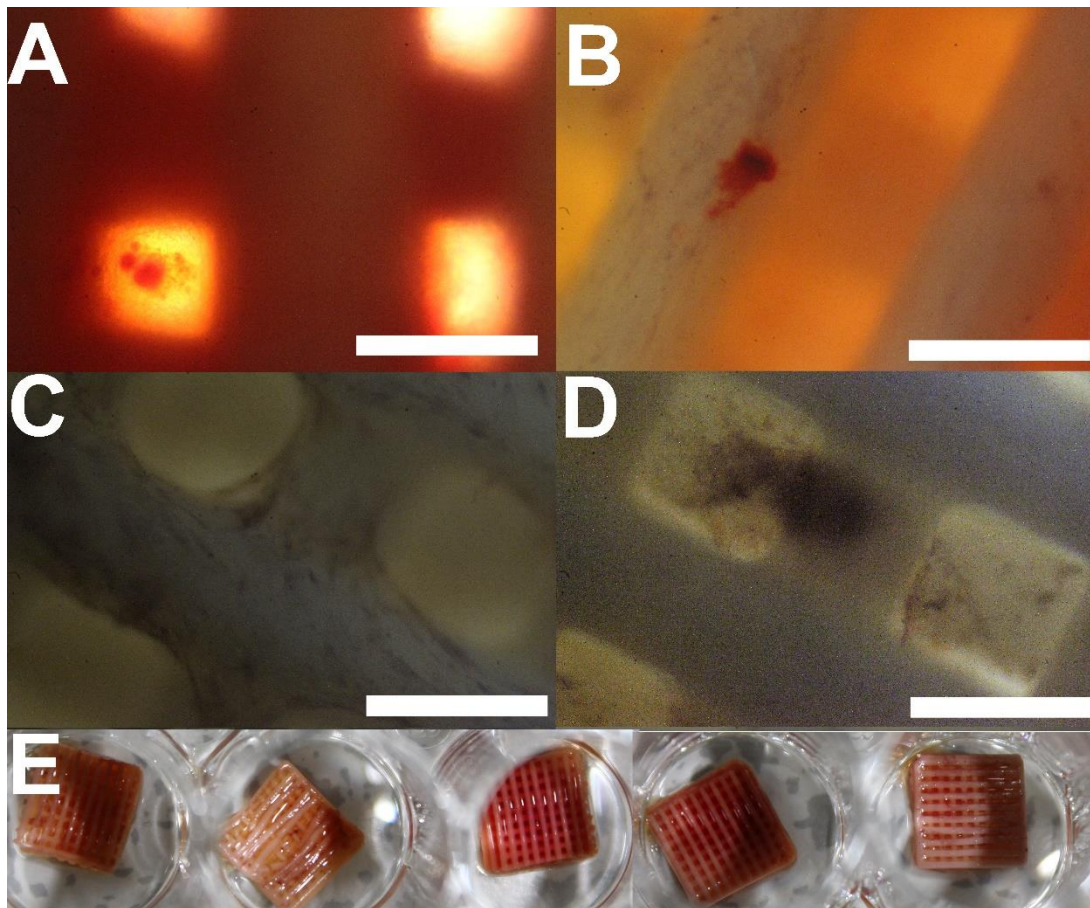


Figure 5.25: Representative photographs of ARS stained single phase PolyHIPE scaffolds ($n=12$). (A & B) show mineralised nodules in the extracellular matrix deposited by hES-MPs present between the fibres. (C & D) show the elongated hES-MP cells aligning with the fibre direction and spanning the fibre spacing. (E) macroscopic photographs of mineralised hES-MP cultures. Scale bars all 400 μm .

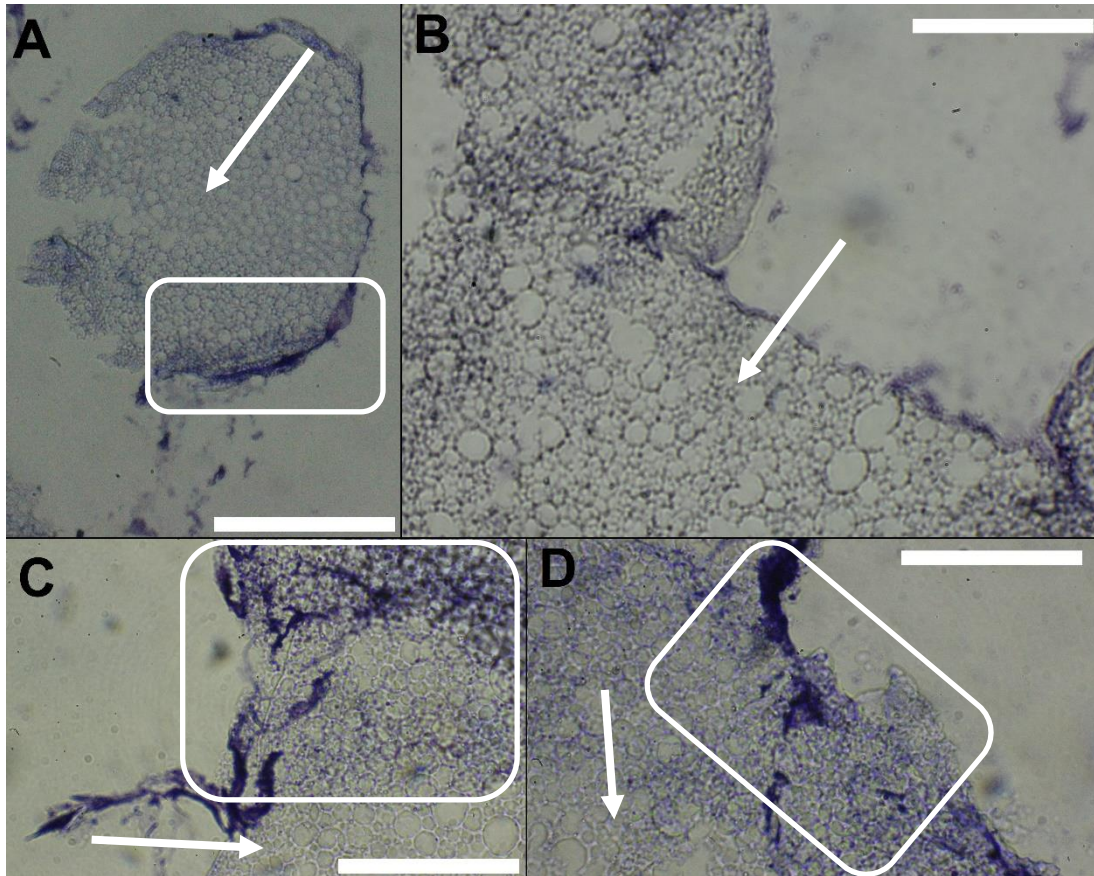


Figure 5.26: Optical microscope images of generation 3 PolyHIPE scaffold sections stained with H&E. (A) cross-section of a single fibre (B) cross-section of two layers of fibres intersecting (C&D) cross sections of scaffold material. Boxes surround darker areas within the fibre where cellular material is present. Arrows point to regions where cells did not penetrate. Images taken at 20 \times magnification. Scale bars 200 μm .

When sectioning it was not possible to retain the woodpile architecture of the scaffold. Due to the presence of extracellular matrix and PBS within the macropores of scaffold, the tissue freezing medium was not fully able to penetrate the porosity resulting in the scaffold rupturing as it was frozen in liquid nitrogen. However, it was possible to stain and image individual pieces of the scaffold. In figure 5.26 it can be seen that the outer perimeter of the scaffold appears dark purple, showing where the cells and matrix have coated the surface of the fibre. In some regions, the immediate layers of pores below the surface of the fibre are also stained dark purple, indicating ingrowth (white boxes). However, despite the large interconnectivity of the PolyHIPE material, cells did not penetrate the full thickness of the fibre, with many regions left without cells (white arrows).

5.5 Discussion

Parts of this discussion have appeared in the author's publication 'Emulsion templated scaffolds with tunable mechanical properties for bone tissue engineering' [240]. A full copy of this publication is available in the appendix, §10.3. Under the Personal Use terms of the publication, the author has used parts of this article in full for this thesis.

The work performed in this chapter primarily aimed to determine a suitable substrate for use in an *in vitro* model of postmenopausal osteoporosis that will be developed in chapter 6. First, the ability of the generation 1 PolyHIPE scaffolds to support bone-cell cultures was evaluated, with the effect of substrate stiffness and plasma treatment examined. Once their suitability was confirmed, they were developed into generation 2 scaffolds that utilised a UV light absorber to improve the printing resolution and no longer required a glass substrate to retain their architecture. This scaffold was then compared to two alternatives; a polyurethane foam and a commercial polycaprolactone woodpile structure produced by 3D Biotek. The cellular performance was assessed as well as the physical properties. The PolyHIPE scaffold was then further developed, with the generation 3 scaffold having superior architecture and reproducibility.

Wet mechanical testing showed that cell culture conditions did not affect the stiffness of the material. However, samples were not plasma treated prior to testing meaning that they were still hydrophobic and PBS may not have fully penetrated the porous network. Despite this, swelling of the polymer which could affect the mechanical properties only occurs in solvents such as acetone; therefore, it is unlikely that full saturation of the PolyHIPE by culture media would have significantly changed the mechanical properties. Furthermore, PolyHIPEs with a high IBOA content are less prone to swelling [408]. It is interesting to note that tensile specimens were not always made from the same batch of HIPE, yet there is a high level of concordance in the results. This indicates that the synthesis method reproducibly creates a PolyHIPE with indistinguishable mechanical properties.

Physical characterisation by determining the DOO for each of the twenty compositions confirmed that the manifestation of these nominal porosities is not affected by monomer proportion. Having the same DOO in each of the three compositions means that variation in internal fibre architecture is minimised between compositions as well

as allowing similar levels of nutrient exchange between the cells and the environment [409]. The compositions selected for scaffold manufacture, EHA0P80, EHA50P80, and EHA100P80, had the highest possible internal phase volume ratio in order to maximise the DOO whilst retaining a viscosity that is amenable to pipetting.

It is known that the porous architecture of a scaffold can affect cell proliferation and osteogenesis, therefore optimising this will enhance the performance of the scaffold [362]. The ease with which porous materials can be fabricated using emulsion templating makes PolyHIPEs excellent materials for 3D cell culture, as exemplified by the commercialisation of Alvetex®, a 200 µm thick polystyrene-based PolyHIPE scaffold [410]. However, cellular penetration into these PolyHIPE monoliths is dependent on their thickness and pore size [372], with Akay, et al., finding that regardless of pore size, cellular penetration in PolyHIPEs was rarely seen beyond 1 mm [373]. Additionally, when plasma treating the PolyHIPE to overcome the intrinsic hydrophobicity, it has been shown that there is a significant depth dependence with regards to its efficiency. Plasma treatments have been shown to coat the inner-surfaces of an 85% porous, 10 mm diameter 3 mm thick disk; however, any porous object beyond a few millimetres thick will not be homogeneously coated, with the least deposition occurring at the core [411], [412]. Therefore, PolyHIPE monoliths need to be thin for optimal cell and plasma penetration. By creating scaffolds from HIPEs using microstereolithography, this depth limit can be overcome as individual fibres will not be too thick for cell ingrowth and plasma penetration (<1 mm), but the overall depth of the scaffold can be much larger than it can be for monoliths.

This allows focus to shift onto the macroscopic structure of the scaffold, resulting in the ability to produce much more complex scaffolds. The minimum void diameter for osseous deposition is considered to be between 50 and 100 µm [363] with the recommended size being 300 µm and larger [364]. The scaffolds fibres fabricated here have pore sizes in the region of 20–30 µm, which is lower than the minimum required for bone deposition. This would be problematic if culturing on a disc of the bulk PolyHIPE material; however, the macroscopic pores formed between the fibres during the fabrication of the generation 1 woodpile scaffold are between 300 µm (vertically) and 650 µm (laterally). This results in a hierarchical porosity, with a range of sizes over an order of magnitude. The presence of micro-pores creates a rougher surface topography, which likely increases cell attachment and may also increase cell migration [373].

It is not surprising that untreated scaffolds were not able to support cell attachment. In order to form a stable emulsion with water, the continuous phase of the HIPE must be hydrophobic and it has been clearly demonstrated that it is necessary to overcome this for a polymer to be used as a biomaterial or tissue engineering scaffold [413]. To do this, two plasma treatments were selected, pcAir and pdAAc. Plasma contains a mixture of electrons, radicals, ions, neutrals and photons [414], and when generated from volatile, organic compounds such as acrylic acid, it can be used to deposit a thin film of 'plasma polymer' onto virtually any solid material. It allows tight control over film thickness, is performed in a clean environment, and can be implemented regardless of the substrate geometry with minimal or no pre-treatment necessary [415].

When plasmas are generated from organic compounds, the molecules are liable to fragment; however, by using a low ratio of power to plasma flow rate, it is possible to retain a similar functionality to the initial compound by preserving functional groups [416]. pdAAc adds negatively charged carboxyl groups to the surface, as well as some hydroxyl groups generated either from atmospheric oxygen or water desorbed from the plasma chamber [417]. pcAir does not generate plasma from an organic compound, instead just drawing in air to the plasma vessel. This results in just oxygen-containing hydroxyl groups being deposited onto the surface, which also have been shown to support protein and cell adhesion and improve wettability [418], [419]. Although scaffolds used in this thesis were not intended for clinical application and therefore were not subjected to the sterilisation techniques necessary for implanted materials, plasma treatments can survive these harsh treatments, with Haddow, et al., demonstrating that plasma polymerised surfaces were not degraded by gamma-irradiation or ethylene oxide sterilisation [417]. The ability of plasma polymers to survive ethylene oxide treatment is an important finding in the study of polymeric materials for tissue engineering as this technique does not degrade the material, whereas gamma-irradiation is likely to do so.

Plasma modification is effective at penetrating the porous network of a 3D scaffold, improving the wettability of the PolyHIPEs and consequently improving the cell adhesion [411]. The inclusion of acrylic acid has been used previously to enhance cell culture on PolyHIPEs. In particular, Hayward et al., introduced it into the internal phase of the HIPE before its addition to the continuous phase. After curing, they showed carboxylic functionality on the PolyHIPE pore surfaces that did not adversely affect the adhesion of human hepatocytes [372].

Similar cell metabolic activity on these scaffolds indicates that both treatments are suitable when improving the adhesion and proliferation on the PolyHIPEs. However, the application of pcAir is less time consuming, requires fewer processing steps (e.g. does not require liquid nitrogen to cool the monomer) and avoids handling of potentially harmful monomers (acrylic acid). Therefore, the results suggest that the simpler, faster plasma modification technique is sufficient when considering cell viability alone.

Metabolic activity on the EHA0 scaffolds made from the stiffest PolyHIPE appears to be lower than the more elastic EHA50 and EHA100 materials on both day 8 and 15. Given that fibre thickness and spacing are maintained throughout, it would be expected that relative scaffold stiffness would follow the same pattern as the material stiffness. The difference in metabolic activity between the two more elastic scaffolds is much less noticeable, which may be due to a much smaller difference in stiffness; the difference between EHA0 and EHA50 is approximately 45 MPa, whereas EHA50 to EHA100 is approximately 4.5 MPa. This lower metabolic activity on the EHA0 composition agrees with the total DNA quantification. The amount of DNA present is also lower on the EHA0 compositions, with little difference between EHA50 and EHA100 (data not shown). Previously published work demonstrated using confocal imaging that on PolyHIPE scaffolds with the highest levels of metabolic activity, groups of cells could bridge the gaps between the fibres and two-photon imaging demonstrated that they could penetrate the fibres (Fig. 5.27).

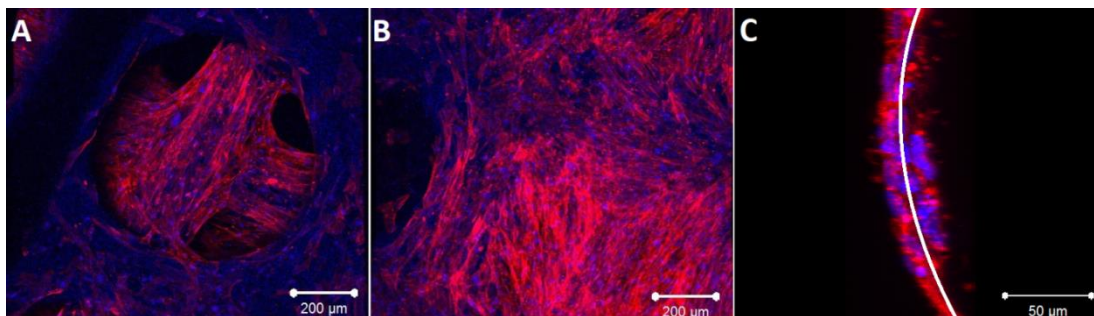


Figure 5.27: Confocal microscopy (A and B) images of a EHA100P80 scaffold showing cells completely covering fibres and filling the spaces between the fibres. (C) Two-photon image showing actin (red) and nuclei (blue) within the fibre, the white line indicates the fibre surface. Adapted and reprinted from Owen, et al., under the Creative Commons Attribution Licence [240].

Neither the composition of the scaffold nor the pdAAc coating had a significant effect on ALP activity. However, cells seeded on EHA0 scaffolds with a pdAAc coating did have significantly higher ALP activity compared to all other scaffolds, indicating this scaffold stimulated osteogenic differentiation. This suggests that the combination of the EHA0P80 PolyHIPE and pdAAc treatment resulted in the best substrate for osteogenic differentiation between those examined here. This is interesting given that EHA0 scaffolds did not result in significantly higher ALP activity than EHA50 and EHA100 scaffolds; neither did pdAAc scaffolds when compared to pcAir.

The stiffest scaffolds (EHA0P80) have a significantly lower amount of DNA ($p < 0.05$) but similar metabolic activity to other scaffolds, which together with the higher ALP activity suggests that more cells in this condition differentiated rather than proliferated. It is possible that this is due to the cell's response to the stiffness of the material, as substrate mechanical properties have been shown to influence stem cell fate [420]–[422]. However, whilst stiffer substrates have been demonstrated to be conducive to osteogenic differentiation, those substrates had much lower Young's moduli than these PolyHIPEs and cells in those previous experiments were cultured in media without dexamethasone. In addition, subsequent work suggests that stiffness alone cannot commit a stem cell to a specific lineage, with other factors such as substrate chemistry and density of cell binding ligands also influencing differentiation [423]. For the PolyHIPEs investigated here, relative stiffness alone did not appear to induce differentiation as significantly higher ALP activity only occurs in conjunction with pdAAc. With regards to the effect of acrylic acid on osteogenic differentiation, conclusive evidence for a relationship is yet to be seen as there is evidence in the literature indicating stimulatory [424] as well as no [425] effects. It has been shown that plasma deposited acrylic acid does not diminish the cells' ability to perceive differences in substrate stiffness when comparing the osteogenic response of MSCs to varied substrate stiffness [426]. Therefore, the reason for the enhanced ALP activity could be that the pdAAc coating provides sufficient ligands for the cells to respond to the stiffer EHA0P80 scaffold fibres whereas pcAir does not. Hence, no significant difference was seen between any pcAir treatments and the stiffer scaffold material only influenced osteogenic differentiation under a specific condition.

Woodpile scaffolds formed from porous and non-porous fibres of the same material were not compared directly in this study. However, it is likely that the differences seen when cells are grown on microporous monoliths in comparison to planar substrates are relevant when trying to understand the potential benefits of microporous scaffold

struts. First, it seems likely that porous fibres will improve diffusion-based processes throughout the PolyHIPE scaffold. Furthermore, scaffolds with non-porous fibres and macro-pores much larger than the cell size, e.g. 100s of microns, are likely to induce the same cellular behaviour as planar surfaces because the cell attaches to the strut in the same manner (shape and orientation) as a tissue culture plate [427], [428]. In contrast, scaffolds with micropores within the fibre allow the cells to have a more physiologically relevant morphology, as demonstrated when Alvetex® PolyHIPE inserts were compared to tissue culture polystyrene. Here it was shown that the use of these substrates profoundly improves the ability of mesenchymal stem cells to differentiate into osteogenic phenotypes, that cells retained a more similar phenotype to that seen *in vivo*, and that they had increased levels of osteogenic markers, such as ALP activity, osteocalcin production, and calcium deposition.

Other groups have demonstrated the benefits of strut microporosity. For example, in selective laser sintered polycaprolactone scaffolds where a microporosity within the fibres of the scaffold was formed during the sintering process [429], [430]. The interconnected network formed was shown to improve cell ingrowth and colonisation of the scaffold. Similar to this, rapid prototyping and particulate leaching have previously been combined to introduce a controllable microporosity into scaffolds with larger macro-channels, allowing the influence of pore architecture on mechanical and biological properties to be explored [431].

Full cellular penetration of the fibres would also enable continuous neo-tissue formation throughout the scaffold, a clear advantage in tissue engineering applications. In the work presented here, partial cell ingrowth was observed into the porous PolyHIPE fibre by two-photon microscopy and histology. Although cells did not fully infiltrate the fibres here, in parallel work by Paterson where the same type of PolyHIPE was used to create microparticles, hES-MPs were observed to fully invade the material. However, this level of penetration was only seen at later time points (day 30 and 60). At a similar time point (day 15), comparable levels of infiltration were observed, indicating that the low level of cell permeation seen here may have been due to the shorter culture period (Fig. 5.28).

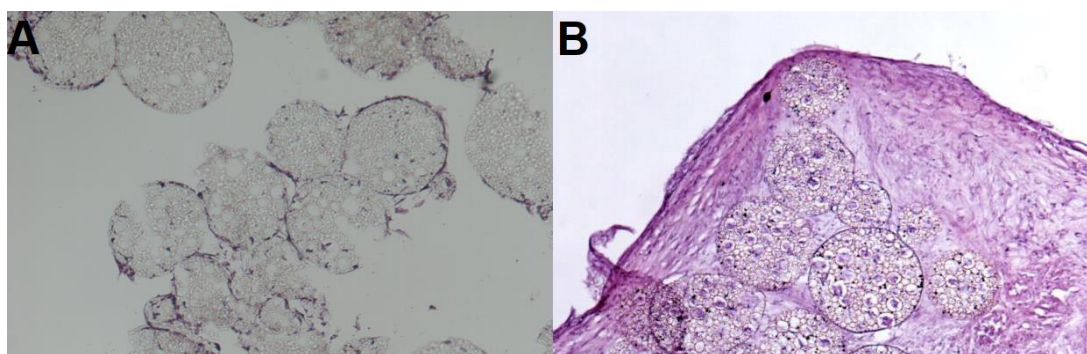


Figure 5.28: *Ingrowth of hES-MPs into PolyHIPE microparticles on day (A) 15 and (B) 60. At day 15, dark bands of cells can be seen around the perimeter of the microparticles, similar to that observed around the fibres in this work. By day 60, cells have fully penetrated the microparticles and deposited large amounts of extracellular matrix outside the particles, binding them together. Adapted and reprinted with the kind permission of Dr. Thomas Paterson, University of Sheffield [396].*

The single-photon technique used to create the scaffolds was not capable of a smaller fibre spacing whilst retaining the fibre diameter as partial polymerisation of the HIPE would occur between the fibres, resulting in a solid sheet or web effect, depending on the distance. To remedy this, a two-photon technique could have been used as this permits a much higher resolution as absorption only occurs within the immediate area surrounding the focal spot. However, the single-photon technique has a manufacture time of approximately 13 minutes for a 13 mm × 13 mm generation 1 woodpile structure, producing each fibre in a single pass. A two-photon setup would take much longer, with each fibre potentially requiring multiple passes to achieve the desired width and depth. Therefore, introduction of Tinuvin, a UV light absorber, into the continuous phase of the emulsion was utilised to reduce out-of-focal spot polymerisation and increase resolution whilst retaining manufacture speed.

Tinuvin® 234 was selected due to the ease with which it can be incorporated into the current synthesis protocol. Due to its solubility in the continuous phase, it can readily be added to the polymer and dissolved with the surfactant by sonicating in a water bath. The ability of Tinuvin to cease polymerisation at 4 wt% even at high laser power shows that is a potent additive. The production of films rather than fibres at 0.5 to 2 wt% is analogous to the work of Sušec et al., who used Tinuvin® CarboProtect® to reduce the penetration depth of light into PolyHIPES, increasing the resolution [387]. This is how ribbons were created rather than fibres, as the laser could only penetrate a

few microns into the HIPE. 0.1 wt% was found to produce fibres rather than ribbons, and SEM analysis of the scaffolds showed a 30% reduction in fibre spacing compared to scaffolds without the light absorber.

Side skin formation is thought to be formed due to a partial polymerisation of the HIPE outside of the focal spot of the laser. Here, the polymer is sub-activated resulting in an incomplete polymerisation which collapses and forms a closed sheet around the fibre. From cross-sectional SEMs, the addition of Tinuvin appears to have partially reduced skin formation, with a larger proportion of the fibre having an open pore surface. However, no effect on side skin thickness was seen. This may be because although out-of-focal spot polymerisation has been minimised by quenching the scattering of UV light through the HIPE, reducing the presence of polymerising free radicals between fibres thereby decreasing spacing, it is still occurring in the immediate vicinity of the fibre to the extent that a skin is formed. This is because Tinuvin is only soluble in the continuous phase, not the internal phase, and therefore transmission of UV light scattered through the water phase is not quenched. These findings agree with the work of Sherborne, whose work focussed on determining why the skin forms when PolyHIPEs are structured using microstereolithography [432].

Metabolic assays performed on PolyHIPE scaffolds fabricated from EHA0P80 either with or without 0.1 wt% Tinuvin had no significant difference, even over an 18 week period, indicating that its addition is not cytotoxic and it does not leach out over time.

Free standing scaffolds that do not require a functionalised glass coverslip were developed as this base acts as a barrier, limiting nutrient diffusion and flow through the scaffold. Although PolyHIPEs which could undergo a large extension at failure were initially selected to allow the possibility of dynamically straining the scaffold during culture, it was immediately found that scaffold stiffness was essential to maintain the complex architecture. As it has been shown that porosity influences the stiffness of the material, attempts to reduce porosity but retain the EHA50 monomer composition were made. This required the use of MIPes; however, the stiffness still was not high enough to maintain the architecture. Additionally, MIPes have negligible pore interconnectivity and therefore have fully enclosed pores within the polymer. As a result, washing will not be able to fully remove uncured polymer from the system, which could leach out during cell culture and contaminate the sample. Without the methacrylate groups on the coverslip for the HIPE to adhere to when curing, it was found that keeping the base layer of fibres parallel was not possible. SEM showed that

with the exception of the bottom layer of fibres, the architecture of the regular scaffold had been retained.

Three scaffolds were compared for use in the *in vitro* model; PolyHIPE, polyurethane and Biotek. In terms of architecture, the PolyHIPE and Biotek scaffolds are preferable to the polyurethane for use in an *in vitro* model due to their reproducible architecture. As their 3D geometry is controlled by additive manufacturing techniques (microstereolithography and extrusion, respectively), there should be less variability between scaffolds in comparison to the foam due to the control available over fibre position. This reproducible, regular architecture should produce more a more consistent cellular response and is also beneficial for computationally modelling fluid flow through the scaffold. However, although polyurethane substrates have a more stochastic architecture, they are a well-characterised scaffold in the field of bone tissue engineering, having been previously been reported to support extensive osteogenesis *in vitro* and *in vivo*, under both static and dynamic conditions [9], [406], [433], [434]. For model development and to have statistically valid results, a large number of scaffolds will be required. Therefore, ease of manufacture must also be considered. Clearly, the Biotek is the superior scaffold in this category as it is bought premade. However, 12 scaffolds cost \$199, making large scale cultures an expensive endeavour. The polyurethane foam is purchased as a large block which is then cut down to size, which is neither financially or time expensive. In comparison, the PolyHIPE raw materials are cheap; however, the largest time investment is required to produce the scaffolds.

With regards to cell performance, both the PolyHIPE and polyurethane scaffold outperformed the Biotek scaffold in terms of cell viability, calcium deposition and collagen production. The Biotek scaffold was seeded and cultured as per manufacturer instructions. However, the relatively low cell number and matrix production is likely due to the hydrophobicity of PCL [435] inhibiting cell proliferation throughout the scaffold, as seen in figure 5.13 where the mineral distribution is patchy and uneven in comparison to the PolyHIPE. It may be that this high hydrophobicity is intended to retain the seeding droplet within the scaffold, improving seeding efficiency in comparison to a more hydrophilic chemistry. However, this ultimately inhibits cell proliferation throughout the scaffold.

Initially, it appears that the PU scaffold has outperformed the other two in all three categories. However, it has a larger volume than the PolyHIPE scaffold. Due to the

complex, stochastic nature of the PU scaffold and the multiscale porosity of the PolyHIPE scaffold it is not possible to normalise the results accurately to scaffold volume. However, were the scaffolds solid blocks, the volume of the polyurethane cylinder and Biotek scaffold would be $\sim 280 \text{ mm}^3$ and the PolyHIPE $\sim 130 \text{ mm}^3$. Therefore, it can be seen that per unit volume the polyurethane scaffold was not greatly superior to the PolyHIPE as mineral deposition was not 2.15 times higher.

From ARS staining, it was clear that mineral distribution was even throughout the PolyHIPE and polyurethane scaffolds, but patchy on the Biotek. However, these differences in mineral distribution were not immediately apparent using MicroCT. Although scans on days 21 and day 28 revealed denser, mineralised regions, MicroCT was not able to detect all of the mineralised regions revealed by histological staining. When differences in the GSI histograms were analysed with a minimum threshold set to include the scaffold, the unseeded polyurethane and PolyHIPE scaffolds had a distribution of GSIs equivalent to a higher density than the seeded scaffolds, with the seeded samples peaking between 65 and 75 GSI and the unseeded at ~ 90 GSI. From the ARS staining it is clear that the seeded scaffold contain more dense material than the unseeded; therefore, a material other than the scaffold and extracellular matrix is influencing the results.

Although samples were mounted in a polystyrene foam holder, the density of this polymer is even less than the scaffold and was chosen due to its x-ray transparency. Therefore, this was not the material impacting the density histogram. As a result, it became clear that PBS retained within the scaffold was skewing the distribution. As the seeded scaffolds had extensive matrix deposition which retains PBS within the substrate, and PBS has a lower density than the scaffold material, they have a lower peak GSI than the unseeded control scaffolds. Control scaffolds retain less PBS and therefore have a higher peak GSI. This effect was not seen in the Biotek scaffolds due to the minimal extracellular matrix deposition allowing the PBS to drain away.

By setting the minimum threshold to a GSI that excludes the scaffold and therefore the PBS, the distribution of GSIs pertaining to the extracellular matrix can be compared. Here we can see that on all three scaffold types at day 28 there is a greater percentage of higher GSIs in the seeded scaffolds than the unseeded. When cultures were maintained in BM rather than SM, there are similar amounts of collagen synthesis as shown by DR80 staining, but negligible mineral staining. When these scaffolds are scanned by MicroCT, there is no difference in GSI distribution between

seeded and unseeded polyurethane scaffolds, confirming that the difference seen in SM is due to mineralised matrix deposition, not just the presence of cells or collagenous extracellular matrix.

The effect of drying the scaffolds prior to scanning is clearly visible. The pores of the polyurethane scaffolds no longer seem to be filled with a similar density material to the polymer due to the absence of PBS. Furthermore, without PBS skewing the GSI distribution, mineral deposits and scaffold material are clearly visible on the same reconstructions, meaning that segmentation to analyse mineral distribution would be possible.

Although the presence of PBS here negatively affected the scan clarity, other groups have successfully discerned mineral from the scaffold material under wet conditions. Vetsch, et al., examined how the curvature of a defect affects tissue formation by cutting different shape channels into a scaffold and examining ingrowth by repeated MicroCT scanning at various time points [436]. By scanning a hydroxyapatite sample, they were also able to determine the GSI equivalent to the bone mineral, allowing for effective segmentation of the scaffold and matrix. Using this protocol, they were able to measure the spatial and temporal change in bone deposition. Repeated MicroCT scanning *in vivo* can affect bone metabolism due to the radiation [437]; however, the protocol used by Vetsch, et al., has been shown to not impact the osteogenic performance of the human MSCs used when total DNA, ALP activity and calcium deposition were compared between irradiated and non-irradiated samples [438]. In addition to this, work by Cartmell, et al., found that mineral deposition on scaffolds can be scanned up to five times by MicroCT without significantly inhibiting the function of the cells [439]. Therefore, it seems that the difficulties presented by the presence of PBS in the scaffold stem from the parameters used to scan the samples.

Scanning operating procedures were determined using dry samples to maximise clarity of the low density polymer scaffolds. When wet experimental conditions were then scanned the presence of PBS skewed the histogram significantly, meaning that it was not possible to determine the presence of mineral without thresholding out the scaffold and water. In the future, scanning parameters would be changed to allow mineral and the scaffold to be accurately segmented. This would mean that in the *in vitro* model the same samples could be repeatedly scanned and areas of formation and resorption could be accurately tracked. In comparison to histological staining, this approach would allow the spatial aspect of bone remodelling to be evaluated as well as the

change in total mineral. Furthermore, it would reduce the number of samples required as separate scaffolds would not be necessary for each time point. It would also reduce inter-sample variability, as the assumption that multiple scaffolds seeded separately and then cultured under the same conditions will behave identically is no longer required.

In addition to comparing mineral deposition, MicroCT can also reveal the scaffold architecture in a non-destructive manner. In comparison to the original design of the Biotek scaffold, it is clear that the fabricated geometry does not match the intended architecture (Fig. 5.29). MicroCT and SEM reveal that the perimeter of the scaffold is not well defined, with all the fibres from each layer merged together. As this scaffold is extrusion-printed, this is likely from where the scaffolds have been stamped from a larger sheet. In addition to the perimeter of the scaffold not matching the original specifications, the scaffold fibres and spacing do not retain the offset originally intended. Instead of each fibre lying above the space in the previous layers, they appear more randomly distributed, often lying directly above each other. This removes the regular macroporosity and defined pore size from the scaffold, resulting in a more stochastic architecture. These variances are not limited to this batch of scaffolds, as these differences have also been noted by Marin, et al., and Brunelli, with the former finding that these discrepancies affect the micromechanical environment of the scaffold [398], [440].

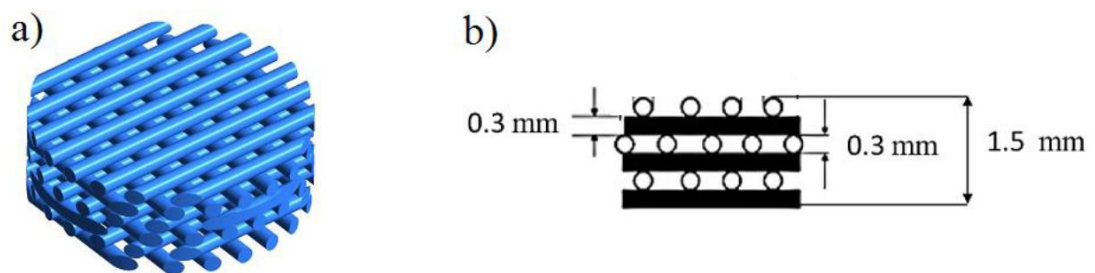


Figure 5.29: a) 3D CAD model of the intended geometry of the Biotek scaffold. b) scaffold design specifications provided by the manufacturer. Adapted from Marin, et al., and reprinted with kind permission of Elsevier [368].

Both the PolyHIPE and Biotek scaffolds are intended to have a woodpile architecture with offset fibres. From MicroCT and SEM it is clear that structuring using microstereolithography rather than extrusion results in an architecture that is much more similar to the original, intended design. However, there is a trade-off between manufacture time and printing resolution, with extrusion based technologies being able to fabricate structures significantly faster than light-based techniques [441].

MicroCT works by generating x-rays, passing them through the sample and then using a detector to determine their intensity. This can be converted into 2D sections of the sample that can be combined during reconstruction into a 3D image. The ability of the sample to attenuate the x-ray beam is related to its atomic number and therefore density [442]. The PolyHIPE scaffold has limited x-ray attenuation capability due to the high level of macroporosity combined with low density of the 80% porous fibres. This results in very poor contrast, with only the fibre edges being clearly defined. Although the background settings were changed to maximise the system's ability to detect low density materials, MicroCT still struggles to generate high quality scans of this material. Despite this, the macroarchitecture is visible and the retention of the fibre offset is clear. However, SEM imaging reveals that the perimeter of the scaffold is merged due to the reliance on surface tension to hold the pre-polymer in place during fabrication.

Taking into account the fabrication costs, cellular performance and architecture, the polyurethane scaffold was selected as the most suitable for creating an *in vitro* model of postmenopausal osteoporosis. The Biotek scaffold was prohibitively expensive to be used on a large scale, failed to support extensive matrix deposition, and had a high level of sample variability. Therefore, the choice was between the PolyHIPE and the polyurethane scaffold. Both were cheap to manufacture in terms of raw materials, but the PolyHIPE was significantly more time intensive for large scale production. Both supported similar levels of mineralised matrix deposition, but despite the PolyHIPE scaffold's superior architecture, the sponge-like behaviour of the polyurethane scaffold means that it would be easier to add a secondary seeding suspension when the osteoclast precursors are introduced.

The PolyHIPE scaffold has been continually developed since its initial conception in late 2014. The first generation was proof of concept; that a multiscale porosity scaffold

could be created using photocurable emulsions that had tunable mechanical properties as well as supporting mineralising bone cells. These scaffolds have since had hydroxyapatite successfully incorporated into the emulsion whilst retaining a similar architecture, which may produce a more clinically relevant scaffold should the result be repeated with a biodegradable polymer [390]. Additionally, they have been used as trabecular bone mimics for studying osteosarcoma [397]. The second generation of PolyHIPE scaffolds focussed on making the scaffold free standing and improving the architecture. Prior to this, they had been attached to a glass coverslip. Whilst this is acceptable for basic 3D cell culture, it does not allow the possibility of dynamic culture or flow through the scaffold and is not clinically relevant. By using IBOA dominated emulsions that give a stiffer scaffold, it was found that they could retain their architecture without relying on a glass base. In addition, the inclusion of a light absorber allowed the production of scaffolds with a greatly improved resolution, reducing the size of the macropores between fibres. Despite these improvements, these scaffolds were limited in height and had fibre merging at the perimeter. Although now improved for *in vitro* culture, they did not have the intended architecture and would not be clinically relevant should different polymers be used.

Due to these limitations, the third generation of PolyHIPE scaffolds was developed. The use of a bespoke fabrication well allowed for excess polymer to be added when each layer was printed. This removed the reliance on surface tension for keeping the uncured polymer in place during fabrication and allowed much larger scaffolds to be fabricated. In addition to increasing the permissible size, it also improved scaffold architecture as fibre layers no longer merged at the perimeter. In addition to this, it improved fabrication reproducibility and has the potential to allow architectures other than woodpile to be fabricated.

Whilst the third generation of the PolyHIPE scaffold was being developed, it was realised that this substrate had alternative applications in the field of osteoarthritis (OA) tissue engineering. Osteoarthritis (OA) affects over 150 million people worldwide and is generally considered the greatest burden musculoskeletal disorder, ranking even above osteoporosis [443]. As the disease progresses, lesions form in the articular cartilage [444], which can be treated by autologous cartilage transplantation, also known as mosaicplasty. This is a surgical procedure aimed at restoring lesions in load bearing regions by transplanting osteochondral plugs to the area from a non-load bearing site. These cylindrical plugs consist of both the articular cartilage and subchondral bone and are typically 12 – 25 mm in length and are suitable for lesions

up to 4 cm in diameter [445]–[447]. Tissue engineered osteochondral plugs are a promising alternative to mosaicplasty as they offer the possibility of implanting full-thickness grafts without donor site morbidity and the need to create additional defect sites. However, this requires creating a biphasic scaffold capable of supporting two functional tissues with appropriate mechanical properties for the osseous and chondral regions, whilst retaining sufficient porosity for nutrient and waste diffusion, as well as angiogenesis in the osseous phase [448], [449]. Biphasic osteochondral scaffolds have been fabricated and shown promising results *in-vitro* [448], and *in-vivo* [450], [451] (Fig. 5.30). However, it has been noted that the most prevalent drawback to multi-phase scaffolds is delamination of the discrete phases due to a non-continuous fabrication technique [452].

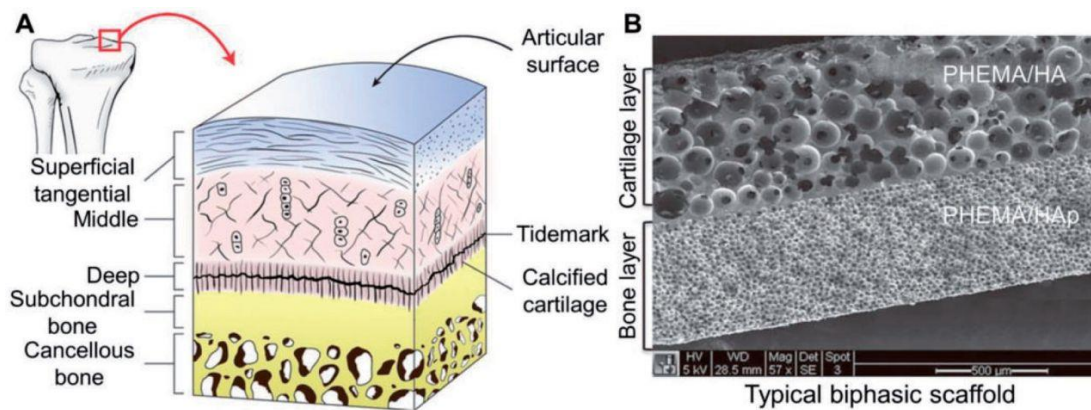


Figure 5.30: (A) typical structure of a mosaicplasty graft (B) SEM image of an example biphasic scaffold produced by a non-continuous fabrication technique. Reprinted from Li, et al., under the Creative Commons Attribution licence [453].

As we have seen here, a multiscale porosity can be easily and quickly introduced into bone tissue engineering scaffolds through emulsion templating. Furthermore, we have seen that the mechanical properties of these scaffolds can be modulated by tuning the composition and porosity of the HIPE [240]. Therefore, a biphasic osteochondral plug can be produced by selecting stiff and soft HIPE compositions, and as microstereolithography is a continuous fabrication technique, the risk of delamination is reduced. This approach to creating a tissue engineered osteochondral plug was explored in a parallel project, where biphasic scaffolds were fabricated, mechanically tested and shown to support bovine articular chondrocytes as well as human osteoblasts [454].

Although this main focus of the work in this thesis is not the clinical applications of the scaffold, the fabrication technique used here could be replicated with biodegradable polycaprolactone PolyHIPEs developed within the group [432]. This has the potential to be an ideal bone tissue engineering scaffold, as it would be made from FDA approved biodegradable materials, be highly porous over multiple length scales allowing excellent cellular performance, and be capable of being produced with a wide range of architectures depending on the application due to the method of manufacture. In addition, the single-photon fabrication technique used has excellent resolution due to the high precision of laser-based manufacture without the long fabrication times associated with two-photon polymerisation, meaning that high throughput manufacture is not unthinkable.

5.6 Summary

- There was no difference in the wet and dry mechanical properties of the PolyHIPEs, meaning that culture conditions can be assumed to not affect the mechanical properties of the 20 previously characterised PolyHIPE materials.
- The degree of openness is determined by the percentage porosity, not the monomer composition.
- PolyHIPE compositions containing EHA facilitated the highest levels of metabolic activity.
- Substrate mechanical properties did not influence osteogenic differentiation, with the exception of the stiffest material in combination with an acrylic acid plasma treatment.
- Printing resolution can be improved by the addition of Tinuvin, a UV light absorber, whilst remaining biocompatible.
- When combined with the stiffest compositions, this allows for highly reproducible, free standing scaffolds to be fabricated.
- In a comparison between the PolyHIPE, Polyurethane and Biotek scaffolds, the polyurethane is the most suitable for the *in vitro* model due to its extensive mineralisation, ease of manufacture and low cost.
- Detection and localisation of scaffold mineralisation by MicroCT is heavily influenced by the presence of water in the sample, although its effects can be reduced by thresholding.
- In comparison to extrusion, microstereolithography is a greatly superior technique with regards to reproducibly fabricating a woodpile architecture.

6. Modelling osteoporosis *in vitro*

6.1 Introduction

In 2015, 89% of musculoskeletal research animal studies were conducted on mice and rats [155]. Their popularity arises from a relatively low public opposition to their use, as well as low cost and ease of housing in comparison to other, larger animal alternatives [128]. However, despite being a fundamental component of pre-clinical research, mouse physiology does not accurately represent the human condition. This is demonstrated by the poor translation of pre-clinical efficacy in animal models to human clinical trials and the vast majority of promising discoveries failing to enter routine clinical use [159]–[162]. A promising alternative to the use of animals is *in vitro* modelling.

A wide range of *in vitro* models of certain skeletal disorders, such as osteoarthritis, have been developed to permit their study with reduced use of animals [163]. *In vitro* systems that study bone remodelling have begun to be developed, offering a human-based cell system that can be used to study the process (§2.3). However, although they have been utilised to study certain disease states, predominantly cancer metastases, no such model of osteoporosis currently exists. Oestrogen has been shown to affect both osteoblasts and osteoclasts *in vitro* in a similar way to that seen *in vivo*; therefore, designing an *in vitro* remodelling model that can respond to oestrogen withdrawal in order to mimic postmenopausal osteoporosis is a realistic aim.

In a co-culture of bone cells it is important that the investigator is able to identify the presence and function of both cell types. For osteoblasts this is typically done through measuring ALP activity, an enzyme involved in mineralisation that can be used as a marker of osteogenic differentiation [22], [455], or quantifying mineralisation directly, for example by ARS staining for calcium [456] or Von Kossa staining for phosphate [457]. Mature osteoclast detection is normally done through microscopy or measuring TRAP or cathepsin K production as both are enzymes involved in the bone remodelling process [40], [352], [354], [458], [459]. Multinucleation and the formation of actin rings, both indicators of a mature osteoclast, can be confirmed using microscopy [267], but this is not feasible for 3D cultures. Therefore, measuring enzyme activity is a better, quantitative method of determining osteoclast activity.

6.2 Aims and objectives

The aim of this chapter was to determine to what extent an *in vitro* model of postmenopausal osteoporosis can be developed. It will combine the results of chapter 4, where IDG-SW3 and RAW264.7 were identified as the most suitable cell lines, with the results of chapter 5, where the polyurethane scaffold was identified as the most suitable substrate, and a regimen of oestrogen withdrawal to mimic the onset of postmenopausal osteoporosis. Ideally, it should respond in the catabolic manner seen *in vivo* when oestrogen levels decline. To achieve this, the following objectives were addressed:

1. Examine the effect of PTH, a drug used in the treatment of osteoporosis, on markers of the constituent cells.
2. Assess whether ALP and TRAP activity and mineralisation are suitable markers of osteoblast and osteoclast activity in the co-culture.
3. Determine the effect of oestrogen exposure on monolayer and 3D co-cultures.
4. Optimise osteoclast seeding density to maximise co-culture duration.
5. Evaluate the effect of oestrogen withdrawal on markers in co-culture.

6.3 Materials and methods

Further to the materials and methods outlined in §3, the following are used in this chapter.

6.3.1 Co-culture medium

All co-cultures were maintained in IDG-SW3 differentiation media (supplemented media, SM) with 50 ng/mL RANKL. Where co-cultures are compared to monocultures of IDG-SW3 or RAW264.7 to analyse differences in ALP and TRAP activity, monocultures have been maintained in the same media; therefore, any differences observed are not due to the presence of absence of β GP and AA2P.

6.3.2 Evaluation of mineral resorption in co-cultures

To ascertain the amount of mineral resorption taking place in the co-cultures, Alizarin Red S (ARS) staining was utilised. ARS is typically used to determine mineralised extracellular matrix deposition by osteoblasts by staining for calcium. However, by determining the amount of mineral present before and after the addition of osteoclasts, it is possible to infer the amount of osteoclastic resorption by the decrease in the mineral staining. This is similar in principle to the work of Hoyte, who used ARS to stain bone sections *in vivo* and then quantified resorption by measuring the removal of the stained bone [460], and Suzuki, et al., who used diminished ARS staining on bone sections to demonstrate increased osteoclast resorption [461].

This method of estimating resorption requires a baseline level of mineral to already be present. Therefore, co-cultures where mineral resorption was ascertained using this technique were only initiated after sufficient mineralisation had already occurred by the IDG-SW3. This was identified as 21 days of IDG-SW3 pre-culture in supplemented media (SM) before the addition of RAW264.7. Co-cultures were performed either in 48 well plates (TCP co-cultures) or 5 × 5 mm polyurethane scaffolds (3D co-cultures). After 21 days of culture, IDG-SW3 were found to have deposited approximately 360 μ g/mL of ARS in the 48 well plates and 370 μ g/mL of ARS in the polyurethane scaffolds (n=6). Any reduction in ARS staining following the subsequent co-culture period was assumed to be the result of osteoclastic resorption of mineral. The estimated baseline levels are indicated on any graphs where mineral resorption is ascertained by this technique.

ARS staining in co-cultures was performed after decellularisation, rather than fixing. Decellularisation was performed in accordance with the protocol of Kusuma, et al. [462]. Briefly, media was removed from the samples which were then washed twice with PBS. 0.5% Triton X-100 and 20 mM ammonium hydroxide in PBS was then added and incubated for either five or ten for tissue culture plastic (TCP) and 3D scaffold cultures, respectively. Samples were then stained in accordance with the ARS staining protocol detailed in §3.2.11.

6.3.3 Parathyroid hormone preparation

Human parathyroid hormone (1-34) (PTH, cat# A1129-1mg) was purchased from Generon, UK. Murine cells have previously been shown to be responsive to human PTH [463], [464]. A 10 μ M stock solution was created by dissolving 1 mg PTH in 24.3 mL of PBS with 0.1 wt/vol% bovine serum albumin. The stock solution was aliquoted and stored at -20°C. The same amount of vehicle was added to all wells regardless of the drug concentration used.

6.4 Results

6.4.1 Parathyroid hormone has a predominantly catabolic effect on IDG-SW3

PTH is a common therapeutic for the treatment of osteoporosis as it has the potential to promote bone formation and inhibit resorption. However, application of parathyroid hormone (PTH) can have either a catabolic or anabolic effect of bone depending on the concentration, frequency and duration of its application. Continuous exposure to PTH, for example in hyperthyroidism, results in bone loss by inhibiting the synthesis of extracellular matrix proteins, including collagen I, osteocalcin, and ALP. Intermittent exposure can increase bone formation by promoting osteoblast differentiation, inhibiting sclerostin in osteocytes, activating and differentiating bone lining cells, and inhibiting osteoblast apoptosis. Despite its effects on osteoblast matrix production, the catabolic effect on bone seen during continuous exposure is stated to be mostly due to its indirect effect on osteoclasts. Continuous exposure to PTH supports a high RANKL:OPG ratio by upregulating RANKL and downregulating OPG synthesis [192], [225], [226].

One potential method of evaluating an *in vitro* model of osteoporosis be to determine whether it responds to PTH in an analogous way to that observed *in vivo*. To do this, a treatment regimen that elicits an anabolic effect needs to be determined. To explore the effects of PTH on IDG-SW3, cells were seeded at 25,000 cells per well in a 48 well plate and cultured until confluent for three days at 33 °C in EM. Cells were then transferred to SM and 37 °C and 0 – 100 nM PTH added either continuously or intermittently (twice a week for either 1 hour or 24 hours). ALP activity was measured on day 7, meaning that intermittently treated wells were exposed to PTH twice (Fig. 6.1).

Concentrations of PTH of 25 nM and above inhibited ALP activity for all treatment durations. Total DNA was significantly lower when cells were exposed to PTH at 50 nM and 100 nM for the 1-hour duration. ALP activity and normalised ALP activity were significantly higher at 1nM compared to 0 nM when the treatment was applied intermittently for 24 hours. For 1 hour and continuous exposures there were no differences between 0 nM and 1 nM for normalised ALP activity and concentrations of 25 nM and above had significantly lower normalised ALP activities for all treatment durations.

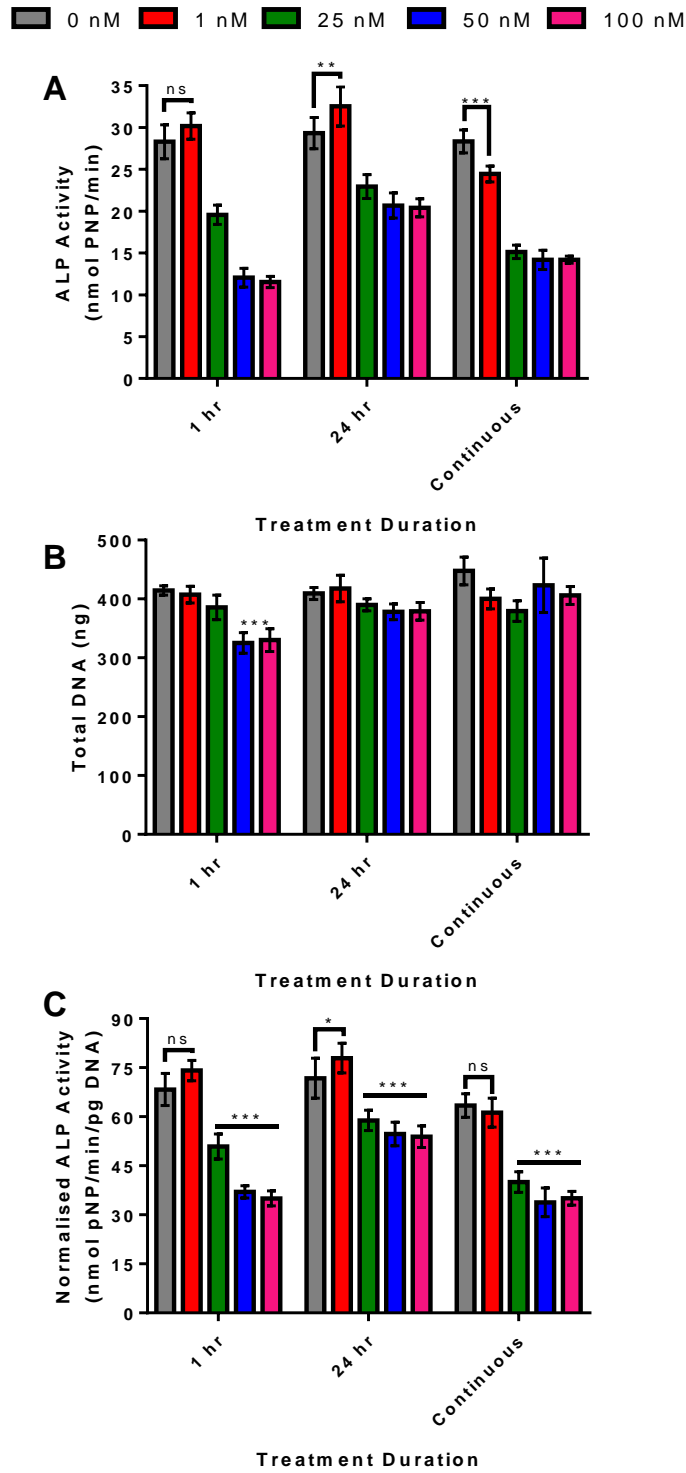


Figure 6.1: Response of IDG-SW3 to a range of PTH concentrations and treatment duration. (A) ALP activity (B) Total DNA (C) Normalised ALP activity of IDG-SW3 exposed to various concentrations and durations of PTH (n=6) (*/**/*** = $p < 0.05/0.01/0.001$).

To investigate further the effect of PTH on mineralisation and osteocytogenesis, IDG-SW3 were seeded at 25,000 cells per well in a 48 well plate and cultured until confluent for three days at 33 °C in EM. Cells were then transferred to SM and 37 °C and concentrations of PTH between 0 nM and 20 nM were applied intermittently either once (1X) or twice (2X) a week for 24 hours. GFP and ALP measurements were taken weekly and mineralisation quantified on day 28 (Fig. 6.2)

Statistical analysis was not performed as this experiment was only repeated once in triplicate. However, with regards to ALP activity, there were minimal differences with regards to concentration or frequency of application at any time point. As with the initial experiment, a higher concentration of PTH led to lower total DNA, and two applications per week appeared to exacerbate this.

By measuring GFP expression to infer osteocyte formation, it appears that all concentrations and frequencies of PTH exposure reduced GFP expression. The 0 nM group was higher from day 14 onwards indicating that osteocytogenesis was inhibited in exposed groups. When comparing mineralisation, it was clear from the staining that as PTH concentration increased mineralisation was lower with no visible staining at concentrations of 10 nM and above in the 1X group and 5 nM and above in the 2X group. However, it is also clear that in comparison to previous experiments, very little mineral was deposited even in the 0 nM group. Therefore, after destaining the ARS for colourimetric quantification, no differences were detectable.

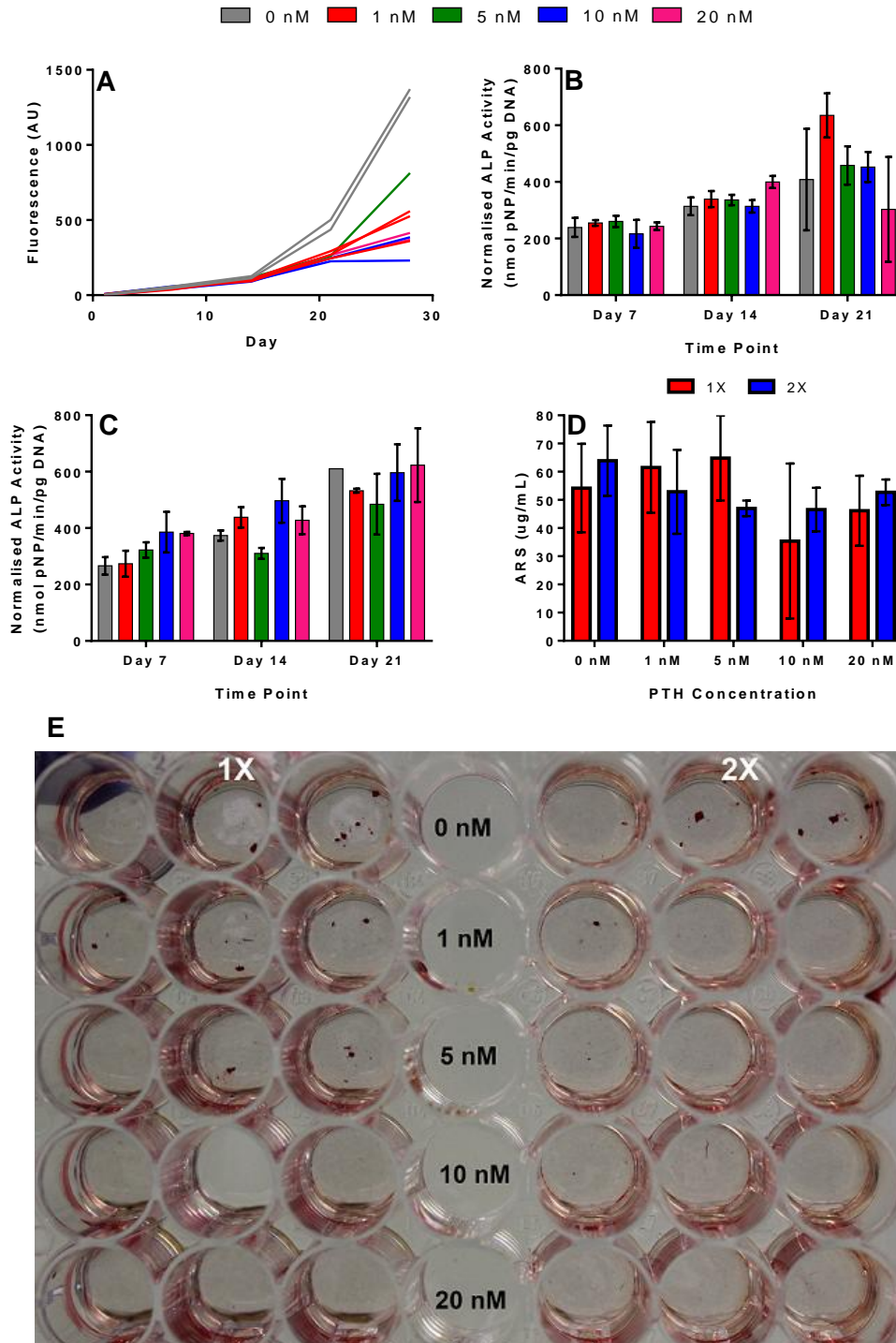


Figure 6.2: Effect of a range of PTH concentrations and treatment frequencies on IDG-SW3 (A) GFP expression (mean only, 1X & 2X combined) (B) normalised ALP activity 1X (C) normalised ALP activity 2X (D) ARS (mineralisation) (E) photograph of ARS before destaining for quantification (n=3).

The current opinion of the scientific community is that PTH can only have an indirect effect on osteoclasts through modulation of the RANKL:OPG ratio in osteoblasts, with only a small number of researchers considering that osteoclast-lineage cells may possess a PTH receptor [465], [466]. To investigate its effect on RAW264.7, cells were seeded at 5,000 per well in a 48 well plate and cultured for ten days in BM supplemented with 25 ng/mL RANKL. Cultures were exposed to 0 – 100 nM PTH which was added either continuously or intermittently (twice a week for either 1 hour or 24 hours). TRAP and metabolic activity were determined on day 10 (Fig. 6.3).

There were no significant differences in TRAP activity in the 1 hr or continuously treated group. When applied for 24 hours, concentrations of 1 nM and above significantly reduced TRAP activity. There was no effect on metabolic activity for any concentration or treatment duration. Normalised TRAP activity was significantly lower in the 25 nM group in comparison to 0 nM for all treatment durations; however, above this concentration normalised activities rose again and were not different to the 0 nM group.

As no combination of PTH concentration, application frequency or treatment duration was found to have an anabolic similar to that observed *in vivo*, PTH treatments were not applied to the co-culture.

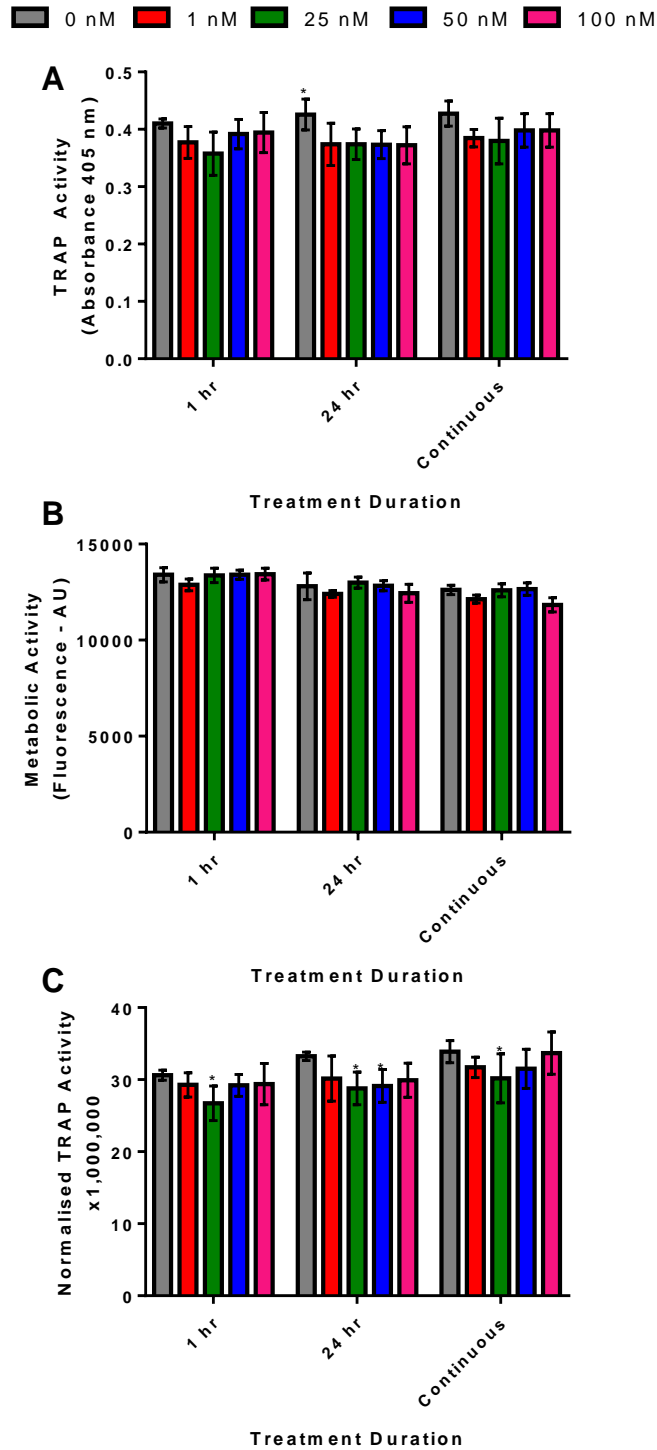


Figure 6.3: Effect of a range of PTH concentrations and treatment frequencies on RAW264.7. (A) TRAP activity (B) Metabolic activity (C) Normalised TRAP activity of RAW264.7 exposed to various concentrations and durations of PTH (n=6) (*= $p < 0.05$).

6.4.2 Mineralisation and ALP and TRAP activity are appropriate co-culture markers

To ensure that ALP activity was specific to osteoblasts and TRAP activity to osteoclasts, monoculture and co-culture activities were compared. Initially, 60,000 IDG-SW3 per well were seeded in 12 well plates, with 20,000 RAW264.7 added 24 hours later and the culture maintained in SM supplemented with 50 ng/mL RANKL for seven days (Fig. 6.4).

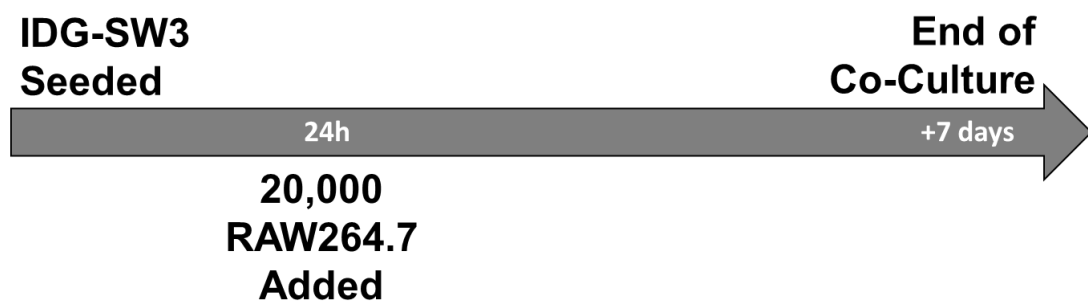


Figure 6.4: Schematic showing the co-culture regimen when RAW264.7 were added after 24 hours.

DNA confirmed that presence of both cell types in the co-culture (Fig. 6.5). IDG monocultures had significantly less DNA after 7 days than RAW264.7 monocultures. ALP activity was not detectable in RAW264.7 monocultures and was significantly higher in IDG-SW3. Conversely, TRAP activity only occurred in RAW264.7 monocultures and was not detectable in IDG-SW3. In co-culture, neither ALP nor TRAP activity was detectable despite high levels of DNA. This was likely due to overgrowth of the osteoblasts by the osteoclasts, stopping them from reaching confluence in co-culture. Although osteoblasts produce ALP whilst sub-confluent, its expression is intensively enhanced when they are confluent [467]. Therefore, if the IDG-SW3 remain sub-confluent due to the presence of the RAW264.7, their expression of ALP may have been undetectable for this reason. Undetectable TRAP activity may have been due to a too high seeding density of osteoclast precursors.

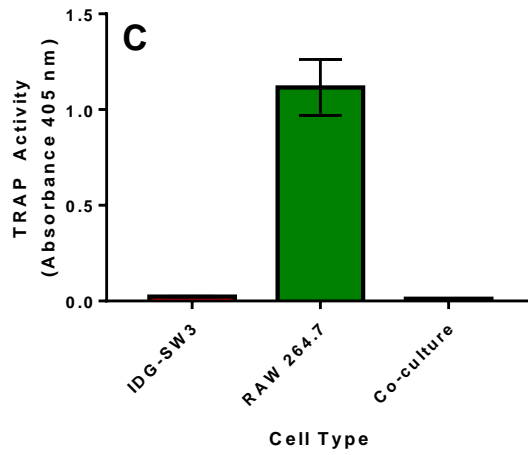
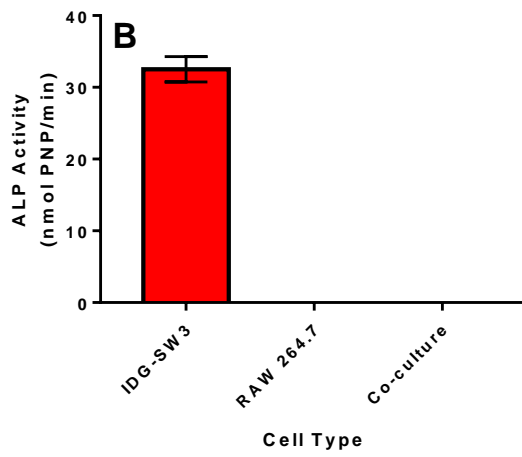
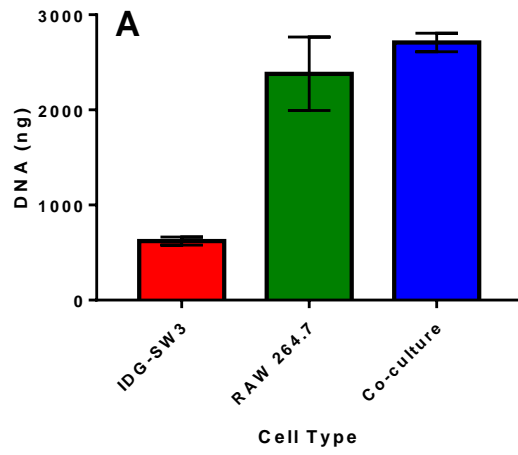


Figure 6.5: Comparison of day 7 (A) DNA (B) ALP activity (C) TRAP activity for co-cultures of IDG-SW3 and RAW264.7 where osteoclasts were added on day 1 (n=6).

To allow the osteoblasts to establish before introducing osteoclasts, IDG-SW3 were cultured for 7 days at confluence in a 12 well plate in SM before adding 10,000 RAW264.7 and maintaining for a further ten days in SM supplemented with 50 ng/mL RANKL (Fig. 6.6).

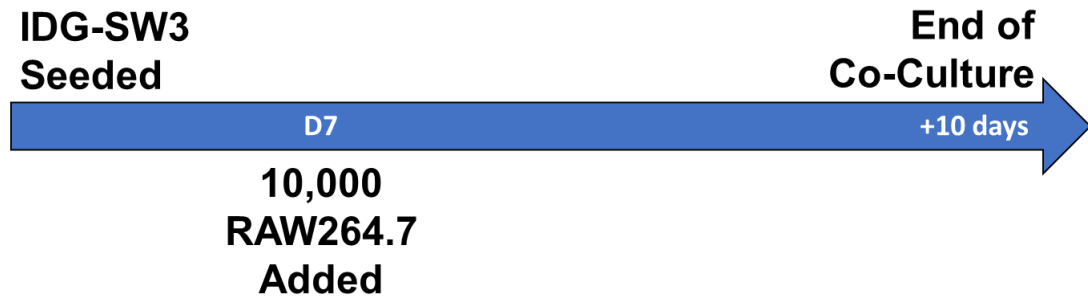


Figure 6.6: Schematic showing the co-culture regimen when RAW264.7 were added after seven days.

Again, DNA confirmed the presence of both cell types in the co-culture (Fig. 6.7). ALP activity was undetectable in RAW264.7 monocultures and TRAP activity was significantly higher in RAW264.7 than IDG-SW3, confirming their suitability as functional markers in a co-culture. ALP activity was significantly reduced in the co-culture in comparison to IDG-SW3 monocultures but remained significantly non-zero. TRAP activity was significantly increased in the co-culture in comparison to the RAW264.7 monoculture. By staining co-cultures with ARS, it was confirmed that co-cultures were able to mineralise (Fig. 6.8).

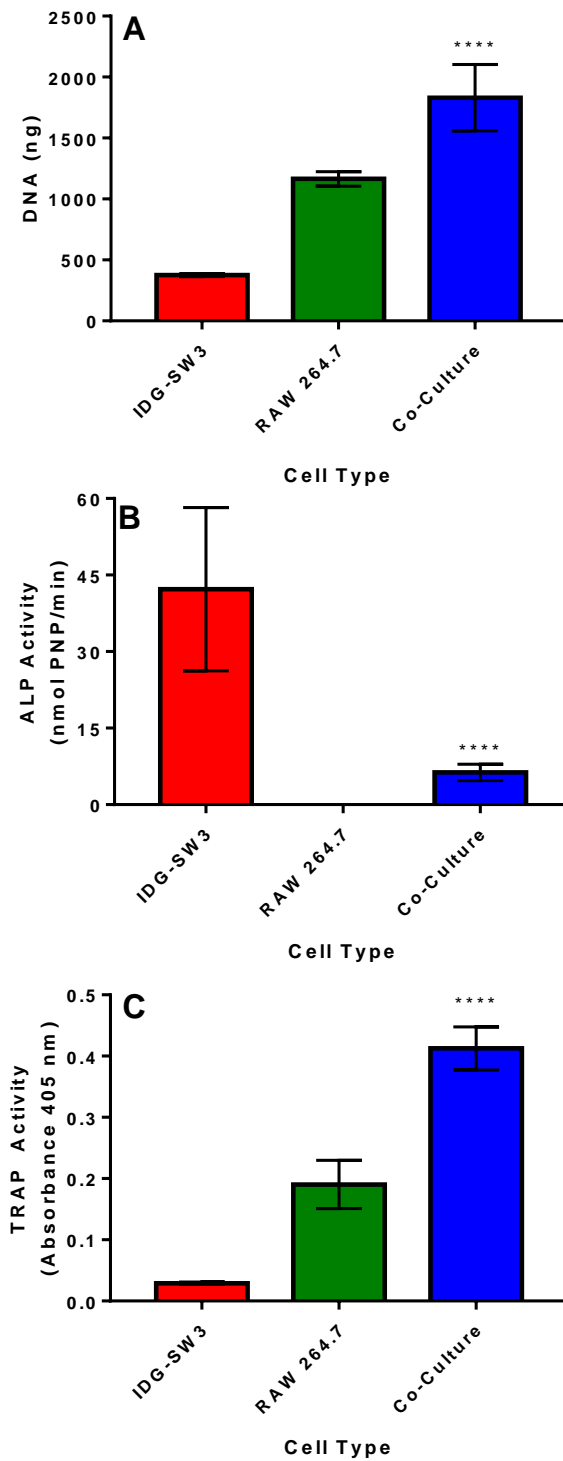


Figure 6.7: Comparison of day 10(+7) (A) DNA (B) ALP activity (C) TRAP activity for co-cultures of IDG-SW3 and RAW264.7 where osteoclasts were added on day 7 (n=6).

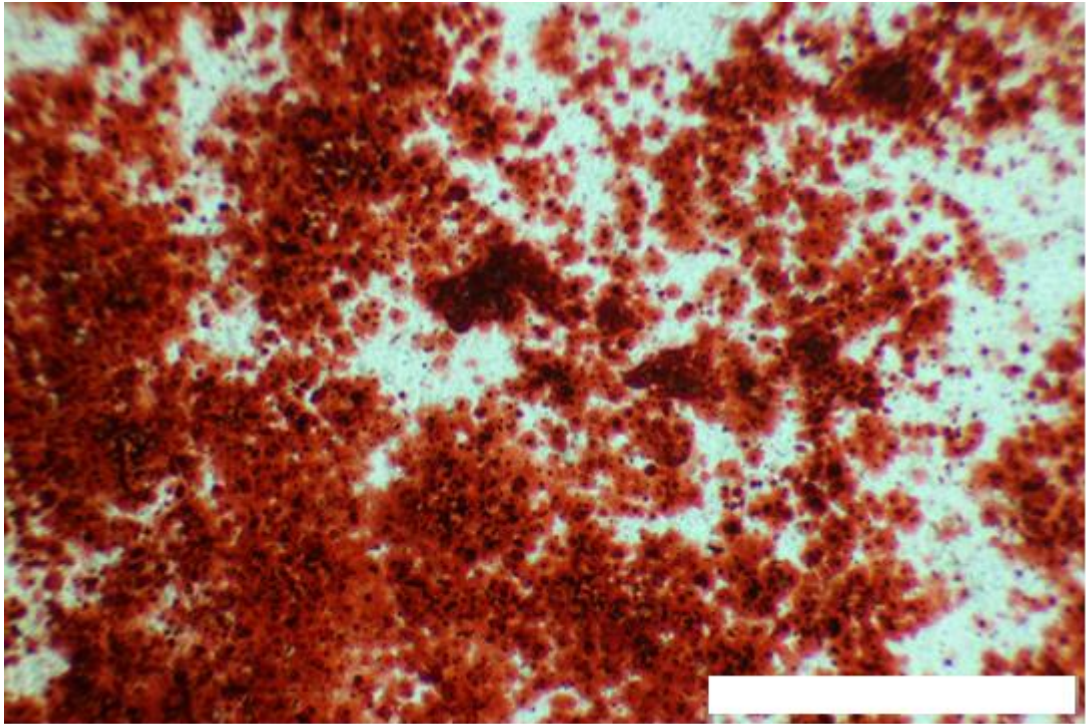


Figure 6.8: *Photograph taken at 10× magnification on an optical microscope of ARS stained day 10(+7) co-cultures of IDG-SW3 and RAW264.7. Scale bar 250 μm.*

6.4.3 Oestrogen affects co-cultures in TCP and scaffolds

For clarity, co-cultures performed in tissue culture plastic (TCP) well plates will be referred to as TCP co-cultures. Ones performed in polyurethane scaffolds will be referred to as 3D co-cultures.

To evaluate the effect of oestrogen on the co-culture, the previous experiment was repeated but either 0 nM or 100 nM 17 β -estradiol was added to the culture at the point of osteoclast addition. In addition to the TCP co-culture, 3D co-cultures were also performed on the 5 \times 5 mm polyurethane scaffold. They were seeded with 60,000 IDG-SW3 and maintained for three days in EM at 33°C before switching to 37°C and SM for a further seven days. Media was then carefully aspirated from the scaffold and replaced with a 60 μ L seeding suspension containing 20,000 RAW264.7. Cells were left to attach for 45 minutes before submerging in SM supplemented with 50 ng/mL RANKL and either 0 nM or 100 nM 17 β -estradiol. The following day, scaffolds and media were transferred to a new well plate to retain only adhered cells and maintained for a further seven days with half media changes every 2-3 days (Fig. 6.9).

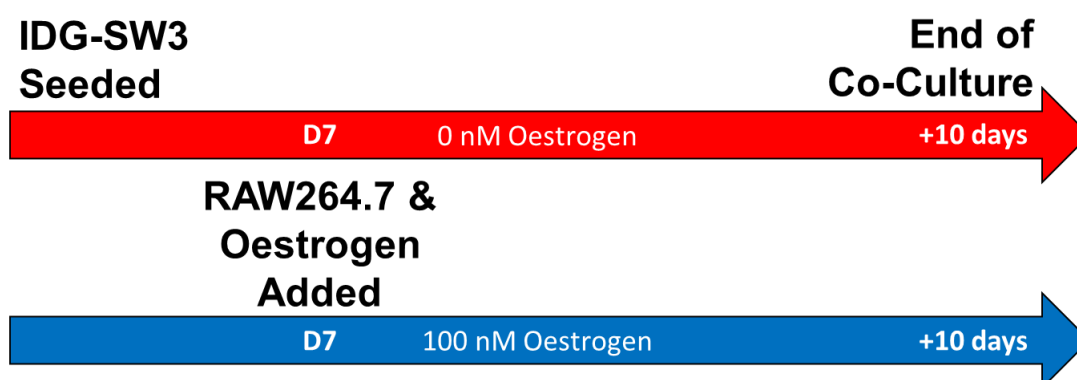


Figure 6.9: Schematic showing the co-culture regimen from preliminary oestrogen-exposed co-cultures.

Oestrogen had no significant effect on cell number in any condition (Fig. 6.10). ALP activity was undetectable in RAW264.7 monocultures and was higher in 100 nM oestrogen cultures in both TCP and 3D, although not significantly. TRAP activity was significantly reduced in RAW264.7 monocultures but not in TCP or 3D co-cultures, indicating that the upregulation of osteoclasts by the osteoblasts may be greater than their inhibition by oestrogen.

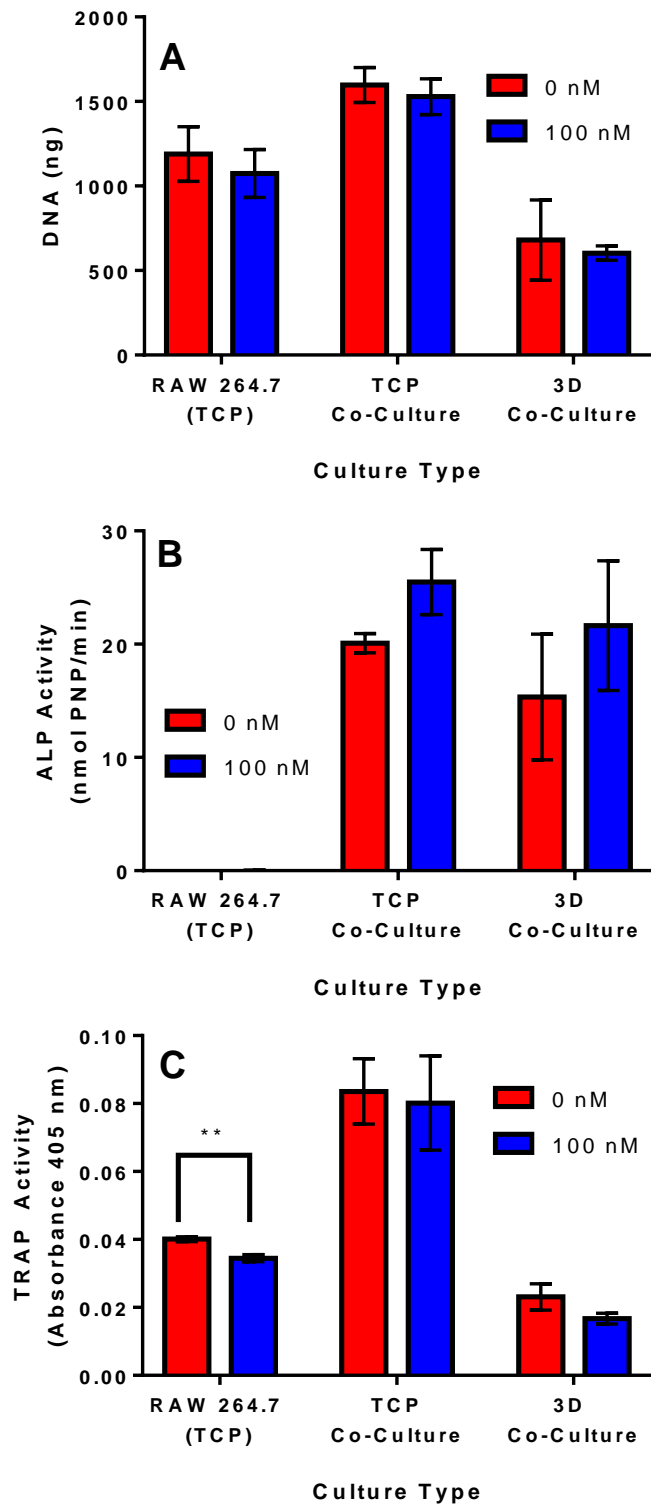


Figure 6.10: Comparison of (A) DNA (B) ALP activity (C) TRAP activity in day 10(+7) co-cultures of IDG-SW3 and RAW264.7 in TCP or 3D (n=3).

6.4.4 Co-cultures are not stable over extended time periods

RAW264.7 are osteoclast precursors. When exposed to RANKL, some fuse and mature to produce osteoclasts whilst others remain as monocytes. As osteoclasts have a finite lifespan of around 12 days, when the first generation of osteoclasts undergo apoptosis, there should be enough residual precursors to fuse and generate a second wave of osteoclasts. To determine whether this was the case, RAW264.7 were seeded at 5,000 per well in a 48 well plate and maintained for 28 days in BM supplemented with 25 ng/mL RANKL. Metabolic and TRAP activity were measured weekly (Fig. 6.11).

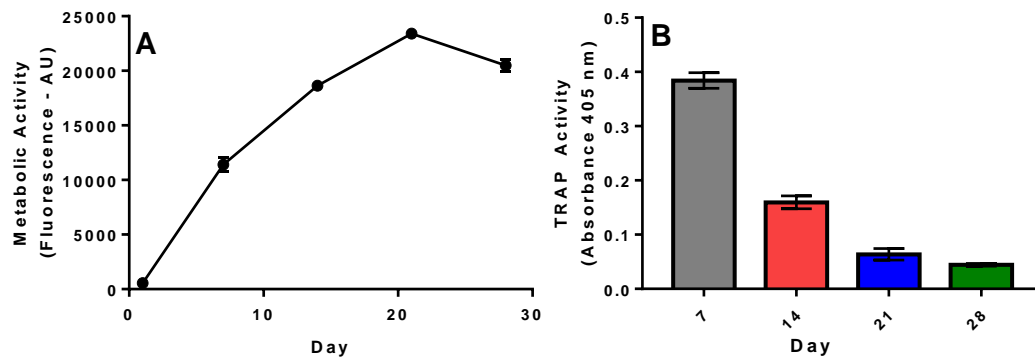


Figure 6.11: (A) Metabolic and (B) TRAP activity of RAW264.7 over 28 days ($n=6$).

Metabolic activity increased for the first three weeks as the RAW264.7 became confluent. TRAP activity was highest on day 7 and reduced at each successive time point, indicating no successive generations of osteoclasts were generated.

As the presence of the IDG-SW3 has been shown to affect osteoclast activity, this experiment was repeated but as a co-culture. They were also exposed to oestrogen and oestrogen withdrawal to determine any long term effects on osteoclast activity. IDG-SW3 were seeded at 25,000 cells per well in a 48 well plate and cultured under standard conditions until day 7 when 5,000 RAW264.7 were added per well and maintained in SM supplemented with 50 ng/mL RANKL for 28 days. Groups were either exposed to 0 nM or 100 nM of 17 β -estradiol at the point of RAW264.7 addition. Oestrogen was either maintained for the entire experiment or withdrawn on day 7 or 14 (Fig. 6.12).

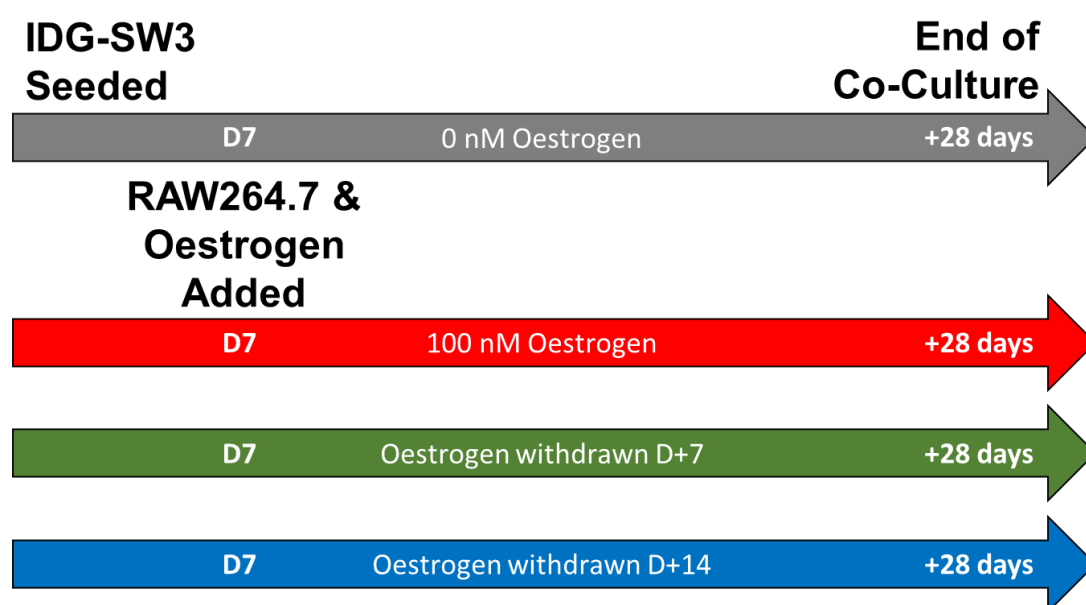


Figure 6.12: Schematic showing the co-culture regimen for oestrogen exposure and staggered withdrawal in TCP co-culture.

Oestrogen treatment has no significant effect on DNA at any time point (Fig. 6.13). DNA changes were due to changes in osteoclast number as IDG-SW3 were confluent and do not proliferate at 37°C. DNA was significantly lower on day 14 than day 7, indicating osteoclast death. Day 21 and 28 were higher than day 14, indicating proliferation of precursors.

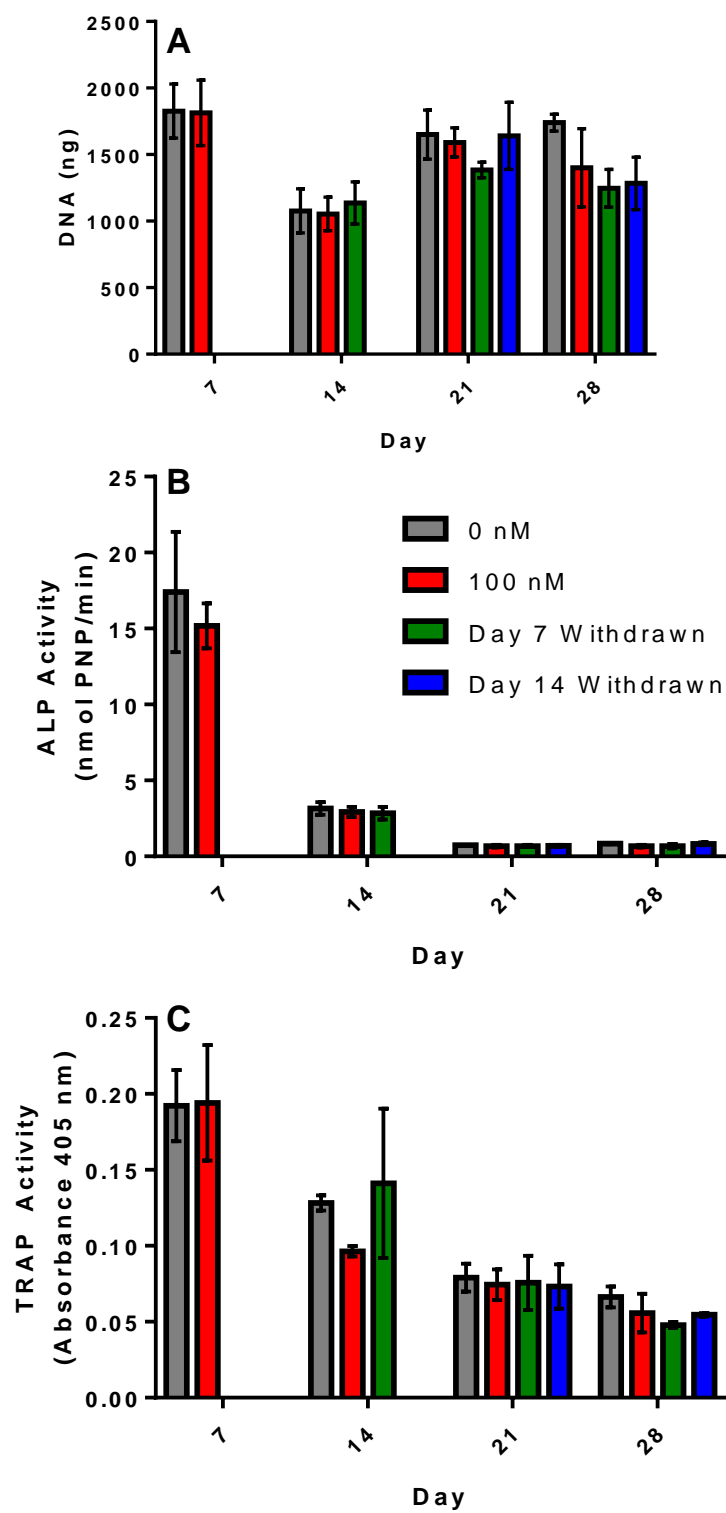


Figure 6.13: (A) DNA (B) ALP activity (C) TRAP activity of IDG-SW3 and RAW264.7 co-cultures over 28 days ($n=3$).

Oestrogen treatment had no significant effect on ALP or TRAP activity at any time point. ALP activity significantly reduced between day 7 and 14 and 14 and 21. This is likely due to overgrowth of the wells by RAW264.7. TRAP activity also steadily decreased, as it did in RAW264.7 monoculture. Comparison of the wells at day 7 and day 28 shows that these declines were due to overgrowth by RAW264.7 monocytes, establishing that generation of multiple waves of osteoclasts did not occur (Fig. 6.14).

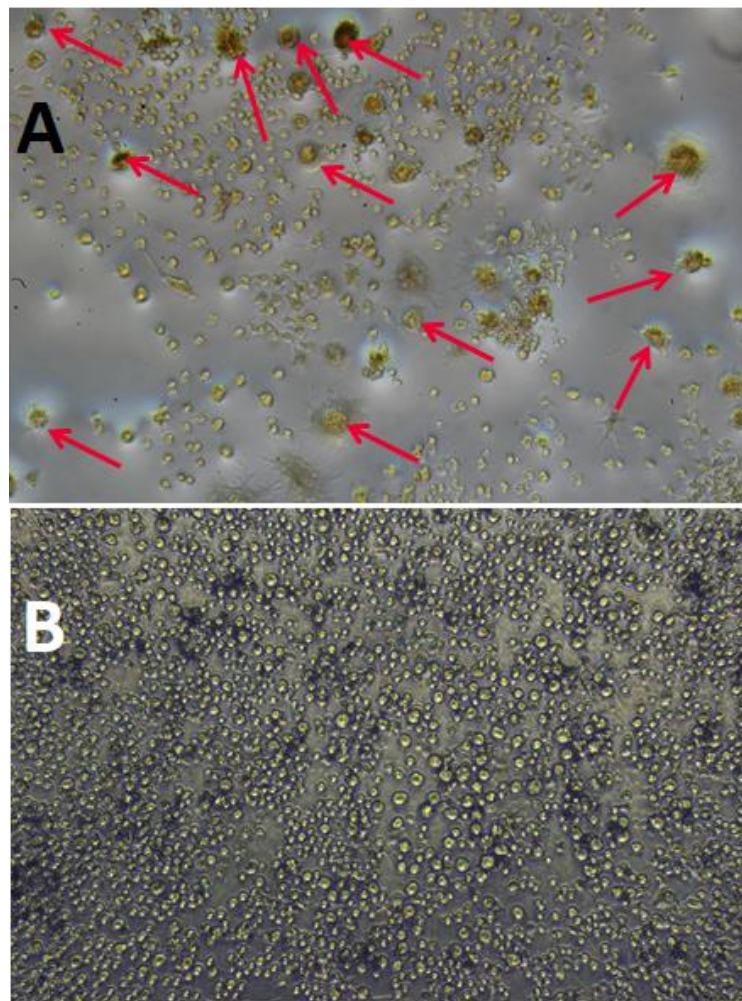


Figure 6.14: Photographs of RAW264.7 cultures on day (A) 7 and (B) 28. Mature osteoclasts (red arrows) only visible on day 7. By day 28, only precursors are present.

6.4.5 Density of osteoclast precursors affects mineral resorption

Due to only a single wave of osteoclasts being generated, attempts to extend the duration of the co-culture were made by varying the precursor seeding number. Co-cultures of IDG-SW3 and RAW264.7 were performed in 48 well plates as before; however, osteoblasts were maintained for 21 days in SM before adding either 2,500, 5,000 or 10,000 RAW264.7 and maintained for a further 14 days in SM supplemented with 50 ng/mL RANKL with either 0 nM or 100 nM of 17 β -estradiol. Osteoblasts were cultured for three weeks before osteoclast addition to allow sufficient mineralised matrix to be deposited so that effects on resorption could also be ascertained. DNA, ALP activity and TRAP activity were quantified 7, 10 and 14 days after osteoclast addition (Fig. 6.15).

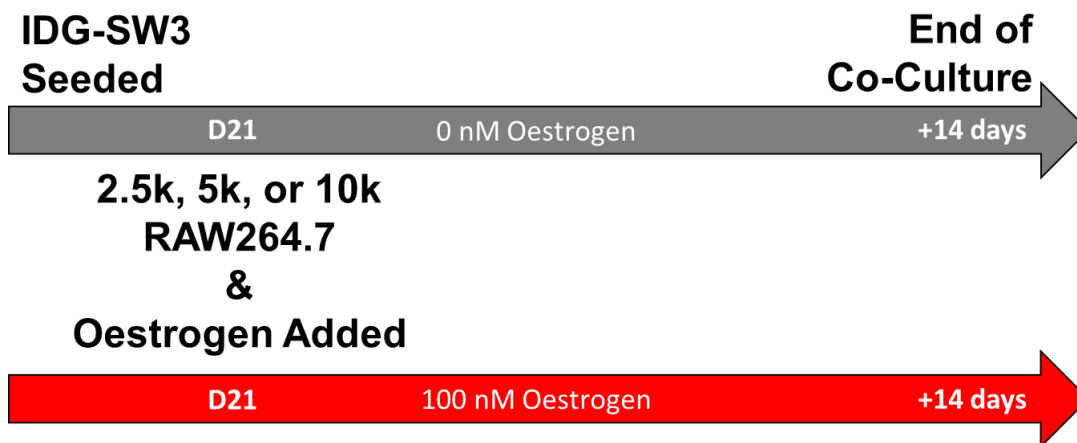


Figure 6.15: Schematic showing the TCP co-culture regimen with varied RAW264.7 seeding number and oestrogen exposure.

In each condition, there was no significant change in DNA at any time point (Fig. 6.16). As expected, co-cultures seeded with the most RAW264.7 had the highest DNA content. Oestrogen had no significant effect on the amount of DNA at the same seeding density, with the exception of 10K at day 14, where the oestrogen exposed group was significantly lower.

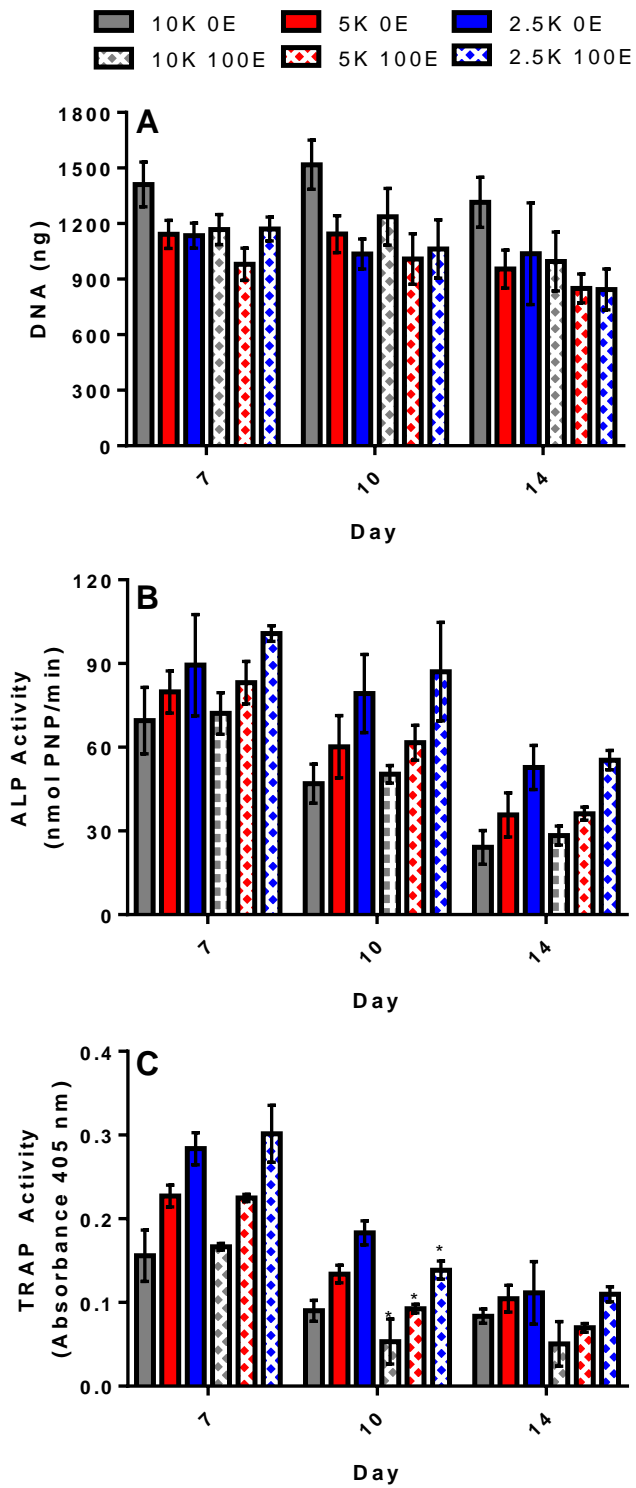


Figure 6.16: Effect of varied RAW264.7 seeding number and oestrogen on (A) DNA (B) ALP activity (C) TRAP activity over time in IDG-SW3 and RAW264.7 co-cultures ($n=3$).

ALP activity was higher when fewer RAW264.7 were present at each time point. The presence of oestrogen had no significant effect on ALP activity at any seeding density or time point.

TRAP activity followed the same pattern as ALP activity, with the highest TRAP activities achieved when the fewest precursors were added. There was no difference in TRAP activity at the same seeding density when oestrogen was applied, with the exception of day 10. From this, day 10 co-cultures were repeated and mineral staining was performed to ascertain resorption (Fig. 6.17). As before, TRAP activity increased with decreased RAW264.7 seeding number. 100 nM oestrogen significantly reduced TRAP activity at each seeding density. TRAP activities were normalised to 10,000 RAW264.7 at 0 nM oestrogen due to batch differences in the exogenous RANKL. Resorption was estimated by measuring the amount of mineral remaining at the end of the co-culture. The lowest number of precursors, which resulted in the highest TRAP activities, had the least remaining mineral at the end of the co-culture, indicating the highest amount of resorption had taken place. Oestrogen only inhibited resorption when 2,500 RAW264.7 were added. At the other seeding densities there were no significant differences.

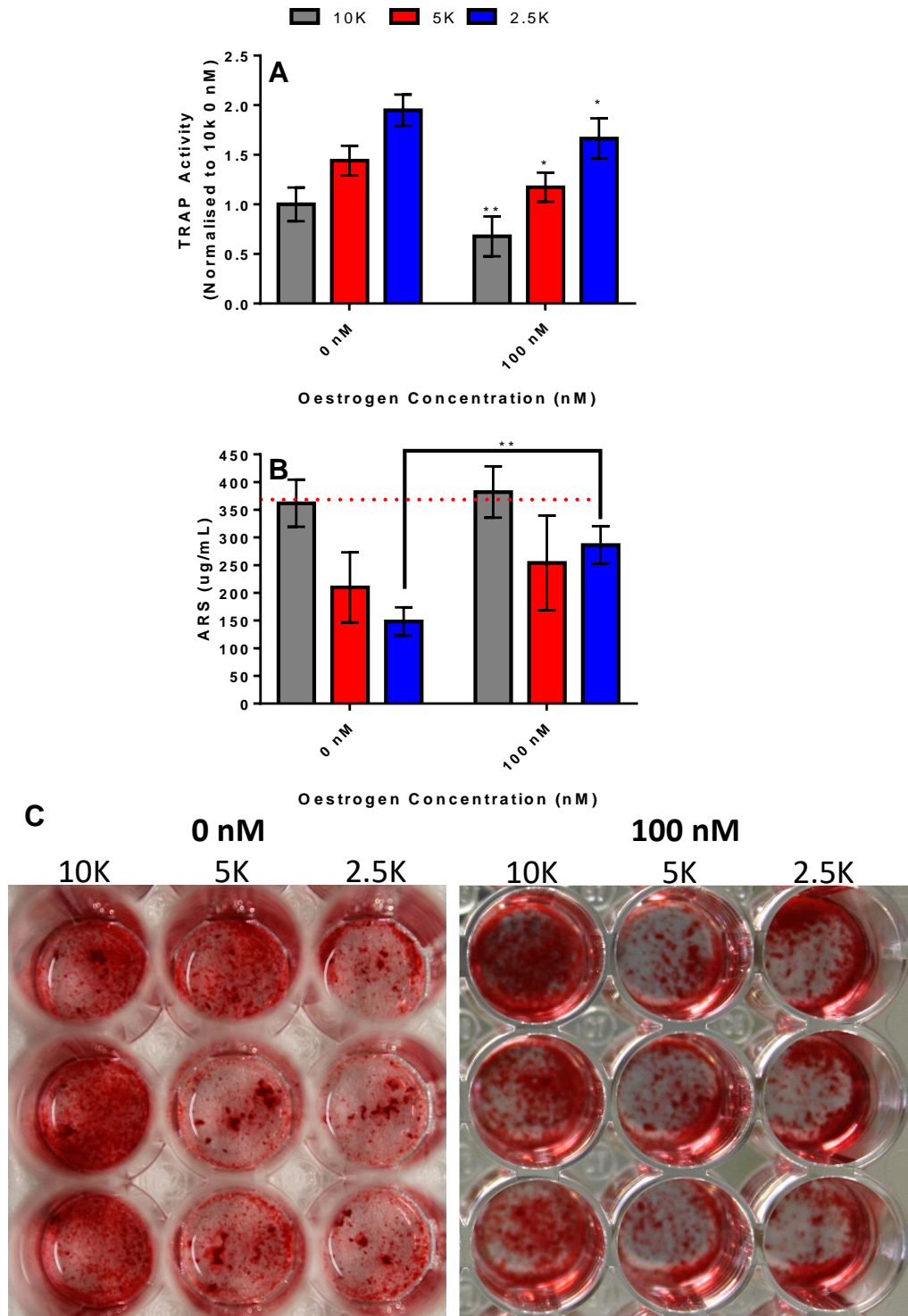


Figure 6.17: Effect of varied RAW264.7 seeding number in TCP co-cultures and oestrogen on (A) TRAP activity (n=7) and (B) resorption by quantifying remaining mineral (n=5) (C) representative images of the ARS staining of each condition. Red dashed line is day 21 staining before osteoclast addition.

6.4.6 Oestrogen pre-treatment of RAW264.7 has lasting effects after seeding

Due to the limited window where the co-culture has functioning mature osteoclasts, there is not sufficient time to expose RAW264.7 to oestrogen and then withdraw it to mimic menopause once the co-culture has been initiated. Therefore, the effect of exposing RAW264.7 to oestrogen prior to seeding was investigated. If they could be conditioned to oestrogen during passage, similar to how MC3T3-E1 have been pre-conditioned, then oestrogen could be withdrawn at the start of the co-culture [308]. To investigate this, RAW264.7 were passaged for one week either in 0 nM or 100 nM of oestrogen. They were then seeded at 2,500 per well in a 48 well plate and maintained for a further 8 days in BM supplemented with 50 ng/mL RANKL and either 0 nM or 100 nM oestrogen before measuring TRAP activity (Fig. 6.18).

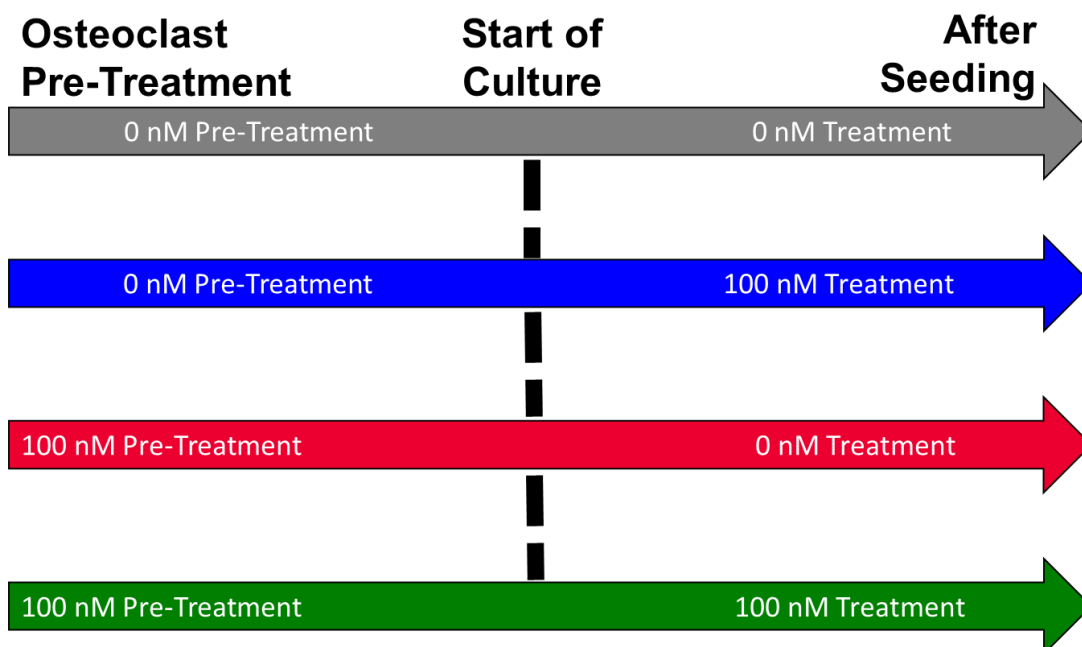


Figure 6.18: Schematic showing the oestrogen pre-treatment regimen for RAW264.7 to determine whether it has lasting effects after withdrawal. Pre-treatment refers to RAW264.7 exposure to oestrogen during passage. After seeding refers to when the osteoclast precursors are added to the culture.

Cultures not exposed to oestrogen had the highest TRAP activity (Fig. 6.19). Cultures only exposed to oestrogen after seeding had significantly lower TRAP activity than unexposed cultures, as previously seen. RAW264.7 with an oestrogen pre-treatment but no oestrogen after seeding had significantly lower TRAP activity than cultures without an oestrogen pre-treatment and no oestrogen after seeding, demonstrating a lasting effect of the pre-treatment. There was no significant difference between maintained oestrogen after seeding and oestrogen withdrawal after seeding.

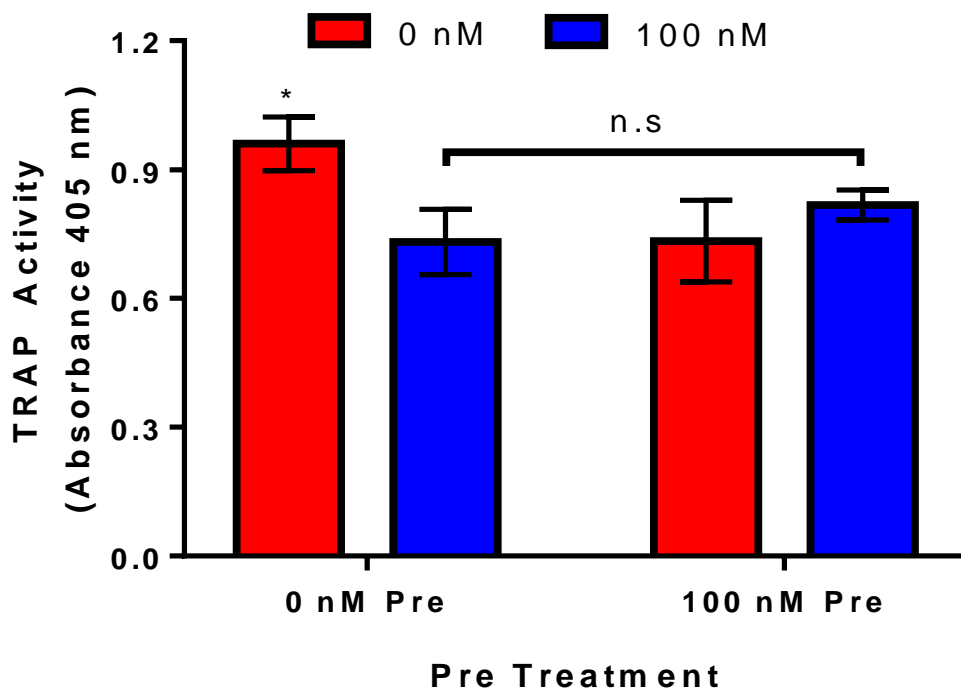


Figure 6.19: Effect of oestrogen pre-treatment on RAW264.7 TRAP activity. RAW264.7 were passaged in either 0 nM (0 nM Pre) or 100 nM (100 nM Pre) oestrogen for one week before seeding. After seeding, cultures were maintained in either 0 nM (red) or 100 nM (blue) oestrogen for 8 days. 0 nM / 0 nM significantly higher than all other groups (n=6) $*=p<0.05$.

6.4.7 Oestrogen withdrawal increases mineral resorption in monolayer co-cultures

The oestrogen pre-treatment regimen was then applied to the co-culture. RAW264.7 were pre-treated with 100 nM 17 β -estradiol during passage for one week prior to their addition to the co-culture. Oestrogen could be either maintained (pre-menopause) or withdrawn (postmenopause) as well as being compared to groups that were never exposed or only exposed to oestrogen after the co-culture was initiated (Fig. 6.20).

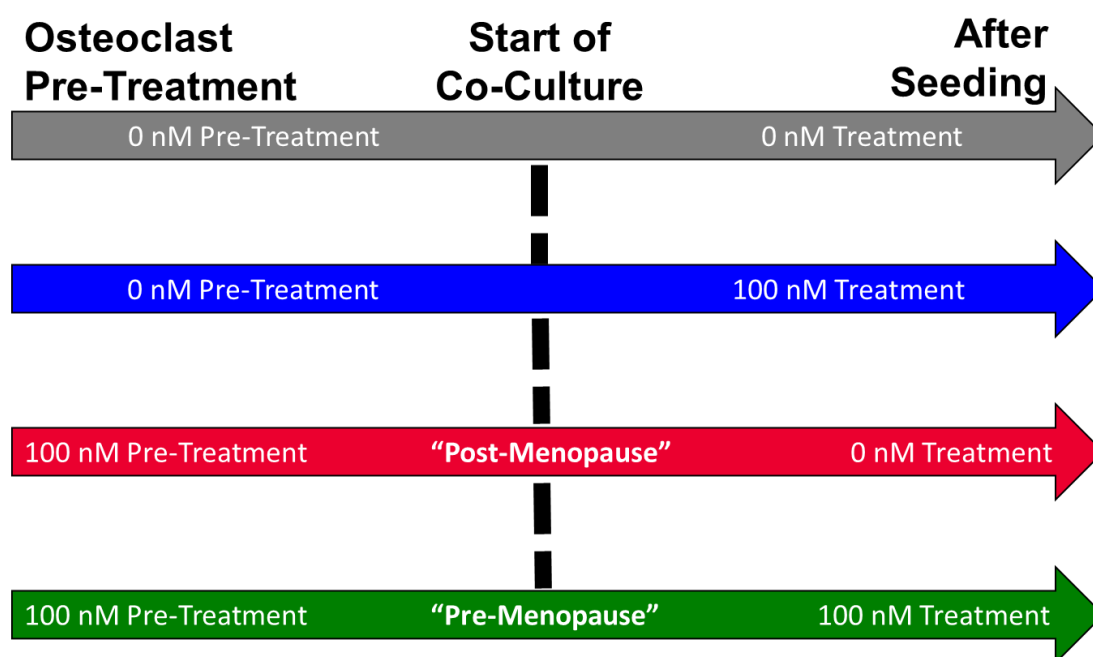


Figure 6.20: Schematic showing the various regimens of oestrogen treatment to be applied to the co-culture. Pre-treatment refers to RAW264.7 exposure to oestrogen during passage. After seeding refers to when the osteoclast precursors are added to the co-culture.

IDG-SW3 were grown for 21 days in SM in 48 well plates before the addition of 5,000 RAW264.7 that had either been exposed to 0 nM or 100 nM for one week during passage. Oestrogen levels were then either maintained or withdrawn, and the co-culture maintained for a further ten days in SM supplemented with 50 ng/mL RANKL (Fig. 6.21).

After ten days of co-culture multinucleated cells were visible (Fig. 6.22). By comparing the co-culture images to Hoechst 33342-stained RAW264.7 cultured with 50 ng/mL RANKL for 12 days, it can be seen that the brighter, round organelles in the brightfield co-culture images are nuclei; therefore, these cells are assumed to be osteoclasts. No oestrogen treatment had a significant effect on DNA, ALP activity or TRAP activity after ten days of co-culture. However, the remaining mineral in the “pre-menopause” (100 nM pre-treatment, 100 nM during co-culture) was significantly higher than the “postmenopause” group (100 nM pre-treatment, 0 nM during co-culture) and the unexposed group (0 nM pre-treatment and during co-culture). This may indicate that withdrawing oestrogen significantly upregulated resorption but not TRAP activity. However, it should be noted that all mineral levels were higher than the baseline level determined for IDG-SW3 after 21 days of culture in SM. Therefore, rather than increased resorption causing the difference between the maintained withdrawn groups, it may have been due to increased deposition in the maintained group.

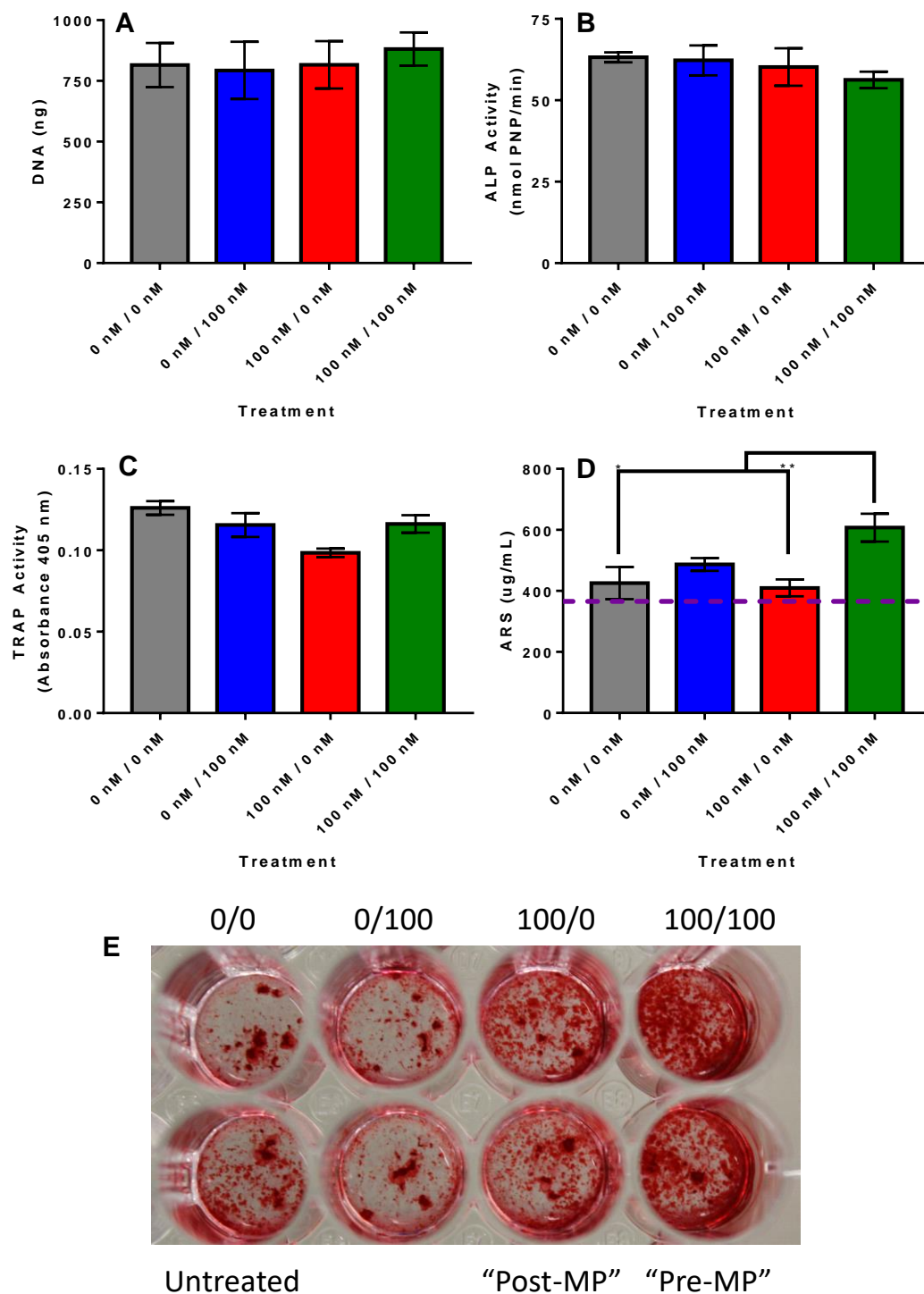


Figure 6.21: Effect of oestrogen pre-treatment and withdrawal on (A) DNA ($n=3$). (B) ALP activity ($n=3$) (C) TRAP activity ($n=6$) (D) remaining mineral ($n=6$). Purple dashed lined is day 21 baseline staining (E) representative images of ARS staining. 100/100 significantly higher than 100/0 and 0/0.

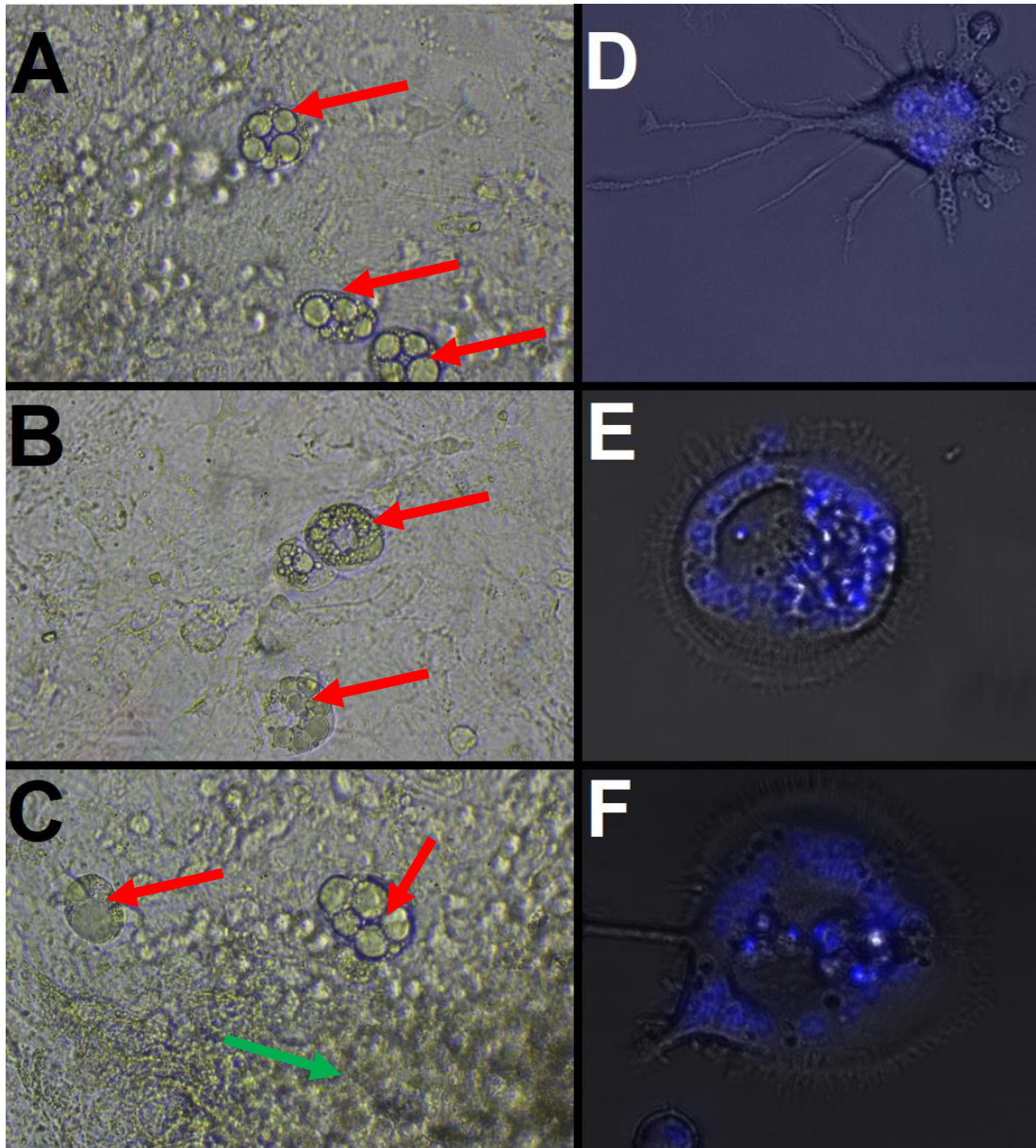


Figure: 6.22: Pictures of multinucleated cells on day 10 of co-culture. (Left) Multinucleated cells presumed to be osteoclasts (red arrows) clearly visible above IDG-SW3 monolayer. In C two osteoclasts border a mineral deposit (green). 20× magnification. (Right) Day 12 RAW264.7 cultured with RANKL and stained with Hoechst 33342 to show nuclei for cell morphology comparison. From this, the brighter, round organelles in the brightfield co-culture images are assumed to be nuclei.

6.4.8 Mineral staining fails to detect changes in resorption following oestrogen withdrawal in 3D

This protocol was then repeated in 3D on the polyurethane scaffold. 60,000 IDG-SW3 were seeded onto 5×5 mm polyurethane scaffolds and cultured for 3 days at 33 °C in EM. Media was then exchanged for SM and the scaffolds maintained for a further 21 days at 37 °C. As the difference in surface area between the scaffold and well plate was not known, either 2,500, 5,000 or 25,000 RAW264.7 that had either been exposed to 0 nM or 100 nM for one week during passage were then added to the scaffold. Oestrogen levels were either maintained or withdrawn, and the co-culture maintained for a further ten days in SM supplemented with 50 ng/mL RANKL (Fig. 6.23).

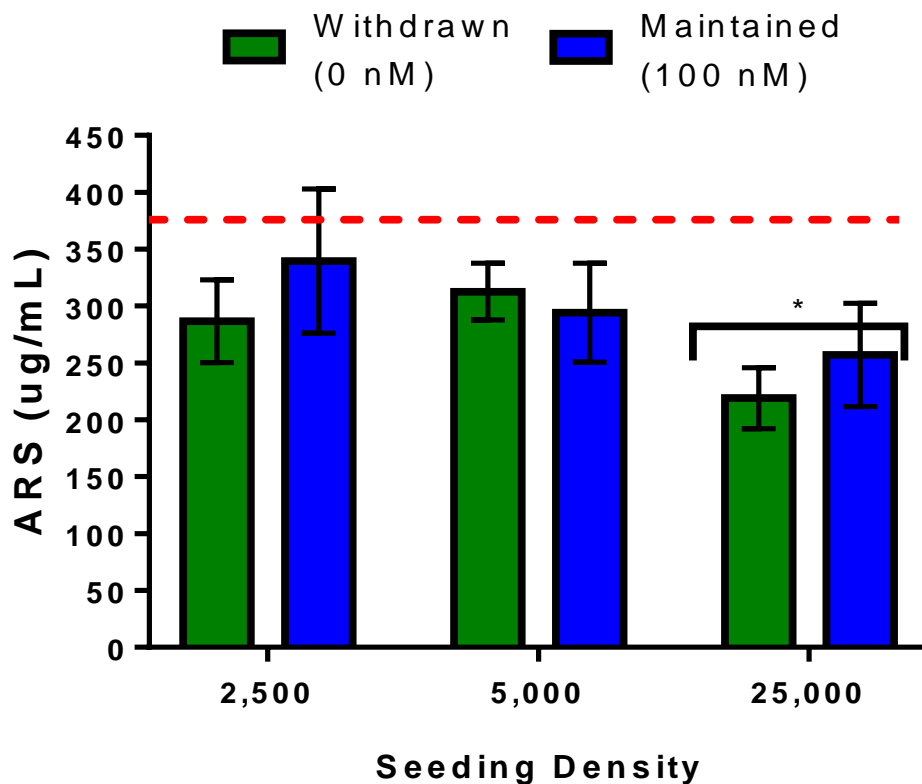


Figure 6.23: Effect of oestrogen pre-treatment and withdrawal on mineral resorption in 3D co-cultures. Either 2,500, 5,000, or 25,000 RAW264.7 added at start of co-culture. Red dashed line is day 21 staining before osteoclast addition. No significant difference between withdrawn and maintained oestrogen at any seeding density. Significantly less mineral in co-cultures seeded with 25,000 RAW264.7 in comparison to the other two conditions ($n=6$).

By day 4, monocytes and multinucleated cells were visible on the extracellular matrix deposited onto the scaffolds by optical microscopy (Fig. 6.24). On day 10, this was also visible on H&E stained histological sections of the co-culture (Fig. 6.25). During sectioning the polyurethane scaffold appeared to pull apart and deposited matrix separated from the scaffold struts. Despite this, the extensive extracellular matrix was still clearly visible (light purple) around the polyurethane sections (light pink). RAW264.7 monocytes and multinucleated cells appear as dark purple and are present on the matrix.

With regards to remaining mineral after ten days of co-culture, there were no significant differences between maintained and withdrawn oestrogen at any seeding density. However, there is significantly less mineral remaining in the 25,000 seeding density in comparison to the other two densities indicating the most resorption took place.

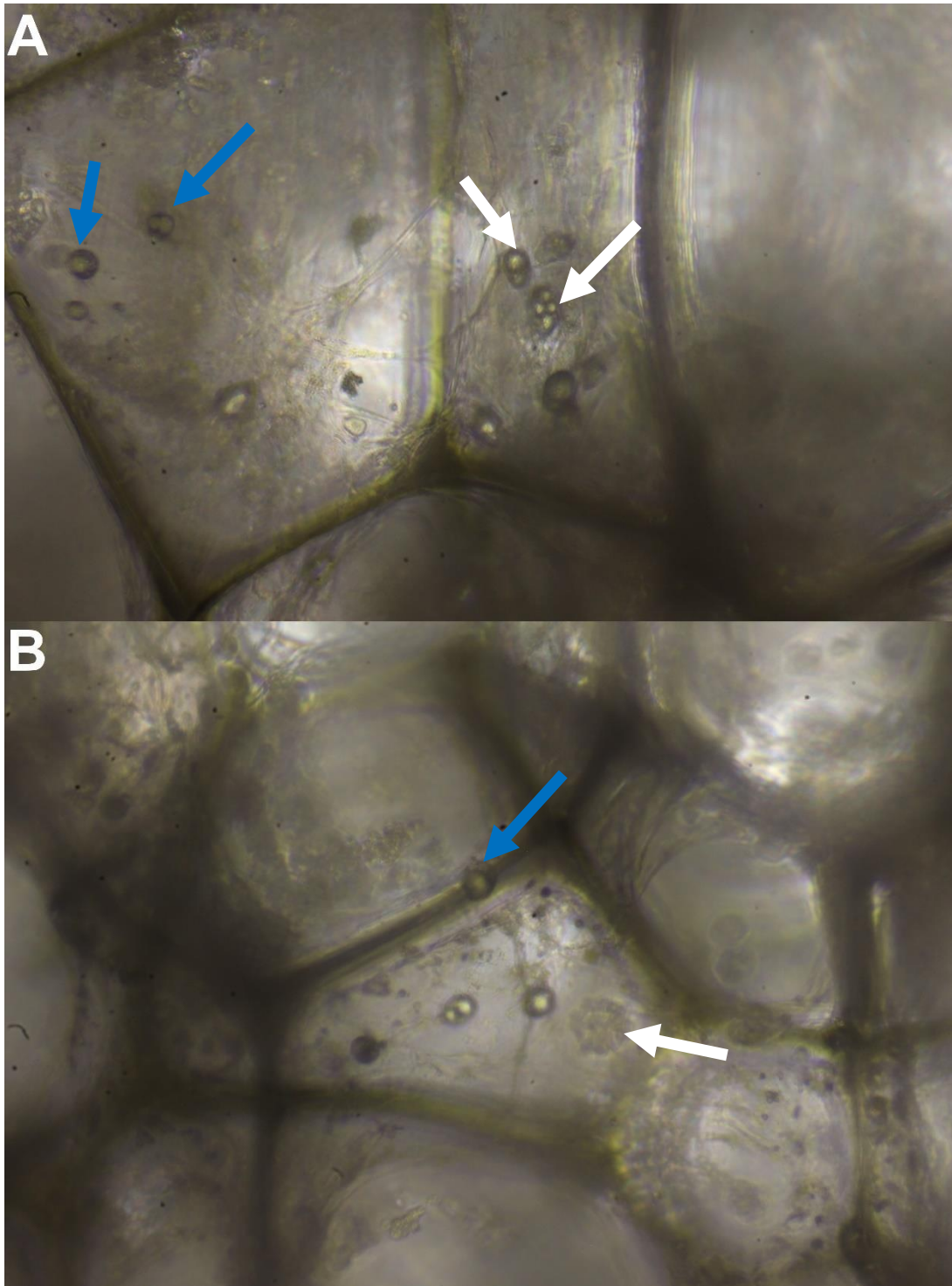


Figure 6.24: Representative optical microscope pictures of the 3D co-culture. Both mononuclear (blue) and multinucleated (white) cells are visible on the extracellular matrix deposited by the IDG-SW3 by day 4 of co-culture.

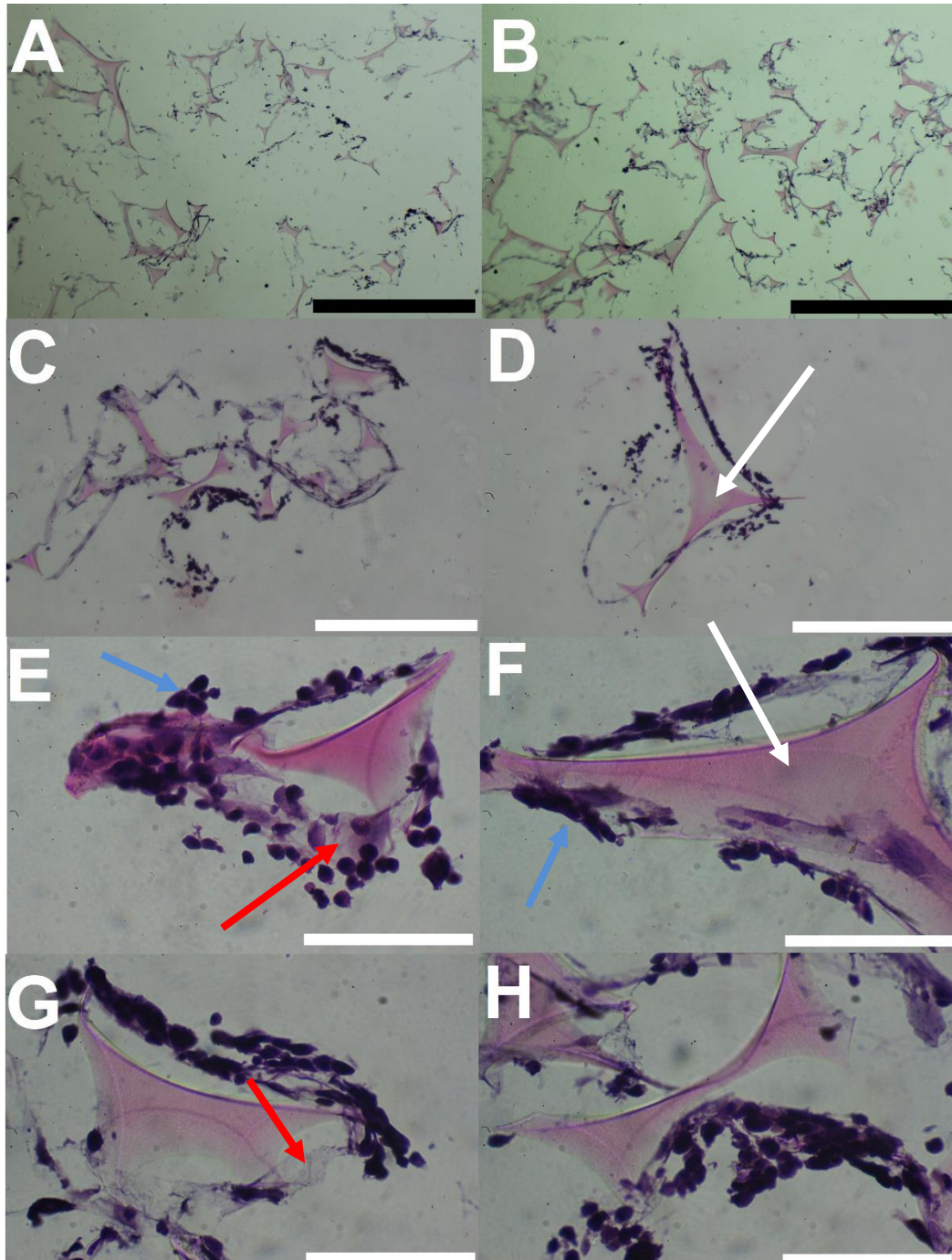


Figure 6.25: Optical microscope images of day 10 3D co-culture sections stained with H&E. (A&B) 4× magnification showing how matrix is pulled from the scaffold during sectioning (scale bar 1 mm) (C&D) 10× magnification RAW264.7 clearly visible on extracellular matrix deposited by IDG-SW3 (scale bar 400 μm) (E-H) 40× magnification RAW264.7 (dark purple / blue arrows) on IDG-SW3 matrix (light purple / red arrows) and polyurethane scaffold struts (light pink / white arrows) (scale bar 100 μm).

6.5 Discussion

The work in this chapter applied the findings of the previous two in an attempt to develop an *in vitro* model of postmenopausal osteoporosis. Initially, the effects of PTH, a common treatment for osteoporosis, were examined on IDG-SW3 and RAW264.7 to determine whether an anabolic effect analogous to that observed *in vivo* could be replicated. Next, markers for osteoblast and osteoclast function in co-culture were determined before evaluating the effect of oestrogen exposure in TCP and 3D co-cultures. The effect of osteoclast seeding density on co-culture duration and mineral content were then evaluated to finalise co-culture parameters. Co-cultures were then subjected to oestrogen withdrawal to mimic postmenopausal osteoporosis in TCP and 3D.

PTH is a common therapeutic for osteoporosis due to its dual action as a promoter of bone formation and an inhibitor of bone resorption and acts both directly and indirectly on cells within bone. Its direct action on cells is initiated by the stimulation of the receptor PTH1R. This receptor is predominantly found on osteoblastic lineage cells as well as tubular cells in the kidney, although there is some evidence that it may also be present on osteoclasts [465], [466]. However, whether PTH has an anabolic or catabolic effect on bone depends on the frequency, concentration and duration of its administration (Fig. 6.26).

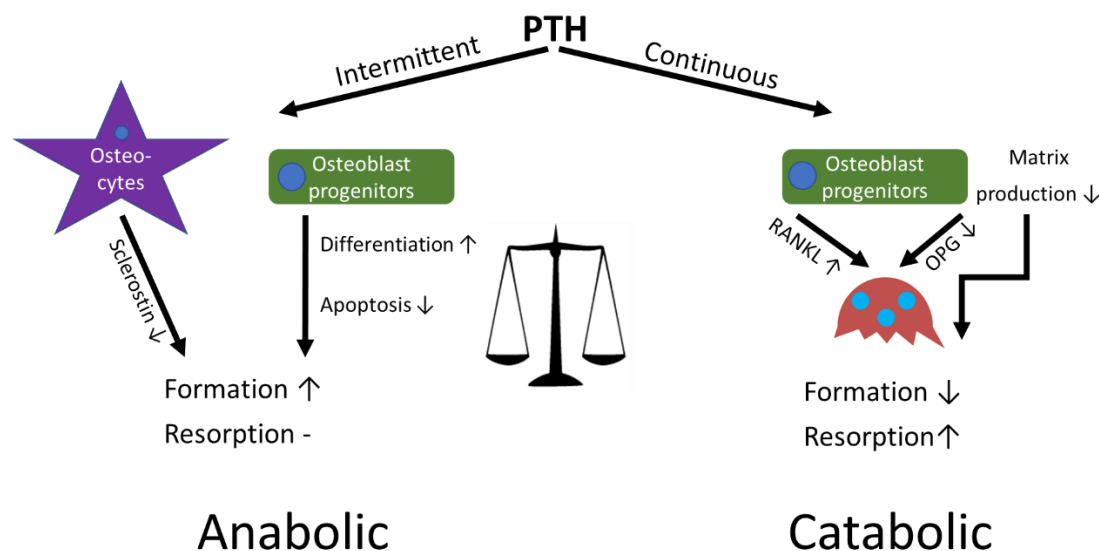


Figure 6.26: PTH can have anabolic or catabolic effects on bone depending on application modality.

Continuous exposure is associated with bone loss due to a downregulation of the expression and synthesis of extracellular matrix proteins and an increase in the RANKL:OPG ratio [226]; whereas intermittent exposure can promote osteoblast differentiation, inhibit their apoptosis and suppress sclerostin synthesis by osteocytes [192], [225], [226]. In the context of this *in vitro* model of osteoporosis, the aim was to find a PTH treatment regimen that would promote IDG-SW3 mineralisation and reduce RAW264.7 resorption. As previously demonstrated, IDG-SW3 do not produce a detectable quantity of RANKL. Therefore, any anabolic or catabolic response will be the result of a direct change to IDG-SW3 mineralisation capacity, rather than an indirect change on RAW264.7 osteoclastogenesis via modulation of the RANKL:OPG ratio as RAW264.7 were found to not respond to direct PTH stimulation.

Initial experiments indicated that a PTH concentration of 1 nM applied intermittently for 1 or 24 hours may elicit an anabolic response, as indicated by an increased ALP activity. The powerful catabolic effect of continuous PTH exposure was apparent even at low concentrations, with a significant reduction in ALP activity. PTH predominantly reduced the ALP activity by reducing expression of these osteoblastic proteins rather than by reducing total cell number, as indicated by minimal differences in total DNA. As IDG-SW3 are an osteoblast-osteocyte cell model, the promotion of osteoblastic differentiation cannot be observed as they have already differentiated past this phenotype. However, as a sub-population of IDG-SW3 will terminally differentiate into osteocytes, it was hypothesised that its effect on sclerostin inhibition and role as an anti-apoptotic would promote mineralisation over longer time periods.

To investigate this, concentrations between 1 and 20 nM were applied intermittently, either once or twice per week, for 24 hours over a three-week period. Interestingly, the highest GFP expression after 21 days was found in the 0 nM group, indicating that PTH exposure inhibited osteocytogenesis and maintained IDG-SW3 in their osteoblastic phenotype. However, despite this, there was no significant increase in ALP activity in treated groups and mineralisation visibly decreased as PTH concentration increased. However, in comparison to previous experiments performed with the same cells over the same duration, mineralisation was visibly less at the same time point, even in the 0 nM group. Although this could have been due to the vehicle, it is very unlikely that a small volume of PBS and BSA would have inhibited mineralisation to this degree, with it being more likely due to variability in cell behaviour, as discussed later in this chapter. As no PTH treatment regimen where an anabolic response analogous to that observed when it is administered as an

osteoporosis therapeutic could be found, no PTH treatment was applied to the *in vitro* model developed.

Work on optimising the co-culture was then performed. Only direct co-cultures were considered for this thesis, as opposed to well plate inserts that separate the osteoblasts and osteoclasts. This was due to osteoblastic cells being able to produce both membrane-bound and soluble isoforms of the cytokines that affect osteoclasts, meaning that indirect co-cultures would preclude membrane-bound cytokines from having an effect. In the literature, groups have co-seeded osteoblasts and osteoclast precursors simultaneously [171], [252], added the precursors 24 hours after seeding the osteoblasts [164], or waited multiple weeks before their addition [241], [249], [250]. In §4.4.13, RAW264.7 were added to IDG-SW3 24 hours after seeding and TRAP activity was detectable after seven days, albeit at a lower level than a RAW264.7 monoculture. However, in this experiment, only 1,500 IDG-SW3 were seeded in a 12 well plate in accordance with the work by Zhao, et al., when co-culturing osteocytes and osteoclast precursors [211]. As the RAW264.7 were added 24 hours later this low seeding density means that the IDG-SW3 had not reached confluence, and as they had now been switched to SM and 37 °C, their ability to proliferate further was diminished.

In an attempt to alleviate this, 60,000 IDG-SW3 were seeded and maintained overnight in EM at 33 °C before the addition of RAW264.7 the following day. Despite this, seven days later, there was no detectable ALP or TRAP activity in the co-culture. Again, it was observed that despite the higher seeding density, the IDG-SW3 did not become confluent in co-culture. In mono-cultures of each cell type the appropriate marker was identifiable and the total DNA in the co-culture confirmed that both cell types were present. Therefore, it appears that the activity of both cell types was inhibited in co-culture.

This inhibition could be due to the IDG-SW3 being unable to achieve confluence due to the addition of the RAW264.7, and therefore not expressing a detectable level of ALP. Although osteoblasts do produce some ALP whilst proliferating, its expression is raised significantly once they are confluent [467], [468]. Therefore, with IDG-SW3 unable to become confluent, their ALP activity and mineralisation was undetectable. Alternatively, the higher metabolic activity of the osteoclastic cell line may have resulted in too few nutrients remaining in the culture media to support their function. The absence of TRAP activity in the co-culture implies that the RAW264.7 were

unable to fuse and generate osteoclasts. As they were seeded onto a non-confluent cell layer, the precursors may have been unable to successfully migrate and fuse with each other due to the IDG-SW3 outnumbering them 3:1. Alternatively, in the co-culture, experiment cells were seeded onto gelatine coated wells, whereas typical RAW264.7 mono-cultures are seeded directly onto the well plate. Gelatine is used as a well plate coating to improve cell attachment; as RAW264.7 is a motile cell line the presence of gelatine could be inhibiting their ability to migrate and find precursors to fuse with. As gelatine is denatured collagen, the major protein in bone, this seems unlikely. However, the denaturing process may affect how well osteoclasts can adhere to gelatine in comparison to collagen *in vivo* by denaturing adhesion proteins on the surface. Furthermore, collagen in native bone tissue is mineralised and consequently would not have the same surface chemistry as a gelatine tissue culture coating. Therefore, it is likely that cell motility would be affected by the concentration of the well plate coating.

Both of these difficulties can be overcome by adding RAW264.7 to a confluent monolayer of IDG-SW3. Here, the osteoblasts are confluent and therefore should express ALP and mineralise, and the osteoclasts are on the same plane and are not attached to a highly adhesive substrate, meaning that they should be able to migrate and fuse. To test this, IDG-SW3 were again seeded at 60,000 cells per well, but were now maintained for three days in EM at 33 °C until confluent. They were then transferred to SM and 37 °C and 10,000 RAW264.7 added before maintaining for ten days. Again, total DNA confirmed that both cell types were present in the co-culture. However, by adding the RAW264.7 once the IDG-SW3 had become confluent, both ALP and TRAP activity were detectable in the co-culture. Importantly, ARS staining of the co-culture revealed that the osteoblasts were still able to mineralise.

Interestingly, ALP activity was lower in the co-culture than in an IDG-SW3 monoculture, and TRAP activity was higher in the co-culture than a RAW264.7 monoculture. The lower ALP activity suggests that the presence of a secondary cell type is inhibiting the function of the osteoblasts. This is most likely due to the effective nutrient availability in the media being lower as another cell type is now also metabolising them. Additionally, in co-culture, only 50% of the media is exchanged during media changes in order to retain factors such as M-CSF produced by the RAW264.7. Therefore, as well as nutrient depletion being enhanced, the accumulation of potentially toxic metabolites that can reduce cell function is likely to be greater in the co-culture as more cells are present [469].

Despite this, the TRAP activity is significantly increased in the co-culture. Without knowledge of the findings of the previous chapters, the assumed reason for this increase would be that the osteoblasts are producing RANKL, thereby stimulating osteoclastogenesis. However, we have seen that co-cultures without exogenous RANKL cannot stimulate osteoclast formation (Fig. 4.19) and ELISAs have shown that IDG-SW3 in mono-culture are not producing RANKL, only OPG. Therefore, rather than increasing the ratio, co-culture should be decreasing it in comparison to monoculture as there is a constant amount of RANKL in the medium, and OPG is only produced by the osteoblasts.

One potential reason for the increase in TRAP activity would be that when IDG-SW3 are co-cultured with RAW264.7 for longer time periods, they are stimulated to produce RANKL, contrasting their behaviour in mono-culture. However, the upregulation of RANKL production is normally associated with vitamin D or PTH exposure and neither of these factors are synthesised by osteoclasts. Despite this, it would be interesting to repeat the co-cultures where osteoclasts were added at later timepoints without exogenous RANKL addition to determine whether there is any osteoclastic stimulation of osteoblasts.

It is more likely that this stimulation of osteoclastogenesis observed in co-culture is due to some other factor being at play. M-CSF is another cytokine produced by osteoblasts that has a role in osteoclastogenesis by promoting the survival and proliferation of osteoclast precursors [48]. In addition to this, Hodge, et al., showed that *in vitro*, it can cause human osteoclast precursors to fuse, form osteoclasts, and become resorptive in a dose dependent manner. They also found that it can modulate the resorptive capability of mature osteoclasts [47]. Although RAW264.7 produce their own M-CSF, a dose-dependent response to the cytokine could explain the further stimulation of the cells by co-culturing with IDG-SW3 if they were also producing the factor [166], [167]. Unfortunately, to date there do not appear to have been any studies discerning whether IDG-SW3 produce M-CSF.

Interleukin-1 (IL-1) is another factor that has been associated with stimulation of osteoclastogenesis. Kim, et al., found that it works in synergy with RANKL to induce osteoclast differentiation as RANKL stimulation upregulates the expression of IL-1 receptor (IL-1R) in bone marrow-derived osteoclast precursors. Before stimulation with RANKL, IL-1R expression is low in this type of precursor, but when it is raised by an alternative mechanism (c-fos stimulation by M-CSF), IL-1 is able to induce

osteoclastogenesis in the absence of RANKL [470]. RAW264.7 have been shown to express IL-1R, and therefore could respond to this stimuli [471]. IL-1 can be produced by osteoblasts as part of the inflammatory response [472], [473]; a response that could have been stimulated in IDG-SW3 by the addition of RAW264.7. This negative reaction of IDG-SW3 is also a potential reason for the reduction in ALP activity observed in co-culture. Alternatively, IL-1 or other inflammatory markers may have been present in the FBS used.

As a suitable co-culture protocol that allowed detectable levels of the three markers to be measured had been developed, co-cultures were next exposed to oestrogen to determine whether similar effects to those seen in mono-cultures would be observed in co-cultures. In addition to TCP co-cultures, 3D co-cultures in PU scaffolds were also performed. Total DNA quantification revealed that both cell types were present and that the presence of oestrogen had no effect on cell number. ALP activity was detectable in both TCP and 3D co-cultures, and although not significant, was higher in oestrogen exposed cultures. As it was not possible to normalise activities to DNA in the co-culture, it was not possible to determine whether this change was due to differences in cell number or a cell-level response to the hormone. Interestingly, the inhibitory response to oestrogen seen in mono-cultures was not observed in co-culture, indicating that the stimulation of osteoclastogenesis by the IDG-SW3 was greater than its inhibition by 17β -estradiol.

To this point, osteoclast cultures had only been maintained over a ten day period. To determine whether the effects seen would continue over longer durations, the changes in activity over a 28 day period were assessed. Although the metabolic activity of RAW264.7 continues to increase over a 4 week period, the TRAP activity decreases each week, indicating fewer mature osteoclasts are present. Not all RAW264.7 fuse and become mature osteoclasts when exposed to RANKL. Therefore, it was expected that when the first generation of mature osteoclasts undergo apoptosis, they would be replaced by subsequent generations formed from the remaining precursors. However, this was not the case, with only an initial generation of osteoclasts being formed. This was due to overgrowth of the culture by the osteoclast precursors. RAW264.7 have a doubling time of approximately 11 hours. This rapid multiplication means that although mature osteoclasts formed initially undergo apoptosis within two weeks, by this stage the density of the precursors is exceptionally high, limiting their ability to fuse and become mature osteoclasts (Fig. 6.27).

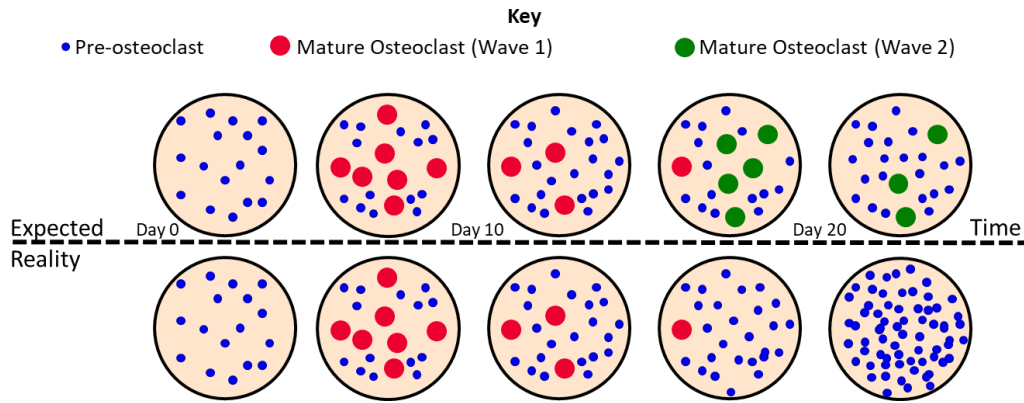


Figure 6.27: Schematic showing the expected and actual ability of RAW264.7 to form multiple generations of mature osteoclasts.

Akchurin, et al., attempted to computationally model the likelihood that RAW264.7 would form multiple generations of mature osteoclasts. They found via *in vitro* experimentation that in 46 long term (15-26 days) RAW264.7 cultures with varied plating densities and RANKL concentrations, only 59% were observed to generate multiple waves of osteoclasts, and that multiple waves of osteoclasts were more likely to occur with very high RANKL concentrations (100 ng/mL) [474]. This agrees with what was observed here, where in monoculture and co-culture only 25 - 50 ng/mL of RANKL was applied and only a single wave was observed. Although the higher concentration of RANKL was used in co-culture, increasing the likelihood of multiple wave formation occurring, the presence of OPG will have reduced the RANKL:OPG ratio, negating the increased probability of subsequent osteoclast waves.

We have seen that seeding with a lower density of RAW264.7 delays the peak TRAP activity and permits a greater number of osteoclasts to be formed. Therefore, with the aim of extending the maximum duration of the co-culture, the effects of reducing the seeding density of RAW264.7 in co-culture was investigated. As expected, the highest total DNA was detected in co-cultures where the greatest number (10,000) of RAW264.7 were added. However, there was no significant difference in total DNA when the middle (5,000) and lowest (2,500) seeding number are compared. This indicates that at the lower seeding density less proliferation occurs, possibly indicating that a larger proportion of precursors had fused. ALP activities have been shown to be lower in co-culture than in monoculture at the same time point. The highest ALP activities are seen in the co-cultures where the fewest RAW264.7 were added at all time points. This indicates a 'dose-response' to the presence of the osteoclast

precursors, where as their number increases, the IDG-SW3 ALP activity decreases. The TRAP activity correlates with the ALP activity with regards to RAW264.7 seeding density; the fewer added the higher the TRAP activity at all time points. This again shows that the maturation of RAW264.7 is space-dependent, and that the efficacy of mature osteoclast generation increases when they are seeded more sparsely.

Interestingly, at day 10, the presence of oestrogen was observed to significantly inhibit the TRAP activity of the co-culture at all seeding densities. However, there was no significant difference in the amount of resorption that occurred, as the quantity of mineral remaining in comparison to the day 21 baseline was the same for treated and untreated cultures despite the difference in TRAP activity. The exception to this is when 2,500 RAW264.7 were added, as the remaining mineral in the oestrogen exposed group is significantly higher than in the untreated group. Therefore, at this seeding density, we observe the protective role of oestrogen on bone that is seen *in vivo*, where the presence of the hormone reduces bone catabolism.

However, this protection of the mineral by oestrogen is only observed when directly staining the extracellular matrix, as there is no reduction in TRAP activity despite less resorption occurring. Therefore, we see that TRAP activity only appears to correlate with mineral content *in vitro* in the absence of oestrogen (Fig. 6.22). When cultures were not exposed to oestrogen, TRAP activity and remaining mineral have a strong negative correlation ($R^2 = 0.9236$), whereas exposure to 100 nM oestrogen results in no correlation ($R^2 = 0.5189$) due to oestrogen preventing resorption at the 2,500 seeding density.

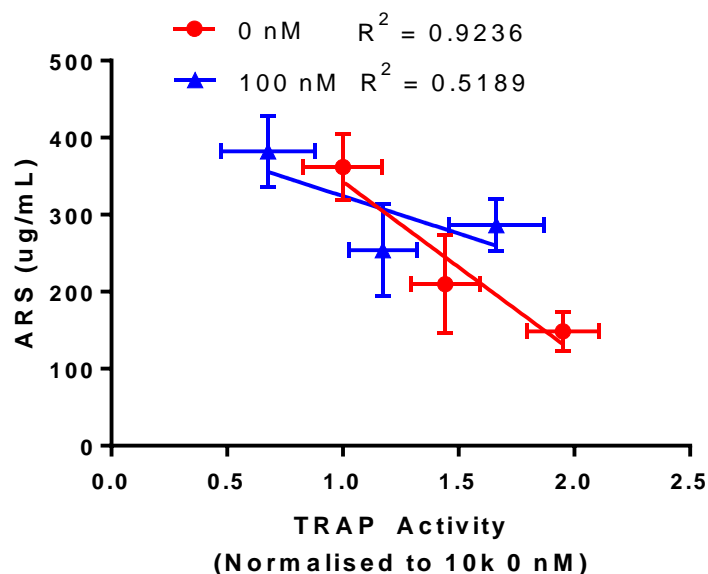


Figure 6.22: XY plot of mean \pm SD of TRAP activity vs. ARS staining for co-cultures exposed to 0 nM or 100 nM oestrogen. Correlation only without oestrogen. R^2 calculated using linear regression.

The strong correlation of serum TRAP concentration with bone resorption seen *in vivo* is the result of TRAP accumulation in the blood as it is secreted by the osteoclasts along with the organic catabolites of bone resorption [350]. When TRAP was measured here *in vitro*, it was after the removal of the media. Therefore, rather than measuring the equivalent of the accumulation of serum TRAP *in vivo*, the activity of intracellular TRAP and TRAP within the extracellular matrix is being quantified. This TRAP measurement gives an indication of the current activity of the osteoclasts, rather than an indication of how resorptive they have been previously. As TRAP has an indirect role in bone resorption, for example by enabling osteoclast migration by disrupting osteopontin rather than directly resorbing the bone surface [349], the lack of correlation seen here could be due to not measuring the same type of TRAP that is quantified *in vivo* (intracellular vs. serum/secreted).

Alternatively, the lack of detectable difference in mineral resorption despite the different TRAP activities could be due to low assay sensitivity when staining for mineral. With regards to the 10,000 and 5,000 seeding density, the day 10 TRAP activities were significantly lower in the presence of oestrogen. As oestrogen affects osteoclast formation and survival, this is presumably due to fewer active osteoclasts

being present. Despite this, there is no difference in the remaining mineral at this time point. We have seen that these higher seeding densities generate fewer mature osteoclasts; therefore, minimal resorption will occur even without oestrogen, so a small decrease in osteoclast number due to oestrogen does not have a large enough effect on mineral resorption to allow this difference to be detected by calcium staining. This effect is further compounded by the small culture surface area of a 48 well plate. For example, consider two culture surfaces, one with an area ten times greater than the other. Both have the same amount of mineral and active osteoclasts per cm², and after ten days the osteoclasts have resorbed 10% of the mineral in both cultures. Although the same percentage has been resorbed, the amount resorbed is ten times greater in the larger surface area culture, meaning that a low sensitivity assay is more likely to detect the change.

At the lowest seeding density (2,500 RAW264.7) we see the highest TRAP activities as more osteoclasts are able to form. Their TRAP activity is still significantly reduced by oestrogen, but in contrast to the higher seeding densities, we see that less mineral is resorbed in the presence of 17 β -estradiol. This may be because having more active osteoclasts overcomes the low sensitivity of using ARS staining as a protocol for quantifying mineral resorption. If we assume oestrogen reduces osteoclast number by x %, having more osteoclasts initially means that a larger number undergo apoptosis in comparison to when fewer are present, and therefore there will be a larger difference in mineral resorption which is more likely to be detected by a low sensitivity assay. This hypothesis agrees with the results seen here, as although we see oestrogen having a protective role when 2,500 RAW264.7 are added, the remaining mineral with oestrogen in this culture is still less than cultures with fewer mature osteoclasts initially, for example those with 10,000 RAW264.7. This is because whilst a large amount have been stimulated to undergo apoptosis by oestrogen, there are still more remaining than in cultures where the conditions were not amenable to effective osteoclastogenesis in the first place.

In the context of postmenopausal osteoporosis, co-culturing osteoblasts and osteoclasts in the presence of oestrogen is the equivalent of the pre-menopause 'healthy' condition when oestrogen levels are still high. Thus far, we have seen that under certain culture durations and seeding densities, it is possible to have a system analogous to this, with oestrogen protecting the deposited mineral in comparison to cultures without oestrogen. However, cultures never exposed to oestrogen do not replicate the postmenopause condition, as their elevated resorption levels are not in

response to a decline in oestrogen. Therefore, for an *in vitro* model of postmenopausal osteoporosis, it is important that the cells are initially conditioned to oestrogen before removing it. This should then result in increased mineral resorption.

Initially it was intended that cells would be exposed to oestrogen whilst in the co-culture. However, as the maximum duration of the co-culture where there are still osteoclasts present is approximately two weeks, this is not feasible, as demonstrated in figure 6.9. Therefore, it was decided to attempt to condition the RAW264.7 to oestrogen prior to seeding whilst they are in passage. Oestrogen levels could then either be maintained or reduced to 0 nM at the point of seeding, replicating the decline in oestrogen seen postmenopause. Conditioning oestrogen during passage prior to seeding has previously been shown to be effective by Brennan, et al., who utilised this approach to simulate pre-menopause whilst examining the effects of oestrogen withdrawal on MC3T3-E1 [308]. Due to the findings of chapter four, where oestrogen had no stimulatory or inhibitory effects on IDG-SW3 proliferation, ALP activity or mineralisation, only pre-treatment of RAW264.7 during passage was considered for these experiments. However, as *in vivo* both cell types are ‘conditioned’ to oestrogen prior to menopause, any further developments of a post-menopausal osteoporosis model should consider this, as it may be affecting markers that were not examined in this study.

This approach to pre-conditioning RAW264.7 with oestrogen prior to their addition to the co-culture is a better representation of what occurs *in vivo*, in comparison to application and withdrawal of oestrogen after seeding, as it is osteoclast precursors circulating in the bloodstream that are conditioned to serum oestrogen levels pre-menopause, rather than mature, active osteoclasts. Osteoclast precursors have the potential to be conditioned by exposure to oestrogen during passage due to its effects on the downstream signalling of RANK. When RANKL binds with RANK, tumour necrosis factor receptor-associated factor 6 (TRAF6) is recruited which in turn activates multiple major downstream signalling pathways that affect the proliferation, differentiation, function and survival of osteoclasts [475]–[477]. The Jun N-terminal kinase (JNK) signalling pathway is one of these, and is responsible for osteoclast precursor differentiation (Fig. 6.28). When stimulated it increases the production of the osteoclastogenic transcription factors c-Fos and c-Jun [478], [479]. This results in the stimulation of nuclear factor-activated T cells c1 (NFATc1), a master transcription factor involved in the terminal differentiation of osteoclasts that regulates osteoclast specific genes for TRAP, cathepsin K and OSCAR [480], [481].

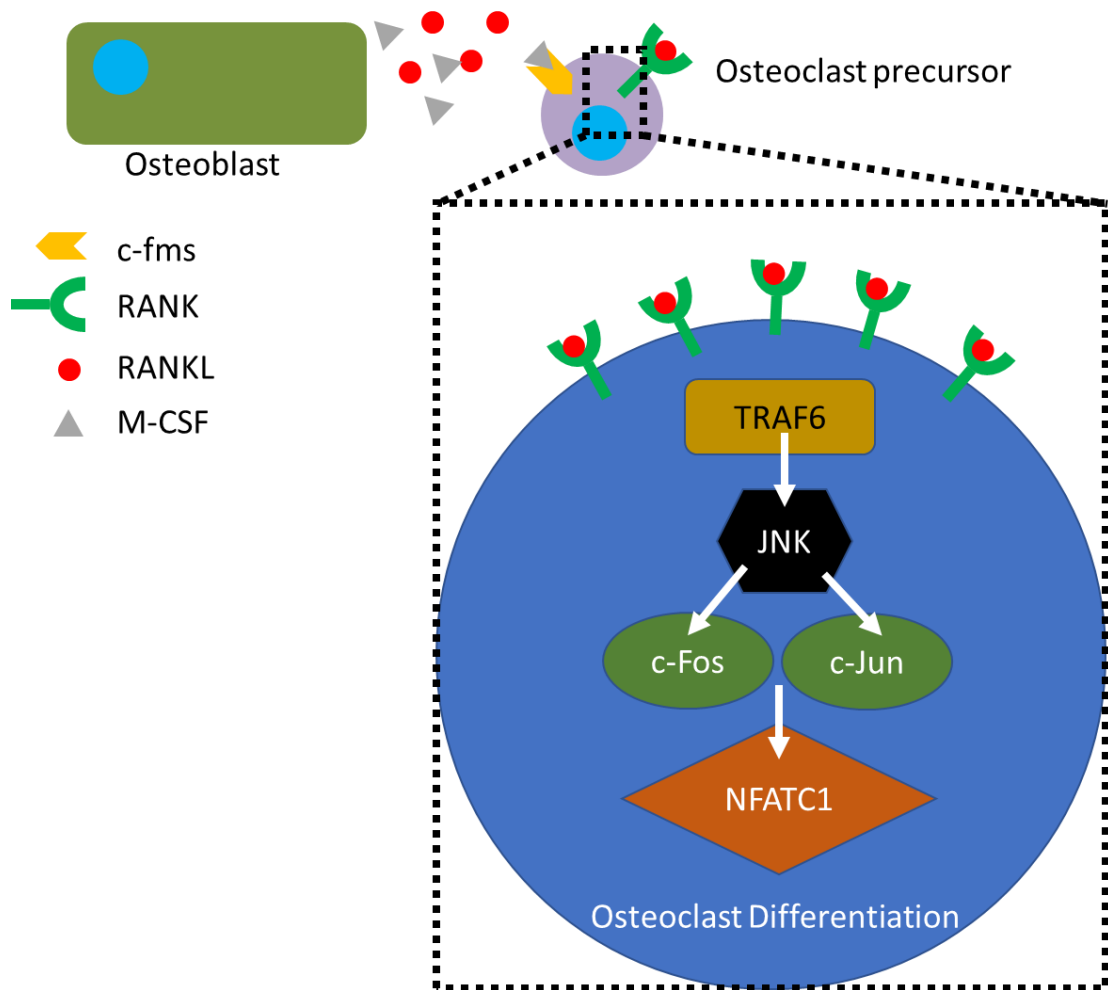


Figure 6.28: A diagram illustrating the role of the JNK pathway on osteoclast precursor differentiation.

Monocytes, the osteoclast precursors in the blood stream, express $ER\alpha$. Its stimulation by oestrogen has the ability to disrupt the JNK signalling pathway, reducing their ability to undergo osteoclastogenesis [479]. This effect on the JNK signalling pathway is also observed in RAW264.7, and in combination with increasing apoptosis, is a key mechanism by which oestrogen reduces osteoclast activity [309].

The different oestrogen treatment regimens applied to RAW264.7 and co-cultures are given in table 6.1. Pre-treatment of RAW264.7 during passage was found to have lasting effects on their ability to undergo osteoclastogenesis. In RAW264.7 monocultures, withdrawn oestrogen was as effective at reducing TRAP activity as oestrogen exposure only after seeding. In TCP co-culture, a similar but not identical response is seen. Again, pre-treatment of RAW264.7 for one week with oestrogen

seems to have had a lasting effect on their ability to become resorptive osteoclasts. However, RAW264.7 with maintained oestrogen had significantly more mineral after ten days than those which had withdrawn oestrogen. This demonstrates that the withdrawal of oestrogen at the start of the co-culture to imitate the cessation of ovarian function results in increased resorption in comparison to maintained oestrogen. This is despite no significant difference in TRAP activity between the two groups, as was observed in RAW264.7 monocultures, again indicating a lack of correlation between TRAP activity and resorption *in vitro*.

Intriguingly, there is no significant difference with regards to mineral content in unexposed co-cultures and withdrawn co-cultures. Furthermore, there is no significant difference in mineral between co-cultures only exposed to oestrogen after seeding and those in maintained oestrogen. This would appear to indicate that the effect of oestrogen during passage is reversible and without constant stimulation by oestrogen its effect on the RAW264.7 diminishes. This contrasts with the effect observed in RAW264.7 monoculture, where oestrogen withdrawal alone was sufficient to have lasting effects on osteoclastogenesis. This difference possibly arises from the extra stimulus of osteoclastogenesis provided by the presence of IDG-SW3 in co-culture. Their upregulation of osteoclast precursor differentiation could be counteracting the inhibition by oestrogen pre-treatment, meaning that without sustained oestrogen after seeding, it is no longer having a lasting effect on their ability to differentiate.

Oestrogen exposure only after seeding the co-culture reduces resorption, but not as effectively as maintained oestrogen after pre-treatment. This is likely because when ER α is stimulated in precursors during passage, the downstream signalling of RANK is already suppressed when RANKL is applied at the start of co-culture. This suppression is maintained by continued stimulation of ER α in addition to oestrogen upregulating apoptosis. However, when ER α is only stimulated at the start of co-culture, the point when RANKL is also applied, the initial effects of RANKL are greater as the JNK pathway is not already inhibited, resulting in RANKL more effectively stimulating osteoclastogenesis.

Table 6.1: A summary of the different oestrogen treatments applied to RAW264.7 monocultures and co-cultures of RAW264.7 and IDG-SW3.

Oestrogen Regimen	Pre-Treatment	After Seeding
Unexposed	0 nM	0 nM
Exposure after seeding	0 nM	100 nM
Withdrawn	100 nM	0 nM
Maintained	100 nM	100 nM

In the TCP co-culture where oestrogen withdrawal was investigated, mineral content after ten days of co-culture was higher than the day 21 baseline level. In all other co-cultures, the addition of RAW264.7 resulted in a reduction in mineral content, assumed to be the result of increased osteoclastic resorption. Therefore, having a higher mineral content after co-culture may seem to imply that rather enhancing mineral resorption by osteoclasts, the addition of RAW264.7 has stimulated matrix deposition by IDG-SW3. Although this is possible as osteoclasts can have an anabolic effect on osteoblasts, for example through the action of bone morphogenetic proteins [235]–[237], it is more likely that in these experiments IDG-SW3 mineralised more than normal prior to osteoclast addition. This increased mineral deposition is assumed to be the result of an increased cell number. Although care was taken to keep seeding density constant, differences in passage number, time between reanimation from liquid nitrogen and seeding, and how confluent the passage flask was before detaching to seed are all factors that will influence cell growth. As IDG-SW3 can only proliferate during their first three days of culture at 33 °C in EM, any difference in their proliferation rate at the point of seeding will have lasting effects on cell number throughout the experiment. Cells visually appeared confluent before switching to the differentiation medium; however, this is a subjective measure and it difficult to discern

accurately the level of confluence when cells are densely packed. This was noted when IDG-SW3 were maintained for 28 days at 33 °C in EM in chapter 4 rather than switching to the differentiation conditions; although total DNA indicates there was four times more DNA by day 7, this was not obvious from optical microscopy.

This lasting effect of initial cell number on mineralisation was also observed by Wittkowske, who found that despite seeding at the same density, day 21 mineralisation of IDG-SW3 varied by up to 37% between repeats [322]. Furthermore, in some instances, they failed to mineralise at all, as seen here in experiments assessing the effects of PTH on IDG-SW3. To overcome this issue in the future, experiments could be seeded at a much higher density so that wells are confluent immediately [283]; however, this approach would require a much larger number of cells to be prepared for each experiment.

The protective role of oestrogen on the deposited mineral observed in monolayer co-culture was not seen when performed in the polyurethane scaffold at any seeding density evaluated. A range of seeding densities were attempted due to the difficulties with approximating the surface area of the scaffold, a problem that is compounded with the deposition of extensive mineralised matrix. Out of the three seeding densities tested, the addition of 25,000 RAW264.7 resulted in the most resorption in comparison to day 21 baseline levels. However, there was no detectable difference between the co-cultures maintained in oestrogen and that which had oestrogen withdrawn at the start of co-culture. As was observed in the TCP co-culture, this is most likely due to a combination of low assay sensitivity and a suboptimal seeding density. Therefore, with larger scaffolds and a wider range of seeding densities tested, it is likely that we would see a response to oestrogen withdrawal. Another issue that arises in the 3D co-culture is the removal of resorption waste products. In the TCP co-culture, metabolites are removed from the culture during media changes and the washing steps before staining. In the scaffold co-culture, mineral-containing products from resorbed matrix secreted by the osteoclasts are likely to be retained in the extensive extracellular matrix still present in the scaffold. These will also stain positive for ARS even if they are not within the matrix giving artificially high results and making differences in the amount of resorption harder to detect.

6.6 Summary

- From the conditions tested, PTH was not found to have catabolic effects on IDG-SW3 mineralisation.
- ALP, TRAP and mineralisation are suitable markers for osteoblast and osteoclast activity in the co-culture due to their cell type specificity.
- In co-culture, mineralisation, ALP activity and TRAP activity are only detectable when RAW264.7 are added to confluent IDG-SW3.
- IDG-SW3 increase TRAP activity in RAW264.7 in comparison to osteoclast monocultures due to production of an unknown factor, possibly M-CSF.
- RAW264.7 decrease ALP activity in IDG-SW3 in comparison to osteoblast monocultures, most likely due to increased competition for nutrients and a higher concentration of metabolites.
- TRAP activity is significantly reduced by the presence of oestrogen in RAW264.7 monocultures but not in TCP and 3D co-cultures initiated at day 7, demonstrating the upregulation of osteoclast activity by IDG-SW3 can overcome the inhibition by oestrogen.
- The maximum culture duration of the co-culture is 14 days as longer time periods result in overgrowth by osteoclast precursors.
- Seeding density when adding RAW264.7 to IDG-SW3 has a significant effect on co-culture activity, with 2,500 RAW264.7 resulting in the highest ALP and TRAP activities and greatest mineral resorption.
- Of the seeding densities investigated, the protective effect of oestrogen on total mineral is only seen when 2,500 RAW264.7 are added to IDG-SW3 after 21 days of pre-culture and 100 nM of oestrogen is applied.
- Treatment with oestrogen during passage before seeding has lasting effects on RAW264.7 TRAP activity after seeding.
- Withdrawal of oestrogen at the point of seeding to mimic the onset of menopause reduces final mineral content in comparison to sustained oestrogen in TCP co-cultures, likely due to stimulation of resorption by RAW264.7.
- Oestrogen withdrawal in 3D co-cultures did not have the same stimulatory effect on mineral resorption as it did in TCP co-cultures, possibly due to non-optimised seeding density and assay sensitivity.

7. General discussion and future work

Postmenopausal osteoporosis is an increasingly prevalent disorder that has major implications for society. These range from the financial costs of treatments to the burden of care on those who look after patients with fractures. There are ethical concerns about the reliance on animal testing to understand the disease further and develop new treatments. The poor translation of pre-clinical efficacy in animal models to human trials means that there is a need for an alternative method of screening and evaluating potential new therapeutics that have a lower financial and ethical costs as well as increased relevance to human physiology [159]–[162]. *In vitro* models of disease are one such alternative, and have the potential to replicate or even improve some aspects of preclinical testing currently done in animals. To date, there has been work developing *in vitro* mimics of healthy bone remodelling, but to the author's knowledge, no research has been performed that aimed to develop an *in vitro* model of postmenopausal osteoporosis. Therefore, the main aim of this thesis was to investigate to what extent such a model can be developed by utilising the principles of bone tissue engineering.

Despite some *in vivo* studies showing that osteoblasts respond to a decline in oestrogen by increasing mineralisation in some parts of the bone [144], [292], [293], reports on the response of osteoblasts to oestrogen *in vitro* vary, with both stimulatory and inhibitory effects reported [299]–[308]. The results of this work found that only MC3T3-E1 are stimulated by exposure to oestrogen, although the subsequent withdrawal of the hormone did not have further stimulatory effects, as has been reported in the literature [308]. Neither MLOA5 nor IDG-SW3 showed any response to oestrogen. To determine why this might be, in the future it would be interesting to assess whether either cell line expresses the gene for ER α by using PCR (polymerase chain reaction) and fluorescent antibody staining to determine protein expression. This would reveal whether the lack of response was due to them not possessing the relevant receptor, the receptor not correctly locating to the membrane, or because the subsequent intracellular pathway activation after its conjugation with 17 β -estradiol does not affect their ALP expression or mineralisation.

A similar approach should also be utilised to investigate the apparent lack of RANKL synthesis. PCR could reveal whether the mRNA transcripts for the protein are being

produced and if there is any fluctuation in their production over time or in response to stimuli. If they are being produced then it would be important to discern why the cell is failing to produce the protein from the transcripts. In the literature, it is common for changes in RANKL and OPG production and the subsequent ratio of the cytokines to only be reported as fold changes in mRNA from PCR with no subsequent analysis at the protein level [208], [270], [331]. Whilst this is an efficient way of determining how a cell is responding at the gene level, these changes do not always translate into changes at the protein level as the fold changes in the mRNA RANKL:OPG ratio do not necessarily match the change seen in the actual RANKL:OPG ratio [172].

Alternatively, although the enhanced cell digestion protocol used to isolate membrane-bound isoforms of the cytokines contains protease inhibitors to minimise protein degradation during digestion, there may have been no mRANKL detection due to the protein being lost or denatured during the digestion process. Therefore, an alternative approach would be to stain for RANKL on the cell membrane using a fluorescent-tagged antibody for the cytokine. This approach has the potential to reveal whether osteocytes generated from IDG-SW3 also possess mRANKL on their cell processes as MLO-Y4 do [211], as some, albeit a very low concentration, of mRANKL was detectable by ELISA at day 35.

IDG-SW3 were found to upregulate the TRAP activity of osteoclasts generated from RAW264.7. However, without the addition of exogenous RANKL they were unable to induce osteoclastogenesis. This means that an unknown factor was being produced by the osteoblasts that had the ability to increase osteoclast formation. Due to its role in osteoclast precursor proliferation and differentiation, this was most likely M-CSF [47], [48]. Future work should therefore focus on determining whether this was indeed the cytokine responsible for the increased TRAP activity by analysing the expression of M-CSF mRNA transcripts as well as protein-level assays, such as ELISAs.

Seeding density of RAW264.7 was found to be perhaps the most influential factor on osteoclast formation, lifespan, and activity. When non-optimised, osteoclast precursors were able to rapidly overgrow the culture, inhibiting the activity of osteoblasts and the formation and activity of osteoclasts. Therefore, it was essential that they were seeded at the correct density for changes in resorption to be detectable *in vitro*. In TCP co-cultures, the ideal seeding density was approximately 2,500 to 5,000 cells per cm². In 3D co-cultures, the addition of 25,000 RAW264.7 resulted in the lowest mineral content on the scaffolds after the co-culture period indicating the

greatest amount of resorption had occurred. However, the difference in remaining mineral between maintained and withdrawn oestrogen was not significant. The difficulty with determining the appropriate seeding density in 3D stems from complexity of the architecture of the scaffold and associated problems with calculating its surface area.

Using a technique such as MicroCT, it is possible to get an accurate reconstruction of the polyurethane scaffold that can then be used to non-destructively discern a wide range of physical properties from pore size to surface area. However, due to the random architecture of the polyurethane foam, each scaffold will have a different surface area. Therefore, using this approach would either require scanning each scaffold prior to seeding, or scanning multiple scaffold initially and using the average surface area. Even if this approach was undertaken, the RAW264.7 were not added to the scaffold until the 21 days of IDG-SW3 pre-culture had been completed. By this time point, the pores of the scaffold are filled with the extracellular matrix deposited by the osteoblasts. This collagenous matrix which fills the scaffold cannot be detected by MicroCT and therefore its effects of surface area cannot be considered using this method. Furthermore, this matrix is likely to act as a sieve upon the addition of the seeding suspension, meaning that it is unlikely that the osteoclast precursors will be evenly distributed throughout the scaffold in comparison to the TCP co-culture. This in turn will result in a variable density of precursors throughout the scaffold. It is because of these difficulties that a more iterative, trial-and-error approach was taken to discern seeding number in 3D, and from the results presented in this thesis it is indicated that a seeding density close to 25,000 RAW264.7 per 5×5 polyurethane scaffold would result in analogous effects to those observed in TCP co-cultures.

Given that the ability of RAW264.7 to undergo osteoclastogenesis is heavily dependent on seeding density, it would be beneficial to use a substrate with a regular geometry over the polyurethane foam scaffold that has a random architecture. This makes it much more straightforward to calculate accurately scaffold surface area. In this thesis, two such scaffolds were investigated; the Biotek 3D Insert-PCL and the PolyHIPE scaffold. Both MicroCT and SEM revealed that despite the Biotek scaffold being advertised and sold as a precisely manufactured woodpile architecture, it does not have a reproducible geometry as both fibre morphology and position are variable. These differences occur both in comparison to the intended design and between samples. In comparison, the PolyHIPE scaffold does have a tightly controlled architecture due to it being fabricated via microstereolithography rather than extrusion

printing. In the generation three scaffold, fibre morphology was consistent between layers and fibre position could be tightly controlled ensuring a consistent offset between layers. However, due to the very high porosity of the scaffold, it has very poor contrast when being analysed by MicroCT. With regards to its use in an *in vitro* model of bone remodelling, this poor contrast has both advantages and disadvantages depending on the study being performed.

When attempting to investigate the physical characteristics of the scaffold in a non-destructive manner, the lack of contrast makes it very difficult to determine properties such as scaffold porosity, surface area, fibre diameter and fibre spacing, due to the difficulties in discerning the edges of each strut. This in turn makes it difficult to generate a computational model of the scaffold, which would be essential when simulating how it would respond to mechanical stimuli via a finite element model, or how fluid would pass through the scaffold using computational fluid dynamics. However, when analysing mineralisation, a scaffold with low x-ray attenuation is beneficial. This is because the densest and therefore most visible material present will be the inorganic mineral deposited by the osteoblasts, making it easier to track bone formation and resorption. Although contrast agents such as osmium tetroxide can be utilised to visualise cells by MicroCT, its use here may mask where mineralised matrix is being deposited due to its high radiopacity, resulting in any areas with cells giving high contrast regardless of how mineralised it is. Furthermore, it is extremely toxic, prohibiting longitudinal scanning of the sample and making it expensive to dispose of safely [482]. Therefore, it would be ideal if the contrast of the PolyHIPE scaffold could be increased when performing physical analysis, but left at its current level during cell culture.

Increasing the x-ray attenuation of polymeric material to increase its contrast in MicroCT can be done through the addition of high atomic number materials. Previously utilised approaches include the incorporation of iodine, barium and tungsten, either by mixing in salts or nanoparticles, or by covalently linking the atoms to the polymer backbone [483], [484]. These approaches increase the radiopacity of polymers, but their inclusion can affect the physical and chemical properties of the polymer, meaning that the amount added should be as low as reasonably possible. With regards to their inclusion in photocurable PolyHIPEs, the presence of such elements is also likely to affect their polymerisation during fabrication, meaning that the standard laser parameters could not be used when they are present. This would result in a different scaffold being fabricated for physical analysis in comparison to

the ones used in cell culture, defeating the purpose of increasing the contrast in the first place. Therefore, an alternative approach may be to apply a coating the scaffold post-fabrication. This could be done via sputter coating with gold using the same protocol as when scaffolds are prepared for SEM analysis. This means that the scaffold contrast can be increased without affecting the architecture, and as the gold films deposited are only nanometres thick, this approach will not influence the physical characteristics derived from the MicroCT scan.

In addition to surface area calculations being more straightforward on a regular geometry substrate such as the PolyHIPE scaffold, performing any future work with a different scaffold may also be beneficial in terms of cellular performance. The polyurethane foam used in this thesis was made from a non-medical grade, non-degradable polyether polyurethane previously shown to support osteogenic differentiation [9]. Subsequent work using this material found that without soaking in media or gelatine coating prior to seeding, cell attachment and distribution throughout the scaffold was poor due to cells forming clumps rather than spreading evenly [402]. Although gelatine coating and media soaking was employed for all polyurethane scaffolds used in this thesis and cells and extracellular matrix were visible throughout the structure, no live/dead analysis of cells seeded onto the scaffold was performed to confirm how many cells remained viable. Therefore, to alleviate any potential concerns with the scaffold, future work should utilise either the PolyHIPE scaffold due to its regular architecture or an alternative polyurethane foam. A potential candidate is the recently developed medical-grade polyurethane scaffolds incorporated with hydroxyapatite that were utilised to make an *in vitro* model of implant fixation [404].

The difficulties in detecting osteoclastic resorption in the co-culture systems presented here were compounded by small culture surface areas used here and the low sensitivity of the assay used to indicate resorption. With regards to the small culture surface areas used, this issue is most easily overcome by increasing the well or scaffold size in which the co-culture is performed. However, this approach increases the amount of culture media and supplements required and therefore the associated cost per experiment. Once it was determined that none of the potential osteoblast cell lines investigated here produced sufficient RANKL to initiate osteoclastogenesis, it was apparent that exogenous RANKL would have to be added to the co-cultures. Supplemented media with a final RANKL concentration of 50 ng/mL costs approximately £1 per mL. TCP co-cultures in a 48 well plate could be maintained in 500 μ L of media with 50% being

exchanged every 2-3 days over a ten-day period. Therefore, increasing the culture surface area by quadrupling the well size (12 well plate) would have increased the media cost per well over the course of an experiment from ~£1.25 to ~£5, or £90 to £360 for the final TCP co-culture experiment presented here alone. Therefore, it was decided to proceed with smaller well sizes to allow more experiments to be performed, to the potential detriment of assay sensitivity.

When a patient's bone loss is being classified and assigned a T score, this calculation is based on their bone mineral density (BMD) computed from a DXA scan [106]. Similarly, when OVX rat models are used to investigate osteoporosis and potential therapeutics, changes in bone morphometry are commonly evaluated by MicroCT, a density based imaging technique that tracks the changes in BMD [156]–[158]. Therefore, although it is not just bone mineral that is resorbed by osteoclasts, the Alizarin Red S assay selected to determine resorption in the co-cultures was chosen as it indicates changes in the mineral content. These changes can be identified qualitatively, as Lutter, et al., demonstrated that resorption pits are visible in mineralised matrix deposited by osteoblasts *in vitro* [485], but more importantly, changes can also be quantitatively determined through destaining and colourimetric analysis. This means that percentage changes in mineral *in vitro* could theoretically be compared to *in vivo* data, to see whether changes seen in response to oestrogen are analogous.

Although this approach can reveal changes in mineral content in comparison to a baseline level, it is an indirect measurement of osteoclastic resorption that examines what is left rather than what is removed. The low sensitivity of this approach stems from the fluctuation in the baseline level of mineral deposited by the IDG-SW3 as discussed in chapter six, as well as the precision of the assay. Through serial dilution, the minimum detection limit of ARS when destaining in 5% perchloric acid was found to be 18.8 µg/mL, similar to the minimum detection limit of 17.1 µg/mL reported when destaining in ammonium acetate [289]. All the ARS assays reported in this thesis had a concentration higher than this; therefore, the issue with the ability of the assay to detect changes in mineral was not that levels were below what could be detected, but rather that colourimetric analysis of the destained solution cannot precisely discern between two similar concentrations. By analysing solutions at 380 to 400 µg/mL at 5 µg/mL increments it was found that only intervals of 10 µg/mL were significantly different, meaning that any concentration of mineral reported could be ± 5 µg/mL (Fig. 7.1). With reported mineral levels after resorption typically being between 250

and 350 µg/mL, this means that errors due to assay precision are between 2.9 and 4%. This means that this approach to determining osteoclastic resorption may not have been powerful enough to detect small differences.

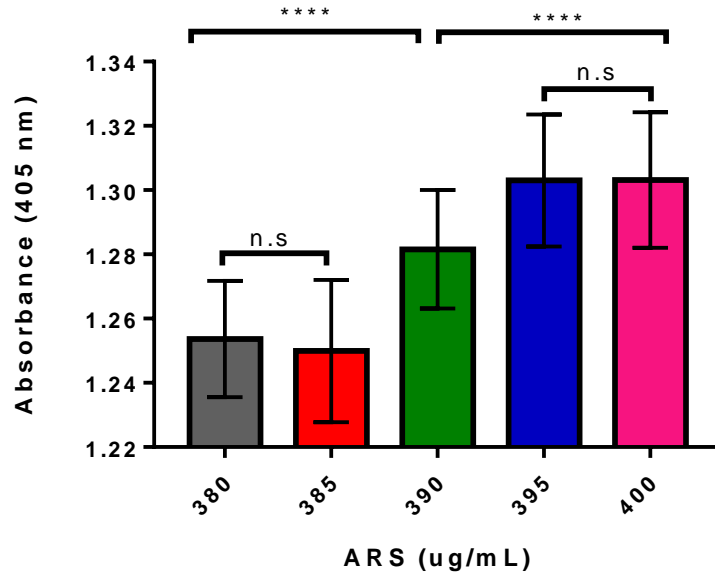


Figure 7.1: Ability of colourimetric analysis to discern between different ARS concentrations ****= $p < 0.0001$ ($n=96$).

When bone is resorbed by osteoclasts, it is not just the inorganic mineral phase that is removed, but also the organic phase consisting of collagen and other proteins. Collagen peptides released into the culture media can be used as biochemical markers of bone formation and resorption *in vitro* as they are *in vivo*, where their concentration in serum or urine correlates with bone turnover [486]. The concentration of carboxy- and amino-terminal propeptides of procollagen type 1 (P1CP and P1NP, respectively) can be used as markers of bone formation. Collagen type 1 in bone is initially synthesised as procollagen. Once released in to the extracellular space, P1CP and P1NP are enzymatically cleaved from both termini of the collagen molecule, and therefore the concentration can be used to quantitatively assess newly formed collagen [487]. Similarly, the carboxy- and amino-terminal telopeptides of collagen type 1 (CTX and NTX, respectively) can be used as markers of bone resorption. CTX is released from the bone matrix by the osteoclastic protease cathepsin K during bone resorption [488], and therefore its concentration correlates with resorption. *In vitro*, the concentration of these peptides can be assessed via ELISA and used as markers of

bone turnover, as demonstrated by Papadimitropoulos, et al., in their *in vitro* bone organ model [250]. Although measurements of these peptides do not reveal the mineral content of *in vitro* cultures, analysis of co-culture supernatants would help confirm that any reduction in mineral was indeed due to osteoclastic resorption without the need for further repeats of any experiment, as media can be taken without terminating the experiment.

TRAP is an enzyme involved in bone resorption that correlates with bone resorption *in vivo* due to its accumulation in the blood during bone turnover. Although its activity *in vitro* has been used extensively to show osteoclast activity as a marker of osteoclastic differentiation, here it was not found to correlate with *in vitro* resorption. This is likely due to the fact that the TRAP activity quantified *in vitro* here is the intracellular activity rather than the serum equivalent of the TRAP activity in the culture media. This means that rather than an indication of how much mineral resorption has occurred in the culture this far, the activity indicates how many osteoclasts are currently active. Due to the short lifespan of osteoclasts and the cyclic nature of their formation, this TRAP activity does not necessarily correlate with historic resorption. TRAP is an osteoclastic enzyme indirectly involved in bone resorption, meaning that whilst it is essential for osteoclasts to resorb bone, it does not degrade the bone matrix. Due to its involvement in collagen hydrolysis, cathepsin K activity could also be used as a measure of how much resorption is currently taking place, and may more strongly correlate with resorption due to its direct involvement in the process. *In vitro* assays for cathepsin K are commercially available for cell lysates and media supernatants. However, as with TRAP activity, its activity only reveals the activity of the osteoclasts currently in the culture, rather than the historic resorption that has taken place.

For any future studies exploring an *in vitro* model of osteoporosis or any model of bone turnover for that matter, it is clear that a range of assays for the activity of both cell types is necessary. Alkaline phosphatase activity is a good indication of osteoblast activity, but does not accurately predict how much mineral will be deposited as it is not directly involved in matrix mineralisation [489]. Therefore, calcium or phosphate quantification are necessary to reveal how much mineralisation has occurred. Similarly, whilst TRAP and cathepsin K activity can reveal how active osteoclasts currently are in the co-culture, without quantifying changes in the extracellular matrix the enzyme activities cannot reveal how much resorption has occurred. Ideally, media and cell lysates would be collected at regular intervals throughout the co-culture.

These supernatants and lysates could then be analysed for P1CP and CTX peptides and ALP, TRAP and cathepsin K activity, both separately at each time point and cumulatively at the end to reveal total resorption and formation. In addition to this, longitudinal scanning of the co-culture using MicroCT to reveal how mineral content and distribution changes throughout the co-culture could demonstrate how changes in the enzyme activities affect the bone matrix on the scaffold. Furthermore, providing that osteoblasts capable of producing RANKL were selected, these supernatants and lysates could also reveal changes in the RANKL:OPG ratio over time. Finally, performing all cultures in serum-free of chemically defined medium would increase reproducibility and remove any effects of unknown factors on bone turnover.

This thesis has demonstrated that it is possible to mimic the onset of postmenopausal osteoporosis *in vitro*; however, the co-cultures developed here are not yet a valid alternative to the work currently performed in OVX animal models. In order to achieve this, long term work should focus on maintaining the co-cultures over extended time periods and using human-origin cells for improved clinical relevance. The main limitation on culture duration in the work presented here was overgrowth by RAW264.7 precursors. One potential solution to this issue would be to have osteoblasts and osteoclasts cultured in separate but connected chambers of a bioreactor system, with osteoblasts cultured on a generation 3 PolyHIPE scaffold in one chamber and osteoclasts on a resorbable calcium phosphate substrate in another (Fig. 7.2). With the two cell types cultured separately, osteoclast precursors would be unable to overgrow the osteoblasts.

An ideal bioreactor for this is the Quasi-Vivo® (Kirkstall Ltd, UK) system as it applies physiologically-relevant levels of oxygen and shear stress at low pressures via laminar flow with chambers that permit 3D cell culture on scaffolds. The chambers are modular, so co-cultures can be in the same or connected chambers, exposing them to the same common medium. This allows circulating levels of drugs and metabolites to be retained, rather than being removed during media changes. The separate culture of OBs and OCs in this system allows them to communicate with each other and would enable the extension of the co-culture to much longer time periods, ideally up to 8 weeks to mimic the OVX procedure in rats [130]–[133]. Such a system would allow all of the assays for an ideal *in vitro* described previously to be performed, as media could still be analysed, lysates generated, and longitudinal MicroCT scans taken. The main limitation of such a system would be that the mineral deposited would not be the mineral resorbed, making it a representation of uncoupled bone remodelling rather

than bone turnover through BMUs, and that only the influence of soluble rather than membrane bound isoforms of cytokines can exert influence on the other cells in the culture.

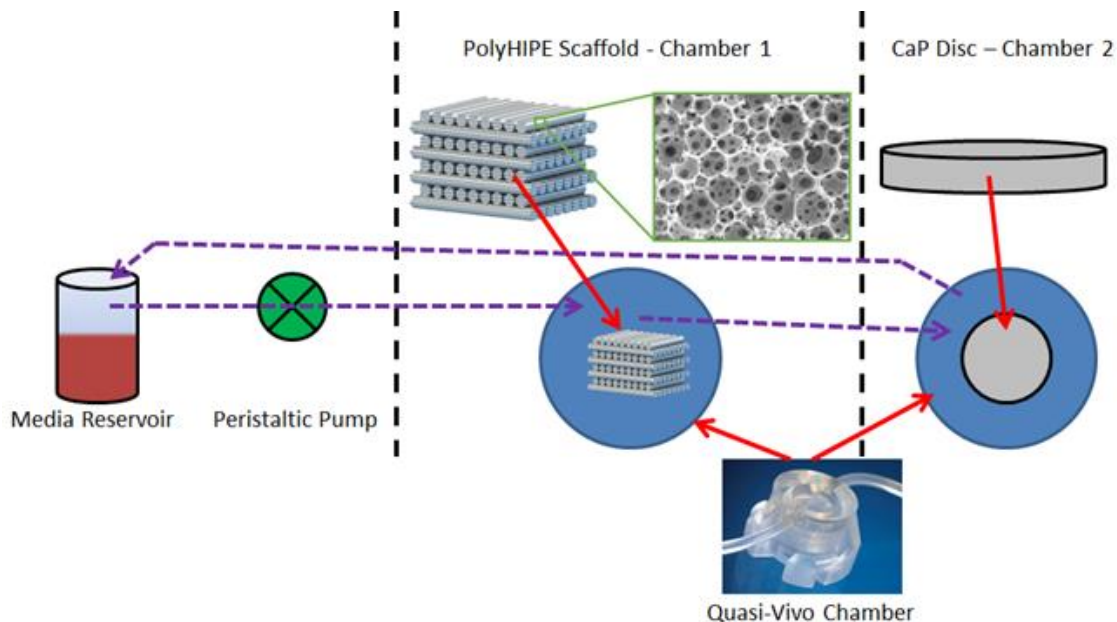


Figure 7.2: Schematic showing a potential layout of a bioreactor system used for long term co-cultures. A peristaltic pump is used to flow and recirculate media through the chambers.

The murine co-cultures performed in this thesis required the exogenous addition of RANKL to stimulate osteoclastogenesis. Therefore, when selecting a suitable cell type for any future studies, it is imperative that they produce RANKL. This means that the concentration of this cytokine can change in response to hormone or drug concentration, better mimicking what occurs *in vivo*. Previous studies have demonstrated that primary human osteoblasts produce sufficient RANKL to induce osteoclast differentiation in co-culture; therefore, identifying a donor capable of this should be the first step when developing any future system [249], [252], [253].

Furthermore, the use of RAW264.7 in the co-culture should be replaced by CD14 and CD45 positive human monocytes derived from peripheral blood (hPBMC) as these have been used extensively to generate osteoclasts in the study of remodelling

fundamentals and *in vitro* models of bone remodelling [164], [165], [169], [170], [206], [209], [234], [244], [249]–[253]. By sourcing monocytes from women both pre- and postmenopause, any difference in osteoclastogenic potential could also be examined.

Co-cultures containing hPBMC precursors have been maintained for three [250], four [249], and five [249] weeks, reporting prolonged osteoclast activity and no overgrowth. Therefore, it seems possible that extending the duration of the co-culture in a bioreactor system over longer time periods is possible. However, should overgrowth or loss of osteoclasts occur due to apoptosis over time, the separate cultures of osteoblasts and osteoclasts in the Quasi-Vivo® system would allow the re-seeding of the hPBMCs at later time points, mimicking the arrival of precursors in the bloodstream. If a single addition of hPBMCs was capable of producing osteoclasts over the entire co-culture then it would not be necessary to culture the osteoclasts and osteoblasts separately. This would allow membrane-bound isoforms of RANKL to stimulate osteoclastogenesis, as well as other molecules dependent on osteoblast-osteoclast contact, such as intercellular adhesion molecule (ICAM)-1 [169]. Furthermore, it would better represent coupled bone remodelling, as the matrix deposited by osteoblasts would then in turn be resorbed by osteoclasts.

8. Conclusion

This thesis explored the feasibility of developing an *in vitro* model of postmenopausal osteoporosis using the principles of bone tissue engineering. In TCP co-cultures with an optimised seeding density, using oestrogen withdrawal to mimic the onset of postmenopausal osteoporosis resulted in increased mineral resorption, analogous to the effect seen *in vivo*. However, out of the conditions assessed in 3D co-cultures, no equivalent response was observed. This indicates further work is required to optimise osteoclast seeding number, as well as using a wider range of assays to monitor bone remodelling over time.

The work presented in this thesis has advanced the field of developing *in vitro* models as alternatives for animal testing. Importantly, it has demonstrated that it will be possible to mimic the onset of postmenopausal osteoporosis *in vitro*. However, additional development and refinement is necessary to create a widely accepted, valid alternative to current animal models. The main areas to be addressed include creating a model that uses human-origin cells and maintaining three-dimensional co-cultures over longer duration. This will result in a more physiologically relevant *in vitro* model that should improve translation from pre-clinical studies to human trials whilst minimising our reliance on animal models.

9. References

- [1] National Osteoporosis Society, “National Osteoporosis Society 25th anniversary report - A fragile fracture,” 2011.
- [2] N. I. of Health, “Osteoporosis Prevention, Diagnosis, and Therapy,” *NIH Consens. Statement*, vol. 17, no. 1, pp. 1–36, 2000.
- [3] R. Eastell, J. S. Walsh, N. B. Watts, and E. Siris, “Bisphosphonates for postmenopausal osteoporosis,” *Bone*, vol. 49, no. 1, pp. 82–88, 2011.
- [4] H. Hamoda and M. Savvas, “What should we be advising women about hormone replacement therapy?,” *InnovAiT Educ. Inspir. Gen. Pract.*, vol. 7, no. 5, pp. 295–300, 2014.
- [5] J. L. Vahle, M. Sato, G. G. Long, J. K. Young, P. C. Francis, J. a Engelhardt, M. S. Westmore, Y. Linda, and J. B. Nold, “Skeletal changes in rats given daily subcutaneous injections of recombinant human parathyroid hormone (1-34) for 2 years and relevance to human safety.,” *Toxicol. Pathol.*, vol. 30, no. 3, pp. 312–321, 2002.
- [6] A. S. Turner, “Animal models of osteoporosis-necessity and limitations.,” *Eur. Cell. Mater.*, vol. 1, pp. 66–81, 2001.
- [7] M. Peric, I. Dumic-Cule, D. Grcevic, M. Matijasic, D. Verbanac, R. Paul, L. Grgurevic, V. Trkulja, C. M. Bagi, and S. Vukicevic, “The rational use of animal models in the evaluation of novel bone regenerative therapies,” *Bone*, vol. 70, pp. 73–86, 2015.
- [8] “Directive 2010/63/EU of the European Parliament and of the Council of 22 September 2010 on the protection of animals used for scientific purposes,” *Off. J. Eur. Union*, 2010.
- [9] A. Sittichockechaiwut, A. M. Scutt, A. J. Ryan, L. F. Bonewald, and G. C. Reilly, “Use of rapidly mineralising osteoblasts and short periods of mechanical loading to accelerate matrix maturation in 3D scaffolds.,” *Bone*, vol. 44, no. 5, pp. 822–9, May 2009.
- [10] G. Iolascon, R. Napolano, M. Gioia, A. Moretti, I. Riccio, and F. Gimigliano, “The contribution of cortical and trabecular tissues to bone strength: Insights from denosumab studies,” *Clin. Cases Miner. Bone Metab.*, vol. 10, no. 1, pp. 47–51, 2013.

- [11] E. Seeman, "Growth and Age-Related Abnormalities in Cortical Structure and Fracture Risk," *Endocrinol. Metab.*, pp. 419–428, 2015.
- [12] R. Pignolo, M. A. Keenan, and N. M. Hebel, Eds., *Fractures in the Elderly: A Guide to Practical Management*. New York: Humana Press, 2010.
- [13] B. Clarke, "Normal bone anatomy and physiology.," *Clin. J. Am. Soc. Nephrol.*, vol. 3 Suppl 3, pp. 131–139, 2008.
- [14] R. Seeley, T. Stephens, and P. Tate, "Skeletal System: Bones and Bone Tissue," in *Anatomy and Physiology*, Sixth Edit., New York: McGraw-Hill Higher Education, 2003, pp. 166–196.
- [15] L. J. Gibson, "The mechanical behaviour of cancellous bone," *J. Biomech.*, vol. 18, no. 5, pp. 317–328, 1985.
- [16] K. Saladin, *Human Anatomy*. New York: McGraw-Hill Higher Education, 2007.
- [17] K. Farbod and M. Nejadnik, "Interactions Between Inorganic and Organic Phases in Bone Tissue as a Source of Inspiration for Design of Novel Nanocomposites," *Tissue Eng. Part B*, vol. 20, no. 2, pp. 173–188, 2013.
- [18] V. I. Sikavitsas, J. S. Temenoff, and A. G. Mikos, "Biomaterials and bone mechanotransduction," *Biomaterials*, vol. 22, no. 19, pp. 2581–2593, 2001.
- [19] A. J. Salgado, O. P. Coutinho, and R. L. Reis, "Bone tissue engineering: State of the art and future trends," *Macromol. Biosci.*, vol. 4, no. 8, pp. 743–765, 2004.
- [20] J. Sodek and M. D. McKee, "Molecular and cellular biology of alveolar bone," *Periodontology*, vol. 24, pp. 99–126, 2000.
- [21] J. M. Roudsari and S. Mahjoub, "Quantification and comparison of bone-specific alkaline phosphatase with two methods in normal and paget's specimens," *Casp. J. Intern. Med.*, vol. 3, no. 3, pp. 478–483, 2012.
- [22] C. D. Hoemann, H. El-Gabalawy, and M. D. McKee, "In vitro osteogenesis assays: Influence of the primary cell source on alkaline phosphatase activity and mineralization," *Pathol. Biol.*, vol. 57, no. 4, pp. 318–323, 2009.
- [23] H. Orimo, "The Mechanism of Mineralization and the Role of Alkaline Phosphatase in Health and Disease," *J. Nippon Med. Sch.*, vol. 77, no. 1, pp. 4–12, 2010.

- [24] J. L. Millan, *Mammalian Alkaline Phosphatases - From Biology to Applications in Medicine and Biotechnology*. Wiley-VCH, 2006.
- [25] J. Y. Rho, L. Kuhn-Spearing, and P. Zioupos, "Mechanical properties and the hierarchical structure of bone," *Med. Eng. Phys.*, vol. 20, no. 2, pp. 92–102, 1998.
- [26] F. Long, "Building strong bones: molecular regulation of the osteoblast lineage," *Nat. Rev. Mol. Cell Biol.*, vol. 13, no. 1, pp. 27–38, 2011.
- [27] J. R. Mauney, V. Volloch, and D. L. Kaplan, "Role of Adult Mesenchymal Stem Cells in Bone Tissue Engineering Applications: Current Status and Future Prospects," *Tissue Eng.*, vol. 11, no. 5–6, pp. 787–802, 2005.
- [28] D. Sommerfeldt and C. Rubin, "Biology of bone and how it orchestrates the form and function of the skeleton," *Eur. Spine J.*, vol. 10, no. SUPPL. 2, pp. 86–95, 2001.
- [29] A. Rutkovskiy, K.-O. Stenslkken, and I. J. Vaage, "Osteoblast Differentiation at a Glance," *Med. Sci. Monit. Basic Res.*, vol. 22, pp. 95–106, 2016.
- [30] D. L. Stocum, *Chapter 6 – Regeneration of Musculoskeletal Tissues*, Second Edi. 2012.
- [31] S. Sell, C. Gaissmaier, J. Fritz, G. Herr, S. Esenweln, W. Ksswetter, R. Volkmann, K. M. Wittkowski, and H. P. Rodemann, "Different behavior of human osteoblast-like cells isolated from normal and heterotopic bone in vitro," *Calcif. Tissue Int.*, vol. 62, no. 1, pp. 51–59, 1998.
- [32] D. Park, J. A. Spencer, B. I. Koh, T. Kobayashi, J. Fujisaki, T. L. Clemens, C. P. Lin, H. M. Kronenberg, and D. T. Scadden, "Endogenous bone marrow MSCs are dynamic, fate-restricted participants in bone maintenance and regeneration," *Cell Stem Cell*, vol. 10, no. 3, pp. 259–272, 2012.
- [33] J. . Lian, G. . Stein, T. . Owen, S. Dworetzky, M. . Tassinari, M. Aronow, D. Collart, V. Shalhoub, S. Peura, L. Barone, J. Bidwell, and S. Pockwinse, "Chapter 6: Gene Expression during Development of the Osteoblast Phenotype: An Integrated Relationship of Cell Growth to Differentiation," in *Molecular and Cellular Approaches to the Control of Proliferation and Differentiation*, Academic Press, Inc, 1992, pp. 165–222.
- [34] K. Tanaka-Kamioka, H. Kamioka, H. Ris, and S. S. Lim, "Osteocyte shape is dependent on actin filaments and osteocyte processes are unique actin-rich projections.," *J. Bone Miner. Res.*, vol. 13, no. 10, pp. 1555–1568, 1998.

- [35] S. B. Doty, "Morphological evidence of gap junctions between bone cells.," *Calcif. Tissue Int.*, vol. 33, no. 5, pp. 509–512, 1981.
- [36] S. L. Dallas, M. Prideaux, and L. F. Bonewald, "The osteocyte: An endocrine cell . . . and more," *Endocr. Rev.*, vol. 34, no. 5, pp. 658–690, 2013.
- [37] A. Santos, A. D. Bakker, and J. Klein-Nulend, "The role of osteocytes in bone mechanotransduction," *Osteoporos. Int.*, vol. 20, no. 6, pp. 1027–1031, 2009.
- [38] B. S. Noble, "The osteocyte lineage," *Arch. Biochem. Biophys.*, vol. 473, no. 2, pp. 106–111, 2008.
- [39] J. E. Aubin, "Bone stem cells," *J Cell Biochem Suppl*, vol. 30–31, pp. 73–82, 1998.
- [40] H. Bull, P. G. Murray, D. Thomas, A. M. Fraser, and P. N. Nelson, "Acid phosphatases," *Mol Pathol*, vol. 55, no. 2, pp. 65–72, 2002.
- [41] O. H. Jeon, S. H. Jeong, Y. M. Yoo, K. H. Kim, D. S. Yoon, and C. H. Kim, "Quantification of temporal changes in 3D osteoclastic resorption pit using confocal laser scanning microscopy," *Tissue Eng. Regen. Med.*, vol. 9, no. 1, pp. 29–35, 2012.
- [42] S. L. Teitelbaum, "Bone Resorption by Osteoclasts," *Science (80-.)*, vol. 289, no. 5484, pp. 1504–1508, 2000.
- [43] G. Stenbeck, "Formation and function of the ruffled border in osteoclasts," *Semin. Cell Dev. Biol.*, vol. 13, no. 4, pp. 285–292, 2002.
- [44] I. Fernández-Tresguerres-Hernández-Gil, M. A. Alobera-Gracia, M. del-Canto-Pingarrón, and L. Blanco-Jerez, "Physiological bases of bone regeneration II. The remodeling process.," *Med. oral, Patol. oral y cirugía bucal.*, vol. 11, no. 2, pp. 151–157, 2006.
- [45] A. M. Parfitt, "Targeted and nontargeted bone remodeling: Relationship to basic multicellular unit origination and progression," *Bone*, vol. 30, no. 1, pp. 5–7, 2002.
- [46] N. A. Sims and T. J. Martin, "Coupling the activities of bone formation and resorption: a multitude of signals within the basic multicellular unit.," *Bonekey Rep.*, vol. 3, no. August 2013, p. 481, 2014.
- [47] J. M. Hodge, M. A. Kirkland, and G. C. Nicholson, "Multiple roles of M-CSF in human osteoclastogenesis," *J Cell Biochem*, vol. 102, no. 3, pp. 759–768,

2007.

- [48] F. P. Ross, “M-CSF, c-Fms, and signaling in osteoclasts and their precursors,” *Ann. N. Y. Acad. Sci.*, vol. 1068, no. 1, pp. 110–116, 2006.
- [49] J. Kular, J. Tickner, S. M. Chim, and J. Xu, “An overview of the regulation of bone remodelling at the cellular level,” *Clin. Biochem.*, vol. 45, no. 12, pp. 863–873, 2012.
- [50] A. Mizuno, N. Amizuka, K. Irie, A. Murakami, N. Fujise, T. Kanno, Y. Sato, N. Nakagawa, H. Yasuda, S. Mochizuki, T. Gomibuchi, K. Yano, N. Shima, N. Washida, E. Tsuda, T. Morinaga, K. Higashio, and H. Ozawa, “Severe osteoporosis in mice lacking osteoclastogenesis inhibitory factor/osteoprotegerin,” *Biochem. Biophys. Res. Commun.*, vol. 247, no. 3, pp. 610–615, 1998.
- [51] R. L. Jilka, “Biology of the basic multicellular unit and the pathophysiology of osteoporosis,” *Med. Pediatr. Oncol.*, vol. 41, no. 3, pp. 182–185, 2003.
- [52] K. Wesseling-Perry, “The BRC canopy: An important player in bone remodeling,” *Am. J. Pathol.*, vol. 184, no. 4, pp. 924–926, 2014.
- [53] J.-M. Delaisse, “The reversal phase of the bone-remodeling cycle: cellular prerequisites for coupling resorption and formation,” *Bonekey Rep.*, vol. 3, no. April, p. 561, 2014.
- [54] T. L. Andersen, T. E. Sondergaard, K. E. Skorzynska, F. Dagnaes-Hansen, T. L. Plesner, E. M. Hauge, T. Plesner, and J.-M. Delaisse, “A physical mechanism for coupling bone resorption and formation in adult human bone,” *Am. J. Pathol.*, vol. 174, no. 1, pp. 239–247, 2009.
- [55] E. F. Eriksen, “Cellular mechanisms of bone remodeling,” *Rev. Endocr. Metab. Disord.*, vol. 11, no. 4, pp. 219–227, 2010.
- [56] L. J. Raggatt and N. C. Partridge, “Cellular and molecular mechanisms of bone remodeling,” *J. Biol. Chem.*, vol. 285, no. 33, pp. 25103–25108, 2010.
- [57] E. M. Hauge, D. Qvesel, E. F. Eriksen, L. Mosekilde, and F. Melsen, “Cancellous bone remodeling occurs in specialized compartments lined by cells expressing osteoblastic markers,” *J. Bone Miner. Res.*, vol. 16, no. 9, pp. 1575–1582, 2001.
- [58] a M. Parfitt, “The bone remodeling compartment: a circulatory function for bone lining cells,” *J. Bone Miner. Res.*, vol. 16, no. 9, pp. 1583–1585, 2001.

- [59] N. Rucci, "Molecular biology of bone remodelling.," *Clin. Cases Miner. Bone Metab.*, vol. 5, pp. 49–56, 2008.
- [60] S. Mahadevan, R. Bharath, and V. Kumaravel, "Calcium and bone disorders in pregnancy," *Indian J. Endocrinol. Metab.*, vol. 16, no. 3, p. 358, 2012.
- [61] U. Kini and B. N. Nandeesh, "Physiology of Bone Formation, Remodeling, and Metabolism," in *Radionuclide and Hybrid Bone Imaging*, I. Fogelman, G. Gnanasegaran, and H. van der Wall, Eds. New York: Springer, 2012, pp. 29–57.
- [62] D. Dempster, "Anatomy and Functions of the Adult Skeleton," in *Primer on the Metabolic Bone Diseases and Disorders of Mineral Metabolism*, 6th ed., M. Favus, Ed. Washington DC: American Society for Bone and Mineral Research, 2006, pp. 7–11.
- [63] X. Feng and J. M. McDonald, "Disorders of bone remodeling.," *Annu. Rev. Pathol.*, vol. 6, pp. 121–145, 2011.
- [64] L. Donaldson, I. Reckless, S. Scholes, J. Mindell, and N. Shelton, "The burden of fractures in England," *J. Epidemiol. Community Health*, vol. 62, no. 2, pp. 174–180, 2008.
- [65] J. Van Der Stok, E. M. M. Van Lieshout, Y. El-Massoudi, G. H. Van Kralingen, and P. Patka, "Bone substitutes in the Netherlands - A systematic literature review," *Acta Biomater.*, vol. 7, no. 2, pp. 739–750, 2011.
- [66] R. M. Nerem, "Tissue Engineering: The Hope, the Hype, and the Future," *Tissue Eng.*, vol. 12, no. 5, pp. 1143–50, 2006.
- [67] T. W. Bauer, "Bone graft substitutes," *Skeletal Radiol.*, vol. 36, no. 12, pp. 1105–1107, 2007.
- [68] G. Grabowski and C. a Cornett, "Bone graft and bone graft substitutes in spine surgery: current concepts and controversies.," *J. Am. Acad. Orthop. Surg.*, vol. 21, no. 1, pp. 51–60, 2013.
- [69] T. E. Mroz, M. J. Joyce, I. H. Lieberman, M. P. Steinmetz, E. C. Benzel, and J. C. Wang, "The use of allograft bone in spine surgery: is it safe?," *Spine J.*, vol. 9, no. 4, pp. 303–308, 2009.
- [70] B. Long, L. Dan, L. Jian, H. Yunyu, H. Shu, and Y. Zhi, "Evaluation of a novel reconstituted bone xenograft using processed bovine cancellous bone in combination with purified bovine bone morphogenetic protein," *Xenotransplantation*, vol. 19, no. 2, pp. 122–132, 2012.

- [71] T. W. Bauer and G. F. Muschler, “Bone graft materials. An overview of the basic science.,” *Clin. Orthop. Relat. Res.*, no. 371, pp. 10–27, 2000.
- [72] M. Łączka, K. Cholewa-Kowalska, and A. M. Osyczka, “Bioactivity and osteoinductivity of glasses and glassceramics and their material determinants,” *Ceram. Int.*, vol. 42, pp. 14313–14325, 2016.
- [73] J. Filipowska, J. Pawlik, K. Cholewa-Kowalska, G. Tylko, E. Pamula, L. Niedzwiedzki, M. Szuta, M. Łączka, and a M. Osyczka, “Incorporation of sol-gel bioactive glass into PLGA improves mechanical properties and bioactivity of composite scaffolds and results in their osteoinductive properties,” *Biomed. Mater.*, vol. 9, no. 6, p. 65001, 2014.
- [74] E. Pamula, J. Kokoszka, K. Cholewa-Kowalska, M. Łączka, L. Kantor, L. Niedzwiedzki, G. C. Reilly, J. Filipowska, W. Madej, M. Kolodziejczyk, G. Tylko, and A. M. Osyczka, “Degradation, bioactivity, and osteogenic potential of composites made of PLGA and two different sol-gel bioactive glasses,” *Ann. Biomed. Eng.*, vol. 39, no. 8, pp. 2114–2129, 2011.
- [75] J. S. Suwandi, R. E. M. Toes, T. Nikolic, and B. O. Roep, “Inducing tissue specific tolerance in autoimmune disease with tolerogenic dendritic cells,” *Clin. Exp. Rheumatol.*, vol. 33, pp. 97–103, 2015.
- [76] J. Filipowska, K. Cholewa-Kowalska, J. Wieczorek, D. Semik, Z. Dąbrowski, M. Łączka, and A. M. Osyczka, “Ectopic bone formation by gel-derived bioactive glass-poly-L-lactide-co-glycolide composites in a rabbit muscle model,” *Biomed. Mater.*, vol. 12, no. 1, p. 15015, 2017.
- [77] P. V Giannoudis, H. Dinopoulos, and E. Tsiridis, “Bone substitutes: an update.,” *Injury*, vol. 36 Suppl 3, pp. S20–S27, 2005.
- [78] G. Ryan, A. Pandit, and D. P. Apatsidis, “Fabrication methods of porous metals for use in orthopaedic applications,” *Biomaterials*, vol. 27, no. 13, pp. 2651–2670, 2006.
- [79] K. A. Hing, L. F. Wilson, and T. Buckland, “Comparative performance of three ceramic bone graft substitutes,” *Spine J.*, vol. 7, no. 4, pp. 475–490, 2007.
- [80] K. A. Hing, “Bioceramic bone graft substitutes: Influence of porosity and chemistry,” *Int. J. Appl. Ceram. Technol.*, vol. 2, no. 3, pp. 184–199, 2005.
- [81] W. R. Moore, S. E. Graves, and G. I. Bain, “Synthetic bone graft substitutes.,” *ANZ J. Surg.*, vol. 71, no. 6, pp. 354–361, 2001.
- [82] D. W. Hutmacher, “Scaffolds in tissue engineering bone and cartilage.,”

Biomaterials, vol. 21, no. 24, pp. 2529–2543, 2000.

- [83] L. G. Griffith, “Polymeric biomaterials,” *Acta Mater.*, vol. 48, no. 1, pp. 263–277, 2000.
- [84] A. Ami R., L. Cato T., and N. Syam P., “Bone Tissue Engineering: Recent Advances and Challenges,” *Crit. Rev. Biomed. Eng.*, vol. 40, no. 5, pp. 363–408, 2012.
- [85] L. G. Griffith and G. Naughton, “Tissue engineering--current challenges and expanding opportunities.,” *Science*, vol. 295, no. 5557, pp. 1009–1014, 2002.
- [86] L. G. Raisz, “Science in medicine Pathogenesis of osteoporosis : concepts , conflicts , and prospects,” vol. 115, no. 12, 2005.
- [87] M. Egermann, J. Goldhahn, and E. Schneider, “Animal models for fracture treatment in osteoporosis,” *Osteoporos. Int.*, vol. 16, no. SUPPL. 2, pp. 129–138, 2005.
- [88] K. Lippuner, “Medical treatment of vertebral osteoporosis,” *Eur. Spine J.*, vol. 12, no. SUPPL. 2, pp. 132–141, 2003.
- [89] N. E. Lane, “Epidemiology, etiology, and diagnosis of osteoporosis,” *Am. J. Obstet. Gynecol.*, vol. 194, no. 2 SUPPL., 2006.
- [90] O. Johnell and J. Kanis, “Epidemiology of osteoporotic fractures,” *Osteoporos. Int.*, vol. 16, no. SUPPL. 2, pp. 6–10, 2005.
- [91] D. T. Gold, “The clinical impact of vertebral fractures: quality of life in women with osteoporosis.,” *Bone*, vol. 18, no. 3 Suppl, p. 185S–189S, 1996.
- [92] R. O. Ritchie, M. J. Buehler, and P. Hansma, “Plasticity and toughness in bone,” *Phys. Today*, vol. 62, no. 6, pp. 41–47, 2009.
- [93] E. F. Eriksen, S. F. Hodgson, R. Eastell, S. L. Cedel, W. M. O’Fallon, and B. L. Riggs, “Cancellous bone remodeling in type I (postmenopausal) osteoporosis: quantitative assessment of rates of formation, resorption, and bone loss at tissue and cellular levels.,” *J. Bone Miner. Res.*, vol. 5, no. 4, pp. 311–319, 1990.
- [94] P. Garnero, E. Sornay-Rendu, M. C. Chapuy, and P. D. Delmas, “Increased bone turnover in late postmenopausal women is a major determinant of osteoporosis.,” *J. Bone Miner. Res.*, vol. 11, no. 3, pp. 337–349, 1996.

- [95] R. Pacifici, "Estrogen, cytokines, and pathogenesis of postmenopausal osteoporosis.," *J. Bone Miner. Res.*, vol. 11, no. 8, pp. 1043–1051, 1996.
- [96] D. L. Lacey, E. Timms, H. L. Tan, M. J. Kelley, C. R. Dunstan, T. Burgess, R. Elliott, a. Colombero, G. Elliott, S. Scully, H. Hsu, J. Sullivan, N. Hawkins, E. Davy, C. Capparelli, a. Eli, Y. X. Qian, S. Kaufman, I. Sarosi, V. Shalhoub, G. Senaldi, J. Guo, J. Delaney, and W. J. Boyle, "Osteoprotegerin ligand is a cytokine that regulates osteoclast differentiation and activation," *Cell*, vol. 93, no. 2, pp. 165–176, 1998.
- [97] M. Saika, I. Daisuke, S. Kido, and T. Matsumoto, "17beta-Estradiol Stimulates Expression by a Mouse Stromal Cell Line, ST-2, via Estrogen Receptor-alpha," *Endocrinology*, vol. 142, no. 6, pp. 2205–2212, 2001.
- [98] G. Eghbali-fatourech, S. Khosla, A. Sanyal, W. J. Boyle, D. L. Lacey, and B. L. Riggs, "Role of RANK ligand in mediating increased bone resorption in early postmenopausal women," *J. Clin. Invest.*, vol. 111, no. 8, pp. 1221–1230, 2003.
- [99] T. Nakamura, Y. Imai, T. Matsumoto, S. Sato, K. Takeuchi, K. Igarashi, Y. Harada, Y. Azuma, A. Krust, Y. Yamamoto, H. Nishina, S. Takeda, H. Takayanagi, D. Metzger, J. Kanno, K. Takaoka, T. J. Martin, P. Chambon, and S. Kato, "Estrogen Prevents Bone Loss via Estrogen Receptor α and Induction of Fas Ligand in Osteoclasts," *Cell*, vol. 130, no. 5, pp. 811–823, 2007.
- [100] P. Ravn, G. Cizza, N. H. Bjarnason, D. Thompson, M. Daley, R. D. Wasnich, M. Mcclung, D. Hosking, a J. Yates, and C. Christiansen, "Low Body Mass Index Is an Important Risk Factor for Low Bone Mass and Increased Bone Loss in Early Postmenopausal Women," *J. Bone Miner. Res.*, vol. 14, no. 9, pp. 1622–1627, 1999.
- [101] E. A. Krall and B. Dawson-Hughes, "Smoking increases bone loss and decreases intestinal calcium absorption.," *J. Bone Miner. Res.*, vol. 14, no. 2, pp. 215–220, 1999.
- [102] T. V Nguyen, J. R. Center, and J. a Eisman, "Osteoporosis in elderly men and women: effects of dietary calcium, physical activity, and body mass index.," *J. Bone Miner. Res.*, vol. 15, no. 2, pp. 322–331, 2000.
- [103] P. Lips, "Vitamin D Deficiency and Secondary Hyperparathyroidism in the Elderly : Consequences for Bone Loss," *Endocr. Rev.*, vol. 22, no. March, pp. 477–501, 2001.
- [104] T. L. Stewart and S. H. Ralston, "Role of genetic factors in the pathogenesis of osteoporosis," *J. Endocrinol.*, vol. 166, pp. 235–245, 2000.

- [105] E. P. Smith, J. Boyd, G. R. Frank, H. Takahashi, R. M. Cohen, B. Specker, T. C. Williams, D. B. Lubahn, and K. S. Korach, "Estrogen resistance caused by a mutation in the estrogen-receptor gene in a man," *N. Engl. J. Med.*, vol. 331, no. 16, pp. 1056–1061, 1994.
- [106] E.-M. Lochmuller, R. Muller, V. Kuhn, C. A. Lill, and F. Eckstein, "Can Novel Clinical Densitometric Techniques Replace or Improve DXA in Predicting Bone Strength in Osteoporosis at the Hip and Other Skeletal Sites?," *J. Bone Miner. Res.*, vol. 18, no. 5, pp. 906–912, 2003.
- [107] J. F. Griffith and H. K. Genant, "Bone mass and architecture determination: state of the art," *Best Pract. Res. Clin. Endocrinol. Metab.*, vol. 22, no. 5, pp. 737–764, 2008.
- [108] E. Dall'Ara, D. Pahr, P. Varga, F. Kainberger, and P. Zysset, "QCT-based finite element models predict human vertebral strength in vitro significantly better than simulated DEXA," *Osteoporos. Int.*, vol. 23, no. 2, pp. 563–572, 2012.
- [109] P. Delmas, R. Eastell, P. Garnero, M. Seibel, J. Stepan, and for the Committee of Scientific Advisors of the International Osteoporosis Foundation, "The use of biochemical markers of bone turnover in Osteoporosis," *Osteoporos. Int.*, vol. 11, no. S6, pp. S2–S17, 2000.
- [110] F. Cosman, S. J. de Beur, M. S. LeBoff, E. M. Lewiecki, B. Tanner, S. Randall, and R. Lindsay, "Clinician's Guide to Prevention and Treatment of Osteoporosis," *Osteoporos. Int.*, vol. 25, pp. 2359–2381, 2014.
- [111] M. J. Gronholz, "Prevention, diagnosis, and management of osteoporosis-related fracture: a multifactorial osteopathic approach," *J. Am. Osteopath. Assoc.*, vol. 108, no. 10, pp. 575–585, 2008.
- [112] C. E. Bowring and R. M. Francis, "National Osteoporosis Society's Position Statement on hormone replacement therapy in the prevention and treatment of osteoporosis," *Menopause Int.*, vol. 17, no. 2, pp. 63–65, 2011.
- [113] E. M. Lewiecki, "Current and emerging pharmacologic therapies for the management of postmenopausal osteoporosis," *J. Womens. Health (Larchmt.)*, vol. 18, no. 10, pp. 1615–1626, 2009.
- [114] J. Burch, S. Rice, H. Yang, A. Neilson, L. Stirk, R. Francis, P. Holloway, P. Selby, and D. Craig, "Systematic review of the use of bone turnover markers for monitoring the response to osteoporosis treatment: the secondary prevention of fractures, and primary prevention of fractures in high-risk groups," *Health Technol. Assess.*, vol. 18, no. 11, pp. 1–180, 2014.

- [115] J. Y. Reginster, J. M. Kaufman, S. Goemaere, J. P. Devogelaer, C. L. Benhamou, D. Felsenberg, M. Diaz-Curiel, M. L. Brandi, J. Badurski, J. Wark, A. Balogh, O. Bruyère, and C. Roux, “Maintenance of antifracture efficacy over 10 years with strontium ranelate in postmenopausal osteoporosis,” *Osteoporos. Int.*, vol. 23, no. 3, pp. 1115–1122, 2012.
- [116] A.-F. Donneau and J.-Y. Reginster, “Cardiovascular safety of strontium ranelate: real-life assessment in clinical practice.,” *Osteoporos. International*, vol. 25, pp. 397–8, 2014.
- [117] “PSUR assessment report: Strontium ranelate,” 2013.
- [118] P. Vestergaard, “New strategies for osteoporosis patients previously managed with strontium ranelate,” *Ther. Adv. Musculoskelet. Dis.*, vol. 6, no. 6, pp. 217–225, 2014.
- [119] S. R. Cummings, J. San Martin, M. R. McClung, E. S. Siris, R. Eastell, I. R. Reid, P. Delmas, H. B. Zoog, M. Austin, A. Wang, S. Kutilek, S. Adami, J. Zanchetta, C. Libanati, S. Siddhanti, and C. Christiansen, “Denosumab for prevention of fractures in postmenopausal women with osteoporosis.,” *N. Engl. J. Med.*, vol. 361, no. 8, pp. 756–765, 2009.
- [120] F. Cosman, D. B. Crittenden, J. D. Adachi, N. Binkley, E. Czerwinski, S. Ferrari, L. C. Hofbauer, E. Lau, E. M. Lewiecki, A. Miyauchi, C. A. F. Zerbini, C. E. Milmont, L. Chen, J. Maddox, P. D. Meisner, C. Libanati, and A. Grauer, “Romosozumab Treatment in Postmenopausal Women with Osteoporosis,” *N. Engl. J. Med.*, vol. 375, no. 16, pp. 1532–1543, 2016.
- [121] K. Kim, A. Svedbom, X. Luo, S. Sutradhar, and J. A. Kanis, “Comparative cost-effectiveness of bazedoxifene and raloxifene in the treatment of postmenopausal osteoporosis in Europe, using the FRAX algorithm,” *Osteoporos. Int.*, vol. 25, no. 1, pp. 325–337, 2014.
- [122] R. Rizzoli, J.-Y. Reginster, S. Boonen, G. Bréart, A. Diez-Perez, D. Felsenberg, J.-M. Kaufman, J. a Kanis, and C. Cooper, “Adverse reactions and drug-drug interactions in the management of women with postmenopausal osteoporosis.,” *Calcif. Tissue Int.*, vol. 89, no. 2, pp. 91–104, 2011.
- [123] M. Arlot, P. J. Meunier, G. Boivin, L. Haddock, J. Tamayo, R. Correa-Rotter, S. Jasqui, D. W. Donley, G. P. Dalsky, J. S. Martin, and E. F. Eriksen, “Differential effects of teriparatide and alendronate on bone remodeling in postmenopausal women assessed by histomorphometric parameters.,” *J. Bone Miner. Res.*, vol. 20, no. 7, pp. 1244–1253, 2005.
- [124] R. Eastell, T. Nickelsen, F. Marin, C. Barker, P. Hadji, J. Farrerons, M. Audran,

- S. Boonen, K. Brixen, J. M. Gomes, B. Obermayer-Pietsch, A. Avramidis, G. Sigurdsson, and C. C. Glüer, "Sequential treatment of severe postmenopausal osteoporosis after teriparatide: final results of the randomized, controlled European Study of Forsteo (EUROFORS).," *J. Bone Miner. Res.*, vol. 24, no. 4, pp. 726–736, 2009.
- [125] J. N. Tsai, A. V. Uihlein, H. Lee, R. Kumbhani, E. Siwila-Sackman, E. a. McKay, S. A. M. Burnett-Bowie, R. M. Neer, and B. Z. Leder, "Teriparatide and denosumab, alone or combined, in women with postmenopausal osteoporosis: The DATA study randomised trial," *Lancet*, vol. 382, no. 9886, pp. 50–56, 2013.
- [126] D. N. Kalu, "Animal Models of the aging skeleton," in *The Aging Skeleton*, C. J. Rosen, J. Glowacki, and J. P. Bilezikian, Eds. San Diego: Academic Press, 1999, pp. 37–50.
- [127] J. B. Rodgers, M.-F. Marie-Claude, and M. Hartmut, "Animal models for the study of bone loss after cessation of ovarian function," *Bone*, vol. 14, pp. 369–377, 1993.
- [128] E. Bonucci and P. Ballanti, "Osteoporosis--Bone Remodeling and Animal Models.," *Toxicol. Pathol.*, pp. 1–13, 2013.
- [129] D. N. Kalu, "The ovariectomized rat model of postmenopausal bone loss," *Bone Miner.*, vol. 15, no. 3, pp. 175–191, 1991.
- [130] M. Li, Y. Shen, and T. J. Wronski, "Time course of femoral neck osteopenia in ovariectomized rats," *Bone*, vol. 20, no. 1, pp. 55–61, 1997.
- [131] T. J. Wronski, L. M. Dann, and K. S. Scott, "Long-term effects of ovariectomy and aging on the rat skeleton," *Calcif. Tissue Int.*, vol. 45, no. 6, pp. 360–366, 1989.
- [132] T. J. Wronski, L. M. Dann, and S. L. Horner, "Time course of vertebral osteopenia in ovariectomized rats," *Bone*, vol. 10, no. 4, pp. 295–301, 1989.
- [133] T. J. Wronski, M. Cintron, and L. M. Dann, "Temporal Relationship between Bone Loss and Increased Bone Turnover in Ovariectomized Rats," *Calcif. Tissue Int.*, vol. 43, pp. 179–183, 1988.
- [134] P. P. Lelovas, T. T. Xanthos, S. E. Thorma, G. P. Lyritis, and I. a. Dontas, "The laboratory rat as an animal model for osteoporosis research," *Comp. Med.*, vol. 58, no. 5, pp. 424–430, 2008.
- [135] W. S. Jee and W. Yao, "Overview: animal models of osteopenia and

- osteoporosis.," *J. Musculoskelet. Neuronal Interact.*, vol. 1, no. 3, pp. 193–207, 2001.
- [136] U. T. Iwaniec and R. T. Turner, "Animal Models for Osteoporosis," in *Osteoporosis 3rd Edition*, R. Marcus, D. Feldman, D. Nelson, and C. Rosen, Eds. Academic Press, 2007, pp. 939–961.
- [137] R. L. Jilka, G. Hangoc, G. Girasole, G. Passeri, D. C. Williams, J. S. Abrams, B. Boyce, H. Broxmeyer, and S. C. Manolagas, "Increased osteoclast development after estrogen loss: mediation by interleukin-6," *Science (80-.)*, vol. 257, no. 5066, pp. 88–91, 1992.
- [138] R. Oheim, M. Amling, A. Ignatius, and P. Pogoda, "Large animal model for osteoporosis in humans: The ewe," *Eur. Cells Mater.*, vol. 24, pp. 372–385, 2012.
- [139] H. J. Wilke, A. Kettler, K. H. Wenger, and L. E. Claes, "Anatomy of the sheep spine and its comparison to the human spine," *Anat. Rec.*, vol. 247, no. 4, pp. 542–555, 1997.
- [140] I. M. Sigrist, C. Gerhardt, M. Alini, E. Schneider, and M. Egermann, "The long-term effects of ovariectomy on bone metabolism in sheep," *J. Bone Miner. Metab.*, vol. 25, no. 1, pp. 28–35, 2007.
- [141] A. S. Turner, M. Alvis, W. Myers, M. L. Stevens, and M. W. Lundy, "Changes in bone mineral density and bone-specific alkaline phosphatase in ovariectomized ewes," *Bone*, vol. 17, no. 4 SUPPL., pp. 395–402, 1995.
- [142] P. Pogoda, M. Egermann, J. C. Schnell, M. Priemel, A. F. Schilling, M. Alini, T. Schinke, J. M. Rueger, E. Schneider, I. Clarke, and M. Amling, "Leptin inhibits bone formation not only in rodents, but also in sheep.," *J. Bone Miner. Res.*, vol. 21, no. 10, pp. 1591–9, 2006.
- [143] P. Augat, S. Schorlemmer, C. Gohl, S. Iwabu, A. Ignatius, and L. Claes, "Glucocorticoid-treated sheep as a model for osteopenic trabecular bone in biomaterials research.," *J. Biomed. Mater. Res. A*, vol. 66, no. 3, pp. 457–62, 2003.
- [144] M. A. Brennan, J. P. Gleeson, M. Browne, F. J. O'Brien, P. J. Thurner, and L. M. McNamara, "Site specific increase in heterogeneity of trabecular bone tissue mineral during oestrogen deficiency," *Eur. Cells Mater.*, vol. 21, no. 353, pp. 396–406, 2011.
- [145] B. I. Newton, R. C. Cooper, J. A. Gilbert, R. B. Johnson, and L. D. Zardiackas, "The ovariectomized sheep as a model for human bone loss," *J. Comp. Pathol.*,

vol. 130, no. 4, pp. 323–326, 2004.

- [146] M. Fini, G. Pierini, G. Giavaresi, G. Biagini, B. M. Mattioli, N. Nicoli Aldini, M. Rocca, L. Martini, and R. Giardino, “The ovariectomised sheep as a model for testing biomaterials and prosthetic devices in osteopenic bone: a preliminary study on iliac crest biopsies,” *Int. J. Artif. Organs*, vol. 23, no. 4, pp. 275–281, 2000.
- [147] R. Oheim, T. Schinke, M. Amling, and P. Pogoda, “Can we induce osteoporosis in animals comparable to the human situation?,” *Injury*, vol. 47, pp. S3–S9, 2016.
- [148] C. P. Jerome and P. E. Peterson, “Nonhuman primate models in skeletal research,” *Bone*, vol. 29, no. 1, pp. 1–6, 2001.
- [149] L. C. Miller, D. S. Weaver, J. A. McAlister, and D. R. Koritnik, “Effects of Ovariectomy on Vertebral Trabecular Bone in the Cynomolgus Monkey (*Macaca fascicularis*),” *Calcif. Tissue Int.*, vol. 38, pp. 62–65, 1986.
- [150] S. Y. Smith, A. Varela, and J. Jolette, “Nonhuman Primate Models of Osteoporosis,” in *Osteoporosis Research*, G. Duque and K. Watanabe, Eds. Springer, 2011, pp. 135–157.
- [151] S. Y. Smith, J. Jolette, and C. H. Turner, “Skeletal health: Primate model of postmenopausal osteoporosis,” *Am. J. Primatol.*, vol. 71, no. 9, pp. 752–765, 2009.
- [152] N. Binkley, D. Kimmel, J. Bruner, a Haffa, B. Davidowitz, C. Meng, V. Schaffer, and J. Green, “Zoledronate prevents the development of absolute osteopenia following ovariectomy in adult rhesus monkeys.,” *J. Bone Miner. Res.*, vol. 13, no. 11, pp. 1775–1782, 1998.
- [153] R. Brommage, C. E. Hotchkiss, C. J. Lees, M. W. Stancill, J. M. Hock, and C. P. Jerome, “Daily Treatment with Human Recombinant Parathyroid Mass in Ovariectomized Monkeys *,” *J. Clin. Endocrinol. Metab.*, vol. 84, no. 10, pp. 3757–3763, 1999.
- [154] R. A. Weiss, “Retroviral Zoonoses,” *Nat. Med.*, vol. 4, pp. 391–392, 1998.
- [155] “Annual Statistics of Scientific Procedures on Living Animals Great Britain 2015,” 2016.
- [156] J. C. van der Linden, J. H. Waarsing, and H. Weinans, “The use of micro-CT to study bone architecture dynamics noninvasively,” *Drug Discov. Today Technol.*, vol. 3, no. 2, pp. 213–219, 2006.

- [157] E. Dall'Ara, M. Boudiffa, C. Taylor, D. Schug, E. Fiegle, A. J. Kennerley, C. Damianou, G. M. Tozer, F. Kiessling, and R. Müller, "Longitudinal imaging of the ageing mouse," *Mech. Ageing Dev.*, vol. 160, pp. 93–116, 2016.
- [158] T. S. Gross, S. Srinivasan, C. C. Liu, T. L. Clemens, and S. D. Bain, "Noninvasive loading of the murine tibia: an in vivo model for the study of mechanotransduction," *J. Bone Miner. Res.*, vol. 17, no. 3, pp. 493–501, 2002.
- [159] P. McGonigle and B. Ruggeri, "Animal models of human disease: Challenges in enabling translation," *Biochem. Pharmacol.*, vol. 87, no. 1, pp. 162–171, 2014.
- [160] A.-M. Malfait and C. B. Little, "On the predictive utility of animal models of osteoarthritis," *Arthritis Res. Ther.*, vol. 17, no. 1, p. 225, 2015.
- [161] A. M. Burkhardt and A. Zlotnik, "Translating translational research: mouse models of human disease," *Cell. Mol. Immunol.*, vol. 10, no. 5, pp. 373–374, 2013.
- [162] K. H. Benam, S. Dauth, B. Hassell, A. Herland, A. Jain, K.-J. Jang, K. Karalis, H. J. Kim, L. MacQueen, R. Mahmoodian, S. Musah, Y. Torisawa, A. D. van der Meer, R. Villenave, M. Yadid, K. K. Parker, and D. E. Ingber, "Engineered In Vitro Disease Models," *Annu. Rev. Pathol. Mech. Dis.*, vol. 10, no. 1, pp. 195–262, 2015.
- [163] C. I. Johnson, D. J. Argyle, and D. N. Clements, "In vitro models for the study of osteoarthritis," *Vet. J.*, vol. 209, pp. 40–49, 2016.
- [164] H. Domaschke, D. Biol, M. Gelinsky, B. Burmeister, D. Biol, R. Fleig, T. Hanke, A. Reinstorf, D. Chem, W. Pompe, and A. Rösen-wolff, "In Vitro Ossification and Remodeling of Mineralized Collagen I Scaffolds," *Tissue Eng.*, vol. 12, no. 4, pp. 949–958, 2006.
- [165] P. K. Anaraki, M. Patecki, S. Tkachuk, Y. Kiyan, H. Haller, and I. Dumler, "Urokinase receptor mediates osteoclastogenesis via M-CSF release from osteoblasts and the c-Fms/PI3K/Akt/NF- κ B pathway in osteoclasts," *J. Bone Miner. Res.*, vol. 30, no. 2, pp. 379–388, 2015.
- [166] Z. Zhang, J. T. Egaña, A. K. Reckhenrich, T. L. Schenck, J. A. Lohmeyer, J. T. Schantz, H. G. MacHens, and A. F. Schilling, "Cell-based resorption assays for bone graft substitutes," *Acta Biomater.*, vol. 8, no. 1, pp. 13–19, 2012.
- [167] P. Collin-Osdoby, X. Yu, H. Zheng, and P. Osdoby, "RANKL-Mediated Osteoclast Formation from Murine RAW 264.7 Cells," in *Methods in Molecular Medicine, Vol. 80: Bone Research Protocols*, M. H. Helfrich and S.

H. Ralston, Eds. 2003, pp. 153–166.

- [168] S. Tsuchiya, M. Yamabe, Y. Yamaguchi, Y. Kobayashi, T. Konno, and K. Tada, “Establishment and characterization of a human acute monocytic leukemia cell line (THP-1).,” *Int. J. Cancer*, vol. 26, no. 2, pp. 171–6, 1980.
- [169] Y. Tanaka, A. Maruo, K. Fujii, M. Nomi, T. Nakamura, S. Eto, and Y. Minami, “Intercellular adhesion molecule 1 discriminates functionally different populations of human osteoblasts: characteristic involvement of cell cycle regulators,” *J Bone Min. Res.*, vol. 15, no. 10, pp. 1912–1923, 2000.
- [170] H. Xie, P. L. Xie, X. H. Luo, X. P. Wu, H. D. Zhou, S. Y. Tang, and E. Y. Liao, “Omentin-1 exerts bone-sparing effect in ovariectomized mice,” *Osteoporos. Int.*, vol. 23, no. 4, pp. 1425–1436, 2012.
- [171] F. Tortelli, N. Pujic, Y. Liu, N. Laroche, L. Vico, and R. Cancedda, “Osteoblast and Osteoclast Differentiation in an In Vitro Three-Dimensional Model of Bone,” *Tissue Eng. Part A*, vol. 15, no. 9, pp. 2373–83, 2009.
- [172] Y. Vinik, H. Shatz-Azoulay, A. Vivanti, N. Hever, Y. Levy, R. Karmona, V. Brumfeld, S. Baraghithy, M. Attar-Lamdar, S. Boura-Halfon, I. Bab, and Y. Zick, “The mammalian lectin galectin-8 induces RANKL expression, osteoclastogenesis, and bone mass reduction in mice,” *Elife*, vol. 4, no. MAY, pp. 1–19, 2015.
- [173] American Type Culture Collection, “Saos-2 (ATCC® HTB-85™),” 2016. [Online]. Available: <https://www.atcc.org/products/all/HTB-85.aspx>. [Accessed: 28-Nov-2017].
- [174] American Type Culture Collection, “MG-63 (ATCC® CRL-1427™),” 2016. [Online]. Available: <https://www.atcc.org/Products/All/CRL-1427.aspx>. [Accessed: 28-Nov-2017].
- [175] K. C. Hicok, T. Thomas, F. Gori, D. J. Rickard, T. C. Spelsberg, and B. L. Riggs, “Development and characterization of conditionally immortalized osteoblast precursor cell lines from human bone marrow stroma,” *J. Bone Miner. Res.*, vol. 13, no. 2, pp. 205–17, 1998.
- [176] E. Otsuka, A. Yamaguchi, S. Hirose, and H. Hagiwara, “Characterization of osteoblastic differentiation of stromal cell line ST2 that is induced by ascorbic acid,” *Am. J. Physiol.*, vol. 277, no. 1, pp. C132–C138, 1999.
- [177] H. Kodama, Y. Amagai, H. Sudo, S. Kasai, and S. Yamamoto, “Establishment of a clonal osteogenic cell line from newborn mouse calvaria,” *J. Oral Biol.*, vol. 23, pp. 899–901, 1981.

- [178] E. K. Basdra and G. Komposch, "Osteoblast-like properties of human periodontal ligament cells: an in vitro analysis," *Eur. J. Orthod.*, vol. 19, no. 6, pp. 615–621, 1997.
- [179] a. M. Chou, V. Sae-Lim, T. M. Lim, J. T. Schantz, S. H. Teoh, C. L. Chew, and D. W. Hutmacher, "Culturing and characterization of human periodontal ligament fibroblasts—a preliminary study," *Mater. Sci. Eng. C*, vol. 20, pp. 77–83, 2002.
- [180] Y. Kato, J. J. Windle, B. A. Koop, G. R. Mundy, and L. F. Bonewald, "Establishment of an Osteocyte-like Cell Line, MLO-Y4," *J. Bone Miner. Res.*, vol. 12, no. 12, pp. 2014–2023, 1997.
- [181] B. F. Boyce and L. Xing, "Biology of RANK, RANKL, and osteoprotegerin," *Arthritis Res. Ther.*, vol. 9, no. Suppl 1, p. S1, 2007.
- [182] T. Komori, "Regulation of bone development and extracellular matrix protein genes by RUNX2," *Cell Tissue Res.*, vol. 339, no. 1, pp. 189–195, 2010.
- [183] K. Nakashima, X. Zhou, G. Kunkel, Z. Zhang, J. M. Deng, R. R. Behringer, and B. De Crombrughe, "The novel zinc finger-containing transcription factor Osterix is required for osteoblast differentiation and bone formation," *Cell*, vol. 108, no. 1, pp. 17–29, 2002.
- [184] F. P. Reinholt, K. Hulthén, A. Oldberg, and D. Heinegård, "Osteopontin—a possible anchor of osteoclasts to bone," *Proc. Natl. Acad. Sci.*, vol. 87, no. 12, pp. 4473–4475, 1990.
- [185] L. . Fisher, W. McBride, J. . Termine, and M. . Young, "Human Bone Sialoprotein," *J. Biol. Chem.*, vol. 265, no. 4, pp. 2347–2351, 1990.
- [186] A. R. Hayman, S. J. Jones, A. Boyde, D. Foster, W. H. Colledge, M. B. Carlton, M. J. Evans, and T. M. Cox, "Mice lacking tartrate-resistant acid phosphatase (Acp 5) have disrupted endochondral ossification and mild osteopetrosis," *Development*, vol. 122, no. 10, pp. 3151–62, 1996.
- [187] N. Bonnet, J. Brun, J. C. Rousseau, L. T. Duong, and S. L. Ferrari, "Cathepsin K Controls Cortical Bone Formation by Degrading Periostin," *J. Bone Miner. Res.*, vol. 32, no. 7, pp. 1432–1441, 2017.
- [188] A. Yabluchanskiy, Y. Ma, R. P. Iyer, M. E. Hall, and M. L. Lindsey, "Matrix Metalloproteinase-9: Many Shades of Function in Cardiovascular Disease," *Physiology*, vol. 28, no. 6, pp. 391–403, 2013.
- [189] K. Nemeth, M. Schoppet, N. Al-Fakhri, S. Helas, R. Jessberger, L. C. Hofbauer,

and C. Goettsch, “The Role of Osteoclast-Associated Receptor in Osteoimmunology,” *J. Immunol.*, vol. 186, no. 1, pp. 13–18, 2011.

- [190] Y. Azuma, K. Kaji, R. Katogi, S. Takeshita, and A. Kudo, “Tumor necrosis factor- α induces differentiation of and bone resorption by osteoclasts.,” *J. Biol. Chem.*, vol. 275, no. 7, pp. 4858–4864, 2000.
- [191] B. F. Boyce, P. Li, Z. Yao, Q. Zhang, I. R. Badell, E. M. Schwarz, R. J. O’Keefe, and L. Xing, “TNF- α and pathologic bone resorption.,” *Keio J. Med.*, vol. 54, no. 3, pp. 127–131, 2005.
- [192] V. Z. C. Borba and N. C. P. Mañas, “The use of PTH in the treatment of osteoporosis.,” *Arq. Bras. Endocrinol. Metabol.*, vol. 54, no. 2, pp. 213–219, 2010.
- [193] N. K. Shevde, L. A. Plum, M. Clagett-Dame, H. Yamamoto, J. W. Pike, and H. F. Deluca, “A potent analog of $1\alpha,25$ -dihydroxyvitamin D3 selectively induced bone formation,” *Proceedings of the National Academy of Sciences*, vol. 99, no. 21, pp. 13487–13491, 2002.
- [194] L. You, S. Temiyasathit, P. Lee, C. H. Kim, P. Tummala, W. Yao, W. Kingery, A. M. Malone, R. Y. Kwon, and C. R. Jacobs, “Osteocytes as mechanosensors in the inhibition of bone resorption due to mechanical loading,” *Bone*, vol. 42, no. 1, pp. 172–179, 2008.
- [195] R. Kitazawa and S. Kitazawa, “Vitamin D(3) augments osteoclastogenesis via vitamin D-responsive element of mouse RANKL gene promoter.,” *Biochem. Biophys. Res. Commun.*, vol. 290, no. 2, pp. 650–5, 2002.
- [196] Y. Ishimi, C. Miyaura, C. H. Jin, T. Akatsu, E. Abe, Y. Nakamura, A. Yamaguchi, S. Yoshiki, T. Matsuda, T. Hirano, T. Kishimoto, and T. Suda, “IL-6 is produced by osteoblasts and induces bone resorption,” *J. Immunol.*, vol. 145, pp. 3297–3303, 1990.
- [197] E. M. Greenfield, J. I. Alvarez, E. A. Mclaurine, M. J. Oursler, H. C. Blair, P. Osdoby, S. L. Teitelbaum, and F. P. Ross, “Avian Osteoblast Conditioned Media Stimulate Bone Resorption by Targeting Multinucleating Osteoclast Precursors,” pp. 317–323, 1992.
- [198] E. Jimi, I. Nakamura, Y. Taguchi, T. Tsurukai, M. Tamura, N. Takahashi, and T. Suda, “Osteoclast function is activated by osteoblastic cells through a mechanism involving cell-to-cell contact,” *Endocrinology*, vol. 137, no. 8, pp. 2187–2190, 1996.
- [199] P. M. J. McSheehy and T. J. Chambers, “Osteoblast-Like Cells in the Presence

- of Parathyroid Hormone Release Soluble Factor that Stimulates Osteoclastic Bone Resorption,” *Endocrinology*, vol. 119, no. 4, pp. 1654–1659, 1986.
- [200] E. C. Weir, M. C. Horowitz, R. Baron, M. Centrella, B. M. Kacinski, and K. L. Insogna, “Macrophage colony-stimulating factor release and receptor expression in bone cells,” *J. Bone Miner. Res.*, vol. 8, no. 12, 1993.
- [201] D. L. Kaplan, C. M. Eielson, M. C. Horowitz, K. L. Insogna, and E. C. Weir, “Tumor necrosis factor-alpha induces transcription of the colony-stimulating factor-1 gene in murine osteoblasts,” *J. Cell. Physiol.*, vol. 168, no. 1, pp. 199–208, 1996.
- [202] G. Yao, B. Sun, E. E. Hammond, E. N. Spencer, C. Mark, K. L. Insogna, and E. C. Weir, “The Cell-surface Form of Colony-stimulating Factor-1 Is Regulated by Osteotropic Agents and Supports Formation of Multinucleated Osteoclast-like Cells *,” *J. Biol. Chem.*, vol. 273, no. 7, pp. 4119–4128, 1998.
- [203] G. Q. Yao, J. J. Wu, N. Troiano, M. L. Zhu, X. Y. Xiao, and K. Insogna, “Selective deletion of the membrane-bound colony stimulating factor 1 isoform leads to high bone mass but does not protect against estrogen-deficiency bone loss,” *J. Bone Miner. Metab.*, vol. 30, no. 4, pp. 408–418, 2012.
- [204] H. W. Smith and C. J. Marshall, “Regulation of cell signalling by uPAR.,” *Nat. Rev. Mol. Cell Biol.*, vol. 11, no. 1, pp. 23–36, 2010.
- [205] M. Komine, a Kukita, T. Kukita, Y. Ogata, T. Hotokebuchi, and O. Kohashi, “Tumor necrosis factor-alpha cooperates with receptor activator of nuclear factor kappaB ligand in generation of osteoclasts in stromal cell-depleted rat bone marrow cell culture.,” *Bone*, vol. 28, no. 5, pp. 474–83, 2001.
- [206] P. Collin-Osdoby, L. Rothe, F. Anderson, M. Nelson, W. Maloney, and P. Osdoby, “Receptor Activator of NF- κ B and Osteoprotegerin Expression by Human Microvascular Endothelial Cells, Regulation by Inflammatory Cytokines, and Role in Human Osteoclastogenesis,” *J. Biol. Chem.*, vol. 276, no. 23, pp. 20659–20672, 2001.
- [207] H. Goto, M. Osaki, T. Fukushima, K. Sakamoto, A. Hozumi, H. Baba, and H. Shindo, “Human bone marrow adipocytes support dexamethasone-induced osteoclast differentiation and function through RANKL expression,” *Biomed Res*, vol. 32, no. 1, pp. 37–44, 2011.
- [208] Y.-M. Lee, N. Fujikado, H. Manaka, H. Yasuda, and Y. Iwakura, “IL-1 plays an important role in the bone metabolism under physiological conditions,” *Int. Immunol.*, vol. 22, no. 10, pp. 805–816, 2010.

- [209] K. Shinoda, E. Sugiyama, H. Taki, S. Harada, T. Mino, M. Maruyama, and M. Kobayashi, "Resting T cells negatively regulate osteoclast generation from peripheral blood monocytes," *Bone*, vol. 33, no. 4, pp. 711–720, 2003.
- [210] F. Gori, L. C. Hofbauer, C. R. Dunstan, T. C. Spelsberg, S. Khosla, and B. L. Riggs, "The Expression of Osteoprotegerin and RANK Ligand and the Support of Osteoclast Formation by Stromal-Osteoblast Lineage Cells Is Developmentally Regulated," *Endocrinology*, vol. 141, no. 12, pp. 4768–4776, 2000.
- [211] S. Zhao, Y. K. Y. Zhang, S. Harris, S. S. Ahuja, and L. F. Bonewald, "MLO-Y4 osteocyte-like cells support osteoclast formation and activation.," *J. Bone Miner. Res.*, vol. 17, no. 11, pp. 2068–2079, 2002.
- [212] C. Wittkowske, G. C. Reilly, D. Lacroix, and C. M. Perrault, "In Vitro Bone Cell Models: Impact of Fluid Shear Stress on Bone Formation," *Front. Bioeng. Biotechnol.*, vol. 4, no. November, 2016.
- [213] R. N. Kulkarni, A. D. Bakker, V. Everts, and J. Klein-Nulend, "Inhibition of osteoclastogenesis by mechanically loaded osteocytes: Involvement of MEPE," *Calcif. Tissue Int.*, vol. 87, no. 5, pp. 461–468, 2010.
- [214] C. H. Kim, L. You, C. E. Yellowley, and C. R. Jacobs, "Oscillatory fluid flow-induced shear stress decreases osteoclastogenesis through RANKL and OPG signaling," *Bone*, vol. 39, no. 5, pp. 1043–1047, 2006.
- [215] X. Zhang, J. Li, Z. Wan, H. Liu, H. Li, L. Liu, R. Li, Y. Guo, W. Chen, and X. Zhang, "Osteoblasts subjected to mechanical strain inhibit osteoclastic differentiation and bone resorption in a Co-culture system," *Ann. Biomed. Eng.*, vol. 41, no. 10, pp. 2056–2066, 2013.
- [216] G. Gu, M. Mulari, Z. Peng, T. A. Hentunen, and H. K. Väänänen, "Death of osteocytes turns off the inhibition of osteoclasts and triggers local bone resorption," *Biochem. Biophys. Res. Commun.*, vol. 335, no. 4, pp. 1095–1101, 2005.
- [217] X. Wang, J. Wu, Y. Shidoji, Y. Muto, N. Ohishi, K. Yagi, S. Ikegami, T. Shinki, N. Udagawa, T. Suda, and Y. Ishimi, "Effects of geranylgeranoic acid in bone: induction of osteoblast differentiation and inhibition of osteoclast formation.," *J. Bone Miner. Res.*, vol. 17, no. 1, pp. 91–100, 2002.
- [218] F. Guillerminet, H. Beaupied, V. Fabien-Soulé, D. Tomé, C. L. Benhamou, C. Roux, and A. Blais, "Hydrolyzed collagen improves bone metabolism and biomechanical parameters in ovariectomized mice: An in vitro and in vivo study," *Bone*, vol. 46, no. 3, pp. 827–834, 2010.

- [219] W. Zhang, H. Guo, H. Jing, Y. Li, X. Wang, H. Zhang, L. Jiang, and F. Ren, "Lactoferrin stimulates osteoblast differentiation through PKA and p38 pathways independent of Lactoferrin's receptor LRP1," *J. Bone Miner. Res.*, vol. 29, no. 5, pp. 1232–1243, 2014.
- [220] F. Lorget, J. Clough, M. Oliveira, M. C. Daury, A. Sabokbar, and E. Offord, "Lactoferrin reduces in vitro osteoclast differentiation and resorbing activity," *Biochem. Biophys. Res. Commun.*, vol. 296, no. 2, pp. 261–266, 2002.
- [221] M. Montesi, S. Panseri, M. Iafisco, A. Adamiano, and A. Tampieri, "Coupling hydroxyapatite nanocrystals with lactoferrin as a promising strategy to fine regulate bone homeostasis," *PLoS One*, vol. 10, no. 7, pp. 1–13, 2015.
- [222] J. Salbach-Hirsch, N. Ziegler, S. Thiele, S. Moeller, M. Schnabelrauch, V. Hintze, D. Scharnweber, M. Rauner, and L. C. Hofbauer, "Sulfated glycosaminoglycans support osteoblast functions and concurrently suppress osteoclasts," *J. Cell. Biochem.*, vol. 115, no. 6, pp. 1101–1111, 2014.
- [223] R. Mashima, Y. Hishida, T. Tezuka, and Y. Yamanashi, "The roles of Dok family adapters in immunoreceptor signaling," *Immunol. Rev.*, vol. 232, no. 1, pp. 273–285, 2009.
- [224] X. Cai, J. Xing, C. L. Long, Q. Peng, and M. Beth Humphrey, "DOK3 Modulates Bone Remodeling by Negatively Regulating Osteoclastogenesis and Positively Regulating Osteoblastogenesis," *J. Bone Miner. Res.*, 2017.
- [225] S. Kousteni and J. P. Bilezikian, "The Cell Biology of Parathyroid Hormone in Osteoblasts," *Curr. Osteoporos. Rep.*, vol. 6, no. 2, pp. 72–76, 2008.
- [226] B. C. Silva and J. P. Bilezikian, "Parathyroid hormone: Anabolic and catabolic actions on the skeleton," *Curr. Opin. Pharmacol.*, vol. 22, pp. 41–50, 2015.
- [227] D. D. Pierroz, A. Rufo, E. N. Bianchi, V. Glatt, M. Capulli, N. Rucci, F. Cavat, R. Rizzoli, A. Teti, M. L. Bouxsein, and S. L. Ferrari, "Beta-Arrestin2 regulates RANKL and ephrins gene expression in response to bone remodeling in mice.," *J. bone Miner. Res.*, vol. 24, no. 5, pp. 775–84, 2009.
- [228] S. Lossdörfer, W. Götz, and A. Jäger, "PTH(1-34)-induced changes in RANKL and OPG expression by human PDL cells modify osteoclast biology in a co-culture model with RAW 264.7 cells," *Clin. Oral Investig.*, vol. 15, no. 6, pp. 941–952, 2011.
- [229] M. Baker, "Reproducibility: Respect your cells," *Nature*, vol. 537, pp. 433–435, 2016.

- [230] G. J. Atkins, P. Kostakis, K. J. Welldon, C. Vincent, D. M. Findlay, and A. C. W. Zannettino, "Human trabecular bone-derived osteoblasts support human osteoclast formation in vitro in a defined, serum-free medium," *J. Cell. Physiol.*, vol. 203, no. 3, pp. 573–582, 2005.
- [231] Y. Shirai, Y. Yoshimura, Y. Yawaka, T. Hasegawa, T. Kikuri, S. Takeyama, A. Matsumoto, and H. Oguchi, "Effect of Extracellular Calcium Concentrations on Osteoclast Differentiation in Vitro," *Biochem. Biophys. Res. Commun.*, vol. 265, no. 2, pp. 484–488, 1999.
- [232] S. Takeyama, Y. Yoshimura, Y. Deyama, Y. Sugawara, H. Fukuda, and A. Matsumoto, "Phosphate Decreases Osteoclastogenesis in Coculture of Osteoblast and Bone Marrow," *Biochem. Biophys. Res. Commun.*, vol. 282, no. 3, pp. 798–802, 2001.
- [233] M. Shin, Y. Kim, S. Kim, G. Kim, and J. Baek, "High extracellular Ca²⁺ alone stimulates osteoclast formation but inhibits in the presence of other osteoclastogenic factors," *Exp. Mol. Med.*, vol. 35, no. 3, pp. 167–174, 2003.
- [234] T. C. Dandajena, M. A. Ihnat, B. Disch, J. Thorpe, and G. F. Currier, "Hypoxia triggers a HIF-mediated differentiation of peripheral blood mononuclear cells into osteoclasts," *Orthod. Craniofacial Res.*, vol. 15, no. 1, pp. 1–9, 2012.
- [235] R. Garimella, S. E. Tague, J. Zhang, F. Belibi, N. Nahar, B. H. Sun, K. Insogna, J. Wang, and H. C. Anderson, "Expression and Synthesis of Bone Morphogenetic Proteins by Osteoclasts: A Possible Path to Anabolic Bone Remodeling," *J. Histochem. Cytochem.*, vol. 56, no. 6, pp. 569–577, 2008.
- [236] L. Pederson, M. Ruan, J. J. Westendorf, S. Khosla, and M. J. Oursler, "Regulation of bone formation by osteoclasts involves Wnt/BMP signaling and the chemokine sphingosine-1-phosphate.," *Proc. Natl. Acad. Sci. U. S. A.*, vol. 105, no. 52, pp. 20764–9, 2008.
- [237] G. Luo, S. J. Sun, T. J. Weng, X. M. Li, Z. G. Wang, and B. Zhang, "Effect of osteoclasts on murine osteoblastic differentiation in early stage of co-culture," *Int. J. Clin. Exp. Med.*, vol. 9, no. 2, pp. 1062–1072, 2016.
- [238] B. M. Baker and C. S. Chen, "Deconstructing the third dimension - how 3D culture microenvironments alter cellular cues," *J. Cell Sci.*, vol. 125, no. 13, pp. 3015–3024, 2012.
- [239] S. Bose, M. Roy, and A. Bandyopadhyay, "Recent advances in bone tissue engineering scaffolds," *Trends Biotechnol.*, vol. 30, no. 10, pp. 546–554, 2012.
- [240] R. Owen, C. Sherborne, T. Paterson, N. H. Green, G. C. Reilly, and F.

- Claeysens, “Emulsion Templated Scaffolds with Tunable Mechanical Properties for Bone Tissue Engineering,” *J. Mech. Behav. Biomed. Mater.*, vol. 54, pp. 159–172, 2015.
- [241] K. Nakagawa, H. Abukawa, M. Y. Shin, H. Terai, M. J. Troulis, and J. P. Vacanti, “Osteoclastogenesis on Tissue-Engineered Bone,” *Tissue Eng.*, vol. 10, no. 1–2, pp. 93–100, 2004.
- [242] A. Bernhardt, S. Thieme, H. Domaschke, A. Springer, A. Rösen-Wolff, and M. Gelinsky, “Crosstalk of osteoblast and osteoclast precursors on mineralized collagen-towards an in vitro model for bone remodeling,” *J. Biomed. Mater. Res. - Part A*, vol. 95, no. 3 A, pp. 848–856, 2010.
- [243] A. Ruggiu, F. Tortelli, V. Komlev, F. Peyrin, and R. Cancedda, “Extracellular matrix deposition and scaffold biodegradation in an in vitro three-dimensional model of bone by X-ray computed microtomography,” *J. Tissue Eng. Regen. Med.*, vol. 8, no. 7, pp. 557–565, 2014.
- [244] M. Rubert, J. R. Vetsch, L. Lehtoviita, S. Hofmann, and R. Muller, “Bone remodelling imaging in a human-based in vitro co-culture model - A proof of concept,” *Eur. Cells Mater.*, vol. 33, no. Suppl. 2, 2017.
- [245] G. L. Jones, A. Motta, M. J. Marshall, A. J. El Haj, and S. H. Cartmell, “Osteoblast: osteoclast co-cultures on silk fibroin, chitosan and PLLA films.,” *Biomaterials*, vol. 30, no. 29, pp. 5376–84, Oct. 2009.
- [246] R. S. Hayden, J. P. Fortin, B. Harwood, B. Subramanian, K. P. Quinn, I. Georgakoudi, A. S. Kopin, and D. L. Kaplan, “Cell-tethered ligands modulate bone remodeling by osteoblasts and osteoclasts,” *Adv. Funct. Mater.*, vol. 24, no. 4, pp. 472–479, 2014.
- [247] R. S. Hayden, K. P. Quinn, C. A. Alonzo, I. Georgakoudi, and D. L. Kaplan, “Quantitative characterization of mineralized silk film remodeling during long-term osteoblast-osteoclast co-culture,” *Biomaterials*, vol. 35, no. 12, pp. 3794–3802, 2014.
- [248] R. S. Hayden, M. Vollrath, and D. L. Kaplan, “Effects of clodronate and alendronate on osteoclast and osteoblast co-cultures on silk-hydroxyapatite films,” *Acta Biomater.*, vol. 10, no. 1, pp. 486–493, 2014.
- [249] C. Heinemann, S. Heinemann, H. Worch, T. Hanke, and C. Heinemann, “Development of an osteoblast/osteoclast co-culture derived by human bone marrow stromal cells and human monocytes for biomaterials testing.,” *Eur Cell Mater.*, vol. 21, pp. 80–93, 2011.

- [250] A. Papadimitropoulos, A. Scherberich, S. Güven, N. Theilgaard, H. J. A. Crooijmans, F. Santini, K. Scheffler, A. Zallone, and I. Martin, “A 3D in vitro bone organ model using human progenitor cells,” *Eur. Cells Mater.*, vol. 21, pp. 445–458, 2011.
- [251] M. S. F. Clarke, A. Sundaresan, C. R. Vanderburg, M. G. Banigan, and N. R. Pellis, “A three-dimensional tissue culture model of bone formation utilizing rotational co-culture of human adult osteoblasts and osteoclasts,” *Acta Biomater.*, vol. 9, no. 8, pp. 7908–7916, 2013.
- [252] L. Penolazzi, A. Lolli, L. Sardelli, M. Angelozzi, E. Lambertini, L. Trombelli, F. Ciarpella, R. Vecchiadini, and R. Piva, “Establishment of a 3D-dynamic osteoblasts-osteoclasts co-culture model to simulate the jawbone microenvironment in vitro,” *Life Sci.*, vol. 152, pp. 82–93, 2016.
- [253] D. Mandatori, L. Penolazzi, C. Pipino, P. Di Tomo, S. Di Silvestre, N. Di Pietro, S. Trevisani, M. Angelozzi, M. Ucci, R. Piva, and A. Pandolfi, “Menaquinone-4 enhances osteogenic potential of human Amniotic Fluid Mesenchymal Stem Cells Cultured in a 2D and 3D dynamic culture system,” *J. Tissue Eng. Regen. Med.*, 2017.
- [254] P. Young, P. Tsimbouri, N. Gadegaard, M. RM, and D. MJ, “Osteoclastogenesis/osteoblastogenesis using human bone marrow-derived cocultures on nanotopographical polymer surfaces,” *Nanomedicine*, vol. 10, no. 6, pp. 949–957, 2015.
- [255] M. Bongio, S. Lopa, M. Gilardi, S. Bersini, and M. Moretti, “A 3D vascularized bone remodeling model combining osteoblasts and osteoclasts in a CaP nanoparticle-enriched matrix,” *Nanomedicine*, vol. 11, no. 9, pp. 1073–1091, 2016.
- [256] N. Giuliani, V. Rizzoli, G. D. Roodman, W. Dc, N. Giuliani, V. Rizzoli, and G. D. Roodman, “Multiple myeloma bone disease : pathophysiology of osteoblast inhibition Review in translational hematology Multiple myeloma bone disease : pathophysiology of osteoblast inhibition,” *Blood*, vol. 108, no. 13, pp. 3992–3996, 2014.
- [257] T. L. Andersen, K. Sjøe, T. E. Sondergaard, T. Plesner, and J. M. Delaisse, “Myeloma cell-induced disruption of bone remodelling compartments leads to osteolytic lesions and generation of osteoclast-myeloma hybrid cells: Research paper,” *Br. J. Haematol.*, vol. 148, no. 4, pp. 551–561, 2010.
- [258] L. Bubendorf, A. Schöpfer, U. Wagner, G. Sauter, H. Moch, N. Willi, T. C. Gasser, and M. J. Mihatsch, “Metastatic patterns of prostate cancer: An autopsy study of 1,589 patients,” *Hum. Pathol.*, vol. 31, no. 5, pp. 578–583, 2000.

- [259] S. N. Pentylala, J. Lee, K. Hsieh, W. C. Waltzer, a Trocchia, L. Musacchia, M. J. Rebecchi, and S. a Khan, “Prostate cancer: a comprehensive review.,” *Med. Oncol.*, vol. 17, no. 2, pp. 85–105, 2000.
- [260] B. I. Carlin and G. L. Andriole, “The natural history, skeletal complications, and management of bone metastases in patients with prostate carcinoma.,” *Cancer*, vol. 88, no. 12 Suppl, pp. 2989–2994, 2000.
- [261] A. Nordstrand, J. Nilsson, Å. ° Tieva, P. Wikström, U. H. Lerner, and A. Widmark, “Establishment and validation of an in vitro co-culture model to study the interactions between bone and prostate cancer cells,” *Clin. Exp. Metastasis*, vol. 26, no. 8, pp. 945–953, 2009.
- [262] Y. Li, D. Kong, A. Ahmad, B. Bao, and F. H. Sarkar, “Targeting bone remodeling by isoflavone and 3,3'-diindolylmethane in the context of prostate cancer bone metastasis,” *PLoS One*, vol. 7, no. 3, 2012.
- [263] C. Desantis, J. Ma, L. Bryan, and A. Jemal, “Breast Cancer Statistics , 2013,” *CA Cancer J. Clin.*, vol. 64, no. 1, pp. 52–62, 2013.
- [264] Y.-C. Chen, D. M. Sosnoski, and A. M. Mastro, “Breast cancer metastasis to the bone: mechanisms of bone loss.,” *Breast Cancer Res.*, vol. 12, no. 6, p. 215, 2010.
- [265] V. Krishnan, R. Dhurjati, E. A. Vogler, and A. M. Mastro, “Osteogenesis in vitro: From pre-osteoblasts to osteocytes,” *Vitr. Cell. Dev. Biol. - Anim.*, vol. 46, no. 1, pp. 28–35, 2010.
- [266] V. Krishnan, E. A. Vogler, D. M. Sosnoski, and A. M. Mastro, “In vitro mimics of bone remodeling and the vicious cycle of cancer in bone,” *J. Cell. Physiol.*, vol. 229, no. 4, pp. 453–462, 2014.
- [267] V. Krishnan, E. A. Vogler, and A. M. Mastro, “Three-Dimensional in Vitro Model to Study Osteobiology and Osteopathology,” *J. Cell. Biochem.*, vol. 116, no. 12, pp. 2715–2723, 2015.
- [268] A. Sophocleous, S. Marino, J. G. Logan, P. Mollat, S. H. Ralston, and A. I. Idris, “Bone cell-autonomous contribution of type 2 cannabinoid receptor to breast cancer-induced osteolysis,” *J. Biol. Chem.*, vol. 290, no. 36, pp. 22049–22060, 2015.
- [269] A. N. Lozano-Ondoua, K. E. Hanlon, A. M. Symons-Liguori, T. M. Largent-Milnes, J. J. Havelin, H. L. Ferland, A. Chandramouli, M. Owusu-Ankomah, T. Nikolich-Zugich, A. P. Bloom, J. M. Jimenez-Andrade, T. King, F. Porreca, M. A. Nelson, P. W. Mantyh, and T. W. Vanderah, “Disease modification of

breast cancer-induced bone remodeling by cannabinoid 2 receptor agonists,” *J. Bone Miner. Res.*, vol. 28, no. 1, pp. 92–107, 2013.

- [270] H. N. Kim, H. Ha, J. H. Lee, K. Jung, D. Yang, K. M. Woo, and Z. H. Lee, “Trichostatin A inhibits osteoclastogenesis and bone resorption by suppressing the induction of c-Fos by RANKL,” *Eur. J. Pharmacol.*, vol. 623, no. 1–3, pp. 22–29, 2009.
- [271] J. Huang, L. Yuan, X. Wang, T. L. Zhang, and K. Wang, “Icaritin and its glycosides enhance osteoblastic, but suppress osteoclastic, differentiation and activity in vitro,” *Life Sci.*, vol. 81, no. 10, pp. 832–840, 2007.
- [272] Y. Q. Liu, X. F. Han, T. Liu, M. C. Cheng, and H. Bin Xiao, “A cell-based model of bone remodeling for identifying activity of icarrin in the treatment of osteoporosis,” *Biotechnol. Lett.*, vol. 37, no. 1, pp. 219–226, 2015.
- [273] T. Negishi-Koga, M. Shinohara, N. Komatsu, H. Bito, T. Kodama, R. H. Friedel, and H. Takayanagi, “Suppression of bone formation by osteoclastic expression of semaphorin 4D,” *Nat. Med.*, vol. 17, no. 11, pp. 1473–1480, 2011.
- [274] Y. Zhang, L. Wei, R. J. Miron, B. Shi, and Z. Bian, “Anabolic bone formation via a site-specific bone-targeting delivery system by interfering with semaphorin 4d expression,” *J. Bone Miner. Res.*, vol. 30, no. 2, pp. 286–296, 2015.
- [275] S. Lossdörfer, B. Abou Jamra, B. Rath-Deschner, W. Götz, R. Abou Jamra, B. Braumann, and A. Jäger, “The Role of Periodontal Ligament Cells in Delayed Tooth Eruption in Patients with Cleidocranial Dysostosis*,” *J. Orofac. Orthop. / Fortschritte der Kieferorthopädie*, vol. 70, no. 6, pp. 495–510, 2009.
- [276] W. J. Yan, C. Y. Zhang, X. Yang, Z. N. Liu, X. Z. Wang, X. Y. Sun, Y. X. Wang, and S. G. Zheng, “Abnormal Differentiation of Dental Pulp Cells in Cleidocranial Dysplasia,” *J. Dent. Res.*, vol. 94, no. 4, pp. 577–583, 2015.
- [277] X. Z. Wang, X. Y. Sun, C. Y. Zhang, X. Yang, W. J. Yan, L. H. Ge, and S. G. Zheng, “RUNX2 Mutation Impairs $1\alpha,25$ -Dihydroxyvitamin D3 mediated Osteoclastogenesis in Dental Follicle Cells,” *Sci. Rep.*, vol. 6, no. April, p. 24225, 2016.
- [278] D. Granchi, E. Cenni, L. Savarino, G. Ciapetti, G. Forbicini, M. Vancini, C. Maini, N. Baldini, and A. Giunti, “Bone cement extracts modulate the osteoprotegerin/osteoprotegerin-ligand expression in MG63 osteoblast-like cells,” *Biomaterials*, vol. 23, no. 11, pp. 2359–2365, 2002.
- [279] H. Jablonski, H. Rekasi, and M. Jäger, “The influence of calcitonin gene-related

- peptide on markers of bone metabolism in MG-63 osteoblast-like cells co-cultured with THP-1 macrophage-like cells,” *BMS Musculoskelet. Disord.*, vol. 17, no. 199, pp. 1–12, 2016.
- [280] L. Wu, F. Feyerabend, A. F. Schilling, R. Willumeit-Römer, and B. J. C. Luthringer, “Effects of extracellular magnesium extract on the proliferation and differentiation of human osteoblasts and osteoclasts in coculture,” *Acta Biomater.*, vol. 27, pp. 294–304, 2015.
- [281] D. Wang, K. Christensen, K. Chawla, G. Xiao, P. H. Krebsbach, and R. T. Franceschi, “Isolation and characterization of MC3T3-E1 preosteoblast subclones with distinct in vitro and in vivo differentiation/mineralization potential,” *J. bone Miner. Res.*, vol. 14, no. 6, pp. 893–903, 1999.
- [282] D. A. Towler and R. St. Arnaud, “Use of Cultured Osteoblastic Cells to Identify and Characterize Transcriptional Regulatory Complexes,” in *Principles of Bone Biology Volume 1*, Second Edi., J. P. Bilezikian, L. G. Raisz, and G. A. Rodan, Eds. 2002, pp. 1503–1527.
- [283] S. M. Woo, J. Rosser, V. Dusevich, I. Kalajzic, and L. F. Bonewald, “Cell line IDG-SW3 replicates osteoblast-to-late-osteocyte differentiation in vitro and accelerates bone formation in vivo,” *J. Bone Miner. Res.*, vol. 26, no. 11, pp. 2634–2646, 2011.
- [284] Y. Kato, a Boskey, L. Spevak, M. Dallas, M. Hori, and L. F. Bonewald, “Establishment of an osteoid preosteocyte-like cell MLO-A5 that spontaneously mineralizes in culture,” *J. Bone Miner. Res.*, vol. 16, no. 9, pp. 1622–33, 2001.
- [285] A. . Stern, M. . Stern, M. . Van Dyke, K. Jähn, M. Prideaux, and L. . Bonewald, “Isolation and culture of primary osteocytes from the long bones of skeletally mature and aged mice,” *Biotechniques*, vol. 52, no. 6, pp. 361–373, 2012.
- [286] C. Karlsson, K. Emanuelsson, F. Wessberg, K. Kajic, M. Z. Axell, P. S. Eriksson, A. Lindahl, J. Hyllner, and R. Strehl, “Human embryonic stem cell-derived mesenchymal progenitors-Potential in regenerative medicine,” *Stem Cell Res.*, vol. 3, no. 1, pp. 39–50, 2009.
- [287] B. L. Cuetara, T. N. Crotti, A. J. O’Donoghue, and K. P. Mchugh, “Cloning and characterization of osteoclast precursors from the RAW264.7 cell line,” *Vitr. Cell. Dev. Biol. - Anim.*, vol. 42, no. 7, pp. 182–188, 2010.
- [288] J. O’Brien, I. Wilson, T. Orton, and F. Pognan, “Investigation of the Alamar Blue (resazurin) fluorescent dye for the assessment of mammalian cell cytotoxicity,” *Eur. J. Biochem.*, vol. 267, no. 17, pp. 5421–5426, 2000.

- [289] C. a. Gregory, W. G. Gunn, A. Peister, and D. J. Prockop, "An Alizarin red-based assay of mineralization by adherent cells in culture: Comparison with cetylpyridinium chloride extraction," *Anal. Biochem.*, vol. 329, no. 1, pp. 77–84, 2004.
- [290] M. N. Dugard, C. A. Sharp, S. F. Evans, J. H. Williams, M. W. Davie, and M. J. Marshall, "A bio-assay for effectors of osteoclast differentiation in serum from patients with bone disease," *Clin Chim Acta*, vol. 356, no. 1–2, pp. 154–163, 2005.
- [291] O. Brennan, O. D. Kennedy, T. C. Lee, S. M. Rackard, and F. J. O'Brien, "Biomechanical properties across trabeculae from the proximal femur of normal and ovariectomised sheep," *J. Biomech.*, vol. 42, no. 4, pp. 498–503, 2009.
- [292] L. M. McNamara, A. G. H. Ederveen, C. G. Lyons, C. Price, M. B. Schaffler, H. Weinans, and P. J. Prendergast, "Strength of cancellous bone trabecular tissue from normal, ovariectomized and drug-treated rats over the course of ageing," *Bone*, vol. 39, no. 2, pp. 392–400, 2006.
- [293] B. Busse, M. Hahn, M. Soltau, J. Zustin, K. Püschel, G. N. Duda, and M. Amling, "Increased calcium content and inhomogeneity of mineralization render bone toughness in osteoporosis: Mineralization, morphology and biomechanics of human single trabeculae," *Bone*, vol. 45, no. 6, pp. 1034–1043, 2009.
- [294] O. Brennan, F. J. Obrien, and L. McNamara, "Estrogen plus estrogen receptor antagonists alter mineral production by osteoblasts in vitro," *Horm. Metab. Res.*, vol. 44, no. 1, pp. 47–53, 2012.
- [295] A. A. Lloyd, B. Gludovatz, C. Riedel, E. A. Luengo, R. Saiyed, E. Marty, D. G. Lorich, J. M. Lane, R. O. Ritchie, B. Busse, and E. Donnelly, "Atypical fracture with long-term bisphosphonate therapy is associated with altered cortical composition and reduced fracture resistance," *Proc. Natl. Acad. Sci.*, vol. 114, no. 33, p. 201704460, 2017.
- [296] S. a Krum, G. a Miranda-Carboni, P. V Hauschka, J. S. Carroll, T. F. Lane, L. P. Freedman, and M. Brown, "Estrogen protects bone by inducing Fas ligand in osteoblasts to regulate osteoclast survival.," *EMBO J.*, vol. 27, no. 3, pp. 535–545, 2008.
- [297] S. Manolagas, S. Kousteni, and R. L. Jilka, "Sex Steroids and Bone," *Recent Prog. Horm. Res.*, vol. 57, pp. 385–409, 2002.
- [298] A. B. Khalid and S. A. Krum, "Estrogen receptors alpha and beta in bone,"

Bone, vol. 87, pp. 130–135, 2016.

- [299] F.-P. Chen, N. Lee, K.-C. Wang, Y.-K. Soong, and K.-E. Huang, “Effect of estrogen and 1[alpha],25(OH)₂- vitamin D₃ on the activity and growth of human primary osteoblast-like cells in vitro,” *Fertility and Sterility*, vol. 77, no. 5. pp. 1038–1043, 2002.
- [300] L. G. Rao, L. J.-F. Liu, T. M. Murray, E. McDermott, and X. Zhang, “Estrogen added intermittently, but not continuously, stimulates differentiation and bone formation in SaOS-2 cells.,” *Biol. Pharm. Bull.*, vol. 26, no. 7, pp. 936–945, 2003.
- [301] J. A. Robinson, S. A. Harris, B. L. Riggs, and T. C. Spelsberg, “Estrogen regulation of human osteoblastic cell proliferation and differentiation,” *Endocrinology*, vol. 138, no. 7, pp. 2919–2927, 1997.
- [302] D. Rickard, S. A. Harris, R. Turner, S. Khosla, and T. C. Spelsberg, “Estrogens and Progestins,” in *Principles of Bone Biology*, Second., vol. 1, J. P. Bilezikian, L. G. Raisz, and G. A. Rodan, Eds. Academic Press, 2002, pp. 655–675.
- [303] N. Patlas, Y. Zadik, P. Yaffe, M. Patlas, Z. Schwartz, and A. Ornoy, “The response to sex steroid hormones and vitamin D of cultured osteoblasts derived from ovariectomized mice with and without 17β-estradiol pretreatment,” *Odontology*, vol. 93, no. 1. pp. 16–23, 2005.
- [304] J. B. Park, “Effects of low doses of estrone on the proliferation, differentiation and mineralization of osteoprecursor cells,” *Exp. Ther. Med.*, vol. 4, no. 4, pp. 681–684, 2012.
- [305] S. Kousteni, J. . Chen, T. Bellido, L. Han, A. . Ali, C. . O’Brien, L. Plotkin, Q. Fu, A. . Mancino, Y. Wen, A. . Vertino, C. . Powers, A. . Stewart, R. Ebert, A. . Parfitt, R. . Weinstein, R. . Jilka, and S. . Manolagas, “Reversal of Bone Loss in Mice by Nongenotropic Signaling of Sex Steroids,” *Science (80-.)*, vol. 298, no. 5594, pp. 843–846, 2002.
- [306] J. B. Park, “The effects of fulvestrant, an estrogen receptor antagonist, on the proliferation, differentiation and mineralization of osteoprecursor cells,” *Molecular Medicine Reports*, vol. 7, no. 2. pp. 555–558, 2013.
- [307] G. Passeri, G. Girasole, R. . Jilka, and S. . Manolagas, “Increased interleukin-6 production by murine bone marrow and bone cells after estrogen withdrawal,” *Endocrinology*, vol. 133, no. 2, pp. 822–828, 1993.
- [308] M. Á. Brennan, M. G. Haugh, F. J. O’Brien, and L. M. McNamara, “Estrogen withdrawal from osteoblasts and osteocytes causes increased mineralization

and apoptosis,” *Horm. Metab. Res.*, vol. 46, no. 8, pp. 537–545, 2014.

- [309] N. K. Shevde, a C. Bendixen, K. M. Dienger, and J. W. Pike, “Estrogens suppress RANK ligand-induced osteoclast differentiation via a stromal cell independent mechanism involving c-Jun repression.,” *Proc. Natl. Acad. Sci. U. S. A.*, vol. 97, no. 14, pp. 7829–7834, 2000.
- [310] V. G. Palacios, L. J. Robinson, C. W. Borysenko, T. Lehmann, S. E. Kalla, and H. C. Blair, “Negative regulation of RANKL-induced osteoclastic differentiation in RAW264.7 cells by estrogen and phytoestrogens,” *J. Biol. Chem.*, vol. 280, no. 14, pp. 13720–13727, 2005.
- [311] I. Kalajzic, A. Braut, D. Guo, X. Jiang, M. S. Kronenberg, M. Mina, M. A. Harris, S. E. Harris, and D. W. Rowe, “Dentin matrix protein 1 expression during osteoblastic differentiation, generation of an osteocyte GFP-transgene,” *Bone*, vol. 35, no. 1, pp. 74–82, 2004.
- [312] Y. Berthois, J. A. Katzenellenbogen, and B. S. Katzenellenbogen, “Phenol red in tissue culture media is a weak estrogen: implications concerning the study of estrogen-responsive cells in culture.,” *Proc. Natl. Acad. Sci. U. S. A.*, vol. 83, no. 8, pp. 2496–500, 1986.
- [313] J. Wesierska-Gadek, T. Schreiner, M. Maurer, A. Waringer, and C. Ranftler, “Phenol red in the culture medium strongly affects the susceptibility of human MCF-7 cells to roscovitine.,” *Cell. Mol. Biol. Lett.*, vol. 12, no. 2, pp. 280–293, 2007.
- [314] W. V. Welshons, M. F. Wolf, C. S. Murphy, and V. C. Jordan, “Estrogenic activity of phenol red,” *Mol. Cell. Endocrinol.*, vol. 57, no. 3, pp. 169–178, 1988.
- [315] M. Ernst, C. Schmid, and E. R. Froesch, “Phenol red mimics biological actions of estradiol: Enhancement of osteoblast proliferation in vitro and of type I collagen gene expression in bone and uterus of rats in vivo,” *J. Steroid Biochem.*, vol. 33, no. 5, pp. 907–914, 1989.
- [316] J. E. Moreno-Cuevas and D. A. Sirbasku, “Estrogen mitogenic action. III. Is phenol red a ‘red herring’?,” *Vitr. Cell. Dev. Biol. - Anim.*, vol. 36, no. 7, pp. 447–464, 2000.
- [317] Z. C. Dang and C. W. G. M. Lowik, “Removal of serum factors by charcoal treatment promotes adipogenesis via a MAPK-dependent pathway,” *Mol. Cell. Biochem.*, vol. 268, no. 1–2, pp. 159–167, 2005.
- [318] L. M. Schäck, S. Noack, R. Winkler, G. Wißmann, P. Behrens, M. Wellmann,

- M. Jagodzinski, C. Krettek, and A. Hoffmann, “The Phosphate Source Influences Gene Expression and Quality of Mineralization during In Vitro Osteogenic Differentiation of Human Mesenchymal Stem Cells,” *PLoS One*, vol. 8, no. 6, 2013.
- [319] J. P. Cassella, N. Garrington, T. B. C. Stamp, and S. Y. Ali, “An Electron-Probe X-ray Microanalytical Study of Bone-Mineral in Osteogenesis Imperfecta,” *Calcif. Tissue Int.*, vol. 56, no. 2, pp. 118–122, 1995.
- [320] D. J. Haisenleder, A. H. Schoenfelder, E. S. Marcinko, L. M. Geddis, and J. C. Marshall, “Estimation of estradiol in mouse serum samples: Evaluation of commercial estradiol immunoassays,” *Endocrinology*, vol. 152, no. 11, pp. 4443–4447, 2011.
- [321] R. M. Delaine-Smith, S. MacNeil, and G. C. Reilly, “Matrix production and collagen structure are enhanced in two types of osteogenic progenitor cells by a simple fluid shear stress stimulus,” *Eur. Cells Mater.*, vol. 24, no. 0, pp. 162–174, 2012.
- [322] C. Wittkowske, “The role of mechanical forces in bone formation: Evaluation of long-term responses by osteoblasts to low fluid shear stress in vitro [PhD Thesis],” Sheffield, 2016.
- [323] V. Rochira, E. Kara, and C. Carani, “The Endocrine Role of Estrogens on Human Male Skeleton Vincenzo,” *Int. J. Endocrinol.*, vol. 2015, 2015.
- [324] E. M. Lewiecki, “Role of sclerostin in bone and cartilage and its potential as a therapeutic target in bone diseases.,” *Ther. Adv. Musculoskelet. Dis.*, vol. 6, no. 2, pp. 48–57, 2014.
- [325] M. Robin, C. Almeida, T. Azaïs, B. Haye, C. Illoul, J. Lesieur, M. M. Giraud-Guille, N. Nassif, and C. Hélyary, “Involvement of 3D osteoblast migration and bone apatite during in vitro early osteocytogenesis,” *Bone*, vol. 88, pp. 146–156, 2016.
- [326] M. Prideaux, N. Loveridge, A. A. Pitsillides, and C. Farquharson, “Extracellular matrix mineralization promotes E11/gp38 glycoprotein expression and drives osteocytic differentiation,” *PLoS One*, vol. 7, no. 5, pp. 1–11, 2012.
- [327] K. Irie, S. Ejiri, Y. Sakakura, T. Shibui, and T. Yajima, “Matrix Mineralization as a Trigger for Osteocyte Maturation,” *J. Histochem. Cytochem.*, vol. 56, no. 6, pp. 561–567, 2008.
- [328] L. C. Hofbauer, S. Kholsa, C. R. Dunstan, D. L. Lacey, T. C. Spelsberg, and B.

- L. Riggs, "Estrogen stimulates gene expression and protein production of osteoprotegerin in human osteoblastic cells," *Endocrinology*, vol. 140, no. 9, pp. 4367–4370, 1999.
- [329] B. L. Riggs, "The mechanisms of estrogen regulation of bone resorption," *The J. Clin. Investig.*, vol. 106, no. 10, pp. 1203–1204, 2000.
- [330] Y. Fujiwara, M. Piemontese, Y. Liu, J. D. Thostenson, J. Xiong, and C. A. O'Brien, "RANKL (Receptor Activator of NFκB Ligand) produced by osteocytes is required for the increase in B cells and bone loss caused by estrogen deficiency in mice," *J. Biol. Chem.*, vol. 291, no. 48, pp. 24838–24850, 2016.
- [331] A. G. Turner, M. A. Hanrath, H. A. Morris, G. J. Atkins, and P. H. Anderson, "The local production of 1,25(OH)₂D₃ promotes osteoblast and osteocyte maturation," *J. Steroid Biochem. Mol. Biol.*, vol. 144, no. PART A, pp. 114–118, 2014.
- [332] J. Delgado-Calle, J. Anderson, M. D. Cregor, M. Hiasa, J. M. Chirgwin, N. Carlesso, T. Yoneda, K. S. Mohammad, L. I. Plotkin, G. D. Roodman, and T. Bellido, "Bidirectional notch signaling and osteocyte-derived factors in the bone marrow microenvironment promote tumor cell proliferation and bone destruction in multiple myeloma," *Cancer Res.*, vol. 76, no. 5, pp. 1089–1100, 2016.
- [333] B. Li, D. Lu, Y. Chen, M. Zhao, and L. Zuo, "Unfractionated heparin promotes osteoclast formation in vitro by inhibiting osteoprotegerin activity," *Int. J. Mol. Sci.*, vol. 17, no. 4, 2016.
- [334] N. Scully, "Differentiation of osteoblasts to osteocytes in 3D type I collagen gels - a novel tool to study osteocyte responses to mechanical loading," Cardiff University, 2015.
- [335] J. M. Spatz, M. N. Wein, J. H. Gooi, Y. Qu, J. L. Garr, S. Liu, K. J. Barry, Y. Uda, F. Lai, C. Dedic, M. Balcells-Camps, H. M. Kronenberg, P. Babij, and P. D. Pajevic, "The Wnt inhibitor sclerostin is up-regulated by mechanical unloading in osteocytes in vitro," *J. Biol. Chem.*, vol. 290, no. 27, pp. 16744–16758, 2015.
- [336] N. Zhao, F. H. Nociti, P. Duan, M. Prideaux, H. Zhao, B. L. Foster, M. J. Somerman, and L. F. Bonewald, "Isolation and Functional Analysis of an Immortalized Murine Cementocyte Cell Line, IDG-CM6," *J. Bone Miner. Res.*, vol. 31, no. 2, pp. 430–442, 2016.
- [337] M. Kogawa, P. H. Anderson, D. M. Findlay, H. A. Morris, and G. J. Atkins,

- “The metabolism of 25-(OH)vitamin D₃ by osteoclasts and their precursors regulates the differentiation of osteoclasts,” *J. Steroid Biochem. Mol. Biol.*, vol. 121, no. 1–2, pp. 277–280, 2010.
- [338] S. Christakos, L. Liebsbet, R. Masuyama, and G. Carmeliet, “Vitamin D endocrine system and the intestine,” *Bonekey Rep.*, vol. 3, no. February, pp. 1–7, 2014.
- [339] A. Zarei, A. Morovat, K. Javaid, and C. P. Brown, “Vitamin D receptor expression in human bone tissue and dose-dependent activation in resorbing osteoclasts,” *Bone Res.*, vol. 4, no. August, p. 16030, 2016.
- [340] H. C. St. John, K. A. Bishop, M. B. Meyer, N. A. Benkusky, N. Leng, C. Kendzioriski, L. F. Bonewald, and J. W. Pike, “The Osteoblast to Osteocyte Transition: Epigenetic Changes and Response to the Vitamin D₃ Hormone,” *Mol. Endocrinol.*, vol. 28, no. 7, pp. 1150–1165, 2014.
- [341] D. Yang, A. G. Turner, A. R. Wijenayaka, P. H. Anderson, H. A. Morris, and G. J. Atkins, “1,25-Dihydroxyvitamin D₃ and extracellular calcium promote mineral deposition via NPP1 activity in a mature osteoblast cell line MLO-A5,” *Mol. Cell. Endocrinol.*, vol. 412, pp. 140–147, 2015.
- [342] L. Song, X. Zhang, and Y. Zhou, “A synergetic role of 1,25-dihydroxyvitamin D₃ in 17β-estradiol induced-proliferation and differentiation of osteoblastic MC3T3-E1 cells,” *European Journal of Pharmacology*, vol. 659, no. 2–3, pp. 273–280, 2011.
- [343] P. H. Anderson and G. J. Atkins, “The skeleton as an intracrine organ for vitamin D metabolism,” *Mol. Aspects Med.*, vol. 29, no. 6, pp. 397–406, 2008.
- [344] Y. Okada, I. Morimoto, K. Ura, K. Watanabe, S. Eto, M. Kumegawa, L. Raisz, C. Pilbeam, and Y. Tanaka, “Cell-to-Cell adhesion via intercellular adhesion molecule-1 and leukocyte function-associated antigen-1 pathway is involved in 1α,25(OH)₂D₃, PTH and IL-1α-induced osteoclast differentiation and bone resorption,” *Endocr. J.*, vol. 49, no. 4, pp. 483–495, 2002.
- [345] G. J. Atkins, P. Kostakis, B. Pan, A. Farrugia, S. Gronthos, A. Evdokiou, K. Harrison, D. M. Findlay, and A. C. W. Zannettino, “RANKL expression is related to the differentiation state of human osteoblasts,” *J. Bone Miner. Res.*, vol. 18, no. 6, pp. 1088–1098, 2003.
- [346] T. Nakashima, M. Hayashi, T. Fukunaga, K. Kurata, M. Oh-hora, J. Q. Feng, L. F. Bonewald, T. Kodama, A. Wutz, E. F. Wagner, J. M. Penninger, and H. Takayanagi, “Evidence for osteocyte regulation of bone homeostasis through RANKL expression,” *Nat. Med.*, vol. 17, no. 10, pp. 1231–1234, 2011.

- [347] C. Vincent, M. Kogawa, D. M. Findlay, and G. J. Atkins, "The generation of osteoclasts from RAW 264.7 precursors in defined, serum-free conditions," *J. Bone Miner. Metab.*, vol. 27, no. 1, pp. 114–119, 2009.
- [348] Y. Lu, G. Wang, W. Xu, P. Tao, X. Lv, and Y. Wang, "Tartrate-resistant acid phosphatase 5b is a marker of osteoclast number and volume in RAW 264.7 cells treated with receptor-activated nuclear κ B ligand.pdf," *Exp. Ther. Med.*, vol. 9, pp. 143–146, 2015.
- [349] B. Ek-Rylander, M. Flores, M. Wendel, D. Heinegard, and G. Andersson, "Dephosphorylation of osteopontin and bone sialoprotein by osteoclastic tartrate-resistant acid phosphatase. Modulation of osteoclast adhesion in vitro," *J. Biol. Chem.*, vol. 269, no. 21, pp. 14853–14856, 1994.
- [350] J. M. Halleen, S. Raisanen, J. J. Salo, V. Sakamuri, G. D. Roodman, T. A. Hentunen, P. P. Lehenkari, H. Kaija, P. Vihko, and H. K. Vaananen, "Intracellular Fragmentation of Bone Resorption Products by Reactive Oxygen Species Generated by Osteoclastic Tartrate-resistant Acid Phosphatase," *J. Biol. Chem.*, vol. 274, no. 33, pp. 22907–22911, 1999.
- [351] A. R. Hayman and T. M. Cox, "Purple Acid Phosphatase of the Human Macrophage and Osteoclast," *J. Bio. Chem.*, vol. 269, pp. 1294–1300, 1994.
- [352] J. M. Halleen, S. L. Alatalo, H. Suominen, S. Cheng, a J. Janckila, and H. K. Väänänen, "Tartrate-resistant acid phosphatase 5b: a novel serum marker of bone resorption.," *J. Bone Miner. Res.*, vol. 15, no. 7, pp. 1337–45, 2000.
- [353] T. Y. Chao, Y. Y. Wu, and A. J. Janckila, "Tartrate-resistant acid phosphatase isoform 5b (TRACP 5b) as a serum maker for cancer with bone metastasis," *Clin. Chim. Acta*, vol. 411, no. 21–22, pp. 1553–1564, 2010.
- [354] a J. Janckila, K. Takahashi, S. Z. Sun, and L. T. Yam, "Naphthol-ASBI phosphate as a preferred substrate for tartrate-resistant acid phosphatase isoform 5b.," *J. Bone Miner. Res.*, vol. 16, no. 4, pp. 788–793, 2001.
- [355] R. Song, X. Liu, J. Zhu, Q. Gao, Q. Wang, J. Zhang, D. Wang, L. Cheng, D. Hu, Y. Yuan, J. Gu, and Z. Liu, "RhoV mediates apoptosis of RAW264.7 macrophages caused by osteoclast differentiation," *Mol. Med. Rep.*, vol. 11, no. 2, pp. 1153–1159, 2015.
- [356] A. H. Lutter, U. Hempel, U. Anderer, and P. Dieter, "Biphasic influence of PGE2 on the resorption activity of osteoclast-like cells derived from human peripheral blood monocytes and mouse RAW264.7 cells," *Prostaglandins Leukot. Essent. Fat. Acids*, vol. 111, pp. 1–7, 2016.

- [357] V. Deepak, A. Kasonga, M. C. Kruger, and M. Coetzee, “Inhibitory effects of eugenol on RANKL-induced osteoclast formation via attenuation of NF- κ B and MAPK pathways,” *Connect. Tissue Res.*, vol. 56, no. 3, pp. 195–203, 2015.
- [358] Y. Zhu, Y. Wu, Y. Liang, W. Tan, Z. Liu, and J. Xiao, “Regulation of expression level of fms-like tyrosine kinase-4 is related to osteoclast differentiation,” *Arch. Med. Sci.*, vol. 3, pp. 502–506, 2016.
- [359] Y.-Q. Liu, Z.-L. Hong, L.-B. Zhan, H.-Y. Chu, X.-Z. Zhang, and G.-H. Li, “Wedelolactone enhances osteoblastogenesis by regulating Wnt/ β -catenin signaling pathway but suppresses osteoclastogenesis by NF- κ B/c-fos/NFATc1 pathway,” *Sci. Rep.*, vol. 6, no. 1, p. 32260, 2016.
- [360] C. Ghayor, R. M. Corroero, K. Lange, L. S. Karfeld-Sulzer, K. W. Grätz, and F. E. Weber, “Inhibition of osteoclast differentiation and bone resorption by N-methylpyrrolidone,” *J. Biol. Chem.*, vol. 286, no. 27, pp. 24458–24466, 2011.
- [361] S. J. Hollister, “Porous scaffold design for tissue engineering,” *Nat. Mater.*, vol. 4, no. 7, pp. 518–524, 2005.
- [362] S. M. Mantila Roosa, J. M. Kemppainen, E. N. Moffitt, P. H. Krebsbach, and S. J. Hollister, “The pore size of polycaprolactone scaffolds has limited influence on bone regeneration in an in vivo model,” *J. Biomed. Mater. Res. - Part A*, vol. 92, no. 1, pp. 359–368, 2010.
- [363] P. Kasten, I. Beyen, P. Niemeyer, R. Luginbühl, M. Bohner, and W. Richter, “Porosity and pore size of beta-tricalcium phosphate scaffold can influence protein production and osteogenic differentiation of human mesenchymal stem cells: an in vitro and in vivo study,” *Acta biomaterialia*, vol. 4, no. 6, pp. 1904–1915, 2008.
- [364] V. Karageorgiou and D. Kaplan, “Porosity of 3D biomaterial scaffolds and osteogenesis,” *Biomaterials*, vol. 26, no. 27, pp. 5474–5491, 2005.
- [365] Y. Cao, G. Mitchell, A. Messina, L. Price, E. Thompson, A. Penington, W. Morrison, A. O’Connor, G. Stevens, and J. Cooper-White, “The influence of architecture on degradation and tissue ingrowth into three-dimensional poly(lactic-co-glycolic acid) scaffolds in vitro and in vivo,” *Biomaterials*, vol. 27, no. 14, pp. 2854–2864, 2006.
- [366] Q. Chen, C. Zhu, and G. a Thouas, “Progress and challenges in biomaterials used for bone tissue engineering: bioactive glasses and elastomeric composites,” *Prog. Biomater.*, vol. 1, no. 1, p. 2, 2012.
- [367] A. Campos Marin and D. Lacroix, “The inter-sample structural variability of

regular tissue-engineered scaffolds significantly affects the micromechanical local cell environment,” *Interface Focus*, vol. 5, no. 2, pp. 20140097–20140097, 2015.

- [368] A. C. Marin, T. Grossi, E. Bianchi, G. Dubini, and D. Lacroix, “ μ -Particle Tracking Velocimetry and Computational Fluid Dynamics study of cell seeding within a 3D porous scaffold,” *J. Mech. Behav. Biomed. Mater.*, 2017.
- [369] D. W. Hutmacher, “Scaffold design and fabrication technologies for engineering tissues--state of the art and future perspectives.,” *J. Biomater. Sci. Polym. Ed.*, vol. 12, no. 1, pp. 107–124, 2001.
- [370] S. A. Bencherif, T. M. Braschler, and P. Renaud, “Advances in the design of macroporous polymer scaffolds for potential applications in dentistry,” *J. Periodontal Implant Sci.*, vol. 43, no. 6, pp. 251–261, 2013.
- [371] J. Kim, M. J. Yaszemski, and L. Lu, “Three-dimensional porous biodegradable polymeric scaffolds fabricated with biodegradable hydrogel porogens.,” *Tissue Eng. Part C. Methods*, vol. 15, no. 4, pp. 583–594, 2009.
- [372] A. S. Hayward, A. M. Eissa, D. J. Maltman, N. Sano, S. A. Przyborski, and N. R. Cameron, “Galactose-functionalized polyHIPE scaffolds for use in routine three dimensional culture of mammalian hepatocytes,” *Biomacromolecules*, vol. 14, no. 12, pp. 4271–4277, 2013.
- [373] G. Akay, M. a. Birch, and M. a. Bokhari, “Microcellular polyHIPE polymer supports osteoblast growth and bone formation in vitro,” *Biomaterials*, vol. 25, no. 18, pp. 3991–4000, 2004.
- [374] R. J. Narayan, A. Doraiswamy, D. B. Chrisey, and B. N. Chichkov, “Medical prototyping using two photon polymerization,” *Mater. Today*, vol. 13, no. 12, pp. 42–48, 2010.
- [375] D. W. Johnson, C. Sherborne, M. P. Didsbury, C. Pateman, N. R. Cameron, and F. Claeysens, “Macrostructuring of emulsion-templated porous polymers by 3D laser patterning,” *Adv. Mater.*, vol. 25, no. 23, pp. 3178–3181, 2013.
- [376] J. a. Lewis and G. M. Gratson, “Direct writing in three dimensions,” *Mater. Today*, vol. 7, no. 7, pp. 32–39, 2004.
- [377] S. Kawata, H. Sun, T. Tanaka, and K. Takada, “Finer features for functional microdevices,” *Nature*, vol. 412, no. 6848, pp. 697–698, 2001.
- [378] J. Stampfl, S. Baudis, C. Heller, R. Liska, A. Neumeister, and R. Kling, “Photopolymers with tunable mechanical properties processed by laser-based

- high-resolution stereolithography,” *J. Micromechanics Microengineering*, vol. 18, no. 12, p. 125014, 2008.
- [379] F. P. W. Melchels, J. Feijen, and D. W. Grijpma, “A review on stereolithography and its applications in biomedical engineering,” *Biomaterials*, vol. 31, no. 24, pp. 6121–6130, 2010.
- [380] J. T. Davies, “A quantitative kinetic theory of emulsion type, I. Physical chemistry of the emulsifying agent,” *Proc. 2nd Int. Congr. Surf. Act.*, vol. 1, pp. 426–38, 1957.
- [381] W. C. Griffin, “Calculation of HLB values of non-ionic surfactants,” *J. Soc. Cosmet. Chem.*, pp. 249–256, 1954.
- [382] N. R. Cameron and D. C. Sherrington, “High internal phase emulsions (HIPEs) --- Structure, properties and use in polymer preparation,” in *Biopolymers Liquid Crystalline Polymers Phase Emulsion*, Berlin, Heidelberg: Springer Berlin Heidelberg, 1996, pp. 163–214.
- [383] K. J. Lissant, “The Geometry of High-Internal-Phase-Ratio Emulsions,” vol. m, pp. 462–468, 1966.
- [384] J. M. Williams and D. A. Wroblewski, “Spatial Distribution of the Phases in Water-in-Oil Emulsions. Open and Closed Microcellular Foams from Cross-Linked Polystyrene?,” pp. 656–662, 1988.
- [385] N. R. Cameron, D. C. Sherrington, L. Albiston, and D. P. Gregory, “Study of the formation of the open-cellular morphology of poly(styrene/divinylbenzene) polyHIPE materials by cryo-SEM,” *Colloid Polym. Sci.*, vol. 274, no. 6, pp. 592–595, 1996.
- [386] A. Menner and A. Bismarck, “New evidence for the mechanism of the pore formation in polymerising high internal phase emulsions or why polyHIPEs have an interconnected pore network structure,” *Macromol. Symp.*, vol. 242, pp. 19–24, 2006.
- [387] M. Sušec, S. C. Ligon, J. Stampfl, R. Liska, and P. Krajnc, “Hierarchically porous materials from layer-by-layer photopolymerization of high internal phase emulsions,” *Macromol. Rapid Commun.*, vol. 34, no. 11, pp. 938–943, 2013.
- [388] I. Cooperstein, M. Layani, and S. Magdassi, “3D printing of porous structures by UV-curable O / W emulsion for fabrication of conductive objects †,” *J. Mater. Chem. C Mater. Opt. Electron. devices*, vol. 0, pp. 1–5, 2015.

- [389] R. Owen, “3-D Structuring for Bone Tissue Engineering Applications,” University of Sheffield, 2014.
- [390] A. Wang, T. Paterson, R. Owen, C. Sherborne, J. Dugan, J. Li, and F. Claeysens, “Photocurable high internal phase emulsions (HIPEs) containing hydroxyapatite for additive manufacture of tissue engineering scaffolds with multi-scale porosity,” *Mater. Sci. Eng. C*, vol. 67, pp. 51–58, Oct. 2016.
- [391] I. Pulko and P. Krajnc, “High internal phase emulsion templating--a path to hierarchically porous functional polymers.,” *Macromol. Rapid Commun.*, vol. 33, no. 20, pp. 1731–46, 2012.
- [392] C. a Schneider, W. S. Rasband, and K. W. Eliceiri, “NIH Image to ImageJ: 25 years of image analysis,” *Nat. Methods*, vol. 9, no. 7, pp. 671–675, 2012.
- [393] R. J. Carnachan, M. Bokhari, S. a. Przyborski, and N. R. Cameron, “Tailoring the morphology of emulsion-templated porous polymers.,” pp. 608–616, 2006.
- [394] L. Polo-Corrales, M. Latorre-Esteves, and J. . Ramirez-Vick, “Scaffold Design for Bone Regeneration,” *J. Nanosci. Nanotechnol.*, vol. 14, no. 1, pp. 15–56, 2014.
- [395] S. Puwanun, R. M. Delaine-Smith, H. E. Colley, J. M. Yates, S. MacNeil, and G. C. Reilly, “A simple rocker-induced mechanical stimulus upregulates mineralization by human osteoprogenitor cells in fibrous scaffolds,” *J. Tissue Eng. Regen. Med.*, no. August 2016, pp. 1–12, 2017.
- [396] T. Paterson, “PolyHIPE Microspheres for Injectable Bone Tissue Engineering Applications,” University of Sheffield, 2017.
- [397] A. Malayeri, C. Sherborne, T. Paterson, S. Mittar, I. O. Asencio, P. V Hatton, and F. Claeysens, “Osteosarcoma growth on trabecular bone mimicking structures manufactured via laser direct write,” *Int. J. Bioprinting*, vol. 2, no. 2, pp. 67–77, 2016.
- [398] M. Brunelli, “A Mechanobiology Study on the Response To Mechanical Compression of Mesenchymal Progenitor Cells Cultured in a Composite Scaffold Made of 3D Insert ® Pcl and Collagen Gel,” University of Sheffield, 2015.
- [399] M. Khandaker, M. B. Vaughan, and B. Starly, “The Influence of MgO Nanoparticles on the Osseointegration of Polycaprolactone - Sodium Alginate Hydrogel Interfaces,” vol. 4, no. 1, pp. 79–88, 2014.
- [400] M. S. Ventura Ferreira, W. Jahnen-Dechent, N. Labude, M. Bovi, T.

- Hieronimus, M. Zenke, R. K. Schneider, and S. Neurs, "Cord blood-hematopoietic stem cell expansion in 3D fibrin scaffolds with stromal support," *Biomaterials*, vol. 33, no. 29, pp. 6987–6997, 2012.
- [401] M. Barbarisi, G. Marino, E. Armenia, Q. Vincenzo, F. Rosso, M. Porcelli, and A. Barbarisi, "Use of polycaprolactone (PCL) as scaffolds for the regeneration of nerve tissue," *J. Biomed. Mater. Res. - Part A*, vol. 103, no. 5, pp. 1755–1760, 2015.
- [402] J. H. Edwards, "The effects of vibration as a mechanical stimulus on osteogenesis of mesenchymal progenitors," University of Sheffield, 2013.
- [403] L. Boyle, "The effect of oscillating and unidirectional flow with and without dexamethasone on hESMP cells seeded on porous polyurethane scaffolds," University of Sheffield, 2015.
- [404] G. Tetteh, "Polyurethane-based Scaffolds for Bone Tissue Engineering," University of Sheffield, 2016.
- [405] G. Tetteh, A. S. Khan, R. M. Delaine-Smith, G. C. Reilly, and I. U. Rehman, "Electrospun polyurethane/hydroxyapatite bioactive Scaffolds for bone tissue engineering: The role of solvent and hydroxyapatite particles," *J. Mech. Behav. Biomed. Mater.*, vol. 39, pp. 95–110, 2014.
- [406] J. Filipowska, G. C. Reilly, and A. M. Osyczka, "A single short session of media perfusion induces osteogenesis in hBMSCs cultured in porous scaffolds, dependent on cell differentiation stage," *Biotechnol. Bioeng.*, vol. 113, no. 8, pp. 1814–1824, 2016.
- [407] X. Tang, S. Teng, C. Liu, and M. Jagodzinski, "Influence of hydrodynamic pressure on the proliferation and osteogenic differentiation of bone mesenchymal stromal cells seeded on polyurethane scaffolds," *J. Biomed. Mater. Res. - Part A*, vol. 105, no. 12, pp. 3445–3455, 2017.
- [408] S. J. Pierre, J. C. Thies, A. Dureault, N. R. Cameron, J. C. M. Van Hest, N. Carette, T. Michon, and R. Weberskirch, "Covalent enzyme immobilization onto photopolymerized highly porous monoliths," *Adv. Mater.*, vol. 18, no. 14, pp. 1822–1826, 2006.
- [409] M. Bokhari, R. J. Carnachan, S. a. Przyborski, and N. R. Cameron, "Emulsion-templated porous polymers as scaffolds for three dimensional cell culture: effect of synthesis parameters on scaffold formation and homogeneity," *J. Mater. Chem.*, vol. 17, no. 38, p. 4088, 2007.
- [410] E. Knight, B. Murrar, R. J. Carnachan, and S. Przyborski, "Alvetex®:

Polystyrene Scaffold Technology for Routine Three Dimensional Cell Culture,” in *3D Cell Culture: Methods and Protocols*, 2011, pp. 323–340.

- [411] J. J. A. Barry, M. M. C. G. Silva, K. M. Shakesheff, S. M. Howdle, and M. R. Alexander, “Using plasma deposits to promote cell population of the porous interior of three-dimensional poly(D,L-lactic acid) tissue-engineering scaffolds,” *Adv. Funct. Mater.*, vol. 15, no. 7, pp. 1134–1140, 2005.
- [412] P. Viswanathan, M. G. Ondeck, S. Chirasatitsin, K. Ngamkham, G. C. Reilly, A. J. Engler, and G. Battaglia, “Biomaterials 3D surface topology guides stem cell adhesion and differentiation,” *Biomaterials*, vol. 52, pp. 140–147, 2015.
- [413] E. J. Chang, H. H. Kim, J. E. Huh, I. A. Kim, J. Seung Ko, C. P. Chung, and H. M. Kim, “Low proliferation and high apoptosis of osteoblastic cells on hydrophobic surface are associated with defective Ras signaling,” *Exp. Cell Res.*, vol. 303, no. 1, pp. 197–206, 2005.
- [414] A. Michelmore, D. A. Steele, J. D. Whittle, J. W. Bradley, and R. D. Short, “Nanoscale deposition of chemically functionalised films via plasma polymerisation,” *RSC Adv.*, vol. 3, no. 33, p. 13540, 2013.
- [415] R. Daw, S. Candan, A. J. Beck, A. J. Devlin, I. M. Brook, S. MacNeil, R. A. Dawson, and R. D. Short, “Plasma copolymer surfaces of acrylic acid/1,7 octadiene: Surface characterisation and the attachment of ROS 17/2.8 osteoblast-like cells,” *Biomaterials*, vol. 19, no. 19, pp. 1717–1725, 1998.
- [416] A. J. Beck, J. Phillips, L. Smith-Thomas, R. D. Short, and S. MacNeil, “Development of a plasma-polymerized surface suitable for the transplantation of keratinocyte-melanocyte cocultures for patients with vitiligo,” *Tissue Eng.*, vol. 9, no. 6, pp. 1123–31, 2003.
- [417] D. B. Haddow, D. A. Steele, R. D. Short, R. A. Dawson, and S. Macneil, “Plasma-polymerized surfaces for culture of human keratinocytes and transfer of cells to an in vitro wound-bed model,” *J. Biomed. Mater. Res.*, vol. 64A, no. 1, pp. 80–87, 2003.
- [418] L. Detomaso, R. Gristina, G. S. Senesi, R. D’Agostino, and P. Favia, “Stable plasma-deposited acrylic acid surfaces for cell culture applications,” *Biomaterials*, vol. 26, no. 18, pp. 3831–3841, 2005.
- [419] L. Safinia, K. Wilson, A. Mantalaris, and A. Bismarck, “Atmospheric plasma treatment of porous polymer constructs for tissue engineering applications,” *Macromol. Biosci.*, vol. 7, no. 3, pp. 315–327, 2007.
- [420] A. J. Engler, S. Sen, H. L. Sweeney, and D. E. Discher, “Matrix Elasticity

- Directs Stem Cell Lineage Specification,” *Cell*, vol. 126, no. 4, pp. 677–689, 2006.
- [421] J. R. Tse and A. J. Engler, “Stiffness gradients mimicking in vivo tissue variation regulate mesenchymal stem cell fate,” *PLoS One*, vol. 6, no. 1, 2011.
- [422] N. D. Evans, C. Minelli, E. Gentleman, V. LaPointe, S. N. Patankar, M. Kallivretaki, X. Chen, C. J. Roberts, and M. M. Stevens, “Substrate stiffness effects early differentiation events in embryonic stem cells,” vol. 18, pp. 1–14, 2009.
- [423] B. Trappmann, J. E. Gautrot, J. T. Connelly, D. G. T. Strange, Y. Li, M. L. Oyen, M. a. Cohen Stuart, H. Boehm, B. Li, V. Vogel, J. P. Spatz, F. M. Watt, and W. T. S. Huck, “Extracellular-matrix tethering regulates stem-cell fate,” *Nat. Mater.*, vol. 11, no. 8, pp. 742–742, 2012.
- [424] M. Mattioli-Belmonte, “Mesenchymal Stem Cells on Plasma-Deposited Acrylic Acid Coatings: An In Vitro Investigation to Improve Biomaterial Performance in Bone Reconstruction,” *Journal of Bioactive and Compatible Polymers*, vol. 20, no. 4, pp. 343–360, 2005.
- [425] H. S. Seo, Y. M. Ko, J. W. Shim, Y. K. Lim, J. K. Kook, D. L. Cho, and B. H. Kim, “Characterization of bioactive RGD peptide immobilized onto poly(acrylic acid) thin films by plasma polymerization,” *Appl. Surf. Sci.*, vol. 257, no. 2, pp. 596–602, 2010.
- [426] H. E. Colley, G. Mishra, A. M. Scutt, and S. L. McArthur, “Plasma polymer coatings to support mesenchymal stem cell adhesion, growth and differentiation on variable stiffness silicone elastomers,” *Plasma Process. Polym.*, vol. 6, no. 12, pp. 831–839, 2009.
- [427] G. C. Reilly and A. J. Engler, “Intrinsic extracellular matrix properties regulate stem cell differentiation,” *J. Biomech.*, vol. 43, no. 1, pp. 55–62, 2010.
- [428] M. M. Stevens and J. H. George, “Exploring and engineering the cell surface interface,” *Science*, vol. 310, no. 5751, pp. 1135–1138, 2005.
- [429] F. E. Wiria, K. F. Leong, C. K. Chua, and Y. Liu, “Poly-epsilon-caprolactone/hydroxyapatite for tissue engineering scaffold fabrication via selective laser sintering,” *Acta biomaterialia*, vol. 3, no. 1, pp. 1–12, 2007.
- [430] W. Y. Yeong, N. Sudarmadji, H. Y. Yu, C. K. Chua, K. F. Leong, S. S. Venkatraman, Y. C. F. Boey, and L. P. Tan, “Porous polycaprolactone scaffold for cardiac tissue engineering fabricated by selective laser sintering,” *Acta Biomater.*, vol. 6, no. 6, pp. 2028–2034, 2010.

- [431] J. Y. Tan, C. K. Chua, and K. F. Leong, “Fabrication of channeled scaffolds with ordered array of micro-pores through microsphere leaching and indirect Rapid Prototyping technique,” *Biomed. Microdevices*, vol. 15, no. 1, pp. 83–96, 2013.
- [432] C. Sherborne, “The development and characterisation of biocompatible emulsion templated foams for additive manufacturing Thesis submitted to the University of Sheffield for the degree of Doctor of Philosophy,” no. November, 2015.
- [433] P. Woźniak, M. Bil, J. Ryszkowska, P. Wychowański, E. Wróbel, A. Ratajska, G. Hoser, J. Przybylski, K. J. Kurzydłowski, and M. Lewandowska-Szumieł, “Candidate bone-tissue-engineered product based on human-bone-derived cells and polyurethane scaffold,” *Acta Biomater.*, vol. 6, no. 7, pp. 2484–2493, 2010.
- [434] W. Yang, S. K. Both, G. J. V. M. Van Osch, Y. Wang, J. A. Jansen, and F. Yang, “Performance of different three-dimensional scaffolds for in vivo endochondral bone generation,” *Eur. Cells Mater.*, vol. 27, pp. 350–364, 2014.
- [435] M. M. Mirhosseini, V. Haddadi-Asl, and S. S. Zargarian, “Fabrication and characterization of hydrophilic poly(ε-caprolactone)/pluronic P123 electrospun fibers,” *J. Appl. Polym. Sci.*, vol. 133, no. 17, pp. 1–11, 2016.
- [436] J. R. Vetsch, R. Mu, S. Hofmann, and S. Hofmann, “The influence of curvature on three-dimensional mineralized matrix formation under static and perfused conditions : an in vitro bioreactor model,” 2016.
- [437] E. D. Ara, M. Boudiffa, C. Taylor, D. Schug, E. Fiegle, A. J. Kennerley, C. Damianou, G. M. Tozer, F. Kiessling, and R. Müller, “Longitudinal imaging of the ageing mouse,” *Mech. Ageing Dev.*, vol. 160, pp. 93–116, 2016.
- [438] H. Hagenmüller, S. Hofmann, T. Kohler, H. P. Merkle, D. L. Kaplan, G. Vunjak-Novakovic, R. Müller, and L. Meinel, “Non-invasive time-lapsed monitoring and quantification of engineered bone-like tissue,” *Ann. Biomed. Eng.*, vol. 35, no. 10, pp. 1657–1667, 2007.
- [439] S. Cartmell, K. Huynh, A. Lin, S. Nagaraja, and R. Guldborg, “Quantitative microcomputed tomography analysis of mineralization within three-dimensional scaffolds in vitro.,” *J. Biomed. Mater. Res. A*, vol. 69, no. 1, pp. 97–104, 2004.
- [440] A. C. Marin, D. Lacroix, and S. Sheffield, “The inter-sample structural variability of regular tissue-engineered scaffolds significantly affects the micromechanical local cell environment,” 2015.

- [441] A.-V. Do, B. Khorsand, S. M. Geary, and A. K. Salem, “3D Printing of Scaffolds for Tissue Regeneration Applications,” *Adv. Healthc. Mater.*, vol. 4, no. 12, p. n/a-n/a, 2015.
- [442] S. T. Ho and D. W. Hutmacher, “A comparison of micro CT with other techniques used in the characterization of scaffolds,” *Biomaterials*, vol. 27, no. 8, pp. 1362–1376, 2006.
- [443] F. C. Breedveld, “Osteoarthritis--the impact of a serious disease.,” *Rheumatology (Oxford)*, vol. 43 Suppl 1, no. suppl_1, pp. i4-8, Feb. 2004.
- [444] S. W. O’Driscoll, “The healing and regeneration of articular cartilage.,” *J. Bone Joint Surg. Am.*, vol. 80, no. 12, pp. 1795–812, Dec. 1998.
- [445] J. Cognault, O. Seurat, C. Chaussard, S. Ionescu, and D. Saragaglia, “Return to sports after autogenous osteochondral mosaicplasty of the femoral condyles: 25 cases at a mean follow-up of 9 years,” *Orthop. Traumatol. Surg. Res.*, vol. 101, no. 3, pp. 313–317, 2015.
- [446] J. W. Alford, “Cartilage Restoration, Part 2: Techniques, Outcomes, and Future Directions,” *Am. J. Sports Med.*, vol. 33, no. 3, pp. 443–460, Mar. 2005.
- [447] W. M. Hussain, M. J. Griesser, B. W. McCoy, and R. D. Parker, “Strategies in Articular Cartilage Restoration—Present Advances in Biologic Intervention for Adult Knee Problems,” *Semin. Arthroplasty*, vol. 23, no. 1, pp. 2–6, 2012.
- [448] J. M. Oliveira, M. T. Rodrigues, S. S. Silva, P. B. Malafaya, M. E. Gomes, C. A. Viegas, I. R. Dias, J. T. Azevedo, J. F. Mano, and R. L. Reis, “Novel hydroxyapatite/chitosan bilayered scaffold for osteochondral tissue-engineering applications: Scaffold design and its performance when seeded with goat bone marrow stromal cells,” *Biomaterials*, vol. 27, no. 36, pp. 6123–6137, 2006.
- [449] J. Clouet, C. Vinatier, C. Merceron, M. Pot-vaucel, Y. Maugars, P. Weiss, G. Grimandi, and J. Guicheux, “From osteoarthritis treatments to future regenerative therapies for cartilage.,” *Drug Discov. Today*, vol. 14, no. 19–20, pp. 913–25, Oct. 2009.
- [450] C.-C. Jiang, H. Chiang, C. Liao, Y.-J. Lin, T.-F. Kuo, C.-S. Shieh, Y.-Y. Huang, and R. S. Tuan, “Repair of Porcine Articular Cartilage Defect with a Biphasic Osteochondral Composite,” *J. Orthop. Res.*, pp. 1277–1290, 2007.
- [451] C.-J. Liao, Y.-J. Lin, H. Chiang, S.-F. Chiang, Y.-H. Wang, and C.-C. Jiang, “Injecting partially digested cartilage fragments into a biphasic scaffold to generate osteochondral composites in a nude mice model.,” *J. Biomed. Mater.*

Res. A, vol. 81, no. 3, pp. 567–77, Jun. 2007.

- [452] N. J. Castro, S. A. Hacking, and L. G. Zhang, “Recent progress in interfacial tissue engineering approaches for osteochondral defects,” *Ann. Biomed. Eng.*, vol. 40, no. 8, pp. 1628–40, 2012.
- [453] X. Li, J. Ding, J. Wang, X. Zhuang, and X. Chen, “Biomimetic biphasic scaffolds for osteochondral defect repair,” *Regen. Biomater.*, vol. 2, no. 3, pp. 221–228, 2015.
- [454] R. Burdis, “Microporous Scaffolds for Osteochondral Repair,” University of Sheffield, 2016.
- [455] J. R. Farley, J. E. Wergedal, and D. J. Baylink, “Fluoride directly stimulates proliferation and alkaline phosphatase activity of bone-forming cells,” *Science*, vol. 222, no. 4621, pp. 330–2, 1983.
- [456] C. M. Stanford, P. a. Jacobson, E. D. Eanes, L. a. Lembke, and R. J. Midura, “Rapidly forming apatitic mineral in an osteoblastic cell line (UMR 106-01 BSP),” *Journal of Biological Chemistry*, vol. 270, no. 16, pp. 9420–9428, 1995.
- [457] L. F. Bonewald, S. E. Harris, J. Rosser, M. R. Dallas, S. L. Dallas, N. P. Camacho, B. Boyan, and A. Boskey, “Von Kossa staining alone is not sufficient to confirm that mineralization in vitro represents bone formation,” *Calcif. Tissue Int.*, vol. 72, no. 5, pp. 537–547, 2003.
- [458] F. Tortelli, N. Pujic, Y. Liu, N. Laroche, and L. Vico, “Osteoblast and Osteoclast Differentiation in an In Vitro Three-Dimensional Model of,” *Eng. Part A*, vol. 15, no. 9, pp. 2373–83, 2009.
- [459] R. a Dodds, “A cytochemical assay for osteolast cathepsin K activity,” *Cell Biochem. Funct.*, vol. 21, no. 3, pp. 231–234, 2003.
- [460] D. A. N. Hoyte, “Alizarin red in the study of the apposition and resorption of bone,” *Am. J. Phys. Anthropol.*, vol. 29, no. 2, pp. 157–177, 1968.
- [461] K. Suzuki, S. Takeyama, T. Kikuchi, S. Yamada, J. Sodek, and H. Shinoda, “Osteoclast responses to lipopolysaccharide, parathyroid hormone and bisphosphonates in neonatal murine calvaria analyzed by laser scanning confocal microscopy,” *J. Histochem. Cytochem.*, vol. 53, no. 12, pp. 1525–1537, 2005.
- [462] G. D. Kusuma, S. P. Brennecke, A. J. O’Connor, B. Kalionis, and D. E. Heath, “Decellularized extracellular matrices produced from immortal cell lines derived from different parts of the placenta support primary mesenchymal stem

- cell expansion,” *PLoS One*, vol. 12, no. 2, pp. 1–18, 2017.
- [463] T. Uchiyama, G. Gronowicz, J. M. Alexander, I. Bab, S. Fish, R. Mu, and A. E. T. Al, “Human Parathyroid Hormone 1 – 34 Reverses Bone Loss in Ovariectomized Mice,” *J. Bone Miner. Res.*, vol. 16, no. 9, pp. 1665–1673, 2001.
- [464] Y. Tian, Y. Xu, Q. Fu, and M. He, “Parathyroid hormone regulates osteoblast differentiation in a Wnt/??-catenin-dependent manner,” *Mol. Cell. Biochem.*, vol. 355, no. 1–2, pp. 211–216, 2011.
- [465] D. W. Dempster, C. E. Hughes-Begos, K. Plavetic-Chee, A. Brandao-Burch, F. Cosman, J. Nieves, S. Neubort, S. S. Lu, A. Iida-Klein, T. Arnett, and R. Lindsay, “Normal human osteoclasts formed from peripheral blood monocytes express PTH type 1 receptors and are stimulated by PTH in the absence of osteoblasts,” *J. Cell. Biochem.*, vol. 95, no. 1, pp. 139–148, 2005.
- [466] S. Liu, W. Zhu, S. Li, J. Ma, H. Zhang, Z. Li, L. Zhang, B. Zhang, Z. Li, X. Liang, and W. Shi, “Bovine parathyroid hormone enhances osteoclast bone resorption by modulating V-ATPase through PTH1R,” *Int. J. Mol. Med.*, vol. 37, no. 2, pp. 284–292, 2016.
- [467] Y. Nakayama, K. Takahashi, S. Nqji, K. Muto, K. Nishijima, and S. Taniguchi, “Functional modes of retinoic acid in mouse osteoblastic clone MC3T3-E1, proved as a target cell for retinoic acid,” *FEBS Lett.*, vol. 261, no. 1, pp. 93–96, 1990.
- [468] C. J. Lengner, H. A. Steinman, J. Gagnon, T. W. Smith, J. E. Henderson, B. E. Kream, G. S. Stein, J. B. Lian, and S. N. Jones, “Osteoblast differentiation and skeletal development are regulated by Mdm2-p53 signaling,” *J. Cell Biol.*, vol. 172, no. 6, pp. 909–921, 2006.
- [469] J. R. Masters and G. N. Stacey, “Changing medium and passaging cell lines,” *Nat. Protoc.*, vol. 2, no. 9, pp. 2276–2284, 2007.
- [470] J. H. Kim, H. M. Jin, K. Kim, I. Song, B. U. Youn, K. Matsuo, and N. Kim, “The mechanism of osteoclast differentiation induced by IL-1,” *J. Immunol.*, vol. 183, no. 3, pp. 1862–1870, 2009.
- [471] G. Wang, M. M. Petzke, R. Iyer, H. Wu, and I. Schwartz, “Pattern of proinflammatory cytokine induction in RAW264.7 mouse macrophages is identical for virulent and attenuated *Borrelia burgdorferi*,” *J. Immunol.*, vol. 180, no. 12, pp. 8306–8315, 2008.
- [472] F.-H. Lin, J. B. Chang, M. H. McGuire, J. A. Yee, and B. E. Brigman, “Biphasic

effects of interleukin-1 β on osteoblast differentiation in vitro,” *J. Orthop. Res.*, no. July, p. n/a-n/a, 2010.

- [473] J. . Lorenzo, S. . Sousa, S. . Van Den Brink-Webb, and J. . Korn, “Production of Both Interleukin-1a and B by Newborn Mouse Calvarial Cultures,” *J. Bone Miner. Res.*, vol. 5, no. 1, pp. 77–83, 1990.
- [474] T. Akchurin, T. Aissiou, N. Kemeny, E. Prosk, N. Nigam, and S. V. Komarova, “Complex dynamics of osteoclast formation and death in long-term cultures,” *PLoS One*, vol. 3, no. 5, 2008.
- [475] X. Feng, “RANKing Intracellular Signaling in Osteoclasts,” *IUBMB Life (International Union Biochem. Mol. Biol. Life)*, vol. 57, no. 6, pp. 389–395, 2005.
- [476] S. L. Teitelbaum, “RANKing c-Jun in osteoclast development,” *J. Clin. Invest.*, vol. 114, no. 4, pp. 463–465, 2004.
- [477] J. Kim and N. Kim, “Signaling Pathways in Osteoclast Differentiation,” *Chonnam Med. J.*, vol. 52, pp. 12–17, 2016.
- [478] E. E. McGrath, “OPG/RANKL/RANK Pathway as a Therapeutic Target in Cancer,” *J. Thorac. Oncol.*, vol. 6, no. 9, pp. 1468–1473, 2011.
- [479] S. Srivastava, G. Toraldo, M. N. Weitzmann, S. Cenci, F. P. Ross, and R. Pacifici, “Estrogen Decreases Osteoclast Formation by Down-regulating Receptor Activator of NF- κ B Ligand (RANKL)-induced JNK Activation,” *J. Biol. Chem.*, vol. 276, no. 12, pp. 8836–8840, 2001.
- [480] J. H. Kim and N. Kim, “Regulation of NFATc1 in Osteoclast Differentiation,” *J Bone Metab*, vol. 21, no. 4, pp. 233–241, 2014.
- [481] E.-J. Chang, J. Ha, H. Huang, H. J. Kim, J. H. Woo, Y. Lee, Z. H. Lee, J. H. Kim, and H.-H. Kim, “The JNK-dependent CaMK pathway restrains the reversion of committed cells during osteoclast differentiation,” *J. Cell Sci.*, vol. 121, no. 15, pp. 2555–2564, 2008.
- [482] I. Papantoniou, M. Sannaert, L. Geris, F. P. Luyten, J. Schrooten, and G. Kerckhofs, “Three-dimensional characterization of tissue-engineered constructs by contrast-enhanced nanofocus computed tomography,” *Tissue Eng. Part C. Methods*, vol. 20, no. 3, pp. 177–87, 2014.
- [483] Y. Yang, S. M. Dorsey, M. L. Becker, S. Lin-Gibson, G. E. Schumacher, G. M. Flaim, J. Kohn, and C. G. Simon, “X-ray imaging optimization of 3D tissue engineering scaffolds via combinatorial fabrication methods,” *Biomaterials*,

- vol. 29, no. 12, pp. 1901–11, 2008.
- [484] S. M. Hasan, G. Harmon, F. Zhou, J. E. Raymond, T. P. Gustafson, T. S. Wilson, and D. J. Maitland, “Tungsten-loaded SMP foam nanocomposites with inherent radiopacity and tunable thermo-mechanical properties,” *Polym. Adv. Technol.*, vol. 27, no. 2, pp. 195–203, 2016.
- [485] A. H. Lutter, U. Hempel, C. Wolf-Brandstetter, A. I. Garbe, C. Goettsch, L. C. Hofbauer, R. Jessberger, and P. Dieter, “A novel resorption assay for osteoclast functionality based on an osteoblast-derived native extracellular matrix,” *J. Cell. Biochem.*, vol. 109, no. 5, pp. 1025–1032, 2010.
- [486] G. Wheeler, M. Elshahaly, S. P. Tuck, H. K. Datta, and J. M. van Laar, “The clinical utility of bone marker measurements in osteoporosis,” *J. Transl. Med.*, vol. 11, no. 1, p. 201, 2013.
- [487] M. J. Seibel, “Biochemical markers of bone turnover: Part I: biochemistry and variability.,” *Clin. Biochem. Rev.*, vol. 26, no. 4, pp. 97–122, 2005.
- [488] P. Garnero, M. Ferreras, M. a Karsdal, R. Nicamhlaibh, J. Risteli, O. Borel, P. Qvist, P. D. Delmas, N. T. Foged, and J. M. Delaissé, “The type I collagen fragments ICTP and CTX reveal distinct enzymatic pathways of bone collagen degradation.,” *J. Bone Miner. Res.*, vol. 18, no. 5, pp. 859–867, 2003.
- [489] E. E. Golub and K. Boesze-Battaglia, “The role of alkaline phosphatase in mineralization,” *Curr. Opin. Orthop.*, vol. 18, no. 5, pp. 444–448, 2007.

10. Appendix

10.1 Standard curves

Standard curves for the ALP, DNA, ARS and DR80 assays are given in figure 10.1.

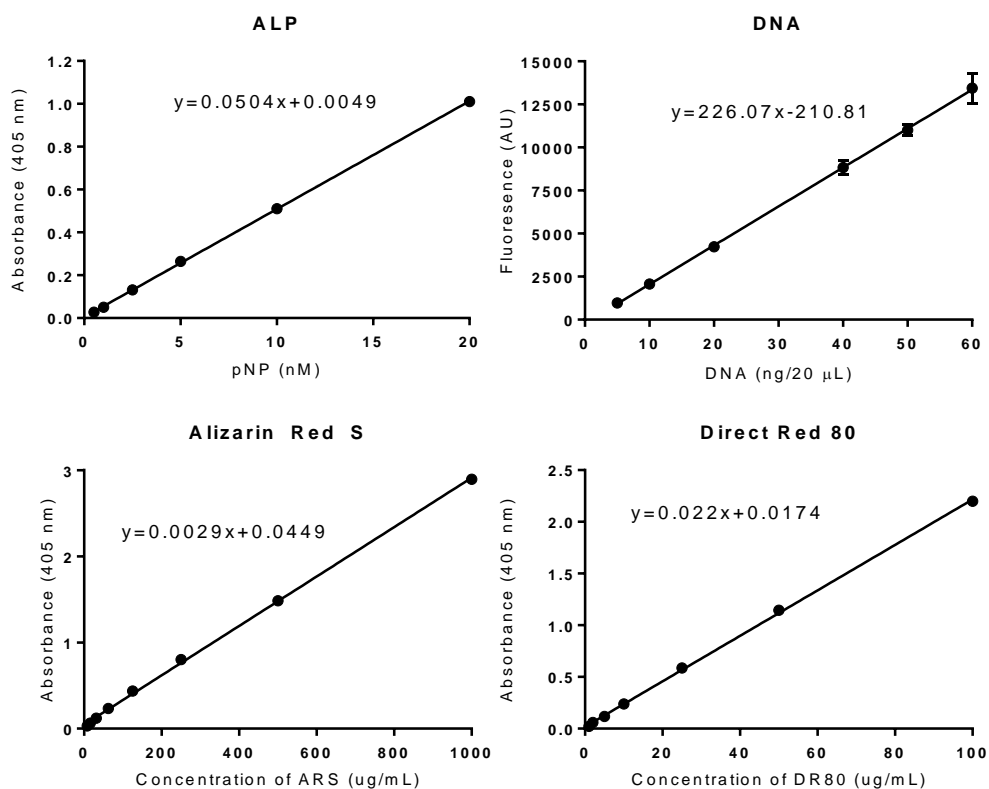


Figure 10.1: Standard curves for the ALP, DNA, ARS and DR80 assays. These can be used to convert plate reader outputs (absorbance/fluorescence) to a known concentration of enzyme product, DNA, or stain.

10.2 Figure permissions

Where figures not covered by the Creative Common Attribution License were reprinted from a publication, permissions were granted via RightsLink® (Fig. 10.2)

The screenshot shows the RightsLink® interface. At the top, there is a navigation bar with 'My Orders', 'My Library', and 'My Profile'. A welcome message for 'roberteowen1992@gmail.com' is displayed. Below the navigation bar, the page title is 'My Orders'. There are tabs for 'Orders', 'Billing History', 'Payable Invoices', and 'Copyright.com Orders'. A search section includes a search bar for 'Order Number', a date range selector (From 1-Jun-2017 to 28-Nov-2017), and a 'Go' button. Below the search section, there are filters for 'View' with checkboxes for 'All', 'Response Required', 'Pending', 'Completed', 'Canceled', 'Denied', and 'Credited'. The results section shows 'Results: 1-5 of 5' and a table with the following data:

Order Date	Article Title	Publication	Type Of Use	Order Status	Order Number
22-Nov-2017	The Osteocyte: An Endocrine Cell ... and More	Endocrine Reviews	Thesis/Dissertation	Completed	4234461221695
16-Sep-2017	Building strong bones: molecular regulation of the osteoblast lineage	Nature Reviews Molecular Cell Biology	reuse in a dissertation / thesis	Completed	4190740301318
21-Aug-2017	μ-Particle tracking velocimetry and computational fluid dynamics study of cell seeding within a 3D porous scaffold	Journal of the Mechanical Behavior of Biomedical Materials	reuse in a thesis/dissertation	Completed	4173780131997
16-Aug-2017	Coupling the activities of bone formation and resorption: a multitude of signals within the basic multicellular unit	BoneKey Reports	reuse in a dissertation / thesis	Completed	4170890685380
16-Aug-2017	Mechanical properties and the hierarchical structure of bone	Medical Engineering & Physics	reuse in a thesis/dissertation	Completed	4170841285564

Figure 10.2: Reprint permissions granted via RightsLink®.

Where figures by Prof. Timothy Arnett, Dr. James Weaver, Dr. Thomas Patterson, Rebecca O'Neill and Ross Burdis were used, permission was confirmed in writing (Fig. 10.3).

Image permission
3 messages

RE Owen <reowen1@sheffield.ac.uk> 18 August 2017 at 20:21
To: James weaver@wyss.harvard.edu

Dear **Dr. Weaver**,

I am a PhD student at the University of Sheffield currently preparing my thesis on an in vitro model of osteoporosis.

I would like to request permission to use one of your images where you compare the bone structure of the vertebrae of a 21 year old male and a 65 year old woman in my introduction, as it appears in Figure 5 of the publication 'Plasticity and Toughness of Bone' by Ritchie, Buehler and Hansma (<http://physicstoday.scitation.org/doi/10.1063/1.3156332>).

Please let me know if this is acceptable.

Yours sincerely,

Robert Owen
PhD Student

Weaver, James C. <James.Weaver@wyss.harvard.edu> 19 August 2017 at 00:03
To: RE Owen <reowen1@sheffield.ac.uk>

Hi Robert,
Thanks for the note and you're welcome to use the image. Do you have everything you need?

Thanks for your interest in our research, James

CAD Permission
1 message

Ross Burdis <rossburdis1@gmail.com> 1 October 2017 at 14:25
To: RE Owen <reowen1@sheffield.ac.uk>

Hi Rob,

Just to confirm you have my permission to use my CAD renders in your thesis.

All the best,

Ross **Burdis**

Image Permission
2 messages

Rebecca O'Neill <rebecca.o.neill91@gmail.com> 1 October 2017 at 14:34
To: RE Owen <reowen1@sheffield.ac.uk>

Hi Rob,

This is to confirm that you have permission to use my bone macro- and micro-structure diagram in your thesis.

Kind regards,
Rebecca O'Neill

RE Owen <reowen1@sheffield.ac.uk> 16 September 2017 at 17:48
To: Tom Paterson <tom_pat2552@hotmail.com>

Hi Tom,

In my discussion I am talking about the differences in ingrowth between your particles, my scaffold fibres and **alvetex**. Would it be ok with you to reprint one of your figures in my discussion to show the level of ingrowth you observed?

All the best,

Robert Owen
PhD Student

Tom Paterson <tom_pat2552@hotmail.com> 20 September 2017 at 11:36
To: RE Owen <reowen1@sheffield.ac.uk>

Looks fine to me, go for it!

And good luck with the writing!

Image permisison
2 messages

RE Owen <reowen1@sheffield.ac.uk> 9 October 2017 at 12:52
To: t.arnett@ucl.ac.uk

Dear Prof. Arnett,

I am a PhD student at the University of Sheffield currently preparing my thesis on an in vitro model of osteoporosis.

I would like to request permission to use one of your images of a resorbing osteoclast in my introduction, as it appears on the boneresearchsociety.org resources page. (http://boneresearchsociety.org/media/gallery/Osteoclast_resorption_03.tif.2000x2000_q85_autocrop.jpg)

Please let me know if this is acceptable.

Yours sincerely,

Robert Owen
PhD Student

Arnett, Timothy <t.arnett@ucl.ac.uk> 9 October 2017 at 14:35
To: RE Owen <reowen1@sheffield.ac.uk>

Hi Robert,

Delighted to grant permission - just acknowledge in the usual way.

Good luck with your thesis!

Tim

Tim Arnett | t.arnett@ucl.ac.uk

Figure 10.3: Written permissions for figures not available through RightsLink®.

10.3 Emulsion templated scaffolds with tunable mechanical properties for bone tissue engineering

JOURNAL OF THE MECHANICAL BEHAVIOR OF BIOMEDICAL MATERIALS 54 (2016) 159–172



Available online at www.sciencedirect.com

ScienceDirect

www.elsevier.com/locate/jmbbm



Research Paper

Emulsion templated scaffolds with tunable mechanical properties for bone tissue engineering



Robert Owen^a, Colin Sherborne^b, Thomas Paterson^b, Nicola H. Green^b,
Gwendolen C. Reilly^a, Frederik Claeyssens^{b,*}

^aDepartment of Materials Science and Engineering, University of Sheffield, INSIGNEO Institute for in silico medicine, The Pam Liversidge Building, Sir Frederick Mappin Building, Mappin Street, Sheffield S1 3JD, United Kingdom

^bDepartment of Materials Science and Engineering, University of Sheffield, The Kroto Research Institute, North Campus, Broad Lane, Sheffield S3 7HQ, United Kingdom

ARTICLE INFO

Article history:

Received 22 April 2015

Received in revised form

9 September 2015

Accepted 14 September 2015

Available online 25 September 2015

Keywords:

Porosity

Free form fabrication

Mechanical properties

PolyHIPEs

Plasma polymerization

Stereolithography

ABSTRACT

Polymerised High Internal Phase Emulsions (PolyHIPEs) are manufactured via emulsion templating and exhibit a highly interconnected microporosity. These materials are commonly used as thin membranes for 3D cell culture. This study uses emulsion templating in combination with microstereolithography to fabricate PolyHIPE scaffolds with a tightly controlled and reproducible architecture. This combination of methods produces hierarchical structures, where the microstructural properties can be independently controlled from the scaffold macrostructure. PolyHIPEs were fabricated with varying ratios of two acrylate monomers (2-ethylhexyl acrylate (EHA) and isobornyl acrylate (IBOA)) and varying nominal porosity to tune mechanical properties. Young's modulus, ultimate tensile stress (UTS) and elongation at failure were determined for twenty EHA/IBOA compositions. Moduli ranged from 63.01 ± 9.13 to 0.36 ± 0.04 MPa, UTS from 2.03 ± 0.33 to 0.11 ± 0.01 MPa and failure strain from $21.86 \pm 2.87\%$ to $2.60 \pm 0.61\%$. Selected compositions were fabricated into macro-porous woodpile structures, plasma treated with air or acrylic acid and seeded with human embryonic stem-cell derived mesenchymal progenitor cells (hES-MPs). Confocal and two-photon microscopy confirmed cell proliferation and penetration into the micro- and macro-porous architecture. The scaffolds supported osteogenic differentiation of mesenchymal cells and interestingly, the stiffest IBOA-based scaffolds that were plasma treated with acrylic acid promoted osteogenesis more strongly than the other scaffolds.

© 2015 The Authors. Published by Elsevier Ltd. This is an open access article under the CC BY license (<http://creativecommons.org/licenses/by/4.0/>).

1. Introduction

3-D tissue scaffold manufacturing processes are divided into techniques that produce 3-D objects with random microstructure

via stochastic processes (e.g. electrospinning, high internal phase emulsions, solvent casting and particulate leaching) (Hutmacher, 2000); and additive manufacturing techniques that produce structures with ordered user-controlled microstructure (e.g.

*Corresponding author. Tel. +44 114 222 5513; fax: +44 114 222 5943.
E-mail address: f.claeyssens@sheffield.ac.uk (F. Claeyssens).

<http://dx.doi.org/10.1016/j.jmbbm.2015.09.019>

1751-6161/© 2015 The Authors. Published by Elsevier Ltd. This is an open access article under the CC BY license (<http://creativecommons.org/licenses/by/4.0/>).

stereolithography, fused deposition modelling and selected laser sintering) via computer aided design/manufacturing (CAD/CAM) (Hutmacher, 2001). Random networks, when compared to user-defined structures, are generally easier to produce in bulk but their microstructure and physical properties are more difficult to control, analyse and interpret. Control over pore distribution and interconnectivity can be achieved using additive manufacturing techniques, which are ideally suited for exploring the relationship between 3-D topography and cell attachment, proliferation and differentiation. This requires optimising the geometrical parameters of the scaffold, i.e. the dimensions of the scaffold fibres vs. the pores (Hollister, 2005; Danilevicius et al., 2015). The fibres ensure the mechanical stability of the scaffold, while the pores allow for mass transport to aid cell/nutrient delivery and tissue generation. High resolution and throughput techniques such as microstereolithography permit the fabrication of scaffolds that have a highly controlled architecture with well-defined pores and interconnectivity, improving cell growth and tissue formation (Lee et al., 2011).

Additive manufacture and emulsion templating have been previously combined to produce structures with multi-scale porosity (Cooperstein et al., 2015; Sušec et al., 2013; Johnson et al., 2013). Materials formed by emulsion templating two immiscible liquids (termed the internal phase and continuous phase) with the internal phase volume ratio (ϕ) exceeding 0.7405, are termed HIPEs. For the majority of photocurable HIPEs, the internal phase is water and the continuous phase is a hydrophobic liquid formed from the monomer(s), crosslinker, surfactant, and photoinitiator (Cameron and Sherrington, 1996; Cameron, 2005). Polymerisation of the continuous phase results in a PolyHIPE; a permeable, highly interconnected, porous network with a low bulk density where the percentage porosity is simply ϕ (Caldwell et al., 2012). We previously showed that a hierarchical porosity can be introduced into scaffolds using microstereolithography through the use of a High Internal Phase Emulsion (HIPE) as a substrate material (Johnson et al., 2013). This hybrid biomaterial manufacturing technique enables the hierarchical structuring of scaffolds where the microstructure is controlled by emulsion templating while the macrostructure is governed by additive manufacturing.

Acrylate-based PolyHIPEs with specific mechanical properties can be fabricated using different monomers. By altering the proportions of the elastomer 2-ethylhexyl acrylate (EHA) and the monomer isobornyl acrylate (IBOA), different stiffness can be obtained (Johnson et al., 2013; Jereñec et al., 2014). The ability to control the mechanical properties of PolyHIPEs allows scaffolds to be tuned depending on the application. For example, flexible scaffolds are needed for mechanical conditioning of cells in compression; however, scaffolds need to be stiff enough to fill a load-bearing defect and to be handled during surgery. In addition, it has been demonstrated that substrate stiffness, nanotopography and binding site spacing all effect stem cell differentiation and matrix production (Engler et al., 2006; Trappmann et al., 2012; Evans et al., 2009; Viswanathan et al., 2015; Stevens and George, 2005).

The ease with which porous materials can be fabricated using emulsion templating makes PolyHIPEs excellent materials for 3-D cell culture, as exemplified by the commercialisation of Alvetex[®], a polystyrene-based PolyHIPE scaffold

(Knight et al., 2011). Cellular penetration into these PolyHIPE monoliths is dependent on their thickness and pore size (Hayward et al., 2013a); however, Akay et al. (2004) found that regardless of pore size, cellular penetration in PolyHIPEs was rarely seen beyond 1 mm. Additionally, when plasma treating the PolyHIPE to overcome the intrinsic hydrophobicity, it has been shown that there is a significant depth dependence with regards to its efficiency. Plasma treatments have been shown to coat the inner-surfaces of an 85% porous, 10 mm diameter 3 mm thick disc; however, any porous object beyond a few millimetres thick will not be homogeneously coated, with the least deposition occurring at the core (Barry et al., 2005; Viswanathan et al., 2014). Therefore, PolyHIPE monoliths need to be thin for optimal cell and plasma penetration. By creating scaffolds from HIPEs using microstereolithography, this depth limit can be overcome as individual fibres will not be too thick for cell ingrowth and plasma penetration (<1 mm), but the overall depth of the scaffold can be much larger than for monoliths. This can have many applications, especially in bone repair, such as a for synthetic bone graft substitutes or as a scaffold for cell-based bone regeneration. In addition, macro-pores can be created in the scaffold that are large enough to permit vascularisation, whereas the smaller micro-pores present on a PolyHIPE monolith would not. In general, cells need to be within 200 μm of a blood vessel to receive oxygen and nutrients, and for sufficient vascularisation of a scaffold, a pore size of at least 300 μm has been recommended (Cao et al., 2006).

Current bone graft substitutes, usually ceramic based, have had some success but are brittle and difficult to shape and therefore are usually provided as granules (Hing et al., 2007; Hing, 2005). Bone tissue engineering is a promising alternative that could overcome many of these complications, but it is yet to proceed to mainstream clinical practise due to limitations such as the need to retain both mechanical strength and adequate porosity for sufficient and timely vascularisation of scaffolds after implantation (Amini and Laurencin, 2012).

Our aim in this study was to synthesise a range of PolyHIPEs with tunable mechanical properties to support bone cells in vitro. PolyHIPEs of different stiffness were selected and used to manufacture hierarchically structured 3-D scaffolds for cell culture using a woodpile design. Scaffolds were seeded with human embryonic stem-cell derived mesenchymal progenitors (hES-MPs), and their ability to support attachment, proliferation and osteogenic differentiation was assessed.

2. Materials and methods

2.1. HIPE synthesis

HIPEs were synthesised with monomer proportions ranging from 100% EHA (Sigma Aldrich, UK) to 100% IBOA (Sigma Aldrich, UK) at 25% intervals. The organic component of the continuous phase was formed from the monomers and a crosslinker (trimethylolpropane triacrylate (TMPTA) Sigma Aldrich, UK) at 26.96 wt% of the monomers. A surfactant (Hypermer B246-SO-(MV), Croda, UK) was added at 3 wt% of

the organic mass and left to dissolve in a sonic water bath. Finally, a photoinitiator (2,4,6-trimethylbenzoyl)-phosphine oxide/2-hydroxy-2-methylpropiophenone, 50/50, Sigma Aldrich, UK) was added at 5 wt% of the organic mass. The internal phase, distilled water, was added at 0.75, 0.80, 0.85 and 0.90 ϕ to each continuous phase, to produce twenty HIPE compositions. These are referred to by their wt% EHA and nominal porosity. For example, EHA50P85 is a HIPE consisting of 50 wt% EHA and 50 wt% IBOA with a ϕ of 0.85, and EHA0P75 is a HIPE formed from 100% IBOA with a ϕ of 0.75.

2.2. Fabrication of PolyHIPE sheets for tensile testing

Sheets of PolyHIPE were fabricated from each composition and laser-cut to size based on ASTM D638-10, the standard test method for tensile properties of plastics (American Society for Testing and Materials, 2010). HIPE was pipetted into a silicone mould and cured to form a sheet using an automated UV belt curer (GEW Mini Laboratory, GEW engineering UV), washed in acetone and dried overnight. The size of the tensile samples was scaled down from the dimensions stated in ASTM D638-10 due to the maximum sample height that could be tested in the extensometer. Therefore, longitudinal dimensions were reduced by a factor of 3.83, but original axial dimensions were not altered to retain the cross-sectional area. Samples were cut using a laser cutter (Mini 18 Laser, Epilog Laser) with an intensity of 8%, speed of 70% and a frequency of 2500 Hz. The number of passes required was dependent on the porosity and thickness of the PolyHIPE.

2.3. Mechanical characterisation of PolyHIPE tensile samples

Samples were tested on a BOSE ElectroForce 3200 mechanical testing machine using a 450 N load cell, an extension rate of 0.02 mm/s, a grip distance of 10 mm, and a maximum extension of 6 mm. Each composition was tested and the Young's modulus (E), ultimate tensile stress (UTS) and percentage elongation at failure determined. The UTS was calculated as the maximum force applied divided by the sample cross sectional area, and percentage elongation at failure expressed as the extension at failure divided by the original distance between the grips (10 mm for all samples). The Young's modulus of each sample was determined using the gradient of the linear-elastic region of the force–displacement curve. For all samples, the initial point from which this was measured was at an extension of 0.02 mm, and the final point taken was at yield. Compositions selected for cell culture were also tested after soaking in PBS for 1 h to investigate whether the stiffness was affected by the sample being wet.

2.4. Physical characterisation of PolyHIPE tensile samples

Scanning electron microscopy (SEM) was used to examine how changes in composition affected the degree of openness (DOO) of the PolyHIPE (Pulko and Krajnc, 2012). For each composition, a sample was mounted on a carbon tab; sputter coated with gold (SC500, emscope) at a pressure of 0.05 atm and a current of 15 mA for two minutes, and then imaged using a Philips XL-20 SEM with an electron beam with energy

of 20 kV. Images at $400\times$ magnification were analysed using the measurement tool in Image J (Schneider et al., 2012).

DOO is the ratio of open surfaces (S_o) to the total surface of a cavity (S_c). S_c is calculated using the measured void diameter (D_m) multiplied by a statistical correction factor to represent the equatorial void diameter (D_e) (Eq. (1)) (Carnachan et al., May 2006)

$$S_c = \pi \left(\frac{2D_m}{\sqrt{3}} \right)^2 \quad (1)$$

To determine S_o , the diameters of the visible interconnects were averaged (D_i) and used to calculate the average area ($\pi(\frac{D_i}{2})^2$). This was multiplied by the number of visible interconnects (N), then by 2 as the void had been cut in half, and by the statistical correction factor as it is not known where the cavity had been bisected. The DOO is simply the ratio of S_o to S_c (Eq. (2))

$$\begin{aligned} \text{Degree of Openness (DOO)} &= \frac{\text{Open Surface of Cavity}}{\text{Total Surface of Cavity}} \\ &= \frac{N * 2 * \frac{2}{\sqrt{3}} * \pi \left(\frac{D_i}{2} \right)^2}{\pi D_e^2} \quad (2) \end{aligned}$$

2.5. Fabrication of PolyHIPE scaffolds

Scaffolds were fabricated onto 13 mm glass coverslips. To functionalise the coverslips so that the polymer adhered, they were treated with piranha solution (80 vol% H_2SO_4 (Sigma Aldrich, UK), 20 vol% H_2O_2 (Sigma Aldrich, UK)), washed in distilled water, methanol-dried, and added to a solution of 10 wt% 3-methylacryloxypropyltrimethoxysilane (MAPTMS, Polysciences Inc.) in toluene. Before use, coverslips were washed in methanol and dried.

Four layer woodpile scaffolds were fabricated from EHA0P80, EHA50P80 and EHA100P80 PolyHIPEs using a single-photon direct-write microstereolithography setup. A subnanosecond pulse duration, passively Q-switched DPSS microchip laser (PULSELAS-P355-300, ALPHALAS, Germany), controlled using a laser diode and thermoelectric cooler driver (LDD1-1BT-D, ALPHALAS, Germany), emitting wavelengths of 1064, 532 and 355 nm was used as a source. A Pellin-Broca prism (ADB-10, THORLABS, UK) was used to separate a single wavelength of 355 nm. Beam delivery was controlled with a shutter (UNIBLITZ LS6, VincentAssociates, Canada) linked to a shutter driver (VCM-D1, VincentAssociates, Canada) and intensity with a pinhole. The beam was focused through a microscope objective (EC-Plan NEOFLUAR $10\times$, Carl Zeiss Ltd, UK), and a high precision stage with the ability to move in all three planes (ANT130-XY (Aerotech, UK) for xy translation & PRO115 (Aerotech, UK) for z translation) commanded by a motion controller and software (A3200 Software-Based Machine Controlled (Aerotech, UK)) was used to translate the focal spot. The laser was focused just above the coverslip-HIPE interface for the bottom layer and the fibre-HIPE interface for each subsequent layer in order to write the scaffold.

For all compositions, a current of 2.20 μA and a pinhole size of 3.1 mm was used, resulting in a measured laser power of 1.5 mW on the sample (measured by a SC310 thermal

power sensor and a PM50 controller, THORLABS, UK). However, for each of the different compositions it was necessary to tune the process parameters (e.g. the volume of HIPE used and write speed) to address differences in curing properties and to ensure that the macrostructure of each scaffold was similar between compositions. To write the scaffold, a layer of HIPE was pipetted onto a functionalised coverslip, placed onto the stage and the first layer fabricated. Additional HIPE was added after the completion of each layer. Once completed, scaffolds were washed with acetone and dried with a heat gun. For this study, in total 336 scaffolds were fabricated, each taking approximately 13 min to produce (Fig. 1).

2.6. Plasma modification of scaffolds

The continuous phase of a HIPE typically utilises a hydrophobic monomer in order to form the emulsion. Therefore, to promote cell adhesion, spreading and proliferation, the surface chemistry of the produced scaffold was altered via plasma modification using either an air plasma clean (pcAir) or air plasma followed by plasma deposited acrylic acid (pdAAc).

Treatments were applied by placing the scaffolds centrally in a cylindrical plasma chamber with stainless steel end-plates, wrapped with a coil of wire connected to a 13.56 MHz frequency generator. For pcAir scaffolds, the pressure was adjusted to 1.8×10^{-1} mbar and the power set to 50 W to generate the plasma. Samples were exposed to the plasma for 5 min. For pdAAc scaffolds, samples were kept in the chamber after exposure to air plasma and liquid nitrogen added to the cold trap. Once the pressure dropped to 3.0×10^{-3} mbar, a flask of acrylic acid (Sigma Aldrich, UK) was attached to the inlet and the pressure adjusted to 3.0×10^{-2} mbar. Acrylic

acid plasma was then generated for 10 min using a power of 15 W and a flow rate of $2.40\text{--}2.50$ sccm⁻¹. If samples were not used immediately, they were kept under vacuum until needed.

2.7. Cell culture

hES-MPs (Cellartis, Sweden), mesenchymal progenitors, were used to assess the suitability of the PolyHIPE scaffolds to support osteogenic precursors. Cells were cultured at 37 °C, 5% CO₂ in basal media (BM), containing Minimum Essential Alpha Medium (α -MEM, Lonza, UK), 10% foetal bovine serum (FBS, Labtech, UK), 2 mM L-glutamine (Sigma Aldrich, UK) and 100 mg/mL penicillin/streptomycin (Sigma Aldrich, UK) and in gelatine-coated T75 flasks. BM was supplemented with human fibroblastic growth factor (Life Technologies, UK) at 4 ng/ml and media was changed every 2–3 days.

Cells were used between the third and sixth passage, and depending on the experiment, cultured in either osteogenesis induction media (OIM) or supplemented media (SM). OIM is BM supplemented with ascorbic acid (50 μ g/mL (Sigma Aldrich, UK)), beta-glycerolphosphate (β GP, 5 mM (Sigma Aldrich, UK)) and dexamethasone (100 nM (Sigma Aldrich, UK)). SM is the same composition as OIM but without dexamethasone.

Scaffolds were sterilised by soaking in 70 vol% ethanol for 2 h before being washed three times in sterile PBS. Scaffolds were seeded with 75,000 cells at a density of 1,500,000 cells/mL in a non-treated 24 well plate, to ensure cell attachment only occurred on the scaffold, and left for 45 min to attach. 1 mL of BM was then added to each well to submerge the scaffolds and incubated overnight. On day 1, scaffolds were transferred to a

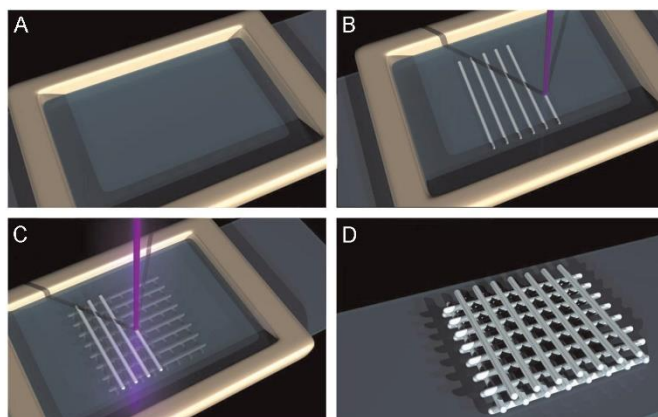


Fig. 1 – Scaffold manufacture process. (A) HIPE is pipetted onto a functionalised coverslip (B) Laser beam is focused onto the coverslip-HIPE interface and writes the bottom layers. These fibres attach to the coverslip (C) Additional HIPE added covering the first layer of fibres. Laser beam focussed to fibre-HIPE interface and second layer is written. These fibres attach to the first fibre layer. This is repeated until scaffold is complete (D) After fabrication excess polymer is removed and the scaffold is washed in acetone before drying.

12 well plate and 2 mL of OIM or SM added to selected scaffolds. Media was changed every 2–3 days.

2.7.1. Assessment of the suitability of acrylate-based PolyHIPEs for bone tissue engineering

To assess the suitability of the PolyHIPE scaffolds for cell culture, resazurin reduction (RR) assays were performed. Resazurin solution is reduced to resorufin by the cells, changing the colour of the media from a non-fluorescent blue to a highly fluorescent pink. The fluorescence is measured using a microplate reader and is correlated with cell viability (O'Brien et al., 2000).

The RR assay was performed at three time points (Day 1, 8, 15). 1 mM Resazurin Sodium Salt (Sigma Aldrich, UK) in dH₂O was diluted in BM (10 vol%) to create a RR solution. Culture media was removed from the samples and replaced with 2 mL of RR solution, the well plates were wrapped in aluminium foil and incubated for 4 h at 37 °C. 200 µL of the reduced solution was added to a 96-well plate and measured using a spectrofluorometer (FLx800, BIO-TEK Instruments, Inc.) at an excitation wavelength of 540 nm and an emission wavelength of 630 nm. Scaffolds were washed twice with PBS before adding fresh media.

2.7.2. Evaluation of the effects of PolyHIPE composition on alkaline phosphatase activity

The activity of ALP, an enzyme involved in the bone mineralisation process, can be used as an early indicator of osteogenic differentiation (Farley et al., 1983; Hoemann et al., 2009). ALP activity was measured on days 8 and 15 on pdAAC and pcAir scaffolds cultured in OIM and SM. Culture media was removed from the scaffolds, they were washed twice in PBS and 500 µL of cell digestion buffer (10 v/v% cell assay buffer (1.5 M Tris-HCl, 1 mM ZnCl₂, 1 mM MgCl₂ in deionised water (dH₂O), 1% Triton-X100 (Sigma Aldrich, UK), in dH₂O) was added to each scaffold and incubated for 30 min. Scaffolds were then removed and the lysates transferred to 1.5 mL tubes, vortexed briefly, then stored overnight at 4 °C. The lysates then underwent a freeze-thaw cycle three times (–80 °C 10 min, 37 °C 15 min), before being vortexed for 15 seconds per sample. Finally, they were centrifuged at 10,000 rpm for 5 min.

10 µL of the lysate was combined with 190 µL of PNPP Phosphatase Substrate (Thermo Scientific, UK) and added to a 96-well plate, then incubated at 37 °C until a slight colour change from colourless to yellow was observed. Absorbance was then measured using a plate reader (ELx800, BIO-TEK) at a wavelength of 405 nm every minute for 30 min. ALP activity is expressed as nmol of *p*-nitrophenol per minute (nmol pNP/min), assuming that one absorbance value equals 22.5 nmol of product.

2.7.3. PicoGreen[®] assay

A Quant-iT[™] PicoGreen[®] dsDNA Assay (PG) Kit (Life Technologies, UK) was used to determine the amount of double stranded DNA (dsDNA) present in the cell lysate, indicating cell number. PG reagent is a fluorochrome which binds with dsDNA. When excited, the fluorescence value correlates to the amount of dsDNA present in the sample (Ahn et al., 1996). 180 µL of the lysate was mixed in a 1:1 ratio with the PG working solution (1:20 Tris-EDTA (TE) buffer (10 mM Tris-HCl,

1 mM EDTA, pH 7.5), 1:200 PG reagent in dH₂O) in a 1.5 mL tube. This mixed solution was transferred to an opaque well plate, wrapped in foil and incubated at room temperature for 10 min. Samples were then read using a spectrofluorometer at an excitation wavelength of 485 nm and an emission wavelength of 528 nm.

2.7.4. Immunolabelling, confocal, and two-photon microscopy

The scaffolds with the highest levels of proliferation, as determined from day 15 RR assay results, were imaged using confocal microscopy to view cell location on the scaffold. Samples were stained with DAPI (4', 6-diamidino-2-phenylindole dihydrochloride (Sigma Aldrich, UK) and Phalloidin-TRITC (Phalloidin-Tetramethylrhodamine B isothiocyanate (Sigma Aldrich, UK)) in order to view nuclei and f-actin, respectively. Two-photon microscopy was used to assess cell penetration into the scaffold pores using the same staining protocol.

To stain the cells, the media was removed and the scaffolds washed twice with PBS. They were then fixed with 1 mL of 3.7% formaldehyde (Sigma Aldrich, UK) and left for 20 min before being washed with PBS a further 2 times. 1 mL of immunocytochemistry (ICC) buffer (1% BSA, 0.1% Triton-X100 in PBS) was then added and left for 20 min before removing the buffer, adding 500 µL of phalloidin working solution (1:1000 phalloidin stock solution (1 mg phalloidin-TRITC, 1.5 mL methanol) in ICC buffer), and wrapping the well plate in foil. After 30 min, the staining solution was removed and the scaffold washed twice with PBS, then 1 mL of DAPI working solution (0.1 vol% DAPI in PBS) was added and left wrapped in foil for 10 min. The DAPI working solution was then removed and the scaffolds washed once in PBS. Samples were submerged in PBS, wrapped in foil, and refrigerated until use.

Confocal images (512 × 512 pixels) were obtained using an upright microscope (Axioskop 2 FS MOT Microscope, Carl Zeiss Ltd, UK) with a 10 × objective (W N-Achroplan 10 × /0.3, Carl Zeiss Ltd, UK) and a pixel dwell time of 2.56 µs. DAPI was detected using a tunable Ti:Sapphire two-photon laser (λ_{ex} 800 nm, λ_{em} 435–485 nm) and Phalloidin-TRITC detected using a single photon laser (λ_{ex} 543 nm, λ_{em} 565–615 nm). 3-D images of the scaffolds were produced using 'z-stacking', with between 25 and 100 images, taken at 8.74 µm intervals. Differential interference contrast (DIC) images were also taken at the middle slice of the z-stack. This shows the position of the scaffold fibres without any cells, which when viewed side by side with the confocal images, allows for the plane of the image within the scaffold to be easily determined.

Two-photon images (512 × 512 pixels) were obtained using the upright microscope with a 40 × objective (Achromplan 40 × /0.75 W, Carl Zeiss Ltd, UK) and a pixel dwell time of 6.39 µs. Both fluorophores and the PolyHIPE material were detected using a tunable Ti:Sapphire two-photon laser (λ_{ex} 800 nm), with the signal detected as follows: DAPI – λ_{em} 435–485 nm, Phalloidin-TRITC – λ_{em} 565–661 nm, and PolyHIPE autofluorescence – λ_{em} > 560 nm. Images were taken at 1 µm intervals to create a Z-stack.

2.7.5. Statistical analysis

All mechanical analysis was performed with ten samples at each composition. If samples slipped or broke in the grips,

the results for that sample were discarded. When calculating DOO, ten voids were selected randomly for measurement from an SEM image of each composition. Cell viability experiments were repeated three times in triplicate. Outliers were removed using the ROUT method (Q=5%). ALP and PicoGreen experiments were repeated twice in triplicate. Two-way ANOVA with Tukey's post-test was used to evaluate significant differences, all graphs are presented at mean ± SD and notable significant differences are indicated on the graphs or in the legends.

3. Results

3.1. Mechanical characterisation of PolyHIPE tensile samples

PolyHIPE sheets had measured stiffness in tension ranging from 63.01 ± 9.13 MPa to 0.36 ± 0.04 MPa, with the highest Young's moduli occurring in the EHA0P75 composition and

the lowest at EHA100P90, as expected (Fig. 2A). Both higher porosity and a higher wt% of EHA resulted in a lower stiffness. However, the monomer composition had the greatest influence.

As with Young's modulus, an increase in ϕ at the same wt% EHA causes a reduction in UTS (Fig. 2B). However, the highest UTS was achieved by EHA25P75 (2.03 ± 0.33 MPa), rather than EHA0P75 (1.64 ± 0.22 MPa). The highest UTS at 0.75, 0.85 and 0.90 ϕ is achieved by an EHA25 composition, although at all four nominal porosities the difference between the EHA0 and EHA25 UTSs is not significant ($p < 0.05$).

The percentage elongation at failure is not affected by the nominal porosity at each composition (Fig. 2C). It is only influenced by the monomer compositions with the ductility increasing with the addition of EHA, peaking around the EHA50 and EHA75 compositions and then declining. As EHA is an elastomer, this is expected.

Tensile samples for each composition were not always made from the same batch of polymer, yet there was a high degree of concordance for the stress-strain curves, indicating that the

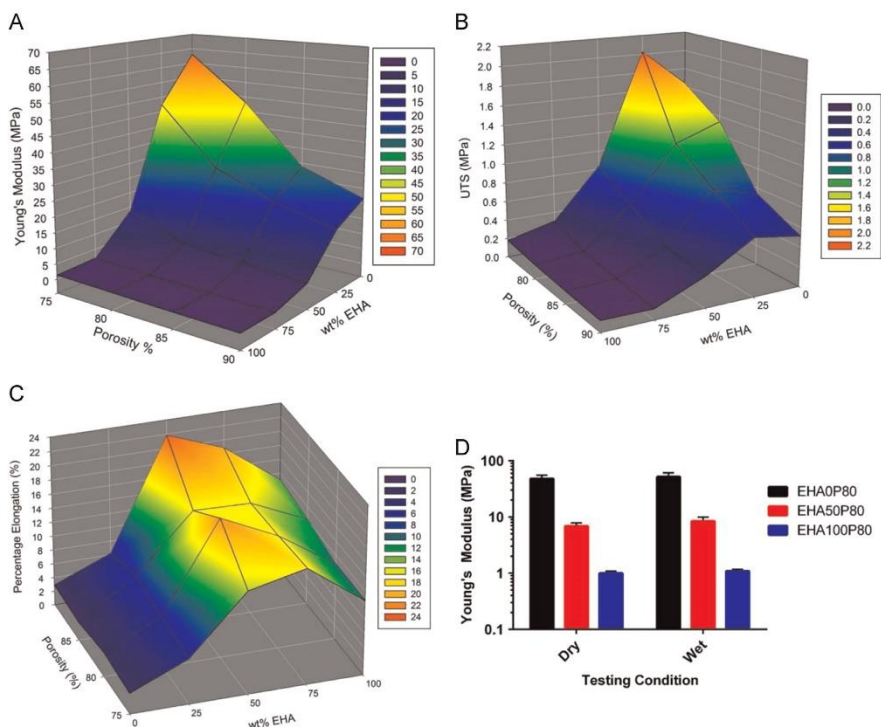


Fig. 2 – Surface plots showing the effects of nominal porosity and wt% EHA on (A) Young's modulus, (B) Ultimate Tensile Stress, (C) percentage elongation at failure (D) mean ± SD of the dry and wet stiffness for the compositions used for cell culture. For A–C, the nodes indicate the mean of ten samples. There were no significant differences for dry vs. wet at any of the compositions.

synthesis method can reproducibly create the same material. Testing of wet samples showed that cell culture conditions had no effect on the stiffness of the material (Fig. 2D).

3.2. Degree of openness

To determine whether the physical effects of the different nominal porosities were the same for each composition, DOO values were compared. In all cases, a higher DOO was observed at higher porosities (Fig. 3A). At a given porosity, there was no significant difference in DOO between monomer proportions for 0.75, 0.80 and 0.90 ϕ ($p < 0.05$), and only EHA25P85 vs. EHA50P85 and EHA50P85 vs. EHA75P85 were significantly different ($p < 0.05$). For each composition, the largest increase in the DOO was observed when ϕ increased from 0.75 to 0.80 and 0.85 to 0.90, with a relatively smaller difference between 0.80 and 0.85. The low DOO at 0.75 ϕ is because the emulsion is only classed as a HIPE at 0.7405 ϕ . If nominal porosity is viewed as the volume of water added per 1ml of continuous phase to achieve this ϕ , a linear relationship can be seen (Fig. 3B). This is because the porosity is reciprocal to the amount of polymer.

3.3. Scaffold fabrication

Scaffolds were reproducibly fabricated from the three compositions (EHA0P80, EHA50P80, EHA100P80), with a fibre diameter and spacing of approximately 350 μm and 650 μm , respectively (Fig. 4). The third and fourth layers were offset so that the top layers lay directly above the gaps of the previous layer.

3.4. Cell metabolic activity assay

Untreated scaffolds were unable to support cell attachment and growth (Fig. 5A). Plasma modification of the scaffolds clearly enhanced viable cell number on all scaffolds (Fig. 5B–D). Metabolic activity was significantly higher on plasma modified scaffolds than on untreated scaffolds for all compositions and media types on day 8 and 15 ($p < 0.05$). Interestingly, there was no significant difference at any time point and composition between pcAir and pdAAc scaffolds, showing that both treatments supported similar levels of metabolic activity. Additionally, there was no significant difference observed between the two cell culture media (OIM and SM), as previously described (Delaine-Smith et al., 2012). Comparisons between scaffolds with the same plasma treatment but different wt% EHA indicated that EHA0 scaffolds supported the lowest metabolic activity, with the highest metabolic activity achieved on pcAir-treated EHA100 scaffolds and pdAAc-modified EHA50 substrates. There were no significant differences between compositions at day 8, but by day 15 significant differences with regards to composition were observed between EHA0P80 pcAir vs. EHA100P80 pcAir and EHA0P80 pdAAc SM vs. EHA50P80 pdAAc SM ($p < 0.05$).

3.5. Confocal and two-photon microscopy

Confocal images were taken of pcAir and pdAAc scaffolds that produced the highest RR value on day 15 (Fig. 6A–D). From the images, it can be observed that cells initially

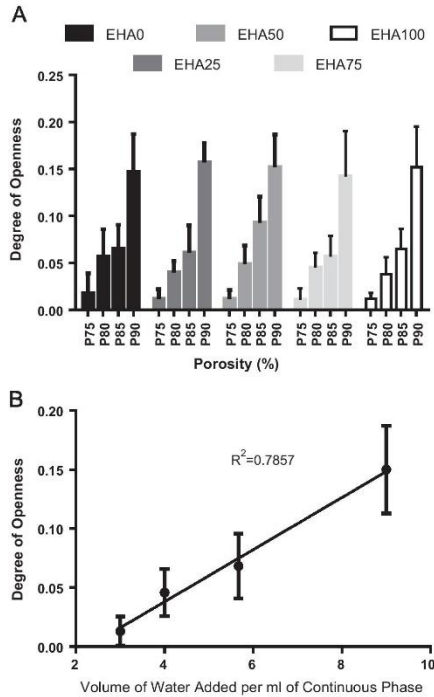


Fig. 3 – (A) Mean \pm SD of the DOO for each of the 20 compositions. (B) Average DOO vs. nominal porosity expressed as volume of water added per 1 mL of continuous phase. Nominal porosities combined for compositions. R2 calculated using linear regression, slope is significantly non-zero ($p < 0.0001$).

adhered and proliferated on the lowest layers indicating that the cell suspension fell to the bottom of the scaffold. On scaffolds with the highest levels of proliferation, cells were able to grow up the scaffold fibres and bridge the gaps between the fibres. Two-photon images of pcAir EHA0P80 images revealed that cells were able to penetrate the fibres (Fig. 6E and F), as shown by the presence of nuclei and actin within the material.

3.6. Osteogenic differentiation assay

In OIM, normalised ALP activity increased over time (Fig. 7). On day 8, normalised ALP activity was similar for both plasma treatments at each composition, with pcAir only being significantly higher on EHA0 scaffolds ($p < 0.05$). On day 15, there was no significant difference between pcAir and pdAAc for EHA50 and EHA100 scaffolds. However, normalised activity on pdAAc EHA0 scaffolds was significantly

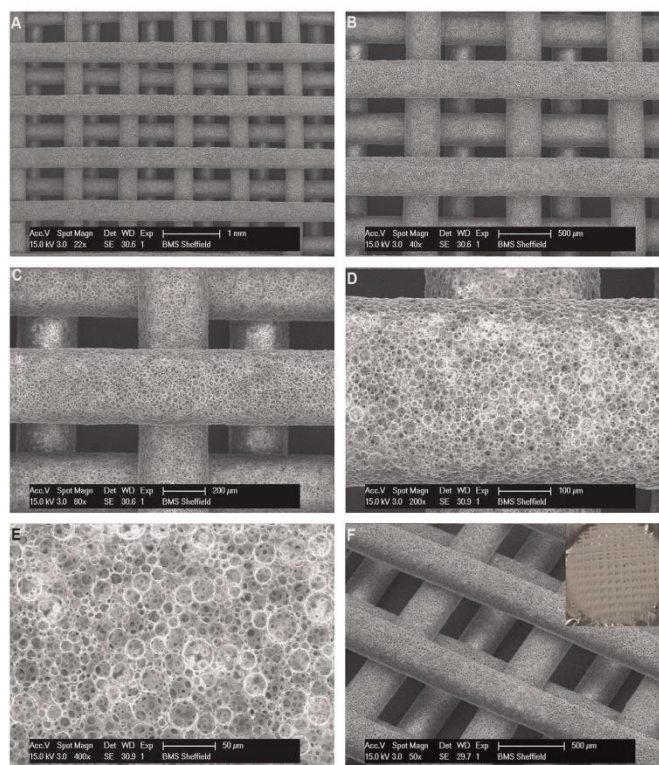


Fig. 4 – SEM images of an EHA0P80 4 layer woodpile scaffold. (A–E) Magnification of the same point from 22 x to 400 x , showing the inherent macroscopic and microscopic porosity of the structure. (F – Main) A side view of one of the fibres showing the offset of the upper two layers. Scale bars A–F: 1 mm, 500 μm, 200 μm, 100 μm, 50 μm, 500 μm. (F-Insert) Photograph of a single scaffold.

higher than pcAir for the same composition ($p < 0.001$), as well as significantly higher than both pdAAc and pcAir EHA50 and EHA100 scaffolds ($p < 0.001$). Normalised activity in SM was lower than in OIM in all instances and did not increase over time. This indicates that the stiffness of the substrate did not affect osteogenic differentiation when dexamethasone was not present in the media.

4. Discussion

This study aimed to assess whether acrylate-based PolyHIPEs with tunable mechanical properties were suitable for bone tissue engineering. To our knowledge, this is the first time that woodpile scaffolds have been created from high internal phase emulsions using microstereolithography resulting in hierarchically porous structures for tissue engineering. A range of

scaffolds was created where the fibre material was modified to give a range of mechanical properties, demonstrating that it is possible to tailor the material's properties to the application, for example, if the application requires the scaffold to undergo load bearing or be able to accommodate a specified strain. The mechanical characterisation generated here can be used as a basic selection chart for the mechanical properties of these PolyHIPEs over a range of monomer compositions and nominal porosities. The mechanical properties describe the struts of the PolyHIPE-based woodpile structures that the cells attach to in this study. For example, a stiffness of ~30 MPa can be achieved using a composition of either EHA25P80 or EHA0P85, but the EHA25 material will undergo greater extension before failure whilst the latter has a higher UTS. A requirement of tissue engineering scaffolds is that they provide adequate mechanical support whilst new tissue is being formed, so inappropriate mechanical properties will result in a failed regeneration. For

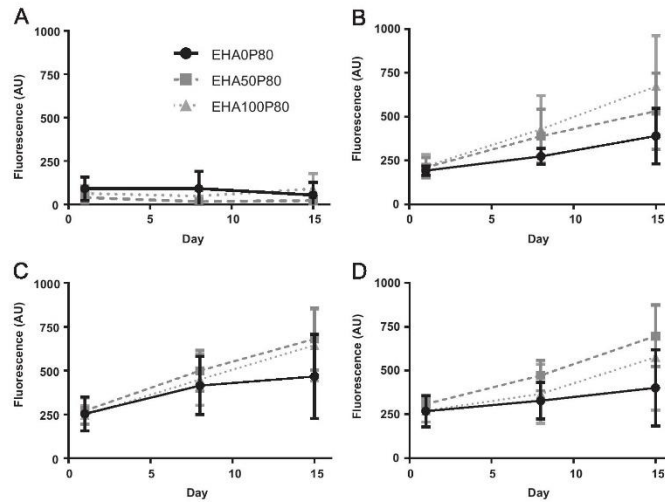


Fig. 5 – Mean \pm SD of resazurin fluorescence for (A) untreated (B) pcAir (C) pdAAc OIM (D) pdAAc SM samples. Untreated scaffolds did not support cell growth, pcAir and pdAAc had similar rates of increase in fluorescence intensity, with the highest proliferation occurring on compositions containing EHA. Cell viability was not affected by media composition.

hard tissues it has been stated that a modulus in the range of 10–1500 MPa is necessary, depending on anatomical location, and for soft tissues 0.4–350 MPa (Hollister, 2005).

The surface plots show that porosity and monomer composition both affected the mechanical performance of the PolyHIPes, but monomer composition had the greatest effect. Increasing ϕ from 0.75 to 0.90 reduced the stiffness by 66–75% at each monomer proportion, with the largest decrease seen between 0.75 and 0.80 ϕ . Increasing from 0 wt% to 100 wt% EHA decreased the stiffness by approximately 98% for all porosities, with 80–85% of this reduction seen as wt% EHA increase from 0% to 50%.

The highest UTS was achieved by an EHA25 sample as the elastomer addition allows the material to plastically deform more than the more brittle EHA0 compositions, thereby allowing it to undergo a higher tensile stress before failure. The EHA50 compositions were not able to achieve an ultimate tensile stress higher than the EHA25 composition, as at this monomer proportion the increased elasticity means that a lower force is required to achieve the same extension.

Percentage elongation at failure is not affected by nominal porosity. For the EHA0 PolyHIPes there is no significant difference in failure strain between any of the porosities; however, by comparing the UTS of these PolyHIPes, it can be seen that the force required to achieve the same level of extension is significantly lower as porosity increases ($p < 0.001$, EHA0P75 (1.64 ± 0.22 MPa) vs. EHA0P90 (0.51 ± 0.10 MPa)). This relationship continues across all compositions, with the UTS for the 0.90 ϕ composition being approximately three times lower than that for the 0.75 ϕ composition. This reduction in force required to achieve the same extension is due to the decrease in cross

sectional area at the microscopic level, resulting in less force being required to achieve the same stress. The macroscopic cross sectional area of the 75% and 90% PolyHIPes is still similar as tensile specimens were all cut to the same shape, hence the reduced UTS of the material but same elongation at failure. EHA100 PolyHIPes are not the most ductile as they are too weak to undergo large extensions. Therefore, the maximum is observed where EHA and IBOA complement each other (EHA50P90, $21.86 \pm 2.87\%$), with the former providing sufficient ductility to allow large extensions whilst the latter strengthens the material, raising the failure stress.

The compositions selected for scaffold manufacture had the highest possible internal phase volume ratio in order to maximise the DOO whilst retaining a viscosity that is amenable to pipetting. The single-photon technique used to create the scaffolds was not capable of a smaller fibre spacing whilst retaining the fibre diameter, as partial polymerisation of the HIPE would occur between the fibres resulting in a solid sheet or web effect, depending on the distance. To remediate this in the future, a two-photon technique could be used as this permits a much higher resolution as absorption only occurs within the immediate area surrounding the focal spot. However, the single-photon technique has a manufacture time of approximately 13 min for a $13 \text{ mm} \times 13 \text{ mm}$ woodpile structure, producing each fibre in a single pass. A two-photon setup would take much longer, with each fibre potentially requiring multiple passes to achieve the desired width and depth. Therefore, a possible alternative would be to introduce biocompatible UV light absorbers into the continuous phase of the emulsion, reducing out-of-focal spot polymerisation and increasing resolution whilst retaining manufacture speed.

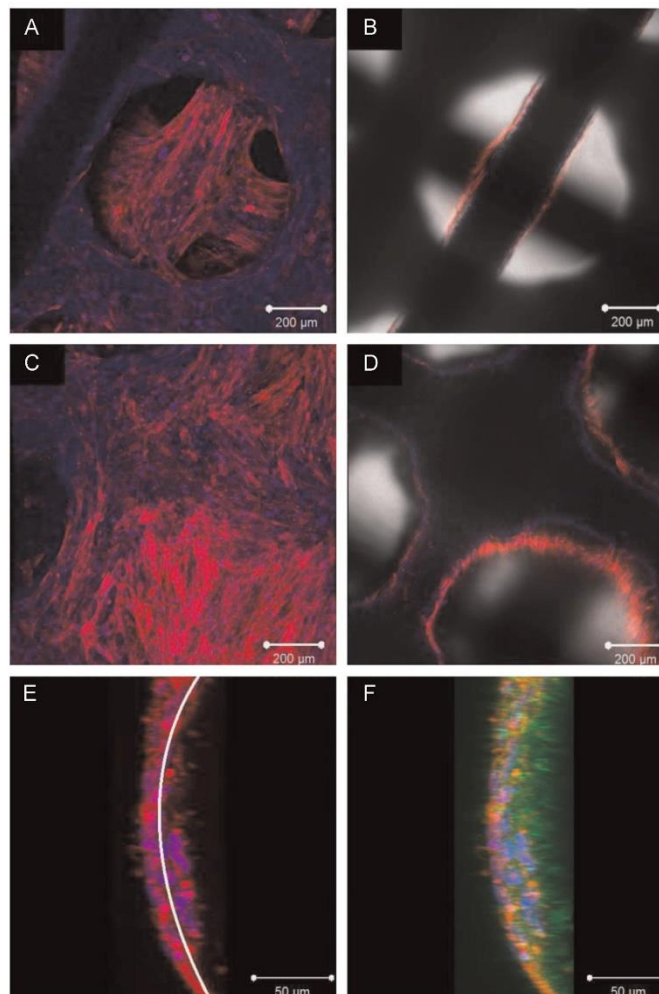


Fig. 6 – Confocal microscopy (A and C) and the corresponding DIC images (B and D) of (A) bottom two layers of a pdAAc EHA100P80 scaffold (C) the same scaffold from a different location showing the upper two layers. Note the fibre intersect is completely covered with cells and gaps between fibres were also filled. Two-photon images with (E) and without (F) the autofluorescence of the PolyHIPE (green). Fibre is viewed side on from a processed z-stack image, the curved line indicates the fibre edge. Both nuclei and actin can be seen within the fibre. (For interpretation of the references to color in this figure legend, the reader is referred to the web version of this article.)

The use of PolyHIPEs in tissue engineering is still at a preliminary stage, but their capability to be used to fabricate scaffolds has begun to be assessed. It is known that the porous architecture of a scaffold can affect cell proliferation

and osteogenesis (Roosa et al., 2010) and therefore optimising this will enhance the performance of the scaffold. Conventional techniques are limited in their ability to produce porous scaffolds as pore interconnectivity is often low,

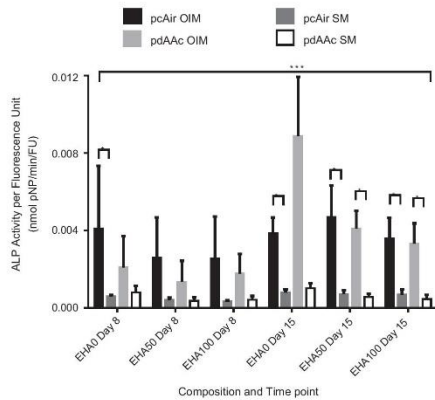


Fig. 7 – ALP activity normalised to PicoGreen fluorescence (dsDNA) present. hES-MPs cultured in OIM had higher ALP activity than their SM counterparts at all time points ($^* = p < 0.05$). None of the substrates or plasma treatments were seen to significantly induce higher osteogenic differentiation, with the exception of pdAAc modified EHA0 scaffolds, which by day 15 were found to be significantly higher than all other groups ($^{***} = p < 0.001$).

achieving regular and evenly dispersed porosity is limited to thin scaffolds, and it is time consuming to remove all solvents from the system (Hutmacher, 2001). PolyHIPE scaffolds produced using microstereolithography are not hampered by these problems as the porosity is formed from emulsion templating. The desired porosity is much more easily achievable and the final product will have regular, interconnected porosity throughout. This allows focus to shift onto the macroscopic structure of the scaffold, resulting in the ability to produce much more complex scaffolds. The minimum void diameter for osseous deposition is considered to be between 50 and 100 μm (Kasten et al., 2008) with the recommended size being 300 μm and larger (Karageorgiou and Kaplan, 2005). The scaffolds fibres fabricated here have pore sizes in the region of 20–30 μm , which is lower than the minimum required for bone deposition. This would be problematic if culturing on a disc of the bulk PolyHIPE material; however, the macroscopic pores formed between the fibres during the fabrication of the woodpile scaffold are between 300 μm (vertically) and 650 μm (laterally). This results in a hierarchical porosity, with a range of sizes over an order of magnitude. The presence of micro-pores creates a rougher surface topography, which increases cell attachment and may also increase cell migration (Akay et al., 2004).

It is not surprising that untreated scaffolds were unable to support cell attachment. In order to form a stable emulsion with water, the continuous phase of the HIPE must be hydrophobic and it has been clearly demonstrated that it is necessary to overcome this for a polymer to be used as a biomaterial or tissue engineering scaffold (Chang et al., 2005). To do this, two plasma treatments were selected, pcAir and

pdAAc. Plasma modification is effective at penetrating the porous network of a 3-D scaffold, improving the wettability of the PolyHIPEs and consequently improving the cell adhesion (Barry et al., 2005). pdAAc adds negatively charged carboxyl groups to the surface to promote cell adhesion, and pcAir deposits oxygen-containing groups, which also have been shown to support protein and cell adhesion and improve wettability (Detomaso et al., 2005; Safinia et al., 2007). Furthermore, the inclusion of acrylic acid has been used previously to enhance cell culture on PolyHIPEs. In particular, Hayward et al. (2013b) introduced it into the internal phase of the HIPE before its inclusion into the continuous phase. After curing, they showed carboxylic functionality on the PolyHIPE pore surfaces that did not adversely affect the adhesion of human hepatocytes.

Similar cell metabolic activity on these scaffolds indicates that both treatments are suitable when improving the adhesion and proliferation on the PolyHIPEs. However, the application of pcAir is less time consuming, requires fewer processing steps (e.g. does not require liquid nitrogen to cool the monomer) and avoids handling of potentially harmful monomers (acrylic acid). Therefore, our results suggest that the simpler, faster plasma modification technique is sufficient when considering cell viability alone.

Metabolic activity on the EHA0 scaffolds made from the stiffest PolyHIPE appears to be lower than the more elastic EHA50 and EHA100 materials on both day 8 and 15. Given that fibre thickness and spacing are maintained throughout, it would be expected that relative scaffold stiffness would follow the same pattern as the material stiffness. The difference in metabolic activity between the two more elastic scaffolds is much less noticeable, which may be due to a much smaller difference in stiffness; the difference between EHA0 and EHA50 is approximately 45 MPa, whereas EHA50 to EHA100 is approximately 4.5 MPa. This lower metabolic activity on the EHA0 composition agrees with the PicoGreen data. The amount of dsDNA present is also lower on the EHA0 compositions, with little difference between EHA50 and EHA100 (data not shown). Confocal imaging demonstrated that these PolyHIPE scaffolds supported cell proliferation, and that on scaffolds with the highest levels of metabolic activity, cells groups could bridge the gaps between the fibres. However, this imaging modality cannot penetrate the scaffold fibres to investigate cell penetration. Therefore, two-photon imaging was utilised due to its ability to obtain optical sections from deeper within the sample. By exploiting the inherent autofluorescence of the material, it could be confirmed that cell ingrowth had occurred. As well as penetrating the PolyHIPE, cell processes were seen to connect through pore interconnects.

Although woodpile scaffolds formed from porous and non-porous fibres were not compared directly in this study, it is likely that differences seen when cells were grown on a microporous monolith as compared to a planar substrate are relevant to understanding the potential benefits of microporous scaffold struts. Cell ingrowth was observed into the porous PolyHIPE fibre, therefore we are confident the structure provided a 3D growth environment which would enable continuous neo-tissue formation throughout the scaffold. This is also evidenced by recent data generated in our group

on microporous PolyHIPE particles (Paterson et al., in preparation). Scaffolds with non-porous fibres and macropores much larger than the cell size, e.g. 100s of microns, are likely to induce the same cellular behaviour as planar surfaces because the cell attaches to the strut in the same manner (shape and orientation) as a tissue culture plate (Stevens and George, 2005; Reilly and Engler, 2010). When Alvetex[®] PolyHIPE inserts were compared to tissue culture polystyrene, it was shown that the use of these substrates profoundly improves the ability of mesenchymal stem cells to differentiate into osteogenic phenotypes. Cells retained a more physiologically relevant morphology and had increased levels of osteogenic markers, such as ALP activity, osteocalcin production, and calcium deposition (Knight et al., 2011; Reinnervate, 2015). We suggest that porous fibres will also improve diffusion-based processes throughout the scaffold.

Other groups have demonstrated the benefits of strut microporosity. For example, in selective laser sintered polycaprolactone scaffolds where a microporosity within the fibres of the scaffold was formed during the sintering process (Wiria et al., 2007; Yeong et al., 2010). The interconnected network formed was shown to improve cell ingrowth and colonisation of the scaffold. Similar to this, rapid prototyping and particulate leaching have previously been combined to introduce a controllable microporosity into scaffolds with larger macro-channels, allowing the influence of pore architecture on mechanical and biological properties to be explored (Tan et al., 2013).

Neither the composition of the scaffold nor the pdAAc coating had a significant effect on ALP activity. However, cells seeded on EHA0 scaffolds with a pdAAc coating did have significantly higher ALP activity compared to all other scaffolds, indicating this scaffold stimulated osteogenic differentiation. This suggests that the combination of the EHAOP80 PolyHIPE and pdAAc treatment resulted in the best substrate for osteogenic differentiation between those examined here. This is interesting given that EHA0 scaffolds did not result in significantly higher ALP activity than EHA50 and EHA100 scaffolds; neither did pdAAc scaffolds when compared to pcAir.

The stiffest scaffolds (EHAOP80) have a significantly lower amount of DNA ($p < 0.05$) but similar metabolic activity to other scaffolds, which together with the higher ALP activity suggests that more cells in this condition differentiated rather than proliferated. It is possible that this is due to the cells response to the stiffness of the material, as substrate mechanical properties have been shown to influence stem cell fate (Engler et al., 2006; Evans et al., 2009; Tse and Engler, 2011). However, whilst stiffer substrates have been demonstrated to be conducive to osteogenic differentiation, those substrates had much lower Young's moduli than these PolyHIPEs and cells in those previous experiments were cultured in media without dexamethasone. In addition, subsequent work suggests that stiffness alone cannot commit a stem cell to a specific lineage, with other factors such as substrate chemistry and density of cell binding ligands also influencing differentiation (Trappmann et al., 2012). For the PolyHIPEs investigated here, relative stiffness alone did not appear to induce differentiation as significantly higher ALP activity only occurs in conjunction with pdAAc. With regards to the effect of acrylic acid on osteogenic differentiation, conclusive evidence for a relationship is yet to be seen as

there is evidence in the literature indicating stimulatory (Mattioli-Belmonte et al., 2005) as well as no (Seo et al., 2010) effects. It has been shown that plasma deposited acrylic acid does not diminish the cells' ability to perceive differences in substrate stiffness when comparing the osteogenic response of MSCs to varied substrate stiffness (Colley et al., 2009). Therefore, the reason for the enhanced ALP activity could be that the pdAAc coating provides sufficient ligands for the cells to respond to the stiffer EHAOP80 scaffold fibres whereas pcAir does not. Hence, no significant difference was seen between any pcAir treatments and the stiffer scaffold material only influenced osteogenic differentiation under a specific condition.

5. Conclusions

To conclude, EHA/BOA PolyHIPEs were fabricated at a range of monomer proportions and porosities demonstrating that it should be possible to predict the mechanical properties of a given composition based on its EHA/BOA ratio. Three compositions with distinct mechanical properties were selected and used to fabricate 3-D, four layer woodpile scaffolds using single-photon microstereolithography and functionalised with either air and/or acrylic acid plasma. Compositions containing EHA were found to facilitate the highest levels of metabolic activity. Interestingly, although substrate mechanical properties alone did not significantly influence osteogenic differentiation, the stiffest scaffold material in combination with an acrylic acid treatment did induce more ALP activity in osteoprogenitor cells compared to all other conditions indicating that this substrate may be able to enhance osteogenic differentiation.

To our knowledge, this is the first time multi-layer woodpile scaffolds have been fabricated from EHA/BOA PolyHIPEs using microstereolithography. The described fabrication method is capable of making bespoke structures from HIPEs and the use of these materials as a substrate for cell culture shows promise for tissue engineering applications where multi-scale porosities and the ability to fill a large defect are required.

Acknowledgements

We acknowledge funding from the Engineering and Physical Sciences Research Council (Grant no. EP/L505055/1) and Biotechnology and Biological Sciences Research Council (Grant no. BB/F016840/1). Confocal and two-photon imaging work was performed at the Kroto Imaging Facility.

REFERENCES

- Akay, G., Birch, M.A., Bokhari, M.A., 2004. Microcellular polyHIPE polymer supports osteoblast growth and bone formation in vitro. *Biomaterials* 25 (18), 3991–4000.
- Amini, A.R., Laurencin, C.T., Nukavarapu, S.P., 2012. Bone tissue engineering: recent advances and challenges. *Crit. Rev. Biomed. Eng.* 40 (5), 363–408.
- American Society for Testing and Materials, 2010. D638-10. Standard Test Method for Tensile Properties of Plastics.

- Available at: (<http://enterprise.astm.org/SUBSCRIPTION/NewValidateSubscription.cgi?D638-HTML>) (accessed 27.02.14).
- Ahn, S.J., Costa, J., Emanuel, J.R., 1996. PicoGreen quantitation of DNA: effective evaluation of samples pre-or post-PCR. *Nucl. Acids Res.* 24 (13), 2623–2625.
- Barry, J.J., Silva, M.M., Shakesheff, K.M., Howdle, S.M., Alexander, M.R., 2005. Using plasma deposits to promote cell population of the porous interior of three-dimensional Poly(D,L-Lactic Acid) tissue-engineering scaffolds. *Adv. Funct. Mater.* 15 (7), 1134–1140.
- Cooperstein, I., Layani, M., Magdassi, S., 2015. 3D printing of porous structures by UV-curable O/W emulsion for fabrication of conductive objects. *J. Mater. Chem. C* 3 (9), 2040–2044.
- Cameron, N.R., Sherrington, D.C., 1996. High Internal Phase Emulsions (HIPEs) – structure, properties and use in polymer preparation. *Adv. Polym. Sci.* 126, 163–214.
- Cameron, N.R., 2005. High internal phase emulsion templating as a route to well-defined porous polymers. *Polymer* 46 (5), 1439–1449.
- Caldwell, S., Johnson, D.W., Didsbury, M.P., Murray, B.A., Wu, J.J., Przyborski, S.A., Cameron, N.R., 2012. Degradable emulsion-templated scaffolds for tissue engineering from thiol-ene photopolymerisation. *Soft Matter* 8 (40), 10344–10351.
- Cao, Y., Mitchell, G., Messina, A., Price, L., Thompson, E., Penington, A., Morrison, W., O'Connor, A., Stevens, G., Cooper-White, J., 2006. The influence of architecture on degradation and tissue ingrowth into three-dimensional poly(lactic-co-glycolic acid) scaffolds in vitro and in vivo. *Biomaterials* 27 (14), 2854–2864.
- Carnachan, R.J., Bokhari, M., Przyborski, S.A., Cameron, N.R., 2006. Tailoring the morphology of emulsion-templated porous polymers. *Soft Matter* 2 (7)608–616.
- Chang, E.-J., Kim, H.-H., Huh, J.-E., Kim, I.-A., Ko, J.S., Chung, C.-P., Kim, H.-M., 2005. Low proliferation and high apoptosis of osteoblastic cells on hydrophobic surface are associated with defective Ras signaling. *Exp. Cell Res.* 303 (1), 197–206.
- Colley, H.E., Mishra, G., Scutt, A.M., McArthur, S., 2009. Plasma polymer coatings to support mesenchymal stem cell adhesion, growth and differentiation on variable stiffness silicone elastomers. *Plasma Process. Polym.* 6 (12), 831–839.
- Danilevicius, P., Georgiadi, L., Pateman, C.J., Claeysens, F., Chatzinikolaïdou, M., Farsari, M., 2015. The effect of porosity on cell ingrowth into accurately defined, laser-made, polylactide-based 3D scaffolds. *Appl. Surf. Sci.* 336, 2–10.
- Delaine-Smith, R.M., MacNeil, S., Reilly, G.C., 2012. Matrix production and collagen structure are enhanced in two types of osteogenic progenitor cells by a simple fluid shear stress stimulus. *Eur. Cells Mater.* 24, 162–174.
- Detomaso, L., Gristina, R., Senesi, G.S., d'Agostino, R., Favia, P., 2005. Stable plasma-deposited acrylic acid surfaces for cell culture applications. *Biomaterials* 26 (18), 3831–3841.
- Engler, A.J., Sen, S., Sweeney, H.L., Discher, D.E., 2006. Matrix elasticity directs stem cell lineage specification. *Cell* 126 (4), 677–689.
- Evans, N.D., Minelli, C., Gentleman, E., LaPointe, V., Patankar, S.N., Kallivretaki, M., Chen, X., Roberts, C.J., Stevens, M.M., 2009. Substrate stiffness affects early differentiation events in embryonic stem cells. *Eur. Cells Mater.* 18, 1–14.
- Farley, J.R., Wergedal, J.E., Bavlink, D.J., 1983. Fluoride directly stimulates proliferation and alkaline phosphatase activity of bone-forming cells. *Science* 222 (4621), 330–332.
- Hutmacher, D.W., 2000. Scaffolds in tissue engineering bone and cartilage. *Biomaterials* 21, 2529–2543.
- Hutmacher, D.W., 2001. Scaffold design and fabrication technologies for engineering tissues – state of the art and future perspectives. *J. Biomater. Sci.* 12 (1), 107–124.
- Hollister, S.J., 2005. Porous scaffold design for tissue engineering. *Nat. Mater.* 4 (7), 518–524.
- Hayward, A.S., Eissa, A.M., Maltman, D.J., Sano, N., Przyborski, S.A., 2013a. Galactose-functionalized polyhiPE scaffolds for use in routine three dimensional culture of mammalian hepatocytes. *Biomacromolecules* 14 (12), 4271–4277.
- Hing, K.A., Wilson, L.F., Buckland, T., 2007. Comparative performance of three ceramic bone graft substitutes. *Spine J.* 7 (4), 475–490.
- Hing, K.A., 2005. Bioceramic bone graft substitutes: influence of porosity and chemistry. *Int. J. Appl. Ceram. Technol.* 2 (3), 184–199.
- Hoemann, C.D., El-Gabalawy, H., McKee, M.D., 2009. In vitro osteogenesis assays: influence of the primary cell source on alkaline phosphatase activity and mineralization. *Pathol. Biol.* 57 (4), 318–323.
- Hayward, A.S., Sano, N., Przyborski, S.A., Cameron, N.R., 2013b. Acrylic-acid-functionalized PolyHIPE Scaffolds for use in 3D cell culture. *Macromol. Rapid Commun.* 34 (23–24), 1844–1849.
- Johnson, D.W., Sherborne, C., Didsbury, M.P., Pateman, C., Cameron, N.R., Claeysens, F., 2013. Macrostructuring of emulsion-templated porous polymers by 3D laser patterning. *Adv. Mater.* 25 (23), 3178–3181.
- Jerenc, S., Šimić, M., Šavnik, A., Podgornik, A., Kolar, M., Turnšek, M., Krajnc, P., 2014. Glycidyl methacrylate and ethylhexyl acrylate based polyHIPE monoliths: morphological, mechanical and chromatographic properties. *React. Funct. Polym.* 78, 32–37.
- Knight, E., Murray, B., Carnachan, R., Przyborski, S., 2011. Alvetex[®]: polystyrene scaffold technology for routine three dimensional cell culture. in: Haycock, J.W. (Ed.), *3D Cell Culture: Methods and Protocols*. Humana Press, New York, pp. 323.
- Kasten, P., Beven, I., Niemeier, P., Luginbühl, R., Bohner, M., Richter, W., 2008. Porosity and pore size of beta-tricalcium phosphate scaffold can influence protein production and osteogenic differentiation of human mesenchymal stem cells: an in vitro and in vivo study. *Acta Biomater.* 4 (6), 1904–1915.
- Karageorgiou, V., Kaplan, D., 2005. Porosity of 3D biomaterial scaffolds and osteogenesis. *Biomaterials* 26 (27), 5474–5491.
- Lee, J.W., Kang, K.S., Lee, S.H., Kim, J., Lee, B., Cho, D., 2011. Bone regeneration using a microstereolithography-produced customized poly(propylene fumarate)/diethyl fumarate photopolymer 3D scaffold incorporating BMP-2 loaded PLGA microspheres. *Biomaterials* 32 (3), 744–752.
- Mattioli-Belmonte, M., Lucarini, G., Virgili, L., Biagini, G., Detomaso, L., Favia, P., D'Agostino, R., Gristina, R., Gigante, A., Bevilacqua, C., 2005. Mesenchymal stem cells on plasma-deposited acrylic acid coatings: an in vitro investigation to improve biomaterial performance in bone reconstruction. *J. Bioact. Compat. Polym.* 20 (4), 343–360.
- O'Brien, J., Wilson, I., Orton, T., Pognan, F., 2000. Investigation of the Alamar Blue (resazurin) fluorescent dye for the assessment of mammalian cell cytotoxicity. *Eur. J. Biochem.* 267 (17), 5421–5426.
- Pulko, I., Krajnc, P., 2012. High internal phase emulsion templating – a path to hierarchically porous functional polymers. *Macromol. Rapid Commun.* 33 (20), 1731–1746.
- Paterson, T.E., Dugan, J.M., Sherborne, C., Green, N.H., Reilly, G.C., Claeysens, F., 2015. Highly controllable porous particle production with tuneable internal porosity with applications in bone tissue engineering. *Tissue Engineering Part A* 21, S287.
- Roosa, S.M., Kemppainen, J.M., Moffitt, E.N., Krebsbach, P.H., Hollister, S.J., 2010. The pore size of polycaprolactone scaffolds has limited influence on bone regeneration in an in vivo model. *J. Biomed. Mater. Res.: Part A* 92 (1), 359–368.
- Reilly, G.C., Engler, A.J., 2010. Intrinsic extracellular matrix properties regulate stem cell differentiation. *J. Biomech.* 43 (1), 55–62.
- Reinnervate, Formation of Mesenchymal Tissues in Alvetex[®] Scaffold Derived From Stem Cells and Established Cell Lines.

- Available at: (<http://reinnervate.com/science-technical-resources/application-notes/formation-of-mesenchymal-tissues-in-alvetexscaffold-derived-from-stem-cells-and-established-cell-lines/>). (accessed 18.08.15).
- Sušec, M., Ligon, S.C., Stampfl, J., Liska, R., Krajnc, P., 2013. Hierarchically porous materials from layer-by-layer photopolymerization of high internal phase emulsions. *Macromol. Rapid Commun.* 34 (11), 938–943.
- Stevens, M., George, J.H., 2005. Exploring and engineering the cell surface interface. *Science* 310 (5751), 1135–1138.
- Schneider, C.A., Rasband, W.S., Eliceiri, K.W., 2012. NIH Image to ImageJ: 25 years of image analysis. *Nat. Methods* 9 (7), 671–675.
- Safinia, L., Wilson, K., Mantalaris, A., Bismarck, A., 2007. Atmospheric plasma treatment of porous polymer constructs for tissue engineering applications. *Macromol. Biosci.* 7 (3), 315–327.
- Seo, H.S., Ko, Y.M., Shim, J.W., Lim, Y.K., Kook, J., Cho, D., Kim, B. H., 2010. Characterization of bioactive RGD peptide immobilized onto poly(acrylic acid) thin films by plasma polymerization. *Appl. Surf. Sci.* 257 (2), 596–602.
- Trappmann, B., Gautrot, J.E., Connelly, J.T., Strange, D.G., Li, Y., Oyen, M.L., Cohen, S.M., Boehm, H., Li, B., Vogel, V., Spatz, J.P., Watt, F.M., Huck, W.T., 2012. Extracellular-matrix tethering regulates stem-cell fate. *Nat. Mater.* 11 (7), 642–649.
- Tan, J.Y., Chua, C.K., Leong, K.F., 2013. Fabrication of channeled scaffolds with ordered array of micro-pores through micro-sphere leaching and indirect Rapid Prototyping technique. *Biomed. Microdevices* 15 (1), 83–96.
- Tse, J.R., Engler, A.J., 2011. Stiffness gradients mimicking in vivo tissue variation regulate mesenchymal stem cell fate. *PLoS One* 6 (1), 1–9.
- Viswanathan, P., Ondeck, M.G., Chirasatitsin, S., Ngamkham, K., Reilly, G.C., Engler, A.J., Battaglia, G., 2015. 3D surface topology guides stem cell adhesion and differentiation. *Biomaterials* 52, 140–147.
- Viswanathan, P., Johnson, D., Hurley, C., Cameron, N., Battaglia, G., 2014. 3D surface functionalization of emulsion-templated polymeric foams. *Macromolecules* 47 (20), 7091–7098.
- Wiria, F.E., Leong, K.F., Chua, C.K., Liu, Y., 2007. Poly-epsilon-caprolactone/hydroxyapatite for tissue engineering scaffold fabrication via selective laser sintering. *Acta Biomater.* 3 (1), 1–12.
- Yeong, W.Y., Sudarmadji, N., Yu, H.Y., Chua, C.K., Leong, K.F., Venkatraman, S.S., Boey, Y.C., Tan, L.P., 2010. Porous polycaprolactone scaffold for cardiac tissue engineering fabricated by selective laser sintering. *Acta Biomater.* 6 (6), 2028–2034.